University of Plymouth

PEARL **https://pearl.plymouth.ac.uk**

04 University of Plymouth Research Theses 01 Research Theses Main Collection

2023

Analysis of Hippo pathway signalling in schwannoma and meningioma

Grimm de Guibert, Julio

http://hdl.handle.net/10026.1/20156

http://dx.doi.org/10.24382/637
University of Plymouth

All content in PEARL is protected by copyright law. Author manuscripts are made available in accordance with publisher policies. Please cite only the published version using the details provided on the item record or document. In the absence of an open licence (e.g. Creative Commons), permissions for further reuse of content should be sought from the publisher or author.

Copyright Statement

This copy of the thesis has been supplied on condition that anyone who consults it is understood to recognise that its copyright rests with its author and that no quotation from the thesis and no information derived from it may be published without the author's prior consent.

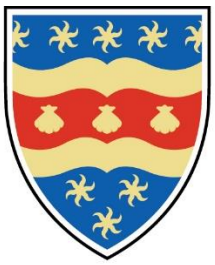

UNIVERSITY OF
PLYMOUTH

Analysis of Hippo pathway signalling in schwannoma and meningioma

by

Julio Grimm de Guibert

A thesis submitted to the University of Plymouth

in partial fulfilment for the degree of

Doctor of Philosophy

Peninsula Medical School

April 2022

Acknowledgements

I would like to thank my supervisory team consisting of Director of Studies Professor David Parkinson and supervisors Professor Oliver Hanemann and Dr Holly Roy for their guidance and support.

I would also like to thank the members of the Parkinson lab for their help and advice.

My appreciation also goes out to Glenn Harper of the EM unit, Professor Christian Mawrin and his group of the University of Magdeburg, Dr David Hilton and Philip Edwards of the Anatomical and Cellular Pathology department of the Derriford Hospital and Dr Emanuela Ercolano.

Finally, I would like to thank my parents and my partner Jayne for always having my back and believing in me.

Author's Declaration

At no time during the registration for the degree of Doctor of Philosophy has the author been registered for any other University award without prior agreement of the Doctoral College Quality Sub-Committee.

Work submitted for this research degree at the University of Plymouth has not formed part of any other degree either at the University of Plymouth or at another establishment.

Word count of main body of thesis (Start of Introduction to End of Discussion): 55360

Signed:

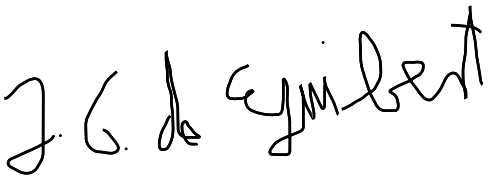

Date: 30/04/22

Abstract

Analysis of Hippo pathway signalling in schwannoma and meningioma by Julio Grimm de Guibert

This project focuses on two tumours of the nervous system, schwannoma and meningioma. A large group of schwannomas and meningiomas display the inactivation of the *NF2* gene. The *NF2* gene codes for the tumour suppressor protein Merlin and its loss is associated with a multitude of pro-tumourigenic mechanisms leading to the occurrence of schwannomas and meningiomas. The loss of Merlin function causes augmented Hippo signaling i.e. interaction of YAP and TAZ, both co-activators of gene expression and the two main effectors of the Hippo signalling pathway, and TEAD, a group of transcription factors binding to YAP and TAZ. There resulting gene expression is associated with increased proliferation and evasion of cell death. This makes the YAP/TAZ-TEAD complex an excellent therapeutic target.

Since therapy options for schwannomas and meningiomas are limited to surgery and radiosurgery, both carrying additional risks for the patient, new therapy approaches are desperately needed. Therefore, we explored if a schwannoma mouse model and cell culture and primary meningioma cells would be suitable systems to allow the testing of two potential new therapy options.

Macrophages, especially tumour associated macrophages (TAMs), have been shown to promote tumour growth in various ways. Therefore, macrophage depletion is considered a promising therapy option. To see whether elimination of macrophages could be effective in our chosen schwannoma mouse model, a connection between increased TAM numbers and equally heightened proliferation within the developing schwannomas would need to be and was established. Additionally, *Nf2* gene knockout and the additional knockout of either *Yap* or *Taz* genes also had distinct effects on proliferation, TAM numbers and overall schwannoma structure and cell numbers.

Macrophage infiltration and resulting support of tumour growth has also been shown to be partly YAP/TAZ-TEAD signaling dependent. Therefore, in order to simultaneously reduce TAM-derived growth support and directly impair tumour cell proliferation, the second approach targets the Hippo signaling pathway using TEAD S-autopalmitoylation inhibitors by Vivace Therapeutics which interfere with YAP/TAZ-TEAD interaction. I could show that these TEAD palmitoylation inhibitors efficiently inhibit cell proliferation of human meningioma cell lines and primary human meningioma cells.

Abbreviations

AMOTL	Angiomotin like
ANOVA	Analysis of Variance
ARID	AT-rich interaction domain
BAX	BCL-2 Associated X
BCA	Bicinchoninic acid
BCL-2	B-cell lymphoma-2
BM-1	Ben-men-1
BSA	Bovine serum albumin
cAMP	Cyclic adenosine monophosphate
CPA	Cerebellopontine angle
CTGF	Connective tissue growth factor
CYR61	Cysteine-rich angiogenic inducer 61
DMEM	Dulbecco's modified eagle medium
DMSO	Dimethyl sulfoxide
Dpi	Days post injury
E10	Embryonic day 10
ECM	Extracellular matrix
EDTA	Ethylenediaminetetraacetic acid
EdU	5-Ethynyl-2’-deoxyuridine
EGFR	Epidermal growth factor receptor
ER	Endoplasmic reticulum
ErbB2/3	Erb-B2/3 receptor tyrosine kinase
ERK	Extracellular signal-regulated kinase
ERM	Ezrin, Radixin and Moesin
FAK	Focal adhesion kinase
FBS	Fetal bovine serum
GLUT3	Glucose transporter 3
HRP	Horseradish peroxidase
ICC	Immunocytochemistry
IGFBP4	Insulin growth factor binding protein 4
IHC-fr	Immunohistochemistry
IOMM-Lee	IntraOsseous Malignant Meningioma-Lee
KIBRA	Kidney and brain expressed protein
LATS1/2	Large tumour suppressor kinase 1/2
LZTR1	Leucine-zipper-like transcriptional regulator 1
MAML2	Mastermind like transcriptional coactivator 2
MEK	Mitogen-activated protein kinase kinase
MOB1A/B	Mps One Binder kinase activator 1A/B
MST1/2	Macrophage stimulating 1/2
mTORC1	Mammalian target of rapamycin complex 1
NuRD	Nucleosome remodelling and deacetylase

NUTM1	NUT midline carcinoma family member 1
OCT	Optimum cutting temperature compound
PAK	p21-activated kinase
PBP	Palmitate binding pocket
PBS	Phosphate buffered saline
PFA	Paraformaldehyde
PGDS	Prostaglandin D_2 synthase
PI3K	Phosphoinositide 3-kinase
Postn-Cre	Periostin-Cre
RAF	Rapidly accelerated fibrosarcoma
Ras	Rat sarcoma virus
RIPA	Radioimmunoprecipitation assay
Rpm	Rounds per minute
RTK	Receptor tyrosine kinase
SAV	Salvador family WW domain containing protein 1
SC	Schwann cell
SDS-PAGE	Sodium dodecyl sulphate polyacrylamide gel electrophoresis
SGC	Satellite glial cell
SMARCB1	SWI/SNF related matrix associated actin dependent regulator of chromatin subfamily B member 1
Src	Proto-oncogene tyrosine-protein kinase
SWI/SNF	SWItch/sucrose non-fermentable
TAMs	Tumour associated macrophages
TAM receptors	Tyro3 (Sky) – Axl – Mer receptors
TAZ	Transcriptional coactivator with PDZ-binding motif
TBS-T	Tris-buffered saline containing 0.5 % Tween
TEAD	TEA domain
TGF-β	Transforming growth factor beta
WNT5A	Wingless-related integration site family member 5A
WT	wild type
YAP	Yes-associated protein
YBD	YAP binding domain

Table of Contents

Copyright statement……1

Title page……2

Acknowledgements……4

Author's declaration……5

Abstract……6

Abbreviations……7

Table of contents……9

1. Introduction……20

1.1 NF2/Merlin……20

1.2 Identification of the NF2 gene……20

1.3 NF2 gene mutations and effects……20

1.4 Neurofibromatoses……21

1.5 Neurofibromatosis type 2……22

1.5.1 Introduction……22

1.5.2 NF2 schwannomas……22

1.5.3 Schwannoma treatment……23

1.5.4 NF2 meningiomas……24

1.5.5 Meningioma treatment……25

1.5.6 Alternative Merlin regulation and schwannoma malignancy……25

1.5.7 Spinal cord ependymomas……26

1.5.8 Ependymoma treatment……26

1.5.9 Peripheral neuropathy……26

1.5.10 Other neurological manifestations in NF2 patients……27

1.5.11 Ocular manifestations……28

1.5.12 Disease course of NF2……28

1.6 Merlin in cancer……30

1.7 Merlin regulation and signalling……31

1.7.1 NF2/Merlin structure……31

1.7.2 Merlin regulation via phosphorylation……33
1.7.3 Merlin's regulation of non-Hippo signalling pathways……33
1.7.4 Merlin's tumour suppressive function……34
1.8 Hippo signalling pathway……36
1.8.1 Canonical Hippo pathway: MST activation……36
1.8.2 Canonical Hippo pathway: LATS activation……38
1.8.3 Canonical Hippo pathway: YAP and TAZ regulation……38
1.8.4 Canonical Hippo pathway: TEAD function……40
1.8.5 VGLL regulation and function……41
1.8.6 Other TEAD cofactors……41
1.8.7 TEAD regulation……42
1.8.8 TEAD post-translational regulation: S-palmitoylation……42
1.8.9 YAP/TAZ-TEAD transcriptional activity……43
1.8.10 YAP/TAZ-TEAD target genes……43
1.8.11 TEAD significance in cancer……44
1.9 Merlin dependent YAP/TAZ/TEAD regulation……45
1.9.1 Metabolism……45
1.9.2 Actin cytoskeleton/Mechanical stress……45
1.9.3 GPCRs……46
1.9.4 Cell polarity proteins/complexes……46
1.9.5 Cell-cell contacts/Angiomotin……46
1.9.6 Integrins/Cell-ECM contacts/FGF……47
1.9.7 Nervous system……47
1.10 Merlin independent YAP/TAZ/TEAD regulation……47
1.10.1 Actin cytoskeleton/Mechanical stress……47
1.10.2 Actomyosin cytoskeleton/Spectrin……48
1.10.3 GPCRs……49
1.10.4 Cell cycle/Src/p53……49
1.10.5 Energy stress……50

1.10.6 Osmotic stress/ER……50
1.10.7 IKKε/PRP4K……51
1.10.8 Immune response……51
1.10.9 mTOR/Lysosomes/Autophagosomes……52
1.10.10 Cell-cell contacts/Cell polarity proteins/complexes……52
1.10.11 Post-translational modifications……52
1.10.12 Integrins /Cell-ECM contacts……53
1.10.13 Wnt-β-catenin……53
1.10.14 EGF/Insulin/Hyaluronan/Oncogenic viruses……53
1.10.15 Organ size regulation……53
1.10.16 Nervous system……54
1.11 Hippo signalling in schwannomas and meningiomas……55
1.12 Hippo signalling in macrophages……55
1.13 Hypothesized effect of Vivace inhibitors on schwannomas and their growth….56
1.14 Role of Hippo signalling in cancer……56
1.15 Compounds targeting the Hippo pathway……59
1.15.1 Introduction……59
1.15.2 Classification of YAP/TAZ drugs……60
1.15.3 Group II drugs……60
1.15.4 Vivace Therapeutics inhibitors……63
1.16 NF2 drug trials……63
1.17 Macrophages……64
1.17.1 Origin and function of macrophages……64
1.17.2 TAMs……65
1.17.3 Depletion of macrophages……67
1.18 Schwannoma mouse models……68
1.19 Meningioma mouse models……69
1.20 Hypotheses and objectives……73
2. Materials and Methods……75

2.1 Clinical samples……75
2.2 Cells……76
2.2.1 General cell culture……76
2.2.2 EdU proliferation experiments……77
2.2.3 EdU staining of coverslips……78
2.2.4 Primary human meningioma cell samples for Western blot analysis…..78
2.3 Mice……79
2.3.1 Mouse breeding……79
2.3.2 PCR genotyping and agarose gel electrophoresis……79
2.3.3 IP EdU injection and tissue extraction……82
2.4 Fluorescent staining……83
2.4.1 Tissue sample preparation……83
2.4.2 Embedding, sectioning and staining of tissue sections/cells……84
2.4.2.1 IHC-fr/ICC……84
2.4.2.2 Agarose EdU staining and IHC……87
2.4.2.3 EdU staining of DRG and VG sections……87
2.5 Western blot……88
2.5.1 BCA assay……88
2.5.2 Sample preparation and SDS-PAGE……88
2.5.3 Electroblotting……89
2.5.4 Immunodetection and secondary probing……89
2.6 Imaging and quantification……91
2.7 Statistical analysis……92
3. Results……93
3.1 Breeding of required mouse genotypes……93
3.2 Examination of antibody functionality in sciatic nerves……95
3.2.1 IHC staining for macrophage markers……95
3.2.2 IHC staining for vascular marker CD31 and pan-macrophage marker Iba1……101
3.3 Sciatic nerve crush experiment with F1 generation of Postn-Cre mice……103

3.4 IHC staining for Iba1 in xenograft meningioma……..108

3.5 Genotyping of Postn-Cre driven mice colonies……110

3.6 Transmission electron microscopy of NF2 sKO sciatic nerves……...112

3.7 H & E staining of Postn-Cre mice DRGs……113

3.8 MSB staining of Postn-Cre mice DRGs……122

3.9 IHC staining for Collagen IV, Iba1 and Edu in Postn-Cre mouse DRGs……126

3.10 IHC staining for Iba1 and EdU in Postn-Cre mouse cochleae……133

3.11 IHC staining for Iba1 and EdU in Postn-Cre mouse vestibular ganglia……..136

3.12 Testing the effect of TEAD palmitoylation inhibitors on the proliferation of human meningioma cell lines.....141

3.13 Testing the effect of Pan-TEAD inhibitors on the proliferation of primary human meningioma cells.....147

3.14 Testing the effect of Pan-TEAD inhibitors on the protein expression of CTGF and Pan-TEAD in primary human meningioma cells……155

4. Discussion and Conclusion……161

4.1 Main results summary……161

4.2 Postn-Cre mouse model……162

4.3 DRG architecture……163

4.4 Schwannoma mouse model comparison……163

4.5 YAP/TAZ-TEAD dependent SGC/SC proliferation in DRGs and VGs……166

4.6 Non-neuronal and neuronal cell quantification results……167

4.7 Difference between YAP and TAZ functions……167

4.8 Role of YAP and TAZ in proliferation and apoptosis……168

4.9 Possible apoptotic effect due to differences of YAP and TAZ knockouts……168

4.10 Link between proliferation and macrophage numbers in injured nerves, schwannoma and meningioma……169

4.11 Link between proliferation and macrophage numbers in Postn-Cre schwannoma mouse model……170

4.12 Loss of neuronal cells……171

4.13 The presence of collagen and collagen IV in different genotypes……171

4.14 Role of collagen in hearing loss……171

4.15 Potential use of losartan in the Postn-Cre schwannoma model……..172

4.16 Interaction of TAMs and collagen……172

4.17 Losartan and Pan-TEAD combination therapy……173

4.18 YAP and TAZ inhibition in meningioma……173

4.18.1 YAP and TAZ inhibition in human meningioma cell lines……174

4.18.2 YAP and TAZ inhibition in primary human meningioma cells……174

4.18.3 VT1 efficacy in meningioma and mesothelioma cells……175

4.18.4 Effect of Pan-TEAD inhibitors on CTGF and TEAD protein expression……175

4.18.5 Faster effect of Pan-TEAD inhibitors on proliferation than on protein expression……176

4.19 Limitations of the used Postn-Cre schwannoma model……177

4.20 Future work……177

4.21 Conclusion……178

5. References……179

6. Appendix……243

List of Figures

Figure 1.1: Domain structure of Merlin and corresponding exons 32

Figure 1.2: CD44/β1 integrin/receptor tyrosine kinase (RTK) signalling and Merlin regulation 35

Figure 1.3: Merlin and the Hippo signalling pathway 36

Figure 1.4: Mammalian Hippo pathway and influences on its activity 37

Figure 1.5: Structure and domains of TEAD1 – 4 and the paralogs YAP and TAZ 39

Figure 1.6: Mutations of different Hippo pathway components in cancer and other diseases 58

Figure 1.7: The three groups of YAP/TAZ-TEAD targeting drugs 62

Figure 1.8: Image displaying schwannoma formation in DRGs and spinal nerves 71

Figure 1.9: Comparison of tumoursphere-derived xenograft in mice and original human patient meningioma 72

Figure 1.10: H & E stained xenograft meningioma consisting of KT21 cells growing in SCID mice for 21 days 74

Figure 3.1: Breeding scheme to generate NF2 single knockout (NF2 sKO), NF2/YAP double knockout (NF2/YAP dKO) and NF2/TAZ double knockout (NF2/TAZ dKO) mice and their littermate controls 94

Figure 3.2.1: CD68 and CD206 staining of a 21 days post injury (21 dpi) sciatic nerve of an adult 3 month old P0-Cre+ $NF2^{fl/fl}$ (NF2 sKO) mouse 96

Figure 3.2.2: CD68+ and CD206+ cells were detected in two 21 dpi sciatic nerves of adult 3 month old NF2 sKO (P0-Cre+ $NF2^{fl/fl}$) mice 97

Figure 3.2.3: 3 layer CD68 and 2 layer CD206 double staining of a 21 dpi sciatic nerve of an adult 3 month old NF2 sKO (P0-Cre+ $NF2^{fl/fl}$) mouse 98

Figure 3.2.4: CD68 and iNOS double staining of four 21 dpi sciatic nerves of adult 3 month old mice 99

Figure 3.2.5: LPS-treated RAW 264.7 macrophage cells displayed cytoplasmic iNOS staining 100

Figure 3.2.6: Iba1 staining of the 21 dpi sciatic nerve sections of five adult 5 month old mice 102

Figure 3.3.1: Semithin sections of intact (INT) and injured (INJ) tibial control (Postn-Cre- $NF2^{wt/fl}$) nerves of adult 2 month old 23 dpi stained with methylene blue 104

Figure 3.3.2: Semithin sections of intact (INT) and injured (INJ) tibial nerves of the Postn-Cre+ $NF2^{wt/fl}$ (= monoallelic for NF2) adult 2 month old mice 23 dpi stained with methylene blue 105

Figure 3.3.3: Semithin sections of intact (INT) and injured (INJ) tibial nerves of the P0-Cre+ $NF2^{fl/fl}$ (NF2 sKO) adult 2 month old mice 23 dpi stained with methylene blue 106

Figure 3.3.4: Quantification of counted myelinated/remyelinated axons in tibial nerves of adult 2 month old mice 23 dpi 107

Figure 3.4.: Iba1 positive cells were found within the IOMM-Lee derived xenograft meningioma 109

Figure 3.5.1: In direct comparison, genotyping with the Gehlhausen primers resulted in clearer differences between Postn-Cre+ and Postn-Cre- samples than using the King's College primers 110

Figure 3.5.2: Examples of Postn-Cre, NF2, YAP and TAZ genotyping of mouse tail snips confirming the flox/flox background of the Postn-Cre driven mouse colonies 111

Figure 3.6: Ultrathin sections of Postn-Cre driven NF2 sKO sciatic nerves stained with uranyl acetate and Reynold's lead citrate under a transmission electron microscope (TEM) 113

Figure 3.7.1: Visual assessment of hematoxylin and eosin (H & E) stained dorsal root ganglia (DRGs) of 3 month old control, NF2 sKO, NF2/YAP dKO and NF2/TAZ dKO mice 114

Figure 3.7.2: H & E staining of the DRGs of 5 month old mice 116

Figure 3.7.3: 9 month timepoint DRGs stained for H & E 118

Figure 3.7.4: Quantification of neuronal cells in H & E stained images of DRGs from all genotypes and timepoints 119

Figure 3.7.5: Counts of non-neuronal cells in DRGs 121

Figure 3.8.1: MSB stained DRGs of the 3 month timepoint 123

Figure 3.8.2: 5 month timepoint DRGs stained with MSB 124

Figure 3.8.3: MSB stained sections of the 9 month DRGs 125

Figure 3.9.1: Neurofilament (NF) and Collagen IV (Coll-IV) stained frozen sections of 9 month timepoint DRGs 127

Figure 3.9.2: Cytoplasmic Iba1 stain of macrophages detected in DRG mouse tissue 128

Figure 3.9.3: Iba1 stained frozen sections of the 3 months, 5 months and 9 months DRGs of all genotypes 129

Figure 3.9.4: Quantification of Iba1 positive macrophages in DRG tissue and subsequent statistical analysis 130

Figure 3.9.5: Frozen DRG sections stained for EdU 132

Figure 3.9.6: Statistical analysis of the quantification of EdU stained frozen DRG sections 133

Figure 3.10.1: Iba1 stained agarose sections of cochleae from 5 month old control and NF2 sKO mice 135

Figure 3.10.2: EdU and Iba1 stained agarose cochlea sections of 5 month old control and NF2 sKO mice 136

Figure 3.11.1: 3 and 5 month NF2 sKO vestibular ganglion (VG) and 5 month NF2 sKO DRG sections stained for Neurofilament (NF) and EdU 138

Figure 3.11.2: Iba1 stained VG sections of 3 month and 5 month old control and NF2 sKO mice 139

Figure 3.11.3: Frozen VG sections of 3 month and 5 month old control and NF2 sKO mice 140

Figure 3.11.4: Quantification of 3 month and 5 month timepoint VGs of control and NF2 sKO mice 141

Figure 3.12.1: After testing the four different EdU pulse incubation times on IOMM-Lee cells 4 hours (4 h) was chosen as a suitable EdU pulse time 143

Figure 3.12.2: Usage of TEAD palmitoylation inhibitors V2, V3 and V5 at a concentration of 1 µM for 48 hours in BM-1 and KT21 cells 145

Figure 3.12.3: Quantification of EdU positive nuclei in BM-1 and KT21 cells after incubation with TEAD palmitoylation inhibitors 146

Figure 3.13.1: Images of Merlin null primary human meningioma cells treated with Pan-TEAD inhibitors VT1 or VT2 at 1 µM for 48 hours 149

Figure 3.13.2: Quantification of EdU positive nuclei in Merlin null primary human meningioma cells after incubation with Pan-TEAD inhibitors VT1 and VT2 150

Figure 3.13.3: Images of Merlin positive primary human meningioma cells after 1 µM of Pan-TEAD inhibitor VT1 or VT2 or Vehicle for 48 hours 151

Figure 3.13.4: Quantification of EdU positive nuclei in Merlin positive primary human meningioma cells after incubation with Pan-TEAD inhibitors VT1 and VT2 152

Figure 3.13.5: Standardized cell division rates of Merlin null and Merlin positive primary human meningioma cells incubated with Pan-TEAD inhibitors VT1 and VT2 154

Figure 3.14.1: Western blotting of CTGF in Merlin null primary human meningioma cells after a 48 hour incubation period with Pan-TEAD inhibitors VT1 or VT2 at 1 µM 156

Figure 3.14.2: Quantification of protein bands in Figure 3.14.1 156

Figure 3.14.3: Immunoblotting of CTGF and Pan-TEAD after incubating Merlin null primary human meningioma cells for 48 hours with 1 µM of Pan-TEAD inhibitors VT1 or VT2 157

Figure 3.14.4: Quantification of protein bands seen in Figure 3.14.3 158

Figure 3.14.5: Western blotting of CTGF and Pan-TEAD in Merlin positive primary human meningioma cells after a 48 hour incubation period with Pan-TEAD inhibitors VT1 or VT2 at 1 µM 159

Figure 3.14.6: Quantification of the protein bands obtained by Western blot (Figure 3.14.5) 160

Figure 4.1: Loss of NF2 gene results in inhibition of YAP/TAZ activity via Motins 165

Figure 6.1: Martius Scarlet Blue (MSB) control stainings on paraffin sections of human tonsil tissue 243

Figure 6.2: Images of frozen DRG tissue stained without primary anti-Collagen IV and anti-Neurofilament antibodies 244

Figure 6.3: Images of frozen DRG and VG sections stained without primary anti-Iba1 antibody 245

Figure 6.4: Agarose cochlea sections stained without primary anti-Iba1 antibody 246

Figure 6.5: Frozen VG tissue stained without primary anti-Neurofilament antibody 247

Figure 6.6: Images of complete PVDF membranes whose bands are seen in Figure 3.14.1 248

Figure 6.7: Images of uncropped PVDF membranes whose bands are seen in Figure 3.14.3 249

Figure 6.8: Images of whole PVDF membranes whose bands are visible in Figure 3.14.5 250

List of Tables

Table 1.1: Comparison of P0-Cre $NF2^{fl/fl}$ and Postn-Cre $NF2^{fl/fl}$ schwannoma models 68

Table 2.1: Clinical information about primary human meningioma cells used in TEAD S-autopalmitoylation inhibitor experiments 75

Table 2.2: TEAD S-autopalmitoylation inhibitors by Vivace Therapeutics 77

Table 2.3: Click-iT reaction mix 78

Table 2.4: PCR master mix for one reaction 80

Table 2.5: P0-Cre PCR program 80

Table 2.6: Postn-Cre PCR program 81

Table 2.7: NF2 PCR program 81

Table 2.8: YAP PCR program 81

Table 2.9: TAZ PCR program 81

Table 2.10: Primers used for PCR Genotyping 82

Table 2.11: Primary antibodies for IHC/ICC 85

Table 2.12: Secondary antibodies for IHC/ICC 86

Table 2.13: Streptavidin-conjugated fluorophore for IHC 86

Table 2.14: Primary antibodies used for Western blot 90

Table 2.15: Secondary antibodies used for Western blot 90

Table 3.1: IC_{50} values calculated for TEAD palmitoylation inhibitors V2, V3 and V5 147

Table 3.2: IC_{50} values calculated for Pan-TEAD inhibitors VT1 and VT2 in Merlin null and Merlin positive primary meningioma cells 153

1. Introduction

1.1 NF2/Merlin

The function of tumour suppressor genes is to tightly regulate cellular processes such as cell proliferation and survival in order to avoid tumourigenesis. When both copies of a given tumour suppressor gene are impaired in their function (according to Knudson's two-hit hypothesis (Knudson, 1971)) due to mutation, epigenetic silencing or chromosomal loss (Agnihotri *et al.*, 2016; Gonzalez-Gomez *et al.*, 2003; Kino *et al.*, 2001) the product of that tumour suppressor gene can no longer carry out its function, resulting in tumour development. Such a tumour suppressor gene is the NF2 (Neurofibromatosis type 2) gene whose protein product is known as Merlin (Moesin-Ezrin-Radixin-Like Protein") or schwannomin (Rouleau *et al.*, 1993; Trofatter *et al.*, 1993). The NF2 gene can be found on the long arm of human chromosome 22, more specifically on 22q12.

1.2 Identification of the NF2 gene

The NF2 gene and its protein product Merlin were correctly classified as tumour suppressors in 1993 by Trofatter et al (Trofatter *et al.*, 1993). They also identified NF2/Merlin to be the tumour suppressor gene/protein whose impairment gives rise to Neurofibromatosis 2 and can also lead to the occurrence of sporadic schwannomas and meningiomas. Furthermore, they found the NF2 gene to be widely expressed in a multitude of tissues including kidney, lung, brain, pancreas, heart and liver and they correctly hypothesized that Merlin belongs to the family of ERM proteins (Trofatter *et al.*, 1993). Finally, they made correct assumptions about Merlin's function as a plasma membrane-cytoskeleton linker protein and Merlin's structure. They described Merlin to consist of an N-terminal region of approximately 200 amino acids homologous to all ERM proteins (later named the FERM domain), an α-helix region (= central coiled coil region) and a 'highly charged' C-terminal domain (= hydrophilic tail) (Trofatter *et al.*, 1993).

1.3 NF2 gene mutations and effects

It seems that the severity of Neurofibromatosis type 2 strongly correlates with type of mutation found in the NF2 gene. Large or in-frame deletions and missense mutations appear to bring about milder symptoms while frameshift or nonsense mutations result in graver illness, i.e. earlier onset of symptoms and greater number of tumours (Evans *et al.*, 1998; Parry *et al.*, 1996). The reason for this is presumably that the former allows the resulting Merlin protein to retain a certain degree of its functionality while the latter most likely severely impairs Merlin function. Splice-site mutations in exons 11-15 (α helical/coiled coil domain and C-terminal domain) appear to have less severe outcomes whereas splice-site

mutations in exons 1-5 (FERM domain) have a greater impact, i.e. earlier onset of symptoms and higher number of intracranial meningiomas (Baser *et al.*, 2005a). A connection between NF2 gene mutation type and mortality risk was also established. A higher risk of mortality was found in patients with NF2 gene frameshift or nonsense mutations compared to patients with NF2 gene missense mutations (Baser *et al.*, 2002b).

NF2 gene *de novo* mutations during embryogenesis can also occur in individuals without a familial NF2 background. This can result in genetic mosaicism where a percentage of the patients' cells (somatic cells, germline cells or both) contain one mutated NF2 allele, putting these cells at risk for forming tumours after losing their remaining intact NF2 gene. In somatic cells, NF2 gene mosaicism has a propensity to cause a milder form of NF2, with a vestibular schwannoma and other NF2 associated tumours growing only on one side of the body. Mosaicism is estimated to be found in up to 60 % of sporadic cases with bilateral vestibular schwannoma and in 33 % of sporadic cases with unilateral vestibular schwannoma (Evans *et al.*, 2007; Kluwe & Mautner, 1998; Moyhuddin *et al.*, 2003). If the NF2 gene mosaicism is present in the germline cells, only a proportion of germline cells will be affected, decreasing the probability of passing down the NF2 gene mutation to the patients' children. In the event a transmission does occur, the affected children have a high chance of developing a more severe form of Neurofibromatosis type 2 than their mosaic parents since the NF2 gene mutation is present in all of their cells.

1.4 Neurofibromatoses

The first description of the illness now called Neurofibromatosis type 2 (previously named bilateral acoustic neurofibromatosis) dates back to the case of a patient in 1822 suffering from hearing loss and brain, dura mater and skull tumours (Wishart, 1822). For decades, it was not recognised as being a separate disease from the more frequently seen illness known as von Recklinghausen's disease, now termed Neurofibromatosis type 1 (NF1) (Cushing, 1917). After studying 2 different families over several generations, two of NF2's characteristics, inheritance of the illness from parent to child and autosomal dominant transmission, were reported in 1920 and 1930, respectively (Feiling & Ward, 1920; Gardner & FRAZIER, 1930). Finally, the underlying cause for NF1 and NF2 could be traced back to separate chromosomes in 1987 via genetic linkage analysis, allowing the distinction as two different diseases (Health, 1988; Rouleau *et al.*, 1987; Seizinger *et al.*, 1987).

Neurofibromatoses are categorized into three types: Neurofibromatosis type 1 (NF1), Neurofibromatosis type 2 (NF2) and schwannomatosis.

NF1 is an autosomal-dominant disorder. It is brought on by a mutated NF1 tumour suppressor gene which can be found on chromosome 17q11. Patients with NF1 can have many afflictions, including skeletal dysplasia, gliomas of the optic pathway, cutaneous, subcutaneous and plexiform neurofibromas and Lisch nodules (Health, 1988; Viskochil *et al.*, 1990; Wallace *et al.*, 1990a; Wallace *et al.*, 1990b).

Schwannomatosis is often associated with mutations in LZTR1 gene and/or the SMARCB1 tumour suppressor gene (Hulsebos *et al.*, 2007; Piotrowski *et al.*, 2014). Both genes are situated on chromosome 22q11, very close to the NF2 gene (22q12).

Schwannomatosis is defined by the occurrence of several schwannomas not located in the skin and the lack of vestibular schwannomas (Baser, Friedman & Evans, 2006).

1.5 Neurofibromatosis type 2

1.5.1 Introduction

The prevalence of the NF2 disorder is 1/25000 people and close to 100 % of affected people will suffer from symptoms by the age of 60 (Evans *et al.*, 1992b; Evans *et al.*, 2005). Patients with this illness inherit a germline mutation of one of the NF2 alleles or spontaneously gain such a *de novo* mutation during or after embryogenesis. When the remaining intact NF2 allele is then compromised in the peripheral nervous system, central nervous system, skin or eye or a combination of these, Neurofibromatosis type 2 develops. Another way of losing the function of both wild type NF2 genes is by somatic mutation. Such sporadic NF2 gene mutations tend to cause the formation of unilateral vestibular schwannomas in patients aged 40 to 60 (Evans *et al.*, 2005; Sobel, 1993).

NF2 symptoms first occur mostly in young adults between the ages of 20 and 30. A common initial symptom of NF2 is unilateral hearing loss, often paired with dizziness, tinnitus and a loss of balance (Evans *et al.*, 1992a; Parry *et al.*, 1994). These symptoms can also be seen in up to 30% of children with NF2 but other features are more common in younger NF2 patients. These include visual impairment (due to intracranial tumours, hamartomas or cataracts), peripheral neuropathy and more atypical tumours such as spinal cord and skin tumours (Evans, Birch & Ramsden, 1999; Nunes & MacCollin, 2003; Ruggieri *et al.*, 2005).

1.5.2 NF2 schwannomas

The hallmark of Neurofibromatosis type 2 is the occurrence of bilateral vestibular schwannomas on cranial nerve VIII (vestibulocochlear nerve), found in 90 – 95 % of NF2 patients (Evans *et al.*, 1992a; Mautner *et al.*, 1996; Parry *et al.*, 1994). As the name suggests, schwannomas originate from Schwann cells of the peripheral nervous system. Schwann cells either produce myelin sheaths to insulate axons (myelinating Schwann cells) or envelop smaller diameter axons by wrapping their cell bodies around them forming a Remak bundle (non-myelinating Schwann cells).

Over 99 % of NF2-associated vestibular schwannomas are benign (Baser *et al.*, 2000) but their growth on cranial nerve VIII causes symptoms. Despite the fact that vestibular schwannoma (VS) growth rates vary greatly between patients, there is some indication that VS growth rates

tend to slow down as the patients get older (Baser *et al.*, 2005b). High resolution contrast-enhanced, T1-weighted magnetic resonance imaging (MRI) is considered the best method of visualizing vestibular schwannomas. From a histological standpoint, NF2 vestibular schwannomas tend to show interweaving patterns of Schwann cell bundles with Antoni A tissue and Antoni B tissue areas, hyalinized vessels and Verocay bodies (Sobel, 1993).

Schwannomas in Neurofibromatosis type 2 patients are defined by NF2 gene inactivation and a lack of Merlin protein expression (Sainz *et al.*, 1994). Additionally, a study reported a strong decrease or absence of Merlin expression in the majority of the examined sporadic schwannomas and sporadic meningiomas (11/14 and 16/19, respectively) and in some of the sporadic ependymomas (3/8) (Gutmann *et al.*, 1997). The combination of Loss Of Heterozygosity (LOH, loss of one gene copy) and inactivation of the remaining NF2 gene due to mutation is the most frequent reason for the development of sporadic schwannomas. NF2 gene deactivation by 22q chromosome loss and/or NF2 mutations was seen in 77 % and 22q loss could be observed in 61 % of sporadic schwannoma samples (Agnihotri *et al.*, 2016).

Nonetheless, examples of DNA methylation of transcriptional elements of the NF2 gene likely affecting NF2 gene transcription via epigenetic silencing were observed in 15.3 % of NF2-associated and 19.3% of sporadic schwannomas (Gonzalez-Gomez *et al.*, 2003). Methylation of three CpG sites found in the NF2 promoter were seen in 60.9 % of the examined vestibular schwannomas, coupled with both a reduction in promoter activity and a diminished NF2 mRNA expression (Kino *et al.*, 2001). However, a different report found unmethylated NF2 promoters in 23 of 35 sporadic vestibular schwannomas (= 65.7 %). In the remaining 12 sporadic vestibular schwannomas, promoter methylation could not be determined (Koutsimpelas *et al.*, 2012).

1.5.3 Schwannoma treatment

One of the classical treatments for bilateral vestibular schwannoma is surgical removal. Doing so in the early stages of the tumour (when tumour diameter has not yet exceeded 3 cm) can safeguard hearing and facial nerve function (Brackmann *et al.*, 2001; Samii, Matthies & Tatagiba, 1997). In patients with NF2-induced deafness, early VS resection has a chance of preserving the cochlea nerve, allowing the fitting of a cochlea implant to regain their sense of hearing. However, given the risk of facial paralysis and/or injury of the lower cranial nerves, early VS removal is only endorsed upon hearing loss or the discovery of a fast VS growth. Unfortunately, the risk of surgery heightens with tumour size. Often VS resection is only performed when absolutely necessary, i.e. in the event of increased intracranial pressure or compression of the brainstem (Asthagiri *et al.*, 2009).

Another option for treatment is stereotactic radiosurgery. Schwannomas smaller than 3 cm in diameter and schwannomas without cysts or peritumoural oedema have the highest probability to result in schwannoma growth inhibition following radiosurgery. Between 74 % and 100 % of NF2-associated VS after treatment were shown to achieve this favourable outcome. For some patients, this resulted in the preservation of auditory (33 – 57 %) and facial nerve (92 – 100 %) function (Kida *et al.*, 2000; Mathieu *et al.*, 2007; Roche *et al.*, 2000;

Rowe *et al.*, 2003). Radiosurgery risks include relapse in tumour growth, occurrence of malignancies due to exposure to radioactivity, formation of scar tissue complicating the continuing facial nerve preservation and detrimental effects on cochlear nerve function, possibly preventing the future insertion of a cochlea implant (Baser *et al.*, 2000; Rowe *et al.*, 2007).

1.5.4 NF2 meningiomas

With schwannomas being by far the most frequent tumour to be found in NF2 patients, meningiomas are the second most common tumour seen in these patients. The meningioma cells of origin are believed to be the cells of the arachnoid mater of the leptomeninges (the arachnoid and pia mater), which extend along the spinal cord and brain (Wiemels, Wrensch & Claus, 2010). The majority of NF2-associated meningiomas are intracranial, found in 45 – 58 % of NF2 patients (Evans *et al.*, 1992a; Mautner *et al.*, 1996; Parry *et al.*, 1994) and are often numerous and tend to form earlier in life than sporadic meningiomas (Evans, Birch & Ramsden, 1999; Mautner *et al.*, 1996; Nunes & MacCollin, 2003; Parry *et al.*, 1994). Furthermore, NF2 patients with intracranial meningiomas have more than double (2.5x) the relative risk of mortality than NF2 patients without intracranial meningiomas (Baser *et al.*, 2002b). Additionally, a sequencing study in a total of 65 meningiomas (percentages of NF2 and non-NF2 meningiomas not disclosed) reported focal NF2 inactivation in 43 % of examined meningiomas (Brastianos *et al.*, 2013).

Interestingly, a connection between the identity of the mutated gene(s) and meningioma location could be found in sporadic meningiomas. Most of the meningioma occurring in the cerebral convexity and spinal canal were seen to possess NF2 mutations and/or chromosome 22 loss (Bi *et al.*, 2016; Brastianos *et al.*, 2013; Clark *et al.*, 2013; Clark *et al.*, 2016; Okano *et al.*, 2021). Furthermore, skull base meningiomas with these genetic alterations were shown to be found largely in the posterior and lateral skull base (Brastianos *et al.*, 2013; Clark *et al.*, 2013; Hartmann *et al.*, 2006; Wellenreuther *et al.*, 1995; Youngblood *et al.*, 2019).

Common symptoms of meningioma tumours are headaches and seizures but symptoms depend on meningioma location and size. Meningiomas in the cerebral convexity need to grow to a considerable size in order to cause symptoms. In contrast, small meningiomas growing in the lower cranial nerves, the optic nerve sheath, at the skull base and in the spinal canal can quickly result in nerve compression, causing a range of symptoms (including visual impairment) with varying severity (Asthagiri *et al.*, 2009; Lloyd & Evans, 2013).

The imaging technique of choice for visualizing meningiomas is contrast-enhanced, T1-weighted MRI (Asthagiri *et al.*, 2009). Neurofibromatosis type 2 can give rise to meningothelial, fibroblastic, psammomatous and transitional meningiomas, with the transitional kind being the most frequent (Perry *et al.*, 2001). NF2 meningiomas also tend to have higher proliferation rates and be more aggressive (higher occurrence of Grade II and Grade III meningiomas) compared to sporadic meningiomas (Antinheimo *et al.*, 1997; Perry *et al.*, 2001).

Genomic sequencing of 300 sporadic meningiomas showed that NF2 mutations were found in 36.0 % and chromosome 22 loss were found in 49.7% of examined meningiomas (Clark *et al.*, 2013). Furthermore, a study on NF2 gene mutations in 88 sporadic meningiomas revealed a variety of causes. 49 % had a chromosome 22 allelic loss, 24 % showed NF2 gene mutations and 26 % exhibited NF2 promoter methylation. In 5.7 %, a combination of LOH and NF2 promoter methylation was identified while in 18.2 % a combination of NF2 gene mutations and LOH was detected. Interestingly, it was found that NF2 gene promoter methylation was the only alteration found in 17 % of the examined meningiomas, suggesting that epigenetic NF2 gene silencing was the sole reason for the lack of Merlin expression (Lomas *et al.*, 2005). Finally, lack of functional Merlin in meningioma cell lines and human meningioma tumours resulted in heightened YAP expression and its increased nuclear localisation. Merlin knockdown could be associated with increased cell proliferation, cyclin E1 expression and S-phase entry in meningioma cell lines. The increased S-phase entry and cell proliferation of NF2-deficient meningioma cells could be reversed with a subsequent YAP knockdown (Striedinger *et al.*, 2008).

1.5.5 Meningioma treatment

The majority of the meningiomas found in the spinal canal and cerebral hemispheres can safely be resected in their entirety. However, complete surgical removal of skull base and optic nerve sheath meningiomas involves considerable neurological risk (Couldwell *et al.*, 1996; Larson *et al.*, 1995). In these cases, alternative treatment methods such as stereotactic radiosurgery can be used after incomplete tumour resection to manage the growth of the residual tumour (Couldwell *et al.*, 2006; Kondziolka *et al.*, 1999). A report stated that radiosurgery resulted in a progression free survival (PFS) of 5 years in 86 % of NF2 meningioma patients (Wentworth *et al.*, 2009). Unfortunately, as was the case with the radiosurgery treatment of schwannomas, radioactive exposure carries the risk of forming new tumours and transforming a benign tumour into a malignant one (Evans *et al.*, 2006).

1.5.6 Alternative Merlin regulation and schwannoma malignancy

In a small group of schwannomas and meningiomas, neither genetic nor epigenetic causes can be found to explain the decrease of Merlin function. It was shown that heightened proteolysis of Merlin by the protease calpain can account for reduced activity of Merlin (Kimura *et al.*, 1998).

Intriguingly, mutations in the TERT (Telomerase reverse transcriptase) promoter causing an augmented TERT protein expression were observed in 28 % of malignant meningiomas and was not associated with NF2 mutation status. The genetic alterations of the TERT promoter were not detected in the benign meningiomas. Therefore, it seems plausible that the presence or absence of TERT promoter mutations could be used as prognostic marker for the malignant transformation of meningiomas (Goutagny *et al.*, 2014).

1.5.7 Spinal cord ependymomas

The prevalence of ependymomas is approximately 2 per million (McGuire, Sainani & Fisher, 2009). Furthermore, ependymomas can be found in 2.5 – 6 % of NF2 patients (Evans *et al.*, 1992a; Mautner *et al.*, 1996; Parry *et al.*, 1994). Over 75 % of intramedullary spinal cord tumours in NF2 patients are ependymomas (Egelhoff *et al.*, 1992; Lee *et al.*, 1996). In NF2 patients, those who harboured frameshift and nonsense NF2 gene mutations were found to be more likely to form ependymomas than those with different NF2 gene mutations (Patronas *et al.*, 2001). Symptoms of NF2 patients with spinal cord ependymomas depend on both tumour location and size. These symptoms include recumbent back pain (in 56 % of cases), weakness (in 28 % of cases) or sensory disturbances (in 16 % of cases) (Chang *et al.*, 2002; Epstein, Farmer & Freed, 1993; Ferrante *et al.*, 1992; Hoshimaru *et al.*, 1999; McCormick *et al.*, 1990). Both contrast-enhanced, T1-weighted MRI and non-contrast-enhanced, T2-weighted MRI allows accurate depiction of spinal cord ependymomas (Mautner *et al.*, 1995; Patronas *et al.*, 2001; Rennie *et al.*, 2008). Histological analysis generally shows WHO grade II tumour with round to oval nuclei, a medium number of cells and intermittent sightings of ependymal rosettes (tumour cells encircling the empty lumen of a tubule) and perivascular pseudorosettes (tumour cells surrounding a blood vessel, visibly clear area between the ring of tumour cells and the blood vessel) (Asthagiri *et al.*, 2009).

In ependymomas, promoter methylation of the NF2 gene is less frequent than in schwannomas and meningiomas (< 10 %) (Alonso *et al.*, 2004).

1.5.8 Ependymoma treatment

Since many NF2 spinal cord ependymomas neither grow nor cause symptoms for a number of years, the risk of surgery is avoided for as long as possible and these ependymomas are actively monitored. However, as soon as symptoms start occurring, surgical removal is necessary to preserve the maximum amount of neurological function (Epstein, Farmer & Freed, 1993; Ferrante *et al.*, 1992; Hoshimaru *et al.*, 1999). Complete resection of these often WHO grade II spinal cord ependymomas tends to render adjuvant therapies superfluous. However, in case of anaplastic ependymomas which are rarely seen in NF2 patients, the use of adjuvant radiotherapy might be warranted (Gilbert, Ruda & Soffietti, 2010; Plotkin *et al.*, 2011).

1.5.9 Peripheral neuropathy

The majority of NF2 patients suffer from peripheral neuropathy. In a number of cases (up to 66 %), these neuropathies cannot always be traced back to tumours either compressing a nerve or growing within it (Evans *et al.*, 1992a; Parry *et al.*, 1994; Sperfeld *et al.*, 2002). Some of these non-tumour neuropathies include distal symmetric sensorimotor neuropathy, mononeuropathy multiplex and focal amyotrophy. They were found to appear at any age between the ages of 7 and 41 years and the associated symptoms lasted between 3 months

and 50 years (Gijtenbeek *et al.*, 2001; Hagel *et al.*, 2002; Iwata, Kunimoto & Inoue, 1998; Kilpatrick, Hjorth & Gonzales, 1992; Kuo *et al.*, 2004; Overweg-Plandsoen *et al.*, 1996; Thomas *et al.*, 1990; Trivedi *et al.*, 2000). Signs of peripheral neuropathies such as foot drop and facial palsy can be seen before tumour formation, making them possible first symptoms leading to a NF2 diagnosis (Evans, Birch & Ramsden, 1999).

If a craniospinal MRI does not detect tumours to explain the existing peripheral neuropathies, electrodiagnostic studies (e.g. needle electromyography, nerve conduction studies) can be used to study the function of the nerve itself (Asthagiri *et al.*, 2009). Furthermore, MR-neurography might be able to detect the underlying causes of focal neuropathies such as tumours in the peripheral nerves (Filler, Maravilla & Tsuruda, 2004).

Underlying causes of NF2-associated peripheral neuropathies are believed to be schwannosis (non-neoplastic Schwann cell proliferation), production of toxins or metabolites by pathological endoneurial cells of nearby nerve fibres, nerve myelination inept Schwann cells due to lack of adequate Merlin expression caused by haploinsufficiency and nerve compression via tumourlets running alongside the affected peripheral nerve (Hanemann, Diebold & Kaufmann, 2007; Sperfeld *et al.*, 2002).

Histological examination of peripheral nerves affected by peripheral neuropathy routinely show pathological Schwann cell proliferation (sometimes arranged in an onion bulb formation around a myelinated nerve fibre, sometimes not) and loss of both myelinated and unmyelinated nerve fibres (Gijtenbeek *et al.*, 2001; Hagel *et al.*, 2002; Hanemann, Diebold & Kaufmann, 2007; Iwata, Kunimoto & Inoue, 1998; Kilpatrick, Hjorth & Gonzales, 1992; Overweg-Plandsoen *et al.*, 1996; Sperfeld *et al.*, 2002; Thomas *et al.*, 1990; Trivedi *et al.*, 2000).

In NF2 patients, treatment of peripheral neuropathies not associated with tumour formation revolves around the alleviation of the resulting symptoms. This includes treatment of neuropathic pain with gabapentin or pregablin and other palliative and preventive measures (Asthagiri *et al.*, 2009).

1.5.10 Other neurological manifestations in NF2 patients

Aside from the cranial nerve VIII (vestibulocochlear), schwannomas can also form on other cranial nerves, spinal nerves and peripheral nerves in NF2 patients. Reports suggest that the highest frequency of non-vestibular schwannomas is seen on cranial nerves III (oculomotor), V (trigeminal) and VII (facial) in up to half (≤ 51 %) of NF2 patients. There appears to be a tendency of schwannomas developing more regularly on the upper cranial nerves (III-VIII, with the notable exception of I and II) and in the rare event schwannomas do arise on the lower cranial nerves, they are more likely to be symptomatic. Schwannomas on cranial nerves I (olfactory) and II (optic) are not found, likely due to the fact that cranial nerves I and II are myelinated by olfactory ensheathing cells (OECs) and oligodendrocytes, respectively, and not by Schwann cells (Fisher *et al.*, 2007; Mautner *et al.*, 1996; Otsuka *et al.*, 2003; Samii, Matthies & Tatagiba, 1997).

Spinal nerve root schwannomas are often numerous and they are by far the most common extramedullary spinal tumour type in NF2 patients (~ 90%) (Mautner *et al.*, 1995; Patronas *et al.*, 2001). About one third (30 %) of these spinal nerve root schwannomas become symptomatic, requiring them to be surgically removed (Evans *et al.*, 1992a; Mautner *et al.*, 1995; Patronas *et al.*, 2001).

Any peripheral nerve in NF2 patients can develop peripheral nerve schwannomas, potentially causing peripheral neuropathies. Nodular subcutaneous schwannomas are particularly common (43 – 48 %). These schwannomas frequently cause pressure sensitivity and pain (Evans *et al.*, 1992a; Mautner *et al.*, 1997). In contrast, neurofibromas in NF2 patients are rare and present histologically as collagen–myxoid matrices containing a chaotic mixture of fibroblasts and Schwann cells. Once any of these peripheral nerve growths (schwannomas, neurofibromas etc.) cause the development of symptoms, they tend to be surgically excised (Asthagiri *et al.*, 2009).

Additionally, the appearance of intramedullary spinal cord astrocytomas and intramedullary schwannomas has been seen in NF2 patients as well (Dow *et al.*, 2005; Egelhoff *et al.*, 1992; Lee *et al.*, 1996; Mautner *et al.*, 1995; Patronas *et al.*, 2001; Siddiqui & Shah, 2004). MRI can be used to visualize and differentiate between them. As before, surgical removal is performed upon the onset of symptoms (Epstein, Farmer & Freed, 1992).

Other neurological oddities found in NF2 patients include meningioangiomatosis (Omeis *et al.*, 2006), intracranial calcified deposits in cerebellum, cerebral parenchyma and choroid plexus (Mayfrank, Mohadjer & Wullich, 1990) and glial micro-hamartomas in basal ganglia and cerebral cortex (Wiestler *et al.*, 1989).

1.5.11 Ocular manifestations

Cataracts (clouding of the eye lens, eventually causing blurred or hazy vision) are a common symptom of NF2, they are reported in 60 – 81 % of NF2 patients (Evans *et al.*, 1992a; Mautner *et al.*, 1996; Parry *et al.*, 1994).

Epiretinal membranes and retinal hamartomas are also associated with NF2. The grey, semitranslucent or transculent epiretinal membranes with their whitish borders have been seen in up to 80% of NF2 patients but they do not tend to cause vision deterioration (Meyers *et al.*, 1995). In contrast, only 6 – 22 % of NF2 patients develop retinal hamartomas but these masses often found in the macula routinely result in visual impairment (Mautner *et al.*, 1996; Parry *et al.*, 1994; Ragge *et al.*, 1995). Retinal hamartomas contain a mixture of retinal and epiretinal tissue and heightened pigmentation (Bouzas *et al.*, 1992).

1.5.12 Disease course of NF2

NF2 patients are 20 years old on average when they first develop symptoms. In contrast, NF2 patients tend to be 27 years of age when they are formally diagnosed (Evans *et al.*, 1992a;

Kanter *et al.*, 1980; Mautner *et al.*, 1996; Parry *et al.*, 1994). In contrast, sporadic and solitary schwannomas and meningiomas tend to occur in patients older than 60 years of age. Therefore, such seemingly sporadically and solitarily occurring schwannomas and meningiomas in patients younger than 25 years of age have been found in many cases to be due to a genetic predisposition (Pathmanaban *et al.*, 2017).

NF2 disease progression can greatly differ from patient to patient. Nevertheless, the majority of NF2 patients will suffer hearing loss and a large number of them will eventually require wheelchair assistance. Symptoms at an early age and detection of intracranial meningiomas upon diagnosis are the signs of more severe cases of NF2, increasing the risk of early mortality (Baser *et al.*, 2002b). A study in 1992 reported the mean actuarial survival to be 62 years, despite the fact that over 40% of the NF2 patients in this study were predicted to only reach a maximum age of 50 years (Evans *et al.*, 1992a). The reported mean actuarial survival after diagnosis of 15 years (Evans *et al.*, 1992a) has most likely increased since then. This is attributed to advancements in treatment and also heightened diagnostic accuracy, more frequently detecting NF2 mosaicism even in patients with only mild symptoms (Asthagiri *et al.*, 2009).

A recently published study made a multitude of observations on the disease course of NF2 (Forde *et al.*, 2021). It was reported that the average age at diagnosis and at death are 28.9 and 45.2 years, respectively. Furthermore, the percentage of patients without functional hearing and the average number of patients requiring NF2-related tumour surgery or radiotherapy has decreased over time. Meanwhile, the average number of patients undergoing bevacizumab treatment has increased.

Moreover, patients asymptomatic at diagnosis did not need the first intervention for a longer period of time and generally had improved survival compared to their symptomatic counterparts. In contrast, those suffering from what is classified as severe genetic NF2 disease (Halliday *et al.*, 2017) showed reduced survival. Patients which were symptomatic and 16-25 years of age at diagnosis were also seen to require the first intervention earlier than their 26-39 year old counterparts. Furthermore, patients diagnosed when younger than 16 years of age and with symptoms were reported to have an increased chance of suffering from an NF2-related death than their asymptomatic and symptomatic older counterparts (Forde *et al.*, 2021).

Additionally, it was determined that those diagnosed in or after 2008 did not need vestibular schwannoma surgery or radiotherapy for a longer period of time than those diagnosed in or before 1998. This is attributed to improved patient management which combines the involvement of specialist knowledge and the reduced tendency of surgical intervention. Finally, it was stated that the identification of asymptomatic individuals and those suffering from mosaic NF2 has heightened over time (Forde *et al.*, 2021).

1.6 Merlin in cancer

Somatic NF2 mutations are frequently found (40 - 50 %) in patients with malignant mesothelioma (MM). The lack of Merlin activity has been shown to promote the formation of MM which is primarily induced by exposure to asbestos (Altomare *et al.*, 2005; Baser *et al.*, 2002a; Bianchi *et al.*, 1995; Bueno *et al.*, 2016; Cheng *et al.*, 1999; Fleury-Feith *et al.*, 2003; Jin *et al.*, 2006; Li *et al.*, 2014b; Li *et al.*, 2010; López-Lago *et al.*, 2009; Poulikakos *et al.*, 2006; Sekido *et al.*, 1995; Smole *et al.*, 2014; Thurneysen *et al.*, 2009; Xiao *et al.*, 2005; Yokoyama *et al.*, 2008).

In contrast, the formation of malignant tumours in NF2 patients, e.g. schwannoma transformation into a malignant peripheral nerve sheath tumour, is rare. Interestingly, the isolated instances in which malignant tumours were seen in NF2 patients have been linked to radiotherapy treatment (King *et al.*, 2018a; King *et al.*, 2018b). Likewise, occurrence of NF2 mutations in other forms of malignant tumours aside from MM is uncommon (Bianchi *et al.*, 1994; Yoo, Park & Lee, 2012).

Generally, the incidence rate of NF2 mutations in breast cancer is very low (around 1 - 2 %) (Arakawa *et al.*, 1994; Bianchi *et al.*, 1994; Yaegashi *et al.*, 1995). Interestingly, PAK1 gene amplification was present in the tumour samples of various human cancers, most frequently in 30 – 33 % of human breast cancer samples. PAK1 was found to stimulate MET signalling (hepatocyte growth factor - receptor tyrosine kinase c-MET signalling) by inhibiting Merlin via Merlin Ser518 phosphorylation (Shrestha *et al.*, 2012). It seems as if despite the low prevalence of somatic NF2 mutations in breast cancers, Merlin inhibition via PAK1 may have a role in allowing the formation/transformation of breast cancers (Petrilli & Fernández-Valle, 2016).

In contrast, NF2 hemizygosity was reported in 113 of 185 sporadic colorectal cancer samples, with 20% of these NF2 hemizygous samples having experienced NF2 LOH. This NF2 LOH was seen more often in less differentiated and larger tumours (Cačev *et al.*, 2014). This indicates that the presence of somatic NF2 mutations/NF2 LOH could be used as prognostic markers in colorectal cancer (Petrilli & Fernández-Valle, 2016).

Furthermore, deletion of Exon 1 or Exons 2-3 in both NF2 alleles were detected in 2 of 74 hepatobiliary tumour cell lines (Pineau *et al.*, 2003). A report showed that while liver-specific deletion of YAP in mice resulted in the loss of biliary epithelial cells and hepatocytes, liver-specific deletion of NF2 caused the formation of bile duct hamartoma and hepatocellular carcinoma. These liver-specific phenotypes due to NF2 deficiency were shown to be mostly prevented by an additional liver-specific heterozygous deletion of YAP (Zhang *et al.*, 2010).

Comparing the genomes of a non-malignant human prostate cell line and its metastatic, malignant descendant revealed 23 structural chromosome variants unique to the malignant cell line. Some of these structural chromosome variants were reported to result in the inactivation of the NF2 gene, suggesting the involvement of Merlin expression loss in prostate cancer progression (Malhotra *et al.*, 2013). These findings suggest that loss of Merlin activity might be affiliated with the progression of prostate tumours (Petrilli & Fernández-Valle, 2016).

Moreover, one study assessed the Merlin mRNA and protein expression in 23 human glioblastoma multiforme (GBM, WHO grade 4 astroytic tumour) samples. It was shown that Merlin protein expression was decreased by more than 50 % in 61 % of samples compared to control brain tissue and absent in 27.4 % of GBMs. Furthermore, 65 % of samples displayed a more than 50 % reduction in Merlin mRNA expression. No decreases of Merlin expression were seen in WHO grade 3 anaplastic astrocytoma samples, indicating that Merlin loss is only linked to grade 4 GBMs (Lau *et al.*, 2008). A different study revealed a lack of Merlin in 32% of the 53 GBM tissue samples and Merlin expression was diminished in the rest (Morales *et al.*, 2010).

Finally, 75 % of 11 medullary thyroid carcinoma patient samples were shown to have suffered an NF2 allelic loss (highest incidence rate among the examined tumour suppressor genes), often combined with the allelic loss of other tumour suppressor genes. Allelic loss of tumour suppressor genes was more frequent in samples of recurrent medullary thyroid carcinoma. Therefore, NF2 allelic loss might play a huge role in predicting the risk of recurrence of medullary thyroid carcinoma (Sheikh *et al.*, 2004).

1.7 Merlin regulation and signalling

1.7.1 NF2/Merlin structure

NF2 gene deactivation in murine embryonic stem cells show that Merlin is vital during early embryogenesis. Merlin loss causes a lack of gastrulation and results in death between embryonic days 6.5 and 7.0 due to the formation of dysfunctional extraembryonic structures (McClatchey *et al.*, 1997).

The NF2 gene consists of 17 exons which translate to the protein Merlin (Rouleau *et al.*, 1993; Trofatter *et al.*, 1993). More precisely, alternate splicing of the NF2 gene gives rise to two main isoforms. The more frequent and longer Merlin isoform 1 has 595 amino acids and contain exons 1 - 15 and 17. It has 3 main domains: the amino (N)-terminal 4.1-Ezrin–Radixin–Moesin (FERM) domain, a hydrophilic carboxyl (C)-terminal domain and an α helical domain in between (Shimizu *et al.*, 2002). The shorter isoform 2 with 590 amino acids includes exons 1 - 16, resulting in a shortened C-terminal domain due the incorporation of a stop codon (Bianchi *et al.*, 1994; Pykett *et al.*, 1994). Therefore, Merlin isoform 2 does not have the carboxy-terminal residues of isoform 1 to form a bridge between the FERM region on the N-terminal end and the C-terminal tail. This theoretically causes isoform 2 to be permanently stuck in an open conformation (Gonzalez-Agosti *et al.*, 1999; Sher *et al.*, 2012; Sherman *et al.*, 1997).

While Merlin isoform 1 has a confirmed tumour suppressive function, there appear to be conflicting reports about Merlin isoform 2 in that regard. Some evidence points towards Merlin isoform 2's lack of tumour suppression activity (Sherman *et al.*, 1997) while others confirm it to be on par with isoform 1 in that regard (Sher *et al.*, 2012; Zoch *et al.*, 2015).

Additionally, isoform 2 was shown to be essential for preserving axon integrity in peripheral nerve pathologies regularly found in NF2 patients (Schulz *et al.*, 2013).

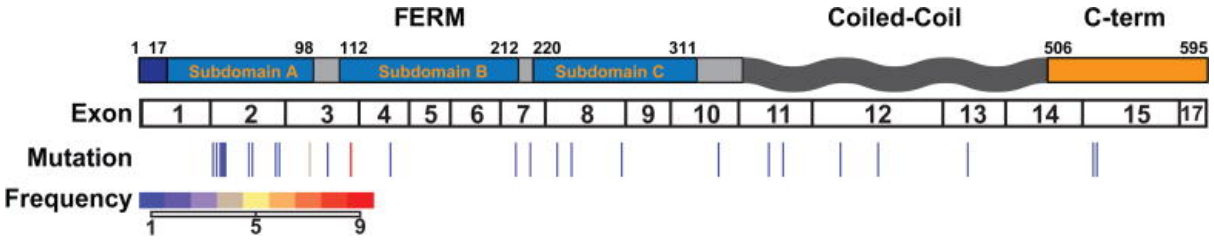

Figure 1.1: Domain structure of Merlin and corresponding exons. *The location and frequency of known mutation sites is displayed. Source: adapted from (Cooper & Giancotti, 2014).*

Proteins containing FERM domains act as linkers between the actin cytoskeleton of the cell cortex and the receptors of the plasma membrane. Merlin's conserved N-terminal FERM domain has been found to have a 63 % sequence similarity with the FERM domains of its other ERM protein family members, namely Ezrin, Moesin, Radixin and Protein 4.1 (Trofatter *et al.*, 1993). In contrast to the other ERM proteins, Merlin contains a unique, conserved 7 residues (residues 177 - 183) called the Blue box motif in the Subdomain B/F2 of the FERM region (Figure 1.1) (LaJeunesse, McCartney & Fehon, 1998).

ERM protein family members are known to associate with one another in head-to-tail heterodimeric and homodimeric intermolecular bonds and also form intramolecular bonds. In comparison to the other ERM protein family members, the intramolecular bonds within Merlin are considered more fragile and dynamic (Grönholm *et al.*, 1999; Nguyen, Reczek & Bretscher, 2001).

The overall majority of truncating (the most common variety of mutation) and non-truncating mutations of Merlin can be found in the FERM region (Ahronowitz *et al.*, 2007) (Figure 1.1).

The FERM region also acts as nuclear localization signal, allowing unphosphorylated and therefore active Merlin to translocate to the nucleus (Li *et al.*, 2010). In its phosphorylated inactive state, Merlin's FERM nuclear localization signal is concealed. As a result, a nuclear export motif found on its C-terminus will cause the exclusion of Merlin from the nucleus via the CRM1-exportin pathway. Losing this export motif results in increased nuclear localization of Merlin (Kressel & Schmucker, 2002; Li *et al.*, 2010).

In contrast to FERM region mutations, mutations in the C-terminal end and the central α-helix (= coiled-coil) of Merlin occur less frequently (Ahronowitz *et al.*, 2007) (Figure 1.1). Overall, the evidence suggests that the FERM region is vital for Merlin's role as tumour suppressor.

The Subdomain B/F2 within the FERM region holds the greatest relevance when it comes to tumour suppression. Replacing Merlin's Subdomain F2 with the F2 subdomain of fellow ERM protein Ezrin completely disables the tumour suppressive ability of Merlin while replacing subdomains F1 or F3 does not change Merlin's inhibitory effect on proliferation. Additionally, the FERM Subdomain A/F1 was demonstrated to be essential for actin colocalization and cytoskeleton reorganization (Lallemand, Saint-Amaux & Giovannini, 2009).

1.7.2 Merlin regulation via phosphorylation

The scaffold protein Merlin is mostly found in the cell cortex, associating with and connecting cell membrane proteins/receptors and parts of the cytoskeleton (Scherer & Gutmann, 1996) (Figure 1.3). Merlin was shown to attach to membrane domains believed to be lipid rafts via phosphoinositide binding (Mani *et al.*, 2011; Stickney *et al.*, 2004). Its protein activity/function is mainly regulated by the phosphorylation of select amino acid residues. AKT (= Ak strain transforming, Protein Kinase B) phosphorylates Merlin serine10 (Ser10), threonine230 (Thr230) and Ser315, causing reduced binding of Merlin to GTPase PIKE-L and Merlin's ubiquitination and subsequent proteasomal degradation. The GTPase PIKE-L is known to augment PI3K signalling (Laulajainen *et al.*, 2011; Tang *et al.*, 2007).

Merlin Ser10 is also phosphorylated by Protein Kinase A (PKA). This results in the alteration of the actin cytoskeleton, causing a change in cell morphology (Laulajainen *et al.*, 2008). The C-terminal Ser518 is the most prominent phosphorylation site. Its phosphorylation is carried out by PKA and p21 activated kinase (PAK), impairing Merlin's function as tumour suppressor protein (Alfthan *et al.*, 2004; Rong *et al.*, 2004a; Shaw *et al.*, 2001; Surace, Haipek & Gutmann, 2004; Xiao *et al.*, 2002) (Figure 1.2). Merlin regulation by PKA is likely to be of central importance in Schwann cells since Schwann cell proliferation is heavily dependent on cAMP-PKA signalling (Kim, DeClue & Ratner, 1997). Additionally, phosphorylation by kinases AKT and PAK permits Merlin Lys76 sumoylation which was shown to be necessary for Merlin's tumour suppressive function (Qi *et al.*, 2014).

Myosin phosphatase MYPT1-PP1δ restores Merlin's tumour suppressive function by catalysing Ser518 dephosphorylation (Jin *et al.*, 2006; Sher *et al.*, 2012). Therefore, activation or inhibition of the mentioned kinases and phosphatases determine Merlin's activity (Shaw *et al.*, 2001) (Figure 1.2).

There is some ambiguity about the conformational state of Merlin due to its Ser518 phosphorylation status. Some reports suggest that Merlin is always in a closed conformational state regardless of its phosphorylation status and only undergoes subtle conformational changes after phosphorylation (Ali Khajeh *et al.*, 2014; Hennigan *et al.*, 2010). In contrast, a different study shows that unphosphorylated Merlin is in an open conformational state and reverts to a more closed conformational state upon phosphorylation (Sher *et al.*, 2012). Additionally, it was reported that Merlin transitions to a slightly less closed confirmation after binding to Phosphatidylinositol 4, 5-bisphosphate (Ali Khajeh *et al.*, 2014).

1.7.3 Merlin's regulation of non-Hippo signalling pathways

Merlin has been shown to regulate the CD44/Rac/PAK/LIMPK pathway (Bai *et al.*, 2007; Bourguignon *et al.*, 2007; Bourguignon *et al.*, 2000; Flaiz *et al.*, 2009; Herrlich *et al.*, 2000; Kaempchen *et al.*, 2003; Kissil *et al.*, 2002; Kissil *et al.*, 2003; Morrison *et al.*, 2001; Nakai *et al.*, 2006; Okada, Lopez-Lago & Giancotti, 2005; Oliferenko *et al.*, 2000; Petrilli *et al.*, 2014a; Sainio *et al.*, 1997; Shaw, McClatchey & Jacks, 1998; Shaw *et al.*, 2001; Thaxton *et al.*, 2007; Xiao *et al.*, 2002) and CD44/ErbB/PKA pathway (Ahmad *et al.*, 2010; Ammoun *et al.*, 2010;

Ammoun *et al.*, 2008; Ammoun *et al.*, 2012; Bashour *et al.*, 2002; Fernandez-Valle *et al.*, 2002; Garcia & Gutmann, 2014; Hansen *et al.*, 2006; Lallemand *et al.*, 2009; Obremski, Hall & Fernandez-Valle, 1998; Pelton *et al.*, 1998; Sherman *et al.*, 2000; Thaxton *et al.*, 2008; Wickremesekera, Hovens & Kaye, 2007; Wickremesekera, Hovens & Kaye, 2010) (Figure 1.2). Furthermore, Merlin plays a role in the Rac1/Wnt pathway (Bosco *et al.*, 2010; Zhou *et al.*, 2011), mTORC1/2 signalling (Cloughesy *et al.*, 2008; Giovannini *et al.*, 2014; James *et al.*, 2009; James *et al.*, 2012; O'Reilly *et al.*, 2006), Ras signalling (Geissler *et al.*, 2013; Li *et al.*, 1993; Morrison *et al.*, 2007; Tikoo *et al.*, 1994), TAM receptors/Src/FAK signalling (Ammoun *et al.*, 2010; Ammoun *et al.*, 2014; Ammoun *et al.*, 2012; Ammoun *et al.*, 2015; Houshmandi *et al.*, 2009), PI3K/AKT/HDAC signalling (Agnihotri *et al.*, 2014; Burns *et al.*, 2013; Bush *et al.*, 2011; Chen *et al.*, 2005; Hilton, Ristic & Hanemann, 2009; Jacob *et al.*, 2008; Jacob *et al.*, 2012; Johnson *et al.*, 2002; Lee *et al.*, 2009; Li *et al.*, 2001; Mawrin *et al.*, 2005; Petrilli *et al.*, 2014b; Rong *et al.*, 2004b; Tang *et al.*, 2007; Ye, 2007) and SIRT signalling (Petrilli, Bott & Fernández-Valle, 2013).

1.7.4 Merlin's tumour suppressive function

As mentioned previously, the exposed FERM region of unphosphorylated and unmutated Merlin allows relocation to the nucleus where Merlin binds to the substrate recognition subunit DCAF1 (DDB1- and Cul4-Associated Factor 1), disrupting the function of E3 ubiquitin ligase $CRL4^{DCAF1}$ and thereby inhibiting proliferation (Figure 1.3). More precisely, the subdomain C of Merlin's FERM domain binds to the hydrophobic IILXLN motif in DCAF1's C-terminal acidic tail (Li *et al.*, 2010; Mori *et al.*, 2014). E3 ubiquitin ligase $CRL4^{DCAF1}$ controls different cell functions such as cell survival, proliferation and DNA repair by conducting the ubiquitination of or interacting with important effectors of said processes such as histone H3, TET proteins and p53 (Kim *et al.*, 2012; Lee *et al.*, 2012; Yu *et al.*, 2013a).

The increased proliferation upon Merlin loss could be counteracted by DCAF silencing. Re-expression of Merlin or DCAF1 knockdown was shown to result in the decreased expression of genes targeted by YAP. Furthermore, DCAF1 silencing in murine primary schwannoma cells (= NF2-deficient primary mouse Schwann cells) inhibits their oncogenic potential while DCAF1 knockdown in human primary schwannoma cells leads to a decrease in proliferation (Li *et al.*, 2010).

Moreover, it was shown that after being relinquished from Merlin's control, $CRL4^{DCAF1}$ inhibits LATS1/2 in the nucleus via ubiquitination. LATS1's poly-ubiquitination results in the decrease of its kinase activity as well as its proteasomal degradation while LATS2's oligo-ubiquitination solely causes the impairment of its kinase activity. LATS1/2 inhibition leads to unphosphorylated and therefore uninhibited YAP/TAZ, inducing the expression of YAP-TEAD target genes such as CTGF and CYR61 and thereby increasing a cell's oncogenic potential (Li *et al.*, 2014b).

Functional Merlin has also been theorized to block the interaction between $CRL4^{DCAF1}$ and LATS1 by obstructing the LATS1 binding site on DCAF1's WD40 domain, thereby preventing

$CRL4^{DCAF1}$ from suppressing LATS1 function. YAP phosphorylation by LATS1/2 results in YAP's expulsion from the nucleus (Li *et al.*, 2014b).

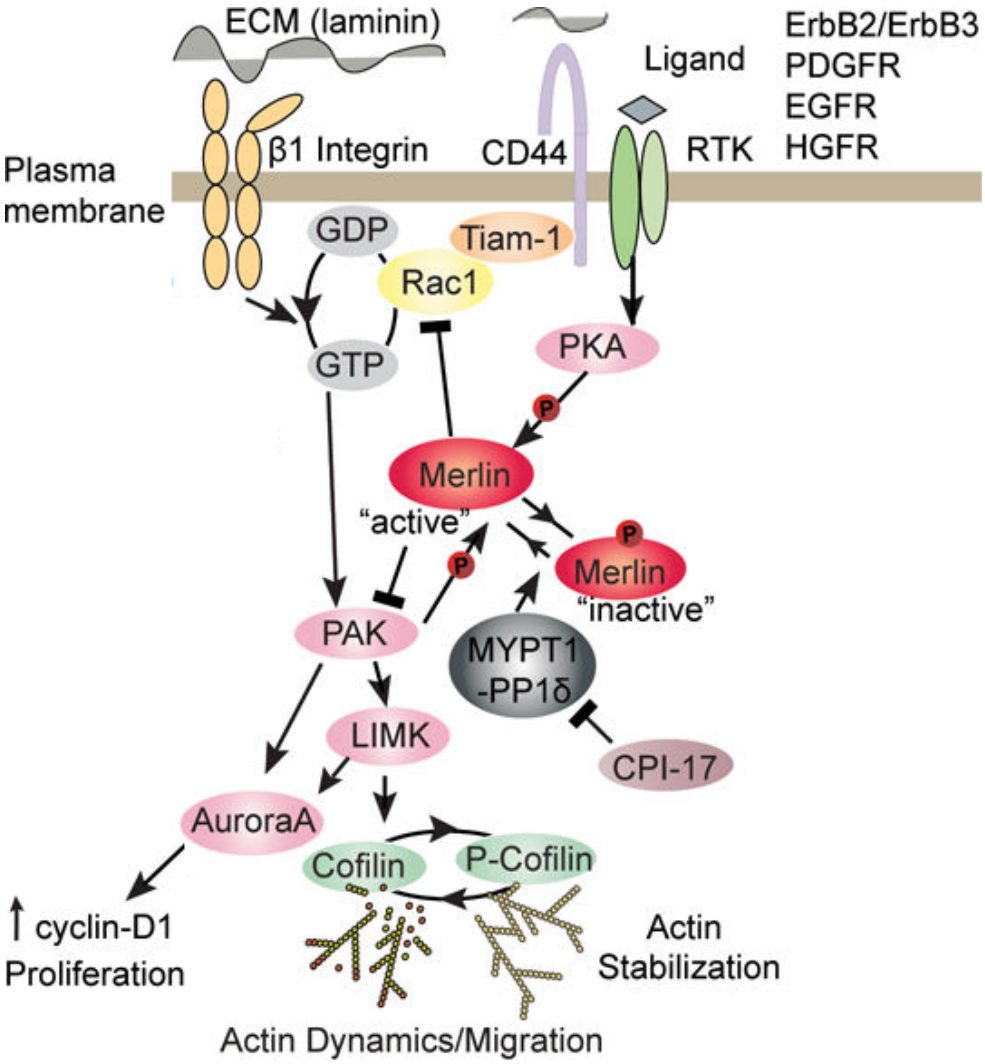

Figure 1.2: CD44/β1 integrin/receptor tyrosine kinase (RTK) signalling and Merlin regulation. *Laminin binding to β1 integrin or hyaluronan binding to CD44 and the resulting Tiam-1 initiation allow Rac1 activation, leading to PAK activity. PAK suppresses Merlin's growth-inhibitory function via Ser518 phosphorylation. PAK also promotes LIMK and Aurora A function, resulting in the upregulation of cyclin-D1 and therefore an increase in cell proliferation. In addition, LIMK phosphorylates actin-depolymerizing enzyme Cofilin and thereby suppresses its function, resulting in actin stabilization. A ligand binding to its RTK, e.g. neuregulin-1 binding to ErbB2/ErBb3, activates PKA which catalyses Merlin Ser518 phosphorylation and thereby suppresses Merlin's growth-restrictive activity. If not inhibited by CPI-17, MYPT1-PP1δ dephosphorylates and thereby allows Merlin to resume its growth-suppressing function. To this end, Merlin inhibits both Rac1 and PAK. Adapted from (Petrilli & Fernández-Valle, 2016).*

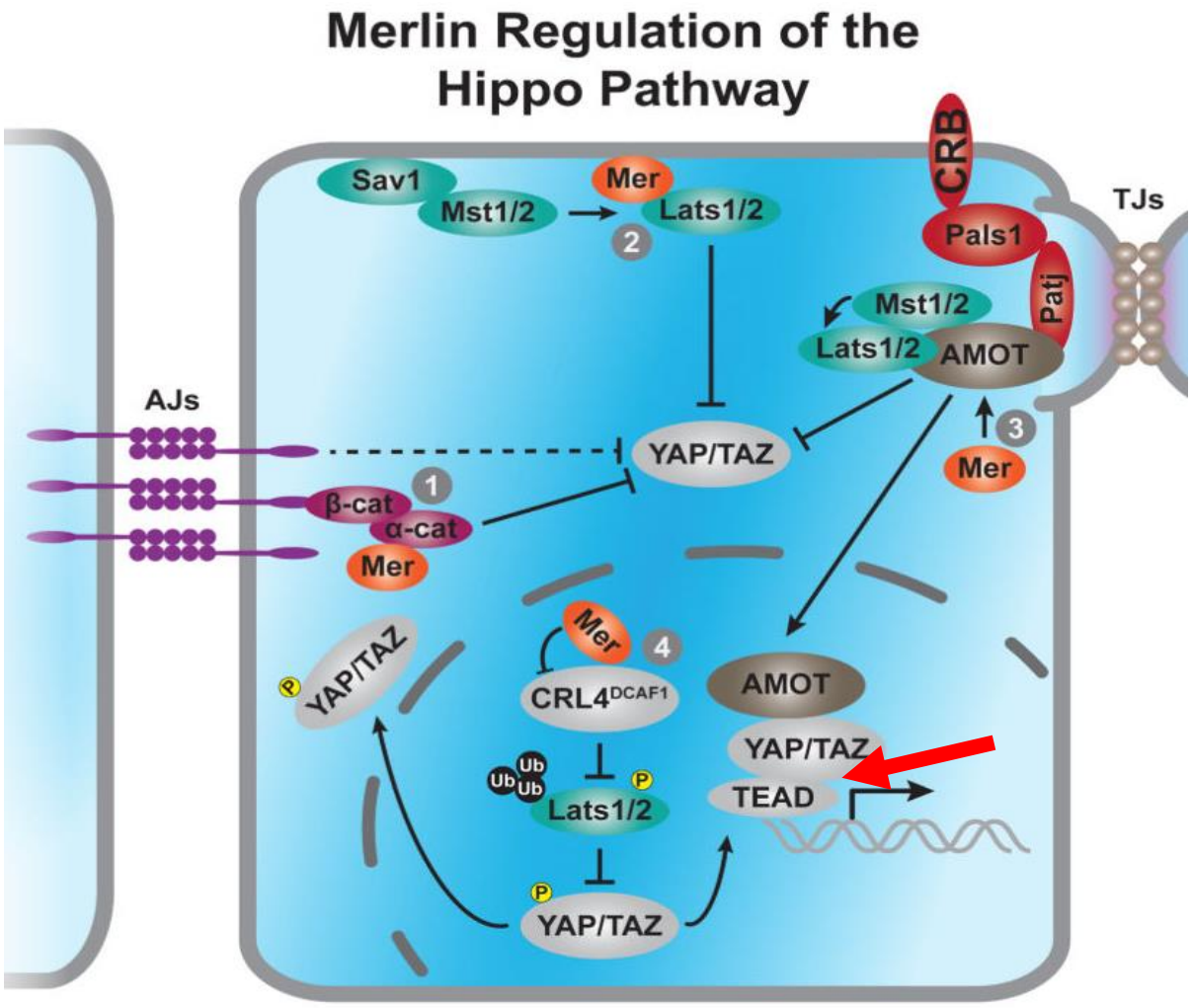

Figure 1.3: Merlin and the Hippo signalling pathway. *Merlin/KIBRA activate LATS1/2 (2) which suppress YAP/TAZ. Additionally, YAP/TAZ is inhibited by angiomotin (AMOT) (3) and a complex of α-catenin, β-catenin, Merlin and 14-3-3 (1). Merlin also suppresses the CRL4^{DCAF1} E3 ubiquitin ligase (4) which would otherwise ubiquitinate and subsequently degrade LATS1/2, resulting in increased YAP/TAZ activity. Upon Merlin loss, YAP/TAZ translocates to the nucleus and binds to different transcription factors (e.g. TEAD1 - 4), activating gene expression. Red arrow shows the YAP/TAZ-TEAD interaction targeted by Vivace inhibitor compounds. Adapted from (Cooper & Giancotti, 2014).*

1.8 Hippo signalling pathway

1.8.1 Canonical Hippo pathway: MST activation

In the mammalian canonical Hippo signalling pathway in, a complex of MST1/2 and SAV1 (also called WW45) phosphorylates and thereby activates the LATS1/2-MOB1A/B complex (Harvey, Pfleger & Hariharan, 2003; Jia *et al.*, 2003; Justice *et al.*, 1995; Lai *et al.*, 2005; Pantalacci, Tapon & Léopold, 2003; Tapon *et al.*, 2002; Udan *et al.*, 2003; Wu *et al.*, 2003; Xu *et al.*, 1995) which in turn inactivates YAP/TAZ via phosphorylation (Figure 1.4).

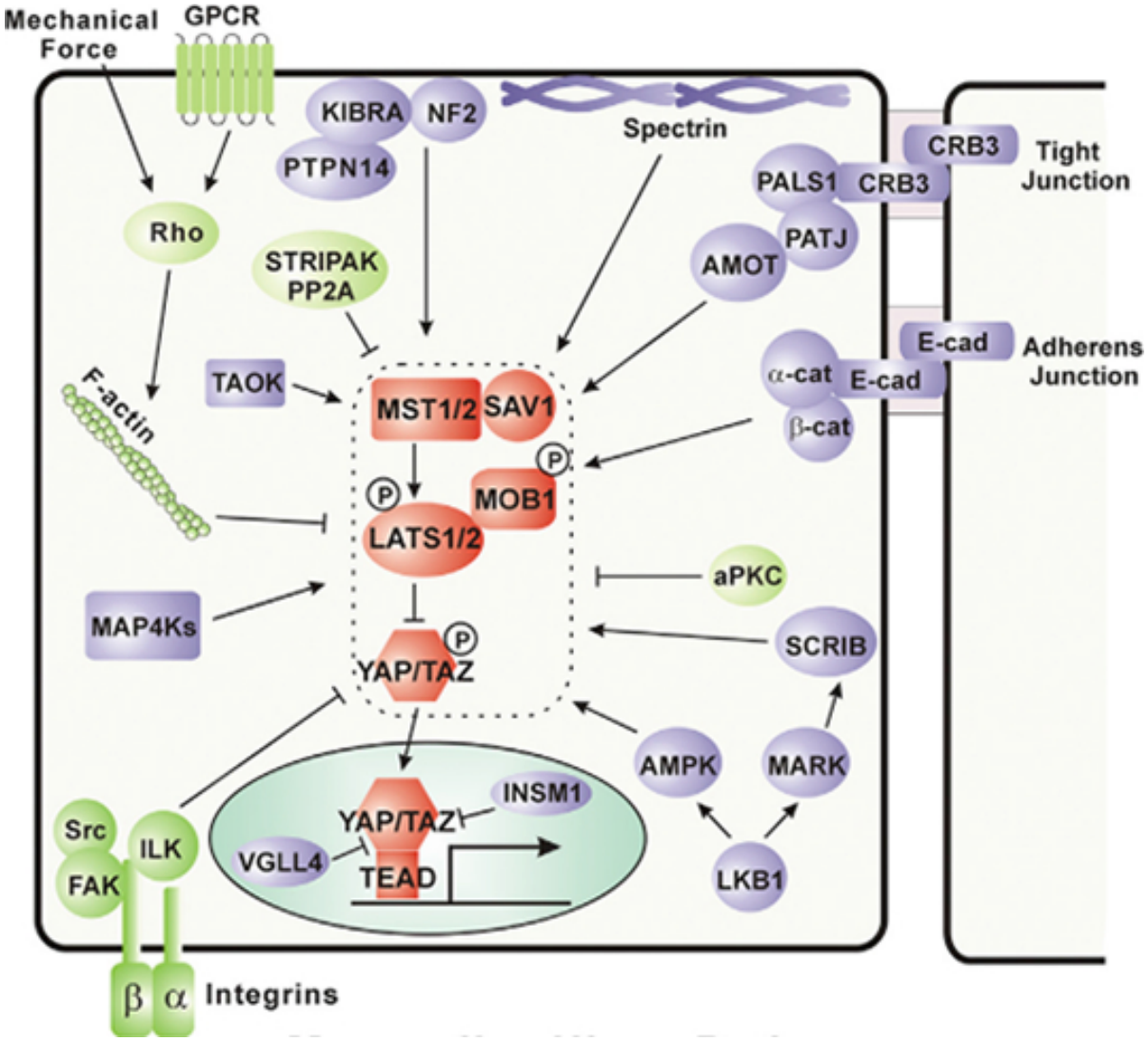

Figure 1.4: Mammalian Hippo pathway and influences on its activity. *Core kinase cascade is within the dotted lines. Arrows indicate effectors activating the core kinase cascade while T-lines inhibit the core kinase cascade. Adapted from (Zheng & Pan, 2019).*

MST1/2 activation requires the phosphorylation of threonine residues found on the activation loop. The TAOK1/3 kinases are indicated to activate MST1/2 by this mechanism (Boggiano, Vanderzalm & Fehon, 2011; Poon *et al.*, 2011) (Figure 1.4). MST monomers can also activate each other via transphosphorylation by forming MST homodimers via their C-terminal SAV-RASSF-Hpo (SARAH) domain (Ni *et al.*, 2013; Ni *et al.*, 2015; Praskova *et al.*, 2004).

This combination of dimerization and transactivation is regulated by SAV1 and RASSF5, both of which have SARAH domains of their own. SAV1 has been found to aid MST autoactivation by facilitating MST transphosphorylation and also suppressing the negative feedback mechanism by the PP2A complex STRIPAK^{SLMAP} (Bae *et al.*, 2017; Goudreault *et al.*, 2009) In contrast, RASSF5 inhibits MST activity by interfering with MST homodimerization and thereby preventing MST transphosphorylation (Ni *et al.*, 2013; Praskova *et al.*, 2004).

1.8.2 Canonical Hippo pathway: LATS activation

LATS1/2 kinases are activated by MST1/2 via phosphorylation of threonine residues at the C-terminal hydrophobic motif (Thr1079 for LATS1, Thr1041 for LATS2) and subsequently LATS1/2 perform an autophosphorylation at their T-loop motif (activation loop) (Hergovich, 2016).

Merlin has been reported to activate the Hippo pathway without participating in the activation of the MST1/2 kinases (Figure 1.4). In a Schwann cell line, cell membrane bound Merlin binds and recruits LATS1/2 to the plasma membrane which allows LATS1/2 phosphorylation/ activation by MST1/2 (Yin *et al.*, 2013). Additionally, it was shown that a complex of Merlin and kidney and brain expressed protein (KIBRA) regulate the Hippo signalling pathway by directly binding to MST1/2 and SAV1 (Baumgartner *et al.*, 2010; Hamaratoglu *et al.*, 2006; Yu *et al.*, 2010).

Interestingly, both the MAP4K family kinases (Li *et al.*, 2014a; Meng *et al.*, 2015; Zheng *et al.*, 2015) and TAOK1/3 are activated by contact inhibition, actin depolymerisation and serum starvation and directly interact and phosphorylate LATS1/2 (Figure 1.4). NF2 gene deletion was seen to severely impede YAP/TAZ phosphorylation, implying that Merlin is likely to also play a chief role in TAOK- and MAP4K-induced LATS1/2 activation. In contrast, Ras homology family member A (RhoA) was shown to convey cell growth signals from GPCRs, negatively impacting LATS1/2 activity and thereby activating YAP/TAZ (Plouffe *et al.*, 2016).

Furthermore, SAV1 has been proposed to promote LATS1/2 activation by acting as an adaptor protein although the precise mechanism is disputed (Bae *et al.*, 2017; Harvey, Pfleger & Hariharan, 2003; Su *et al.*, 2017; Yin *et al.*, 2013).

The second adaptor protein MOB1A/B directly binds to LATS and promotes LATS kinase activation via allosteric regulation and scaffolding, thereby facilitating YAP/TAZ phosphorylation (Lai *et al.*, 2005; Ni *et al.*, 2015; Praskova, Xia & Avruch, 2008).

1.8.3 Canonical Hippo pathway: YAP and TAZ regulation

The paralogues YAP and TAZ contain approximately 45% amino acid identity to one another. They both possess an N-terminal TEAD-binding domain, WW domain(s) and a C-terminal transactivation domain (Kanai *et al.*, 2000) (Figure 1.5). Analysis of the proteomes of 68 human schwannomas revealed activation of YAP and its transcriptional targets PDGFRβ, ErbB2 and ErbB3 (Boin *et al.*, 2014). Mostly cytoplasmic YAP is found under high cell density or confluent conditions while mainly nuclear YAP is observed under low cell density (Zhao *et al.*, 2007). Furthermore, it has been suggested that when YAP is perpetually dephosphorylated, cells counteract this increased YAP activity by reducing YAP protein expression levels (Chen et al., 2015b). Additionally, it was reported in Drosophila that the majority of transcription coactivators YAP/TAZ (Yorkie in Drosophila) quickly oscillate between nucleus and cytoplasm and the subcellular localization of YAP is regulated by controlling YAP's nuclear import rate via LATS1/2-caused YAP phosphorylation (Manning *et*

al., 2018). Activated LATS1/2 kinases phosphorylate and thereby inactivate the transcription coactivators YAP and TAZ, preventing them from fulfilling their roles as co-activators of the TEAD transcription factors (Figure 1.4).

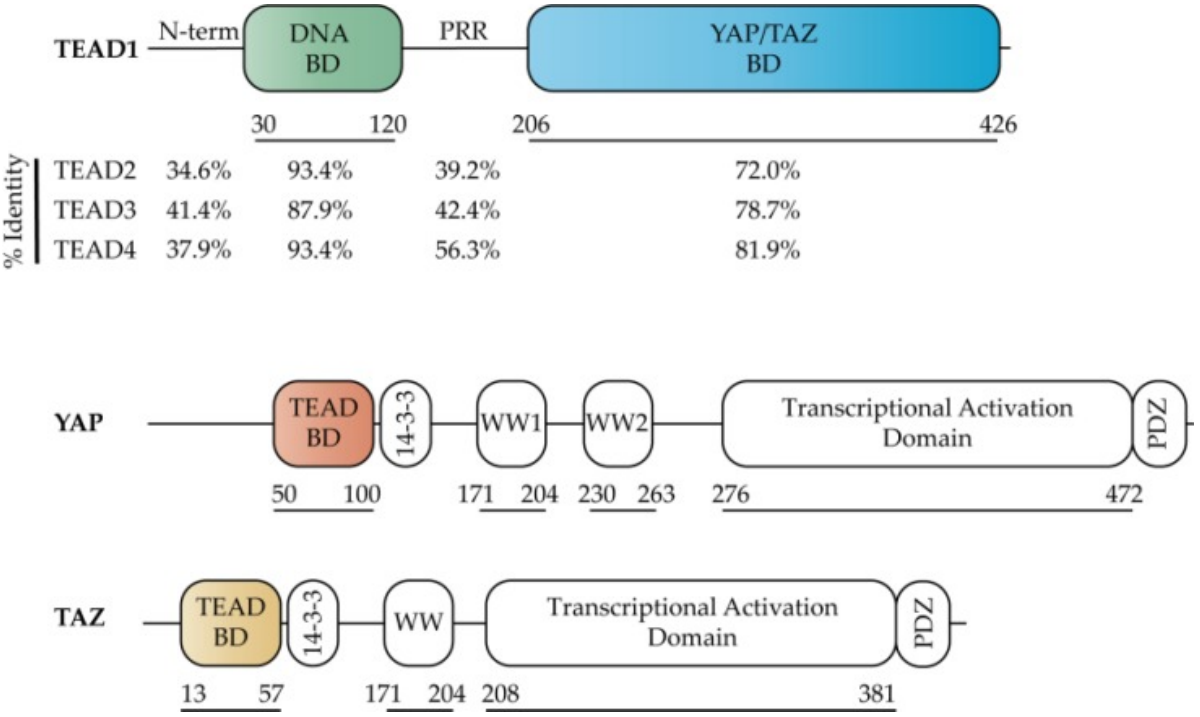

Figure 1.5: Structure and domains of TEAD1 – 4 and the paralogs YAP and TAZ. *% depict sequence identity shared by the TEADs in the above shown domain. Adapted from (Holden & Cunningham, 2018).*

Differences in the regulation of YAP and TAZ activity by LATS were shown. Phosphorylation of YAP Ser127 by LATS influences YAP localization, resulting in 14–3–3 binding and therefore cytoplasmic retention and inactivation of YAP (Zhao *et al.*, 2007). Phosphorylation of YAP Ser381 by LATS on the other hand causes YAP degradation. The Ser381 phosphorylation in one of the five HXRXXS motifs triggers the phosphorylation of the phosphodegron Ser384 (potentially plus Ser387) by CK1δ/ε. Phosphodegrons are characterized as phosphorylated residues which allow recognition and ubiquitination by E3 ubiquitin ligases (Nash *et al.*, 2001). Subsequently, this phosphorylated phosphodegron is recognized and bound by F-box protein β-TrCP and subsequently the SCF/β-TrCP E3 ligase, performing YAP ubiquitination and thereby marking YAP for proteasomal degradation (Zhao *et al.*, 2010).

In the case of TAZ, phosphorylation of multiple serine residues by LATS (Ser89 plus potentially Ser66, Ser117 and Ser311) found in the four conserved HXRXXS motifs generates the binding site for the 14-3-3 protein, resulting in TAZ cytoplasmic retention and deactivation (Lei *et al.*, 2008). Phosphorylation of TAZ Ser311 by LATS prompts subsequent phosphorylation of the phosphodegron Ser314 by CK1ε. This allows the recognition and binding by F-box protein β-TrCP and ubiquitination by the SCF/β-TrCP E3 ligase, eventually leading the degradation of TAZ (Lei *et al.*, 2008; Liu *et al.*, 2010). Interestingly, the NDR1/2 kinases share LATS1/2's

capacity to regulate YAP activity via phosphorylation (Meng *et al.*, 2015; Zhang *et al.*, 2015b; Zheng *et al.*, 2015).

1.8.4 Canonical Hippo pathway: TEAD function

The primary transcription factors (TFs) bound and activated by unphosphorylated, nuclear transcription coactivators YAP/TAZ are the Transcriptional enhanced associate domain (TEAD) family transcription factors (Goulev *et al.*, 2008; Ota & Sasaki, 2008; Stein *et al.*, 2015; Wu *et al.*, 2008; Zanconato *et al.*, 2015; Zhang *et al.*, 2008; Zhao *et al.*, 2008) (Figure 1.4). Mammals possess four TEADs, TEAD1 (TEF-1/NTEF), TEAD2 (TEF-4/ETF), TEAD3 (TEF-5/ETFR-1) and TEAD4 (TEF-3/ETFR-2/FR-19) (Bürglin, 1991; Yasunami, Suzuki & Ohkubo, 1996). TEAD1 - 4 are expressed to varying degrees in developing mice and in the organs of adult mice (Yasunami, Suzuki & Ohkubo, 1996). TEADs share a strongly conserved, 68 amino acid N-terminal TEA/ATTS DNA-binding (TEAD) domain which allows them to bind to the MCAT element (5'-CATTCCA/T-3') in regulatory DNA sequences (Anbanandam *et al.*, 2006; Huh *et al.*, 2019; Jacquemin *et al.*, 1996; Jiang *et al.*, 2000). Additional TEAD binding elements were identified as well (Benhaddou *et al.*, 2012; Zanconato *et al.*, 2015).

TEADs are homologous in both their N-terminal TEA DNA binding domain (87.9 %) and their C-terminal YAP binding domain (YBD) (72 %), separated by a proline rich region (Holden & Cunningham, 2018) (Figure 1.5). YAP contains an N-terminal TEAD-interacting domain which binds to the C-terminal YAP binding domain (YBD) of TEAD1 – 4, forming YAP/TEAD dimers (Chen *et al.*, 2010; Tian *et al.*, 2010; Vassilev *et al.*, 2001). Interestingly, several studies demonstrate that TEAD interaction with YAP/TAZ is necessary for YAP/TAZ nuclear retention. TEAD knockout completely prevented YAP nuclear accumulation (Lin *et al.*, 2017) while impaired TAZ-TEAD interaction resulted in heightened TAZ cytoplasmic retention (Chan *et al.*, 2009). Accordingly, TEAD2 overexpression promoted YAP/TAZ nuclear accumulation (Diepenbruck *et al.*, 2014).

Since the overwhelming majority of TEAD2 molecules are seen in the chromatin fraction, TEADs appear to be predominantly found in a DNA-bound state (Li *et al.*, 2015b) but they only show extremely low transcriptional activity on their own (Xiao *et al.*, 1991). To modulate gene transcription, TEAD uses its C-terminal transactivation domain to recruit co-activators YAP/TAZ (Mahoney *et al.*, 2005; Vassilev *et al.*, 2001; Zhang *et al.*, 2009a; Zhao *et al.*, 2008), cofactors VGLL1/2/3/4 (Chen *et al.*, 2004; Chen, Mullett & Stewart, 2004; Figeac *et al.*, 2019; Honda *et al.*, 2017; Koontz *et al.*, 2013; Pobbati *et al.*, 2012) and the Nucleosome Remodelling and Deacetylase (NuRD) complex (Kim *et al.*, 2015). Additionally, TEADs can recruit the Mediator complex via YAP (Galli *et al.*, 2015).

In the absence of YAP/TAZ binding, TEAD has been found to function as a default repressor by binding to the co-repressor VGLL4 which causes the repression of YAP-targeted genes such as CTGF (Figure 1.4). This TEAD-VGLL4 mediated repression inhibited YAP overexpression-induced and Merlin deficiency-induced hepatomegaly and hepatocellular carcinoma development in transgenic mice (Koontz *et al.*, 2013; Zhang *et al.*, 2010). TEAD's default repressor function was also demonstrated via the heightened expression of CTGF in TEAD4

silenced C2C12 cells (Benhaddou *et al.*, 2012) and in TEAD1/2 double null mouse embryos (Ota & Sasaki, 2008). Furthermore, it was shown that both of the VGLL4 Tondu domains (T1 and T2) are necessary to convey its growth inhibitory function. VGLL4 T1 and T2 domains, like YAP, bind to the C-terminal YBD of TEAD. Despite the primary sequence differences between YAP's TEAD binding domain and VGLL4's Tondu domains, the resulting 3D structures are similar, allowing them to bind to the same domain on TEAD. This leads to competitive binding between YAP and VGLL4 to exert their respective effects on gene expression (Jiao *et al.*, 2014; Koontz *et al.*, 2013; Zhang *et al.*, 2014a). Furthermore, TEAD4 complexes with corepressors C-terminal binding protein 2 (CtBP2) and VGLL4 to form a gene repression complex during adipogenesis (Zhang *et al.*, 2018b).

1.8.5 VGLL regulation and function

VGLL4 function is regulated via microRNA (Liu, Kong & Zhang, 2018), phosphorylation (Zeng *et al.*, 2017), acetylation (Lin *et al.*, 2016), deubiquitination (Zhang *et al.*, 2016) and nuclear export (Chen, Mullett & Stewart, 2004). While VGLL4 predominantly functions as a corepressor via its TEAD interactions in various tissues, the effect of TEAD cofactors VGLL1/2/3 is more tissue-dependent. Depending on the tissue, they appear to bind to different TEADs and act as either TEAD coactivators or corepressors, targeting the same or different genes as the YAP/TAZ-TEAD complexes in those tissues. Within the same tissue, VGLL1/2/3 often are differentially expressed and control different groups of genes via their different TEAD binding partners (Currey, Thor & Piper, 2021; Simon *et al.*, 2016; Zheng & Pan, 2019). Interestingly, it could be shown that YAP, TAZ and cofactor VGLL1 (and presumably also cofactors VGLL2/3/4) share a similar affinity for TEAD1 – 4 (Bokhovchuk *et al.*, 2019). While VGLL1/2/3 contain only a single TEAD-interacting C-terminal Tondu domain, VGLL4 possesses two of these domains which are also necessary for VGLL4 nuclear localization (Chen, Mullett & Stewart, 2004).

1.8.6 Other TEAD cofactors

The nuclear receptor coactivators of the p160 family SRC1, TIF2 (SRC2) and RAC3 (SRC3) were reported to act as TEAD1 and TEAD2 coactivators and augment TEAD-induced gene transcription (Belandia & Parker, 2000). Furthermore, TEAD4 associates with SRC1 – 3 coactivators to activate the expression of genes promoting cell migration and invasion (Liu *et al.*, 2016a).

Other TEAD interactors include the paralogs FAM181A and FAM181B which, similar to YAP/TAZ, bind to TEAD via an Ω-loop (Bokhovchuk *et al.*, 2020). High FAM181A and FAM181B neural expression in mice embryos and adults points towards a role in the developing and developed nervous system (Marks *et al.*, 2016). Additionally, TEAD1 was shown to bind and cooperate with the transcription factors myc-associated factor X (Max), serum response factor (SRF) and myocyte enhancer factor-2 (MEF2) in myocytes (Gupta *et al.*, 2001; Gupta, Kogut & Gupta, 2000; Maeda, Gupta & Stewart, 2002).

Additionally, the protein INSM1 has also been shown to act as repressor of YAP-TEAD transcription by binding to TEAD (Guo *et al.*, 2019) (Figure 1.4).

1.8.7 TEAD regulation

Post-translational modifications can also regulate TEAD activity. Phosphorylation of TEAD1 Ser102 by PKA was seen to inhibit TEAD1's DNA-binding ability but had no effect on its ability to bind to Max (Gupta, Kogut & Gupta, 2000). Similarly, phosphorylation by PKC was also shown to negatively impact the DNA-binding ability of TEAD1 (Jiang *et al.*, 2001).

Furthermore, it was shown that TEAD4 is alternatively spliced. The resulting truncated splicing variant TEAD4-S suppresses YAP activity in a dominant negative manner, leading to inhibition of cancer cell migration and proliferation *in vitro* and xenograft tumour growth *in vivo* (Qi *et al.*, 2016).

1.8.8 TEAD post-translational regulation: S-palmitoylation

Furthermore, TEADs undergo S-autopalmitoylation which results in the attachment of the fatty acid palmitate to the conserved cysteine residue found in the palmitate binding pocket (PBD) of the C-terminal YAP-binding domain (YBD) of TEAD. The YBDs of TEAD1-4 share more than 70% sequence identity (Holden & Cunningham, 2018). Structural studies show that the palmitoyl group is deeply embedded in an equally conserved hydrophobic pocket of the protein core. TEAD S-palmitoylation is not required for the nuclear localization of TEAD (Tang *et al.*, 2021). Additionally, the allosteric effects of S-palmitoylation on TEADs appear to differ depending on the TEAD family member.

TEAD1 S-palmitoylation was shown to be vital for YAP/TAZ (but interestingly, not for VGLL4) binding. In contrast, TEAD4 S-palmitoylation is important for TEAD4 protein stability but dispensable for YAP/TAZ binding. TEAD2 S-palmitoylation was shown to be a requirement for TEAD2 to assume its correct protein structure and maintain its stability (Chan *et al.*, 2016; Kim & Gumbiner, 2019; Mesrouze *et al.*, 2017; Noland *et al.*, 2016).

Moreover, activation of Merlin due to high cell density/contact inhibition results in the decreased expression of two enzymes of palmitate biosynthesis, namely acetyl-CoA carboxylase and fatty acid synthase in a LATS1/2 independent manner. This reduces palmitate levels and therefore also TEAD S-palmitoylation, causing decreased gene transcription of YAP-TEAD target genes such as CTGF and CYR61. Additionally, TEAD4 S-palmitoylation is regulated by depalmitoylases such as APT2 and to a lesser extent, ABHD17A and RBBP9. Unpalmitoylated TEAD4 was shown to be marked for proteasomal degradation by the E3 ubiquitin ligase CHIP, thereby decreasing TEAD4 protein levels (Kim & Gumbiner, 2019).

1.8.9 YAP/TAZ-TEAD transcriptional activity

Upon binding a coactivator, TEADs activate gene transcription by binding to gene promoters (Tamm, Böwer & Annerén, 2011) and enhancers (Cebola *et al.*, 2015; Ribas *et al.*, 2011; Zhu *et al.*, 2019) (Figure 1.4). TEADs can interact and cooperate with the transcription factors of other signalling pathways such as SMAD2/3, OCT4, TCF4, AP-1 and MRTF (Beyer *et al.*, 2013; Jiao *et al.*, 2017; Kim *et al.*, 2017; Liu *et al.*, 2016a). Furthermore, it was shown that YAP/TAZ-TEAD binds together with TFs such as E2F, Myc and AP-1 at distal enhancers. Such a distal enhancer bound ternary complex then interacts with target gene promoters via chromatin looping (Croci *et al.*, 2017; Kapoor *et al.*, 2014; Zanconato *et al.*, 2015).

After binding to the chromatin via its transcription factor e.g. TEAD, YAP recruits the MLL H3K4 methyltransferase complex by using the WW domains of YAP to bind to Nuclear receptor coactivator 6 (Ncoa6), a subunit of the MLL H3K4 methyltransferase complex. This results in histone H3K4 methylation and thereby in chromatin remodelling, allowing the transcription of YAP target genes (Oh *et al.*, 2014; Qing *et al.*, 2014). YAP was found to also recruit the Mediator complex to the enhancers, resulting in the additional recruitment of the CDK9 elongating kinase. This allows YAP to activate transcription by releasing the promoter-proximal pausing of RNA polymerase II (Galli *et al.*, 2015). Furthermore, TAZ was shown to interact with the SWI/SNF chromatin remodelling complex to allow gene expression (Skibinski *et al.*, 2014).

Interestingly, YAP/TAZ have also been shown to act as TEAD corepressors. YAP/TAZ bound to TEAD can recruit the nucleosome remodelling and deacetylase (NuRD) complex. This results in histone deacetylation and changes in nucleosome occupancy, causing the repression of certain genes such as tumour-suppressor genes TNF-related apoptosis-inducing ligand (TRAIL) and DNA-damage-inducible transcript 4 (DDIT4). The repression of these two genes was to seen to be a requirement of the activation of the mTORC1 complex, leading to the promotion of cell survival (Kim *et al.*, 2015).

1.8.10 YAP/TAZ-TEAD target genes

It has been established that the YAP/TAZ-TEAD complex activates the expression of a number of genes influencing cell proliferation. Among these TEAD target genes are the genes of integrin ligands, CTGF (Lai *et al.*, 2011; Zhao *et al.*, 2008) and CYR61 (Lai *et al.*, 2011; Zhang, Pasolli & Fuchs, 2011), alternative Wnt ligand WNT5A (Park *et al.*, 2015), EGFR ligand amphiregulin (AREG) (Yang *et al.*, 2012), EGFR (Song *et al.*, 2015), Wnt/β-catenin antagonists DKK1 and IGFBP4 (Park *et al.*, 2015; Seo *et al.*, 2013), cytokine TGFβ2 (Lee *et al.*, 2016), growth factor BMP4 (Lai & Yang, 2013; Park *et al.*, 2015), amino acid transporters SLC7A5 and SLC38A1 (causing increased AA uptake which in turn activates mTORC1 complex and thereby promotes cell growth, a requirement for prolonged cell proliferation) (Hansen *et al.*, 2015; Park *et al.*, 2016b), transcription factor Myc (Cai *et al.*, 2018; Neto-Silva, de Beco & Johnston, 2010; Rajbhandari *et al.*, 2018; Zanconato *et al.*, 2015), glucose transporter GLUT3 (Wang *et al.*, 2015c), NF2, AMOTL2 and LATS2 (Dai *et al.*, 2015; Moroishi

et al., 2015) and immune checkpoint molecule PD-L1 (Feng *et al.*, 2017; Janse van Rensburg *et al.*, 2018; Kim *et al.*, 2018a; Miao *et al.*, 2017).

Some of these ligands/transporters are part of positive feedback loops. The YAP/TAZ-TEAD expressed ligands TGF-β2, WNT5A/B and AREG in turn activate YAP/TAZ via the receptors TGF-βR (Hiemer, Szymaniak & Varelas, 2014; Pefani *et al.*, 2016; Varelas *et al.*, 2008), Frizzled/ROR (Park *et al.*, 2015; Samanta *et al.*, 2018; Zhang *et al.*, 2019) and EGFR (Fan, Kim & Gumbiner, 2013; He *et al.*, 2015), respectively. Similarly, the YAP/TAZ-TEAD expressed glucose transporter GLUT3 and amino acid transporters SLC7A5 and SLC38A1 activate YAP/TAZ via glycolytic enzymes such as phosphofructokinase 1 (Enzo *et al.*, 2015; Wang *et al.*, 2015c) and the mTORC1 complex (Liang *et al.*, 2014b), respectively. In contrast, the YAP/TAZ-TEAD mediated expression of NF2, AMOTL2 and LATS2 (Dai *et al.*, 2015; Moroishi *et al.*, 2015) inhibit YAP/TAZ activity, making the expression of these proteins a part of negative feedback loops.

1.8.11 TEAD significance in cancer

High levels of TEAD expression have been shown to be associated with a poor prognosis in colorectal cancer (Liang *et al.*, 2014a; Liu *et al.*, 2016b), breast cancer (Wang *et al.*, 2015a), head and neck squamous cell carcinoma (Zhang *et al.*, 2018a), gastric cancer (Zhou *et al.*, 2013; Zhou *et al.*, 2017) and prostate cancer (Knight *et al.*, 2008). Similarly, nuclear YAP and heightened YAP expression correlates with decreased disease-free survival and overall survival in many cancer types (Sun *et al.*, 2015).

YAP/TAZ-TEAD mediated gene expression promotes a number of oncogenic cellular mechanisms such as cancer cell proliferation (Lamar *et al.*, 2012; Zhang *et al.*, 2009a; Zhao *et al.*, 2008) and oncogenic transformation (Lamar *et al.*, 2012; Zhao *et al.*, 2008). Furthermore, YAP/TAZ-mediated transcription promotes epithelial-mesenchymal transition (EMT) (Zhang *et al.*, 2009a; Zhao *et al.*, 2008), anoikis resistance (Haemmerle *et al.*, 2017; Zhao *et al.*, 2012) and migration and invasion (Kim *et al.*, 2017; Lamar *et al.*, 2012; Lee *et al.*, 2017), all of which are important for metastasis (Hiemer, Szymaniak & Varelas, 2014; Kim *et al.*, 2017; Lamar *et al.*, 2012; Lee *et al.*, 2017).

The YAP fusion genes YAP-MAML2 and YAP-NUTM1 were very frequently identified in poromas and porocarcinomas while the only TAZ fusion gene TAZ-NUTM1 was found in only one of the poroma samples. The YAP and TAZ fusion proteins were shown to retain their function as TEAD coactivators, thereby granting the oncogenic trait of soft agar colony formation (Sekine *et al.*, 2019).

1.9 Merlin dependent YAP/TAZ/TEAD regulation

1.9.1 Metabolism

In NF2-deficient tumours, YAP/TAZ induced growth factors bind growth factor receptor tyrosine kinases (RTKs), activating AKT signalling and thereby causing aerobic glycolysis to be maintained at a high rate (White *et al.*, 2019). This ensures that the high energy demand necessary for heightened proliferation is met. While YAP/TAZ does stimulate aerobic glycolysis, they have been proven to inhibit other cellular functions. YAP/TAZ suppress oxidative phosphorylation to avoid the threat of reactive oxygen species (ROS) formation which can put a cancer cell at risk of oxidative stress induced cell death. This is likely to be the case, particularly in cancer cells starved of nutrients who might struggle to express antioxidants as a countermeasure (White *et al.*, 2019).

Furthermore, both lysosomal biogenesis and the cAMP-PKA/EPAC pathway in NF2-deficient tumours are inhibited by YAP/TAZ (White *et al.*, 2019) since both of these mechanisms can trigger Hippo signalling and therefore suppress YAP/TAZ activity (Iglesias-Bartolome *et al.*, 2015; Kim *et al.*, 2013; Yu *et al.*, 2013b). Interestingly, it has been shown that after the loss of both NF2 and YAP/TAZ, the now uninhibited cAMP-PKA/EPAC pathway activates the RAF-MEK-ERK pathway, which permits tumour cells deprived of YAP/TAZ to survive (White *et al.*, 2019).

1.9.2 Actin cytoskeleton/Mechanical stress

A multitude of findings indicate that actin cytoskeleton deregulation due to Merlin loss promotes cell proliferation (Ammoun *et al.*, 2008; Bashour *et al.*, 2002; Flaiz *et al.*, 2009; Flaiz *et al.*, 2008; Pelton *et al.*, 1998; Petrilli *et al.*, 2014a), including through the Hippo pathway (Yin *et al.*, 2013). There is an indication that Merlin loss induced cytoskeletal alterations causing high mechanical stress might be stronger inducers of YAP/TAZ activation than the loss of regulation by LATS1/2 due to Merlin loss (Aragona *et al.*, 2013; Dupont *et al.*, 2011).

Some studies suggest that YAP regulation due to cell morphology/cytoskeleton reorganization is LATS dependent, with LATS being activated by F-actin stress fibres (Wada *et al.*, 2011) and the reorganization of the cytoskeleton (Zhao *et al.*, 2012). Since it has been shown that actin cytoskeleton disruption promotes Merlin-LATS interaction, it is possible that LATS-dependent cytoskeleton-induced regulation (in this case suppression) of YAP activity functions via LATS association with Merlin (Yin *et al.*, 2013).

1.9.3 GPCRs

The Hippo pathway can be activated or inhibited via G-protein-coupled receptors (GPCRs) and their agonists depending on the Gα subunit type, resulting in higher or lower YAP phosphorylation, respectively. $G\alpha_s$ is the only Gα subunit to activate Hippo signalling and thereby heighten YAP phosphorylation. Epinephrine and glucagon stimulate $G\alpha_s$-coupled receptors, leading to the activation of cAMP and thereby the activation of PKA which in turn inhibits Rho GTPases and activates LATS1/2, resulting in increased YAP Ser127 and YAP Ser381 phosphorylation and the subsequent inhibition of YAP. This pathway was shown to be promoted by Merlin (Kim *et al.*, 2013; Yu *et al.*, 2012).

1.9.4 Cell polarity proteins/complexes

There are indications that Merlin, KIBRA and PTPN14 associate and form a complex in the apical side of epithelial cells (Baumgartner *et al.*, 2010; Genevet *et al.*, 2010; Poernbacher *et al.*, 2012; Yu *et al.*, 2010) (Figure 1.4). Non-receptor tyrosine phosphatase PTPN14 promotes the export of YAP to the cytoplasm during contact inhibition. PTPN14 was found to perform its inhibitory function by using its PPxY domain to directly bind to the WW domain of YAP. PTPN14 stability is maintained at high cell density and targeted for degradation by $CRL2^{LRR1}$ (cullin2 RING ubiquitin ligase complex/leucine-rich repeat protein 1) complex at low cell density (Liu *et al.*, 2013; Wang *et al.*, 2012).

1.9.5 Cell-cell contacts/Angiomotin

Cell-cell contact components have been shown to regulate Hippo signalling activity and vice versa (Figures 1.2 and 1.3). Merlin organizes and binds to specific membrane domains and intercellular contacts such as adherens junctions (AJs) and tight junctions (TJs) (Gladden *et al.*, 2010; McClatchey & Giovannini, 2005). At AJs of keratinocytes, Merlin binds α-catenin and Par3, resulting in the assembly of a matured adherens junction (Gladden *et al.*, 2010). Furthermore, E-cadherin and β-catenin are involved in contact inhibition by inducing YAP phosphorylation via Merlin, KIBRA and LATS1/2 activation, thereby restricting cell proliferation (Kim *et al.*, 2011).

Furthermore, Merlin can form a tight junction complex consisting of Merlin, angiomotin (AMOT), PATJ and PALS1. Merlin has been shown to competitively bind to AMOT, thus freeing the small GTPase Activating Protein Rich1 from the Angiomotin-inhibitory complex. Rich1 then inhibits Rac1, suppressing Rac1-PAK and Ras-MAPK signalling and their oncogenic potential. Angiomotin knockout in NF2-deficient Schwann cells inhibited the Ras-MAPK pathway, disrupting proliferation *in vitro* and tumour xenograft growth *in vivo* (Okada, Lopez-Lago & Giancotti, 2005; Wells *et al.*, 2006; Yi *et al.*, 2011).

In general, the function of AMOT is strongly associated with cell-cell contacts and AMOT protein stability and thereby function has been shown to be Merlin dependent (Wang *et al.*, 2021). AMOT was seen to be highly expressed in 10 human schwannoma samples while the

control human nerve only contained low levels of AMOT (Yi *et al.*, 2013). AMOT and angiomotin-like 1 and 2 (AMOTL1 and AMOTL2) were shown to directly interact with YAP and TAZ to suppress their function. The N-terminal PPxY motif of angiomotin proteins binds to YAP's first/TAZ's only WW domain, sequestering YAP/TAZ at tight junctions and thereby preventing their nuclear localization and associated YAP/TAZ dependent gene expression (Chan *et al.*, 2011; Zhao *et al.*, 2011). Additionally, AMOTL2 was suggested to act as a scaffold protein by binding MST2, LATS2 and YAP, thereby promoting LATS2 activation and YAP deactivation (Paramasivam *et al.*, 2011).

In contrast, p130 splicing isoform of AMOT (AMOT-p130) was reported to promote YAP activity. The PPxY and LPxY motifs of cytoplasmic AMOT-p130 binds to YAP's WW domains, denying LATS1's access to these domains and thereby blocking YAP phosphorylation. Nuclear AMOT-p130 forms a complex with YAP and TEAD, promoting the expression of YAP-TEAD target genes (Yi *et al.*, 2013).

1.9.6 Integrins/Cell-ECM contacts/FGF

Focal adhesions (FAs) also play a role in regulating the Hippo signalling pathway. Integrin-linked kinase (ILK) promotes YAP/TAZ-TEAD activity via Merlin inactivation (Figure 1.4) and ErbB2 signalling (Serrano *et al.*, 2013). In contrast, FGF15 mediates Merlin-RAF1 binding, releasing MST1/2 from RAF1's inhibitory effect and thereby allowing MST1/2 activation and YAP inactivation (Ji *et al.*, 2019).

1.9.7 Nervous system

Merlin was demonstrated to affect the expression of an axonal surface protein crucially determining Schwann cell differentiation and myelination, neuregulin 1, both *in vitro* (primary DRG cells and P19 neuronal cell line) and *in vivo*. Merlin deficient nerve tissue from Merlin knockout animals and Neurofibromatosis type 2 patients showed a decreased expression of neuregulin 1 type III and a (possibly compensatory) heightened expression of neuregulin 1 receptor ErbB2 (Schulz *et al.*, 2014).

1.10 Merlin independent YAP/TAZ/TEAD regulation

1.10.1 Actin cytoskeleton/Mechanical stress

Mechanical stimuli produced by ECM elasticity/rigidity, cell density, cell geometry/shape and cytoskeletal tension regulate YAP/TAZ activity, identifying YAP and TAZ as mechanosensors (Dupont *et al.*, 2011; Zhao *et al.*, 2007).

In NF2-deficient breast cancer cell lines, re-introduction of Merlin expression causes the suppression of YAP-TEAD signalling. This is reversible by LATS1/2 knock down except in the vicinity of a soft extracellular matrix which causes a low mechanical stress on the cells attached to it. This imitates the low mechanical stress cells experience when they are forced to change their cell geometry under high cell density conditions, adopting a smaller cell size/shape which would only allow them to adhere to a small ECM area. Accordingly, cells growing in low cell density will adopt a flat and spread-out cell morphology and permit them to occupy a larger ECM area, resulting in high mechanical stress. Similarly, cells attached to/growing on ECM with high rigidity will experience high mechanical stress whereas growing on soft ECM will result in low mechanical stress. Changes from low cell density/high mechanical stress to high cell density/low mechanical stress requires Rho GTPase (central regulators of actin remodelling) activity and will activate the F-actin capping/severing proteins CapZ, Gelsolin and Cofilin, causing them to reduce F-actin stress fibres. This F-actin remodelling decreases YAP/TAZ activity independent of LATS1/2, inhibiting the promotion of cell proliferation by YAP/TAZ and enforcing contact inhibition. Therefore, cells experiencing high mechanical stress contain nuclear YAP/TAZ promoting cell proliferation while cells under low mechanical stress show cytoplasmic accumulation of YAP/TAZ, inhibiting proliferation. YAP/TAZ regulation by this mechanism was found to be more efficient than YAP/TAZ regulation by activated LATS1/2.

Another mechanism of LATS independent YAP regulation via mechanical stress involves the ARID1A-containing SWI/SNF protein complex (ARID1A-SWI/SNF). At low mechanical stress, ARID1A of the SWI/SNF protein complex binds to YAP/TAZ, preventing YAP/TAZ and TEAD bonding and thereby YAP/TAZ-TEAD target gene expression and associated effects. Under high mechanical stress, ARID1A-SWI/SNF is bound by nuclear F-actin instead, allowing YAP/TAZ-TEAD association and gene expression and thereby leading to increased cell proliferation and oncogenic transformation (Chang *et al.*, 2018). Interestingly, mutations inactivating the ARID1A or ARID1B genes were reported in 29 % of sporadic schwannomas (Agnihotri *et al.*, 2016).

Additionally, a study reported that the high mechanical forces in a stiff cell environment increase the opening of the nuclear pores, allowing a heightened nuclear import of YAP (Ege *et al.*, 2018; Elosegui-Artola *et al.*, 2017).

1.10.2 Actomyosin cytoskeleton/Spectrin

The Rho-associated protein kinase (ROCK)-non-muscle myosin II light chain (MLC) pathway is one of the main regulators of the actomyosin cytoskeleton. This signalling pathway was suggested to connect actomyosin rearrangement and YAP regulation, causing YAP dephosphorylation/activation under high mechanical stress conditions (Cai *et al.*, 2018; Dupont *et al.*, 2011; Zhao *et al.*, 2012). Accordingly, a different study showed that low ECM stiffness (= low mechanical stress) induces the stimulation of Ras-related GTPase RAP2 which in turn binds to and activates MAP4K4/6/7 and Rho inhibitor ARHGAP29. This allows LATS1/2 activation and subsequent YAP/TAZ suppression (Meng *et al.*, 2018). Interestingly, spectrin, a

protein belonging to the spectrin-based membrane skeleton (SBMS) which is located at the cytoskeleton-plasma membrane border, is suggested to antagonize MLC phosphorylation /activation or bind to the Crumbs complex, either resulting in the activation of the Hippo pathway and the promotion of YAP phosphorylation/deactivation or YAP cytoplasmic retention in a LATS dependent manner, respectively (Deng *et al.*, 2015; Fletcher *et al.*, 2015) (Figure 1.4).

1.10.3 GPCRs

As mentioned previously, the Hippo pathway has been shown to be either activated or inhibited by G-protein-coupled receptors (GPCRs) and their agonists depending on the type of Gα subunit, causing an increase or decrease of YAP phosphorylation, respectively. $G\alpha_{12}$ and $G\alpha_{13}$ cause the strongest Hippo pathway inhibition and reduction of YAP phosphorylation, followed by $G\alpha_q$, $G\alpha_{11}$, $G\alpha_{14}$ and $G\alpha_{15}$ and to a lesser extent, $G\alpha_i$, $G\alpha_t$ and $G\alpha_o$. It was reported that Sphingosine 1-phosphophate (S1P) or lysophosphatidic acid (LPA), both present in the blood serum, can be used to stimulate $G\alpha_{12/13}$ - or $G\alpha_{q/11}$ -coupled receptors. This causes the activation of Rho GTPases such as RhoA and actin cytoskeleton alterations, resulting in LATS1/2 suppression and thereby in decreased YAP Ser127 and Ser381 phosphorylation. This allows increased YAP activity and expression of YAP target genes e.g. CTGF (Yu *et al.*, 2012).

1.10.4 Cell cycle/Src/p53

A number of other signalling effectors can regulate Hippo signalling activity. During the G2-M phase, cell-cycle kinase CDK1 can phosphorylate YAP at Thr119, Ser289 and Ser367, promoting YAP-induced cancer cell migration and invasion (Yang *et al.*, 2013b).

Furthermore, the SRC tyrosine kinase, activated by β4 integrin and IL-6, phosphorylates YAP at Tyr341, Tyr357 and Tyr394 found in its transcription domain, resulting in YAP activation and allowing oncogenic transformation. This β4 integrin-SRC signalling pathway was shown to be inhibited by cell-cell adhesion protein αE-catenin (Li *et al.*, 2016a; Taniguchi *et al.*, 2017).

Hippo signalling also connects tetraploid cells (found in a substantial fraction of human tumours) and p53 signalling leading to G1/S arrest. Genome duplication during S-phase and subsequent cytokinesis failure creates binuclear tetraploid cells containing an additional centromere. The microtubules of the extra centromere cause an increase and decrease of Rac1 and RhoA activity, respectively. Decreased RhoA activity levels activates LATS2 which both phosphorylates/inactivates YAP and inhibits the E3 ubiquitin ligase MDM2 by direct binding. This prevents p53 proteasomal degradation, allowing p53 accumulation in the nuclei. The combination of YAP deactivation and nuclear p53 accumulation triggers G1/S cell cycle arrest, preventing the proliferation of tetraploid cells (Aylon *et al.*, 2006; Ganem *et al.*, 2014).

1.10.5 Energy stress

Hippo signalling has also been reported to respond to a multitude of cellular stresses. Energy stress/glucose deprivation results in a heightened AMP:ATP ratio. This activates the main metabolic sensor AMP-activated protein kinase (AMPK) which catalyses AMOTL1 Ser793 phosphorylation. AMOTL1 Ser793 phosphorylation leads to increased AMOTL1 protein stability and expression, promoting LATS1/2 induced YAP Ser127 phosphorylation, YAP cytoplasmic retention and suppression of YAP target gene transcription (Figure 1.4). Interestingly, YAP transcriptional activity causes the upregulation of glucose-transporter 3 (GLUT3) expression. AMPK also phosphorylates YAP directly at Ser366 and Ser463 and more importantly, at Ser94 which is a residue vital for YAP-TEAD binding. Therefore, Ser94 phosphorylation was shown to interfere with YAP-TEAD interaction (DeRan *et al.*, 2014; Mo *et al.*, 2015; Wang *et al.*, 2015c).

In contrast, hypoxia inactivates Hippo signalling by activating the E3 ubiquitin ligase SIAH2 which prevents hypoxia-inducible factor 1α (HIF1α) degradation but also induces LATS2 proteasomal degradation. This results in reduced YAP phosphorylation and allows YAP-HIF1α and YAP-TEAD binding and gene expression, e.g. VEGF (YAP-HIF1α) and CTGF and CYR61 (YAP-TEAD) (Ma *et al.*, 2015). Hippo signalling also plays a role in the cellular response to oxidative stress in mammalian neurons. In these cells, oxidative stress causes MST1 activation which phosphorylates Ser207 in the conserved forkhead domain of the FOXO3 transcription factor. Ser207 phosphorylation interferes with FOXO3-14-3-3 binding, promoting FOXO3 translocation to the nucleus to trigger apoptosis (Lehtinen *et al.*, 2006).

1.10.6 Osmotic stress/ER

During the acute phase of osmotic stress, NLK catalyses YAP Ser128 phosphorylation, preventing YAP-14-3-3 interaction despite YAP Ser127 phosphorylation. This allows YAP nuclear accumulation and YAP-TEAD target gene expression (Hong *et al.*, 2017; Moon *et al.*, 2017). In contrast, high cell density, the adaptation phase of osmotic stress and cell detachment cause cytoplasmic translocation of YAP/TAZ and TEAD. During the adaptation phase of osmotic stress, p38 MAPK is activated whose direct interaction with TEAD promotes TEAD and YAP/TAZ cytoplasmic translocation, thereby interfering with YAP/TAZ-TEAD target gene transcription in a MST1/2 and LATS1/2 independent manner. Interestingly, p38 MAPK binds to a putative TEAD D domain close to the TEAD nuclear localization signal and TEAD nuclear export was shown to be dependent on both a putative TEAD nuclear export signal and exportin CRM1 (Huh *et al.*, 2019; Lin *et al.*, 2017). TEAD cytoplasmic translocation was shown to negatively affect the proliferation of YAP-driven cancer cells such as GNAQ mutant uveal melanoma cells and LATS1/2 mutant mesothelioma cells but had no effect on the proliferation of their YAP-independent counterparts. Additionally, TEAD was mostly cytoplasmic in normal kidney tissue but became increasingly nuclear in malignant renal clear cell carcinoma nuclear (Lin *et al.*, 2017). Taken all together and given that the presence of TEAD in the nucleus is necessary for YAP/TAZ nuclear accumulation as mentioned before (Chan *et al.*, 2009; Diepenbruck *et al.*, 2014; Lin *et al.*, 2017), this suggests that YAP/TAZ-TEAD

signalling inhibition via TEAD cytoplasmic translocation supersedes activation signals directly targeting YAP/TAZ (Huh *et al.*, 2019).

Furthermore, the deregulation of the ER stress induced unfolded protein response (UPR) has been found in a significant number of human hepatocellular carcinoma (HCC). ER stress due to misfolded proteins induces the UPR which taps into Hippo signalling. During the initial adaptive UPR phase, the kinase PERK phosphorylates elF2α which heightens ATF4 expression which in turn increases YAP expression. This augmentation in YAP activity results in an increase of UPR and ER size to ease ER stress. If ER stress cannot be alleviated and therefore persists, a modulation of the UPR occurs, activating MST/LATS signalling. This promotes the formation of the GADD34/protein phosphatase 1 (PP1) complex which allows elF2α dephosphorylation by PP1 in the cytoplasm (= adaptive UPR inhibition) while preventing YAP dephosphorylation in the nucleus. This results in increased levels of YAP phosphorylation, thereby promoting apoptosis to prevent tumourigenesis (Wu *et al.*, 2015).

1.10.7 IKKε/PRP4K

Moreover, virus-activated kinase IKKε phosphorylates YAP Ser403, resulting in lysosomal YAP degradation (Wang *et al.*, 2017). YAP is also phosphorylated by the PRP4 kinase which plays in role in mRNA splicing. PRP4 kinase induced YAP Ser111 and Ser250 phosphorylation (sites also phosphorylated by LATS1/2), resulting in the suppression of YAP-TEAD interaction and YAP export into the cytoplasm (Cho *et al.*, 2018).

1.10.8 Immune response

Hippo signalling was also seen to be involved in the innate immune response. MST1/2 stimulate the GTPase Rac to foster the Toll-like receptor (TLR)-induced formation of the TRAF6-ECSIT complex. This complex is necessary for mitochondria recruitment to the phagosomes, thereby allowing the production of reactive oxygen species (ROS) to destroy pathogens. This has been shown to be particularly important for the cellular defence against bacteria (Geng *et al.*, 2015).

The viral defence of the cell relies heavily on cytosolic DNA/RNA sensing and interferon production, both of which require the function of transcription factor interferon regulatory factor 3 (IRF3). MST1 (not MST2) catalyses IRF3 Thr75 and Thr253 phosphorylation, preventing IRF3 homodimerization, chromatin binding and IRF3 target gene transcription (Meng *et al.*, 2016). Interestingly, upon viral infection YAP activity has been shown to impede IRF3 dimerization and nuclear translocation. As mentioned before, viral infection activates the kinase IKKε which phosphorylates YAP Ser403, triggering YAP degradation in lysosomes and counteracting the described YAP-induced effects (Wang *et al.*, 2017). In addition, MST1 interferes with the activation of the virus-induced TANK-binding kinase 1 (TBK1), resulting in additional IRF3 suppression (Meng *et al.*, 2016).

1.10.9 mTOR/Lysosomes/Autophagosomes

Activation of mTOR was shown to result in the accumulation of YAP and thereby in increased proliferation and attenuated apoptosis *in vitro* and *in vivo*. YAP accumulation was caused by mTOR-induced inhibition of YAP degradation in lysosomes and autophagosomes. This YAP and mTOR dependent mechanism was suggested to play an important role in the development of perivascular epithelioid cell tumours (PEComas) (Liang *et al.*, 2014b). Interestingly, under high/low mechanical stress (= contact inhibition) YAP/TAZ have been shown to induce/fail to induce myosin II expression which contributes to/inhibits F-actin polymerization and F-actin stress fibre formation. In turn, this allows the formation of autophagosomes (Pavel *et al.*, 2018). This shows that contact inhibition of cell proliferation also impairs autophagy and suggests that YAP/TAZ at least in part control their own degradation through the lysosome/autophagosome system.

1.10.10 Cell-cell contacts/Cell polarity proteins/complexes

A-catenin binds to the 14-3-3/phosphorylated Ser127 YAP1 complex and recruits this complex to AJs, resulting in increased YAP phosphorylation and cytoplasmic retention and thereby decreased YAP activity. It is suggested that α-catenin binding might stabilize the 14-3-3/YAP1 complex and thereby prevent phosphatase PP2A from YAP dephosphorylation, both effects resulting in the promotion of YAP cytoplasmic retention and degradation (Schlegelmilch *et al.*, 2011; Silvis *et al.*, 2011). As mentioned before, αE-catenin inhibits β4 integrin-mediated YAP Tyr341, Tyr357 and Tyr394 phosphorylations and thereby suppresses YAP1 activation (Li *et al.*, 2016a).

Hippo pathway signalling molecules have also been found at TJs. The C-terminal PDZ-binding motif of YAP2 and the first PDZ domain of tight junction protein zonula occludens-2 (ZO-2) can bind, allowing ZO-2 to promote the nuclear localization and pro-apoptotic effect of YAP2 (Oka *et al.*, 2010). Furthermore, the apical Crumbs polarity complex has been shown to localize at TJs. Crumbs 3 (CRB3) has been found to promote the assembly and apical localization of the Crumbs complex and to be vital for correct TJ formation (Fogg, Liu & Margolis, 2005; Makarova *et al.*, 2003). The Crumbs polarity complex which includes CRB3, PALS1, PATJ, AMOT, LIN7C and MUPP1 phosphorylates YAP/TAZ under high cell density conditions (Figure 1.4) (Varelas *et al.*, 2010).

Additionally, the planar cell polarity (PCP) regulator FAT4 has been shown to reduce YAP activity by sequestering the scaffold protein AMOTL1, resulting in YAP cytoplasmic retention (Ragni *et al.*, 2017).

1.10.11 Post-translational modifications

Various post-translational modifications have also been shown to regulate Hippo pathway signalling. Monomethylation of YAP reduces YAP activity (Oudhoff *et al.*, 2013) while YAP O-GlcNAcylation (Peng *et al.*, 2017) and K63-linked polyubiquitination (Yao *et al.*, 2018) enhance

YAP function. Finally, as mentioned previously, TEAD autopalmitoylation was shown to be important for TEAD function (Chan *et al.*, 2016; Noland *et al.*, 2016).

1.10.12 Integrins /Cell-ECM contacts

Integrin activates focal adhesion kinase (FAK)-Src-PI3K signalling, resulting in LATS1/2 inhibition and therefore YAP nuclear accumulation and activation (Kim & Gumbiner, 2015). In contrast, integrin activation in endothelial cells under unidirectional shear stress increases YAP phosphorylation/inhibition (Wang *et al.*, 2016b).

1.10.13 Wnt-β-catenin

Links between Hippo signalling and Wnt-β-catenin signalling pathway have also been reported. When Wnt signalling is activated, both YAP/TAZ and β-catenin are released from the β-catenin destruction complex, allowing both to translocate to the nucleus and induce YAP/TAZ-TEAD and β-catenin-TCF target gene expression (Azzolin *et al.*, 2014). Furthermore, WNT3a and WNT5a/b were seen to activate the GTPase Rho, causing LATS1/2 inhibition and therefore YAP/TAZ activation and YAP/TAZ-TEAD target gene transcription (Park *et al.*, 2015).

1.10.14 EGF/Insulin/Hyaluronan/Oncogenic viruses

Moreover, EGF signalling can suppress the Hippo pathway. EGF treatment causes LATS inactivation, YAP dephosphorylation and nuclear accumulation, CTGF gene transcription and cell proliferation (Fan, Kim & Gumbiner, 2013). Similarly, Insulin treatment results in YAP dephosphorylation via LATS suppression (Straßburger *et al.*, 2012).

In contrast, the ECM component high-molecular-weight hyaluronan (HMW-HA) binds to CD44, permitting the recruitment of Partitioning defective-1b (PAR1b, also named microtubule affinity-regulating kinase 2 (MARK2)) to CD44. Now released from PAR1b's control, MST1/2 can initiate Hippo signalling and suppress YAP-induced effects including cell proliferation. Interestingly, this HMW-HA induced Hippo signalling activation can be counteracted by low-molecular-weight hyaluronan (LMW-HA) (Ooki *et al.*, 2019).

Finally, oncogenic viruses can also induce YAP activation. Infection of cells with the Kaposi sarcoma causing herpesvirus (Liu *et al.*, 2015b) and the Merkel cell carcinoma causing Merkel cell polyomavirus (Nguyen *et al.*, 2014) result in YAP activation.

1.10.15 Organ size regulation

One of the main functions of the Hippo signalling pathway is controlling organ size via a balance of cell proliferation and apoptosis. Deregulation of the Hippo pathway can lead to organ overgrowth and oncogenesis which has been extensively shown in the liver (Camargo

et al., 2007; Chen *et al.*, 2015b; Dong *et al.*, 2007; Hermann *et al.*, 2018; Lee *et al.*, 2010; Lu *et al.*, 2010; Nishio *et al.*, 2016; Song *et al.*, 2010; Yi *et al.*, 2016; Zhang *et al.*, 2010; Zhou *et al.*, 2009). Similarly, an organ overgrowth phenotype upon Hippo pathway deregulation was seen in the heart (Heallen *et al.*, 2011; von Gise *et al.*, 2012; Xin *et al.*, 2011) and the spleen and stomach (Cotton *et al.*, 2017; Song *et al.*, 2010).

In contrast, it was reported that Hippo signalling pathway deactivation in mammary gland, lung and intestines has no effect on organ size (Chen *et al.*, 2014; Song *et al.*, 2010). Interestingly, Hippo signalling loss in the pancreas and kidney reduces pancreas size due to an artificially occurring metaplasia and decreases kidney size due to impeded cell differentiation, respectively (Gao *et al.*, 2013; George *et al.*, 2012; McNeill & Reginensi, 2017).

1.10.16 Nervous system

During neural tube development, MST1/2 and LATS1/2 have been found to regulate the neural progenitor cell pool by controlling YAP activity. YAP-TEAD target gene expression can drive neural progenitor cell proliferation via cyclin D1 expression and suppress differentiation by inhibiting expression of the TF NeuroM. Loss of YAP or TEAD function results in increased apoptosis among the neural progenitor cells while YAP-TEAD target gene repression inhibits proliferation and initiates neuronal differentiation (Cao, Pfaff & Gage, 2008).

YAP function also plays a fundamental role in avoiding foetal non-communicating hydrocephalus which can occur due to a blockage in the cerebral aqueduct between the third and fourth ventricle of the brain. YAP activity allows the generation of functional ependymal cells and preserves the integrity of the apical cells lining the cerebral aqueduct by promoting cell junction protein localization (e.g. N-cadherin) during mouse development. Intriguingly, preservation of cellular lining integrity by YAP appears to be due to cytoplasmic and/or junctional YAP localization and not due to nuclear YAP (Park *et al.*, 2016a).

Furthermore, YAP/TAZ in Schwann cells are shown to be important in two crucial steps in peripheral nerve development, namely radial sorting and myelination. For that purpose, YAP/TAZ are activated by mechanical stimuli and subsequently promote Schwann cell proliferation and induce YAP/TAZ-TEAD-mediated expression of basal laminin receptor genes e.g. dystroglycan and integrins α6β1 and α6β4. Interestingly, YAP is unable to entirely compensate for the loss of TAZ while TAZ alone is sufficient to allow correct radial sorting and myelination. Additionally, upon complete loss of both YAP and TAZ, development of the peripheral nerves stops at the radial sorting stage, unable to complete that stage of nerve development. Mice with such a YAP/TAZ dKO genotype were shown to develop a very severe phenotype which leaves them with almost completely paralyzed hind legs (Poitelon *et al.*, 2016).

1.11 Hippo signalling in schwannomas and meningiomas

Analysing the proteomes of 68 NF2-related and sporadic schwannomas unveiled a link between YAP expression levels and tumour cell proliferation (Boin *et al.*, 2014). Furthermore, LATS1/2 gene mutations and promoter methylations were found in 82 sporadic schwannomas (Oh *et al.*, 2015). A different study showed decreased MST2 and LATS2 protein expression in sporadic vestibular schwannomas compared to normal nerve controls. A correlation between nuclear YAP levels and tumour cell proliferation was found as well (Zhao *et al.*, 2018a). Moreover, SAV1 mutations were identified in spinal schwannomas (Gao *et al.*, 2020).

Additionally, YAP fusion genes such as YAP1-MALM2, YAP1-LMO1, YAP1-PYGO1 and YAP1-FAM118B were identified in sporadic meningiomas (Schieffer *et al.*, 2021; Sievers *et al.*, 2020). YAP1-MALM2 fusion gene containing meningiomas were seen to exert similar gene expression patterns to NF2-mutant meningiomas and engage in YAP-TEAD induced gene expression, unaffected by Hippo signalling. *Ex vivo* usage of verteporfin and Vivace inhibitors (see section 1.15.4) VT104 and VT107 reduced cell viability of cuboids derived from extra-cranial mouse tumours induced by YAP1-MAML2 (Szulzewsky *et al.*, 2022). Furthermore, one study showed the abundant presence of nuclear YAP in human meningiomas and suggested an important role of YAP in meningioma tumourigenesis (Baia *et al.*, 2012), which was later supported by (Szulzewsky *et al.*, 2022).

1.12 Hippo signalling in macrophages

In the murine RAW264.7 macrophage cell line and in bone marrow-derived macrophages, YAP/TAZ inhibition was seen to impair M2-like macrophage polarization (Feng *et al.*, 2018). Similarly, it was shown that YAP in human monocytic THP-1 cells promotes M2-like TAM polarization and YAP inhibition impedes this process without interfering with M1-like TAM macrophage polarization (Huang *et al.*, 2017). In contrast, a different study showed that a myeloid cell-specific knockout of YAP promotes M2-like macrophage polarization and impairs IL-6 production of M1-like macrophages (Zhou *et al.*, 2019). Furthermore, nuclear translocation of YAP in human monocytic THP-1 cells was seen to play a role in macrophage migration and recruitment (Zhang *et al.*, 2018c). In bone-marrow derived macrophages, YAP-TEAD activity was linked to differentiation into osteoclasts (Zhao *et al.*, 2018b).

Moreover, YAP has been demonstrated to adversely affect the antiviral immune defence in primary peritoneal macrophages and in cell line macrophages and monocytes (RAW264.7 and THP-1 cells, respectively). As a result, YAP inhibition elicited a strengthened antiviral immune response (Wang *et al.*, 2017; Zhang *et al.*, 2017). Using macrophage cell lines such as U937 and RAW264.7 and human monocyte-derived macrophages, it was shown that the MST-like kinase LegK7, expressed after *Legionella pneumophila* infection, activates MOB1 and therefore the Hippo signalling pathway, causing YAP/TAZ degradation. This results in altered gene expression within macrophages including PPARγ-mediated transcription (TAZ acts as corepressor to the transcription factor PPARγ (Hong *et al.*, 2005)), allowing enhanced replication of the *L. pneumophila* pathogen (Lee & Machner, 2018).

Also, MST1/2 activity in RAW264.7 cells and murine bone marrow derived macrophages was demonstrated to promote ROS production by controlling the recruitment of mitochondria to phagosomes (Geng *et al.*, 2015) which is of great importance to the antibacterial immune response (West *et al.*, 2011). Additionally, MST1 was seen to inhibit pro-inflammatory cytokine secretion and heighten IFN- γ synthesis in primary murine peritoneal and bone-derived macrophages and human peripheral blood mononuclear cells (Li *et al.*, 2015a).

1.13 Hypothesized effect of Vivace inhibitors on schwannomas and their growth

YAP is implicated in a number of protumourigenic mechanisms such as schwannoma cell proliferation (Boin *et al.*, 2014; Oh *et al.*, 2015), macrophage/TAM recruitment (Kim *et al.*, 2018b; Zhang *et al.*, 2018c; Zhou *et al.*, 2018) (one of which was shown to be TEAD dependent (Guo *et al.*, 2017)), M2-like macrophage and TAM polarization (Feng *et al.*, 2018; Huang *et al.*, 2017; Murakami *et al.*, 2017), CAF-induced tumour microenvironment formation (Calvo *et al.*, 2013; Liu *et al.*, 2015a) and immunosuppression (An *et al.*, 2018; Ni *et al.*, 2018; Wang *et al.*, 2016a). Additionally, TAZ-TEAD signalling was demonstrated to promote myeloid cell infiltration and tumour development (Hagenbeek *et al.*, 2018). Therefore, using Vivace inhibitors (see section 1.15.4) would inhibit YAP/TAZ-TEAD signalling in schwannoma cells and macrophages alike. This is likely to result in the impairment of tumour growth both directly and indirectly by interfering with the protumourigenic mechanisms mentioned above.

1.14 Role of Hippo signalling in cancer

The Hippo signalling pathway is described as one of 10 canonical pathways associated with tumourigenesis (Sanchez-Vega *et al.*, 2018). As mentioned before, NF2 gene inactivation gives rise to Neurofibromatosis type 2, characterized by the formation of nervous system tumours such as schwannomas, meningiomas and more rarely, ependymomas (Rouleau *et al.*, 1993).

Furthermore, a 30% prevalence of somatic NF2 mutations in 20 human melanoma samples was reported (Bianchi *et al.*, 1994). It was shown that Merlin silencing in human melanoma cell lines increased their proliferation, migration and invasion *in vitro* and augmented their growth as subcutaneous melanoma xenograft tumours *in vivo* (Murray, Lau & Yu, 2012). Furthermore, mutations in the GNAQ and GNA11 genes, responsible for roughly 80 – 83 % of uveal melanoma (UM), have been reported to activate YAP and thereby promoting both proliferation of UM cell lines *in vitro* and their growth as xenograft tumours *in vivo* (Feng *et al.*, 2014; Yu *et al.*, 2014). Interestingly, Merlin loss was shown to confer vemurafenib (PLX4032) resistance to melanoma cells (Petrilli & Fernández-Valle, 2016; Reinhold *et al.*, 2014; Shalem *et al.*, 2014).

Also, NF2 gene inactivation was seen in 40 – 50% of malignant mesotheliomas (MMs) (Baser *et al.*, 2002a; Bianchi *et al.*, 1995; Cheng *et al.*, 1999; Sekido *et al.*, 1995), in 22% of a rare subtype (mucinous tubular and spindle cell carcinoma, MTSCC) of renal cell carcinoma (RCC)

(Mehra *et al.*, 2016) and in cervical squamous cell carcinomas (CSCCs) (Wang *et al.*, 2018b) (Figure 1.6).

Moreover, LATS1 and LATS2 mutations were found in MM (Miyanaga *et al.*, 2015; Murakami *et al.*, 2011) and LATS2 and SAV1 mutations were observed in papillary renal cell carcinoma (PRCC), CSCCs and mesothelioma (Wang *et al.*, 2018b). Moreover, PTPN14 mutations were seen in 31% of MTSCCs (Mehra *et al.*, 2016) and 23% of basal cell carcinoma (BCC) (Bonilla *et al.*, 2016).

Aside from mutations in upstream regulators of the Hippo signalling pathway, YAP/TAZ activation, detectable by YAP/TAZ nuclear accumulation and/or increased protein expression, might also be attributable to different YAP/TAZ gene alterations. YAP gene amplification was reported in numerous cancers including medullablastoma, CSCC and hepatocellular carcinoma (HCC) (Fernandez *et al.*, 2009; Wang *et al.*, 2018b; Zender *et al.*, 2006) (Figure 1.6). Furthermore, YAP or TAZ fusion genes due to chromosomal translocation giving rise to YAP or TAZ fusion proteins have been observed in ependymomas (Pajtler *et al.*, 2015), epithelioid hemangioendotheliomas (Antonescu *et al.*, 2013; Tanas *et al.*, 2011) and breast cancer (Li *et al.*, 2013). Moreover, possession of an activating YAP R331W missense mutation was shown to cause a predisposition to lung adenocarcinoma (Chen *et al.*, 2015a).

Finally, YAP/TAZ activity could be increased due to involvement of other signalling pathways. YAP activation is frequently found in the tubular adenomas of patients with familial adenomatous polyposis (FAP) which is caused by Adenomatous polyposis coli (APC) gene mutations. APC inactivation would disrupt the formation of the β-catenin destruction complex, preventing said complex from retaining YAP/TAZ in the cytoplasm. Therefore, YAP/TAZ would be free to accumulate in the nucleus to activate transcription (Azzolin *et al.*, 2014; Cai *et al.*, 2015).

Intriguingly, YAP activation has also been suggested as compensatory mechanism in order to escape $Kras^{G12D}$ mutation dependency in human pancreatic ductal adenocarcinoma (PDAC) (Kapoor *et al.*, 2014) and lung adenocarcinoma (Shao *et al.*, 2014). Furthermore, inactivation of tumour suppressor LKB1 (also named STK11) gene, found in 34% of lung adenocarcinoma (Ji *et al.*, 2007), was shown to result in YAP activation (Mohseni *et al.*, 2014).

Interestingly, YAP gene deletion or low YAP expression levels were seen in a large number of multiple myeloma (MM) samples. It was shown that decreased or lack of YAP activity prevented DNA damage-induced ABL1-mediated apoptosis in MM cells (Cottini *et al.*, 2014). Mechanistically, detection of DNA damage triggers the activation of ABL1 (also called c-Abl) which catalyses YAP Tyr357 phosphorylation, increasing both YAP stability and its affinity for p73. YAP binding to the PPPY motif of p73 interferes with the binding of E3 ubiquitin ligase Itch to p73 (Itch also binds to the p73 PPY motif), thereby suppressing Itch-mediated proteasomal degradation of p73. This allows the YAP-p73 complex to induce the expression of p73 proapoptotic target genes (Levy *et al.*, 2007; Levy *et al.*, 2008).

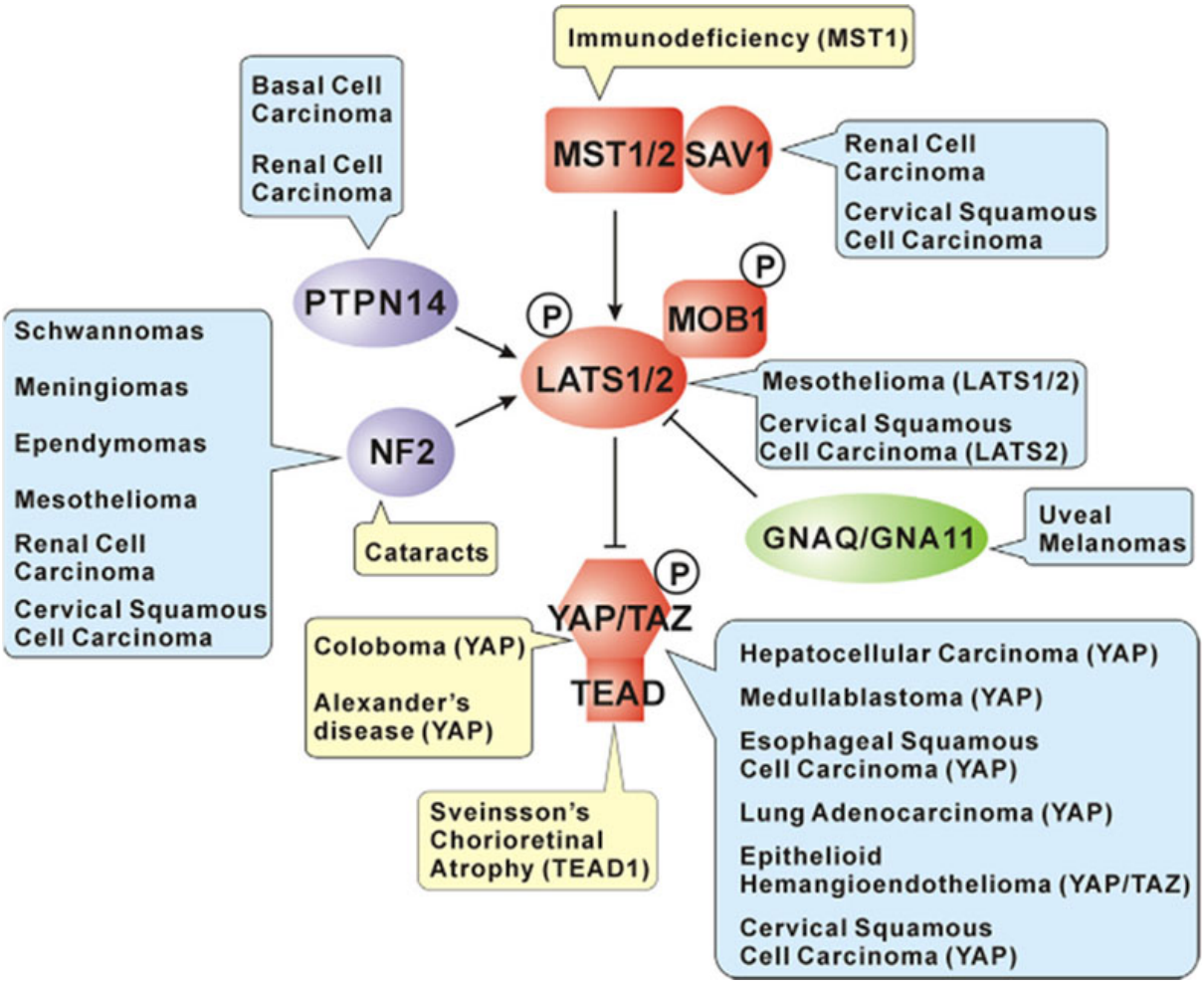

Figure 1.6: Mutations of different Hippo pathway components in cancer (blue boxes) and other diseases (yellow boxes). *Adapted from (Zheng & Pan, 2019).*

YAP/TAZ function can allow the development of cancer-associated abilities in tumour cells aside from increased cell proliferation and cell survival. TAZ activity was shown to impart tumour-initiating and self-renewal abilities to breast cancer stem cells (CSCs). TAZ suppression via phosphorylation mediated by the adaptor protein Scribble complexing with MST and LATS can be counteracted by Scribble displacement from the cell membrane (Cordenonsi *et al.*, 2011). Furthermore, YAP-TEAD activity promotes epithelial-to-mesenchymal transition (EMT), oncogenic transformation and metastasis in melanoma and breast cancer cells (Lamar *et al.*, 2012). In breast cancer cells, YAP has also been suggested to induce the expression and secretion of epidermal growth factor receptor (EGFR) ligand AREG to increase the proliferation and migration abilities of surrounding cells (Zhang *et al.*, 2009b). Moreover, YAP activation in cancer-associated fibroblasts (CAFs) is vital for CAFs' promotion of ECM remodelling/stiffening and cancer cell invasion. ECM stiffening in turn will augment YAP activation through the actomyosin cytoskeleton, establishing a self-reinforcing loop to preserve the CAF function (Calvo *et al.*, 2013). In liver tumour-initiating cells (TICs), YAP activation and subsequent YAP-TEAD gene expression trigger the production and secretion of the cytokine CCL2 to recruit M2-like macrophages to promote tumourigenesis (Guo *et al.*, 2017). Similarly, activation of YAP and YAP-TEAD transcription in prostate cancer cells allow

the expression of the CXCL5 chemokine to attract CXCR2-expressing myeloid-derived suppressor cells (MDSCs) to promote tumour progression (Wang *et al.*, 2016a).

YAP also has functions permitting tumour immune evasion. In regulatory T cells (Tregs), YAP-TEAD activity upregulates activin/TGFβ/SMAD signalling, resulting in enhanced transcription factor Foxp3 expression and thereby augmented T cell suppression (Ni *et al.*, 2018). Additionally, YAP/TAZ-TEAD function increases the expression of the T cell function inhibiting transmembrane protein PD-L1 in lung and breast cancer cell lines, enhancing T cell suppression (Janse van Rensburg *et al.*, 2018).

1.15 Compounds targeting the Hippo pathway

1.15.1 Introduction

All in all, most of Merlin's contact growth inhibitory and tumour suppressive functions converge on the Hippo signalling pathway which makes it a promising target for the treatment of NF2 null schwannomas and meningiomas and other of tumour/cancer types. Therefore, many Hippo pathway effectors have previously been used as cancer drug targets.

Some compounds target Hippo pathway upstream regulators. Tankyrases TNKS1 and TNKS2 ribosylate AMOT family proteins, allowing them to be recognized and ubiquitinated by the E3 ubiquitin ligase RNF146 and thereby marking them for proteasomal degradation. The tankyrase inhibitor XAV939 increases the stability of AMOT family proteins, allowing them to inhibit the oncogenic effects of YAP, as shown *in vitro* (Wang *et al.*, 2015b).

Statins have also been shown to have anti-tumourigenic effects. The metabolic mevalonate pathway produces geranylgeranyl pyrophosphate which is necessary for Rho GTPase activation. As mentioned previously, certain Rho GTPases promote YAP/TAZ activity by stimulating PAK which catalyses Merlin Ser518 phosphorylation and thereby inhibits the Merlin/MST1/2/LATS1/2 mediated phosphorylation/inactivation of YAP/TAZ. The use of statins which inhibit HMG-CoA reductase, a key enzyme in the mevalonate cascade, decreased YAP/TAZ nuclear accumulation and transcription, resulting in reduced proliferation and self-renewal in breast cancer cells *in vitro* (Sorrentino *et al.*, 2014). Since one of these YAP target genes in breast cancer cells is the receptor for hyaluronan-mediated motility (RHAMM), simvastatin was shown to impair ERK-dependent breast cancer cell migration and invasion *in vitro* (Wang *et al.*, 2014).

Additionally, complexes involved in YAP-induced transcription such as the previously mentioned MLL H3K4 methyltransferase complex (Oh *et al.*, 2014; Qing *et al.*, 2014) and the Mediator complex (Galli *et al.*, 2015) might also make promising cancer drug targets (Zheng & Pan, 2019).

As mentioned previously, $G\alpha_s$-coupled receptors activate LATS1/2 via cAMP-PKA signalling, thereby mediating YAP phosphorylation/inactivation. Therefore, inhibitors of the

phosphodiesterases (which break down cAMP) such as ibudilast and rolipram were seen to induce YAP phosphorylation in breast cancer cells *in vitro* which points to their potential as anti-cancer drugs (Yu *et al.*, 2013b). Moreover, as described before, metabolic sensor AMPK causes YAP phosphorylation and thereby suppression of YAP transcriptional activity. Therefore, the AMPK activating type 2 diabetes drug metformin has been shown to heighten YAP and TAZ phosphorylation *in vitro* and inhibit the growth of LATS1/2 dKO mouse embryonic fibroblast xenograft tumours *in vivo*, suggesting metformin's potential as a cancer drug (Mo *et al.*, 2015).

1.15.2 Classification of YAP/TAZ drugs

Chemical compounds inhibiting YAP/TAZ activity can be divided into three groups (Pobbati & Hong, 2020) (Figure 1.7). Members of Group I interfere with upstream YAP/TAZ activators and augment LATS-mediated YAP/TAZ inactivation via phosphorylation. Therefore, Group I drugs inhibit cell receptors (e.g. integrins, GPCRs and VEGFRs), intracellular kinases (e.g. integrin linked kinase (ILK), Src and PI3K), actin and actomyosin cytoskeleton polymerization, YAP/TAZ phosphatases (e.g. PP1 and PP2A), the mevalonate pathway, HDACs or increase cellular energy stress levels (e.g. mitochondrial complex I inhibitors). Group III compounds inhibit the proteins upregulated by YAP/TAZ gene expression such as certain ligands (e.g. CTGF, CYR61 and CXCL5), kinases (e.g. Axl and NUAK2), metabolic enzymes (e.g. ALDH1A1 and COX-2) and different effectors such as FOXM1, BCL-xL and Transglutaminase 2 (Pobbati & Hong, 2020).

1.15.3 Group II drugs

The drug compounds of Group II directly interact with YAP/TAZ or TEAD, thereby inhibiting TEAD function or interfering with YAP/TAZ-TEAD complex formation. In general, compounds either target YAP, the YAP/TAZ binding pocket on TEAD's surface or TEAD's palmitate binding pocket (PBP) (Pobbati & Hong, 2020).

The proteotoxic benzoporphyrin derivative verteporfin targets YAP. It suppresses YAP-TEAD binding and thereby YAP-TEAD target gene expression, preventing the YAP overexpression-induced overgrowth of the liver *in vivo*. Mechanistically, it was suggested that by binding to YAP, verteporfin induces a YAP conformational change, thereby disrupting YAP-TEAD interactions (Liu-Chittenden *et al.*, 2012). Interestingly, verteporfin was reported to induce some of its detrimental effects on cancer cell proliferation/survival in a YAP-independent manner (Dasari *et al.*, 2017; Zhang *et al.*, 2015a). Additionally, a divinyldipyrrine derived from verteporfin was shown to reduce YAP protein levels and inhibit TEAD dependent gene expression (Gibault *et al.*, 2017).

YAP-TEAD interaction can also be disrupted by using a modified short (17mer) YAP-like peptide (Zhou *et al.*, 2015) or a peptide fragment (Kaan *et al.*, 2017).

Chemical compounds discovered by Inventiva Pharma bind to the YAP/TAZ binding pocket on the surface of TEAD, thereby disrupting YAP/TAZ-TEAD complex formation (Barth,

Montalbetti & Spitzer, 2017; Pobbati & Hong, 2020). Furthermore, the small inhibitor peptide 'Super-TDU', designed after and imitating the corepressor VGLL4, was shown to bind to the TEAD YBD and inhibit gastric cancer growth *in vitro* and *in vivo* (Jiao *et al.*, 2014).

Similarly, a cystine-dense peptide termed TB1G2 and a YAP cyclic peptide called peptide 17 were able to inhibit YAP-TEAD interaction by targeting the YAP/TAZ binding pocket but lacked cell penetrating abilities (Crook *et al.*, 2017; Zhang *et al.*, 2014b).

Non-steroidal anti-inflammatory drugs (NSAIDs) such as the fenamate flufenamic acid (FA) were shown to target the PBP. FA binds the hydrophobic palmitate binding central pocket of TEAD2 YBD and thereby inhibiting YAP-TEAD mediated gene expression, cell proliferation and migration without disrupting YAP-TEAD interaction (Pobbati *et al.*, 2015). Mechanistically, FA competes with palmitate for binding to the palmitate binding pocket (PBD) in the YBD of TEAD. FA binding to the PBD was shown to inhibit TEAD S-autopalmitoylation (Li *et al.*, 2018). Using FA as template, a small molecule (chloromethyl-FA) was designed which covalently binds to the conserved cysteine in the PBD of TEAD4 normally used for S-autopalmitoylation. This covalent bond results in an irreversible disruption of YAP-TEAD4 binding and thereby interferes with its transcriptional activity, as shown by decreased CTGF gene expression (Bum-Erdene *et al.*, 2019).

Furthermore, a compound termed Compound 2 has seen to bind hydrophobic lipid pocket of TEAD and impede TEAD S-palmitoylation, thereby reducing TEAD target gene transcription and inhibiting tumour growth *in vivo* (Holden *et al.*, 2020).

Vinylsulfonamide derivatives, especially the one named DC-TEADin02, also covalently bind to the PBP of TEAD, thereby impairing YAP-TEAD target gene transcription while only having a minimal impact on YAP-TEAD interaction (Lu *et al.*, 2019).

Aside from FA, other compounds occupying the PBD and thus disrupting YAP-TEAD interaction include alkylthio-triazole scaffold compounds and the small molecule K-975 (Kaneda *et al.*, 2019; Pobbati & Hong, 2020; Wu, 2020).

It is unclear why FA and DC-TEADin02 are unable to interfere with YAP-TEAD interaction while the chloromethyl-FA, alkylthio-triazole scaffold compounds and the small molecule K-975 can. Theoretically, compounds binding the YAP/TAZ binding pocket or PBP of TEAD can be converted into TEAD degraders by making them a part of a proteolysis-targeting chimeric (PROTAC) molecule, causing increased targeting of TEAD for proteasomal degradation. Reduced levels of available TEAD would then impair YAP/TAZ-TEAD target gene transcription. Such degraders can only target unbound TEAD since binding to YAP/TAZ would conceal both TEAD's YAP/TAZ binding pocket and PBP (Pobbati & Hong, 2020; Sakamoto *et al.*, 2001).

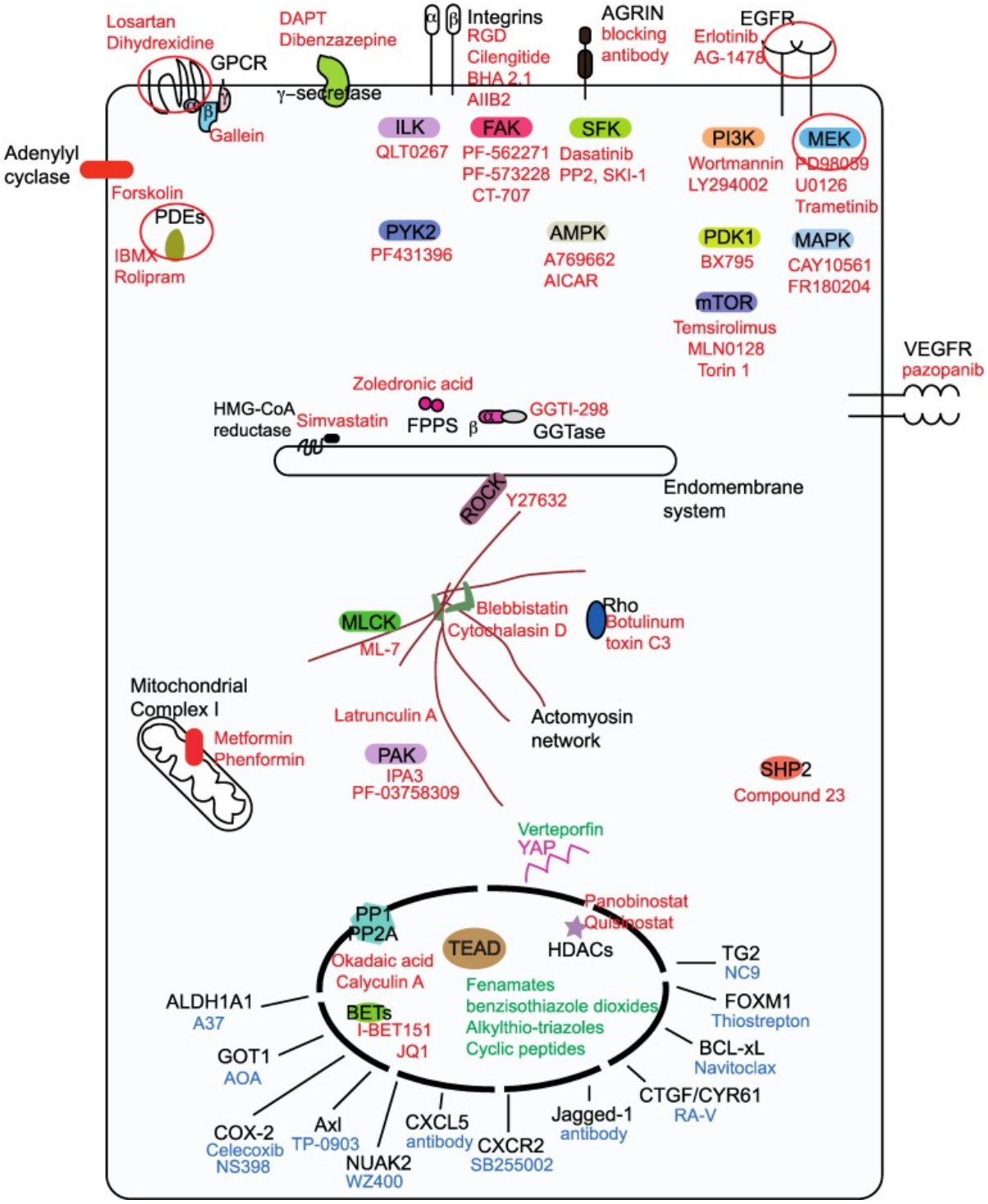

Figure 1.7: The three groups of YAP/TAZ-TEAD targeting drugs. *Compounds targeting upstream YAP/TAZ activators (Group I, compound names in red), drugs directly interacting with YAP/TAZ or TEAD (Group II, compound names in green) and inhibitors interfering with the function of effectors expressed by YAP/TAZ gene transcription (Group III, compound names in blue). Known drugs to be repurposed as Group I compounds are circled in red. Adapted from (Pobbati & Hong, 2020).*

1.15.4 Vivace Therapeutics inhibitors

In this work, inhibitor compounds produced by Vivace Therapeutics were used to suppress the deregulated Hippo signalling pathway caused by NF2 loss. Potentially, some of the effects of NF2 loss can thereby be reversed, resulting in a slower tumour growth rate.

Compounds developed by Vivace Therapeutics (VT) were shown to specifically interfere with TEAD S-autopalmitoylation (Ras palmitoylation was unaffected) and thereby disrupt YAP/TAZ-TEAD interaction by non-covalently binding/occupying the TEAD PBP normally binding to palmitoyl-CoA. The VT compounds efficiently inhibit the cell proliferation of NF2-deficient (e.g. NCI-H226), NF2-deleted (e.g. NCI-H2373) or NF2-mutant (e.g. NCI-H2052) mesothelioma cell lines while the NF2 wild type mesothelioma cell lines displayed decreased sensitivity. *In vivo* experiments confirm an oral bioavailability of over 75% and a half-life of more than 12 hours without detected toxicity (no changes in mouse body weight). The VT compounds halt or reverse the growth of NF2-deficient and NF2-deleted mesothelioma xenografts *in vivo* in a dose-dependent manner. Additionally, the VT inhibitors were seen to decrease levels of TEAD1 S-autopalmitoylation and CTGF and CYR61 expression in NF2-deleted and NF2-deficient mesothelioma xenografts *in vivo* (Tang *et al.*, 2021).

One of the VT compounds used in this report was VT104 which I used in meningioma cell lines and primary meningioma cells. VT104 was shown to be a Pan-TEAD S-autopalmitoylation inhibitor, displaying a stronger binding to TEAD1 and 3 than to TEAD2 and 4. As Pan-TEAD inhibitor, it also managed to suppress the proliferation of mesothelioma cell lines with mutations in Hippo pathway effector genes but without NF2 mutations. With an oral bioavailability of 78 % and a half-life of 24.2 hours, VT104 was reported to cause growth arrest or even tumour shrinkage of NF2-deficient mesothelioma xenografts *in vivo* in a dose-dependent manner (Tang *et al.*, 2021).

1.16 NF2 drug trials

In a clinical trial with 10 NF2 patients using bevacizumab (humanized anti-VEGF monoclonal antibody), 9 patients showed a reduction in progressive vestibular schwannoma size and 4 patients an improvement of hearing (Plotkin *et al.*, 2009). Unfortunately, sustained bevacizumab treatment was found to be necessary to maintain these effects (Plotkin *et al.*, 2012). Additionally, bevacizumab efficacy could also be seen in a case study treating 2 NF2 patients with progressive vestibular schwannomas (Mautner *et al.*, 2010). Another bevacizumab phase II clinical trial with 14 NF2 patients with progressive vestibular schwannomas resulted in a decrease in tumour size in 6 and ameliorated hearing in 7-8 participants (Blakeley *et al.*, 2016; Huang *et al.*, 2018). Bevacizumab was also used in a phase II clinical trial with 22 NF2 patients with progressive vestibular schwannomas. A tumour volume decrease was noted in 7 patients while improved hearing was seen in 9 patients (Plotkin *et al.*, 2019). Interestingly, a different drug trial also chose the VEGF/VEGFR signalling axis as its target. Using a VEGFRs peptide vaccine in 7 NF2 patients with progressive

schwannomas, 2 participants showed tumour volume decrease and 2 participants an improvement of hearing (Tamura *et al.*, 2019).

Furthermore, a phase II clinical trial in 17 NF2 patients treated with the ErbB1/2 receptor tyrosine kinase inhibitor lapatinib resulted in a progressive vestibular schwannoma volume decrease in 4 participants and ameliorated hearing in the same number of participants (Karajannis *et al.*, 2012). Some of these trial participants also had progressive meningiomas. It was observed that 8 of 17 measured meningiomas exhibited a reduction in tumour volume (Osorio *et al.*, 2018).

Moreover, using the mTOR kinase inhibitor everolimus in a phase II clinical trial with 10 NF2 patients with progressive vestibular schwannomas was reported to have no noteworthy effect on tumour size or hearing (Karajannis *et al.*, 2014). In contrast, a different phase II clinical trial treating 10 NF2 patients with everolimus resulted in 5 treated patients exhibiting temporarily suppressed tumour growth which recommenced 3 to 6 months after treatment conclusion (Goutagny *et al.*, 2015). A different phase II clinical trial used a combination therapy consisting of everolimus and the somatostatin agonist octreotide in 20 patients (including 4 NF2 patients) with progressive meningiomas. A tumour volume decrease was observed in 4 patients and tumour growth rate reduction was seen in 78% and 68 % of studied tumours and meningiomas with NF2 mutations, respectively (Graillon *et al.*, 2020).

1.17 Macrophages

1.17.1 Origin and function of macrophages

Macrophages can be classified as either being resident macrophages or infiltrating macrophages (Griffin, George & Ho, 1993). Resident macrophages can be found in their respective tissues while infiltrating macrophages only gain entry to a given tissue following a physical injury which causes production of inflammatory factors. Infiltrating macrophages derive from monocytes circulating the blood stream. Microglia are the resident macrophages of the CNS whose embryonic predecessors originated in the yolk sac (Schulz *et al.*, 2012). In contrast, the origin of the resident macrophages of the PNS is yet to be determined. Macrophages are vital for both the innate and adaptive immunity and in the event of injury. They can be identified using antibodies to various markers including CD68, Iba-1 and F4/80.

Macrophages are generally categorized as either M1-like or M2-like macrophages. M1-like macrophages are activated by IFN-γ, LPS or granulocyte macrophage colony stimulating factor (GM-CSF) and secrete cytokines such as IL-1, IL-6, IL-12 and TNF-α which promote inflammatory responses. They also secrete chemokines such as CXCL10 and CCL5 which enhance activation of cytotoxic T cells. Furthermore, M1 macrophages produce 2 distinct radicals, reactive nitrogen and reactive oxygen species, and they express MHCII, making them efficient antigen presenting cells (APCs). As APCs, they also assist the Th1 immune response. In general, M1-like macrophages exhibit anti-microbial and anti-tumoural activity. M2-like

macrophages are seen as the other side of the coin when it comes to M1 macrophage functions. Activated by signalling molecules such as IL-4, IL-13, IL-10 and macrophage colony stimulating factor (M-CSF aka CSF-1), they secrete anti-inflammatory cytokines including IL-10 and PGE_2. They produce chemokines such as CCL2 and CCL22 which allow recruitment of regulatory T cells (Tregs), which in turn suppress T cell activity. M2-like macrophage chemokines also promote tissue repair and tumour progression. Cell markers for M2 macrophages include CD206 (mannose) and CD163 (Mantovani *et al.*, 2013; Sica & Mantovani, 2012).

The characteristics mentioned above also appear to distinguish M1-like tumour associated macrophages (TAMs) and M2-like TAMs.

1.17.2 TAMs

As far as the origin of TAMs is concerned, the current hypothesis states that they are derived from blood-borne monocytes produced in the bone marrow. These are drawn to the location of the tumour and subsequently transform into TAMs upon activation of certain signalling pathways. Differentiation into TAMs involves downregulation of Ly6C and CD11b and upregulation of MHCII and Vcam1 (Franklin *et al.*, 2014). Molecules such as VEGF-A, CSF1 (M-CSF) and CCL2 are believed to cause chemoattraction of macrophages (Linde *et al.*, 2012; Qian *et al.*, 2011; Quail & Joyce, 2013).

In order to convert macrophages in M2-like TAMs with immunosuppressive abilities, different cell types use cytokines to activate distinct signalling pathways. CD4+ T cells and tumour cells release IL-4 and IL-13 to activate STAT6/PI3K signalling while Tregs secrete IL-10 to target the STAT3 signalling pathway. Tumour cells can also secrete CSF1 (M-CSF), lactic acid and TGF-β to promote macrophage differentiation into M2-like TAMs (Colegio *et al.*, 2014; Lawrence & Natoli, 2011; Noy & Pollard, 2014).

TAMs are known to aid tumour growth and maintenance by a number of different mechanisms.

One of these mechanisms involves angiogenesis, the process by which new blood vessels are produced. It can be divided into 2 steps: 1. Degradation of the basement membrane and 2. Proliferation and migration of the endothelial cells flanking the blood vessels. TAMs produce and release matrix metalloproteinases (MMPs) and cathepsins to degrade the basement membrane (Kessenbrock, Plaks & Werb, 2010) and secrete growth factors (e.g. VEGF and PDGF) and chemokines (CCL2 and CXCL8) to support blood vessel formation (Murdoch *et al.*, 2008). Furthermore, additional growth factors promoting angiogenesis become available when extracellular matrix (ECM) heparin-bound growth factors are released by MMP activity. Additionally, VEGF and CCL2 were also found to act as chemoattractants for monocytes (Murdoch *et al.*, 2008).

TAMs also play a role in metastasis. TAMs produce and release TGF-β which support epithelial-mesenchymal transition (EMT), a process allowing tumour cells to change into metastasizing cells (Bonde *et al.*, 2012). TAMs are also thought to promote metastasis by

entering into direct cell contact with tumour cells (Wyckoff *et al.*, 2007). Tumour cell secretion of CSF-1 and macrophage secretion of EGF secretion cause perivascular macrophages and tumour cells to surround blood vessels, facilitating blood-borne metastasis (Sangaletti *et al.*, 2008). Moreover, TAMs are also responsible for the preparation of the pre-metastatic niche which permits metastasizing tumour cells to grow in a secondary organ (Chanmee *et al.*, 2014). Such a pre-metastatic niche is created by TAMs via secretion of cathepsins, serine proteases and MMPs. Additionally, some macrophages are found to actively assist the survival and proliferation of tumour cells in the metastatic niche after successful metastasis (Qian *et al.*, 2009).

TAMs also support the welfare of cancer stem cells (CSCs), particularly by secreting pro-inflammatory molecules such as TNF-α and IL-6 (Korkaya, Liu & Wicha, 2011; Schwitalla *et al.*, 2013; Wan *et al.*, 2014). Similar to what was seen before, TAMs engaging in direct cell contact with CSCs via CD90 and Eph4A receptors also aids in CSC maintenance (Lu *et al.*, 2014). Furthermore, TAMs were shown to secrete factors such as EGF and MFG-E8 during chemotherapy, activating several pro-survival mechanisms to heighten CSCs' chances of survival (Jinushi *et al.*, 2011; Yang *et al.*, 2013a).

Aside from promoting CSC survival, TAMs also enhance both the disposal of the chemotherapeutic drug and the repair of the tissue surrounding the CSCs during chemotherapy. All in all, TAMs were found to be heavily involved in CSCs' resistance to chemotherapeutic agents (Mantovani & Allavena, 2015).

On top of all the TAM-assisted pro-tumourigenic mechanisms listed above, TAMs also fulfil an immunosuppressive function within the tumour microenvironment (TME) by impeding the function of cytotoxic CD8+ T cells (the most efficient anti-tumourigenic immune cells) in a number of ways. Firstly, TAMs release anti-inflammatory cytokines such as IL-10, TGF-β and PGE_2 (Kalinski, 2012; Oh & Li, 2013; Ruffell *et al.*, 2014). Secondly, TAMs trigger the stimulation of inhibitory receptors found on T cells (e.g. PD-1, CTLA-4) by expressing the corresponding ligands (Kuang *et al.*, 2009; Ojalvo *et al.*, 2009). Thirdly, TAMs deprive T cells of nutrients to prevent them from proliferating by expressing metabolizing enzymes (Mazzoni *et al.*, 2002). Aside from T-cell suppression, TAMs are believed to interfere with the functions of natural killer (NK) and natural killer T (NKT) cells (Krneta *et al.*, 2017; Liu *et al.*, 2012).

TAMs can also exert their immunosuppressive functions in more indirect ways, for example by attracting different types of immunosuppressive cells., TAMs have been proven to secrete certain chemokines (e.g. CCL20 and CCL22) to recruit Tregs to the tumour site to inhibit effector T cell activity (Curiel *et al.*, 2004; Liu *et al.*, 2011). Other immunosuppressive cells which can be recruited by TAMs are myeloid-derived suppressor cells (MDSCs). The main function of this diverse group of immune cells is to inhibit the activity of other immune cells which they will fulfil upon their arrival in the TME. Another way TAMs can make use of MDSCs is by differentiating some of them in TAMs. It has been shown that macrophage produced CSF-1 can convert monocytic MDSCs into TAMs (Lesokhin *et al.*, 2012; Wynn, Chawla & Pollard, 2013). TAMs are also able to trigger the expression of transcription factor Foxp3 in CD4+ T cells to turn them into Tregs. This is accomplished via activation of IL-10 and TGF-β signalling pathways (Denning *et al.*, 2007; Savage *et al.*, 2008).

1.17.3 Depletion of macrophages

In a paper by de Vries et al. in 2013 (de Vries *et al.*, 2013), a positive correlation was found in human vestibular schwannomas between M2-like macrophage numbers and tumour growth rate, i.e. the faster growing schwannomas contained a greater number of macrophages.

Based on that observation, a colony stimulating factor receptor 1 (CSFR1) inhibitor called PLX5622 could theoretically be used to great effect. This inhibitor crosses the blood-brain/blood-nerve barrier and greatly reduces macrophage numbers within peripheral nerves by blocking CSFR1 signalling which is essential for macrophage/microglial survival. It was shown that usage of PLX5622 results in the decrease of peripheral nerve macrophages by approximately 70 % (and reduction of microglia by ca. 50 %) without causing any noticeable adverse effects (no changes in behaviour, activity, appearance and weight) (Klein *et al.*, 2015; Yuan *et al.*, 2018). This is a more direct way of diminishing TAM support than using Vivace inhibitors (see sections 1.12 and 1.15.4). One can argue that macrophage depletion in this manner would, along with the tumour supporting M2-like macrophages, also affect the antitumourigenic M1-like macrophages which could be seen as counterproductive. An opposing argument would be that the M2-like macrophages are probably dominant over or at the very least equally matched with the M1-like macrophages since tumour growth still persists despite M1-like macrophage involvement. Interestingly, it has been found that a whole spectrum of macrophage phenotypes exists, stretching far beyond the oversimplified M1 versus M2 polarization model (Xue *et al.*, 2014). Additionally, macrophage depletion is a potential treatment option regardless of which gene mutation(s) it possesses and as a result which signalling pathway(s) the tumour relies on. This is especially important when treating sporadic schwannomas which are known to possess a variety of different gene mutations (Clark *et al.*, 2013; Mei *et al.*, 2017). Taken together, depletion of all macrophage populations via PLX5622 to impair TAM-induced tumour growth support appears to be a sound strategy.

The CSF1 receptor (CSF1R, CD115) is a tyrosine kinase receptor capable of binding CSF1 (=M-CSF) and IL-34. CSF1R signalling is vital for the proliferation, survival and differentiation of cells of the mononuclear phagocyte system, especially macrophages and TAMs (Stanley & Chitu, 2014). Upon binding its ligand, a homodimer is formed and the receptor signalling cascade is activated (Achkova & Maher, 2016). Other cells found in the TME express CSF1R as well, including neutrophils (Shin *et al.*, 2010), dendritic cells (MacDonald *et al.*, 2005) and MDSCs (Holmgaard *et al.*, 2016).

The basic concept would include measuring schwannoma growth rates in DRGs before and after macrophage elimination via PLX5622. This would allow us to determine whether strong reduction of macrophage numbers results in a tumour growth rate decline in the Gehlhausen Postn-Cre driven mouse model (Gehlhausen *et al.*, 2015). The same approach could theoretically be used to investigate whether microglia elimination in meningioma would have a similar effect.

1.18 Schwannoma mouse models

The mouse model used for studying the effects of NF2 and YAP/TAZ loss in schwannomas is driven by a Cre-Recombinase controlled by the Periostin promoter (Periostin-Cre or Postn-Cre in short). First described and published in 2015 (Gehlhausen *et al.*, 2015), it is considered a superior Neurofibromatosis type 2 mouse model compared to Giovannini et al.'s P0-Cre driven model (Giovannini *et al.*, 2000). In addition to causing spontaneous development of numerous schwannomas in dorsal root ganglia (DRGs), vestibular ganglia (VGs) and spinal (Figure 1.8), peripheral and cranial nerves (especially the 8th cranial nerve), the resulting mouse schwannomas mimic the schwannomas of human NF2 patients very closely regarding schwannoma morphology and the resulting symptoms (Gehlhausen *et al.*, 2015).

Similar to human NF2 patients, the mice were shown to have developed impaired hearing. In these mice, the impaired hearing was seen the first time at 3 months of age and it increased in severity as the mice grew older. At 13 months of age, the mice were also confirmed to have an impaired sense of balance (Gehlhausen *et al.*, 2015).

	P0-Cre NF2$^{fl/fl}$ (Giovannini *et al.*, 2000)	Postn-Cre NF2$^{fl/fl}$ (Gehlhausen *et al.*, 2015)
Cre activation	E9.5 in neural crest cells, E12.5 in Schwann cell precursors (Giovannini *et al.*, 2000)	E10 in Schwann cell precursors (Lindsley *et al.*, 2007) E12.5 in Schwann cell precursors (Gehlhausen *et al.*, 2015)
Cre Recombinase deletion	Exon 2 of NF2 gene	Exon 2 of NF2 gene
Schwannoma (benign) incidence rate	24 %	100 %
Schwannoma location	Atypical including stomach and uterus	Typical sites such as DRGs, VGs and cranial, spinal and peripheral nerves
Other tumours?	Large variety of different tumours in tissues containing cells of neural crest origin including bone, lens and kidney (→neurocristopathy)	Malignant peripheral nerve sheath tumours (MPNSTs)
Reduced survival rate compared to wild type (WT)-like littermates	Yes	Yes
Schwann cell hyperplasia	In basal and spinal ganglia(= DRGs), possibly peripheral nerve	In DRGs, proximal spinal nerve roots, spiral ganglion

Table 1.1: Comparison of P0-Cre NF2$^{fl/fl}$ and Postn-Cre NF2$^{fl/fl}$ schwannoma models.

Previous attempts to establish an NF2 mouse model using genetic tools were less successful. In models with a deletion of exon 2 or exon 3 on one NF2 allele (leaving the other NF2 allele intact) the mice developed osteomas and osteosarcomas. Global deletion of either exon 2 or exon 3 on both NF2 alleles resulted in embryonic lethality (Giovannini *et al.*, 2000). Another attempt by the same group was the combination of one NF2 allele with an exon 3 deletion together with a floxed exon 2 on the other NF2 allele which would then be excised upon activation of the P0 promoter. The mouse model with this combination gave rise to similar characteristics and tumours as found in the P0-Cre $NF2^{fl/fl}$ model (Giovannini *et al.*, 2000) (Table 1.1). Aside from these gene deletion models, transgenic models were investigated as well, bearing the possibility of a dominant negative phenotype in mind. Expression of an NF2 transgene without C-terminal region under the control of the P0 promoter in combination with the expression of both wild type (WT) NF2 alleles showed no effect compared to its WT-like littermates (Giovannini *et al.*, 1999). Survival rates were similar and the tumours which eventually developed were age-related (Mahler *et al.*, 1996). In contrast, P0 promoter driven expression of an NF2 transgene missing exon 2 and 3 together with the expression of both WT NF2 alleles had a pronounced effect. A reduced survival rate compared to WT-like littermates and the occurrence of schwannomas in atypical and typical locations were noted. Atypical locations included the stomach, intestine, pancreas and uterus while a more sensible location such as the DRGs and even a typical location such as the trigeminal nerve were represented as well (Giovannini *et al.*, 1999).

In the Gehlhausen mouse model (Gehlhausen *et al.*, 2015) a Cre-Recombinase is placed under the control of the 3.9-kb upstream promoter region of the Periostin gene which is switched on at E10 in Schwann cell precursors (Lindsley *et al.*, 2007). After its expression, the Cre-recombinase excises and therefore deletes the parts of the gene(s) flanked by loxP sequences (Gehlhausen *et al.*, 2015). In the three genetically modified mice that we bred, the gene parts to be flanked and excised were either exon 2 of both alleles of the NF2 gene alone ($NF2^{fl(ox)/fl(ox)}$ (Giovannini *et al.*, 2000) = NF2 sKO) or in combination with exons 1 and 2 of both YAP alleles ($NF2^{fl/fl}$ and $YAP^{fl/fl}$ (Zhang *et al.*, 2010) = NF2/YAP dKO) or exons 1 and 2 of both TAZ genes ($NF2^{fl/fl}$ and $TAZ^{fl/fl}$ (Azzolin *et al.*, 2014) = NF2/TAZ dKO). This resulted in NF2-deficient, NF2- and YAP-deficient and in NF2- and TAZ-deficient mice, respectively. The Postn-Cre negative mice are similar to WT mice and were used as control.

1.19 Meningioma mouse models

Meningiomas occur either in the cortical convexity, the skull base or the spinal cord. Since spinal meningiomas only account for 10% of all meningiomas, meningioma mouse models focus on cranial meningiomas. In general, meningioma mouse models can be divided between genetic and xenograft models.

All genetic meningioma models by the Michel Kalamarides group rely on the excision of floxed parts in both NF2 alleles in leptomeningeal cells of newborn pups, leading to NF2 sKO leptomeningeal cells. This is achieved by injecting a Cre-recombinase carrying adenovirus into the CSF found in the subarachnoid space via the eyes (transorbital) or the frontal convexity

(subdural). Unfortunately, these transorbital (t.o.) and subdural (s.d.) Cre- recombinase injections resulted in the development of intracranial meningiomas at low frequencies (t.o. = 29 % and s.d. = 19 %) (Kalamarides *et al.*, 2002). If meningiomas did develop, most of them were shown to mimic the various Grade I meningioma subtypes, namely the meningothelial, fibroblastic and transitional (mixture of the two former subtypes) Grade I meningioma. Pups with meningiomas tended to survive for 8 months after injection. Combining this procedure with the global deletion of one of the two p53 alleles (= p53 hemizygosity) significantly shortened survival time but had no notable effect in regards to the frequency of meningioma induction or the progression of the developing meningiomas (Kalamarides *et al.*, 2002). Loss-of-function mutations in both $p16^{INK4a}$ alleles (= nullzygosity) in addition to biallelic NF2 gene inactivation significantly heightened the meningioma induction frequency (from 13 to 37 %) and the proliferation rate of the meningothelial cells (from 47 to 77 %). Both of these changes did not alter the tumour grade of the resulting meningiomas (Kalamarides *et al.*, 2008). Furthermore, pairing biallelic NF2 gene inactivation with the monoallelic or biallelic inactivation of the CDKN2AB locus (containing 3 open reading frames = $p16^{Ink4a}$, $p15^{Ink4b}$ and $p19^{Arf}$) in leptomeningeal cells was found to raise the meningioma induction frequency (50 % and 72 %, respectively), decrease the time it took for meningiomas to develop (= latency, 7.8 and 3.5 months, respectively) and cause the development of Grade II and III meningiomas (Peyre *et al.*, 2013).

Prostaglandin D_2 synthase (PGDS) has been found to be expressed in arachnoid cells (Kawashima *et al.*, 2001). Therefore, yet another approach by the same group involved using a Cre-Recombinase under the control of the PGDS promoter to cause a biallelic NF2 inactivation in all PGDS expressing cells, including arachnoid cells. This gave rise to Grade I meningothelial and fibroblastic meningiomas, confirming that PGDS positive cells as the cells of origin in this genetic meningioma mouse model (Kalamarides *et al.*, 2011).

Finally, overexpression of platelet-derived growth factor B (PDGF-B) in PGDS positive arachnoid cells was shown to induce Grade I meningiomas with short latency. Additional biallelic NF2 inactivation (by subdural adenovirus injection as described earlier) resulted in the appearance of Grade II meningiomas. Furthermore, compared to biallelic NF2 inactivation alone, the combination of biallelic inactivation of NF2 and CDKN2AB was sufficient to heighten meningioma occurrence from 16 % to 72 %, reduce survival time from 6.4 to 3.5 months and cause the formation of Grade III meningiomas. Combining PDGF-B overexpression and biallelic inactivation of NF2 and CDKN2AB shortened survival once more (to 1.8 months) and significantly increased the incidence of Grade II (from approx. 23 % to 47 %) and Grade III (from ca. 3 % to 20 %) meningiomas (Peyre *et al.*, 2015; Peyre *et al.*, 2013).

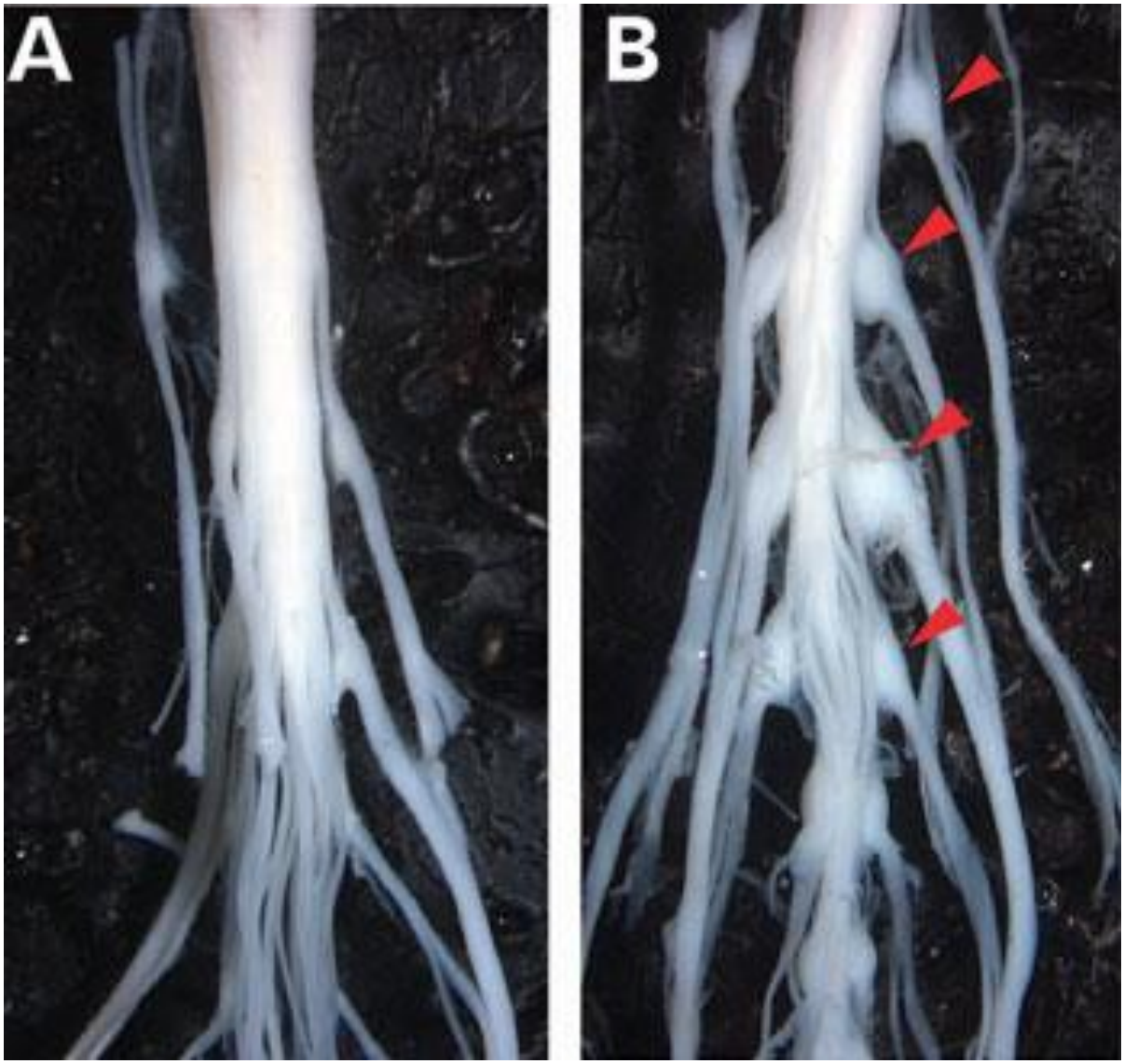

Figure 1.8: Image displaying schwannoma formation in DRGs and spinal nerves. *A: Spinal cord of 15-month-old NF2$^{fl/fl}$ Postn-Cre negative (control) mouse with normal DRGs and spinal nerves. B: Spinal cord of 15-month-old Postn-Cre positive NF2$^{fl/fl}$ mouse (NF2 sKO) with swollen DRGs (indicated by red arrow heads) and spinal nerves. Adapted from (Gehlhausen et al., 2015).*

In an alternative way to approximate meningiomas growing in the human patients, orthotopic xenotransplantation of human primary meningioma cells or human meningioma cell lines is performed in the cerebral convexity or the skull base of mice. Xenograft meningioma mouse models tend to have a high tumour induction rate. Using primary cells, successful establishment of benign meningiomas in the cerebral convexity of immunosuppressed ('nude') mice has been shown before (Friedrich *et al.*, 2012).

Nonetheless, the overwhelming majority of xenograft meningioma models are created using meningioma cell line cells. The malignant NF2 positive IOMM-Lee (Lee, 1990; Mei *et al.*, 2017) and malignant NF2 negative CH-157-MN (Mei *et al.*, 2017) cells appear to be especially versatile since they can be used for both convexity and skull base implantation models (Gogineni *et al.*, 2011; Ragel *et al.*, 2008). Unfortunately, the mice have a predisposition to only live a limited number of days (23-28 days) after xenograft implantation before excessive

tumour burden necessitates euthanasia. Aside from the two aforementioned malignant cell lines, benign meningioma cell line cells such as BenMen1 (BM-1) cells also allow establishment of meningioma tumours in the convexity and skull base of nude mice (Burns *et al.*, 2013; Puttmann *et al.*, 2005). A newer method involves using primary cells derived from malignant meningiomas of human patients and encouraging them under cell culture conditions to form tumour spheres. Transplantation of said tumour spheres into the convexity of immunosuppressed mice resulted in the formation of meningiomas with similar histological features to the original meningioma (Nigim *et al.*, 2016) (Figure 1.9).

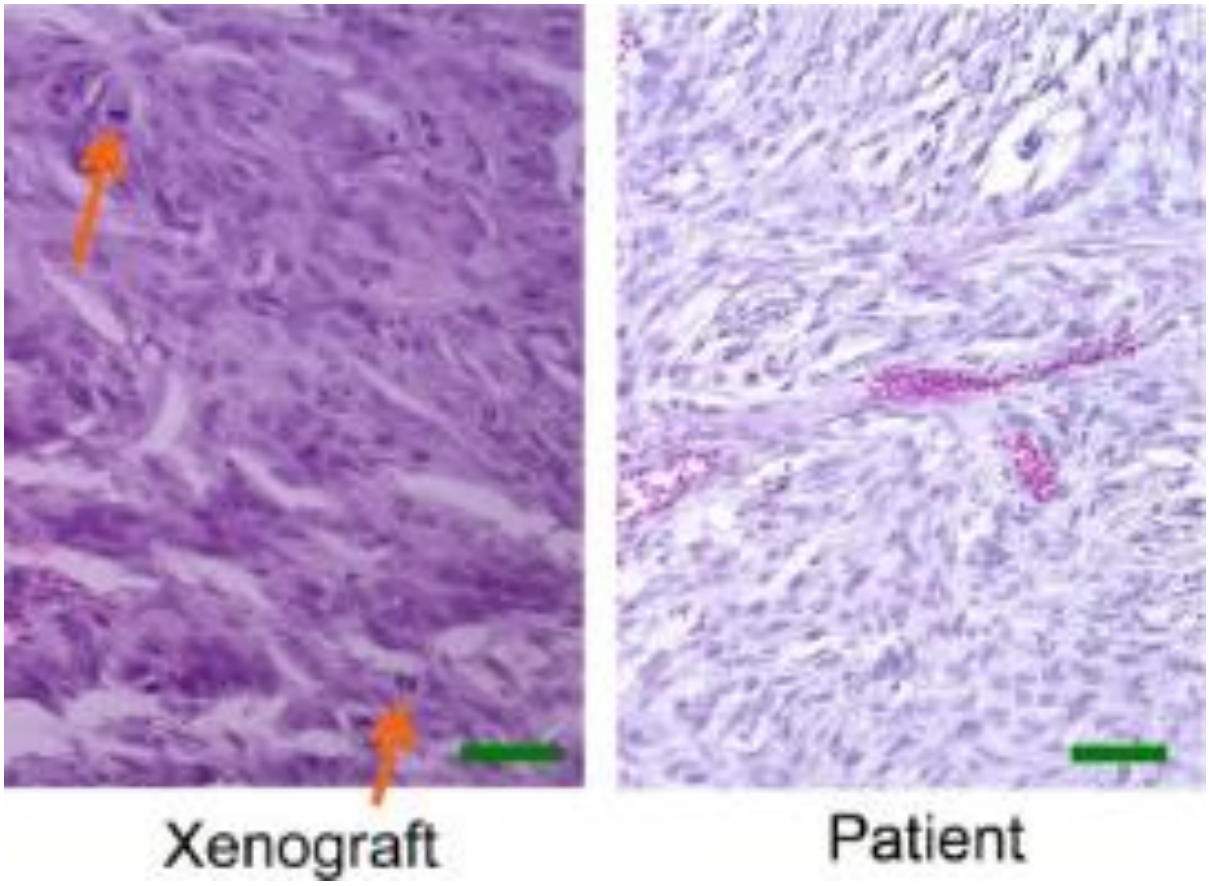

Figure 1.9: Comparison of tumoursphere-derived xenograft in mice and original human patient meningioma. *Primary MN3 meningioma cells obtained from a recurrent sporadic malignant meningioma patient cultured in vitro as tumourspheres and subsequently transplanted into in severe combined immunodeficient (SCID) mice, resulting in the growth of MN3 xenograft meningioma. H & E stained section of MN3 xenograft meningioma seen on the left (= Xenograft), red arrows marking cells in the process of mitosis. As comparison, H & E stained sections of original patient meningioma on the right (= Patient). Scale bars = 100 µm. Adapted from (Nigim et al., 2016).*

In order to monitor the growth of both genetically induced and cell implantation based meningiomas, either magnetic resonance imaging (MRI) (Pachow *et al.*, 2013) or bioluminescent imaging (BLI) (Peyre *et al.*, 2013) can be applied. While BLI is dependent on fluorescent dyes or the expression of fluorescent proteins such as GFP (Iwami *et al.*, 2013) and bioluminescence producing enzymes such as luciferase (Ragel *et al.*, 2008) in meningioma

cells to monitor tumour size changes, the more expensive MRI is not. Therefore, both imaging options have their merits.

The meningioma mouse model which we were planning on using relies on the implantation of meningioma cell line cells straight onto the cortical convexity (superolateral surface of the cerebrum touching the pia mater) of immunocompromised mice, resulting in the growth of xenograft meningiomas. The steps of this procedure as described in literature are as follows (Pachow *et al.*, 2013). After anaesthetization of the immunocompromised 8 - 10 week old mice, their heads are fixed using a stereotactic headframe. 2 mm anterior (towards the front) of the bregma (exact point where the coronal suture and sagittal suture of the skull meet) and 1.5 mm left and right of the sagittal suture, drilling creates 2 tunnels through the skull and the three meninges while avoiding damage to the neocortex as much as possible. Subsequently, a syringe is used to inject the meningioma cell line cells (e.g. IOMM-Lee or KT21) in PBS 1 mm beneath the surface onto the cortical convexity of the cerebrum to cause the rapid formation and growth of xenograft meningiomas (see Figure 1.10).

1.20 Hypotheses and objectives

It was hypothesized that macrophages support schwannoma growth. Therefore, antibodies (anti-CD68 or anti-Iba1) to detect macrophages and the artificial nucleotide EdU to quantify proliferation rates were to be used in the schwannomas of the Postn-Cre driven schwannoma mouse model to uncover a possible correlation between the respective macrophage numbers and proliferation rates.

Furthermore, it was strongly suspected that YAP/TAZ signalling is a requirement for schwannoma growth. To investigate the role of YAP/TAZ signalling in schwannomas, the differences between schwannomas of NF2 sKO, NF2/YAP dKO and NF2/TAZ dKO animals regarding proliferation rates (EdU staining), macrophage presence (CD68/Iba1 staining) and cellular content (H & E staining) was to be elucidated.

Finally, YAP/TAZ function was similarly believed to be of importance in meningioma cell proliferation. In order to verify this, TEAD S-autopalmitoylation inhibitors from Vivace Therapeutics were to be utilized, allowing the determination (using EdU) and comparison of meningioma cell proliferation rates with and without YAP/TAZ signalling disruption.

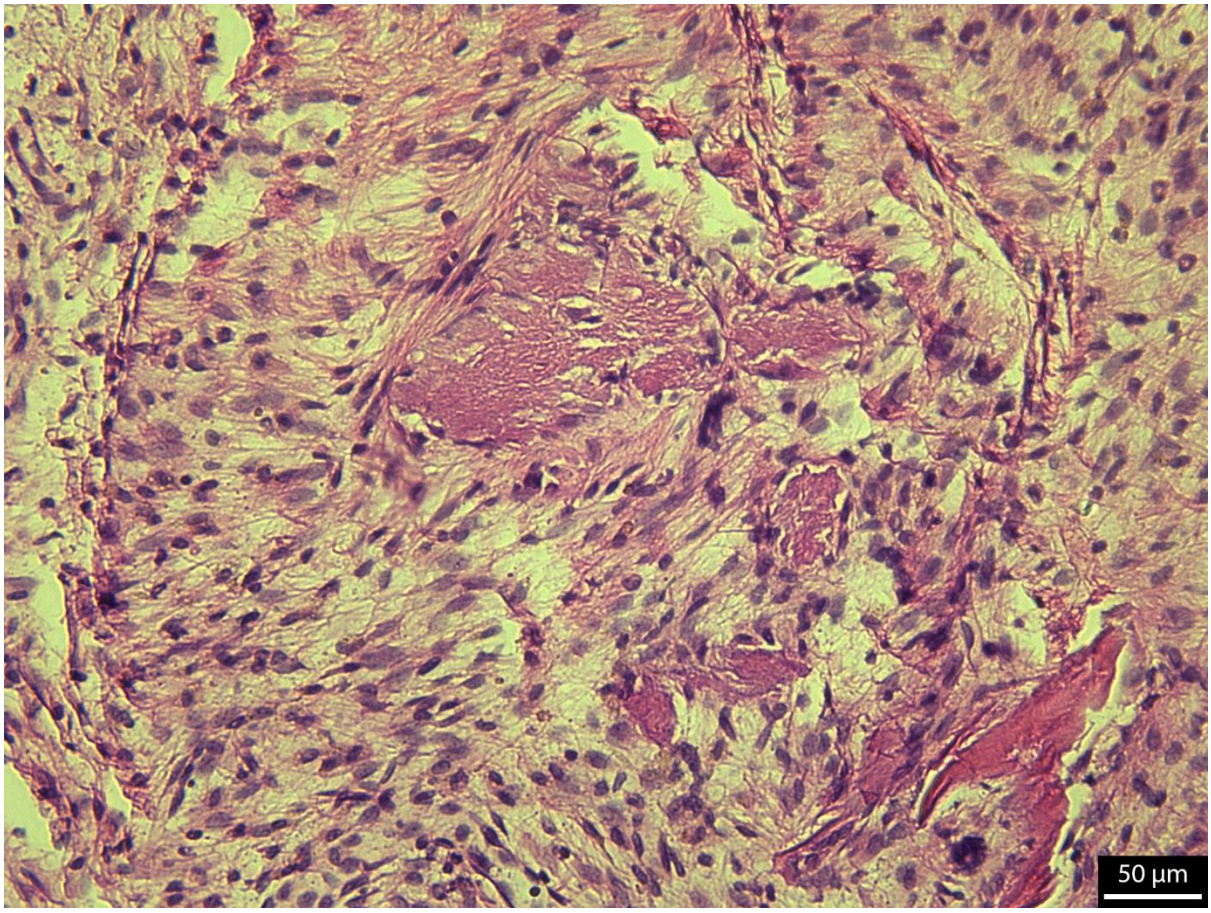

Figure 1.10: H & E stained xenograft meningioma consisting of KT21 cells growing in SCID mice for 21 days. *Image was kindly provided by Dr Liyam Laraba. Scale bar = 50 µm.*

2. Materials and Methods

2.1 Clinical samples

The primary meningioma cells used in this work are derived from the surgically removed meningiomas of anonymised human patients. Patients agreed for the meningioma to be used in this fashion by consenting to the 'Identifying and validating molecular targets in low grade brain tumours' study. Ethical approval was given by Plymouth Hospitals NHS Trust (R&D No: 14/P/056), North Bristol NHS Trust (R&D No: 3458) and the South West research ethics committee (REC No: 14/SW/0119; IRAS project ID: 153351).

These acquired primary human meningioma cells were then assigned an MOT and MN number and listed with other clinical data in the Plymouth Brain tumour database. Some of the clinical information regarding the primary human meningioma cells used by me are listed in Table 2.1.

	Tumour location	**Subtype**	**Grade**	**Age**	**Gender**	**NF2 status by Western blot**	**Genotyping**
MOT 148 /MN091	Middle cranial fossa floor	Not reported	I	62	F	Negative for NF2 and pNF2	TRAF7 N520S hetero
MOT 161 /MN126	Anterior cranial fossa floor	Transitional	I	41	F	Negative for NF2 and pNF2	WT for non-NF2 panel and POLR2A
MOT 172 /MN160	Anterior cranial fossa	Meningothelial	I	48	F	ND	NF2 WT *(by next generation sequencing (= NGS))*
MOT 240 /MN214	Planum sphenoidale	Meningothelial	I	59	F	Positive for NF2 and pNF2	Heterozygous for AKT1 E17K and TRAF7 N520S
MOT 273 /MN243	L frontal convexity	Transitional	I	73	F	Negative for NF2 and pNF2	No SMARCB1 hotspots/WT for POLR2A
MOT 310 /MN268	Bilateral olfactory groove	Meningothelial	I	67	F	Positive for NF2 and pNF2	ND
MOT 357 /MN308	Parasagittal and interosseus vertex	Meningothelial	I	NK	NK	Positive for NF2	ND
MOT 447 /MN345	Middle cranial fossa floor	Meningothelial	I	52	F	Positive for NF2	Heterozygous for TRAF7 N520S and PIK3CA H1047R

Table 2.1: Clinical information about primary human meningioma cells used in TEAD S-autopalmitoylation inhibitor experiments. *Information derived from Plymouth Brain Tumour database provided by Hanemann group. NK = not known; ND = not determined; WT = wild type; age = age at presentation/diagnosis.*

The respective gene mutations shown in the Genotyping column (see Table 2.1) were detected by Dr Claire Adams of the Hanemann group using endpoint genotyping, as described previously (Adams *et al.*, 2020). The only exception in said column is in regards to MOT 172 whose NF2 gene was found to be WT via next generation sequencing by the Manchester Centre for Genomic Medicine.

2.2 Cells

2.2.1 General cell culture

Two human meningioma cell lines were used. Ben-Men-1 is a Merlin-negative Grade I meningioma cell line which was immortalized by the retroviral transduction of the human telomerase reverse transcriptase (hTERT) gene (Puttmann *et al.*, 2005). KT21-MG1 (KT21) cells are Merlin-negative Grade III meningioma cells, which were derived from a malignant meningioma grown in immunosuppressed mice (Tanaka *et al.*, 1989).

All cells were cultured in Dulbecco's Modified Eagle's Medium (DMEM; Thermo Fisher Scientific) containing 10 % foetal bovine serum (FBS; Thermo Fisher Scientific), 2 mM L-alanyl-L-glutamine dipeptide (GlutaMAX, Thermo Fisher Scientific) and 100 U/ml Penicillin-Streptomycin (Thermo Fisher Scientific). The medium for the primary human meningioma cells received an additional 1 g of D-glucose (200 g/L glucose solution, Gibco). All cells were kept in T25 and T75 cell culture flasks at 37°C at 5 % CO_2 in a humidified cell incubator.

To passage the cells or use them for experiments, they were washed with phosphate buffered saline (PBS, Gibco), incubated with a trypsin/ethylenediaminetetraacetic acid (EDTA) mix (0.025 % trypsin and 0.01 % EDTA, Gibco) at 37°C until the cells detached (approx. 3 - 4 minutes) and then the trypsin was neutralized with twice the volume of cell culture media. The cells were spun down at 1500 rpm (rounds per minute)/400 x g for 3 min, the supernatant was removed and the cells were resuspended in 1 ml cell culture media. 10 µl of the cell suspension was diluted 1:5 in 40 µl Trypan blue (0.4 % Trypan blue stain, Gibco) and 10 µl of the cell/Trypan blue mix was pipetted into a Neubauer haemocytometer. The outer 4 squares of the Neubauer chamber were counted separately, not counting the cells found on the bottom border and on the right border lines. The results of the four squares were averaged and multiplied by 5 (accounting for the 1:5 dilution in the Trypan blue) and by 10000 (to adjust the counts to cell number/ml).

Name	Manufacturer	Stock solution
V2	Vivace Therapeutics	10 mM
V3	Vivace Therapeutics	10 mM
V5	Vivace Therapeutics	10 mM
VT1 (VT03534/VT104)	Vivace Therapeutics	10 mM
VT2 (VT03989)	Vivace Therapeutics	10 mM

Table 2.2: TEAD S-autopalmitoylation inhibitors by Vivace Therapeutics.

2.2.2 EdU proliferation experiments

A single 15 µl droplet of cells in a cell media suspension at a cell concentration depending on the cell type were pipetted onto each coverslip. The Ben-Men-1 (BM-1) and the primary human meningioma cells were seeded at a cell density of 5000 cells per coverslip while KT21 cells were seeded at a cell density of 2000 cells/coverslip. The uncoated coverslips (VWR) were placed beforehand into the wells of 24 well plates (Nunclon Delta surface, Thermo Scientific) (one coverslip/well). The cells were left on the coverslips in the incubator for 2 hours to allow the cells to attach themselves to the coverslip. Afterwards, the indicated TEAD S-autopalmitoylation inhibitor (10 mM stock concentration, see Table 2.2) was diluted in cell culture media to reach the indicated concentration and carefully added to and incubated with the cells for 48 hours.

The cells used for the measurement of baseline proliferation were given cell media containing dimethyl sulfoxide (DMSO, Sigma) of the same volume as the 1 µM TEAD palmitoylation inhibitor solution received from the TEAD palmitoylation inhibitor stock solution and incubated for the same amount of time. 5-Ethynyl-2´-deoxyuridine (EdU, Thermo Fisher Scientific) was diluted in cell culture media to a final concentration of 10 µM and then added for a 4 hour pulse into the media after 44 hours. During these last four hours, EdU nucleotides are incorporated into the replicating DNA of dividing cells where they can later be detected, serving as an indicator of proliferation.

At the end of the experiments, the media was removed from all the wells, the coverslips were washed with PBS once and fixed with 500 µl 4 % paraformaldehyde (PFA, Sigma) in PBS (pH 7.4) for 15 min. After one last PBS wash, the cells were kept in 1 ml PBS at 4°C until ready for staining.

2.2.3 EdU staining of coverslips

The coverslips were stained for EdU with the Click-iT EdU Alexa Fluor 488 or 594 Imaging Kit (Thermo Fisher Scientific) according to the manufacturer's instructions. All liquids/reagents were pipetted onto the coverslips away from the centre to wash off the least amount of cells possible. While still inside the 24 well plate, the coverslips were washed once with 3 % bovine serum albumin (BSA; Thermo Scientific) in PBS and permeabilized with 300 µl 0.5 % Triton X-100 (Sigma) in PBS for 20 minutes in the dark at room temperature (RT). Subsequently, the coverslips were washed 3 times with 3 % BSA in PBS. After lifting the coverslips with the cells out of the wells onto coverslip holders (consisting of petri dishes with attached Eppendorf tube caps), the Click-iT reaction mix was made. The recipe for 1 ml can be found in Table 2.3.

Volume	Reagent	Preparation
860 µl	Reaction buffer	1:10 dilution of 10x RB stock solution in dH_2O
40 µl	100 mM $CuS0_4$	
2.5 µl	Alexa Fluor 488 or 594 Azide	Stock solution dissolved in 70 µl DMSO
100 µl	RB additive	1:10 dilution of 10x buffer additive stock solution in dH_2O

Table 2.3: Click-iT reaction mix.

80 µl EdU Click-iT mixture per coverslip was added for 30 min at RT in the dark. Afterwards, the coverslips were washed in PBS by dipping them into four 50 ml Falcon tubes filled with PBS and then incubated with 80 µl of 1 µg/ml Hoechst (Invitrogen) diluted 1:500 in 3 % BSA in PBS for 15 minutes at RT in the dark. After a final wash by dipping the coverslips into PBS as before, the coverslips were mounted on glass slides (VWR) with CitiFluor-AF1 mounting medium (one drop per coverslip, Science Services) and the edges of the coverslips were sealed with nail polish.

2.2.4 Primary human meningioma cell samples for Western blot analysis

Primary meningioma cells were seeded in 6 well plates (Nunclon™ Delta surface, Thermo Scientific) at a concentration of 30,000 cells/well, one 6 well plate per MOT cell type and condition (DMSO vehicle control/1 µM VT1/1 µM VT2). After seeding, the cells were left to grow, adding fresh media every 2 days. As soon as a confluency of approximately 70 % had been reached, the media was replaced with cell media containing 1 µM VT1 or 1 µM VT2 or with cell media containing an equal volume of DMSO for control samples. The cells were incubated with these Pan-TEAD inhibitors or DMSO for 48 hours. At the end of this 48 h period,

the cells were harvested on ice by removing the media and washing the wells twice with ice-cold PBS. 10x Radioimmunoprecipitation assay (RIPA) buffer (EMD Millipore) was diluted 1:10 and protease and phosphatase inhibitor cocktail (100x, Thermo Scientific) was diluted 1:100 in distilled H_2O (dH_2O). After removing the PBS, 50 µl of dH_2O/RIPA/PPIC mixture was added per well (300 µl per 6 well plate in total).

Within each 6 well plate, a cell scraper was used to detach the cells of a well and subsequently this cell lysate was collected and transferred to the next well. This process was repeated until all wells were harvested, with the combined cell lysate of the 6 well plate being pipetted into an Eppendorf tube. The cell lysates were spun down for 15 min at 10,000 rpm/9300 x g at 4°C to pellet the cell debris. The supernatant was then carefully transferred into new Eppendorf tubes and stored at -20°C until used for bicinchoninic acid assay (BCA) protein concentration measurement and Western blot analysis (see section 2.5).

2.3 Mice

2.3.1 Mouse breeding

Mice of 3 different genotypes were used, namely Periostin-Cre positive (Postn-Cre+) $NF2^{fl(ox)/fl(ox)}$, Postn-Cre+ $NF2^{fl/fl}$ $YAP^{fl/fl}$ and Postn-Cre+ $NF2^{fl/fl}$ $TAZ^{fl/fl}$. The Postn-Cre negative (Postn-Cre-) $NF2^{fl/fl}$ littermates were used as controls. The genotypes were obtained by crossing Postn-Cre positive driver line mice with $NF2^{fl/fl}$, $NF2^{fl/fl}$ $YAP^{fl/fl}$ and $NF2^{fl/fl}$ $TAZ^{fl/fl}$ mice (Azzolin *et al.*, 2014; Giovannini *et al.*, 2000; Zhang *et al.*, 2010) and then back crossing the Postn-Cre positive F1 generation mice with the $NF2^{fl/fl}$, $NF2^{fl/fl}$ $YAP^{fl/fl}$ and $NF2^{fl/fl}$ $TAZ^{fl/fl}$ once more. Only the mice of the F2 generation with the floxed ($^{fl/fl}$) versions of the respective genes were then breed amongst themselves to maintain the desired genotypes (Figure 3.1).

The mice were kept under prescribed conditions in a 12/12 hours light/dark cycle. Pups were weaned at 3 weeks of age and ear notched to both mark them and to use the ear tissue sample(s) for polymerase chain reaction (PCR) genotyping (Figure 3.5.2).

2.3.2 PCR genotyping and agarose gel electrophoresis

The ear notches and tail snips were used for the genotyping of the P0-Cre, Postn-Cre, NF2, YAP and TAZ genes. The HotSHOT protocol (Truett *et al.*, 2000) was used for DNA extraction. First, the ear notches or tail snips were suspended in 75 µl alkaline lysis buffer (25 mM NaOH and 0.2 mM EDTA in dH_2O) and heated at 95°C for 90 minutes in a PTC-100 Peltier Thermal Cycler (MJ Research). Afterwards, the samples were neutralized with 75 µl of neutralisation buffer (40 mM Tris-HCl (Sigma) in dH_2O) and stored at -20°C before and after usage. The PCR

master mix for one sample (see Table 2.4) multiplied by the number of samples was mixed and 23 µl of the PCR master mix was added to each PCR tube.

Each PCR tube then received 2 µl of HotSHOT extracted DNA and placed in a G-Storm GS0004M Thermal Cycler (Labtech) and subjected to the appropriate PCR reaction program for the gene in question (see Tables 2.8 – 2.12).

Volume	**Reagent**	**Manufacturer**
15 µl	ddH_2O	Sigma #W4502
5 µl	5x Green Go Taq Buffer	Promega #M891A
1.5 µl	25 mM $MgCl_2$	Promega #A351H
1 µl	Primers (1:1 forward and reverse primer) see Table 2.10	Eurofins
0.5 µl	Deoxyribonucleotide triphosphates (dNTPs) (60 µl ddH_2O + 10 µl each of adenosine triphosphate (ATP), cytosine triphosphate (CTP), guanosine triphosphate (GTP) and thymidine triphosphate (TTP)	Promega #U120A-U123A
0.1 µl	Taq Polymerase	Promega #M740B

Table 2.4: PCR master mix for one reaction.

P0-Cre	Temperature	Time	Repeats
Step 1	95 °C	5 min	X 1
Step 2	94 °C 57 °C 72 °C	30 s 40 s 40 s	X 38
Step 3	72 °C	5 min	X 1
Step 4	8 °C	∞	-

Table 2.5: P0-Cre PCR program.

Postn-Cre	Temperature	Time	Repeats
Step 1	95 °C	5 min	X 1
Step 2	94 °C 57 °C 72 °C	30 s 40 s 40 s	X 36
Step 3	72 °C	5 min	X 1
Step 4	8 °C	∞	-

Table 2.6: Postn-Cre PCR program.

NF2	Temperature	Time	Repeats
Step 1	95 °C	5 min	X 1
Step 2	95 °C 55 °C 72 °C	30 s 30 s 1 min	X 38
Step 3	72 °C	5 min	X 1
Step 4	8 °C	∞	-

Table 2.7: NF2 PCR program.

YAP	Temperature	Time	Repeats
Step 1	95 °C	5 min	X 1
Step 2	94 °C 58 °C 72 °C	30 s 40 s 1 min	X 38
Step 3	72 °C	5 min	X 1
Step 4	8 °C	∞	-

Table 2.8: YAP PCR program.

TAZ	Temperature	Time	Repeats
Step 1	95 °C	2 min	X 1
Step 2	95 °C 60 °C 72 °C	30 s 59 s 1 min	X 38
Step 3	72 °C	5 min	X 1
Step 4	8 °C	∞	-

Table 2.9: TAZ PCR program.

Gene product	Forward (Fwd) primer 5’ – 3’	Reverse (Rev) primer 3’ – 5’
P0-Cre	CCA-CCA-CCT-CTC-CAT-TGC-AC	GCT-GGC-CCA-AAT-GTT-GCT-GG
Postn-Cre (Gehlhausen)	CAT-TTG-GGC-CAG-CTA-AAC-AT	CCC-GGC-AAA-ACA-GGT-AGT-TA
Postn-Cre (King’s College London)	GGC-TCT-AGC-GTT-CGA-ACG-CAC-TGA-T	CGG-ATC-ATC-AGC-TAC-ACC-AGA-GAC-G
NF2	GGG-GCT-TCG-GGA-AAC-CTG-G	GTC-TGG-GAA-GTC-TGT-GGA-GG
YAP	CCA-GAC-GAC-TTC-CTC-AAC-AGT-G	GCA-TCT-CCT-TCC-AGT-GTG-CCA-A
TAZ	CTT-CCA-AGG-TGC-TTC-AGA-GA	GGA-GAG-GTA-AAG-CCC-ACC-AG

Table 2.10: Primers used for PCR Genotyping.

The PCR products were run on an agarose gel, made by dissolving 2 % (w/v) agarose in 1x Tris-acetate-EDTA (TAE) buffer (Sigma) and subsequently boiling the agarose/TAE suspension in the microwave. After the heat caused the agarose to dissolve in the 1x TAE buffer, GelRed (Biotum) was added in a concentration of 1:50000. Afterwards, the solution was poured into a gel casting frame and the comb was inserted before allowing the solution to cool off and solidify into a gel. The comb was then carefully removed and 20 µl of each PCR product was pipetted into a separate well. Using a Power Pac 300 (Bio-Rad), the samples were run at 120 V for approximately 1 h and imaged afterwards using the Syngene PXi4 imager and the GeneSys software to detect the PCR bands.

2.3.3 IP EdU injection and tissue extraction

EdU powder was diluted with DMSO to a solution with a concentration of 0.1 mg/µl (e.g. weighing 2 mg EdU powder and mixing it with 20 µl DMSO). This solution was subsequently diluted 1:10 with sterile PBS (PBS used in cell culture) to a final volume of 200 µl injection mix per mouse containing 2 mg EdU powder. The mice used for proliferation experiments received one intraperitoneal (IP) EdU injection per mouse 24 hours prior to dissection.

In order to extract the needed tissue, mice with the appropriate genotype and age were asphyxiated with CO_2. Death was confirmed either via cervical dislocation or by severing the axillary artery to cause terminal blood loss following Home Office regulations and guidelines.

Depending on the experiment and mouse model and genotype, sciatic nerves, tibial nerves, spinal columns, cochleae and/or head halves containing the middle and posterior cranial fossa were dissected. The sciatic nerves (placed on a piece of filter paper after dissection), spinal columns and head halves were fixed in 4 % PFA in PBS for 24 h at 4 °C. The cochleae were first uncovered and then fixed by initially rinsing the inside of the cochleae with 4 % PFA in PBS using a syringe and subsequently incubating the dissected cochleae in 4 % PFA in PBS at RT for 30 min. Afterwards, the cochleae were washed in PBS 3 times and then submerged in 4 %

EDTA in PBS for an initial 24 hours at 4 °C to start the decalcification of the cochleae.

The tibial nerves for electron microscopy (EM) were placed on pieces of filter paper after dissection and stored in glutaraldehyde (2.5 % glutaraldehyde in 0.1 M sodium cacodylate pH 7.2) at 4 °C until handed over to EM unit at the University of Plymouth for further tissue preparation. A post-mortem tail snip from each mouse to confirm initial genotyping was taken as well. The ear notches and tail snips were stored at -20°C until they were used for PCR genotyping.

2.4 Fluorescent staining

2.4.1 Tissue sample preparation

The sciatic nerves in 4 % PFA in PBS were washed 3 times with PBS and then left in 30 % sucrose in PBS for at least 48 h to ensure cryoprotection of the tissue prior to embedding.

The spinal columns were washed with PBS 5 times and left in PBS at 4 °C until the dissection of the dorsal root ganglia (DRGs). L3 DRGs were isolated by cutting through the spinal column along the centre line and locating the L3 DRGs by counting down the DRGs beginning at the T12 DRGs found next to the most caudal rib. The L3 DRGs were carefully extracted and either immersed in 30 % sucrose in PBS for at least 48 hours at 4 °C to ensure cryoprotection or put back into 4 % PFA in PBS. The L3 DRGs which were returned to 4 % PFA in PBS were handed over to Dr Phil Edwards of the Neuropathology Department in Derriford Hospital to be formalin fixed paraffin embedded (FFPE), sectioned and stained with a hematoxylin and eosin (H&E) stain.

The fixed cochleae, initially left in 4 % EDTA in PBS at 4 °C for 24 hours, were left in 4 % EDTA in PBS for an additional 48 hours, replacing the 4 % EDTA in PBS solution every 24 hours. The EDTA treatment of a total of 72 hours decalcified the cochleae which can then be sectioned.

The head halves in 4 % PFA in PBS were washed 3 times with PBS and then remained in PBS at 4 °C until the vestibular ganglia (VGs) were dissected. After removing the brain remnants and superfluous pieces of skull, gaining access to the internal auditory meatus extending from the inner ear allowed the retrieval of the VGs. As done before with the sciatic nerves and DRGs, the VGs were immersed in 30 % sucrose in PBS for a minimum of 48 hours at 4 °C to assure cryoprotection.

2.4.2 Embedding, sectioning and staining of tissue sections/cells

2.4.2.1 IHC-fr/ICC

For frozen immunohistochemistry (IHC-fr), sciatic nerves, DRGs and VGs were embedded in OCT Tissue Tek embedding matrix (CellPath) and snap-frozen in liquid nitrogen. The blocks were stored at -80 °C until and after sectioning. 10 µm sections were obtained from the blocks using a Leica CM 1860 cryostat and placed on positively charged cryostat glass slides (SuperFrost Plus slides, VWR).

In order to hold the liquid reagents in place a liquid barrier was drawn around the tissue sections on the slides using an ImmEdge pen (Vector Laboratories). The slides were placed in a slide moisture chamber, with the trays at the bottom filled with tap water. This provided moisture, thereby preventing the rapid evaporation of reagents and the drying out of the tissue.

The OCT was dissolved by pipetting PBS inside the liquid barrier (not directly onto the tissue section as this might cause it to detach from the slide) and then removing the PBS after 10 min by tilting the slide, causing the PBS to run off. All liquids/reagents were added and removed in this manner throughout the IHC-fr aside from the mounting medium at the end.

For immunocytochemistry (ICC), the coverslips holding the cells were extracted from the wells and placed on coverslip holders. As mentioned before, all liquids and reagents were pipetted onto the coverslips as far from the centre as possible to avoid washing off too many cells.

Afterwards, the steps for IHC-fr/ICC were similar. The tissue/the cells were permeabilized by adding 1 % BSA/0.25 % Triton X-100 in PBS for 45/30 minutes, respectively. Unspecific binding sites were blocked using 3 % BSA/0.05 % Triton X-100 in PBS for 1 hour/45 min. The liquid barrier for the IHC-fr was replenished/reinforced whenever necessary. Per slide/coverslip, 100 µl/80 µl of primary antibodies diluted in 3 % BSA/0.05 % Triton X-100 in PBS (see Table 2.11) were added overnight at 4 °C in the dark.

The next day, the tissue sections were washed with PBS three times for 10 minutes each to remove any unbound primary antibody. The coverslips were washed with PBS for the same reason by immersing them into 4 falcon tubes filled with PBS. Afterwards, the tissue sections/coverslips were incubated with 100 µl/80 µl per slide/coverslip of the secondary antibodies diluted in 1 % BSA/0.25 % Triton X-100 for 1 hour in the dark at RT (see Table 2.12). Afterwards, three 10 min PBS washes/one immersion into each of 4 PBS falcon tubes were/was performed to remove all unbound secondary antibodies.

Antigen	Antibody	Characteristics	Used concentration
CD68	[FA-11] ab53444 Abcam	Rat Monoclonal Antibody	1:100
Macrophage mannose receptor (MMR)/CD206	#AF2535 Mouse MMR/CD206 R&D Systems	Goat Polyclonal Antibody	1:100
Platelet endothelial cell adhesion molecule (PECAM-1) /CD31	#550274 Clone MEC 13.3 BD Biosciences	Rat Monoclonal Antibody	1:50
Inducible nitric oxide synthase (iNOS)	ab15323 Abcam	Rabbit Polyclonal Antibody	1:100
Ionized calcium binding adaptor molecule 1 (Iba1)	#019-19741 Fujifilm WAKO	Rabbit Polyclonal Antibody	1:500
Collagen IV	[EPR22911-127] ab236640 Abcam	Rabbit Monoclonal Antibody	1:100
Neurofilament (NF)	ab4680 Abcam	Chicken Polyclonal Antibody	1:1000

Table 2.11: Primary antibodies for IHC/ICC.

If a 3 layer antibody system consisting of primary antibody, biotinylated secondary antibody and Streptavidin-conjugated fluorophore was used on tissue sections in an attempt to

increase the signal to background ratio, the Streptavidin-conjugated fluorophore was diluted in 1 % BSA/0.25 % Triton X-100 (see Table 2.13) and 100 µl per slide of this dilution were incubated with the sections for 1 hour in the dark at RT followed by three 10 min PBS washes.

Hoechst nuclear DNA dye was used as counterstain on tissue sections and coverslips, diluted 1:500 in 1 % BSA/0.25 % Triton X-100 in PBS and incorporated in the last incubation step (with the secondary antibodies in a 2 layer system or with the Streptavidin-conjugated fluorophores in a 3 layer system).

Finally, the tissue sections were mounted by adding a drop of CitiFluor-AF1 mounting medium (Science Services) directly onto the tissue and carefully placing a coverslide on top whose edges were subsequently sealed using nail polish. The ICC stained coverslips with the cells were mounted as described previously (see section 2.2.3).

α-Species and conjugate	**Antibody**	**Used concentration**
α-Chicken Alexa Fluor 488	#A-11039 Invitrogen	1:200
α-Goat Alexa Fluor 488	#A-11055 Invitrogen	1:500
α-Goat Alexa Fluor 568	#A-11057 Invitrogen	1:500
α-Goat biotinylated IgG	BA-5000 Vector Laboratories	1:500
α-Rabbit Alexa Fluor 488	#A-11034 Invitrogen	1:500
α-Rabbit Alexa Fluor 568	#A-11011 Invitrogen	1:200
α-Rat Alexa Fluor 488	#A-21208 Invitrogen	1:500
α-Rat Alexa Fluor 568	#A-11077 Invitrogen	1:500
α-Rat biotinylated IgG	BA-4000 Vector Laboratories	1:500

Table 2.12: Secondary antibodies for IHC/ICC.

Conjugated Fluorophore	**Manufacturer**	**Used concentration**
Streptavidin Alexa Fluor 568	#S11226 Invitrogen	1:1000

Table 2.13: Streptavidin-conjugated fluorophore for IHC

2.4.2.2 Agarose EdU staining and IHC

To embed the decalcified cochleae, 4 % agarose w/v (weight by volume, e.g. 4 g agarose in 100 ml PBS) was dissolved in PBS by heating up the suspension in the microwave. After slightly cooling down, the hot but no longer boiling agarose solution was poured into petri dishes and the cochleae were placed into the agarose. After the agarose cooled down and solidified, a scalpel was used to cut out agarose blocks containing the cochleae. These agarose blocks were mounted on a vibratome (Leica VT 1200S) which was used to cut 200 µM sections. These sections were stored by keeping them floating in a petri dish filled with PBS at 4 °C.

To stain the agarose sections, they were placed in the wells of 24 well plates and permeabilized with 0.5 % Triton X-100 in PBS for 20 min at RT in the dark (which is achieved by wrapping the 24 well plates in aluminium foil). After two 10 min washes with 3 % BSA in PBS, the same Click-iT cocktail to stain EdU was used as above (see Table 2.3), adding 200 µl per well for 30 min in the dark at RT on a shaker. After one 10 min PBS wash, the agarose sections were blocked with 3 % BSA in PBS for 1 hour in the dark at RT and then left with 200 µl of the primary antibody (here the Iba1 antibody 1:100 in 3 % BSA in PBS, Table 2.11) overnight on a shaker at 4 °C in the dark. The next day, the sections were washed with PBS 3 times for 10 min each and incubated with 200 µl of the diluted secondary antibody (anti-Rabbit Alexa Fluor 568 1:500 in 3 % BSA in PBS, Table 2.12) and Hoechst (1 µg/ml Hoechst, 1:50 in 3 % BSA in PBS) for 1 hour at RT in the dark on a shaker. After the final three 10 min washes with PBS, the agarose sections were placed on labelled glass slides and covered with the CitiFluor-AF1 mounting medium (Science Services). A drop of vacuum grease was put into each corner forming a rectangle onto which the coverslide was lowered. Finally, the coverslides were sealed with nail polish and kept in the dark at RT until imaging.

2.4.2.3 EdU staining of DRG and VG sections

A similar approach to the EdU staining of coverslips and agarose sections was followed here. After drawing the liquid barriers around the DRG and VG sections, the OCT was dissolved with PBS for 10 min at RT as before. A permeabilization step with 0.5 % Triton X-100 in PBS for 15 - 20 min at RT in the dark and 2 washes with 3 % BSA in PBS for 10 min each followed. Afterwards, the above mentioned Click-iT cocktail to stain EdU was used (see Table 2.3) in the dark at RT for 30 min, 100 µl per section. After three 10 min PBS washes, the section's cell nuclei were stained using 1 µg/ml Hoechst nuclear dye for 1 hour, diluted 1:500 in 3 % BSA in PBS and 100 µl per slide. 3 final 10 min PBS washes followed and then sections were mounted as mentioned above and sealed off with nail polish.

2.5 Western blot

2.5.1 BCA assay

Protein concentrations of standards and primary meningioma cell lysates were determined using the Pierce BCA Protein Assay Kit (Thermo Fisher Scientific) kit following the manufacturer's instructions.

The standards were diluted using ddH_2O (Sigma #W4502) in Eppendorf tubes to acquire standard protein samples of known protein concentration. Each protein standard was pipetted into 4 wells (10 µl/well) of a 48 well plate to be measured in quadruple.

The primary meningioma cell lysates were diluted 1:3 in RIPA buffer (EMD Millipore) (12 µl protein sample + 24 µl RIPA buffer) in Eppendorf tubes and pipetted into 3 wells each (10 µl/well) of a 48 well plate to be measured in triplicate.

Afterwards, Reagent A and Reagent B were mixed 1:50 and 200 µl were added to each well. The 48 well plate was then wrapped in tinfoil and left in the cell culture incubator for 30 minutes. This allowed the initially green liquid in the wells to change to a shade of purple whose intensity is directly proportional to the protein concentration in the respective wells. Finally, the 48 well plate was retrieved, placed in the photometric plate reader (FLUOstar Omega, BMG LABTECH) and measured at a wavelength of 560 nm. Using the preinstalled Reader Control/MARS Data Analysis software (BMG LABTECH), the standard measuring curve was constructed, thereby allowing the determination of the protein concentration of the primary meningioma cell lysates.

2.5.2 Sample preparation and SDS-PAGE

1x running buffer was made by mixing 28.8 g Glycine (Sigma), 6 g Tris Base (Sigma), 1990 ml dH_2O and 10 ml of 20 % SDS (sodium dodecyl sulphate, Fisher Bioreagents) and homogenising the mixture with a magnetic stirring bar.

Afterwards, the cell samples defrosted on ice were used to mix the Western blot samples. Using the protein concentrations of the cell samples obtained by BCA assay, the volume of each sample to reach a protein amount of 30 µg was calculated. This volume, together with 6.6 µl 2x Laemmli buffer (diluted with dH_2O from 6x Laemmli buffer, Alfa Aesar) and the corresponding dH_2O volume to reach a final volume of 25 µl, were pipetted into labelled Eppendorf tubes to create the Western blot samples. These samples were then boiled at 100 °C for 5 min to reduce and denature the proteins and then kept on ice until they were transferred onto the polyacrylamide gel.

The gel electrophoresis chamber was assembled, one pre-cast polyacrylamide gel (Bio-Rad, #4561093) per antibody were prepared and inserted and the chamber was filled with 1x

running buffer. 10 µl of the pre-stained dual colour protein ladder (Bio-Rad, #1610374) was pipetted into one of the wells of each gel while the Western blot samples were added to the rest of the wells (9 wells), 1 sample per well. The loaded polyacrylamide gel(s) was/were then run at a constant voltage of 150 - 200 V for 30 - 40 min until the lowest protein standard of the protein ladder was close to the end of the gel(s).

2.5.3 Electroblotting

While the gel(s) ran, the materials for the next steps were prepared. First, 1x transfer buffer was made by mixing 14.4 g Glycine, 3 g Tris Base, 200 ml methanol (VWR Chemicals) and 800 ml dH_2O and subsequent homogenisation with a magnetic stirring bar. Second, one trap apparatus, 2 sponges, 4 Whatman filter papers (Thermo Scientific) and 1 polyvinylidene difluoride (PVDF) membrane (GE Healthcare Life Sciences Amersham) per gel were readied. The Whatman papers were thoroughly soaked in 1x transfer buffer while the PVDF membrane(s) was activated in methanol. Third, the components of the wet transfer chamber for the protein transfer from the polyacrylamide gel to the PVDF membrane were assembled.

After the gel electrophoresis had concluded, each gel was retrieved and the top part of each gel (stacking gel) was removed. Subsequently, a PVDF membrane was put on top of each gel after which the air bubbles were removed using a Western blot roller. Each gel/PVDF combination was then flanked/sandwiched by 2 soaked Whatman papers on each side and once again freed from air bubbles via roller. Afterwards, each 'sandwich' was fixed in place using a trap apparatus. Each trap apparatus was then inserted into protein transfer chamber and a freezer block was added. The chamber was filled with 1x transfer buffer and the protein transfer from polyacrylamide gel to PVDF membrane was run on a constant electric current (electroblotting) of 300 mA for 90 min. Halfway through the transfer (after 45 min), the freezer block was replaced with a new one.

2.5.4 Immunodetection

During the protein transfer, 1x TBS-T was made by mixing 900 ml dH20, 100 ml 10x TBS and 0.5 ml Tween (Fisher Scientific) and 5 % BSA blocking buffer by solving 2.5 g BSA in 50 ml TBS-T. Upon the completion of the protein transfer, each PVDF membrane was recovered and the overhanging edges were cut with a scalpel. Each PVDF membrane were dipped first into methanol, then dH_2O and finally TBS-T. Afterwards, each PVDF membrane was placed into 5 ml of 5 % BSA blocking buffer for 1 hour at RT on a shaker to block unspecific binding sites. Subsequently, 5 µl of the utilized primary antibody (CTGF and/or Pan-TEAD, see Table 2.14) was added directly into the 5 ml blocking buffer covering each PVDF membrane and left to incubate overnight at 4 °C in the dark on a shaker.

Antigen	Antibody	Characteristics	Used concentration
CTGF	ab6992 Abcam	Rabbit Polyclonal Antibody	1:1000
Pan-TEAD	D3F7L Cell Signaling Technology	Rabbit Monoclonal Antibody	1:1000
GAPDH	ab8245 Abcam	Mouse Monoclonal Antibody	1:10000

Table 2.14: Primary antibodies used for Western blot.

The next day, each membrane underwent three 10 min TBS-T washes on a shaker to remove any unbound primary antibodies. Each membrane was then incubated with 2 µl of HRP conjugated anti-Rabbit secondary antibody (see Table 2.15) in 10 ml of 5 % BSA blocking buffer for 1 hour at RT on a shaker.

α-Species and conjugate	Antibody	Used concentration
α-Rabbit HRP	#1706515 Bio-Rad	1:5000
α-Mouse HRP	#1706515 Bio-Rad	1:5000

Table 2.15: Secondary antibodies used for Western blot.

To remove any unbound secondary antibody, the membrane(s) were subsequently washed with TBS-T 3 times, 10 min each on a shaker.

Each membrane was imaged one at a time using Pierce ECL Western Blotting Substrate (Thermo Scientific). Only for the membrane about to be imaged, 400 µl of Reagent A and 400 µl of Reagent B were mixed in an Eppendorf tube. Excess TBS-T was removed by holding the

membrane by a corner with forceps and carefully dabbing one of the short edges of the membrane against a paper towel. Afterwards, the membrane was covered with the Reagent A and B mixture and the chemiluminescent protein bands were imaged using the Syngene PXi4 imager and GeneSys software.

Given the successful visualization of the CTGF or Pan-TEAD protein bands, the loading control (GAPDH band) of each membrane was determined. After two 10 min washes with TBS-T on a shaker, each membrane was stripped using 5 ml stripping buffer (Thermo Scientific) for 15 min at RT, followed by 2 more 10 min TBS-T on a shaker washes. The previously described membrane blocking (here with 10 ml of 5 % BSA blocking buffer), primary antibody incubation (here 1 µl anti-GAPDH primary antibody, see Table 2.14), TBS-T washing, secondary antibody incubation (here 2 µl HRP conjugated anti-mouse secondary antibody in 10 ml of 5 % BSA blocking buffer, see Table 2.15), TBS-T washing and chemiluminescence imaging steps were repeated to allow the imaging of the GAPDH protein bands.

2.6 Imaging and quantification

Images of mouse tissue sections (sciatic nerves, tibial nerves, DRGs, cochleae and VGs) and cells (cell culture cells and primary human cells) were obtained using a Leica IM8 or Leica SPE microscope (or in one case a TEM, see Figure 3.6). When imaging EdU stained cells on coverslips, it was always attempted to image a section of the coverslip which had similar amounts of cells and where the cells were as evenly spaced out as possible (where they had the space to proliferate freely).

Photoshop CC and ImageJ software were used to count

1. Neuronal and non-neuronal cells in H & E stained paraffin sections
2. Hoechst positive nuclei, EdU positive nuclei and Iba1 positive cells in frozen tissue sections
3. Hoechst positive nuclei and EdU positive nuclei of cell line and primary cells on coverslips

ImageJ was also used to measure the DRG tissue area in H & E paraffin sections using scale bars as reference for the calculations. Microsoft Excel then allowed the determination of the number of neuronal and non-neuronal cells per mm^2 DRG tissue and the percentage of EdU positive nuclei/Iba1 positive cells. When quantifying the DRG and VG sections, only the area with the large neuronal cell bodies was quantified.

For Western blot analysis/quantification, the densities of the protein bands (CTGF, Pan-TEAD and GAPDH) were measured using ImageJ and subsequently the normalized densities were calculated via Microsoft Excel.

The panels/figures were prepared using Photoshop CC and the graphs were plotted with GraphPad Prism 9.

2.7 Statistical analysis

The data in Figures 3.3.4, 3.11.4 and 3.13.5 was analysed by two-way ANOVA since 3 or more groups were compared and 2 categorical independent variables were present (Mishra *et al.*, 2019). Šídák's pair-wise multiple comparisons test was chosen as post-hoc test because it had greater statistical power than other post-hoc tests on these occasions.

The data in Figures 3.7.4, 3.7.5, 3.9.4, 3.9.6, 3.13.5, 3.14.4 and 3.14.6 was analysed by two-way ANOVA since 3 or more groups were compared and 2 categorical independent variables were present. Tukey pair-wise multiple comparisons test was used as post-hoc test since it was recommended by GraphPad Prism 9.

The data in Figures 3.12.3, 3.13.2, 3.13.4 and 3.14.2 was analysed by one-way ANOVA since 3 or more groups were compared and only 1 categorical independent variables was present (Mishra *et al.*, 2019). Tukey pair-wise multiple comparisons test was chosen as post-hoc test because it was recommended by GraphPad Prism 9.

3. Results

3.1 Breeding of required mouse genotypes

In order to obtain mice with the correct genetic make up to spontaneously develop schwannomas according to the Gehlhausen mouse model (Gehlhausen *et al.*, 2015), mice had to be bred in several steps (Figure 3.1). As mentioned before, the animals with the correct genotype for breeding purposes were identified by PCR genotyping (see Materials and Methods section 2.3.2) using the ear notches which were collected after the animals were weaned.

The three genotypes used for this work were NF2 single knockout (NF2 sKO), NF2/YAP double knockout (NF2/YAP dKO) and NF2/TAZ double knockout (NF2/TAZ dKO). More precisely, the NF2 sKO mice are Periostin-Cre positive (Postn-Cre+) $NF2^{fl/fl}$, the NF2/YAP dKO mice are Postn-Cre+ $NF2^{fl/fl}/YAP^{fl/fl}$ and the NF2/TAZ dKO mice are Postn-Cre+ $NF2^{fl/fl}/TAZ^{fl/fl}$ (Figure 3.1). The breeding of these three genotypes involved similar steps.

First, Postn-Cre negative (Postn-Cre-) mice with respective floxed genes ($NF2^{fl/fl}$ or $NF2^{fl/fl}/YAP^{fl/fl}$ or $NF2^{fl/fl}/TAZ^{fl/fl}$ (Azzolin *et al.*, 2014; Giovannini *et al.*, 2000; Zhang *et al.*, 2010)) were crossed with PS animals (Postn-Cre driver line) which were heterozygous for Postn-Cre positive (Postn-Cre+) and wild type for the targeted genes ($NF2^{wt/wt}/YAP^{wt/wt}/TAZ^{wt/wt}$). The resulting F1 generation were all heterozygous ($^{wt/fl}$) for NF2, YAP or TAZ alleles and were either Postn-Cre+ or Postn-Cre-. Some of the $NF2^{wt/fl}$ were used for sciatic nerve crush experiments (see Figure 3.3.1 and 3.3.2). The Postn-Cre+ mice of this F1 generation were then backcrossed with the Postn-Cre- mice with the double floxed genes ($NF2^{fl/fl}$ or $NF2^{fl/fl}/YAP^{fl/fl}$ or $NF2^{fl/fl}/TAZ^{fl/fl}$) which yielded F2 generation litters with a multitude of genotypes with the desired genotypes among them (marked with * in Figure 3.1). The desired genotypes were then bred with one another (Figure 3.1) to maintain the mouse colonies for experimental use.

It is worth mentioning that to maintain the colonies of the NF2 sKO and NF2/YAP dKO mice the female mouse of the breeding pair always needed to be Postn-Cre- and the male therefore Periostin-Cre+ . This was necessary since the knockout (Periostin-Cre+) animals always were smaller, never reaching the size of their Periostin-Cre- littermates. Therefore, it was safer to use the Postn-Cre- females for breeding to avoid any complications of gestation or birth which may have occurred due to the reduced weight of the female NF2 sKO and NF2/YAP dKO mice. This was not the case for NF2/TAZ dKO mice whose size approximated the size of their Postn-Cre- littermates, allowing both the female NF2/TAZ dKO and female Postn-Cre- littermates to be used for breeding.

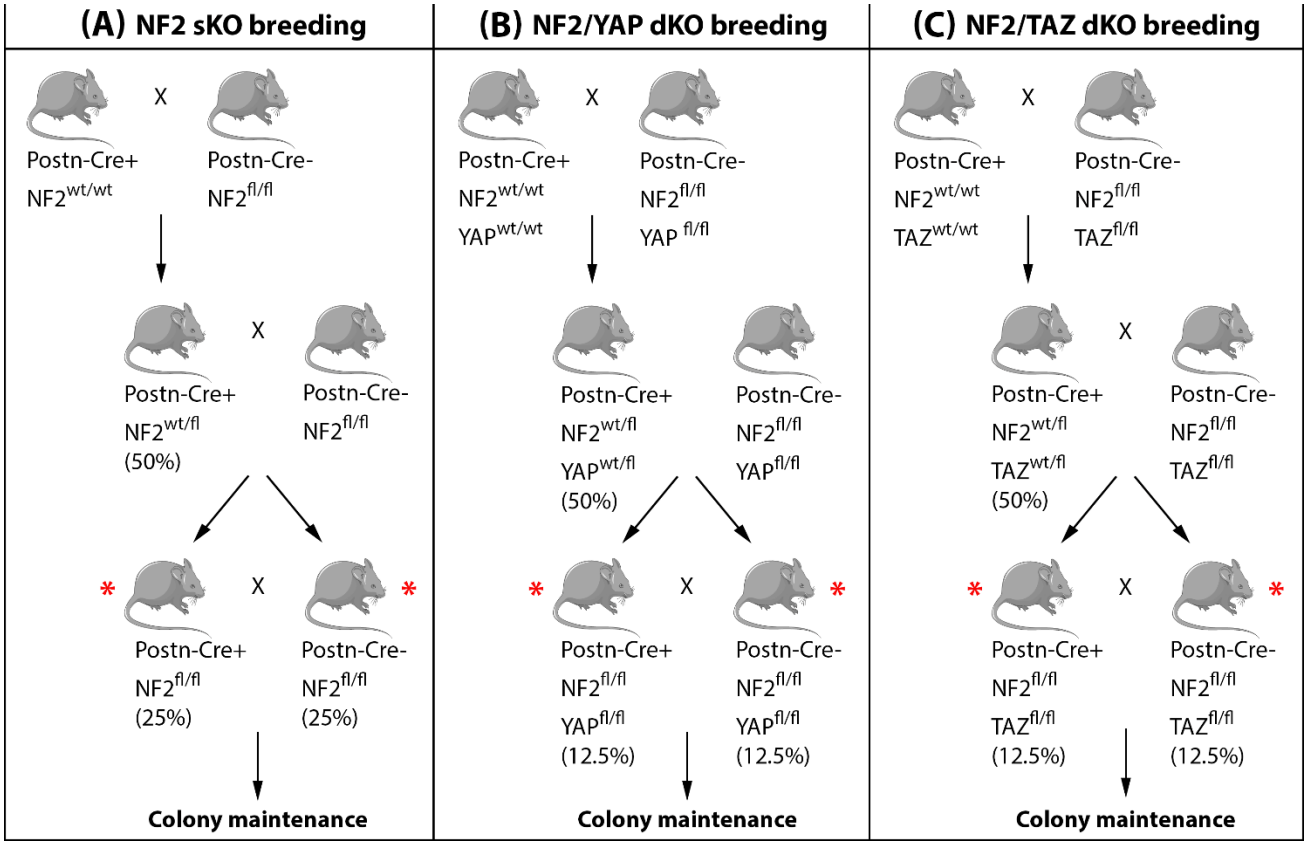

Figure 3.1: Breeding scheme to generate NF2 single knockout (NF2 sKO), NF2/YAP double knockout (NF2/YAP dKO) and NF2/TAZ double knockout (NF2/TAZ dKO) mice and their littermate controls. *(A) Periostin-Cre positive mice (expressing Postn-Cre on one allele, Postn-Cre+) with wild type ($^{wt/wt}$) copies of NF2 were crossed with Postn-Cre negative (Postn-Cre-) mice with floxed ($^{fl/fl}$) NF2 genes. The resulting F1 generation were heterozygous for the NF2 gene (NF2$^{wt/fl}$). Postn-Cre+ mice of F1 generation were back crossed with Postn-Cre- NF2$^{fl/fl}$ mice giving rise to F2 generation with 4 different genotypes, 2 of which would be used both for experiments and maintenance of the NF2 sKO mice colony. These 2 desired genotypes are marked with asterisks (*). (B) A similar approach was used when creating NF2 YAP dKO mice. Postn-Cre+ mice were bred with Postn-Cre- mice with floxed NF2 and YAP genes (NF2$^{fl/fl}$/YAP$^{fl/fl}$). Their F1 generation litters were heterozygous for both NF2 and YAP (NF2$^{wt/fl}$ /YAP$^{wt/fl}$), either Postn-Cre+ or - . Postn-Cre+ F1 mice were then back crossed with Postn-Cre- NF2$^{fl/fl}$/YAP$^{fl/fl}$ mice resulting in an F2 generation with 8 different genotypes of which 2 were once again used for both experiments and colony maintenance (*) (C) To obtain the desired NF2/TAZ dKO mice the same breeding strategy used for the NF2/YAP dKO mice was employed here. Postn-Cre+ mice with wild type NF2 and TAZ genes were crossed with Postn-Cre- mice with floxed NF2 and TAZ genes. The resulting Postn-Cre+ F1 mice with heterozygous NF2 and TAZ genes were bred once more with Postn-Cre- mice with floxed NF2 and floxed TAZ genes. This resulted in an F2 generation with 8 genotypes with the 2 desired genotypes among them (*), used for experiments and continuation of the mouse line. Percentages in brackets (%) show predicted genotype distribution of the shown genotype within that generation.*

3.2 Examination of antibody functionality in sciatic nerves

3.2.1 IHC staining for macrophage markers

While the mouse breeding was under way to acquire the desired genotypes, other experiments were conducted in the meantime. Since I was attempting to find a link between macrophage numbers and proliferation rates which was proposed previously (de Vries *et al.*, 2013; Lewis *et al.*, 2019), a reliable antibody against a pan-macrophage marker such as CD68 to detect and quantify macrophages in the examined schwannomas was needed. Furthermore, an antibody against M1-like or M2-like macrophage markers was required as well to differentiate between the two macrophage types and to detect a possible difference in their proportions. It has been shown that M1-like macrophages generally exhibit pro-inflammatory and anti-tumourigenic activity while M2-like macrophages are described as anti-inflammatory and involved in tumour progression (Ivashkiv, 2013; Mantovani *et al.*, 2013; Martinez & Gordon, 2014; Murray *et al.*, 2014; Sica & Mantovani, 2012) (see Introduction section 1.17.1). Therefore, a possible increase in M2-like macrophages might explain a possibly enhanced proliferation/tumour formation. On this occasion an anti-CD206 (CD206 being an M2-like marker) antibody was used.

The antibodies were tested on injured sciatic nerves of P0-Cre+ $NF2^{fl/fl}$ (NF2 sKO) and P0-Cre- $NF2^{fl/fl}$ (littermate control) mice. In fact, up until stated otherwise, P0-Cre mice were used for the following experiments since the Postn-Cre mice were still in the process of being bred. The sciatic nerve crush surgery was performed by Dr Xin-Peng Dun since I had not yet received my animal license and the necessary training to do the surgery myself. The dissection of the injured sciatic nerves 21 days after the crush injury distal of the crush site were done by Professor David Parkinson for the same reason. Afterwards, the processing and staining of the dissected nerves were performed by me.

Injury to P0-Cre+ $NF2^{fl/fl}$ (NF2 sKO) nerves are known to cause tumours distal to the injury site with a strong macrophage presence and injured NF2 sKO nerves have been shown to contain a substantial amount of macrophages 21 days after injury (Schulz *et al.*, 2016). Macrophages remain in the NF2 sKO nerves 7, 21 and 60 dpi (Mindos *et al.*, 2017) and even 8 months after injury (Schulz *et al.*, 2016). Therefore, sections of 21 days post injury (21 dpi) sciatic nerves of 3 month old (adult) P0-Cre driven NF2 sKO mice were used as positive control.

It was also attempted to verify whether there were differences in M1-like vs M2-like macrophage populations in the injured sciatic nerve between NF2 sKO mice and controls. This was part of an ongoing project with Dr Aditya Shivane of the Department of Cellular & Anatomical Pathology at Derriford Hospital to compare the macrophage populations of human tumours to the mouse model.

For the CD68 primary antibody a 2 layer system was chosen while for the CD206 primary antibody a 3 layer system was used since in preliminary experiments the signal created by the CD206 antibody in a 2 antibody system resulted in weak staining (data not shown). The stained sections were imaged using a Leica IM8 microscope (Figures 3.2.1 – 3.2.3).

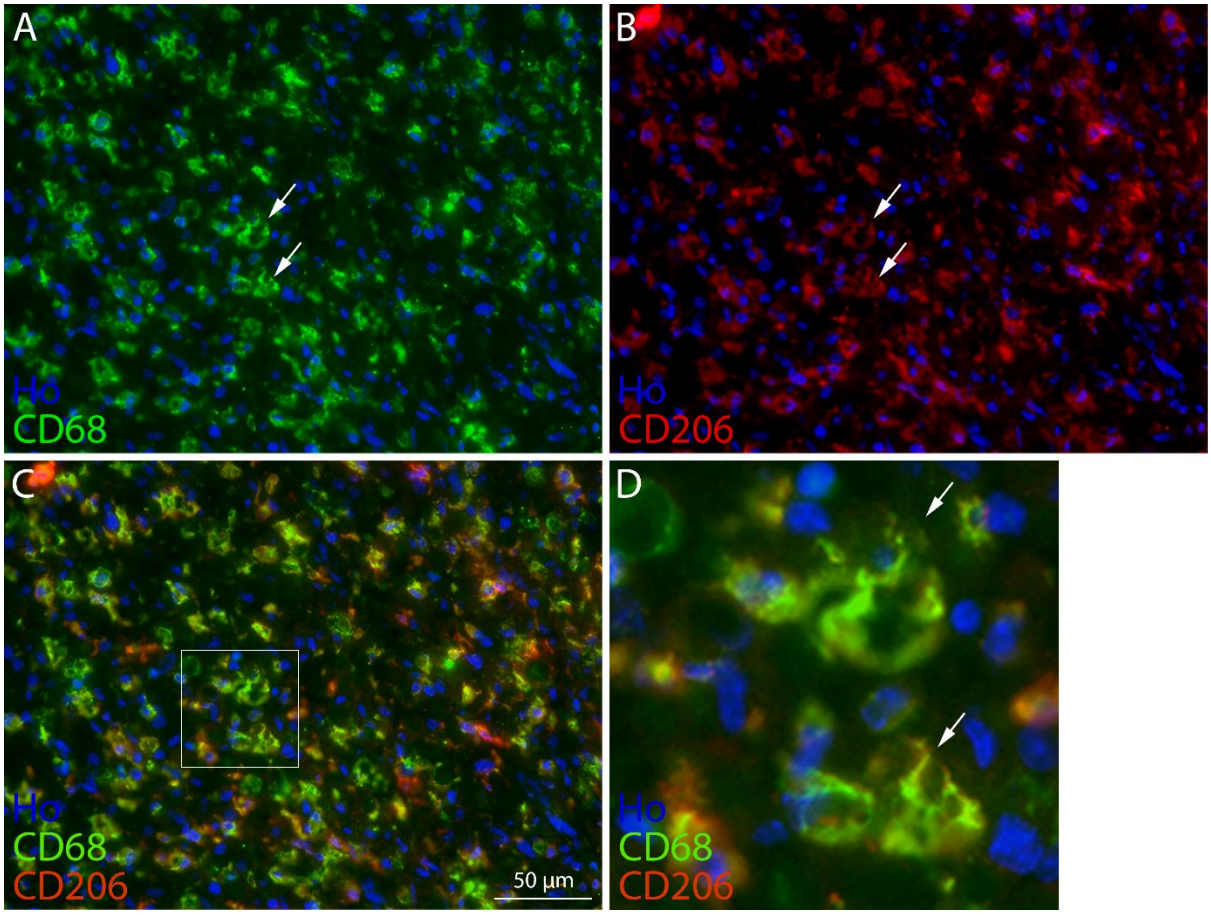

Figure 3.2.1: CD68 and CD206 staining of a 21 days post injury (21 dpi) sciatic nerve of an adult 3 month old P0-Cre+ NF2$^{fl/fl}$ (NF2 sKO) mouse *revealed most macrophages to be M2-like macrophages. A large number of CD68/CD206 double positive (CD68+ CD206+) cells were identified. A: CD68+ macrophages in green. B: CD206+ macrophages in red. C: CD68/CD206 double positive macrophages are seen in yellowish green. Scale bar = 50 µm (micrometres) in A, B and C. D: Enlarged image of white framed area in C. Counterstain DNA dye Hoechst (Ho) used to show cell nuclei in blue. White arrows mark the same two CD68+ CD206 + M2-like macrophages in all 3 images. n = 3 mice. Representative image are shown.*

Figure 3.2.1 shows the representative image of one of the 21 dpi NF2 sKO sciatic nerves. A large number of CD68/CD206 double stained M2-like macrophages (see white arrows in Figure 3.2.1 C and D), macrophages in yellowish green) were observed. Figure 3.2.1 D is an enlarged image of the white framed area of Figure 3.2.1 C. Therefore, according to these images, most macrophages in the 21 dpi NF2 sKO nerve appeared to be M2-like macrophages.

In an attempt to obtain a clearer staining of CD68 and CD206 the 21 dpi sciatic nerve sections were stained with either CD68 or CD206 antibodies separately. The same 2 layer system for CD68 and the 3 layer system for CD206 were used as before. Representative images of the 4 NF2 sKO sciatic nerves stained for either CD68 or CD206 are shown in Figure 3.2.2. A large amount of CD68 positive cells (macrophages, Figure 3.2.2 A and B) and also CD206 positive cells (M2-like macrophages, Figure 3.2.2 C and D) were seen in the respective images. The quality of the staining was comparable to the 2 layer CD68 3 layer CD206 double staining.

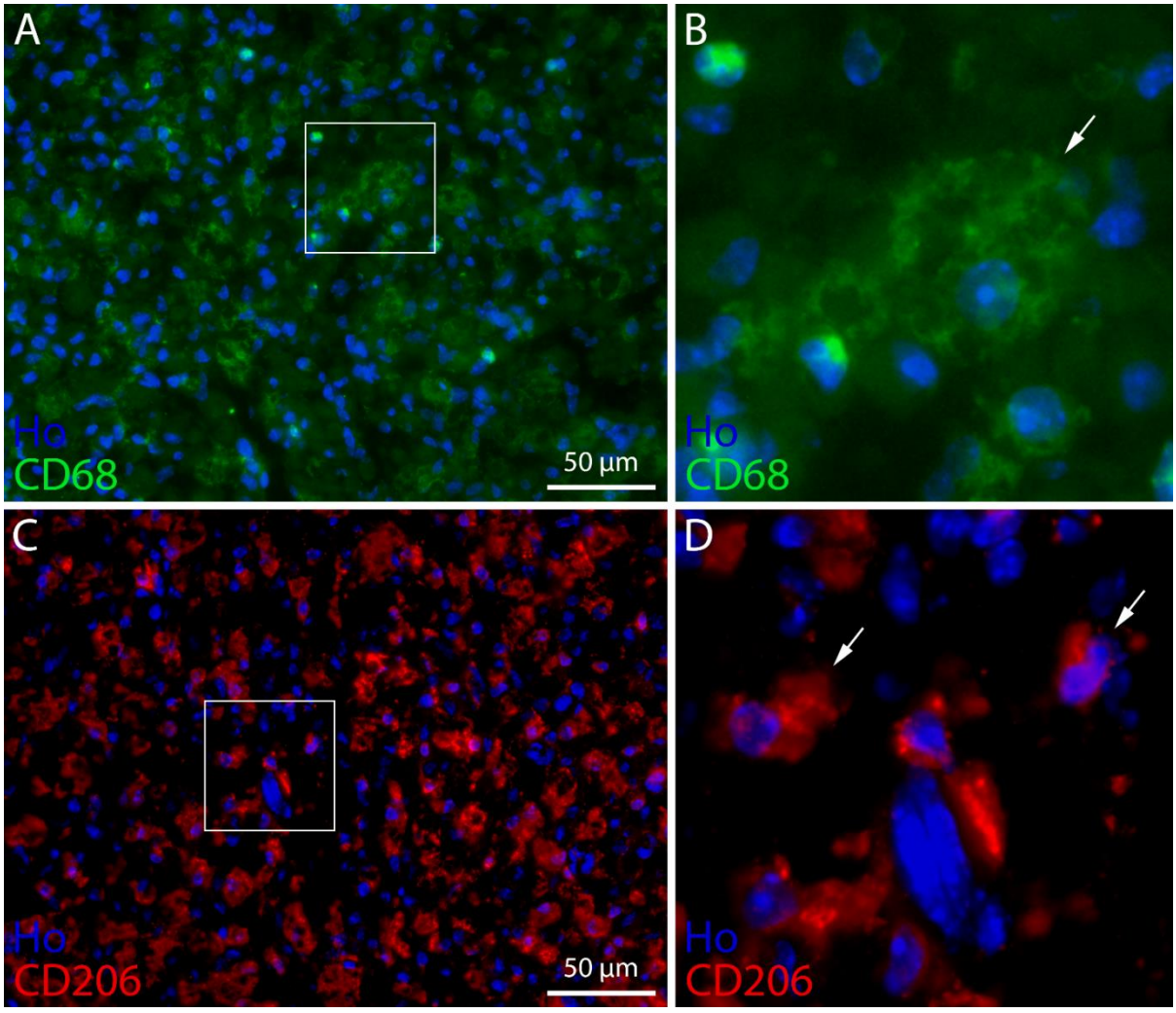

Figure 3.2.2: CD68+ and CD206+ cells were detected in two 21 dpi sciatic nerves of adult 3 month old NF2 sKO (P0-Cre+ NF2$^{fl/fl}$) mice. *Representative pictures of one of the two nerves are shown. A large number of CD68 or CD206 positive cells were detected. A and B display the CD68 positive cells in green. B shows enlarged area within white box in A. C and D display the CD206 positive cells within the same injured nerve in red. D shows enlarged image of white framed area in C. DNA dye Hoechst (Ho) marking all cell nuclei used as counterstain. White arrows mark some of the suspected macrophages. Scale bars in A and C = 50 µm within the two images. n = 4 mice. Representative images are shown.*

Given the strong background stain by the anti-CD68 antibody (see Figures 3.2.1 and 3.2.2 A), ways to improve the staining were explored. One possibility was to reverse the staining system, i.e. use a 2 layer stain for CD206 and a 3 layer for CD68 staining, as shown in Figure 3.2.3. A representative image of one of the stained 21 dpi NF2 sKO nerves is shown. Yet again, the staining was not significantly different from the two previous attempts. Large numbers of CD68+ CD206+ macrophages were detected once more. After comparing the two staining approaches it can be concluded that both of them resulted in staining of similar quality.

As mentioned before, due to the contrasting roles of anti-tumourigenic M1-like and pro-tumourigenic M2-like macrophages it would also be useful to have an antibody capable of recognizing an M1-like macrophage marker. Inducible nitric oxide synthase (iNOS) was chosen as M1-like marker (Jablonski *et al.*, 2015) to hopefully complement the already chosen M2-like marker CD206.

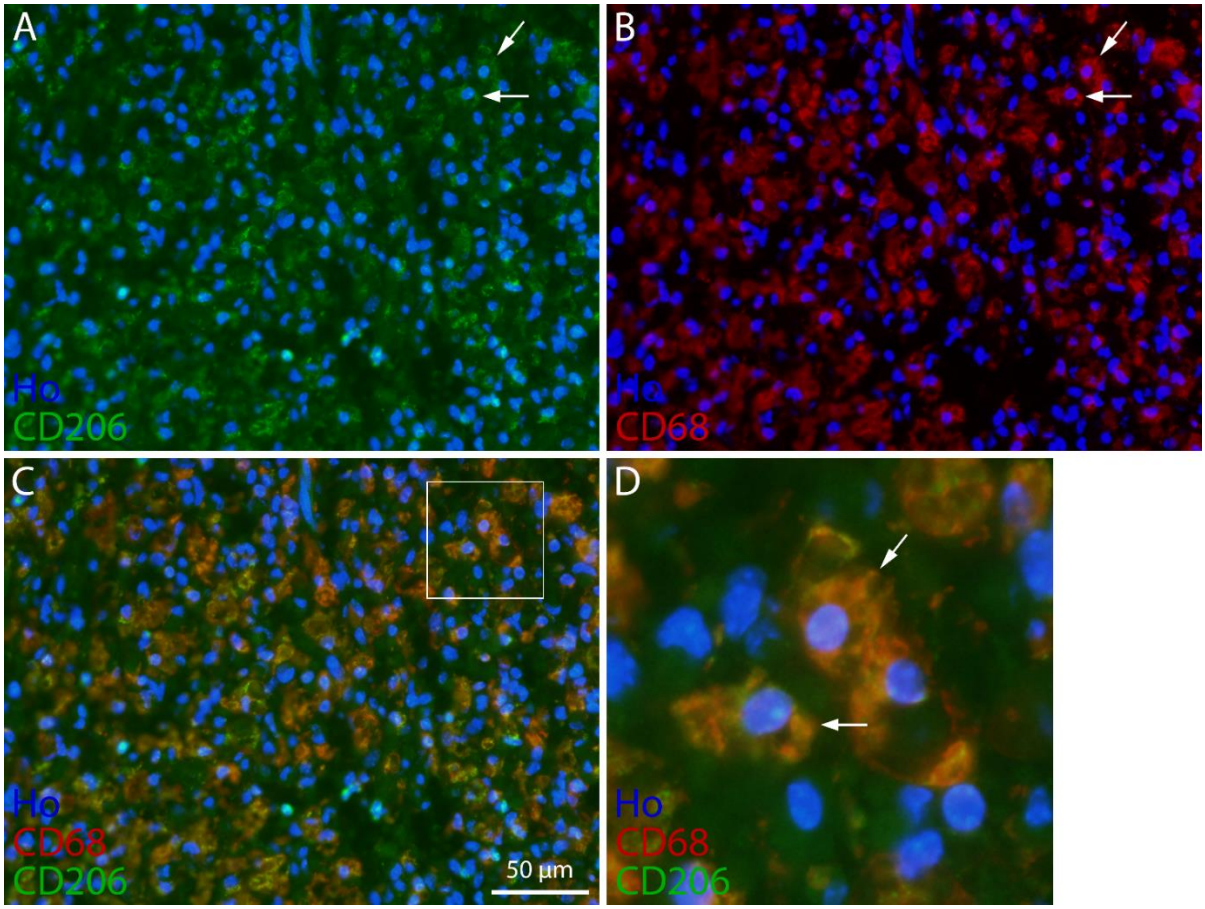

Figure 3.2.3: 3 layer CD68 and 2 layer CD206 double staining of a 21 dpi sciatic nerve of an adult 3 month old NF2 sKO (P0-Cre+ NF2$^{fl/fl}$) mouse *displayed similar results as before, exhibiting mostly M2-like macrophages in the injured nerve. A: CD206+ macrophages in green. B: CD68+ macrophages in red. C: CD206 and CD68 staining overlapping showing CD206+ CD68+ M2-like macrophages in orange. D: Zoomed in image of area in white box in A. Counterstain DNA dye Hoechst (Ho) used to mark cell nuclei. White arrows mark the same two CD68+ CD206+ macrophages in all 4 images. Scale bar in C = 50 µm in A, B and C. n = 2 mice. Representative images are shown.*

Testing the iNOS antibody on the sections of the 21 dpi NF2 sKO nerves, the iNOS staining appeared to be nuclear (Figure 3.2.4). Furthermore, not a single one of the macrophages appeared to be double positive for both CD68 (in green) and iNOS (in red). This could mean that either every single macrophage in the injured nerves was of the M2-like phenotype or that the iNOS staining did not work correctly. While it has been shown that nerve injury in wild type mice results in a shift towards an M2-like macrophage phenotype allowing improved neuroprotection/ repair (Ydens *et al.*, 2012) it is highly unlikely that every single macrophage in our NF2 sKO nerves would switch from M1-like to M2-like even 21 dpi, especially given that nerve repair does not take place in NF2 sKO nerves. Therefore, it was concluded that option 2, namely that the iNOS staining did not work as it should, was far more likely. The CD68 stain on the other hand was working well and on this occasion was quite distinct with minimal background (Figure 3.2.4 white arrows).

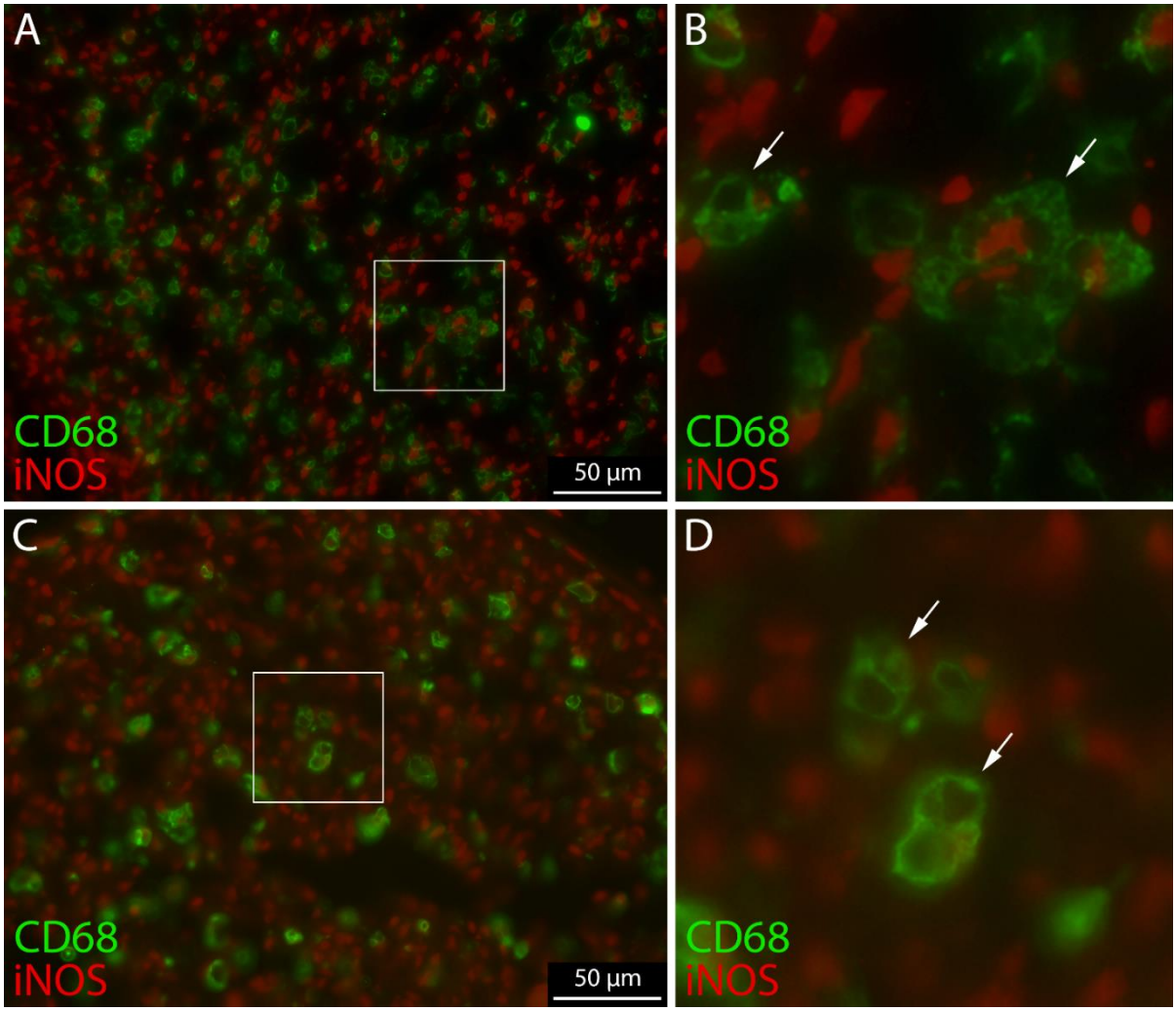

Figure 3.2.4: CD68 and iNOS double staining of four 21 dpi sciatic nerves of adult 3 month old mice *revealed nuclear iNOS stain. Representative images of one of the NF2 sKO (P0-Cre+ NF2$^{fl/fl}$) and one of the control (P0-Cre- NF2$^{fl/fl}$) nerves are shown. A and B: 21 dpi control sciatic nerve illustrating the CD68+ macrophages in green and the red, on this occasion exclusively nuclear iNOS stain. B shows enlarged image of white framed area in A. C and D: 21 dpi NF2 sKO nerve with green CD68+ macrophages and the red iNOS stain marking only cell nuclei. D shows enlarged picture of area enclosed by white box in C. On this occasion, Hoechst counterstaining was not included due to an oversight. White arrows show some of the CD68+ macrophages. Scale bars in A and C = 50 µm. n = 4 mice. Representative images are shown.*

To confirm that the iNOS antibody was functioning correctly it was tested on a positive control (Lowenstein *et al.*, 1993). Our positive control were cells from the RAW 264.7 macrophage cell line treated with lipopolysaccharides (LPS) at a final concentration of 100 ng/ml for 4 hours, kindly provided by former lab member Dr Patricia Woodley. LPS is generally found on the surface of Gram-negative bacteria and is a pathogen-associated molecular pattern which activates the innate immune response. It has been shown that the presence of LPS causes the expression of iNOS, an expression which can be strongly augmented by the combined treatment of LPS and IFN-γ (Lorsbach *et al.*, 1993; Lowenstein *et al.*, 1993; Stuehr & Marletta, 1985). Untreated cells of the same cell line were used as control (Figure 3.2.5).

Although there was some weak staining visible in the untreated controls (faint red staining in Figure 3.2.5 A and B), LPS-treated cells displayed a stronger, clearly cytoplasmic red iNOS staining surrounding the cell nuclei in blue. This proved that the antibody appeared to be working (red stain in Figure 3.2.5 C and D). When comparing the number of iNOS+ cells with the total number of cells it seems that only a small group (19 %) of macrophage cell line cells expressed iNOS after a 4 hour LPS treatment, a percentage which presumably would have increased with a longer LPS incubation period and/or possibly by using a higher concentration of LPS. Additionally, when comparing Figure 3.2.4 and Figure 3.2.5, it appeared that the iNOS antibody worked on the macrophage cell line but not on the frozen sections of the 21 dpi nerves. The reason for this is unknown.

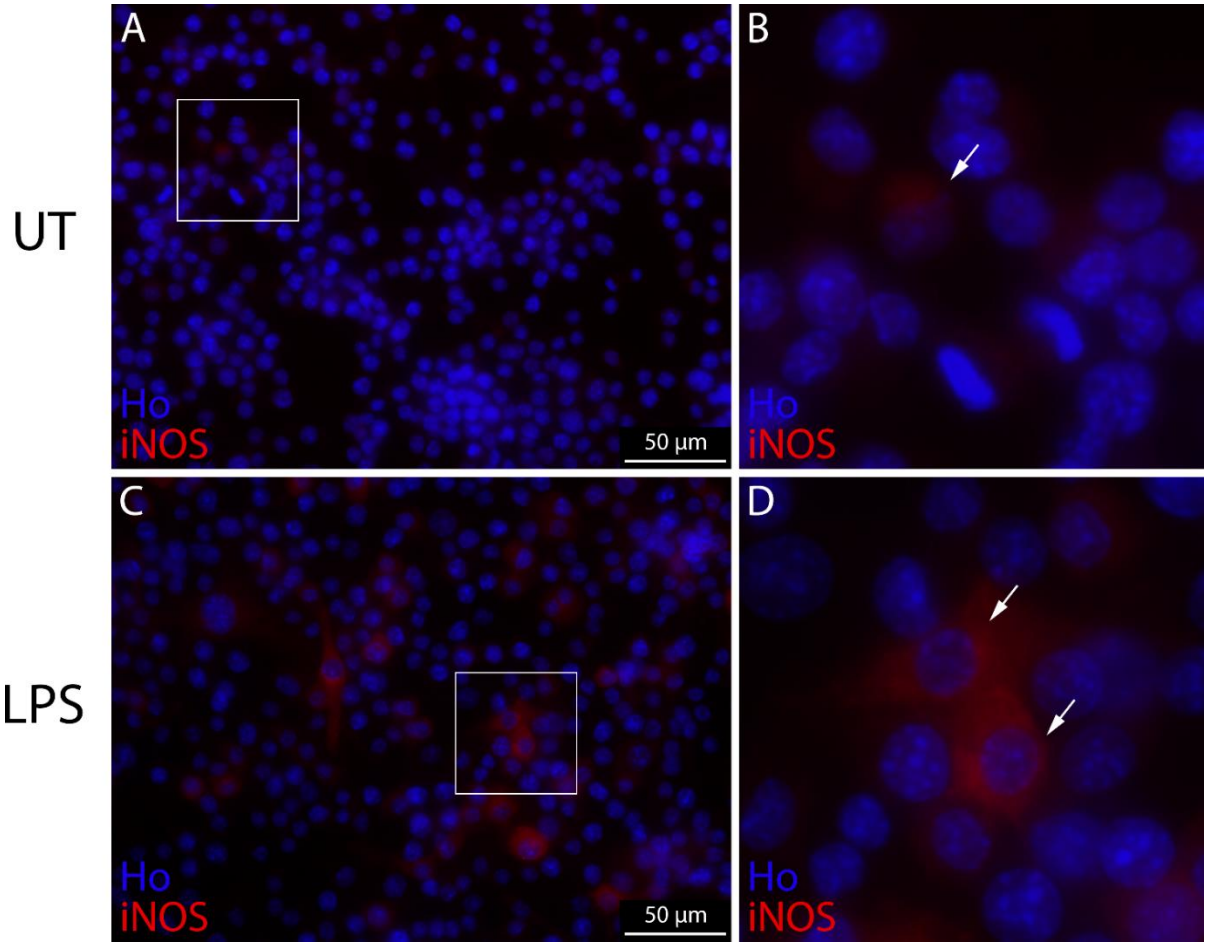

Figure 3.2.5: LPS-treated RAW 264.7 macrophage cells displayed cytoplasmic iNOS staining. *A and B: Untreated (UT) RAW 264.7 macrophage cells only showing a very faint iNOS staining. B displays enlarged image of area inside white frame in A. C and D: RAW 264.7 macrophage cells treated with lipopolysaccharides (LPS) at a final concentration of 100 ng/ml for 4 hours with a strong cytoplasmic iNOS stain. D shows area within white frame in C at greater magnification. Counterstaining with DNA dye Hoechst (Ho) marked cell nuclei. White arrows point out examples of iNOS positive macrophages. Scale bars in A and C = 50 µm in these two images. n = 3 replicate wells per treatment, n = 1 repeats. Representative images are shown.*

3.2.2 IHC staining for vascular marker CD31 and pan-macrophage marker Iba1

Aside from looking for macrophages we also wanted to see whether I would be able to visualize blood vessels in the sciatic nerves. If successful, that would allow us to detect blood vessels in the developing schwannomas in the Postn-Cre mouse model and compare the numbers of counted blood vessels between the different timepoints and genotypes.

There are some indications that the number/presence of macrophages in tumour nerve tissue and its vascularization are connected. It was shown that human schwannomas with great amounts of CD68+ cells had augmented microvessel densities. These higher microvessel densities correlated with both increased tumour size and tumour growth rate (de Vries *et al.*, 2012). It was also reported that microvessel densities and M2-like macrophage numbers were significantly higher in faster-growing vestibular schwannomas and also that schwannomas with higher M2-like macrophage counts contain higher microvessel densities (de Vries *et al.*, 2013). Furthermore, stronger concentrations of vascular endothelial growth factor (VEGF) and of one of its receptors (VEGFR-1) was linked to a faster tumour growth rate in vestibular schwannomas (Cayé-Thomasen *et al.*, 2005). Additionally, it was proven that macrophages are capable of inducing vascularization within the nerve bridge after cut injury by secreting VEGF-A into the nerve bridge (Cattin *et al.*, 2015).

Finally, in unpublished experiments from lab members, mice were intravenously injected (tail vein injection) with fluorescently labelled dextran after nerve injury. This was done to test whether the blood-nerve barrier remained intact in the injured nerve. A blood-nerve barrier disruption would allow the fluorescent dye dextran to leak from the circulatory system into the nervous tissue distal of the injury site causing fluorescence to be picked up in the nerve tissue after injury. Fluorescence detected in the nerve tissue confirmed that the blood-nerve barrier had indeed been broken after nerve injury. These experiments also revealed that new blood vessels were formed distal from the injury site and that a greater number of blood vessels was detected compared to the uninjured nerve.

Additionally, macrophages, more specifically tumour-associated macrophages (TAMs) have been shown to be involved in tumour angiogenesis and metastasis (Bonde *et al.*, 2012; Kessenbrock, Plaks & Werb, 2010; Murdoch *et al.*, 2008; Wyckoff *et al.*, 2007). Therefore, being able to stain for blood vessels would allow us to detect possible differences in vascularization in schwannomas between genotypes and possibly correlate those differences with distinct macrophage quantities between genotypes.

To that end, an anti-CD31 antibody marking endothelial cells was used on the 21 dpi P0-Cre-$NF2^{fl/fl}$ control and NF2 sKO sciatic nerves. Unfortunately, the CD31 stain was unsuccessful, coupled with strong background staining (data not shown). Therefore, I did not have a functioning CD31 antibody to be able to detect blood vessels/vascularization in tissue samples.

Since the original cryosections used previously (see previous figures) had run out another sciatic nerve crush experiment was performed on 3 P0-Cre+ $NF2^{fl/fl}$ (NF2 sKO) and 2 P0-Cre-

$NF2^{fl/fl}$ control mice. The 5 mice were subjected to sciatic nerve crush surgery and the injured sciatic nerves harvested 21 dpi. Since I had been trained for my Home Office personal license and signed off for sciatic nerve injury I performed the surgery myself. Using these new tissue sections, an antibody targeting an alternative pan-macrophage marker called ionized calcium-binding adapter molecule 1 (Iba1) was successfully tested on all 5 of the 21 dpi nerves (Figure 3.2.6). Given the much clearer Iba1 staining with little background both the CD68 and the Iba1 antibody presented viable choices to detect macrophages in frozen tissue sections.

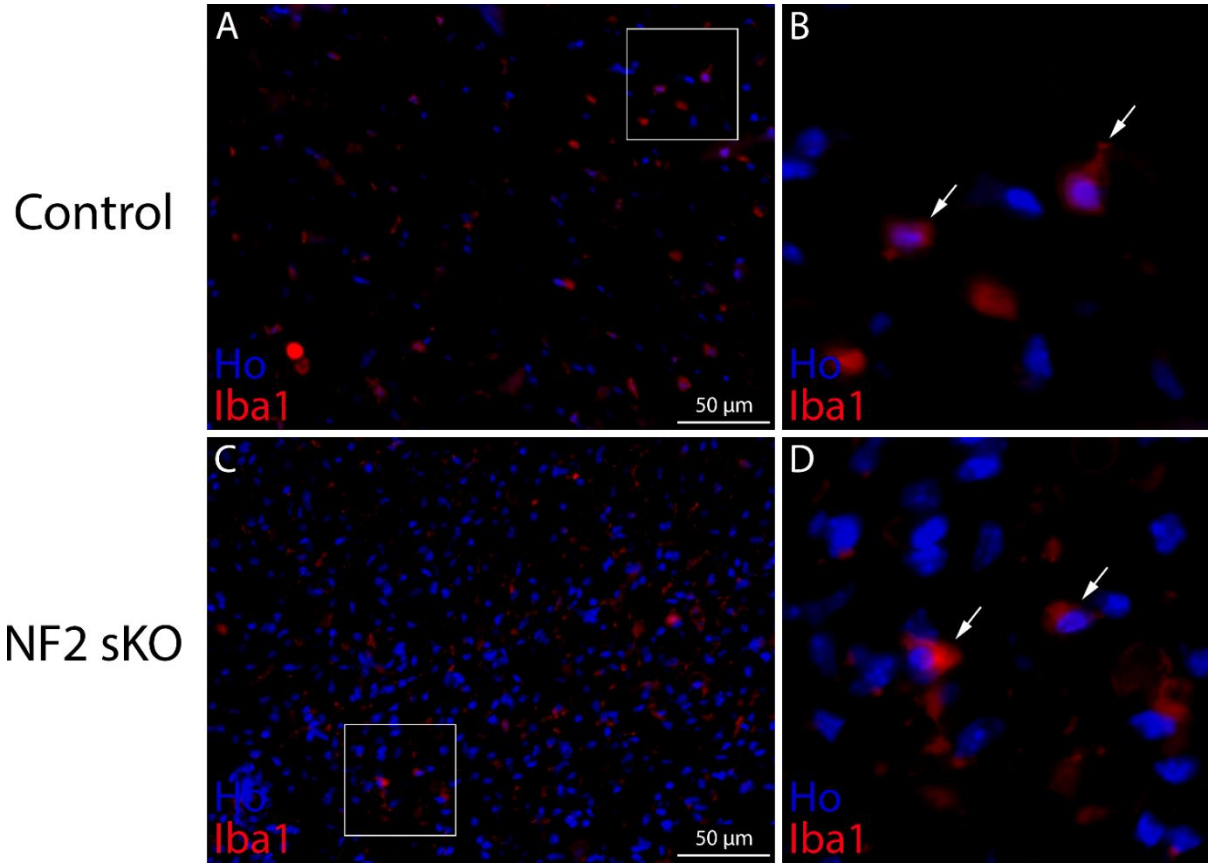

Figure 3.2.6: Iba1 staining of the 21 dpi sciatic nerve sections of five adult 5 month old mice *showed distinct Iba1 positive macrophages. Representative images of a control (P0-Cre- $NF2^{fl/fl}$) nerve (A, B) and a NF2 sKO (P0-Cre+ $NF2^{fl/fl}$) nerve (C, D). A and B: Control 21 dpi sciatic nerve displaying Iba1-stained macrophages. B shows magnified view of area within white box in A. C and D: NF2 sKO 21 dpi sciatic nerve with macrophages with Iba1 staining. D shows enlarged image of white framed area in C. DNA dye Hoechst (Ho) was used to detect all nuclei. White arrows in panels B and D mark some of the Iba1 positive macrophages. Scale bar in A and C = 50 µm in these two images. n = 2 mice for each genotype (Control and NF2 sKO). Representative images are shown.*

In summary, several antibodies were tested on frozen sections to determine their functionality (Figures 3.2.1 – 3.2.6). Unfortunately, some of the antibodies did not appear to work well under the described conditions (see Materials and Methods section 2.4.2.1). The CD31 antibody was unable to pick up any blood vessels while in tissue sections the iNOS antibody only ever showed a nuclear staining (Figure 3.2.4) which, given the published literature, seems rather unconvincing. Thankfully, the CD68 antibody (Figures 3.2.1 – 3.2.4),

the CD206 antibody (Figures 3.2.1 – 3.2.3) and the Iba1 antibody (Figure 3.2.6) displayed reliable staining. Furthermore, it could be concluded that using the Iba1 antibody was a more reliable way to detect macrophages than the CD68 antibody (Figures 3.2.6, 3.4., 3.9.2, 3.93 and 3.11.2).

3.3 Sciatic nerve crush experiment with F1 generation of Postn-Cre mice

Having bred the mice to the intermediate state (F1 generation, see Figure 3.1) some of them were used for a sciatic nerve crush experiment. Schulz et al. (Schulz *et al.*, 2016) published a paper showing that the previously reported impaired repair after nerve injury due to a loss of both wild type copies of NF2 in Schwann cells can also be achieved by the deletion of one wild type copy of NF2 in both Schwann cells and peripheral nerve axons. This genotype also increased the likelihood of tumour formation after injury compared to the aforementioned traditional mouse model with biallelic NF2 loss in Schwann cells (Schulz *et al.*, 2016). Since it was not yet confirmed that the Postn-Cre promoter is only active in Schwann cells and not in neurons as well (Helen Morrison personal communication), it is conceivable that Postn-Cre positive animals of the F1 generation ($NF2^{wt/fl}$) have lost one copy of NF2 in both Schwann cells and neurons, possibly causing a repair deficiency similar to what was described in the paper (Schulz *et al.*, 2016). To test that, I performed sciatic nerve crush injury on 3 Postn-Cre- $NF2^{wt/fl}$ (= control), 3 Postn-Cre+ $NF2^{wt/fl}$ (= heterozygous/monoallelic for NF2) and 3 P0-Cre+ $NF2^{fl/fl}$ (= NF2 sKO). 23 days post injury (23 dpi) tibial nerves of the injured and uninjured sides of adult 2 month old animals were dissected and fixed in glutaraldehyde. The 23 dpi timepoint was chosen since it has been established that 3 weeks after nerve injury, repairs in genetically unmodified mice are completed. At this point in time one would be able to clearly see any possible differences in repair capabilities between control and knockout mice. Furthermore, tibial nerves were chosen to be examined in semithin sections because a) sciatic nerves was already being used for frozen sections IHC staining and b) tibial nerves were distal from the nerve crush injury site meaning they had already undergone axon and myelin sheath degeneration (part of Wallerian degeneration) and subsequent axon regrowth and remyelination 3 weeks after the crush injury. As mentioned before, this would allow us to determine obvious nerve repair deficiencies when comparing the three genotypes.

The fixed tibial nerves were handed over to Glenn Harper of the EM unit at Plymouth University, who proceeded to embed them, cut semithin sections and stain some of those sections with methylene blue which detects myelin in the nerve sheath. Unfortunately, one of the WT samples was lost during processing. The sections were imaged under the Leica IM8 microscope (Figures 3.3.1 - 3.3.3). Eventually, the images were quantified using ImageJ and Microsoft Excel and tested for statistical significance using GraphPad Prism 9 (Figure 3.3.4).

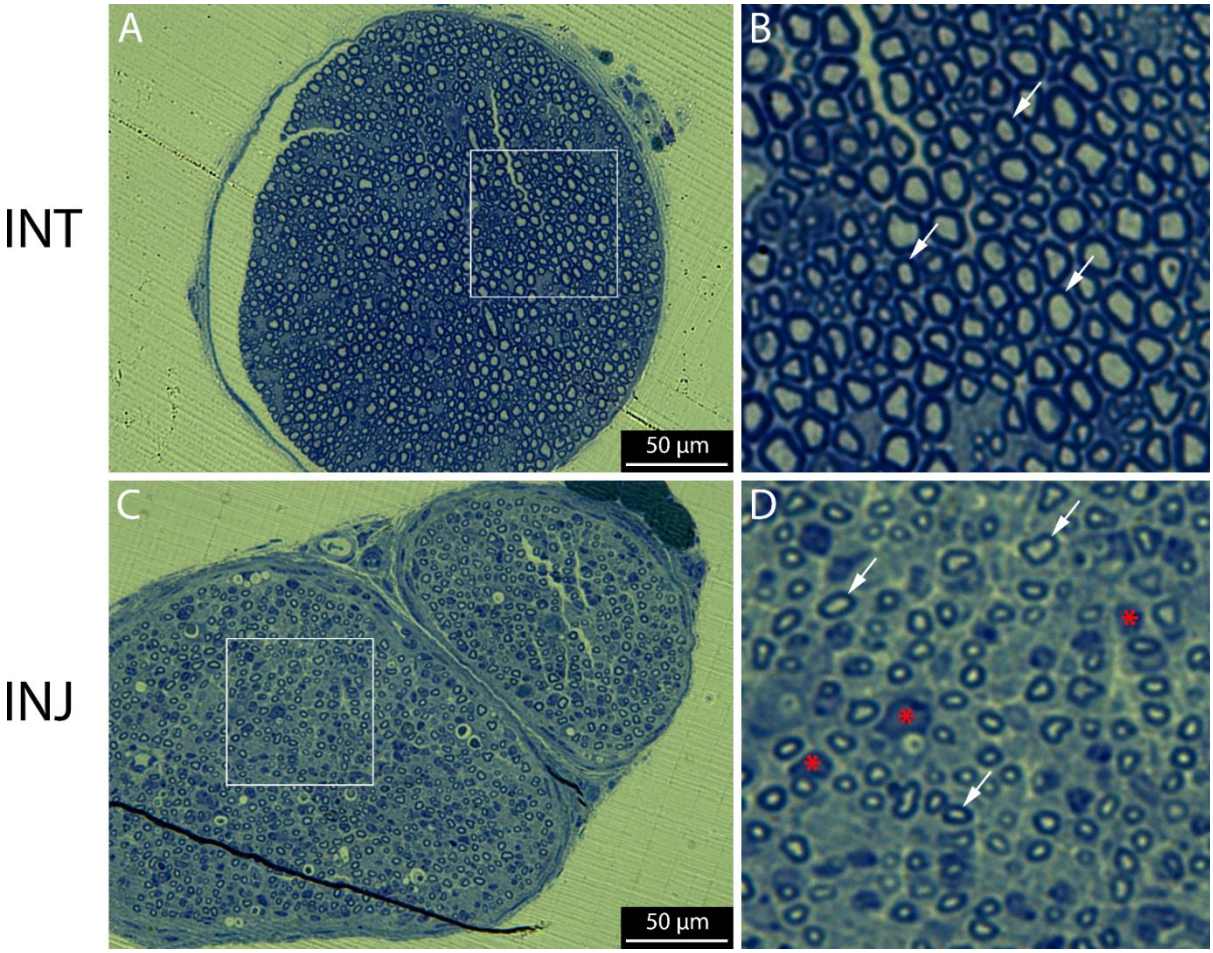

Figure 3.3.1: Semithin sections of intact (INT) and injured (INJ) tibial control (Postn-Cre- NF2$^{wt/fl}$) nerves of adult 2 month old 23 dpi stained with methylene blue *showed a large number of myelinated axons (INT) or remyelinated axons (INJ)**.** A and B: Intact control nerve with myelinated axons stained blue by methylene blue. B shows enlarged image of area encompassed by white frame in A. C and D: Injured control nerve 23 dpi with methylene blue stained remyelinated axons. D displays magnified image of area within white box in C. White arrows point to myelinated and remyelinated axons, respectively, red asterisks (*) mark what appear to be Schwann cell nuclei. Scale bars in A and C = 50 µm in both images. n = 2 mice. Representative images are shown.*

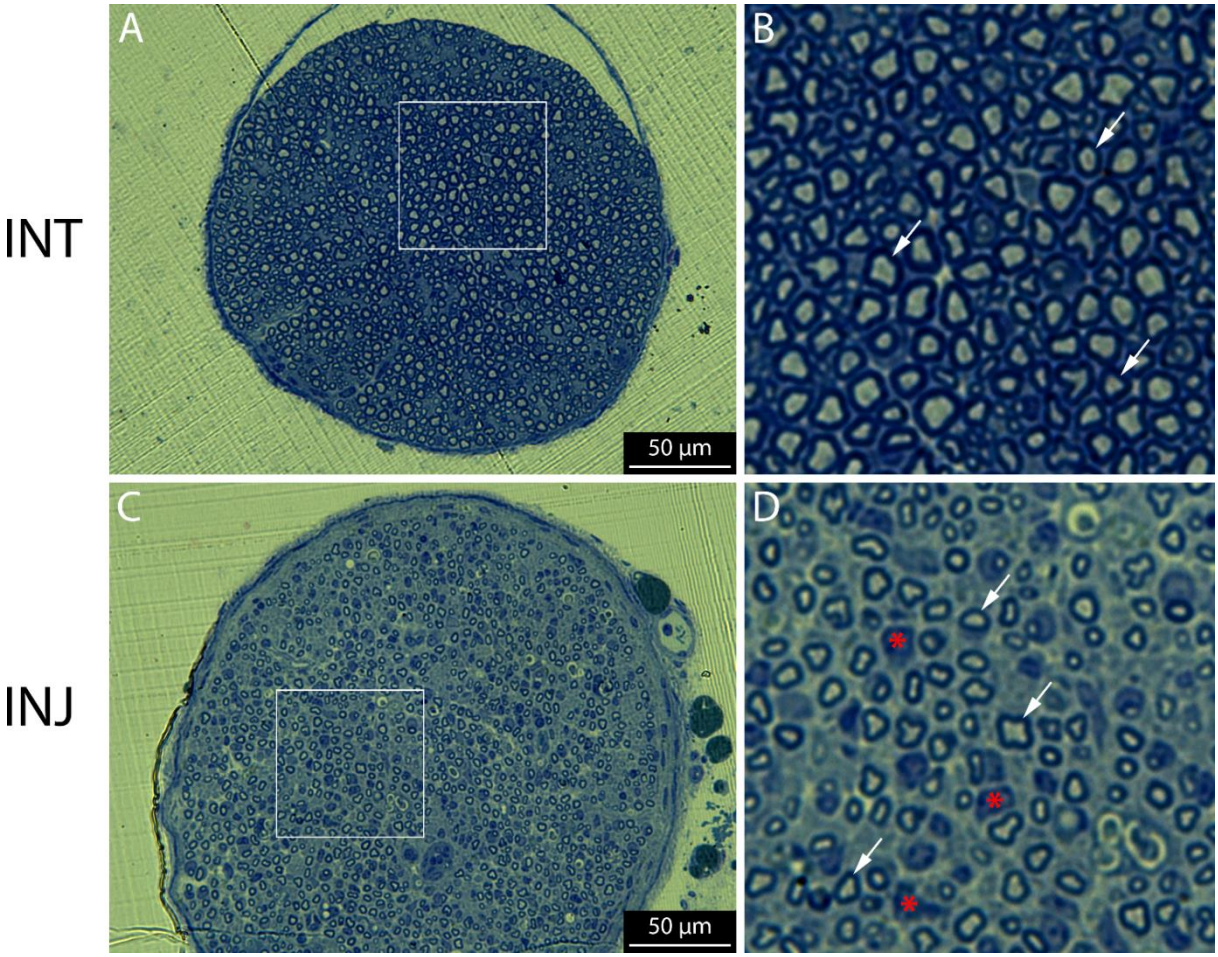

Figure 3.3.2: Semithin sections of intact (INT) and injured (INJ) tibial nerves of the Postn-Cre+ NF2$^{wt/fl}$ (= monoallelic for NF2) adult 2 month old mice 23 dpi stained with methylene blue *displayed large amounts of myelinated axons (INT) or remyelinated axons (INJ). A and B: Intact monoallelic NF2 (only one intact NF2 allele) tibial nerves with methylene blue stained myelinated axons. B shows enlarged image of white framed area in A. C and D: Injured monoallelic NF2 (with only one intact NF2 gene) tibial nerves with remyelinated axons stained with methylene blue. D displays magnified view of area within white box in C. White arrows show myelinated and remyelinated axons, respectively, red asterisks (*) mark what are assumed to be Schwann cell nuclei. Scale bars in A and C = 50 µm in both images. n = 3 mice. Representative images are shown.*

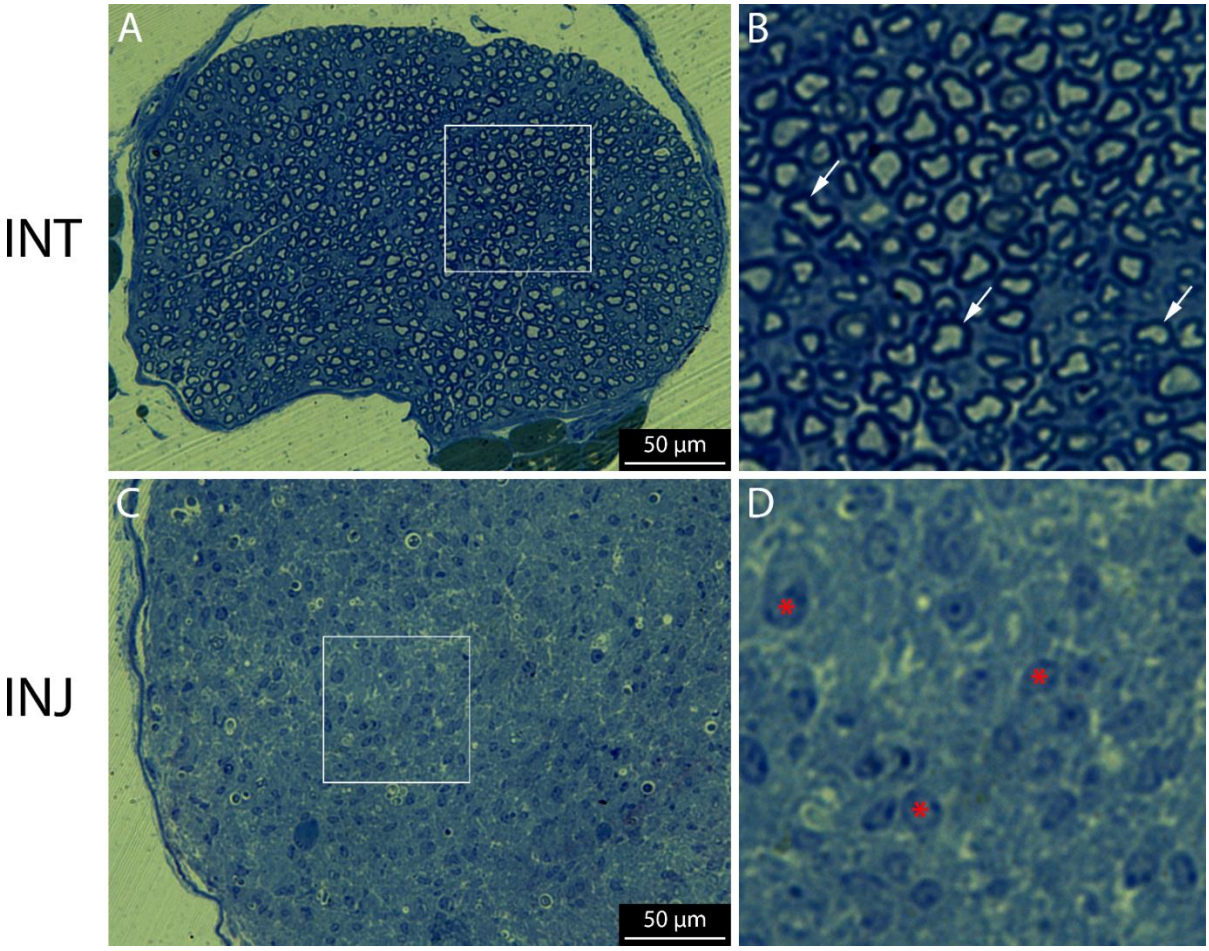

Figure 3.3.3: Semithin sections of intact (INT) and injured (INJ) tibial nerves of the P0-Cre+ NF2$^{fl/fl}$ (NF2 sKO) adult 2 month old mice 23 dpi stained with methylene blue *revealed a large difference in numbers of myelinated axons (INT) compared to remyelinated axons (INJ). A and B: Intact NF2 sKO nerve 23 dpi containing large numbers of methylene blue stained myelinated axons. B depicts area framed by white box in A in greater magnitude. C and D: Injured NF2 sKO nerve apparently without any visible remyelinated axons 23 dpi (even though thinly remyelinated axons were found by others (Mindos et al., 2017)). D shows enlarged image of area within the white square in C. White arrows point out myelinated axons, red asterisks (*) mark what appear to be Schwann cell nuclei. Scale bars in A and C = 50 µm in both images. n = 3 mice. Representative images are shown.*

In order to determine whether there was any difference in repair capacity after injury between the three genotypes, the numbers of myelinated axons were counted using ImageJ and the resulting data was illustrated as a bar chart and analysed with GraphPad Prism 9 software (Figure 3.3.4). Surprisingly, P0-Cre+ NF2 sKO tibial nerves on the injured side had no visible myelinated axons showing an almost complete lack of nerve repair (see Figure 3.3.3 INJ C and D). Mindos et al. (Mindos *et al.*, 2017) showed a similar defect in sciatic nerve repair 21 dpi but they detected some thinly myelinated axons in the repaired NF2 sKO nerves. The P0-Cre driven NF2 sKO nerves on the contralateral uninjured side (Figure 3.3.3 INT A and B), the control nerves (Figure 3.3.1 A-D) and the Periostin-Cre+ NF2$^{wt/fl}$ nerves of both injured (Figure 3.3.2 C and D) and uninjured sides (Figure 3.3.2 A and B) displayed similar numbers of myelinated or remyelinated axons, respectively. Statistical analysis revealed that there was no significant difference in counts of myelinated and remyelinated axons when comparing intact and injured nerves in control and monoallelic NF2 mice (p-values: Control intact vs.

injured = 0.70; Monoallelic NF2 intact vs. injured = 0.11) and a significant difference in myelinated and remyelinated axon numbers between intact and injured nerves in NF2 sKO animals as expected ($p < 0.001$) (Figure 3.3.4). Therefore, monoallelic NF2 nerves displayed no visible phenotype.

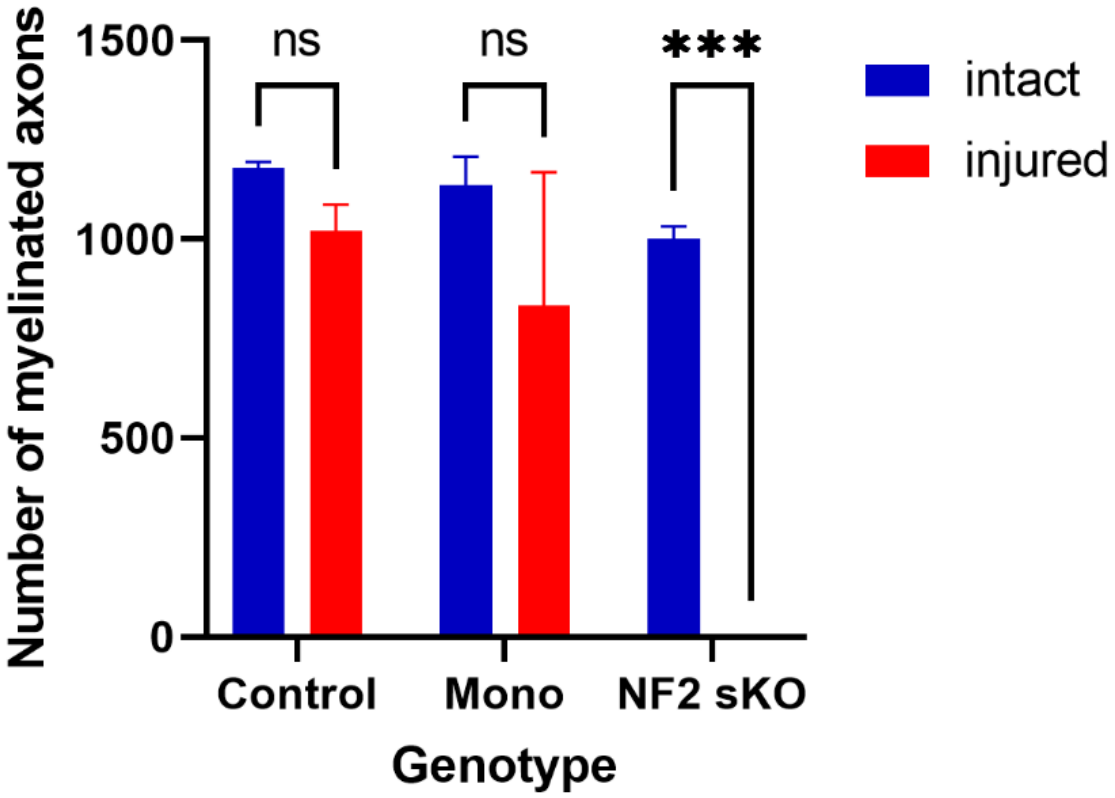

Figure 3.3.4: Quantification of counted myelinated/remyelinated axons in tibial nerves of adult 2 month old mice 23 dpi *revealed a significant difference between the injured (INJ) and intact (INT) NF2 sKO (P0-Cre+ NF2$^{fl/fl}$) nerves ($p < 0.001$). No significant (ns) change in myelinated axon numbers between intact and injured nerves of control (Postn-Cre- NF2$^{wt/fl}$) and monoallelic NF2 (Postn-Cre+ NF2$^{wt/fl}$) mice. Graph shows number of myelinated/remyelinated axons as means ± SD tested for significance using two-way ANOVA with Šídák's multiple comparisons test. * $p \leq 0.05$; ** $p \leq 0.01$; *** $p \leq 0.001$. n = 2 for control mice, n = 3 for the monoallelic NF2 mice and the NF2 sKO mice.*

In short, the sciatic nerve crush experiments (Figures 3.3.1 - 3.3.3) on Postn-Cre- NF2$^{wt/fl}$ (control), Postn-Cre+ NF2$^{wt/fl}$ and P0-Cre+ NF2$^{fl/fl}$ (NF2 sKO) revealed that the loss of a single NF2 copy while retaining a functioning intact NF2 copy did not have a significant effect on repair efficiency after nerve crush injury (Figure 3.3.4).

Therefore, the repair deficiency effects seen when only one WT NF2 gene copy remains in both Schwann cells and peripheral nerve axons (Schulz *et al.*, 2016) could not be replicated. This suggests that the Periostin promoter and thereby Periostin-Cre is not active in neurons, causing the neurons to retain both of their NF2 gene alleles.

In order to confirm this hypothesis, one possibility would be to cross Postn-Cre+ mice with a mouse strain carrying a modified Rosa26 locus. This Rosa26 locus contains a ubiquitous CAG promoter and a fluorescent protein gene which is interrupted by a floxed STOP cassette (Madisen *et al.*, 2010). In these Postn-Cre+ Rosa26 locus mice, only in Postn-Cre expressing cells the STOP cassette would be removed, resulting in the expression of the fluorescent protein. This would allow a visible distinction between Postn-Cre+ (= fluorescent) and Postn-Cre- (= non-fluorescent) cells in these mice, making it simple to determine if Postn-Cre and therefore the Periostin promoter is active in neurons. Such a mouse cross has been done using Rosa26 tdTomato (an intensely red fluorescent protein) mice. This allowed Amy Hewitt of our lab to observe a lack of red fluorescence in the neurons of DRGs, confirming the absence of expressed Postn-Cre and thereby Periostin promoter activation in these neurons (Laraba *et al.*, 2022).

3.4 IHC staining for Iba1 in xenograft meningioma

With the mouse breeding (Figure 3.1) still in progress we decided to test our chosen Iba1 antibody further. We aimed to see if, after detecting murine macrophages in the mice sciatic nerves, the Iba1 antibody would also be able to identify murine macrophages in murine xenograft meningioma tumours. These xenograft meningioma tumours in immunocompromised mice can be created by planting human meningioma cell line cells into various parts of the mouse skull, e.g. the skull convexity (Michelhaugh *et al.*, 2015; Pachow *et al.*, 2013; Tuchen *et al.*, 2017) and skull base (Burns *et al.*, 2013; Chow *et al.*, 2015). Professor Christian Mawrin, our collaborator from Otto-von-Guericke University in Magdeburg, Germany, and his group use IOMM-Lee cells (Lee, 1990) implanted in the skull convexity for their xenograft meningioma mouse model (Pachow *et al.*, 2013; Tuchen *et al.*, 2017). They kindly send us paraffin blocks with both xenograft meningioma tumours, consisting of genetically unmodified IOMM-Lee cells or IOMM-Lee cells with a K409Q mutation in the KLF4 gene (2 blocks each). The paraffin blocks were then cut, stained and imaged by the Cellular and Anatomical Pathology Department of Derriford Hospital. The IHC staining was performed using the anti-Iba1 antibody we provided.

Figure 3.4 shows representative images of the Iba1 stained xenograft meningioma paraffin sections. One of the xenograft meningioma tumours formed by IOMM-Lee cells with a K409Q mutation in the KLF4 gene (top row, top KLF4 K409Q) showed a strong, local aggregation of Iba1 positive cells. This was not seen neither in the other xenograft meningioma made by IOMM-Lee cells with the same genotype (bottom row, bottom KLF4 K409Q) nor in the xenograft meningioma comprised of genetically unmodified wild type IOMM-Lee cells (middle row, WT). Both of these xenografts contained lesser amounts of Iba1 positive macrophages which were more widely distributed. Therefore, I could ascertain that the Iba1 antibody could indeed reliably identify Iba1 positive cells in xenograft meningiomas in mice. Furthermore, the Iba1 antibody proved to be functional in formalin fixed paraffin embedded (FFPE) sections as well. In general, there also did not appear to be a visible difference in macrophage numbers between WT and KLF4 K409Q IOMM-Lee xenograft meningiomas. Finally, I was told that these

IOMM-Lee xenograft meningiomas contained far less macrophages than one would routinely find in human meningioma samples (David Hilton, personal communication).

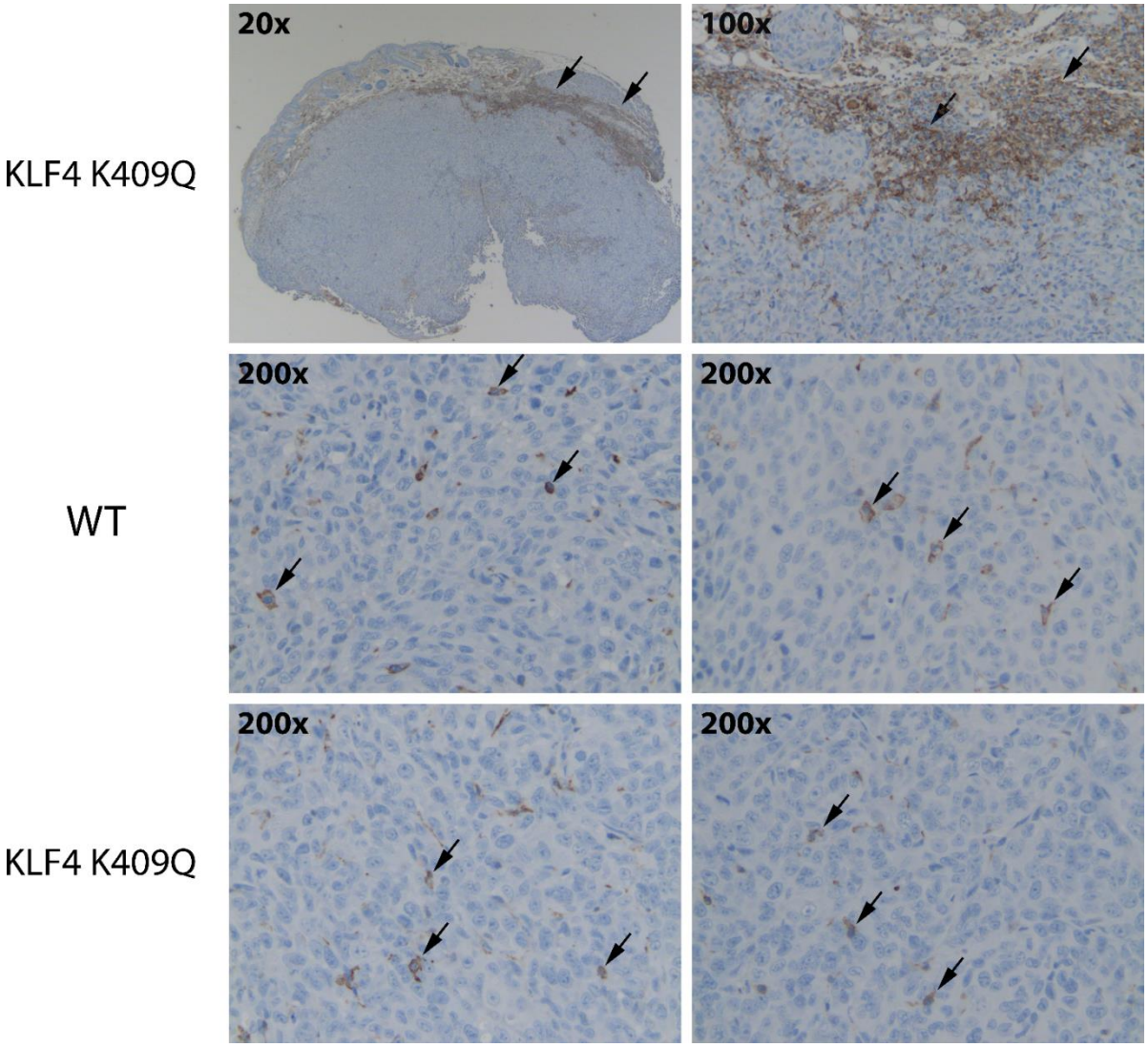

Figure 3.4: Iba1 positive cells were found within the IOMM-Lee derived xenograft meningioma. *Genetically unmodified (wild type, WT) and modified (KLF4 K409Q) IOMM-Lee cells were planted in the skull convexity of immunocompromised mice to grow xenograft meningioma tumours. Once extracted, they were formalin fixed and paraffin embedded (FFPE). Paraffin blocks were then cut, stained with our anti-Iba1 antibody and the DNA dye DAPI and imaged. Top row (top KLF4 K409Q): Xenograft meningioma formed by IOMM-Lee cells with K409Q mutation in KLF4 gene exhibiting large accumulation of Iba1 positive cells at 20x and 100x magnification. Middle row (WT): Xenograft meningioma comprised of genetically unmodified IOMM-Lee cells containing widely dispersed, few Iba1 positive macrophages at 200x magnification. Bottom row (bottom KLF4 K409Q): Second xenograft meningioma made by KLF4 K409Q IOMM-Lee cells lacked macrophage accumulation, showing similar distribution and Iba1 positive macrophage numbers to WT. DNA dye DAPI was used to mark all cell nuclei. Black arrows mark examples of Iba1 positive cells. Magnification shown in top left corner of each image. n = 2 xenograft meningioma per genotype. Representative images are shown.*

3.5 Genotyping of Postn-Cre driven mice colonies

After the mouse breeding (Figure 3.1) was completed I sought to determine whether the Postn-Cre gene primers recommended by the Gehlhausen paper (Gehlhausen *et al.*, 2015) or the Postn-Cre gene primers used by the Genome Editing and Embryology Core, Biological Services division of King's College London (original supplier of the Postn-Cre carrying mice, see Table 2.10 for primer sequences) provided better results. To that end, I used the primers from both sources under same conditions (reagents, PCR program etc.) to genotype the same mice to be able to adequately compare the performance of both primers.

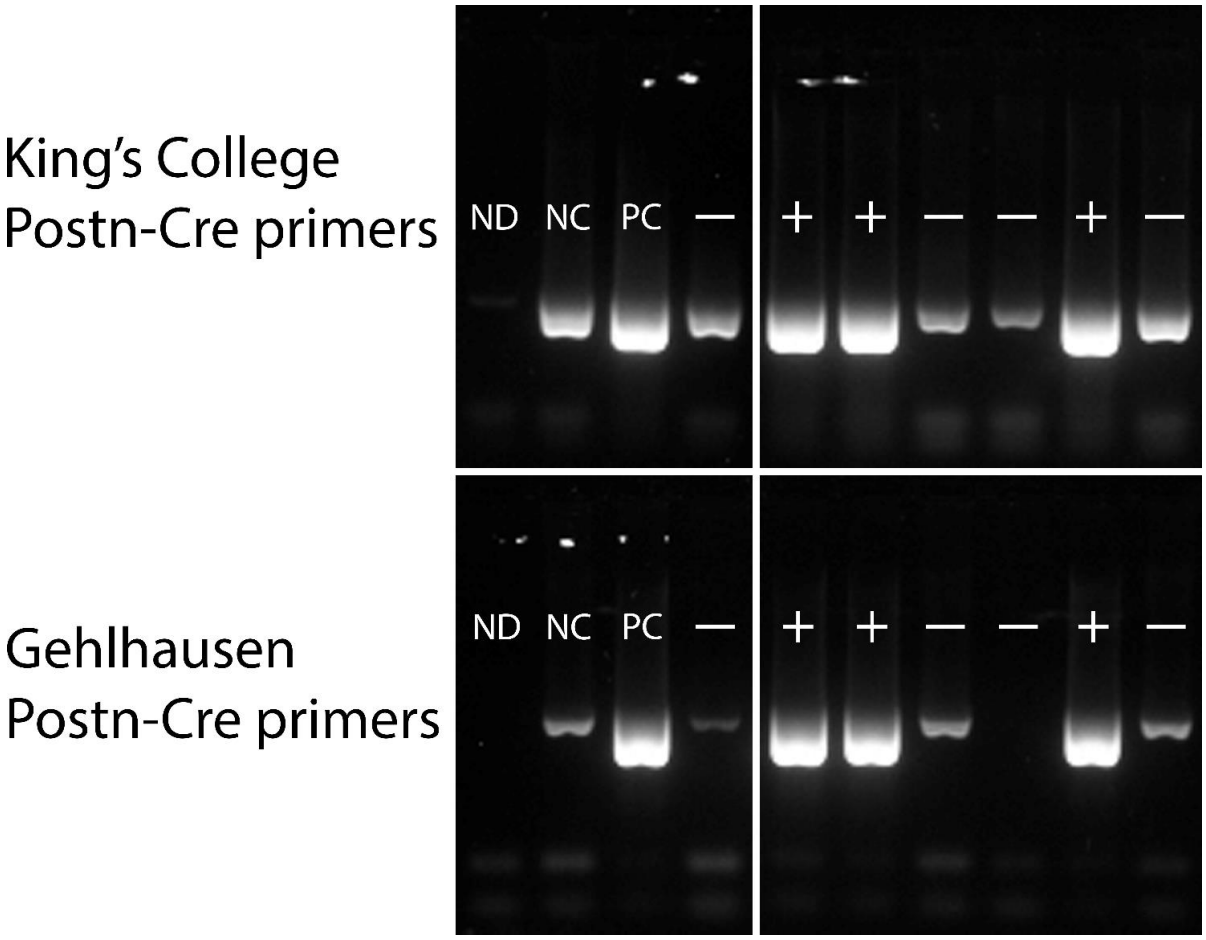

Figure 3.5.1: In direct comparison, genotyping with the Gehlhausen primers resulted in clearer differences between Postn-Cre+ and Postn-Cre- samples than using the King's College primers. *King's College Postn-Cre primers: faint band in the No DNA control (ND), distinct band in the Postn-Cre- control (NC). Strong bands in Postn-Cre+ control (PC) and the Postn-Cre+ (+) samples. Distinct bands in the Postn-Cre- (-) samples. Gehlhausen Postn-Cre primers: no band in the ND, faint band in the NC sample. Strong bands in the PC and + samples. Faint or no bands in the – samples. n = 1 experimental repeats.*

Genotyping with the King's College primers displayed a faint band in the No DNA control (ND) and a strong band in the Postn-Cre- control (NC) while the Gehlhausen primers did not show a band in the ND column and the band seen in the NC was fainter and appeared unspecific (Figure 3.5.1).

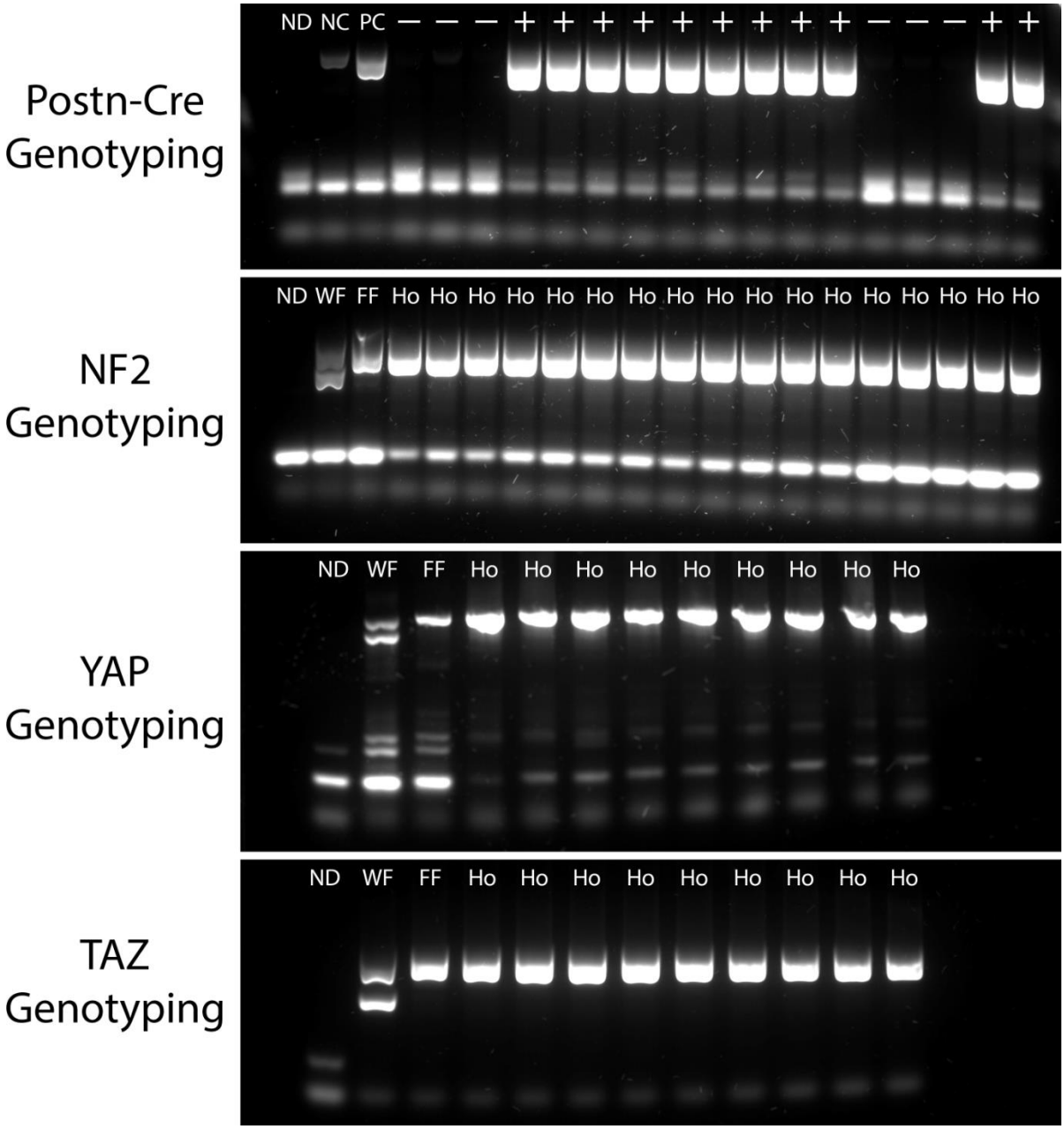

Figure 3.5.2: Examples of Postn-Cre, NF2, YAP and TAZ genotyping of mouse tail snips confirming the $^{flox/flox}$ background of the Postn-Cre driven mouse colonies. *General appearance of genotyping samples run on an agarose gel with controls and tail snip samples. Postn-Cre (top row, from left to right): No DNA control (ND), Postn-Cre- control (NC), Postn-Cre+ control (PC), Postn-Cre- (-) samples and Postn-Cre+ (+) samples. NF2, YAP and TAZ genotyping (other three rows, left to right): ND, one wild type allele and one floxed allele control (WF), both alleles floxed control (FF), both alleles floxed/homozygous (Ho) samples.*

Usage of either primer pair resulted a similarly strong bands for the Postn-Cre+ control (PC) and the samples derived from Postn-Cre+ mice (+). The main difference between the two primer pairs seemed to be found in the samples of the Postn-Cre- mice (-). The distinction between Postn-Cre+ and Postn-Cre- samples was clearer with the Gehlhausen primers compared to the King's College primers with which it was sometimes uncertain if a given sample was Postn-Cre+ or - (e.g. the first sample from the right). Therefore, I decided to

continue to use the Gehlhausen primers as before since they provided clearer genotyping results.

Soon after the Postn-Cre cell lines were fully established, i.e. there were only double floxed ($^{fl/fl}$) animals in the colony causing mouse breeding to always result in $^{fl/fl}$ offspring, mice which were not used to sample collection were only genotyped for Postn-Cre+ or - status. The mice whose tissue was taken for IHC staining were also genotyped for NF2 and furthermore YAP or TAZ if they were from the NF2/YAP or NF2/TAZ dKO colonies. This final confirmation of genotype was derived using tail snip samples from the corresponding tissue donor mice (see Materials and Methods section 2.3.2). An example of such a genotyping is shown in Figure 3.5.2. For the Periostin-Cre genotyping, the same controls as before (Figure 3.5.1) were always used, namely a No DNA control (ND), a Postn-Cre- control (NC) and a Postn-Cre+ control (PC). The additional genotyping for NF2 or YAP or TAZ as necessary were set up in a similar manner with the usage of 3 controls. First, the No DNA control (ND) without any DNA. Second, the $^{wt/fl}$ control (WF) which was a sample from a mouse which had one wild type allele and one allele where the part of the gene in question was flanked by flox sites. This would allow us to see two bands, one for each allele, which were used to determine the height in which the $^{fl/fl}$ bands should run. The third control, the $^{fl/fl}$ control (FF), was used for the same purpose and was originally derived from an animal whose two alleles both contained the floxed version of the gene in question. Both the existence of only a single band and the position of both WF and FF controls then permitted us to confirm the $^{fl/fl}$/homozygous (Ho) nature of the respective gene.

3.6 Transmission electron microscopy of NF2 sKO sciatic nerves

As seen in Figure 3.3.4, I did not observe a significant difference between the number of remyelinated axons in injured tibial nerves and the number of myelinated axons in uninjured/intact tibial nerves of monoallelic NF2 mice. Therefore, in a last attempt to spot phenotypical differences, we wanted to investigate whether uninjured sciatic nerves from Postn-Cre driven NF2 sKO mice would show any morphological anomalies when inspected under an electron microscope. As mentioned before, until now NF2 sKO referred to P0-Cre+ $NF2^{fl/fl}$ mice. From this moment forth, NF2 sKO equals Postn-Cre+ $NF2^{fl/fl}$ mice. We dissected the intact sciatic nerves of two adult 3 week old NF2 sKO mice and fixed them in glutaraldehyde. Afterwards, the fixed nerves were handed over to Glenn Harper of the EM unit at Plymouth University who proceeded to embed the nerves and cut ultrathin sections. These were then viewed under a transmission electron microscope (TEM, Figure 3.6).

Once more, phenotypical changes could not be detected. The large diameter axons (Ax) wrapped by thick myelin sheaths (Ms), small diameter axons (ax) and Schwann cells (Sc) appeared normal after visual scrutinisation.

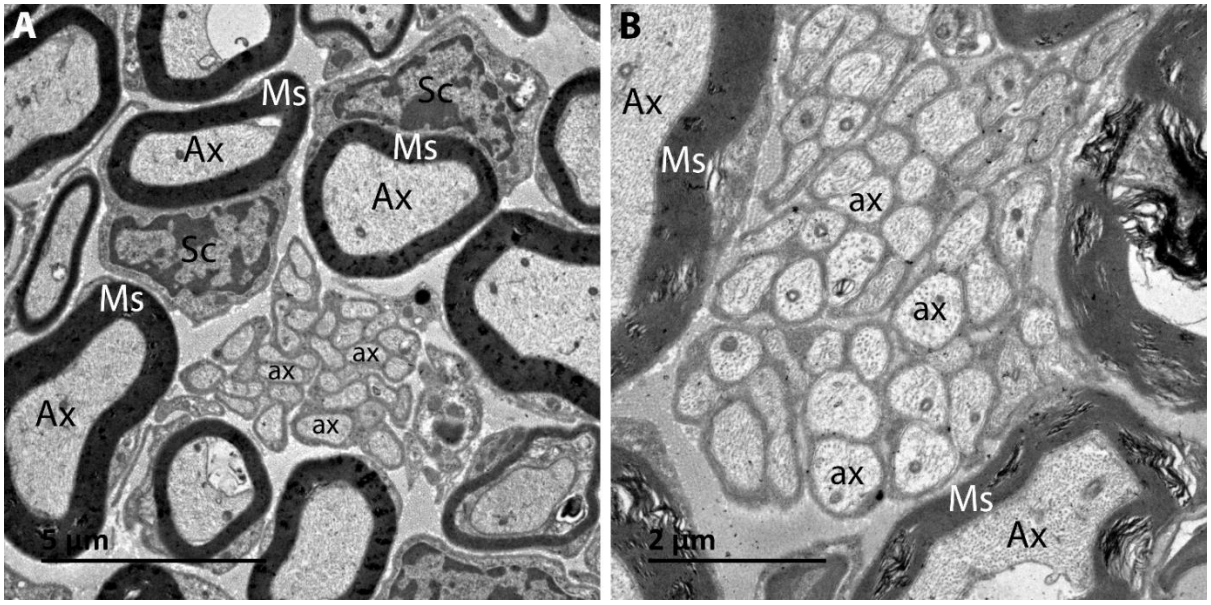

Figure 3.6: Ultrathin sections of Postn-Cre driven NF2 sKO sciatic nerves stained with uranyl acetate and Reynold's lead citrate under a transmission electron microscope (TEM) *revealed no apparent morphological anomalies. A and B show the same NF2 sKO sciatic nerve at 6000x and 12000x magnification, respectively. Large diameter axons (Ax) enveloped by thick myelin sheaths (Ms), small diameter axons (ax) and Schwann cells (Sc) can be seen. Scale bars = 5 µm (in A) and 2 µm (in B). n = 2 mice. Representative images are shown.*

3.7 H & E staining of Postn-Cre mice DRGs

When the mice of the fully established Postn-Cre driven lines were numerous enough we decided to take a look the architecture of the developing schwannomas in the dorsal root ganglia (DRGs) at 3, 5 and 9 months of age in control (Postn-Cre- $NF2^{fl/fl}$), NF2 sKO (Postn-Cre+ $NF2^{fl/fl}$), NF2/YAP dKO (Postn-Cre+ $NF2^{fl/fl}$ $YAP^{fl/fl}$) and NF2/TAZ dKO (Postn-Cre+ $NF2^{fl/fl}$ $TAZ^{fl/fl}$) mice. In short, the mice were euthanized by asphyxiation with CO2 and bled out by severing the brachial artery. Their spinal columns were then excised and fixed in 4 % paraformaldehyde (PFA) for 24 hours at 4 °C. After three PBS washes both L3 DRGs of each spinal column were dissected and one DRG from each spinal column was left in 4 % PFA in PBS at 4 °C. These DRGs in 4 % PFA in PBS were given to Philip Edwards of the Cellular and Anatomical Pathology Department of Derriford Hospital who proceeded to embed the DRGs in paraffin, cut sections and stain them with hematoxylin and eosin (H & E) or later Martius Scarlet Blue (MSB). I imaged the sections using the Leica IM8 microscope.

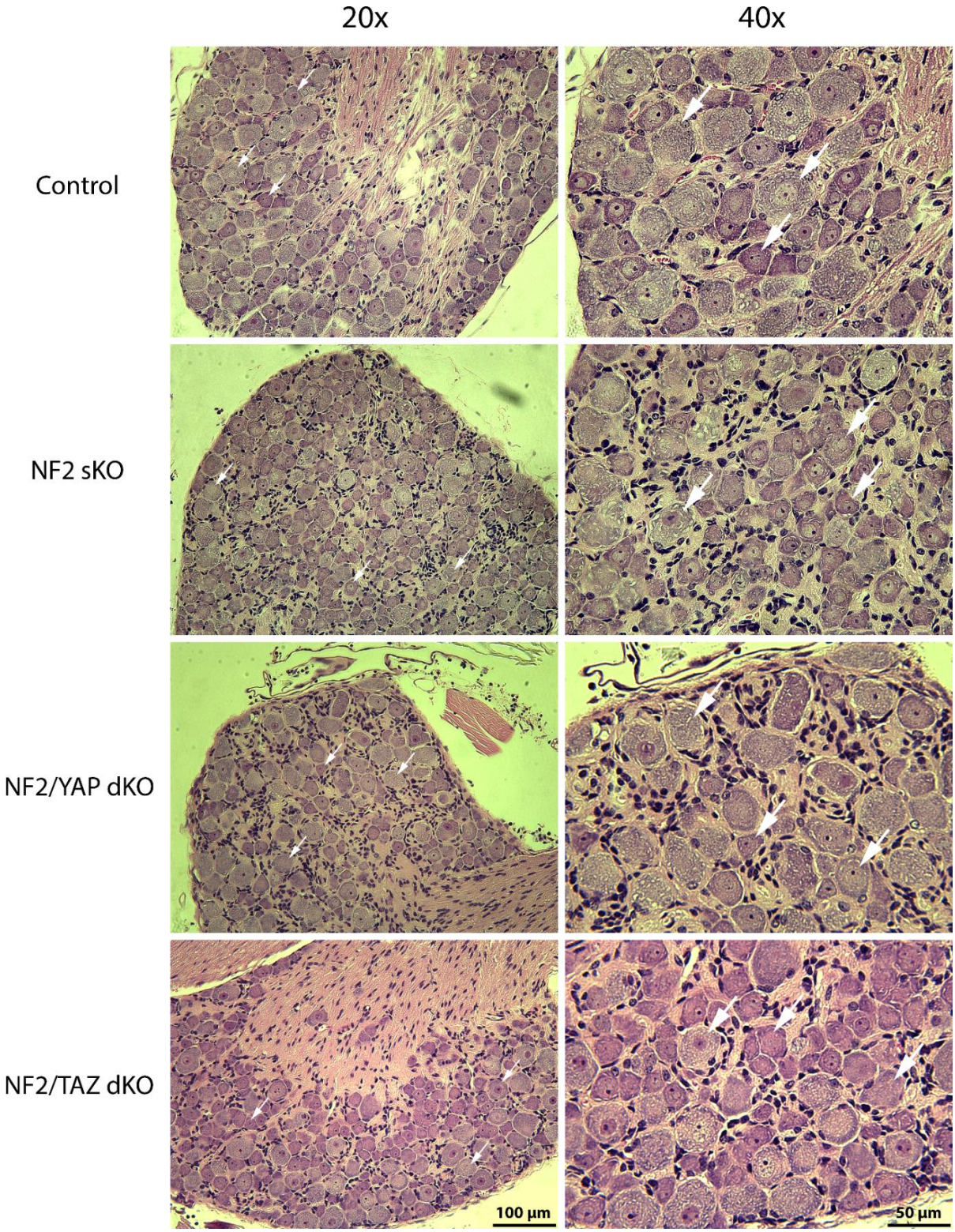

Figure 3.7.1: Visual assessment of hematoxylin and eosin (H & E) stained dorsal root ganglia (DRGs) of 3 month old control, NF2 sKO, NF2/YAP dKO and NF2/TAZ dKO mice *exposed perceived differences in distance between neuronal cell bodies and number of non-neuronal cells. Closely packed neurons seen in the control DRGs, along with low number of smaller non-neuronal cells. Distance between neuronal cells seemingly slightly wider in NF2 sKO DRGs, paired with a hypercellularity of non-neuronal cells, often pooling in certain areas. Neuron spacing and amount of non-neuronal cells in NF2/YAP dKO DRGs similar to the NF2 sKO DRGs. Non-neuronal cells amassing in certain locations observed here as well. Spaces between neurons in NF2/TAZ dKO DRGs appearing similar to control, with non-neuronal*

cell numbers seemingly halfway between control and the other two knockout DRGs. Images as seen with 20x and 40x microscope objectives. White arrows mark neuronal cell bodies. Scale bars = 100 µm (in 20x) and 50 µm (in 40x). n = 3 mice per genotype. Representative images are shown.

In our sections, hematoxylin stained cell nuclei appeared black while eosin showed both the cytoplasm and extracellar matrix in purple/pink. As can be seen in the 3 month timepoint DRGs (Figure 3.7.1), the relatively large neuronal cell bodies (white arrows) in the control DRGs were closely packed with only relatively few non-neuronal cells among them. In contrast, the neurons in NF2 sKO and NF2/YAP dKO DRGs seemed further apart from one another. Additionally, they displayed greater amounts of non-neuronal cells spread throughout the tissue, often concentrating in certain locations. The distance between neurons in NF2/TAZ dKO DRGs appeared similar to control and the numbers of non-neuronal cells found seemed to be more than in control DRGs but less than in the other knockout DRGs.

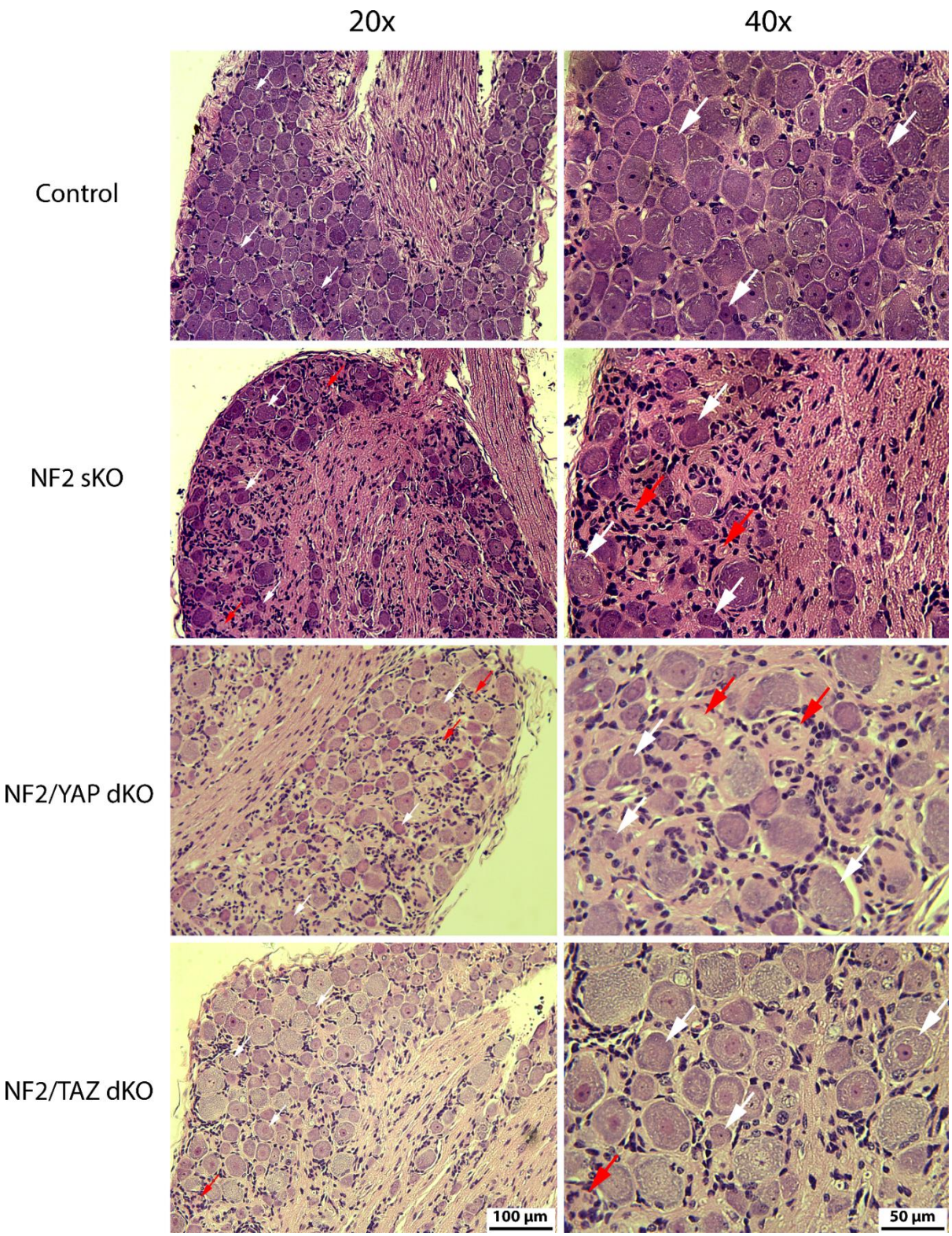

Figure 3.7.2: H & E staining of the DRGs of 5 month old mice *revealed an increased severity of the changes previously noted in 3 months NF2 sKO and NF2/YAP dKO DRGs while NF2/TAZ dKO DRGs only showed minor alterations. Control DRGs remained unchanged. Heightened distance between neurons in NF2 sKO and NF2/YAP dKO DRGs seemingly due to decreased number of visible neurons. Also, seemingly higher number of non-neuronal cells compared to 3 month timepoint counterparts. Cell arrangements possibly indicating neuron loss (red arrows) were observed. NF2/TAZ dKO DRGs only showing minor increases in distance between neurons and non-neuronal cell amounts, with possible*

signs of neuron loss (red arrow) spotted as well. Images as seen with 20x and 40x microscope objectives. White arrows point out neuronal cell bodies. Scale bars = 100 µm (in 20x) and 50 µm (in 40x). n = 3 mice per genotype. Representative images are shown.

At 5 months of age (Figure 3.7.2), control DRGs appeared unchanged. In contrast, the features previously seen in 3 months NF2 sKO and NF2/YAP dKO DRGs had become more striking in their 5 months counterparts. The overall number of neurons appeared to have decreased, creating pronounced spaces between the remaining neurons. Cell arrangements perceived to be possible signs of neuron loss (red arrows, Figure 3.7.2) were found as well. Additionally, the non-neuronal cells seemed to be even more numerous. NF2/TAZ dKO DRGs of the same timepoint seemed to show these changes to a lesser extent. Compared to their 3 months counterparts, they appeared to contain slightly higher numbers of non-neuronal cells and slightly fewer neurons, causing the spaces between neurons to widen. Possible signs of neuron loss (red arrow) could now be perceived as well, although seemingly less frequently than in the other knockout DRGs of the same timepoint.

At the final 9 month timepoint, DRGs of the control mice once again did not differ in any way from controls of previous timepoints (Figure 3.7.3). In stark contrast, both NF2 sKO and NF2/YAP dKO DRGs at 9 months appeared to display both a strong increase in the number of non-neuronal cells and a large decrease of neuronal cell numbers compared to their 5 month counterparts. Only a small number of remaining neurons could still be identified. Furthermore, what is believed to be sites of neuronal loss (red arrows) were seen more frequently. NF2/TAZ dKO DRGs at 9 months also displayed a reduction of neuronal numbers and increased amount of non-neuronal cells, although to lesser extent. Arrangements of cells hinting at neuron loss (red arrow) were observed here as well.

After imaging all the DRGs it became clear that there was a certain variability in appearance found even among DRGs of the same genotype and timepoint (with the exception of the control DRGs). Therefore, choosing representative images and describing them adequately while also considering the appearance of the other DRGs of the same genotype and timepoint proved to be a challenging task. Taking this variability into account, we decided to quantify the number of neurons and the number of non-neuronal cells in order to be able to make more accurate statements of the effects seen in the DRGs for each genotype and timepoint. Using ImageJ, the areas of clearly identified DRG tissue were measured and the neurons and non-neuronal cells within were counted. These values were then used to calculate the number of neurons and non-neuronal cells per mm^2 DRG tissue.

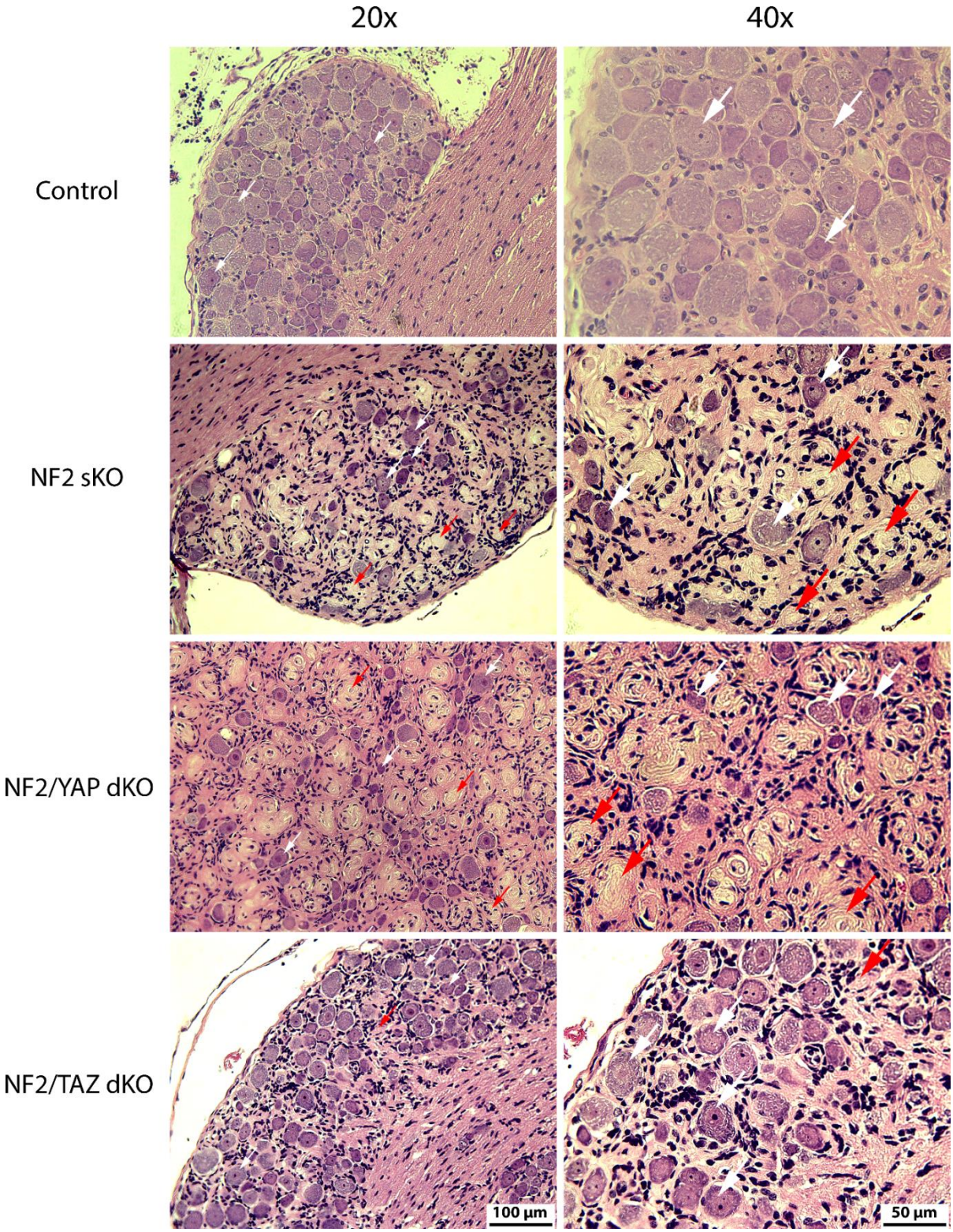

Figure 3.7.3: 9 month timepoint DRGs stained for H & E *unveiled that the effects previously seen in NF2 sKO and NF2/YAP dKO DRGs increased in intensity while the NF2/TAZ dKO DRGs appeared to display these effects to a reduced degree. Once again, appearance of control DRGs did not change. NF2 sKO and NF2/YAP dKO DRGs showing strongly reduced number of neurons and heightened amounts of non-neuronal cells compared to previous timepoints. Increased frequency of perceived signs of neuronal loss (red arrows) in both genotypes. As before, NF2/TAZ dKO DRGs displaying all of aforementioned effects to a diminished degree. Images as seen with 20x and 40x microscope*

objectives. White arrows mark neuronal cell bodies. Scale bars = 100 µm (in 20x) and 50 µm (in 40x). n = 3 mice per genotype. Representative images are shown.

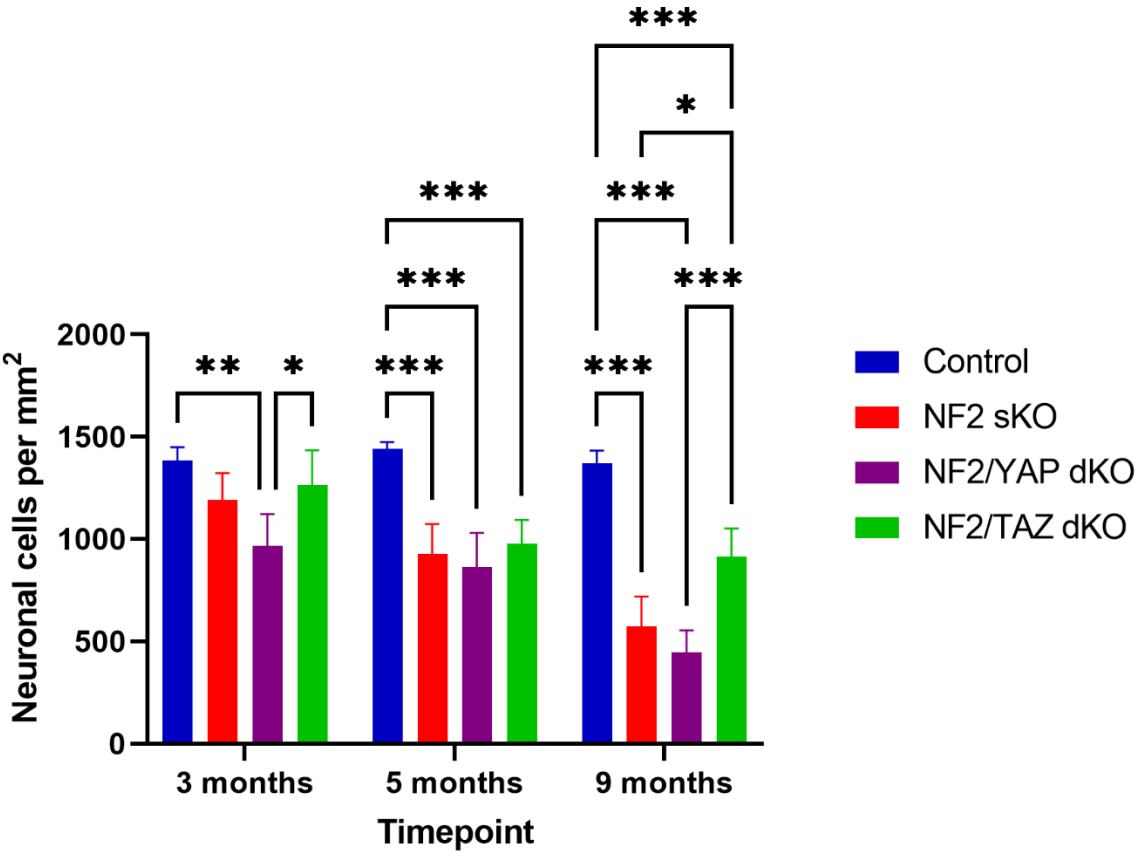

Figure 3.7.4: Quantification of neuronal cells in H & E stained images of DRGs from all genotypes and timepoints *suggested a moderate neuroprotective effect caused by the additional knockout of TAZ. Quantification of neuronal cell numbers per mm² DRG tissue in control, NF2 sKO, NF2/YAP dKO and NF2/TAZ dKO DRGs of 3, 5 and 9 month old mice. 3 month timepoint: Significantly less neurons in NF2/YAP dKO DRGs than in control and NF2/TAZ dKO DRGs (p-values: 3 months NF2/YAP dKO vs. Control = 0.003; NF2/YAP dKO vs. NF2/TAZ dKO = 0.04). 5 month timepoint: Significantly decreased numbers of neurons in all knockout DRGs compared to control (p < 0.001 for all mentioned comparisons). 9 month timepoint: Amounts of neuronal cells reduced significantly in NF2 sKO and NF2/YAP dKO DRGs compared to control and NF2/TAZ dKO DRGs (p-values: 9 months NF2 sKO or NF2/YAP dKO vs. Control = <0.001; NF2 sKO vs. NF2/TAZ dKO = 0.02; NF2/YAP dKO vs. NF2/TAZ dKO = <0.001). Significantly fewer neurons in NF2/TAZ dKO DRGs than in the control DRGs (p < 0.001). No significant difference in neuron numbers between respective NF2 sKO and NF2/YAP dKO DRGs at any timepoint. n = 3 mice per genotype and timepoint. Graph shows numbers of neurons per mm² DRG tissue as means ± SD tested for significance using two-way ANOVA with Tukey's multiple comparisons test. * p ≤ 0.05; ** p ≤ 0.01; *** p ≤ 0.001. Not significant (ns) pairwise comparison brackets were excluded from the graph.*

Quantifying the neurons in DRG tissue (Figure 3.7.4) revealed a significant decrease of neuron numbers in NF2/YAP dKO DRGs at 3 months compared to control and NF2/TAZ dKO DRGs (p-values: 3 months Control vs. NF2/YAP dKO = 0.003; NF2/YAP dKO vs. NF2/TAZ dKO = 0.04). At

the 5 month timepoint, all knockout DRGs displayed a significant reduction in neuronal cell numbers compared to control (p-values: 5 months Control vs. NF2 sKO, NF2/YAP dKO or NF2/TAZ dKO = <0.001). Finally, comparing 9 months DRGs showed that NF2 sKO and NF2/YAP dKO DRGs contained significantly less neurons than control and NF2/TAZ dKO DRGs (p-values: 9 months Control vs. NF2 sKO or NF2/YAP dKO = <0.001; NF2 sKO vs. NF2/TAZ dKO = 0.02; NF2/YAP dKO vs. NF2/TAZ dKO = <0.001). Furthermore, 9 month timepoint NF2/TAZ dKO DRGs also showed a significant decrease in neuron numbers compared to control DRGs ($p < 0.001$). It is also worth pointing out that there never was a significant difference in neuron numbers between NF2 sKO and NF2/YAP dKO DRGs at any of the chosen timepoints.

In summary, according to the quantification the knockout of TAZ along with NF2 resulted in a certain degree of neuroprotection compared to the knockout of NF2 alone or in combination with YAP but was not sufficient to retain neuron numbers similar to the control DRGs.

The quantification of the neuronal cells in DRG tissue (Figure 3.7.4) was followed by the quantification of the non-neuronal cells (Figure 3.7.5). It was found that the same situation applied at each timepoint. The numbers of non-neuronal cells in the NF2 sKO and NF2/YAP dKO DRGs were always significantly higher than in the control and NF2/TAZ DKO of the same timepoint ($p < 0.001$ for all mentioned comparisons except 3 months NF2 sKO vs. NF2/TAZ dKO $p = 0.002$). Similarly, the NF2/TAZ dKO DRGs always contained significantly greater amounts of non-neuronal cells than their respective control DRGs ($p < 0.001$ for all mentioned comparisons). Reminiscent of what was seen before in the quantification of the neuronal cells (Figure 3.7.4), the non-neuronal cell numbers in NF2 sKO and NF2/YAP dKO DRGs of the same timepoint never showed a significant difference.

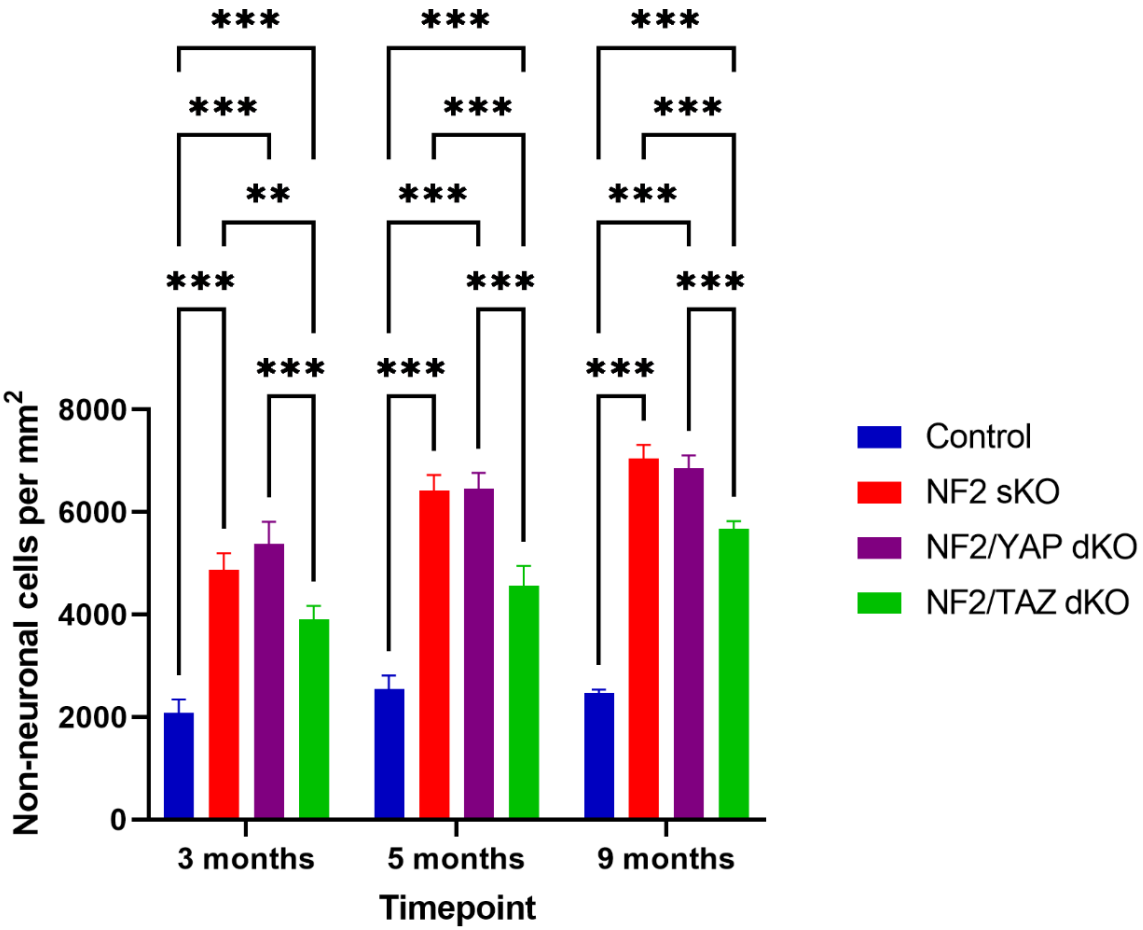

Figure 3.7.5: Counts of non-neuronal cells in DRGs *showed that combined loss of NF2 and TAZ significantly reduced the number of non-neuronal cells found, compared to both the loss of NF2 alone or combined with the loss of YAP. Quantification of non-neuronal cell numbers per mm^2 DRG tissue in control, NF2 sKO, NF2/YAP dKO and NF2/TAZ dKO DRGs of 3, 5 and 9 month old mice. At all timepoints: Significantly more non-neuronal cells in NF2 sKO and NF2/YAP dKO DRGs than in control and NF2/TAZ dKO DRGs of the same timepoint ($p < 0.001$ for all mentioned comparisons except 3 months NF2 sKO vs. NF2/TAZ dKO $p = 0.002$). Also, amounts of non-neuronal cells in NF2/TAZ dKO DRGs significantly higher than in control DRGs of the same timepoint ($p < 0.001$ for all mentioned comparisons). No significant difference in non-neuronal cell numbers between respective NF2 sKO and NF2/YAP dKO DRGs at any timepoint. n = 3 mice per genotype and timepoint. Graph shows numbers of non-neuronal cells per mm^2 DRG tissue as means ± SD tested for significance using two-way ANOVA with Tukey's multiple comparisons test. * $p \leq 0.05$; ** $p \leq 0.01$; *** $p \leq 0.001$. Not significant (ns) pairwise comparison brackets were excluded from the graph.*

3.8 MSB staining of Postn-Cre mice DRGs

As mentioned previously, DRG paraffin sections of all timepoints and genotypes were also stained with Martius Scarlet Blue (MSB). MSB is a stain used for the visualization of a number of different tissue types including collagen (Figure 6.1). Figure 3.8.1 shows the MSB stained DRGs of the 3 month timepoint, with the collagen in light blue. Among the tightly packed neurons of the control DRGs only miniscule amounts of collagen could be observed. In comparison, larger quantities of collagen were visible in the spaces between the neurons of NF2 sKO, NF2/YAP dKO and NF2/TAZ dKO DRGs, along with the previously mentioned increased number of non-neuronal cells.

At the 5 months timepoint (Figure 3.8.2), the MSB stain of the DRGs revealed an only small amount of change. Control DRGs still contained little collagen whereas knockout DRGs maintained or possibly even increased their heightened amounts of collagen compared to control. Additionally, the arrangement of non-neuronal nuclei surrounding what appeared to be the former location of a neuron (as seen before in the H & E staining) could be observed in NF2 sKO and NF2/YAP dKO DRGs of 5 months (Figure 3.8.2, red arrows). Although it did seem as if NF2 sKO and NF2/YAP dKO DRGs possessed slightly more collagen than the NF2/TAZ dKO DRGs the differences were too subtle to be certain.

In the MSB stained 9 month timepoint DRGs (see Figure 3.8.3), the difference became clearer. NF2 sKO and NF2/YAP dKO DRGs of this timepoint showed vastly more collagen than NF2/TAZ dKO DRGs. This strong collagen increase was paired with the previously witnessed severe decrease of visible neurons, a heightened number of non-neuronal cells and more frequent sightings of the locations which are assumed to have previously harboured neurons (Figure 3.8.3, red arrows). As seen before in both the H & E and now in the MSB staining, control DRGs once again remained unchanged, containing only very low amounts of collagen.

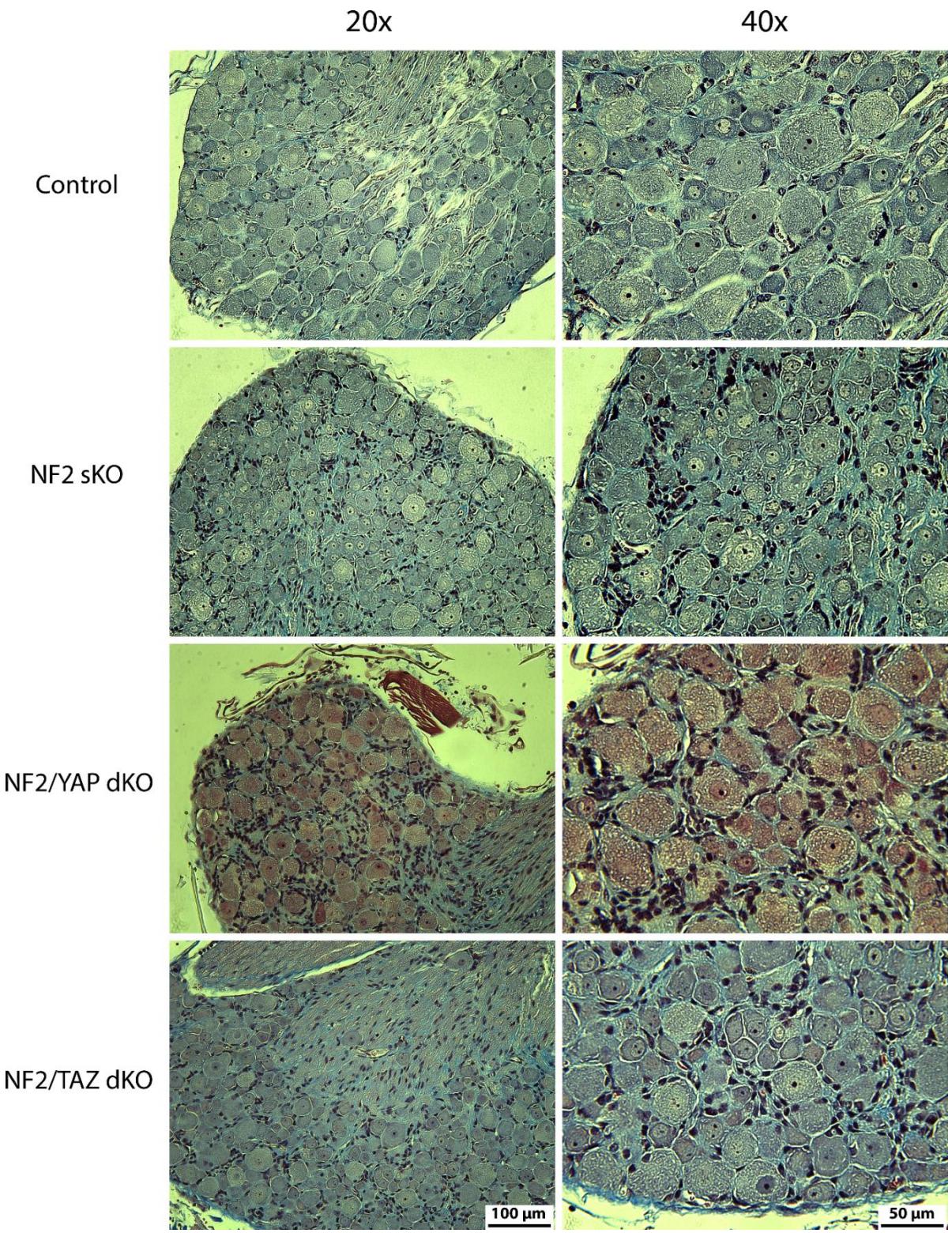

Figure 3.8.1: MSB stained DRGs of the 3 month timepoint *displayed considerable amounts of collagen among the neuronal cell bodies of all knockout DRGs and only small amounts of collagen among the closely stacked neurons in the control DRGs. Majority of hypercellular non-neuronal cells co-localising with the collagen within knockout DRGs. Collagen visible in blue. Images as seen with 20x and 40x microscope objectives. Scale bars = 100 µm (in 20x) and 50 µm (in 40x). n = 3 mice per genotype. Representative images are shown.*

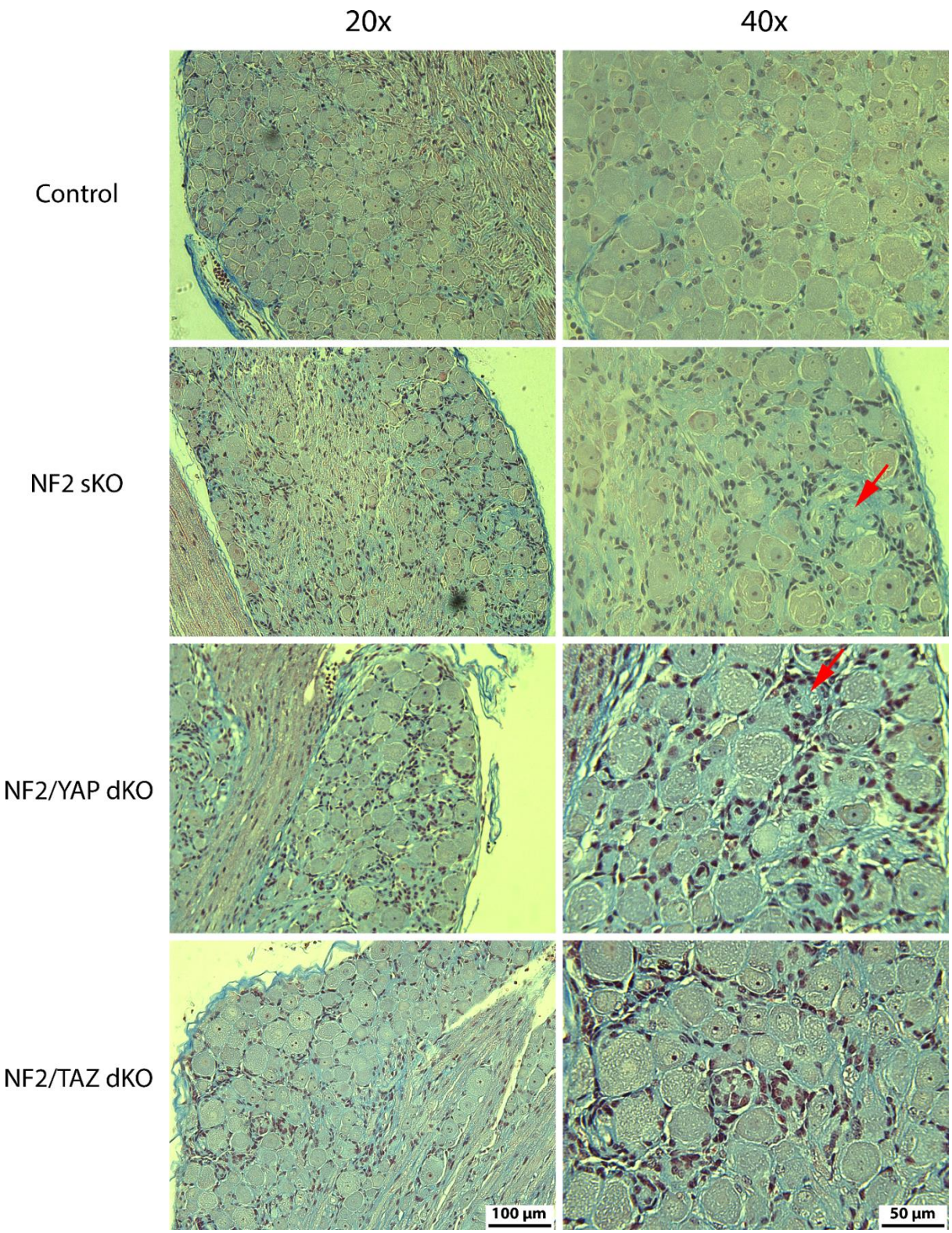

Figure 3.8.2: 5 month timepoint DRGs stained with MSB *revealed only minor changes compared to 3 month DRGs, with control DRGs containing very little and knockout DRGs possessing increased amounts of collagen as before. Collagen visible in blue. Non-neuronal cell arrangements believed to be signs of neuron loss visible within NF2 sKO and NF2/YAP dKO DRGs (red arrows). Images as seen with 20x and 40x microscope objectives. Scale bars = 100 µm (in 20x) and 50 µm (in 40x). n = 3 mice per genotype. Representative images are shown.*

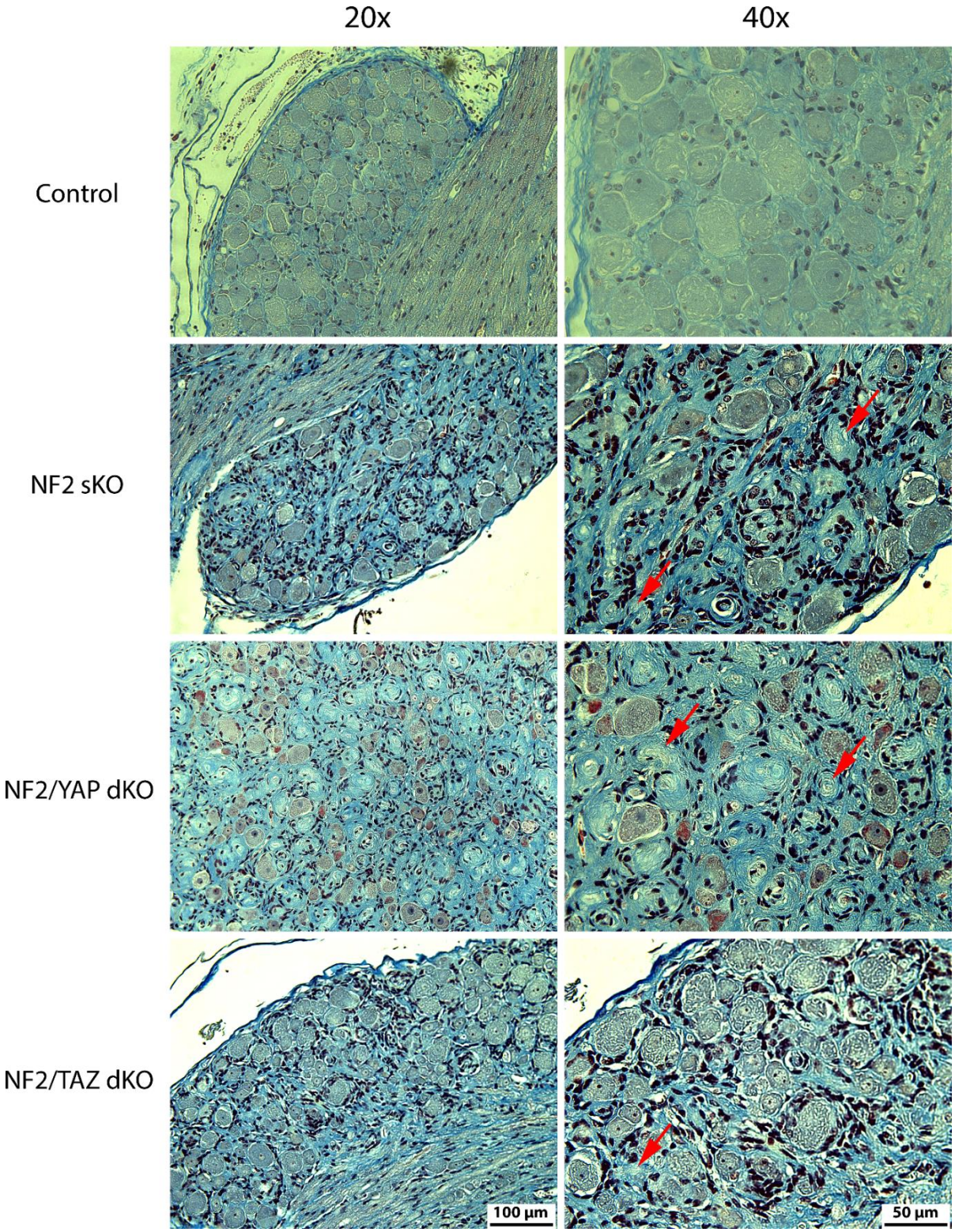

Figure 3.8.3: MSB stained sections of the 9 month DRGs *showed a profound increase of collagen in knockout DRGs, with NF2 sKO and NF2/YAP dKO DRGs displaying a substantially stronger collagen increase than NF2/TAZ dKO DRGs. Potent decrease of neurons and similarly strong increase of non-neuronal cell numbers seen in NF2 sKO and NF2/YAP dKO once again. Non-neuronal cell arrangements perceived as signs of neuron loss now observed more frequently (red arrows). Unchanged appearance of control DRGs, containing only a minimal amount of collagen. Images as seen with 20x and 40x microscope objectives. Scale bars = 100 µm (in 20x) and 50 µm (in 40x). n = 3 mice per genotype. Representative images are shown.*

In the end, it seemed as if in NF2 sKO and NF2/YAP dKO DRGs, and also in NF2/TAZ dKO DRGs to a far lesser extent, the neurons were slowly replaced by collagen over time. Whether the invading collagen had a role in destroying the neurons or the collagen was simply occupying the empty space after the neurons were gone is unknown.

3.9 IHC staining for Collagen IV, Iba1 and EdU in Postn-Cre mouse DRGs

In order to determine whether I could also detect collagen in our frozen sections, we decided to stain our 9 months DRGs for Neurofilament (NF) and Collagen IV using anti-NF and anti-Collagen IV antibodies (Figure 3.9.1). Frozen DRG sections were acquired by same method as the frozen nerve sections before, as described in Materials and Methods section 2.4.2.1. In short, spinal columns were fixed in 4 % PFA in PBS for 24 hours and then washed with PBS. Afterwards, the DRGs were dissected and left in 30 % sucrose in PBS for 48 hours for tissue cryoprotection. Afterwards, the DRGs were embedded in OCT, frozen in liquid nitrogen and sectioned using a cryostat. NF was used to allow easier distinction between neuronal tissue and nerve tissue in DRGs. Collagen IV was chosen since it was found to be strongly upregulated in the sciatic nerves of NF2 sKO mice 21 dpi (Mindos *et al.*, 2017). The antibody stained sections were then imaged using a confocal microscope.

What I found was fairly similar to what was noted before in the MSB stained paraffin sections. Control DRGs showed low amounts of Collagen IV, most of which seemed to be confined to the DRGs' outer layer. In contrast, knockout mice DRGs contained high levels of Collagen IV which seemed to occupy the space previously taken up by DRG neurons. Going by visual observations alone it appeared that there were no apparent differences in Collagen IV amounts between NF2 sKO, NF2/YAP dKO and NF2/TAZ dKO DRGs.

Afterwards, I stained the DRGs of all timepoints and genotypes for Iba1 using an anti-Iba1 antibody in order to detect macrophages. Imaging was once again performed using a confocal microscope. Figure 3.9.2 displays an example of such a staining, with one part of the image magnified to show the morphology of the Iba1 positive macrophages. The Iba1 stain was cytoplasmic and suggested an oval cell body, often possessing cell extensions. Representative images of the Iba1 positive macrophages in the DRGs of all genotypes and timepoints is shown in Figure 3.9.3.

Visual inspection suggested that control DRGs of 3 months, 5 months and 9 months always contained the least amount of Iba1 positive macrophages, compared to the knockout DRGs of the corresponding timepoints. There was also some indication that the NF2/YAP dKO and NF2/TAZ dKO DRGs of each timepoint appeared to possess slightly less Iba1 positive macrophages than the NF2 sKO DRGs of the same timepoint. Quantifying the images by determining the percentage of Iba1 positive macrophages of all counted non-neuronal cells within DRG tissue and conducting analysis for statistical significance gave us a better understanding of the differences among genotypes within the respective timepoints (Figure 3.9.4).

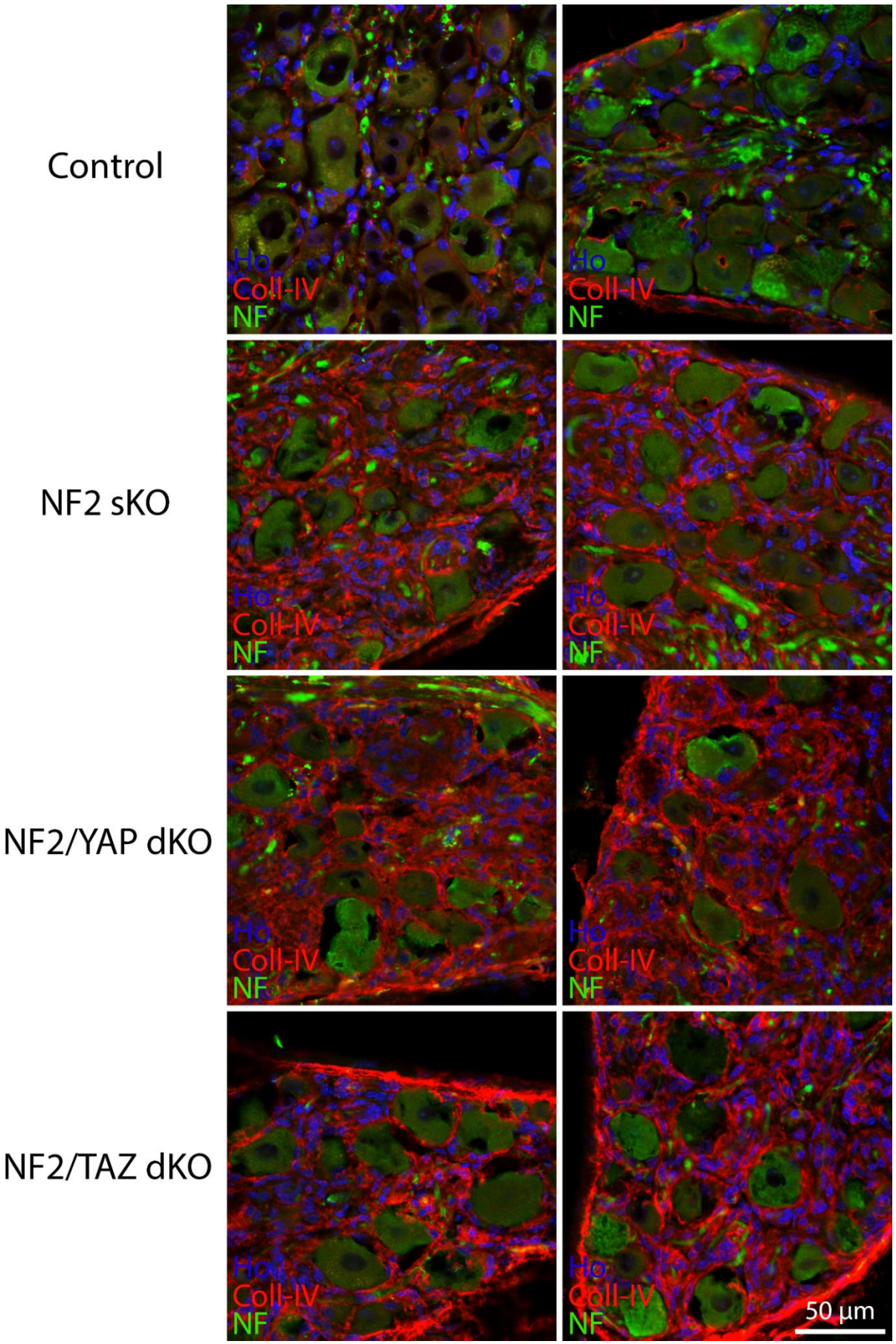
Control
NF2 sKO
NF2/YAP dKO
NF2/TAZ dKO
Ho
Coll-IV
NF
50 µm

Figure 3.9.1: Neurofilament (NF) and Collagen IV (Coll-IV) stained frozen sections of 9 month timepoint DRGs *revealed vast amounts of Collagen IV in knockout DRGs whereas control DRGs only contained very low amounts of Collagen IV. Anti-NF and anti-Coll-IV antibodies were used to detect NF and Coll-IV. Differences in Collagen IV quantity between NF2 sKO, NF2/YAP dKO and NF2/TAZ dKO DRGs difficult to determine by visual assessment alone. As seen in MSB stained paraffin sections before, areas previously held by the large neuronal bodies now occupied by Collagen IV. DNA dye Hoechst (Ho) used as counterstain to mark cell nuclei. Scale bar = 50 µm in all images. n = 3 mice per genotype. Two representative images per genotype are shown.*

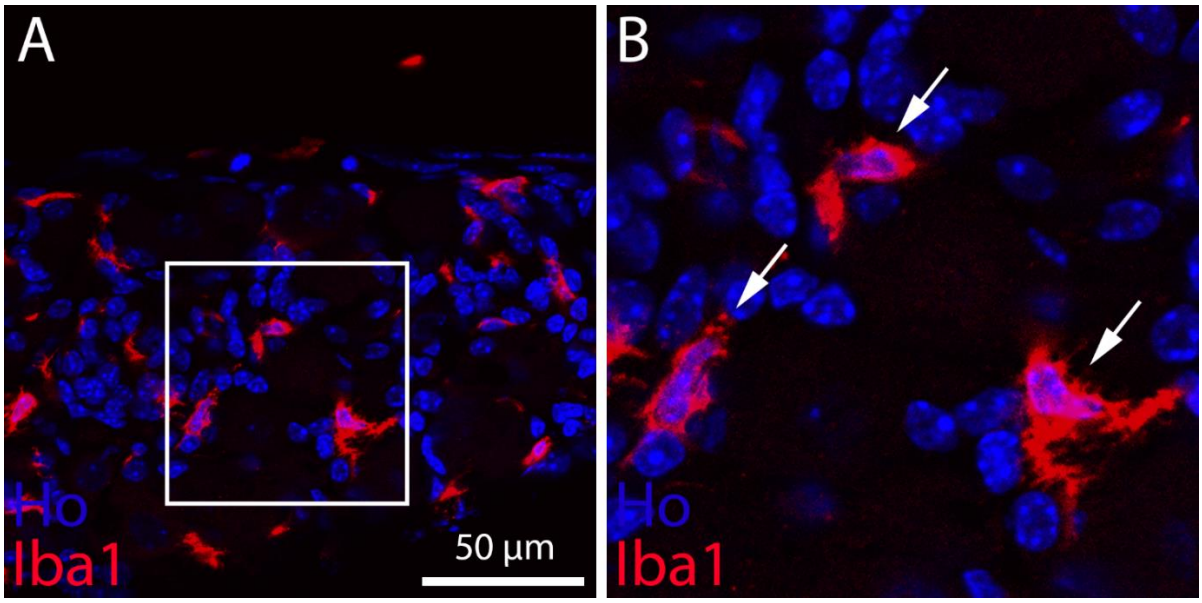

Figure 3.9.2: Cytoplasmic Iba1 stain of macrophages detected in DRG mouse tissue *revealed an oval cell body, frequently seen with cell extensions. A: Image of an Iba1 stained 3 month timepoint NF2/YAP dKO DRG using an anti-Iba1 antibody. Image was chosen to illustrate macrophage morphology. DNA dye Hoechst (Ho) displaying cell nuclei in blue. Scale bar = 50 µm. B: Enlarged image of white framed area in A. White arrows point out examples of Iba1 positive macrophages.*

At the 3 months timepoint, percentages of Iba1 positive macrophages in control DRGs were significantly lower compared to the knockout DRGs (p-values: 3 months Control vs. NF2 sKO = <0.001; Control vs. NF2/YAP dKO = 0.02; Control vs. NF2/TAZ dKO = 0.001). NF2 sKO DRGs were also found to have significantly higher relative macrophage numbers than NF2/YAP dKO DRGs (p = 0.02). In 5 month DRGs, significantly increased relative numbers of macrophages were found in NF2 sKO compared to the three other genotypes ($p < 0.001$ for all mentioned comparisons).

At the final timepoint of 9 months, once again NF2 sKO DRGs contained significantly higher percentages of Iba1 positive macrophages than DRGs of the other genotypes ($p < 0.001$ for all mentioned comparisons). Additionally, significantly larger macrophage percentages were observed in NF2/YAP dKO and NF2/TAZ dKO DRGs compared to control (p-values: 9 months Control vs. NF2/YAP dKO = 0.008; Control vs. NF2/TAZ dKO = 0.04). It is noteworthy that a significant difference in macrophage percentages between the corresponding NF2/YAP dKO and NF2/TAZ dKO DRGs was not found at any timepoint.

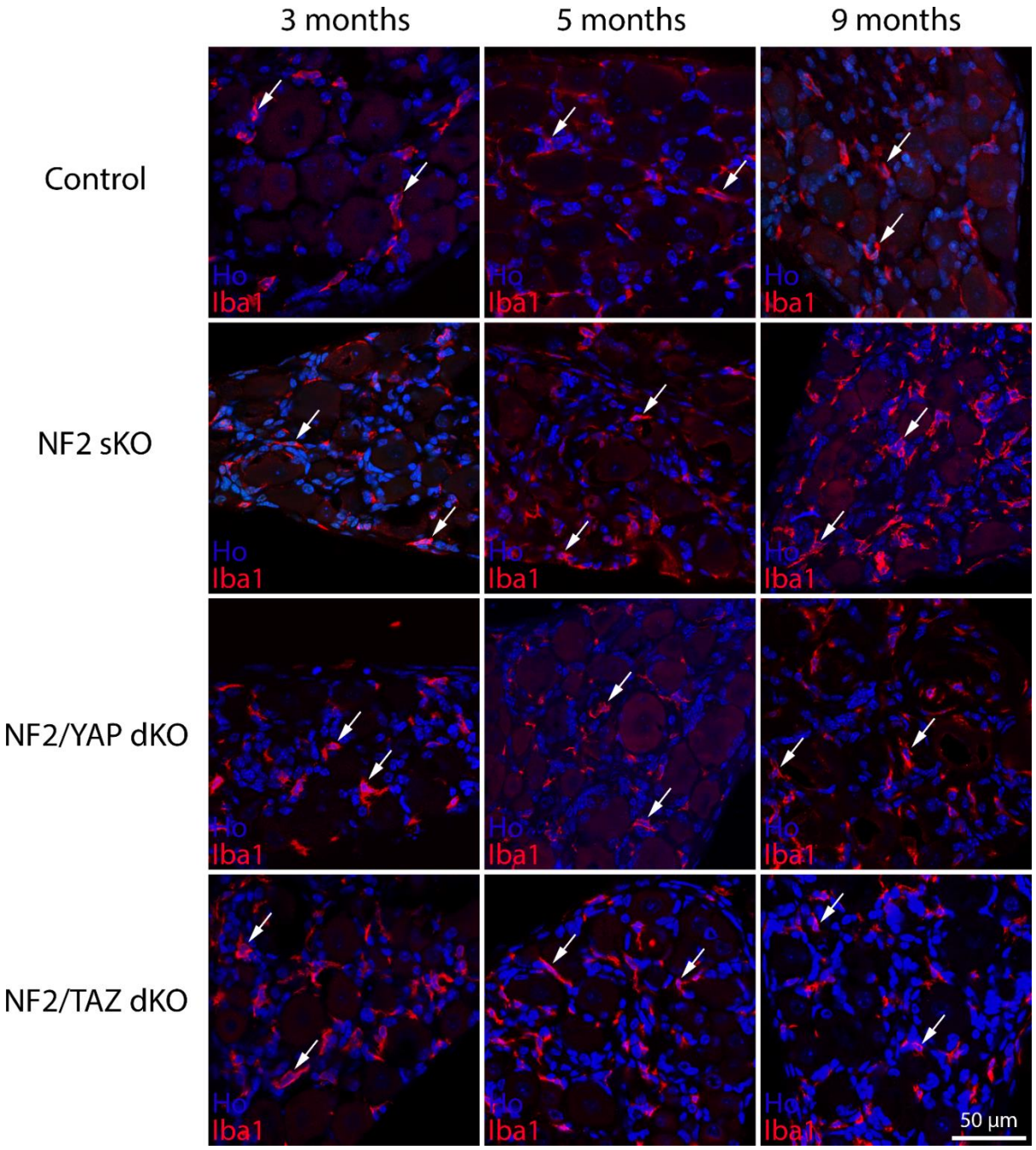

Figure 3.9.3: Iba1 stained frozen sections of the 3 months, 5 months and 9 months DRGs of all genotypes *hinted at a decreased number of Iba1 positive macrophages in control DRGs compared to respective knockout DRGs. As before, an anti-Iba1 antibody was used. NF2/YAP dKO and NF2/TAZ dKO DRGs seemingly containing slightly less Iba1 positive macrophages than NF2 sKO DRGs of the same timepoint. Counterstain DNA dye Hoechst (Ho) employed to visualize all cell nuclei. Scale bar = 50 µm in all images. White arrows in each image mark examples of Iba1 positive macrophages. n = 3 mice per genotype and timepoint. Representative images are shown.*

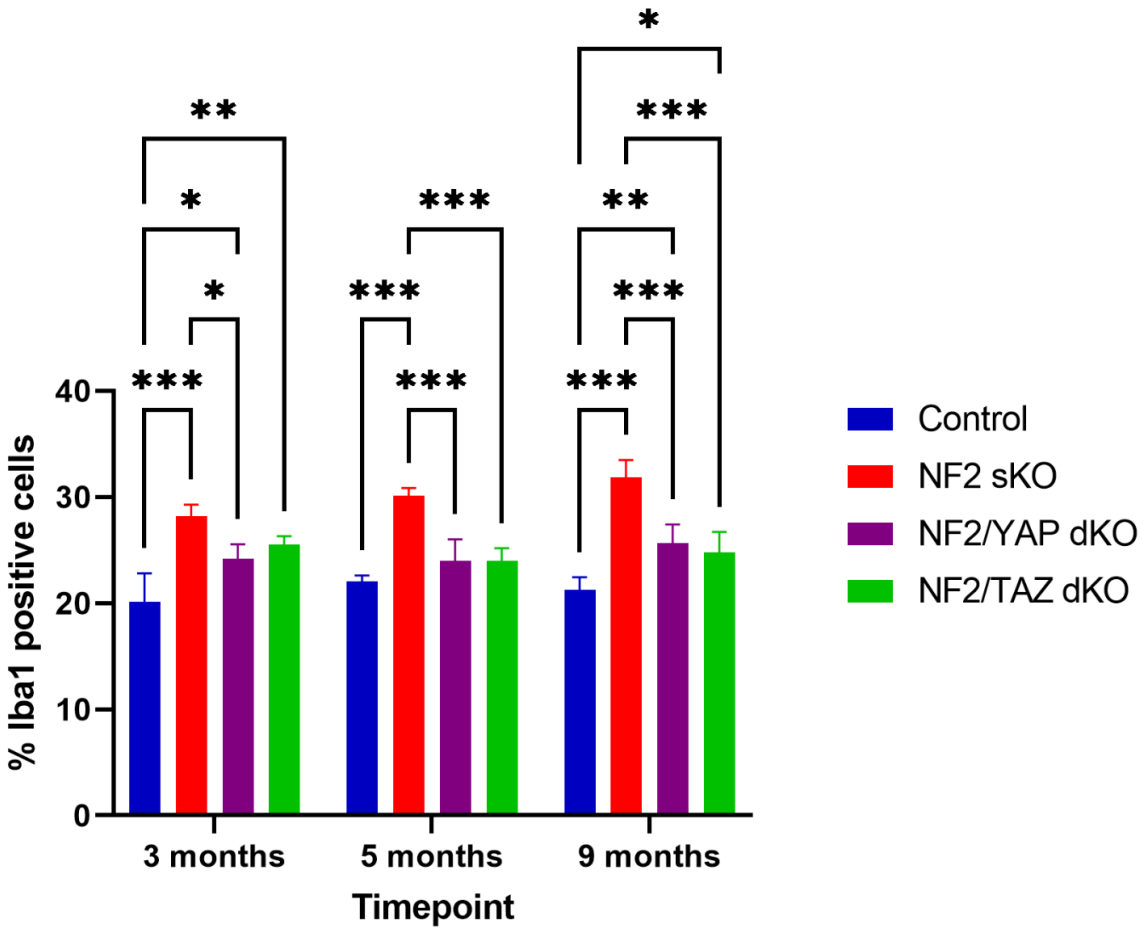

Figure 3.9.4: Quantification of Iba1 positive macrophages in DRG tissue and subsequent statistical analysis *revealed that NF2 loss resulted in a heightened percentage of Iba1 positive macrophages while the added loss of either YAP or TAZ reduced the NF2 knockout driven relative macrophage increase. Quantification of Iba1 positive cells as % of all non-neuronal cells in DRG tissue of control, NF2 sKO, NF2/YAP dKO and NF2/TAZ dKO DRGs of 3, 5 and 9 month old mice. 3 months: Control DRGs contained significantly lower relative macrophage numbers than knockout DRGs (p-values: 3 months Control vs. NF2 sKO = <0.001; Control vs. NF2/YAP dKO = 0.02; Control vs. NF2/TAZ dKO = 0.001). Significantly increased percentages of macrophages in NF2 sKO DRGs compared to NF2/YAP dKO DRGs (p = 0.02). 5 months: Significantly higher percentages of macrophages in NF2 sKO DRGs than in DRGs of other genotypes (p < 0.001 for all mentioned comparisons). 9 months: NF2 sKO DRGs possessed significantly heightened relative macrophage numbers compared to DRGs of other genotypes (p < 0.001 for all mentioned comparisons). Significantly larger percentages of macrophages in NF2/YAP dKO and NF2/TAZ dKO DRGs compared to control (p-values: 9 months Control vs. NF2/YAP dKO = 0.008; Control vs. NF2/TAZ dKO = 0.04). No significant difference in relative macrophage numbers seen between respective NF2/YAP dKO and NF2/TAZ dKO DRGs at any timepoint. n = 3 mice per genotype and timepoint. Graph shows % Iba1 positive cells in DRG tissue as means ± SD tested for significance using two-way ANOVA with Tukey's multiple comparisons test. * p ≤ 0.05; ** p ≤ 0.01; *** p ≤ 0.001. Not significant (ns) pairwise comparison brackets were excluded from the graph.*

In conclusion, the data suggests that the loss of NF2 alone heightened the relative numbers of macrophages found in the DRGs while the additional loss of either YAP or TAZ managed to diminish relative macrophages numbers, although it did not seem to be enough to reduce relative macrophage numbers back down to control DRG levels at the end of the experiment.

Subsequently, we decided to establish the proliferation rates of the cells inside the DRGs of the same timepoints and genotypes. As described before (Materials and Methods section 2.3.3), the artificial nucleotide 5-Ethynyl-2'-deoxyuridine (EdU) was given to all cells of the mice by injecting the mice with 2 mg EdU per mouse (dissolved in DMSO and diluted in PBS, Materials and Methods section 2.3.3) 24 hours before tissue extraction. In these 24 hours, the EdU would then be incorporated into the DNA of cells being in or entering the S-phase of the cell cycle. By subsequently detecting the EdU, a fraction of the proliferating cells can be identified which would allow us to gauge the proliferative activity of any given tissue. Frozen DRG sections were acquired as before and EdU positive cell nuclei were identified by conjugating a fluorophore to the EdU nucleotides via a Click-iT reaction. Imaging was performed using a confocal microscope.

It was previously determined that the EdU positive cells in the DRGs are glial cells (see Discussion section 4.2). Therefore, these EdU positive cells are considered to be the proliferating schwannoma tumour cells. Visual inspection of the amount of EdU positive cells found within the DRGs (Figure 3.9.5) showed that control DRGs of 3 months, 5 months and 9 months never contained any EdU positive cells, consistent with the postmitotic nature of adult, uninjured nerve tissue. Conversely, NF2 sKO DRGs appeared to have the most EdU positive nuclei compared to DRGs of other genotypes of the respective timepoints. EdU positive nuclei in NF2 sKO and NF2/YAP dKO DRGs seemingly heightened over time which was not noted in NF2/TAZ dKO DRGs. In order to provide us with more reliable results, quantification of the images was performed to determine the percentage of EdU positive nuclei among all the nuclei of non-neuronal cells in DRG tissue, followed by statistical analysis (see Figure 3.9.6).

It was revealed that at every measured timepoint the mean proliferation rate in the NF2 sKO DRGs was more than twice as high and also significantly higher compared to the corresponding control, NF2/YAP dKO and NF2/TAZ dKO DRGs ($p < 0.001$ for all mentioned comparisons). Furthermore, given that no EdU positive nuclei were found in the control DRGs, the knockout DRGs always possessed significantly heightened cell division rates compared to control ($p < 0.001$ for all mentioned comparisons). Additionally, the proliferation found in NF2/YAP dKO and NF2/TAZ dKO DRGs did not show a significant difference at 3 months and 5 months. However, at the 9 month timepoint NF2/YAP dKO DRGs had significantly larger cell proliferation rates than NF2/TAZ dKO DRGs.

Reminiscent to what was observed in the Iba1 stained DRGs (Figure 3.9.4), NF2 loss alone increased the proliferation in the DRGs considerably. This increase in proliferation was then reduced by the additional loss of either YAP or TAZ. Moreover, the additional loss of YAP appeared to have a lesser impact on proliferation over time than the additional loss of TAZ.

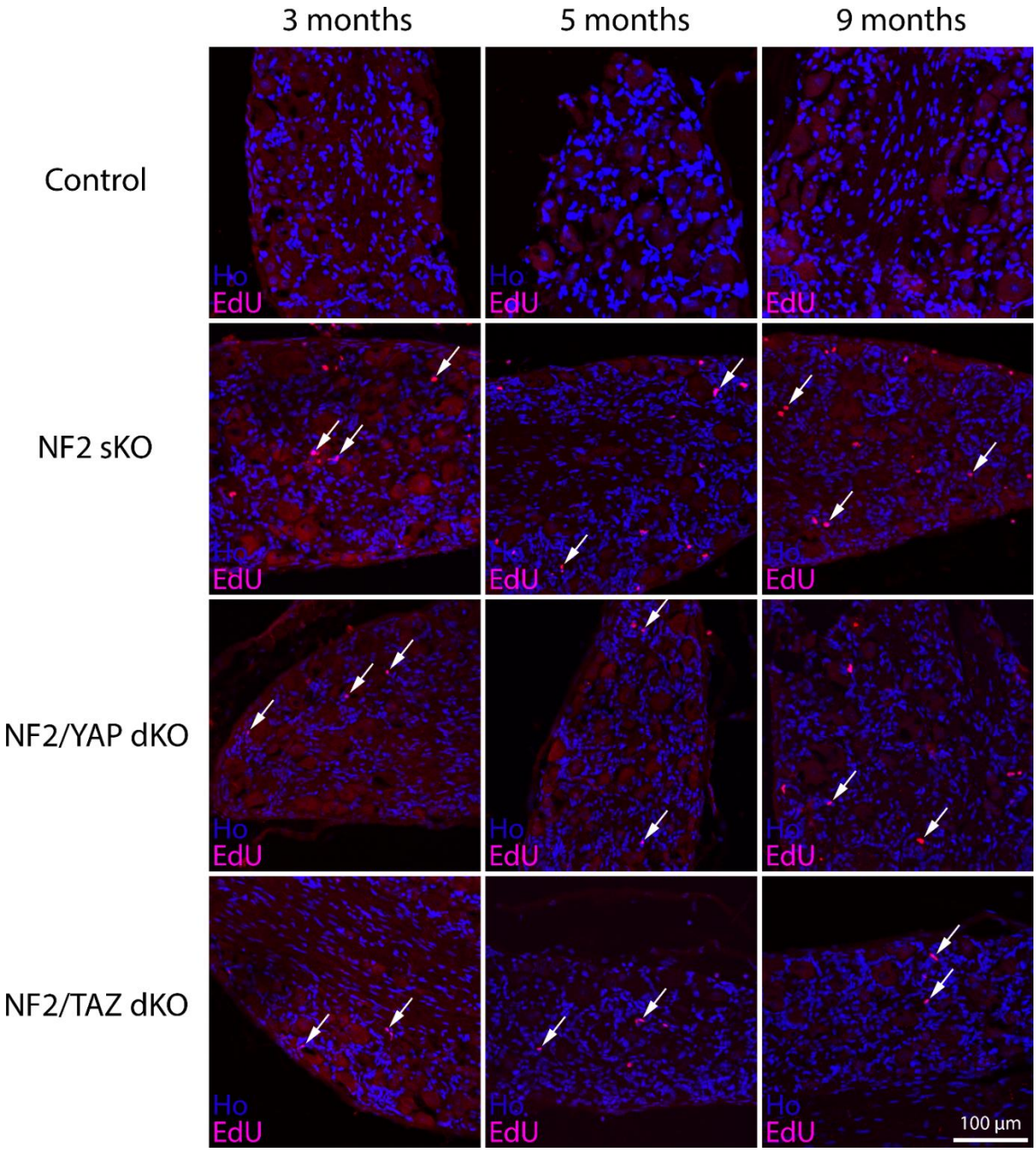

Figure 3.9.5: Frozen DRG sections stained for EdU *revealed that NF2 sKO DRGs appeared to contain the largest amount of EdU positive nuclei compared to DRGs of other genotypes of the same timepoint. Control DRGs found to be without detectable EdU positive nuclei. Perceived increase of EdU positive nuclei in NF2 sKO and NF2/YAP dKO DRGs over time not observable in NF2/TAZ dKO DRGs. DNA dye Hoechst (Ho) used as counterstain marking all cell nuclei. Scale bar = 100 µm in all images. White arrows in each image point out examples of EdU positive nuclei. n = 3 mice per genotype and timepoint. Representative images are shown.*

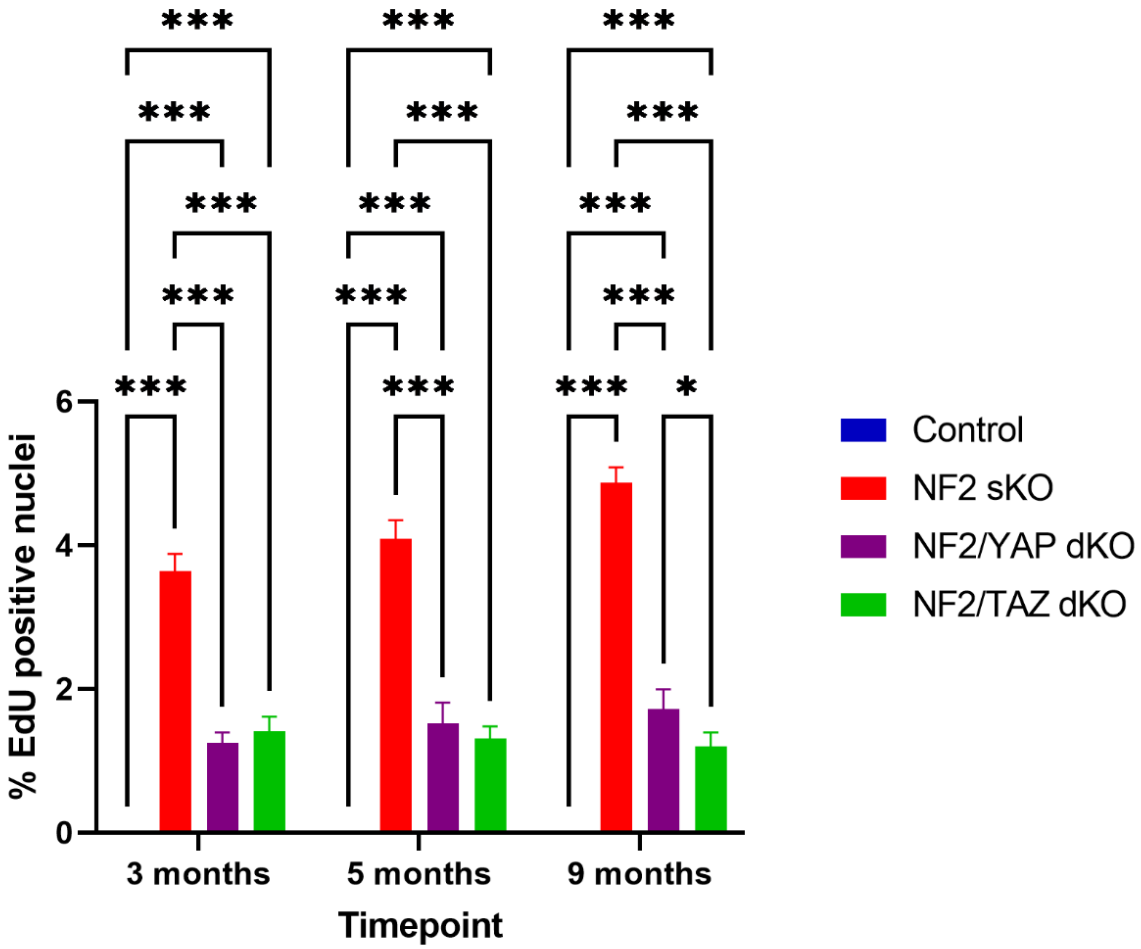

Figure 3.9.6: Statistical analysis of the quantification of EdU stained frozen DRG sections *showed NF2 loss resulted in a statistically significantly increased proliferation, an increase which was counteracted to a certain degree by the added loss of either YAP or TAZ. Quantification of EdU positive nuclei as % of non-neuronal cell nuclei in DRG tissue of control, NF2 sKO, NF2/YAP dKO and NF2/TAZ dKO DRGs of 3, 5 and 9 month old mice. All timepoints: Significantly higher proliferation rates found in NF2 sKO DRGs than in DRGs of other genotypes of the same timepoint ($p < 0.001$ for all mentioned comparisons). Control DRGs contained significantly lower cell division rates compared to same timepoint knockout DRGs ($p < 0.001$ for all mentioned comparisons). No significant difference in proliferation rates between NF2/YAP dKO and NF2/TAZ dKO DRGs at 3 and 5 month timepoint. At 9 months, NF2/YAP DRGs harboured significantly higher cell division rates than NF2/TAZ dKO DRGs ($p = 0.02$). n = 3 mice per genotype and timepoint. Graph displays % EdU positive nuclei in DRG tissue as means ± SD tested for significance using two-way ANOVA with Tukey's multiple comparisons test. * $p \leq 0.05$; ** $p \leq 0.01$; *** $p \leq 0.001$. Not significant (ns) pairwise comparison brackets were excluded from the graph.*

3.10 IHC staining for Iba1 and EdU in Postn-Cre mouse cochleae

Afterwards, we decided to look for developing schwannomas in other tissues of our mouse model mice. Interestingly, the creators of the original Postn-Cre driven NF2 sKO schwannoma mouse model were not able to find any physiological abnormalities within the cochleae of

their NF2 sKO mice. However, when testing the NF2 sKO mice's hearing using click-evoked auditory brainstem response (ABR) Gehlhausen et al. found changes in the ABR waveforms in 10 month old NF2 sKO mice, suggesting the hair cells of the cochlea might play a role in hearing loss at a later stage of Neurofibromatosis type 2 (Gehlhausen *et al.*, 2015). Therefore, we decided to examine the cochleae of recently dissected 5 month old control and NF2 sKO mice to determine whether any differences between these genotypes can be picked up at this earlier timepoint by staining for Iba1 (macrophages) and EdU (proliferating cells). For that purpose, Professor Dan Jagger from University College London (UCL) personally showed us how to dissect and then to process the mice cochleae (see Materials and Methods sections 2.3.3 and 2.4.2.2). In short, the cochleae were carefully exposed and subsequently fixed by first flushing 4 % PFA in PBS through the cochleae using a syringe and then leaving the extracted cochleae in 4 % PFA in PBS for 30 min. Subsequently, the fixed cochleae were PBS washed and decalcified in 4 % EDTA for 72 hours. The decalcified cochleae were then embedded in 4 % agarose blocks which were sectioned using a vibratome. The agarose sections were then stained for Iba1 and EdU and imaged using a confocal microscope.

Unfortunately, Iba1 stained agarose sections of cochleae of control and NF2 sKO (Figure 3.10.1) did not result in a clear Iba1 staining. The strong background staining made it difficult to distinguish between genuinely Iba1 positive cells and cells encompassed by tissue falsely stained for Iba1.

Therefore, I tried the Iba1 staining once more, combined with the EdU staining (Figure 3.10.2). As before, the Iba1 antibody did not seem to be working properly on agarose cochlea sections, despite using a different secondary antibody. EdU staining was more conclusive. It showed EdU positive nuclei belonging to proliferating cells within nuclei-dense regions of the NF2 sKO cochlea. In contrast, the control cochlea did not exhibit any EdU positive nuclei. The same was found by other members of the lab. Upon presenting similar EdU staining sections to Professor Dan Jagger he concluded that the EdU positive cells were located in the bony labyrinth (the outer layer of the cochlea comprised of bone). It is unknown if these proliferating, presumably tumourigenic cells were originally Schwann cells. It is also possible that these EdU positive cells are former osteoblasts which started proliferating after having experienced a Postn-Cre driven NF2 knockout. Since the bony labyrinth was the only location within the cochlea sections found to contain EdU positive nuclei, I and other members of the lab were unable to find any traces of schwannoma in or around the hair cells (within the Organ of Corti). Therefore, we decided to look for developing schwannomas in other locations.

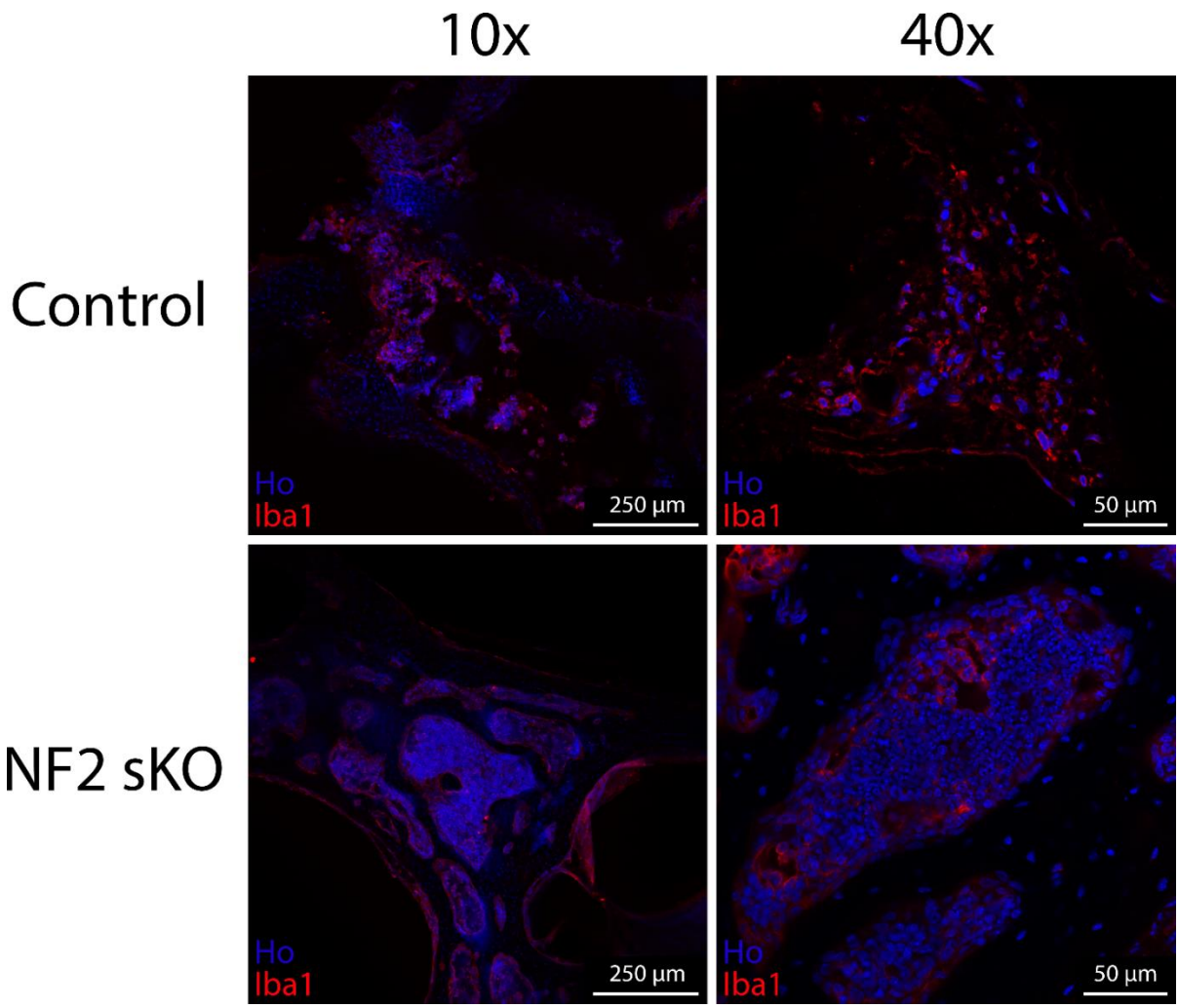

Figure 3.10.1: Iba1 stained agarose sections of cochleae from 5 month old control and NF2 sKO mice *did not show a clear Iba1 staining. If present, Iba1 positive cells could not be clearly identified. Sections were counterstained using DNA dye Hoechst. Images as seen with 10x and 40x microscope objectives. Scale bars = 250 µm (in 10x) and 50 µm (in 40x). n = 1 mouse per genotype.*

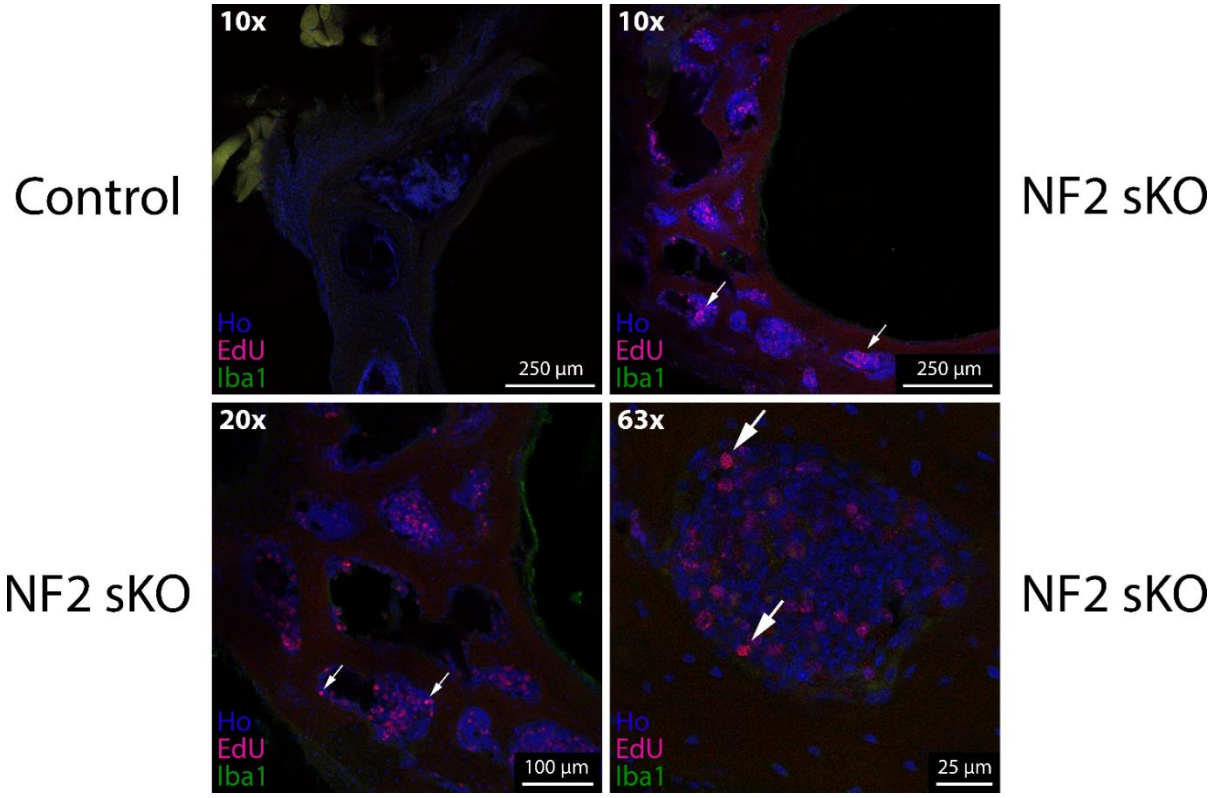

Figure 3.10.2: EdU and Iba1 stained agarose cochlea sections of 5 month old control and NF2 sKO mice *revealed EdU positive nuclei of proliferating cells in the NF2 sKO cochlea. Control cochlea did not contain any EdU positive nuclei. Iba1 staining was unsuccessful once more. DNA dye Hoechst used as counterstain to mark cell nuclei. Images as seen with 10x, 20x and 63x microscope objectives, indicated in upper left corner of each image. Scale bars = 250 µm (in 10x), 100 µm (in 20x) and 25 µm (in 63x). White arrows mark examples of EdU positive nuclei. n = 1 mouse per genotype.*

3.11 IHC staining for Iba1 and EdU in Postn-Cre mouse vestibular ganglia

The discoverers of the original Postn-Cre driven NF2 sKO mouse model were able to detect vestibular schwannomas growing in the vestibular ganglia (= Scarpa's ganglia) in 10 month old NF2 sKO mice (Gehlhausen *et al.*, 2015). Therefore, we decided to look for developing schwannomas in the vestibular ganglia (= VGs). Due to time constraints towards the end of the PhD laboratory period, 3 and 5 month old control and NF2 sKO mice (3 mice per genotype and timepoint) were injected with EdU 24 hours before tissue extraction, as described before (Materials and Methods section 2.3.3). In short, the skulls of the euthanized mice were freed of brain tissue, cut down to size and then fixed for 24 hours in 4 % PFA in PBS. Afterwards, they were PBS washed and the VGs were carefully removed from the bone. Henceforth, the methods of cryoprotection, embedding and frozen sectioning were identical to the ones used in the DRGs. VG cryosections were IHC stained as usual and imaged using a confocal microscope.

First, I stained the frozen vestibular ganglion (VG) sections of 3 and 5 month old NF2 sKO mice for Neurofilament (NF) and EdU. Neurofilament staining was performed to gain a better understanding of the structure of VGs and highlight possible differences to previously

examined DRG tissue. The preliminary EdU staining served to determine the presence of EdU positive nuclei. As comparison, sections of 5 month timepoint NF2 sKO DRGs were stained as well (Figure 3.11.1).

It was discovered that VGs looked almost indistinguishable from DRGs, containing the known ganglia tissue with the large neuronal cell bodies surrounded by non-neuronal cells. The presence of EdU positive nuclei of proliferating cells could be confirmed as well. Therefore, we decided to stain our frozen VG sections for Iba1 and EdU.

Figure 3.11.2 shows Iba1 stained VG sections of control and NF2 sKO 3 month and 5 month old mice. Visual assessment suggested a similar number of Iba1 positive macrophages in the 3 and 5 months control VGs. In contrast, it seemed unclear whether the same applied to NF2 sKO VGs of 3 and 5 months. Moreover, NF2 sKO VGs also appeared to possess more Iba1 positive macrophages than their control VGs counterparts.

Subsequently, I EdU stained my frozen VG sections to identify the EdU positive nuclei of proliferating cells (Figure 3.11.3). As seen before in DRGs, control VGs of the 3 and 5 month timepoint did not contain any EdU positive nuclei, pointing towards extremely low, if any, proliferative activity. NF2 sKO VGs on the other hand exhibited EdU positive nuclei. As before, quantification and statistical analysis followed (Figure 3.11.4).

Quantification of the Iba1 positive cells and EdU positive nuclei confirmed some of our observations (Figure 3.11.4). At the 3 and 5 month timepoints, the NF2 sKO VGs had significantly larger percentages of Iba1 positive macrophages and EdU positive nuclei than the corresponding control VGs ($p < 0.001$ for all mentioned comparisons). There was no significant increase of % Iba1 positive macrophages or % EdU positive nuclei over time in either genotype. As seen before in DRGs, the loss of NF2 both caused an increase of macrophage numbers and induced proliferation in VGs.

NF2 sKO

3 month VG

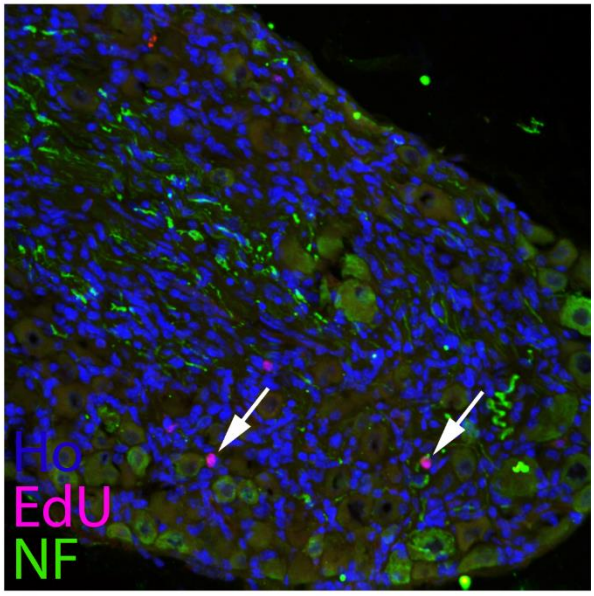

5 month VG

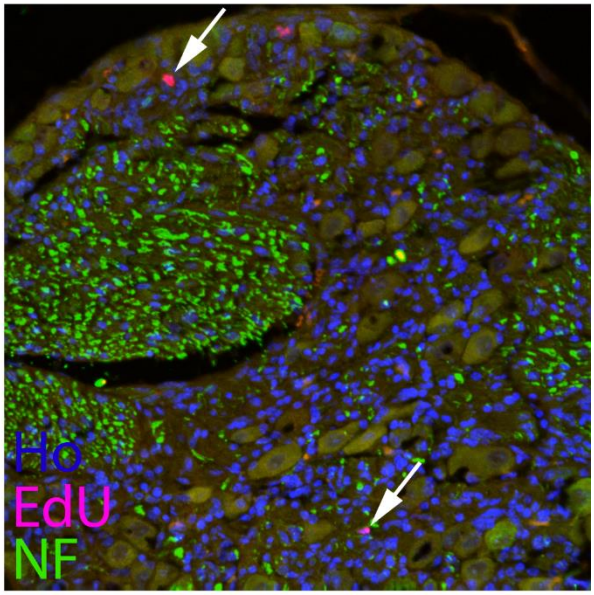

5 month DRG

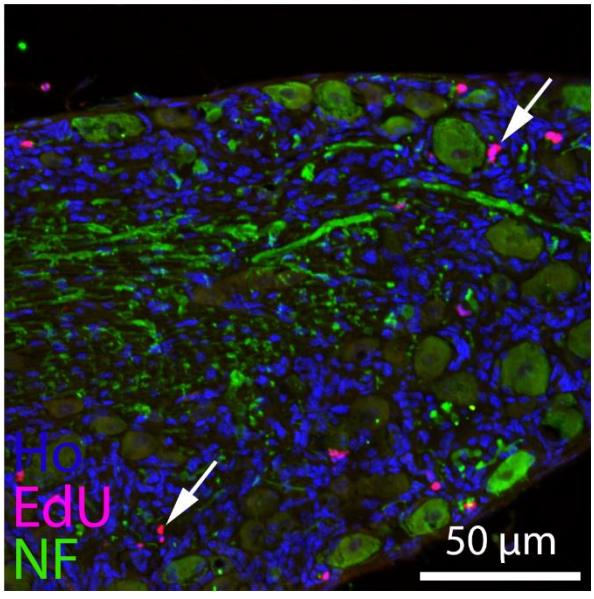

Figure 3.11.1: 3 and 5 month NF2 sKO vestibular ganglion (VG) and 5 month NF2 sKO DRG sections stained for Neurofilament (NF) and EdU *revealed striking similarities between ganglia. Typical large neuronal cell bodies encompassed by non-neuronal cells and EdU positive nuclei found in both ganglia. Sections counterstained with DNA dye Hoechst (Ho) to detect all cell nuclei. Scale bar = 50 µm in all images. White arrows in each image mark examples of EdU positive nuclei. n = 3 mice per genotype and timepoint. Representative images are shown.*

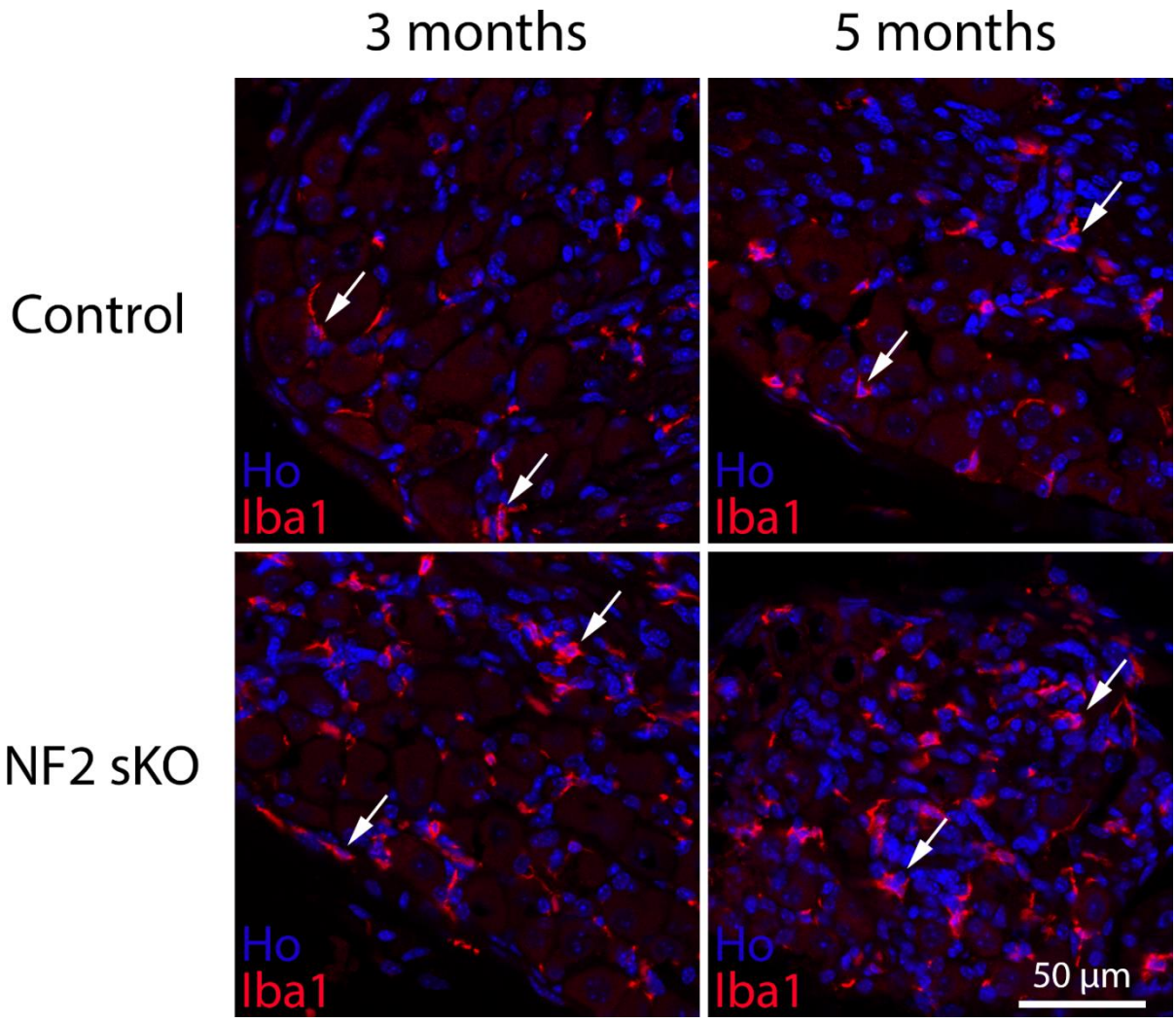

Figure 3.11.2: Iba1 stained VG sections of 3 month and 5 month old control and NF2 sKO mice *suggested that NF2 sKO VGs contained more Iba1 positive macrophages than corresponding control VGs. DNA dye Hoechst (Ho) used as counterstain to mark all cell nuclei. Scale bar = 50 µm in all images. White arrows in each image point out examples of Iba1 positive cells. n = 3 mice per genotype and timepoint. Representative images are shown.*

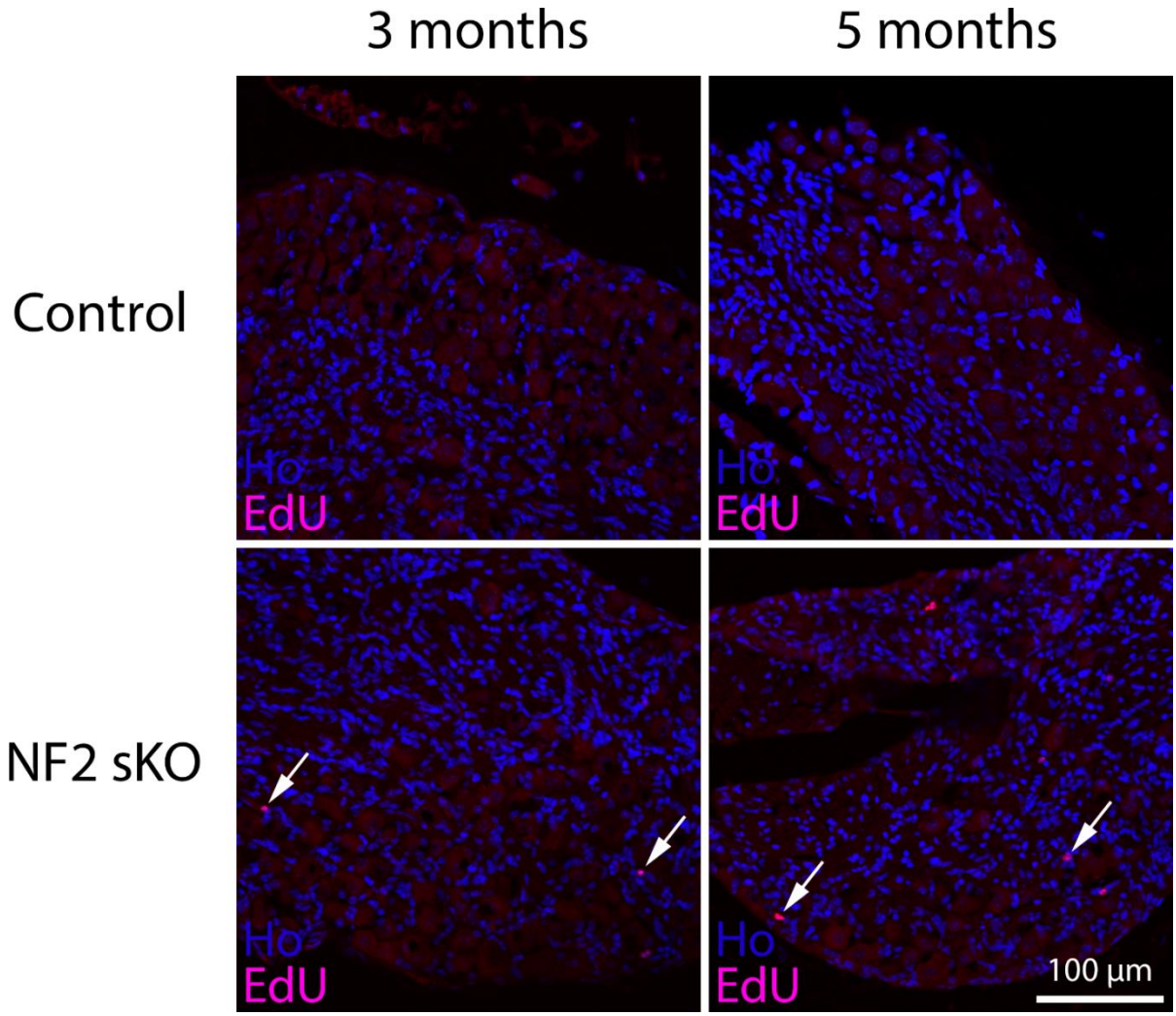

Figure 3.11.3: Frozen VG sections of 3 month and 5 month old control and NF2 sKO mice *revealed EdU positive nuclei in NF2 sKO VGs while control VGs contained none. Sections counterstained using DNA dye Hoechst (Ho) identifying all cell nuclei. Scale bar = 100 µm in all images. White arrows in each image mark examples of EdU positive nuclei. n = 3 mice per genotype and timepoint. Representative images are shown.*

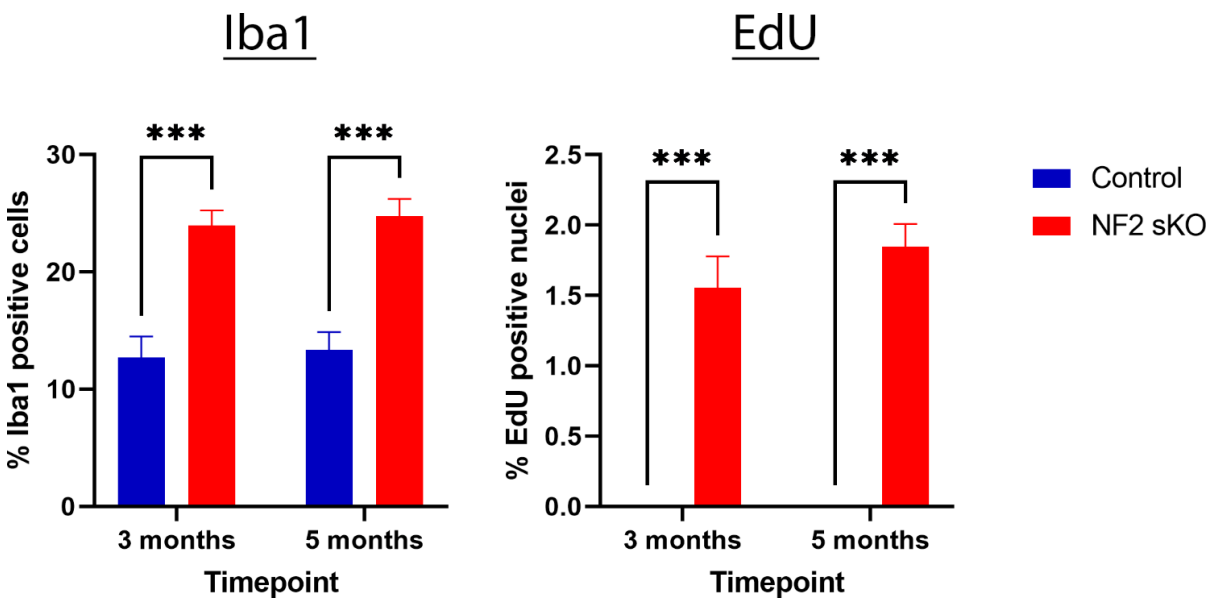

Figure 3.11.4: Quantification of 3 month and 5 month timepoint VGs of control and NF2 sKO mice *revealed significantly higher percentages of Iba1 positive macrophages and EdU positive nuclei in NF2 sKO VGs compared to respective control VGs ($p < 0.001$ for all mentioned comparisons). Quantification of Iba1 positive cells as % of non-neuronal cells (left) and EdU positive nuclei as % of non-neuronal cell nuclei (right) in VG tissue of control and NF2 sKO of 3 and 5 month old mice. No significant difference in % Iba1 positive macrophages and % EdU positive nuclei found between 3 and 5 months VGs of the same genotype (pairwise comparison brackets not shown). n = 3 mice per genotype and timepoint. Graphs shows % Iba1 positive cells (left) or % EdU positive nuclei (right) in VG tissue as means ± SD tested for significance using two-way ANOVA with Šídák's multiple comparisons test * $p \leq 0.05$; ** $p \leq 0.01$; *** $p \leq 0.001$.*

3.12 Testing the effect of TEAD palmitoylation inhibitors on the proliferation of human meningioma cell lines

Dr Liyam Laraba of our lab had previously shown that TEAD S-autopalmitoylation inhibitors by Vivace Therapeutics managed to significantly reduce proliferation in the DRGs and VGs of NF2 sKO mice in the Postn-Cre driven *in vivo* schwannoma model (Laraba *et al.*, 2022). As described previously (see Introduction sections 1.5.2, 1.5.4 and 1.5.7), Neurofibromatosis type II can cause schwannomas, meningiomas and more rarely, ependymomas. Therefore, we also decided to test these newly developed Vivace TEAD palmitoylation inhibitors (see Introduction section 1.15.4) on human meningioma cell lines in cell culture to see whether they would have any effects on their proliferation. If that would be the case, further use in primary meningioma cells and eventually in an *in vivo* meningioma mouse model would be warranted.

In short, the various groups of compounds developed by Vivace (e.g. VT1, named VT104 in literature) are characterized as a bicyclic compounds (Tang *et al.*, 2021) which allosterically inhibit TEAD interaction with YAP and TAZ by interfering with the S-autopalmitoylation of TEAD proteins (Bum-Erdene *et al.*, 2019; Chan *et al.*, 2016; Kaneda *et al.*, 2020; Lu *et al.*, 2019; Noland *et al.*, 2016). Disrupting YAP/TAZ-TEAD mediated gene expression would likely lead to

a decrease in several cell functions including cell survival and proliferation, thereby impairing tumour formation as demonstrated before (Chan *et al.*, 2016; Holden *et al.*, 2020; Li *et al.*, 2020).

As explained previously (Material and Methods section 2.2.2), proliferation of cells was measured by adding EdU to reach a final concentration of 10 µM EdU in each well. It was therefore necessary to determine an appropriate incubation time for the EdU, i.e. an incubation time that would not be too long as to cause nearly or possibly all cells to become EdU positive and also not too short causing too few cells to be EdU positive, both being conditions which would make it impossible to detect differences in proliferation. For this test, the extremely fast growing and robust IOMM-Lee cell line (Lee, 1990) was chosen due to its high proliferation rate, ensuring that the incubation time chosen would never be too long to distinguish differences in cell growth rates even in rapidly proliferating cells. IOMM-Lee cells are an NF2 positive human Grade III meningioma cell line (Mei *et al.*, 2017).

After EdU incubation, the EdU positive cell nuclei were detected by conjugating a fluorophore to the EdU nucleotides via a Click-iT reaction and imaged using a Leica IM8 microscope (Figures 3.12.1, 3.12.2, 3.13.1 and 3.13.3). Finally, the captured images were quantified using ImageJ and Microsoft Excel. The resulting percentages of EdU positive nuclei were subjected to statistical testing using GraphPad Prism 9 (Figures 3.12.3, 3.13.2, 3.13.4 and 3.13.5).

As shown in Figure 3.12.1, 1, 2, 4 and 24 hour incubation times were used plus a control to which EdU was never added. As expected, the nuclei of the control (Ctrl) cells were EdU negative while after 1 hour (1 h) and 2 hours of EdU incubation (2 h) a fairly similar number of EdU positive nuclei were seen (40.4 % and 34.6 %, respectively). A slightly increased percentage of EdU positive nuclei (51.4 %) could be seen after 4 hours of incubation (4 h). Finally, 24 hours of incubation (24 h) resulted in almost all nuclei being EdU positive (98.1 %) showing that a 24 hour EdU incubation period might make it very difficult to see differences in proliferation between different conditions. The incubation period of 4 hours was a chosen as a suitable middle ground allowing the detection of an increase or a decrease of EdU positive nuclei within reasonable margins and thereby picking up differences in proliferation depending on the given cell type and condition.

After finding an appropriate EdU incubation period I tested the aforementioned TEAD palmitoylation inhibitors in two NF2 null human meningioma cell lines, Grade I meningioma cell line BM-1 (Chow *et al.*, 2015; Mei *et al.*, 2017; Puttmann *et al.*, 2005) and Grade III meningioma cell line KT21-MG1 (KT21) (Chow *et al.*, 2015; Tanaka *et al.*, 1989). I used one of the first generation TEAD palmitoylation inhibitors (named V1 - V6) supplied by Vivace. Previous experiments showed that V2, V3 and V5 seemed to work the most efficiently when it came to inhibiting proliferation so these three inhibitors were used at 3 different concentrations, namely 10 nM, 100 nM and finally 1 µM as the highest concentration. 1 µM was chosen to be the highest concentration because 1 µM of TEAD palmitoylation inhibitor was previously shown to be sufficient to impair TEAD S-autopalmitoylation (Tang *et al.*, 2021) and therefore effects on cell proliferation are very likely to be seen at this inhibitor concentration.

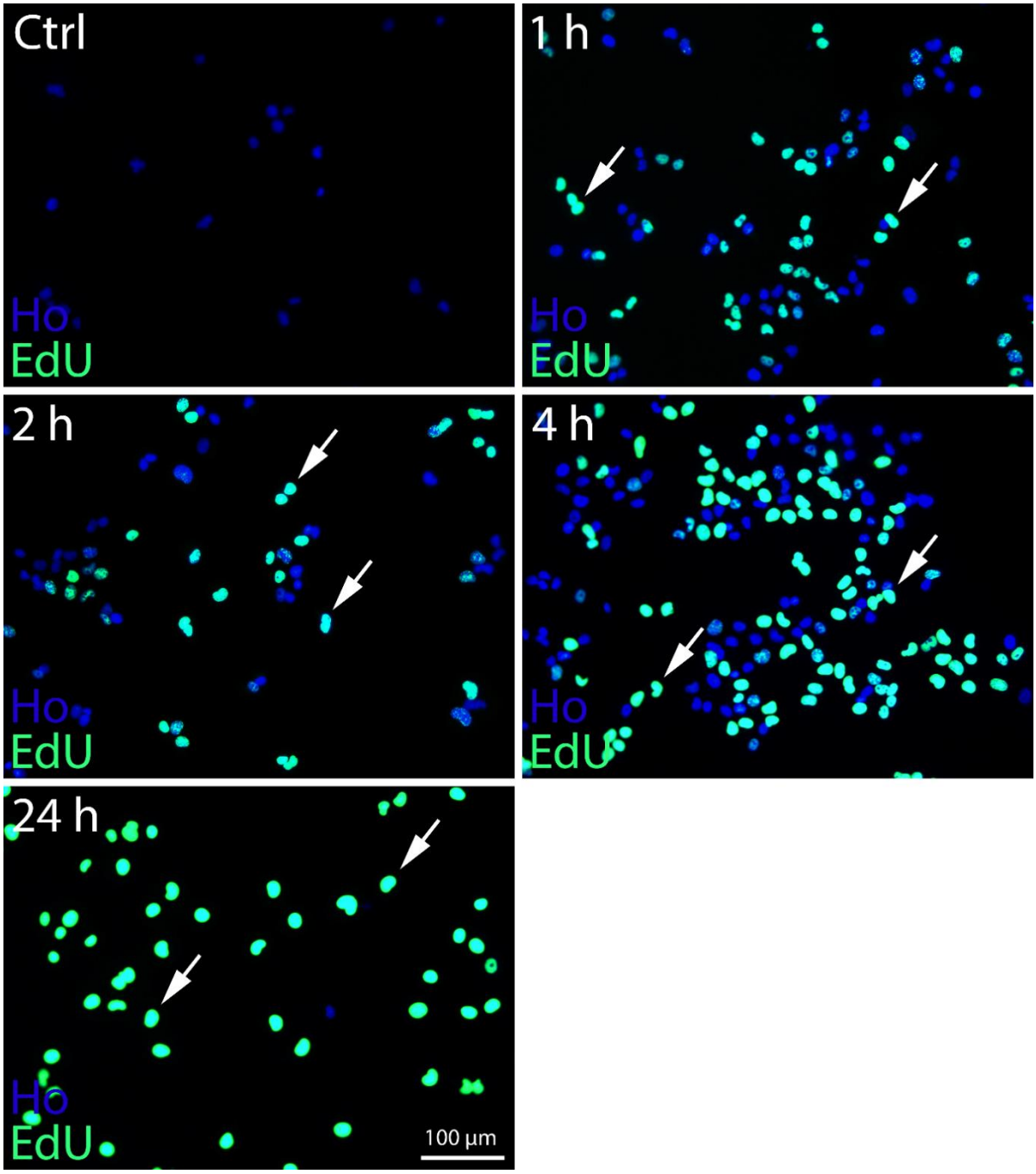

Figure 3.12.1: After testing the four different EdU pulse incubation times on IOMM-Lee cells 4 hours (4 h) was chosen as a suitable EdU pulse time. *IOMM-Lee cells incubated with 10 µM of EdU for 1 hour (1 h), 2 hours (2 h), 4 hours (4 h) and 24 hours (24 h) to determine the standard EdU incubation period. Control (Ctrl) was not given EdU. Similar numbers of EdU positive nuclei seen after 1 h and 2 h EdU pulse, increase of EdU positive nuclei after 4 h EdU pulse. Almost all nuclei EdU were positive after 24 h pulse. DNA dye Hoechst (Ho) counterstain marked all nuclei. White arrows show examples of EdU positive nuclei. Scale bar = 100 µm. n = 1 replicate wells per treatment in each cell line, n = 1 experiment repeats.*

As mentioned in Materials and Methods (Materials and Methods section 2.2.2), the cells were left to attach to the coverslips in the 24 well plates for 2 hours and then treated for 48 hours with media containing either V2, V3 or V5 at 10 nM, 100 nM or 1 µM or with media containing the vehicle DMSO as control. 3 wells per concentration and inhibitor were used as well as 3

wells for the vehicle control. After 44 hours, EdU was added into the media of all wells to achieve a final concentration of 10 µM of EdU in each well. 4 hours later the cells were washed, fixed and subjected to a Click-iT reaction to fuse an Alexa Fluor 594 fluorophore to the EdU. This allowed the identification of the fraction of cells which were in the S phase of the cell cycle at any point in the last 4 hours of the experiment, marking them as proliferating cells. This experiment was repeated 3 times for each cell line to reach an n of 3 repeats.

As can be seen in the DMSO vehicle controls in Figure 3.12.2, the KT21 cells appeared to have a larger amount of cells with EdU positive nuclei than the BM-1 cells. This pointed towards a higher proliferation rate of KT21 cells compared to the BM-1 cells, later confirmed after quantification (Figure 3.12.3). All three inhibitors (V2, V3 and V5) at a concentration of 1 µM had a clearly visible effect on both BM-1 and KT21 cells, causing a decrease in the percentage of EdU positive nuclei.

Quantification of the three repeated experiments (see Figure 3.12.3) showed that untreated BM-1 cells (vehicle control) had an average proliferation rate of 34.1% ± 7.1 % SD (=standard deviation). 10 nM of V3 and V5 reduced the proliferation rate to 26.0 % ± 4.8 % and 30.0 % ± 3.6 %, respectively, which proved to be not significant. Only V2 at a 10 nM concentration managed to decrease the proliferation to 22.7 % ± 4.6 %, a difference which was significant (* $p = 0.04$). At the concentration of 100 nM and 1 µM all three inhibitors displayed significant reductions in cell proliferation compared to the DMSO vehicle control (p-values: Vehicle vs. V2 100 nM = 0.002; Vehicle vs. V3 100 nM = <0.001; Vehicle vs. V5 100 nM = 0.004; Vehicle vs. V2 1 µM, V3 1 µM or V5 1 µM = <0.001) while having non-significant differences when being compared to each other within the same concentrations.

The greatest decrease in cell proliferation within the BM-1 cells was seen with 1 µM of V3, reducing the proliferation rate from 34.1 % ± 7.1 % in the vehicle to 10.7 % ± 2.4 %.

In contrast, the KT21 cells had a higher average base proliferation rate of 43.4 % ± 6.0 % but seemed to be more resistant to the TEAD palmitoylation inhibitors than the BM-1 cells (Figure 3.12.3). While all three inhibitors used at 10 and 100 nM concentrations appeared to decrease the rate of cell growth to a certain degree, none of these differences were significant (ns) compared to the vehicle control.

Only when subjected to the inhibitors at the highest concentration (1 µM) the three TEAD palmitoylation inhibitors showed significant decreases in cell growth compared to the DMSO vehicle control (p-values: Vehicle vs. V2 1 µM = 0.04; Vehicle vs. V3 1 µM = 0.02; Vehicle vs. V5 1 µM = 0.009) although they did not display such a significant difference when compared to each other at the same concentration.

The most efficient inhibitor here appeared to have been V5 at 1 µM which caused the proliferation rate to drop to 24.8 % ± 5.5 % and exhibit a more significant difference (** $p = 0.009$) than the other two inhibitors at the same concentration compared to the vehicle control.

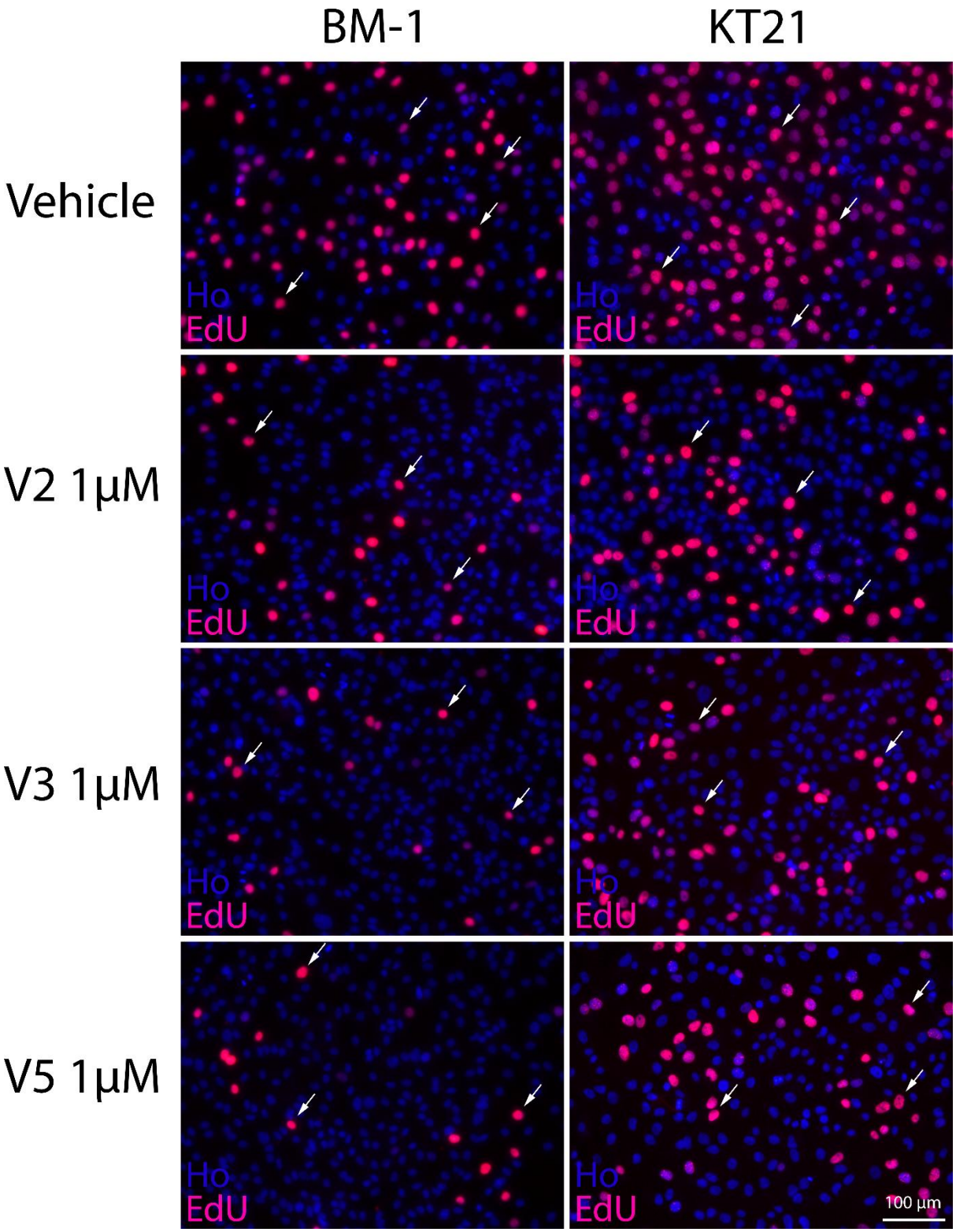

Figure 3.12.2: Usage of TEAD palmitoylation inhibitors V2, V3 and V5 at a concentration of 1 µM for 48 hours in BM-1 and KT21 cells *visibly reduced the number of EdU positive nuclei in BM-1 and KT21 cells compared to the DMSO vehicle control (Vehicle). More EdU positive nuclei were also noted in control KT21 cells compared to the control BM-1 cells. Counterstaining with DNA dye Hoechst (Ho) allowed visualization of all nuclei. White arrows point out examples of EdU positive nuclei. Scale bar = 100 µm. n = 3 replicate wells per treatment in each cell line, n = 3 experiment repeats. Representative images are shown.*

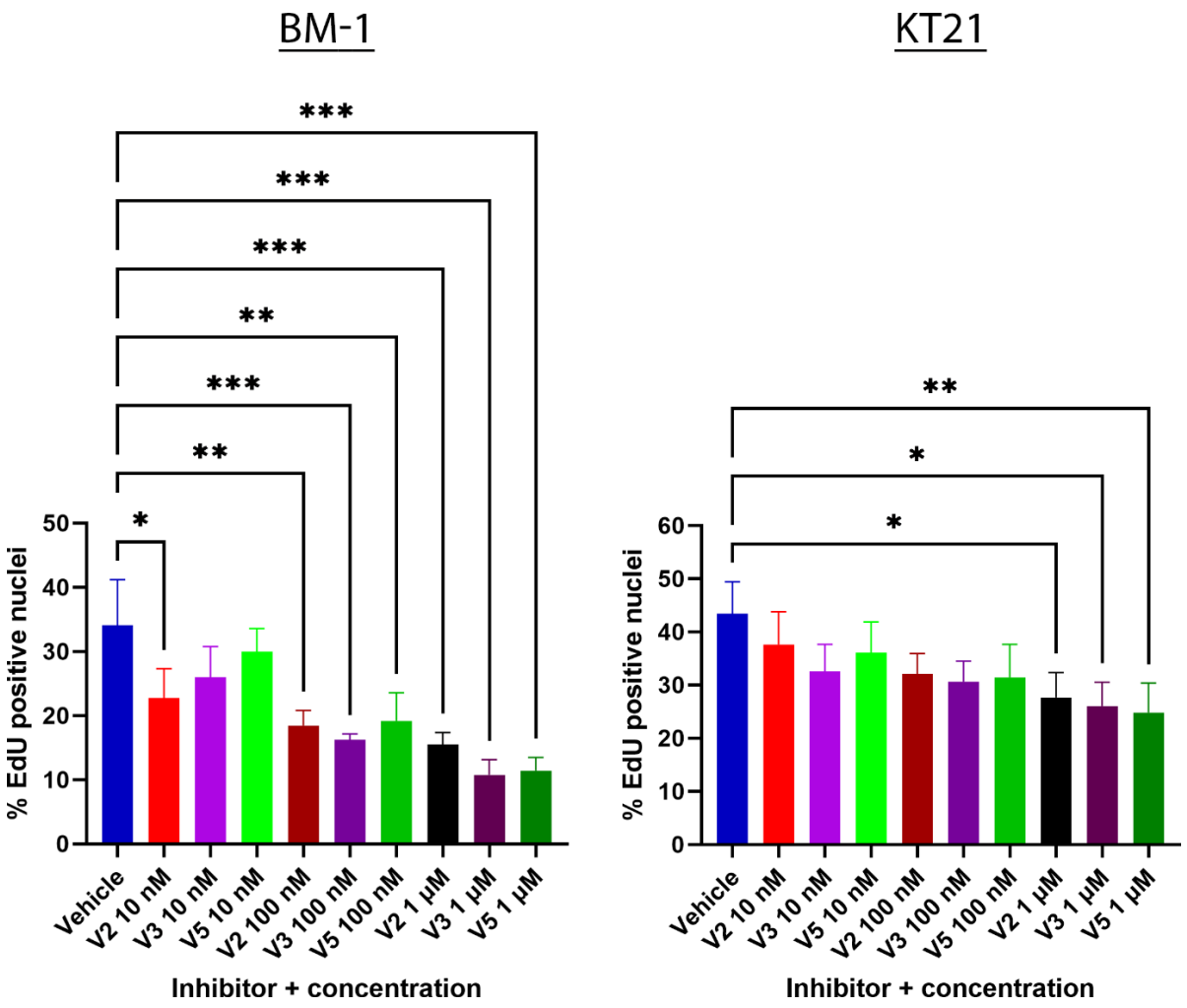

Figure 3.12.3: Quantification of EdU positive nuclei in BM-1 and KT21 cells after incubation with TEAD palmitoylation inhibitors *revealed that TEAD palmitoylation inhibitors V2, V3 and V5 significantly decreased cell proliferation of both BM-1 and KT21 cells. Quantification of the EdU positive nuclei as % of all nuclei in BM-1 and KT21 cells treated with TEAD palmitoylation inhibitors V2, V3 and V5 at 10 nM, 100 nM and 1 µM concentrations or vehicle for 48 hours.* ***BM-1****: Significant reduction in cell proliferation found after treatment with 10 nM V2 (* p = 0.04) compared to control (Vehicle). Same applied to all tested inhibitors at 100 nM and 1 µM (p-values: Vehicle vs. V2 100 nM = 0.002; Vehicle vs. V3 100 nM = <0.001; Vehicle vs. V5 100 nM = 0.004; Vehicle vs. V2 1 µM, V3 1 µM or V5 1 µM = <0.001). Difference in % EdU positive nuclei was not significant between inhibitors within same concentrations.* ***KT21:*** *Significant decrease in cell proliferation compared to vehicle control only seen after treatment with inhibitors at 1 µM (p-values: vehicle vs. V2 1 µM = 0.04; vehicle vs. V3 1 µM = 0.02; vehicle vs. V5 1 µM = 0.009). As observed before, no significant difference in effect between inhibitors at the same concentrations. n = 3 replicate wells per treatment and concentration in each cell line, n = 3 experiment repeats per cell line. Graphs show % EdU positive nuclei as means ± SD tested for significance using one-way ANOVA with Tukey's multiple comparisons test. * p ≤ 0.05; ** p ≤ 0.01; *** p ≤ 0.001. Not significant (ns) pairwise comparison brackets were excluded from the graphs.*

The relative half-maximal inhibitory concentration (relative IC_{50}) for the three inhibitors in the two cell lines was determined as well (Table 3.1). Here the relative IC_{50} is the concentration of inhibitor at which the inhibition of the cell proliferation would be halfway between the

minimum inhibition defined as the proliferation rate at 10 nM of inhibitor concentration and the maximum inhibition defined as the proliferation rate at 1 µM of inhibitor concentration.

IC_{50} in nM			
	V2	**V3**	**V5**
BM-1	64.02	48.71	66.42
KT21	76.76	296.8	153.9

Table 3.1: IC_{50} values calculated for TEAD palmitoylation inhibitors V2, V3 and V5 *reveal a stronger inhibitory effect in BM-1 cells compared to KT21 cells. The IC_{50} values in nanomolar (nM) concentrations were calculated by applying a nonlinear regression (curve fit) to the quantification values of Figure 3.12.3. As expected, the IC_{50} values of the three inhibitors in the BM-1 cells were always lower than the IC_{50}s of the inhibitors found in the KT21 cells reconfirming a higher susceptibility of the BM-1 to the effects of the TEAD palmitoylation inhibitors.*

Calculation of the IC_{50} values (Table 3.1) confirmed V3 to be the most potent TEAD palmitoylation inhibitor in BM-1 cells. Also, IC_{50} values in BM-1 cells were always lower than in the KT21 cells, again pointing towards a higher overall susceptibility of the BM-1 cells to the inhibitors. According to the IC_{50} values, the inhibitor V2 had the strongest effect in the KT21 cells, contradicting the earlier finding made suggesting V5 was the most effective inhibitor of proliferation in this cell line. In light of both observations it can be concluded that both V2 and V5 were the most potent inhibitors in KT21 cells.

In summary, after determining the appropriate EdU incubation time to adequately assess proliferation rates in cell culture (Figure 3.12.1) I tested some of the first generation Vivace TEAD selective palmitoylation inhibitors at different concentrations on NF2 null BM-1 and KT21 cells (Figure 3.12.2). Quantification paired with statistical analysis (Figure 3.12.3) revealed that TEAD palmitoylation inhibitors V2, V3 and V5 were far more efficient in inhibiting proliferation in BM-1 cells than in KT21 cells (also see Table 3.1) where only the highest inhibitor concentration of 1 µM caused a significant decrease in proliferation rates compared to vehicle control.

3.13 Testing the effect of Pan-TEAD inhibitors on the proliferation of primary human meningioma cells

Having concluded our work on meningioma cell lines I moved on to primary meningioma cells kindly provided to us by Dr Emanuela Ercolano. These primary meningioma cells were originally derived from surgically removed meningiomas of human patients (see Table 2.1).

I tested TEAD palmitoylation inhibitors on 3 Merlin null and 5 Merlin positive primary human meningioma cells (see Table 2.1). The previously used TEAD S-autopalmitoylation inhibitors V2, V3 and V5 which were developed to specifically inhibit one of the TEADs (TEAD 1, 2, 3 or 4) over the others were replaced by two Pan-TEAD S-autopalmitoylation inhibitors, in this work termed VT1 (VT104 in literature (Tang *et al.*, 2021)) and VT2. VT1 and VT2 as Pan-TEAD inhibitors effectively target and impair the function of all four TEADs similarly (information

provided by Vivace Therapeutics). VT1/VT104 was confirmed to be a Pan-TEAD inhibitor and a bicyclic aromatic compound which efficiently blocks the proliferation of NF2 negative mesothelioma cells both *in vitro* and *in vivo* (Tang *et al.*, 2021). VT2 aka VT3989 officially does not have a reported chemical structure or compound classification and will be used in a phase I clinical trial with human patients diagnosed with treatment-resistant (refractory) malignant pleural mesotheliomas and other refractory metastatic solid tumours (see *https://clinicaltrials.gov/ct2/ show/NCT04665206*).

Recent findings via Western blot by Postdoctoral Researcher Liyam Laraba suggest that TEAD1 - 4 expression in different primary human schwannoma cells is highly heterogeneous. This is also assumed to be the case in primary human meningioma cells. Therefore, to more effectively impair the proliferation of primary meningioma cells regardless of the TEADs they preferentially signal through, the Pan-TEAD inhibitors VT1 and VT2 were used. Aside from changing to Pan-TEAD inhibitors VT1 and VT2 and using Merlin null and Merlin positive primary meningioma cells, the experimental methodology remained identical. Once again, inhibitor concentrations of 10 nM, 100 nM and 1 µM for 48 hours and 3 wells per inhibitor and concentration plus 3 DMSO vehicle control wells were used.

As seen in Figure 3.13.1, the three Merlin null primary meningioma cells used were MOT 148, MOT 161 and MOT 273 (see also Table 2.1). Visual comparison of the DMSO vehicle controls of all three MOT cells (Figure 3.13.1, Vehicle) to each other showed that MOT 148 appeared to have the largest amount of EdU positive nuclei and therefore the highest proliferation rate of the three, followed by MOT 161 and finally MOT 273 with the lowest proliferation rate. This visual assessment was later confirmed by quantification (Figure 3.13.2). Furthermore, both VT1 and VT2 at 1 µM reduced the number of EdU positive nuclei in these Merlin null primary meningioma cells.

Figure 3.13.2 shows the quantification of the EdU positive nuclei as percentage of all counted nuclei found in the three Merlin null primary meningioma cells after incubation with VT1 or VT2 at three different concentrations or with the vehicle DMSO as control. MOT 148 presented with an average proliferation rate of 38.9 % ± 3.4 % while MOT 161 and MOT 273 had cell division rates of 20.7 % ± 3.0 % SD and 10.7 % ± 0.8 %, respectively. It was determined that 10 nM, 100 nM and 1 µM of either VT1 or VT2 for 48 hours caused a significant decrease in proliferation compared to vehicle baseline control in all of these Merlin null primary meningioma cells ($p < 0.001$ for all of them, Figure 3.13.2). Furthermore, no significant difference in proliferation could be ascertained between the two inhibitors when comparing the same concentrations in the same MOT cells.

The Merlin positive primary meningioma cells used for testing were MOT 172, MOT 240, MOT 310, MOT 357 and MOT 447 (see Table 2.1). MOT 172 under control conditions seemed to have the highest cell proliferation rate by possessing the biggest number of EdU positive nuclei while the opposite appeared to be true for MOT 310 (Figure 3.13.3). This was not supported by quantification (see Figure 3.13.4). 1 µM of either inhibitor decreased the amount of EdU positive nuclei in all five MOT cells.

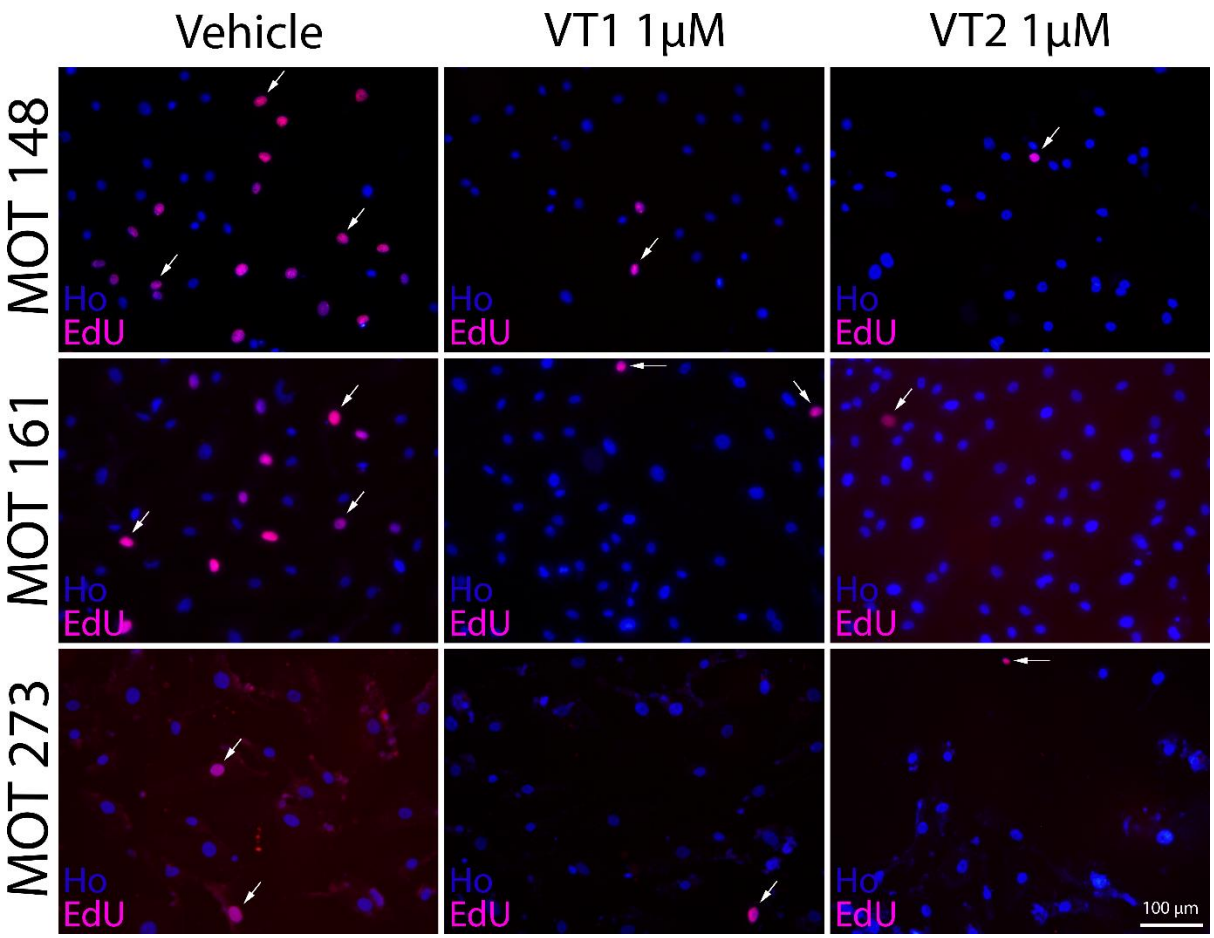

Figure 3.13.1: Images of Merlin null primary human meningioma cells treated with Pan-TEAD inhibitors VT1 or VT2 at 1 µM for 48 hours *showed decreased amounts of EdU positive nuclei compared to vehicle controls (Vehicle). Comparing controls showed control MOT 148 cells exhibited the most EdU positive nuclei while control MOT 273 had the least. DNA dye Hoechst (Ho) counterstain allowed detection of all nuclei. White arrows mark examples of EdU positive nuclei. Scale bar = 100 µm. n = 3 replicate wells per treatment and MOT cell, n = 1 experiment repeats. Representative images are shown.*

Quantification and testing for statistical significant differences of proliferation rates in Merlin positive primary meningioma cells is shown in Figure 3.13.4. In MOT 172 and MOT 357 cells, VT1 and VT2 at 10 nM both exhibited significant distinctions of cell proliferation rates compared to vehicle control (p-values for MOT 172: Vehicle vs. VT1 10 nM = 0.004; Vehicle vs. VT2 10 nM = <0.001; p-values for MOT 357: Vehicle vs. VT1 10 nM or VT2 10 nM = <0.001) and to one another (p-value for MOT 172: VT1 10 nM vs. VT2 10 nM = 0.02; p-value for MOT 357: VT1 10 nM vs. VT2 10 nM = 0.009). Furthermore, both inhibitors at 100 nM and 1 µM in these MOT cells showed significant differences of cell division rates to control ($p < 0.001$ for all mentioned pairwise comparisons) but not to each other at these concentrations within the same MOT cells.

In MOT 240, MOT 310 and MOT 447 cells both inhibitors at all tested concentrations caused a significant difference in proliferation rates (Figure 3.13.4) compared to vehicle control ($p < 0.001$ for all of them) but never to each other when comparing the effects within the same concentration and MOT cell.

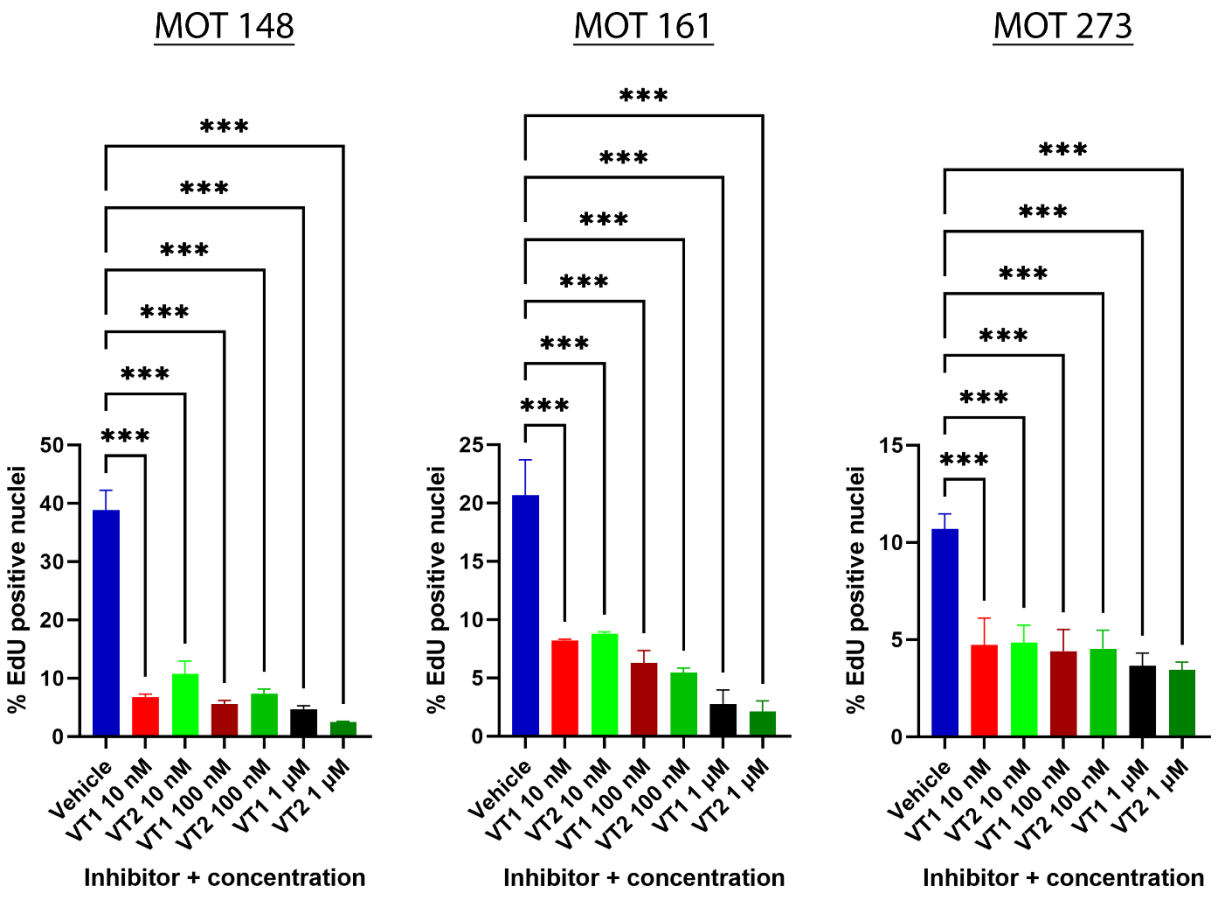

Figure 3.13.2: Quantification of EdU positive nuclei in Merlin null primary human meningioma cells after incubation with Pan-TEAD inhibitors VT1 and VT2 *showed significantly impaired proliferation. Quantification of the EdU positive nuclei as % of all nuclei in Merlin null primary meningioma cells treated with Pan-TEAD inhibitors VT1 and VT2 at 10 nM, 100 nM and 1 µM concentrations or vehicle (Vehicle). MOT 148, MOT 161 and MOT 273 cells had varying baseline cell division rates (vehicle control) which were significantly reduced by all used concentrations of both inhibitors (p-value < 0.001 for all). No significant difference in efficacy found between VT1 and VT2 at the same concentrations in the same cells. n = 3 replicate wells per treatment and MOT cell, n = 1 experiment repeats. Graphs show % EdU positive nuclei as means ± SD tested for significance using one-way ANOVA with Tukey's multiple comparisons test. * p ≤ 0.05; ** p ≤ 0.01; *** p ≤ 0.001. Not significant (ns) pairwise comparison brackets were excluded from the graphs.*

All in all, even the lowest examined concentration of 10 nM of either VT1 or VT2 for 48 hours in both the Merlin null and Merlin positive primary meningioma cells resulted in a significant reduction of cell proliferation compared to vehicle controls and increasing the inhibitor concentrations tended to enhance the proliferation suppressing effect of the Pan-TEAD palmitoylation inhibitors.

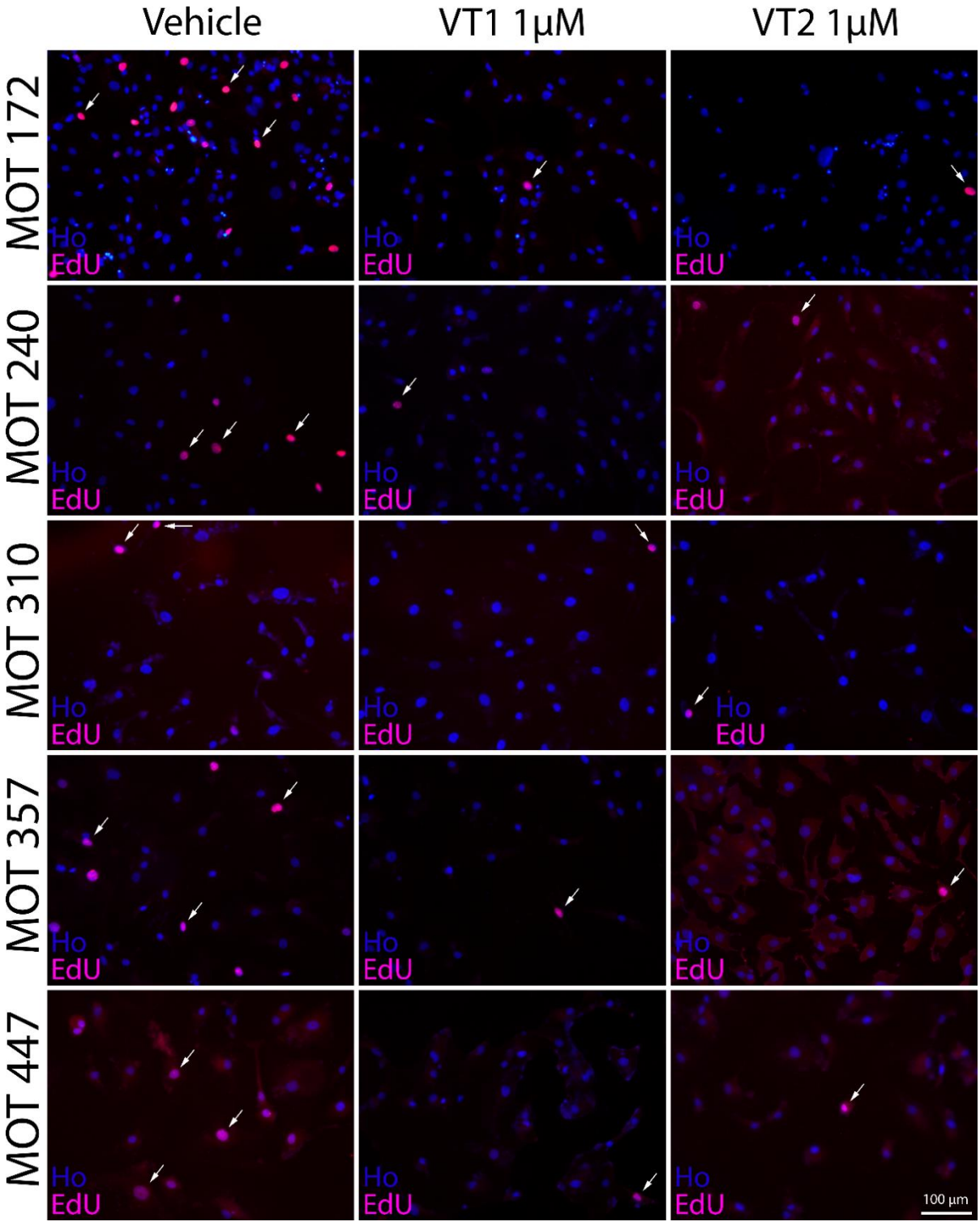

Figure 3.13.3: Images of Merlin positive primary human meningioma cells after 1 µM of Pan-TEAD inhibitor VT1 or VT2 or Vehicle for 48 hours *showed a reduction in the number of EdU positive nuclei compared to vehicle control (Vehicle). Using DNA dye Hoechst (Ho) as a counterstain permitted visualization of all cell nuclei. White arrows point out examples of EdU positive nuclei. Scale bar = 100 µm. n = 3 replicate wells per treatment and MOT cell, n = 1 experiment repeats. Representative images are shown.*

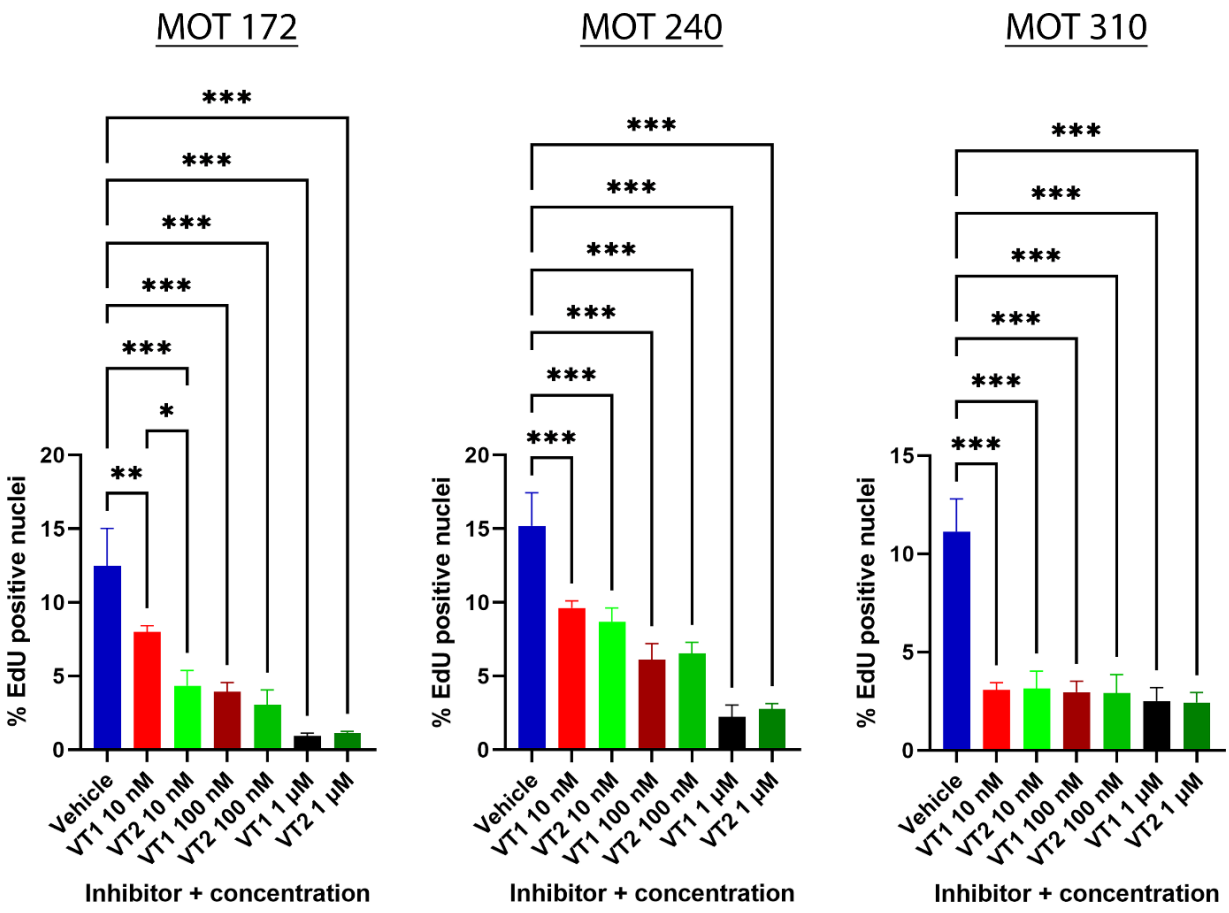
MOT 172
MOT 240
MOT 310
% EdU positive nuclei
Vehicle
VT1 10 nM
VT2 10 nM
VT1 100 nM
VT2 100 nM
VT1 1 µM
VT2 1 µM
Inhibitor + concentration

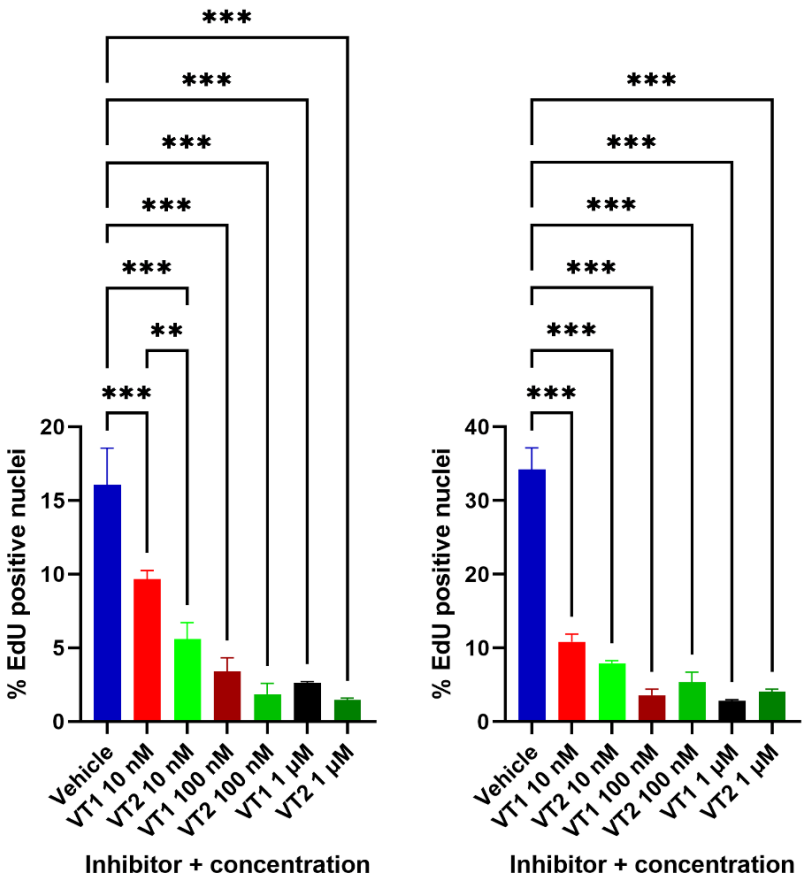
MOT 357
MOT 447
% EdU positive nuclei
Vehicle
VT1 10 nM
VT2 10 nM
VT1 100 nM
VT2 100 nM
VT1 1 µM
VT2 1 µM
Inhibitor + concentration

Figure 3.13.4: Quantification of EdU positive nuclei in Merlin positive primary human meningioma cells after incubation with Pan-TEAD inhibitors VT1 and VT2 *revealed significantly decreased proliferation. Quantification of the EdU positive nuclei as % of all nuclei in Merlin null primary meningioma cells treated with Pan-TEAD inhibitors VT1 and VT2 at 10 nM, 100 nM and 1 µM concentrations or vehicle (Vehicle). Cell proliferation rates of MOT 172, MOT 240, MOT 310, MOT 357 and MOT 447 significantly reduced by both Pan-TEAD inhibitors at all tested concentrations (p-values for MOT 172: Vehicle vs. VT1 10 nM = 0.004; Vehicle vs. VT2 10 nM = <0.001; Vehicle vs. VT1 or VT2, 100 nM or 1 µM = <0.001; p-values for MOT 240, MOT 310, MOT 357 and MOT 447: Vehicle vs. VT1 or VT2 at all concentrations = <0.001). Significant difference in inhibitor efficiency was overall not detected, with the notable exceptions being in MOT 172 and MOT 357 cells at 10 nM inhibitor concentration (p-value for MOT 172: VT1 10 nM vs. VT2 10 nM = 0.02; p-value for MOT 357: VT1 10 nM vs. VT2 10 nM = 0.009). n = 3 replicate wells per treatment and MOT cell, n = 1 experiment repeats. Graphs show % EdU positive nuclei as means ± SD tested for significance using one-way ANOVA with Tukey's multiple comparisons test. * p ≤ 0.05; ** p ≤ 0.01; *** p ≤ 0.001. Not significant (ns) pairwise comparison brackets were excluded from the graphs.*

Table 3.2 displays the relative IC_{50} values of both the Merlin null and Merlin positive primary meningioma cells. As mentioned before, the relative IC_{50} here is the inhibitor concentration at which the inhibition of the cell growth would be halfway between the proliferation rate at 10 nM inhibitor concentration defined as minimum inhibition and the proliferation rate at 1 µM inhibitor concentration defined the maximum inhibition. Differences could be seen in inhibitor susceptibility both between the MOT cells within their respective groups (Merlin status) and between the two inhibitors within said Merlin status groups (Table 3.2) but given the uncorrelated appearance of the calculated relative IC_{50} values a conclusion based on these values could not be drawn.

IC_{50} in nM			
		VT1	**VT2**
Merlin null	MOT 140	77.83	149.3
	MOT 161	211.3	99.22
	MOT 273	311.7	495.6
Merlin positive	MOT 172	68.42	165.0
	MOT 240	112.1	199.4
	MOT 310	796.5	268.7
	MOT 357	2.140	0.4666
	MOT 447	0.4088	41.14

Table 3.2: IC_{50} values calculated for Pan-TEAD inhibitors VT1 and VT2 in Merlin null and Merlin positive primary meningioma cells. *The IC_{50} values in nM concentrations were calculated by applying a nonlinear regression (curve fit) to the quantification values found in Merlin null and Merlin positive primary meningioma cells (Figures 3.13.2 and 3.13.4).*

Finally, the quantifications of % EdU positive nuclei (Figures 3.13.2 and 3.13.4) were standardized by dividing the % values by the % values of their respective DMSO vehicle controls, resulting in the vehicle control cell proliferation to be defined as 100 %. The resulting percentages were then grouped according to their Merlin status (Figure 3.13.5).

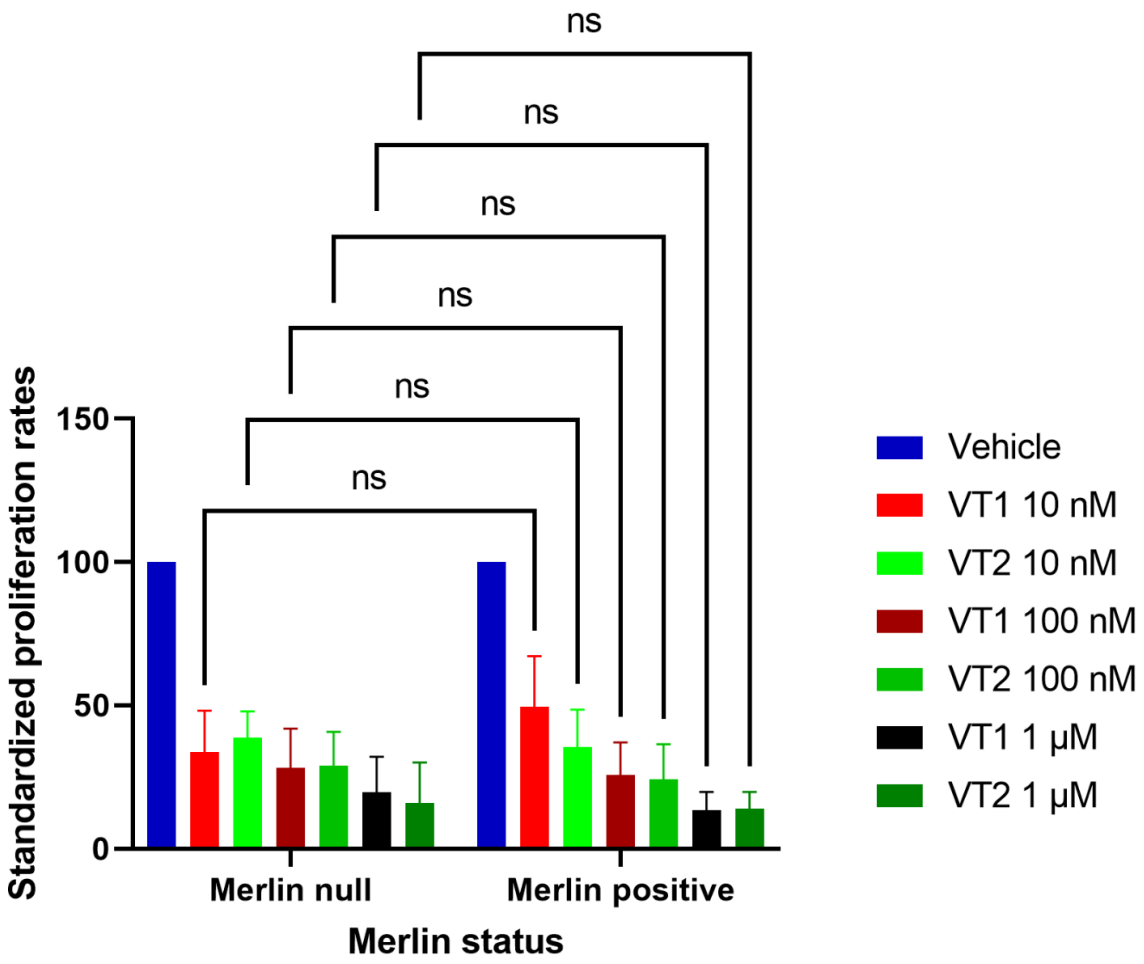

Figure 3.13.5: Standardized cell division rates of Merlin null and Merlin positive primary human meningioma cells incubated with Pan-TEAD inhibitors VT1 and VT2 *revealed equal efficacy of both inhibitors at inhibiting proliferation. Standardization was achieved by dividing each % EdU positive nuclei value by their respective DMSO vehicle control % value. No significant differences (ns) seen when comparing the proliferation inhibitory effects of the two tested Pan-TEAD inhibitors in Merlin null and Merlin positive primary meningioma cells (pairwise comparison brackets shown in graph), by means of two-way ANOVA with Šídák's multiple comparisons test. Same lack of significant distinctions found when comparing the effects of VT1 and VT2 to one another within the same inhibitor concentration and Merlin status group (pairwise comparison brackets not shown) via two-way ANOVA with Tukey's multiple comparisons test. Graph displays standardized cell proliferation rates as means ± SD. n = 3 for Merlin null, n = 5 for Merlin positive primary meningioma cells.*

Comparing the effects of VT1 and VT2 in Merlin null vs. Merlin positive primary meningioma cells or comparing the effects of one inhibitor to the other within the same inhibitor concentration and Merlin status group revealed no significant difference. Henceforth, one can conclude that the Pan-TEAD inhibitors VT1 and VT2 appear to be equally efficient in primary meningioma cells regardless of their Merlin status.

3.14 Testing the effect of Pan-TEAD inhibitors on the protein expression of CTGF and Pan-TEAD in primary human meningioma cells

After verifying the effect which the Pan-TEAD inhibitors had on primary meningioma cells we decided to see whether an incubation with the said inhibitors for 48 hours would also have change the expression of downstream effectors of the Hippo pathway, e.g. TEAD and CTGF. For that purpose primary meningioma cells were seeded in 6-well plates (3 wells per cell line and inhibitor plus 3 wells for the DMSO vehicle control) and then allowed to reach approximately 70 - 80 % confluency. Afterwards, they were treated for 48 hours with media either containing 1 µM VT1, 1 µM VT2 or the DMSO vehicle and then harvested, combining the three wells of each cell line and condition into a single sample to increase protein quantity. After processing the protein samples (see Materials and Methods section 2.2.4) they were measured by BCA assay and then kept at -20 degrees Celsius. For each Western blot, a corresponding volume of each sample equalling 30 µg of protein was loaded. The primary antibodies used were anti-Pan-TEAD and anti-CTGF antibodies. 1 gel/membrane per antibody was run to avoid as much as possible the need to strip antibodies and afterwards reapply others to detect different target proteins. Such a practice can increase the risk of detecting remnant bands. Therefore, by sticking to one gel/membrane per antibody, the chances of accurately placing the resulting bands on the right height of the protein ladder corresponding to their respective molecular weights was maximized. Subsequently, the membranes were stripped only once (an unpreventable step) and then incubated with anti-GAPDH antibody in order to pick up the housekeeping protein GAPDH, here used as a loading control. The protein bands detected by the combination of primary antibodies, secondary antibodies and chemiluminescence were then visualized by a CCD (charge-coupled device) camera (Figures 3.14.1, 3.14.3 and 3.14.5). Afterwards, the protein bands of interest were quantified using ImageJ and Microsoft Excel (Materials and Methods section 2.6) and underwent statistical testing via GraphPad Prism 9 (Figures 3.14.2, 3.14.4 and 3.14.6).

In the first Western blot attempt (Figure 3.14.1) the samples of Merlin null primary meningioma cells MOT 273 and MOT 161 displayed a notable reduction of the CTGF protein band at 37 kDa between the DMSO vehicle control (Ctrl) and the samples from the cells treated with Pan-TEAD inhibitors (VT1 and VT2). Such a difference in CTGF protein band intensity was not detected in the MOT 148 samples, 2 of which (Ctrl and VT1) unfortunately appeared to have mixed during the running of the gel (Figure 3.14.1). The bands of the loading control gene GAPDH also ran at 37 kDa and displayed acceptable variance, allowing subsequent quantification of the uncorrupted MOT 161 and MOT 273 protein bands. The normalized quantified values were grouped into vehicle, VT1 or VT2 treated to create an n of 2 repeats (Figure 3.14.2).

Statistical testing using a one-way ANOVA revealed a significant reduction in CTGF protein levels after using VT1 or VT2 (p-values for Vehicle vs. VT1 1 µM and Vehicle vs. VT2 1 µM = <0.001). However, the two inhibitor treatments caused no significant difference in CTGF protein expression when compared to each other (Figure 3.14.2).

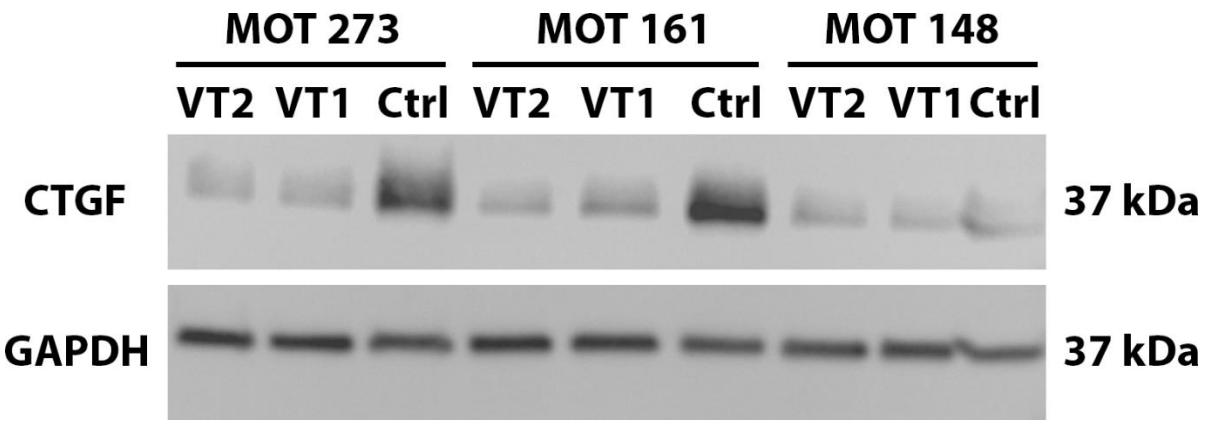

Figure 3.14.1: Western blotting of CTGF in Merlin null primary human meningioma cells after a 48 hour incubation period with Pan-TEAD inhibitors VT1 or VT2 at 1 µM *exposed a pronounced decrease in CTGF protein band intensity in MOT 161 and MOT 273 cells compared to DMSO vehicle control (Ctrl). CTGF and GAPDH bands were detected at 37 kilodalton (kDa) in MOT 273, MOT 161 and MOT 148 cells. A difference in CTGF band intensity between Ctrl and VT1/VT2 was noted in MOT 273 and MOT 161 cells. This difference was not seen in MOT 148 samples, possibly due to visible intermixing of samples. GAPDH bands revealed variability in protein loading amounts within reasonable limits. n = 1 experiment repeats.*

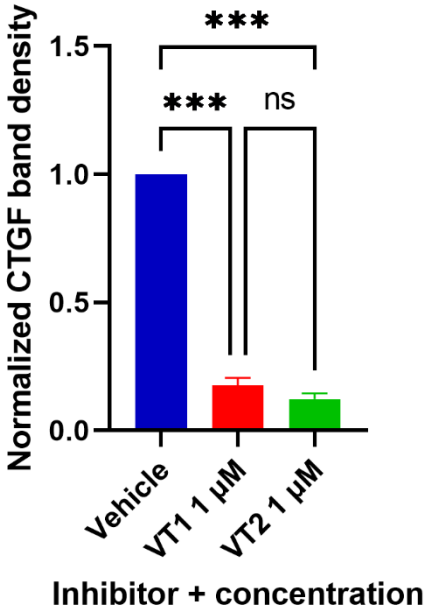

Figure 3.14.2: Quantification of protein bands in Figure 3.14.1 *revealed that there were significant differences in CTGF protein expression between Vehicle and VT1 or VT2 treated Merlin null primary meningioma cells. The normalized quantified protein band density values of MOT 161 and MOT 273 of Figure 3.14.1 were grouped into vehicle treated (Vehicle), VT1 treated (VT1) or VT2 treated (VT2) and underwent statistical analysis. Significant decrease of CTGF protein expression after VT1 or VT2 treatment (p-values for Vehicle vs. VT1 1 µM and Vehicle vs. VT2 1 µM = <0.001). No significant (ns) difference in CTGF protein levels between the treated samples. n = 2 Merlin null MOT cells per treatment. Graph displays data as means ± SD tested for significance using one-way ANOVA with Tukey's multiple comparisons test. * p ≤ 0.05; ** p ≤ 0.01; *** p ≤ 0.001.*

Attempting to achieve an n = 3, the Western blot was repeated with the same samples, looking at both CTGF and Pan-TEAD protein expression (Figure 3.14.3). No discernible differences in Pan-TEAD protein band appearance were seen after VT1 or VT2 treatment (Figure 3.14.3). Conversely, two CTGF protein bands could be confirmed in the vehicle treated controls in contrast to only one CTGF band in the VT1 or VT2 treated samples. The GAPDH control bands appeared fairly similar. Regrettably, the MOT 161 samples appeared to have mixed, making them ineligible for quantification. At first, the MOT 148 VT2 sample seemed to be slightly affected as well. Upon closer inspection, it became clear that it was fairly uncorrupted and rather distinct from the MOT 161 Ctrl sample next to it, making it unlikely that intermixing between these two samples occurred. Thus, all protein bands of MOT 148 and MOT 273 cells were included in the quantification and statistical analysis (Figure 3.14.4).

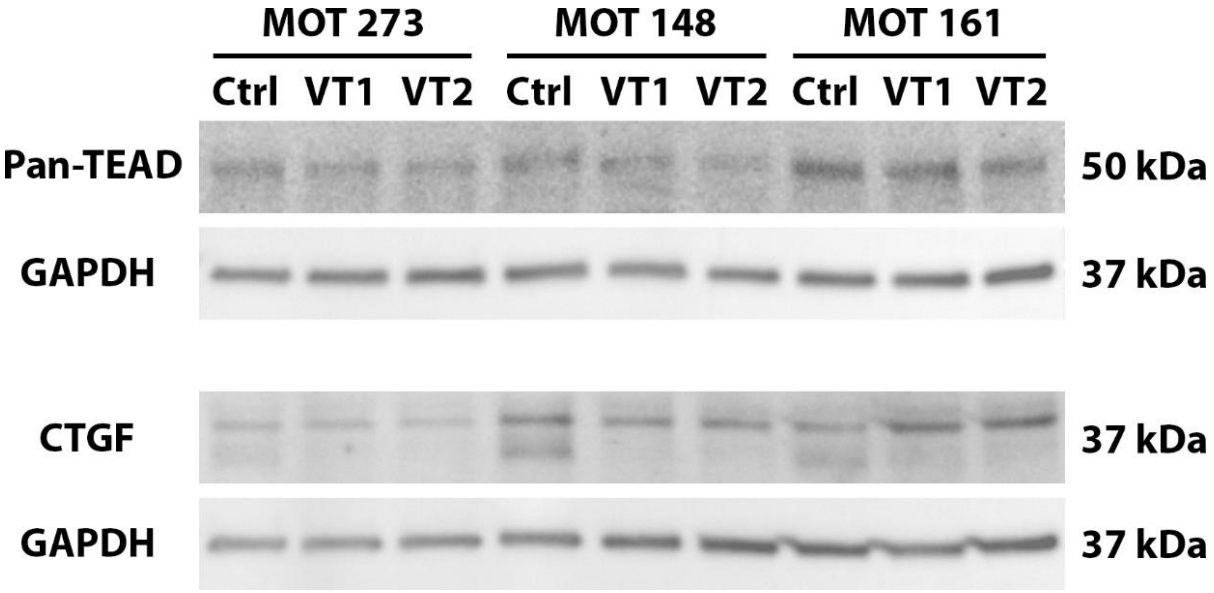

Figure 3.14.3: Immunoblotting of CTGF and Pan-TEAD after incubating Merlin null primary human meningioma cells for 48 hours with 1 µM of Pan-TEAD inhibitors VT1 or VT2. *Pan-TEAD protein bands appeared to be unaffected by incubation with the Pan-TEAD inhibitors while the CTGF bands seemed diminished by Pan-TEAD inhibition. CTGF and the Pan-TEAD protein bands were found at 37 kDa and 50 kDa, respectively. Two CTGF bands were seen in the vehicle controls (Ctrl) but only one in VT1 and VT2 treated samples. GAPDH bands at 37 kDa were fairly uniform, unveiling an unfortunate mixing of the MOT 161 protein samples, possibly also affecting the MOT 148 VT2 sample. n = 1 experiment repeats.*

Due to the fact that 2 independent parameters were present (protein of interest and sample treatment with either DMSO vehicle, VT1 or VT2) a two-way ANOVA was carried out (Figure 3.14.4). As before, a significant decrease of CTGF protein levels could be noted after inhibitor treatment (p-values for CTGF: Vehicle vs. VT1 1 µM = 0.02 and Vehicle vs. VT2 1 µM = 0.010), with no significant difference notable when comparing the two treatments. Furthermore, VT1 or VT2 treatment did not have any significant effect on Pan-TEAD protein expression (Figure 3.14.4).

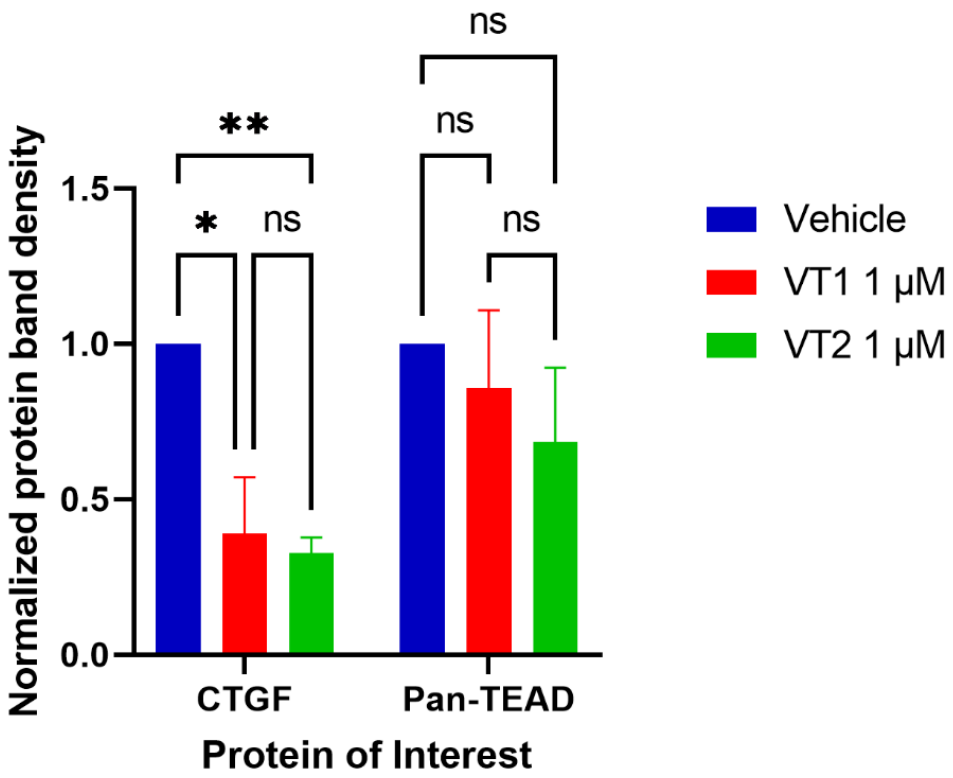

Figure 3.14.4: Quantification of protein bands seen in Figure 3.14.3 *showed significant differences in CTGF protein expression between vehicle and VT1 or VT2 treated Merlin null primary meningioma cells. CTGF and Pan-TEAD protein bands of MOT 148 and MOT 273 of Figure 3.14.3 were quantified, grouped by treatment and underwent statistical analysis. Significant reduction of CTGF protein levels after treatment with VT1 or VT2 (p-values for CTGF: Vehicle vs. VT1 1 µM = 0.02 and Vehicle vs. VT2 1 µM = 0.010). As seen before, no significant (ns) difference in CTGF protein expression when comparing the treated samples. Likewise, lack of significant differences in Pan-TEAD protein levels between vehicle, VT1 or VT2 treated samples. n = 2 Merlin null MOT cells per treatment for CTGF, n = 3 Merlin null MOT cells per treatment for Pan-TEAD. Graph shows data as means ± SD tested for significance via two-way ANOVA with Tukey's multiple comparisons test. * p ≤ 0.05; ** p ≤ 0.01; *** p ≤ 0.001.*

Next, the Merlin positive primary meningioma cells were treated in the exact same manner as the Merlin null primary meningioma cells and the resulting samples were blotted for CTGF and Pan-TEAD (Figure 3.14.5). Bands for both of these proteins of interest appeared unaffected by treatment with the exception of the MOT 240 samples. In these cells, the vehicle control sample contained two CTGF protein bands while the samples incubated with VT1 or VT2 only had one CTGF band. GAPDH bands varied within reasonable margins and revealed undisturbed sample integrity. As before, quantification of protein bands and statistical analysis followed (Figure 3.14.6).

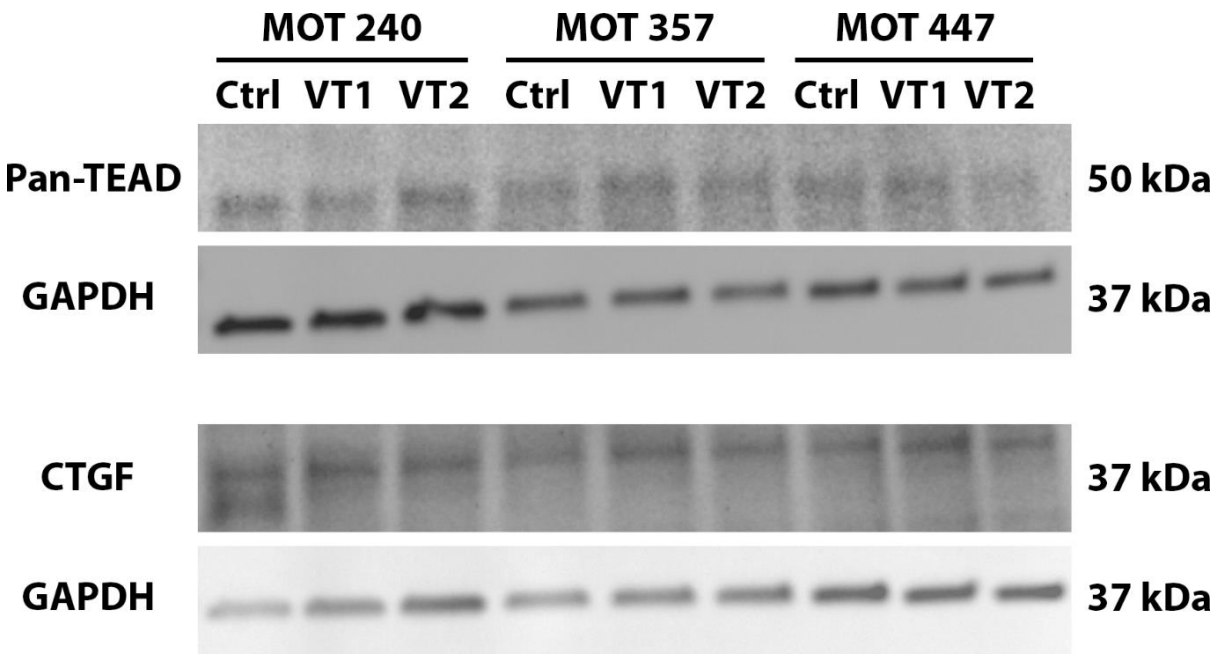

Figure 3.14.5: Western blotting of CTGF and Pan-TEAD in Merlin positive primary human meningioma cells after a 48 hour incubation period with Pan-TEAD inhibitors VT1 or VT2 at 1 µM. *In Merlin positive primary meningioma cells, Pan-TEAD (at 50 kDa) and CTGF (at 37 kDa) protein bands appeared unchanged after Pan-TEAD inhibition except in MOT 240 cells where a decrease in CTGF protein band amount seemed to have occurred after Pan-TEAD inhibitor incubation. In MOT 240 cells, two CTGF bands could be seen in the vehicle control (Ctrl) treated sample while only one CTGF band was present in the VT1 or VT2 treated samples. GAPDH protein bands at 37 kDa appeared uniform and their visible integrity ruled out sample intermixing. n = 1 experiment repeats.*

Quantification of protein bands was carried out as before. Statistical testing showed no significant difference in CTGF and Pan-TEAD protein expression between the three treatment groups.

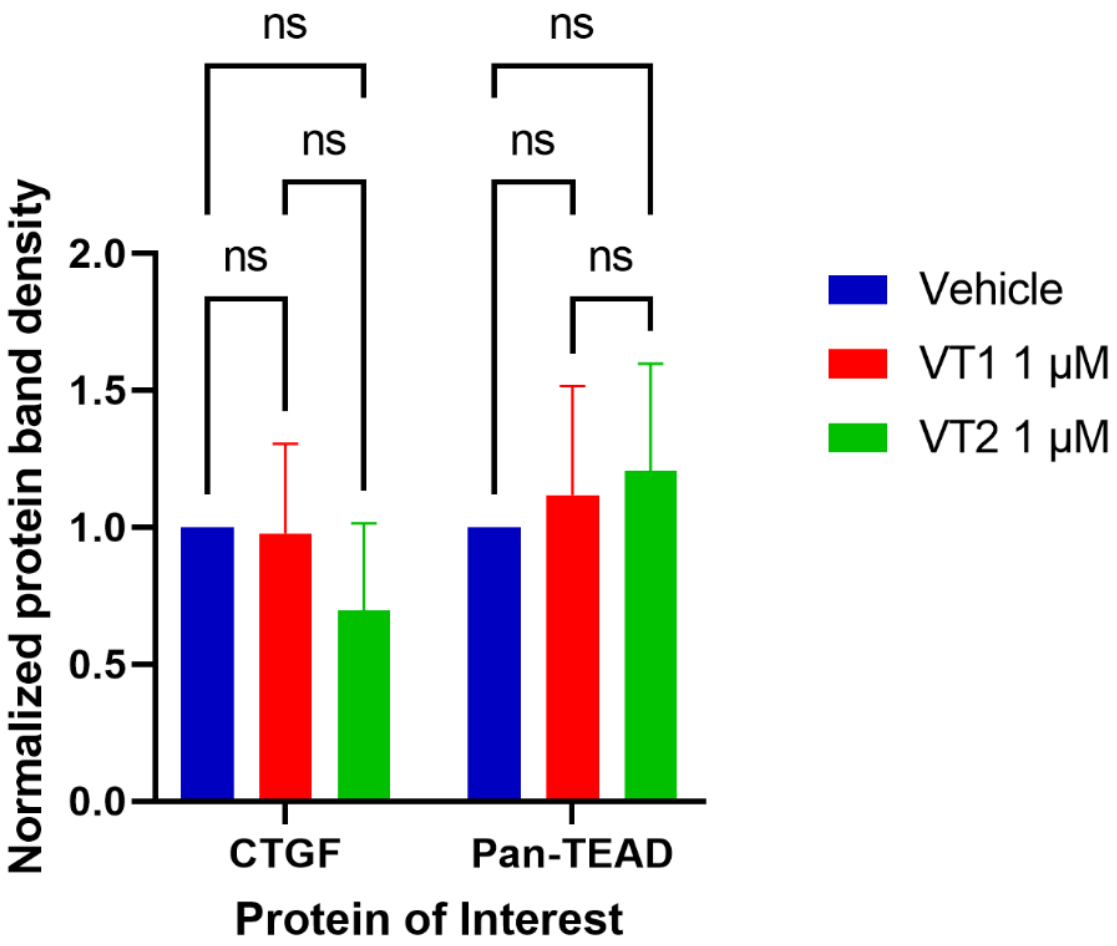

Figure 3.14.6: Quantification of the protein bands obtained by Western blot (Figure 3.14.5) *determined that no significant (ns) changes in CTGF and Pan-TEAD protein expression between Vehicle, VT1 or VT2 treated Merlin positive primary meningioma cells. Values obtained by quantification of the CTGF and Pan-TEAD protein bands of MOT 240, MOT 357 and MOT 447 cells were divided into groups based on treatment and were subjected to statistical analysis. Graph displays data as means ± SD tested for statistical significance via two-way ANOVA with Tukey's multiple comparisons test. n = 3 Merlin positive MOT cells per treatment.*

To summarize, according to these results Pan-TEAD inhibition had a significant detrimental effect on CTGF but not on Pan-TEAD protein expression in Merlin null primary meningioma cells. In contrast, TEAD S-autopalmitoylation suppression did not affect CTGF or Pan-TEAD protein levels in Merlin positive primary meningioma cells.

4. Discussion and Conclusion

4.1 Main results summary

This work sought to examine some of the effects which the inhibition of the Hippo signaling pathway would have in schwannoma and meningioma. Therefore, the effects of NF2 loss alone or in combination with YAP or TAZ loss in schwannoma of a Postn-Cre driven schwannoma mouse model were studied, as well as the effects of YAP/TAZ-TEAD inhibition in meningioma cell lines and primary meningioma cells.

Compared to controls, NF2 loss in satellite glial cells (SGCs)/Schwann cells (SCs) in the Postn-Cre driven schwannoma mouse model was associated with significantly increased proliferation and significantly heightened relative amounts of macrophages in DRGs and VGs. Furthermore, NF2 sKO resulted in significantly increased numbers of non-neuronal cells and significantly decreased relative numbers of neuronal cells in DRGs. Additionally, NF2 sKO caused the appearance of increased amounts of collagen in the DRGs compared to control, one of which was confirmed to be collagen IV.

Given that YAP is reported to promote proliferation in NF2 null Schwann cells, the effects of the additional loss of YAP (NF2/YAP dKO) or the additional loss of YAP's paralog TAZ (NF2/TAZ dKO) in SGCs/SCs were also examined. Combined loss of NF2 and YAP had no striking effect on the relative number of neuronal and non-neuronal cells and the amounts of collagen/collagen IV found in the DRGs compared to NF2 sKO. However, NF2/YAP dKO DRGs possessed significantly reduced relative amounts of macrophages and proliferating cells compared to NF2 sKO DRGs.

Furthermore, NF2/TAZ dKO DRGs possessed similar relative numbers of macrophages and proliferating cells as NF2/YAP dKO DRGs with the exception of the 9 month timepoint where the proliferation in the NF2/TAZ dKO DRGs was significantly lower than in the NF2/YAP dKO DRGs. Also, NF2/TAZ dKO DRGs appeared to contain less collagen in general than the NF2 sKO and NF2/YAP dKO DRGs (but still more than the control DRGs) while the levels of Collagen IV found in the three knockout genotypes seemed comparable. Interestingly, NF2/TAZ dKO DRGs possessed significantly less non-neuronal cells and significantly more neuronal cells than NF2 sKO and NF2/YAP dKO DRGs at the 3 month and 9 month timepoints.

Finally, Pan-TEAD S-autopalmitoylation inhibitors VT1 and VT2 from Vivace Therapeutics were shown to significantly diminish the proliferation of both Merlin null and Merlin positive primary human meningioma cells and also significantly reduce the CTGF protein expression in Merlin null primary human meningioma cells.

4.2 Postn-Cre mouse model

After the Postn-Cre driven NF2 sKO, NF2/YAP dKO, NF2/TAZ dKO and their Postn-Cre negative littermate controls (Postn-Cre- $NF2^{fl/fl}$) were successfully bred (Figure 3.1), DRGs and VGs were examined. The chosen timepoints were 3 months, 5 months and the latest possible timepoint, 9 months after birth. A later timepoint could not be acquired since the mice had to be sacrificed at 9 months of age according to our Home Office project license. It was shown that beyond 9 months of age, Postn-Cre driven NF2 sKO mice experience an increased mortality rate, potentially due to the occurrence of sizeable schwannomas or malignant peripheral nerve sheath tumours in some of the mice (Gehlhausen *et al.*, 2015). Commencing DRG/VG analysis at 3 months of age would allow us to examine the developing schwannomas even earlier than described in the Gehlhausen paper. Looking at 5 months would give us a glimpse at more developed schwannomas while the last timepoint of 9 months would provide us with a good chance of studying the effects of a fully developed schwannoma.

In comparison, Gehlhausen et al. found that at 5 months of age, the Postn-Cre+ $NF2^{fl/fl}$ (NF2 sKO) mice had developed enlarged masses with certain schwannoma characteristics on both DRGs and proximal spinal nerve roots. In 8 month old NF2 sKO mice, these enlargements on both locations had turned into frank schwannomas with histologically visible concentric circles of proliferating cells and positivity for S100 (marker for mature Schwann cells). At 10 months of age, NF2 sKO mice were found to harbour schwannomas on peripheral, spinal and cranial nerves and VGs. Evidence of hearing loss was found in mice which were 6 months or older (Gehlhausen *et al.*, 2015).

As mentioned previously, it has been demonstrated that the Periostin promoter is switched on in Schwann cell (SC) precursors at E10 (Lindsley *et al.*, 2007) and E12.5 (Gehlhausen *et al.*, 2015), resulting in the expression of the Postn-Cre Recombinase and thereby in the knockout of the floxed genes in SC precursors and their descendants. Furthermore, satellite glial cells (SGCs) are the predominant glial cells found in peripheral ganglia including DRGs and VGs and have been shown to share many morphological and transcriptional similarities with SCs. SGCs are hypothesized to be derived through the SC lineage (George, Ahrens & Lambert, 2018) and can also differentiate into SCs (Fex Svenningsen, Colman & Pedraza, 2004). Additionally, by using NF2 sKO mice expressing GFP in glial cells (= PLP-GFP Postn-Cre+ $NF2^{fl/fl}$ mice) the EdU positive proliferating cells in the DRGs were revealed to be glial cells (Laraba *et al.*, 2022), so either SGCs, SCs or both. Furthermore, the previously mentioned Postn-Cre Rosa26 tdTomato mice (Madisen *et al.*, 2010) were used by Amy Hewitt of our lab to reveal efficient Postn-Cre expression within the SGCs/SCs of DRGs (Laraba *et al.*, 2022).

Taken together, this suggests that in the DRGs (and presumably also in the VGs) the SGCs or SCs or both are subjected to the respective gene knockouts depending on the mouse genotype, affecting SGC/SC proliferation and thereby causing schwannoma formation.

4.3 DRG architecture

While the TEM images of NF2 sKO sciatic nerves did not show a notable difference in morphology (Figure 3.6), the H & E stained paraffin sections of the 3 months, 5 months and 9 months control, NF2 sKO, NF2/YAP dKO and NF2/TAZ dKO mouse L3 DRGs (Figures 3.7.1 – 3.7.5) revealed visible and significant differences between timepoints and genotypes.

Remarkably, areas in the images of the 9 month NF2 sKO and NF2/YAP dKO DRGs bear strong resemblance to what is marked as Antoni A tissue within mouse and human schwannomas in a recent paper (Chen *et al.*, 2020) and also what is found in the images of 7 month and 10 month Postn-Cre driven NF2 sKO DRGs (Gehlhausen *et al.*, 2015; Hawley *et al.*, 2021). Since hypercellular Antoni A tissue is a typical histological feature in schwannomas (Sobel, 1993), their appearance in the DRGs suggests that tumours growing there are indeed schwannomas. As previously mentioned, this is also supported in PLP-GFP Postn-Cre NF2 sKO mouse line where the proliferating tumour cells were shown to be of glial origin, again suggesting the growth of schwannomas.

The paper by Chen et al. (Chen *et al.*, 2020) contains H & E stained DRG sections from Postn-Cre driven NF2 sKO, NF2/YAP dKO and YAP sKO mice. Comparing the representative images reveals striking similarities to our own H & E stained DRG section images. As with our findings, their NF2 sKO and NF2/YAP dKO DRGs (Chen *et al.*, 2020) look indistinguishable from each other as well as from our NF2 sKO and NF2/YAP dKO DRGs and the NF2 sKO DRGs of others (Gehlhausen *et al.*, 2015; Hawley *et al.*, 2021). Furthermore, no significant difference between Postn-Cre driven NF2 sKO and NF2/YAP dKO DRGs was found in regards to DRG size and impact on mice survival (Chen *et al.*, 2020). Additionally, their YAP sKO DRGs appear similar to their controls (Chen *et al.*, 2020) and ours and the controls of others (Gehlhausen *et al.*, 2015; Hawley *et al.*, 2021). It was also observed that control and YAP sKO mice show no distinctions when it comes to mouse survival and DRG size (Chen *et al.*, 2020).

Taken together, this indicates that the additional YAP knockout does not cause a visibly different phenotype in regards to DRG architecture compared to NF2 sKO DRGs. As mentioned in the paper, this suggests that a YAP knockout alone is not sufficient to cause a visible phenotype, presumably because TAZ might be able to compensate for the loss of YAP (Chen *et al.*, 2020). In summary, it can be argued that a Postn-Cre driven YAP knockout does not lead to a visible change in DRG phenotype due to TAZ's perceived compensatory function, regardless whether it is a YAP knockout alone or a NF2/YAP dKO.

4.4 Schwannoma mouse model comparison

I used a schwannoma mouse model which relies on the Postn-Cre driven knockout of the NF2 gene (Gehlhausen *et al.*, 2015) while recently a different schwannoma mouse model depending on the Hoxb7-Cre driven knockout of LATS1/2 was reported (Chen *et al.*, 2020). Several differences between these two schwannoma mouse models can be seen.

As mentioned previously, the Postn-Cre driven NF2 sKO and NF2/YAP dKO mice were smaller than their Postn-Cre negative littermates while the NF2/TAZ dKO mice were very close in size to theirs. In contrast, neither the initial LATS1/2 knockout nor the additional YAP/TAZ knockout had any effect on the size of the mice in the Hoxb7-Cre driven LATS1/2 knockout schwannoma mouse model (Chen *et al.*, 2020).

Furthermore, the promoters driving the Cre recombinase in both schwannoma models have slightly different expression profiles. Hoxb7 was shown to be expressed at E9.5 in neural crest cells and at E10.5 to E11.5 in SC precursors (Chen *et al.*, 2019) while the Periostin promoter is activated in SC precursors at E10 and E12.5 (Gehlhausen *et al.*, 2015; Lindsley *et al.*, 2007). The combination of a slightly earlier expression of the Cre recombinase and the excision of LATS1/2 genes instead of the NF2 gene would provide an explanation as to why tumours in soft tissue and skin were found in addition to DRG schwannomas. In contrast, all the tumours in the Postn-Cre driven schwannoma model were found in the peripheral nervous system, namely on peripheral, spinal and cranial nerves, DRGs, VGs and proximal spinal nerve roots. Interestingly, some schwannomas in both mouse models were shown to be malignant, leading them to be classified as malignant schwannomas/malignant peripheral nerve sheath tumours (MPNSTs) (Chen *et al.*, 2020; Gehlhausen *et al.*, 2015).

In LATS1/2 knockout schwannoma cells implanted subcutaneously in mice and growing as a tumour xenograft *in vivo*, YAP or TAZ knockdown did not significantly impair tumour growth. In contrast, YAP or TAZ knockout in addition to NF2 knockout resulted in reduced proliferation in the DRGs (this work and (Laraba *et al.*, 2022)) and VGs (Laraba *et al.*, 2022) of the Postn-Cre driven schwannoma mouse model.

Furthermore, using LATS1/2/YAP/TAZ quadruple knockout mice, it was shown via IHC that at least one functional allele of either YAP or TAZ remained, allowing schwannoma formation (Chen *et al.*, 2020). Moreover, despite attempting a complete YAP and TAZ knockdown, the LATS1/2 knockout schwannoma xenografts retained strong TAZ expression, hypothesized to be due to clonal selection and expansion of TAZ positive tumour cells. Interestingly, this complete YAP and partial TAZ knockdown in these LATS1/2 knockout schwannoma xenografts resulted in significantly augmented tumour growth. Finally, a complete termination of LATS1/2, YAP and TAZ expression was shown to significantly suppress schwannoma cell proliferation *in vitro* (Chen *et al.*, 2020).

There are several reasons as to why results obtained from the Hoxb7-Cre driven LATS1/2 knockout schwannoma mouse model and from the Postn-Cre driven NF2 sKO schwannoma mouse model may differ from one another. The YAP and TAZ related effects in the Hoxb7-Cre driven LATS1/2 knockout schwannoma mouse model were seen in schwannoma xenografts growing subcutaneously, which is a far less natural environment for schwannomas than the DRGs and VGs in the Postn-Cre driven mouse model I used. Furthermore, LATS1/2 knockout derived schwannomas are very rare. A study reported merely 2 % and 1 % of LATS1 and LATS2 mutations in 82 cases of sporadic schwannoma, respectively. In contrast, the same study revealed an NF2 mutation frequency of 55 % (Oh *et al.*, 2015).

Additionally, Merlin has been shown to promote the interaction between Motin family proteins, TNKS1/2 and E3 ubiquitin ligase RNF146 in a LATS1/2 independent manner, resulting the polyubiquitination and subsequent proteasomal degradation of the Motin family members. Upon loss of Merlin activity via NF2 gene loss, Motin family proteins are stabilized and thereby increase their protein levels and activity, allowing them to increase their YAP and TAZ inhibition (Figure 4.1). This is suggested as a failsafe mechanism to impair tumour growth in case of NF2/Merlin loss, contributing to the benign nature and slow growth of NF2-deficient schwannomas (Wang *et al.*, 2021).

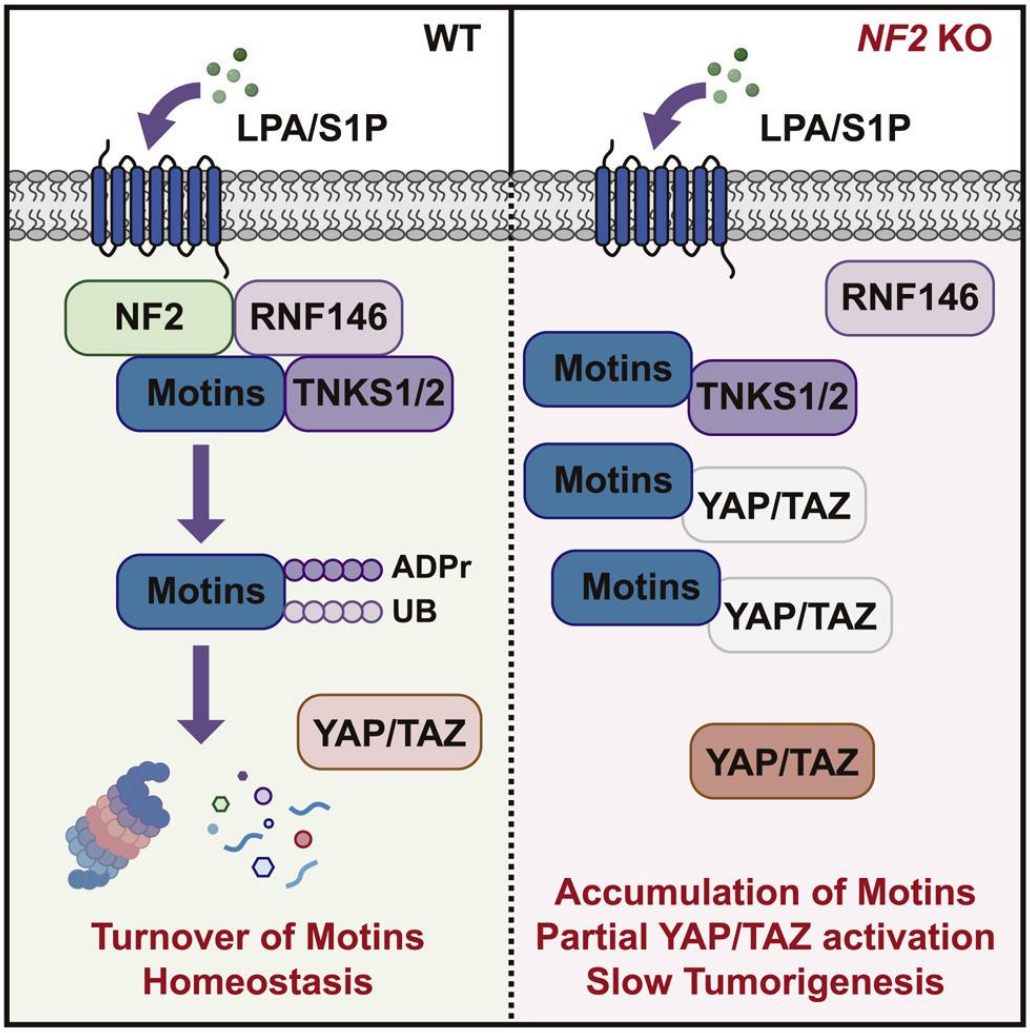

Figure 4.1: Loss of NF2 gene results in inhibition of YAP/TAZ activity via Motins. *Left side: In WT cells, LPA and S1P via membrane receptors promote Merlin (here called NF2) interaction between RNF146, TNKS1/2 and Motins. This leads to Motin PARsylation and subsequent polyubiquitination and proteasomal degradation, preventing Motin-mediated YAP/TAZ inhibition. Right side: NF2 gene loss and thereby lack of Merlin activity results in reduced Motin degradation, allowing Motins to inhibit YAP/TAZ and therefore promote a slowed tumourigenesis. Obtained from (Wang et al., 2021).* https://doi.org/10.1016/j.celrep.2021.109596. http://creativecommons.org/licenses/by-nc-nd/4.0/.

Consequently, a schwannoma mouse model relying on LATS1/2 knockout would not be subject to this regulation and therefore the resulting schwannomas would behave differently.

In contrast, this regulatory mechanism is in effect in our NF2 sKO schwannoma mouse model, as it would be in Neurofibromatosis type 2 patients and patients with spontaneously occurring NF2-deficient schwannomas.

Taken together, the Postn-Cre driven schwannoma mouse model phenocopies Neurofibromatosis type 2 in human patients more accurately than the Hoxb7-Cre driven LATS1/2 knockout schwannoma mouse model. This suggests that results obtained in the Postn-Cre driven mouse model hold greater value and therefore provide a more accurate portrayal of schwannomas and the role of YAP and TAZ in them.

4.5 YAP/TAZ-TEAD dependent SGC/SC proliferation in DRGs and VGs

Quantification in the DRGs with subsequent testing for statistical significance revealed that the loss of NF2 alone at 3, 5 and 9 months caused a significant increase in EdU positive proliferating cells (Figure 3.9.6) compared to the other genotypes. This aligned with heightened amounts of nuclear YAP and TAZ (Laraba *et al.*, 2022) due to NF2 knockout-mediated Hippo pathway dysregulation, driving SGC/SC proliferation.

In contrast, loss of either YAP or TAZ after NF2 loss significantly diminished the increase of cell proliferation seen after NF2 loss at later timepoints. Similar effects could be shown by others lab members at the 3 month (NF2 sKO mediated significant increase in proliferation confirmed) and 5 month (NF2 sKO mediated significant increase in proliferation and significant decrease in proliferation due to additional YAP or TAZ loss confirmed) timepoints (Laraba *et al.*, 2022).

Interestingly, while there was not a significant difference in SGC/SC proliferation rates between 3 months NF2/YAP and NF2/TAZ dKO and 5 months NF2/YAP and NF2/TAZ dKO DRGs, there was a significantly lower rate of proliferation in the NF2/TAZ dKO DRGs compared to the NF2/YAP dKO DRGs at the 9 month timepoint (Figure 3.9.6). This could mean that the heightened proliferation due to NF2 loss was over time mitigated more strongly by the additional loss of TAZ than the additional loss of YAP.

Moreover, a similar YAP/TAZ dependent effect on proliferation could also be established in VGs. Loss of NF2 significantly augmented the relative number of EdU positive proliferating cells in VGs compared to control (Figure 3.11.4). This significantly enhanced proliferation in VGs after NF2 sKO was also observed by others at the 5 month timepoint, as well as significantly enlarged 9 month NF2 sKO VGs compared to controls (Laraba *et al.*, 2022). Laraba et al. also showed that the cell proliferation in 5 months Postn-Cre driven NF2/YAP dKO and NF2/TAZ dKO VGs was significantly decreased compared to NF2 sKO VGs of the same timepoint (Laraba *et al.*, 2022).

This significant reduction of proliferation could also be seen in 3 and 5 months NF2 sKO DRGs and VGs after using Pan-TEAD palmitoylation inhibitors VT1 and VT2 for 21 days. Additionally, such a 21 day treatment with VT1 or VT2 managed to significantly reduce the size of the 9 months NF2 sKO DRGs and VGs (Laraba *et al.*, 2022).

4.6 Non-neuronal and neuronal cell quantification results

The distinct appearances of the DRGs depending on genotype and timepoint prompted me to conduct a quantification and statistical analysis of neuronal and non-neuronal cell numbers in the DRGs of all used genotypes and timepoints (Figures 3.7.4 and 3.7.5). It could be determined that, especially at later timepoints, the loss of NF2 alone or in combination with the loss of YAP caused significant increases in the relative amounts of non-neuronal cells and significant decreases of relative numbers of neurons compared to the corresponding control and NF2/TAZ dKO DRGs (Figures 3.7.4 and 3.7.5). Interestingly, the additional loss of YAP had no significant effect on the relative quantities of neuronal and non-neuronal cells in the NF2/YAP dKO DRGs compared to NF2 sKO DRGs, despite showing a significant decrease of SGC/SC proliferation in the DRGs of NF2/YAP dKO mice compared to the NF2 sKO mouse DRGs (Figure 3.9.6). Apparently, the significantly diminished proliferation due to additional YAP loss only had a very limited effect on neuronal and non-neuronal cell numbers.

In contrast, while the loss of NF2 paired with the loss of TAZ also caused a significant reduction of neuronal cells and significant increase of non-neuronal cells, these changes were significantly less pronounced than in the NF2 sKO and NF2/YAP dKO DRGs (Figures 3.7.4 and 3.7.5). Therefore, the additional loss of TAZ appeared to diminish the effects on the neuronal and non-neuronal cells seen in the NF2 sKO and NF2/YAP dKO DRGs but not reverse them, seemingly occupying the middle ground between the unchanging controls and the rapidly changing NF2 sKO and NF2/YAP dKO DRGs at later timepoints. In general, it appears as if the additional TAZ knockout merely delayed the NF2 sKO-induced development of schwannoma which was seen in the NF2 sKO and NF2/YAP dKO DRGs. Treatment with the Vivace Pan-TEAD S-autopalmitoylation inhibitors might slow down the schwannoma formation even further or, in combination with other drugs such as losartan (= anti-inflammatory/macrophage reducing, see sections 4.14 and 4.17), halt it altogether.

Interestingly, the NF2/TAZ dKO DRGs exhibited significantly decreased SGC/SC proliferation compared to the NF2 sKO DRGs (Figure 3.9.6). At 3 and 5 months, this significant reduction in proliferation in the NF2/TAZ dKO DRGs was similar to the one seen in the NF2/YAP dKO DRGs. A possible explanation for these seemingly contradicting results could be differences between YAP and TAZ functions.

4.7 Difference between YAP and TAZ functions

The knockout of YAP and TAZ in the NF2/YAP dKO and NF2/TAZ dKO mice, respectively, was shown by Laraba et al. (Laraba *et al.*, 2022). Furthermore, there is no indication of a difference between YAP knockout and TAZ knockout efficiencies. Interestingly, while YAP and TAZ as paralogs possess many overlapping functions, they also have some distinct roles from one another in many aspects including cancer (LeBlanc, Ramirez & Kim, 2021; Reggiani *et al.*, 2021). Similarly, TAZ activity in SCs was shown to fulfil a role in nerve development which YAP activity cannot fully compensate for after the loss of TAZ ((Poitelon *et al.*, 2016), see Introduction section 1.10.16). Continuing this line of thought, such differences in YAP and TAZ

function would provide a possible explanation as to why the NF2/TAZ dKO DRGs showed a comparatively milder phenotype than the NF2/YAP dKO DRGs of the same timepoints while the NF2/YAP dKO DRGs were often almost indistinguishable from their NF2 sKO counterparts. This points towards a different mechanism at play here whose effect seems far greater than what could be explained by a significant reduction in proliferating SGCs/SCs alone. Seeing that a significant increase in apoptotic activity was reported in 9 month NF2 sKO DRGs and VGs after a 10 day VT2 treatment (Laraba *et al.*, 2022), it is conceivable that the additional TAZ knockout might cause an increase of apoptotic activity in the SGCs/SCs of VGs and DRGs while the YAP knockout does not.

4.8 Role of YAP and TAZ in proliferation and apoptosis

YAP and TAZ are well known for affecting proliferation and apoptosis in different cancer types, linking them to these 2 hallmarks of cancer (Hanahan & Weinberg, 2000). TAZ has been reported as a driver of proliferation and an inhibitor of apoptosis in numerous tumours such as glioma (Li *et al.*, 2016b), head and neck squamous cell carcinoma (HNSCC) (Li *et al.*, 2019a), breast cancer (Ding *et al.*, 2019), pancreatic cancer (Zhan *et al.*, 2018), acute myeloid leukaemia (Hu *et al.*, 2020) and alveolar rhabdomyosarcoma (Deel *et al.*, 2018). Pharmacological or genetic inhibition of TAZ activity was shown to impair tumour cell proliferation and increase the rate of apoptosis. Similarly, YAP was shown to promote proliferation and suppress apoptotic activity in non-small cell lung cancer (NSCLC) (Shreberk-Shaked *et al.*, 2020), gastric cancer (Zhou *et al.*, 2016), hepatocellular carcinoma (Li *et al.*, 2019b; Wang, Wu & Zhong, 2018), clear cell renal cell carcinoma (Cao *et al.*, 2014), prostate cancer (Jin *et al.*, 2018; Sheng *et al.*, 2015; Shi *et al.*, 2019) and rhabdomyosarcoma (Slemmons *et al.*, 2015), with YAP inhibition using drugs or siRNA knockdown counteracting these effects.

4.9 Possible apoptotic effect due to differences of YAP and TAZ knockouts

Taken together, it is conceivable that similar to some tumour types and in contrast to others, only TAZ activity might inhibit apoptosis in schwannoma, rendering the YAP knockout irrelevant in regards to affecting apoptosis rates. Therefore, it is plausible to assume that, while the additional YAP knockout only negatively affects tumour cell proliferation, the additional TAZ knockout both decreases tumour cell proliferation and heightens apoptosis. As was found in a human colon adenocarcinoma cell line, overexpression of YAP or TAZ resulted in increased expression of the antiapoptotic protein BCL-2, decreased expression of the proapoptotic proteins BAX and Caspase-3 and also heightened proliferation (Li *et al.*, 2017). If TAZ but not YAP would have a similar apoptosis-inhibiting function in schwannoma, the loss of TAZ would naturally lead to enhanced apoptotic cell death, as hypothesized in the NF2/TAZ dKO DRGs. Using IHC and/or Western blot to compare the expression of the above mentioned proteins in NF2/TAZ dKO DRGs/VGs and NF2 sKO and NF2/YAP dKO DRGs/VGs would prove or disprove this proposed mechanism.

As mentioned previously, the usage of Pan-TEAD S-autopalmitoylation inhibitors simultaneously decreased tumour cell proliferation and DRG/VG size and promoted apoptosis as observed by Laraba et al. (Laraba *et al.*, 2022). Looking at the literature reveals a possible mechanism by which the Pan-TEAD inhibitors might trigger apoptosis. DNA damage in cancer cells has been shown to lead to c-Abl-catalysed YAP Tyr357 phosphorylation. This reduces the ability of YAP to activate YAP-TEAD mediated transcription and at the same time causes YAP via its WW domain to bind to the TF p73, resulting in the YAP-p73 induced expression of the proapoptotic protein BAX and therefore increased rates of apoptosis (Basu *et al.*, 2003; Ehsanian *et al.*, 2010; Keshet *et al.*, 2015; Strano *et al.*, 2001). It is possible that by using the Vivace Pan-TEAD S-autopalmitoylation inhibitors and therefore impairing TEAD function, YAP is more likely to bind to other transcription factors including p73 and thereby promote BAX-mediated apoptosis. Using IHC, this could theoretically be confirmed by detecting BAX in the SGCs/SCs of the DRGs and VGs after Pan-TEAD inhibitor treatment while also observing the absence of BAX after vehicle treatment. Another way to verify this hypothesis would be to discover elevated BAX protein levels in the DRGs and VGs via Western blot after Pan-TEAD inhibitor treatment in contrast to lower BAX protein expression after vehicle treatment.

4.10 Link between proliferation and macrophage numbers in injured nerves, schwannoma and meningioma

The presence of macrophages in an overwhelming majority of NF2-related and sporadic vestibular schwannomas (VSs) and also NF2-related meningiomas was reported (Sagers *et al.*, 2019; Schulz *et al.*, 2016; Wang *et al.*, 2018a). Furthermore, a positive correlation between macrophage numbers and VS growth has been observed (de Vries *et al.*, 2013; de Vries *et al.*, 2012; Lewis *et al.*, 2019). Increased numbers of M2-like macrophages have also been associated with a reduced risk of sporadic VS progression (Perry *et al.*, 2019). Additionally, it was shown that NF2 negative meningioma contain higher amounts of M2-like macrophages than meningioma harbouring an AKT1 E17K mutation (Adams *et al.*, 2020). A different study reported a positive correlation between macrophage amounts and meningioma size. Additionally, WHO grade II meningiomas possessed increased amounts of macrophages compared to WHO grade I meningiomas (Proctor *et al.*, 2019).

Moreover, a link between Hippo signaling and macrophage numbers/proliferation has been reported. In injured NF2 sKO sciatic nerves (= 7 dpi P0-Cre+ $NF2^{fl/fl}$), it was shown that macrophage infiltration and cell proliferation were strongly elevated compared to control. In contrast, both macrophage infiltration rate and cell proliferation were decreased in injured NF2/YAP dKO sciatic nerves (= 7 dpi P0-Cre+ $NF2^{fl/fl}$ $YAP^{fl/fl}$) compared to controls (Mindos *et al.*, 2017).

Therefore, it was decided to look for differences in macrophage numbers and SGC/SC proliferation rates in the mouse L3 DRGs to see if there is a positive correlation between macrophage numbers and tumour cell proliferation within the developing schwannomas of the Gehlhausen mouse model (Gehlhausen *et al.*, 2015). The L3 DRGs were chosen since they are one of the biggest DRGs in the mouse spinal column, providing us more tissue sample to

work with. Theoretically, any DRG could have been chosen, given that the Gehlhausen paper reported schwannoma development in all DRGs in their mouse model (Gehlhausen *et al.*, 2015).

Following the detection of macrophages in meningioma xenografts (Figure 3.4) DRG sections of all timepoints and genotypes were stained for pan-macrophage marker Iba1 (Figures 3.9.2 and 3.9.3) and proliferation marker EdU (Figure 3.9.5) to ascertain potential differences in relative macrophage numbers and proliferation within DRGs among genotypes.

4.11 Link between proliferation and macrophage numbers in Postn-Cre schwannoma mouse model

As seen in literature, a link between increased proliferation and higher macrophage numbers could also be established using the Postn-Cre schwannoma mouse model (Figures 3.9.4, 3.9.6, 3.11.4 and (Laraba *et al.*, 2022)).

Since the different genotypes trace back to gene knockouts in SGCs/SCs, it stands to reason that in this case the glial cells determined the relative macrophage amounts at all 3 timepoints. Based on our results, it can be hypothesized that a significantly increased glial cell proliferation and a resulting heightened number of glial cells will lead to the recruitment of significantly more macrophages which could then be classified as TAMs. Of course, the opposite would apply as well, with significantly decreased glial cell proliferation and thereby glial cell amounts recruiting significantly fewer macrophages/TAMs.

It would be interesting to determine whether these significant changes in macrophage numbers are also accompanied by a change of macrophage polarity, i.e. whether the M1-like to M2-like macrophage ratio remains relatively constant or shifts between genotypes and timepoints. To that end, the anti-CD206 antibody marking M2-like macrophages which was used in sciatic nerve tissue (Figures 3.2.1 – 3.2.3) could be utilized.

As outlined before, TAMs support the growth of tumours in a multitude of ways (see Introduction section 1.17.2). Significantly less TAMs would also decrease their tumour-promoting effects, thereby possibly further impairing glial cell proliferation and schwannoma growth, creating a negative feedback loop. The opposite might be true for the significant increase of glial cell numbers and thereby also macrophages/TAMs, enhancing each other to promote schwannoma growth.

Taking all of this into account, it could be beneficial to eliminate these tumour-promoting macrophages, for example by targeting the CSF1 receptor (CSF1R) (see Introduction section 1.17.3). CSF1R inhibitors such as PLX3397 have been shown to either shift TAM polarization towards an M2-like phenotype in hepatocellular carcinoma (Ao *et al.*, 2017) or cause macrophage depletion in melanoma (Erkes *et al.*, 2020), both suppressing the TAM's tumour growth-promoting effect. Additionally, treatment with anti-CSF1 or anti-CSF1R antibodies resulted in the growth inhibition of malignant meningiomas (Yeung *et al.*, 2021).

4.12 Loss of neuronal cells

It is unclear what the cause of the loss of neurons in the NF2 sKO, NF2/YAP dKO and (to a lesser degree) in the NF2/TAZ dKO DRGs over time is (Figure 3.7.4). It is possible that the proliferating tumour cells of SGC/SC origin are responsible. Their significantly increased numbers could gradually displace the neurons and also deprive them of the nutrients the SGCs would normally provide, ultimately leading to neuronal cell death. This could, in theory, also be caused or merely promoted by the significantly heightened numbers of macrophages (Figure 3.9.4) and/or the augmented amount of collagen (Figures 3.8.1 – 3.8.3, 3.9.1). It is also conceivable that the collagen does not play a role in the significantly reduced numbers of neuronal cells but simply takes up the space after the neurons are gone.

4.13 The presence of collagen and collagen IV in different genotypes

Martius Scarlet Blue (MSB) staining can be used to detect various tissue components including collagen (Figure 6.1). The collagen found in the knockout DRGs via MSB staining (Figures 3.8.1 – 3.8.3) appeared to increase in quantity over time, seemingly occupying the space previously taken up by neuronal cells. This collagen increase over time appeared to be stronger in NF2 sKO and NF2/YAP dKO DRGs and weaker in NF2/TAZ dKO DRGs while the collagen amount in the control DRGs remained unchanged throughout the experiment.

Figure 3.9.1 verified that collagen IV could be found in great quantity in all knockout 9 month DRGs. Collagen IV was previously seen to be strongly upregulated in 21 dpi NF2 sKO sciatic nerves (Mindos *et al.*, 2017). Collagen IV was also observed in the Hoxb7-Cre driven LATS1/2 knockout schwannoma mouse model and in schwannomas from human patients (Chen *et al.*, 2020). Furthermore, collagen IV was found in classical, cellular and melanotic schwannomas (Huang *et al.*, 2004; Oda *et al.*, 1988; Zhang *et al.*, 2005). Additionally, collagen I, III, V, VI and VIII are present in schwannomas (Oda *et al.*, 1988; Paulus *et al.*, 1991; Wu *et al.*, 2021). Interestingly, collagen IV, along with collagen IV, VI, VIII and XVIII, were also observed in meningiomas (Caffo *et al.*, 2008; Han, Daniel & Pappas, 1996; Kwon *et al.*, 2013; Ogawa *et al.*, 1989; Salokorpi *et al.*, 2013). All things considered, collagen IV and other types of collagen appear to be a typical feature of schwannomas and meningiomas. Therefore, it might be worthwhile to look for other types of collagen (aside from collagen IV) in DRGs/VGs of the Postn-Cre schwannoma mouse model using IHC.

4.14 Role of collagen in hearing loss

Interestingly, a link between hearing loss and fibrosis (accumulation of extracellular matrix e.g. hyaluronan and collagen) or intratumoural microhemorrhage within vestibular schwannoma was found in 274 patients (Sughrue *et al.*, 2011) and also in the cerebellopontine angle schwannoma model.

The cerebellopontine angle (CPA) vestibular schwannoma mouse model relies on the insertion of transparent cranial windows in the CPA (located between cerebellum and pons)

of immunocompetent or immunosuppressed mice, allowing the simulation of the vestibular schwannoma tumour microenvironment. The subsequent implantation of NF2 null mouse schwannoma cells or human patient derived schwannoma cells into the CPA tumour microenvironment causes the formation of vestibular schwannoma and schwannoma-induced hearing loss (Wu *et al.*, 2021; Zhao *et al.*, 2018c).

In this CPA schwannoma model, the anti-inflammatory, angiotensin receptor blocking drug losartan reduces collagen I and hyaluronan expression, normalizes blood vessels allowing increased perfusion and decreases vestibular schwannoma-induced inflammation (e.g. by downregulating inflammatory cytokines and chemotactic chemokines) compared to saline treated controls, leading to decreased recruitment and therefore significantly lower number of TAMs (Wu *et al.*, 2021). TAMs promote hearing loss by damaging cochlear hair cells via a number of inflammatory mechanisms including expression of IL-6 (ototoxic), reactive oxygen species (ROS, increases fibrosis and also directly damages hearing) and Toll-like receptor 4 (TLR4, activation results in further ROS production). The expression of these ototoxic effectors in TAMs was shown to be through angiotensin II receptor 1 (AT1) signaling, AT1 being the target of losartan (Wu *et al.*, 2021). In agreement with these results, losartan treatment was shown to prevent vestibular schwannoma-mediated hearing loss *in vivo* and in clinic.

4.15 Potential use of losartan in the Postn-Cre schwannoma model

In comparison to the more artificial CPA schwannoma model, it would be interesting to see whether losartan can also decrease inflammation/macrophage numbers and thereby prevent or at the very least reduce the severity of hearing loss in the Postn-Cre schwannoma mouse model which naturally develops hearing deficiencies over time. As mentioned before, hearing loss is found in Postn-Cre driven NF2 sKO mice (6 months of age and onwards) (Gehlhausen *et al.*, 2015). Given that I noted significantly heightened amounts of macrophages in our NF2 sKO DRGs and VGs compared to controls (Figures 3.9.4 and 3.11.4), it seems logical that macrophages/TAMs also promote hearing impairment in the Postn-Cre schwannoma mouse model and lowering TAM numbers might have an otoprotective effect.

Additionally, the Postn-Cre schwannoma mouse model would allow the study of the effects of losartan on schwannoma-induced hearing loss over a longer time period (for approximately 3 months) while the mice after the CPA procedure need to be euthanized after only 3 weeks due to developing neurological symptoms such as ataxia (Wu *et al.*, 2021).

4.16 Interaction of TAMs and collagen

The presence of TAMs is associated with increased levels of collagen I and collagen IV in colorectal cancer (Afik *et al.*, 2016). Collagen production by macrophages/TAMs would explain why I saw visibly increased amounts of collagen (MSB staining, Figure 3.8.3) and collagen IV (Figure 3.9.1) in 9 months NF2 sKO DRGs which contained significantly heightened numbers of macrophages compared to control (Figure 3.9.4).

In this context, it would also be interesting to see whether strongly diminished TAM numbers by using either losartan or PLX5622 (Klein *et al.*, 2015) would cause a drastic reduction in detectable collagen. If that was the case, it could be confirmed that TAMs are indeed responsible for producing the collagen which can be found first surrounding and, at later timepoints, also seemingly occupying the space where DRG neurons were previously located.

Interestingly, the significant reduction of macrophage numbers in 9 months NF2/YAP dKO DRGs and NF2/TAZ dKO DRGs compared to 9 months NF2 sKO DRGs (Figure 3.9.4) appeared insufficient to visibly reduce the collagen IV amounts (Figure 3.9.1). However, the significant decrease of macrophage numbers in NF2/TAZ dKO DRGs did seem to cause a visible reduction of collagen in general (MSB staining, Figure 3.8.3) while the significantly reduced macrophage amounts in the NF2/YAP dKO DRGs did not. This would suggest that only the combined loss of NF2 and TAZ would somehow alter the communication between SGCs/SCs and macrophages, causing them to produce less collagen. It would be worth investigating if the significantly reduced macrophage numbers and the accompanying decrease in collagen would also contribute to prevent hearing loss to a certain extent in the Postn-Cre schwannoma mouse model.

4.17 Losartan and Pan-TEAD combination therapy

In regards to its effects, losartan treatment is likely to be beneficial in promoting and augmenting the effect of the Pan-TEAD palmitoylation inhibitors. Losartan normalizes blood flow, thereby enhancing the delivery and thereby efficacy of the Pan-TEAD palmitoylation inhibitors which would suppress proliferation of schwannoma cells. Additionally, losartan would significantly decrease schwannoma macrophage numbers, likely both impacting proliferation even further by disrupting macrophage-mediated support of schwannoma growth and also preventing hearing loss. Therefore, a combination therapy consisting of losartan and Pan-TEAD palmitoylation inhibitors has the potential to attack from two fronts, targeting both the schwannoma cell proliferation and tumour microenvironment. Such a treatment could turn out to be very effective, possibly decreasing or even halting schwannoma growth and guarding against hearing loss.

4.18 YAP and TAZ inhibition in meningioma

Finally, I sought to examine the effect of YAP and TAZ inhibition in the second most common tumour associated with Neurofibromatosis type 2, namely meningioma. To that end, I studied the effect of TEAD and Pan-TEAD S-autopalmitoylation inhibitors by Vivace Therapeutics on the proliferation of meningioma cell culture cells and primary meningioma cells.

4.18.1 YAP and TAZ inhibition in human meningioma cell lines

Interestingly, it could be determined in BM-1 cells that, while TAZ knockdown has no effect on YAP expression, a YAP knockdown triggers a compensatory upregulation of TAZ expression. Furthermore, TAZ knockdown in BM-1 cells was shown to significantly inhibit BM-1 cell proliferation compared to scramble control (from roughly 35% to around 15%) (Laraba *et al.*, 2022).

Taken together, these results reveal that only the knockdown of TAZ causes an increased expression of the paralog YAP in primary human meningioma cells, presumably negating some of the effects of the knockdown. However, this compensatory mechanism does not appear sufficient to maintain normal cell proliferation rates. Nonetheless, in order to impact cell proliferation even further, Pan-TEAD palmitoylation inhibitors could be used. Via the impairment of the function of all TEADs, these inhibitors have a negative impact on the transcriptional activities of both YAP and TAZ, likely counteracting this suggested compensatory mechanism to a pronounced degree.

4.18.2 YAP and TAZ inhibition in primary human meningioma cells

Subsequently, I moved onto Merlin null and Merlin positive primary human meningioma cells using Pan-TEAD palmitoylation inhibitors VT1 and VT2 at the same concentrations as before (Figures 3.13.1 and 3.13.3). As mentioned before, TEAD1 - 4 expression was shown to be highly variable among primary human schwannoma cells (Laraba *et al.*, 2022), necessitating the usage of Pan-TEAD palmitoylation inhibitors to ensure efficacy regardless of TEAD expression patterns. Statistically testing the proliferation rates gained by quantification for statistical significance (Figures 3.13.2 and 3.13.4) showed that both VT1 and VT2 significantly reduced the cell division rates at all concentrations in Merlin null and Merlin positive primary human meningioma cells compared to vehicle control. Both Pan-TEAD palmitoylation inhibitors were found to be similarly efficient at inhibiting cell proliferation (Figure 3.13.5). Accordingly, YAP or TAZ knockdown in NF2 null human primary schwannoma cells was demonstrated to significantly reduce cell proliferation (Laraba *et al.*, 2022). Furthermore, in comparison to vehicle control, 1 µM of VT1 or VT2 significantly decreased the proliferation of the NF2 null schwannoma cell line HEI193 and treatment with VT1, VT2 or VT3 also significantly suppressed the proliferation of NF2 null primary human meningioma cells (Laraba *et al.*, 2022). VT3 (VT107), similar to VT1 (VT104) and VT2, is a Pan-TEAD palmitoylation inhibitor (Tang *et al.*, 2021). VT3 was previously shown to effectively impair the proliferation of NF2-deficient (NCI-H226), NF2-deleted (NCI-H2373) or NF2-mutant (NCI-H2052) mesothelioma cell lines (Tang *et al.*, 2021). 100 nM and 1 µM of VT3 were able to significantly decrease cell proliferation in primary human schwannoma cells, with an IC_{50} of 39 nM (Laraba *et al.*, 2022).

4.18.3 VT1 efficacy in meningioma and mesothelioma cells

VT1 (VT104) had IC_{50}s of 16.1, 25.6 and 31.6 nM in NF2-deficient, NF2-mutant and NF2-deleted human mesothelioma cell lines, respectively, while the VT1 IC_{50}s in NF2 wild type cell lines were considerably higher, namely more than 3 µM (Tang *et al.*, 2021). Therefore, human mesothelioma cell lines with impaired Merlin function were far more susceptible than human mesothelioma cell lines with intact Merlin activity. In contrast, 6 of the 8 VT1 IC_{50}s measured in our Merlin null and Merlin positive primary human meningioma cells (see Table 3.2) can be found between these two extremes while 2 of the IC_{50} values were far below 16.1 nM. Furthermore, there appeared to be no significant difference in susceptibility to Pan-TEAD inhibitors VT1 and VT2 between the Merlin null and Merlin positive primary human meningioma cells (Figure 3.13.5).

It has to be kept in mind that the IC_{50} values in Table 3.2 were calculated with only 3 data points (concentration-proliferation index pairs) in triplicate. In contrast, the IC_{50} values in the mesothelioma cell lines were determined using 10 data points in duplicate (Tang *et al.*, 2021), making these values more accurate. Furthermore, many of the Merlin null and Merlin positive primary human meningioma cells I used were shown to possess mutations in other genes (see Table 2.1), likely influencing proliferation rates as well. Additionally, Tang et al. used tumour cell lines which are further removed from the original tumour than the primary tumour cells I used.

Taken together, it appears as if human mesothelioma cell lines with inhibited Merlin expression are strongly reliant on YAP/TAZ-TEAD function for cell proliferation while human mesothelioma cell lines with functional Merlin activity are less so. In contrast, primary human meningioma cell lines seem to depend on YAP/TAZ-TEAD activity for cell proliferation, regardless of their NF2/Merlin status.

4.18.4 Effect of Pan-TEAD inhibitors on CTGF and TEAD protein expression

After treatment with 1 µM of VT1 or VT2 for 48 hours, the protein expression of downstream Hippo signaling targets TEAD (TEAD1 – 4) and CTGF in primary human meningioma cells was determined. It was concluded that treatment with 1 µM of Pan-TEAD S-autopalmitoylation inhibitors for 48 hours significantly decreased CTGF but not TEAD protein expression in Merlin null primary meningioma cells compared to control (Figures 3.14.2 and 3.14.4).

Conversely, the Vivace inhibitors did not significantly change CTGF and TEAD protein levels in Merlin positive primary meningioma cells (Figure 3.14.6). It is conceivable that these Merlin positive meningioma cells might not rely on CTGF but instead on other YAP/TAZ-TEAD effectors to drive proliferation. Such effectors could be e.g. CYR61, EGFR and/or its ligand AREG (see Introduction section 1.8.10) whose protein expression would then most likely be significantly affected by TEAD S-autopalmitoylation. Another possibility could be that CTGF has an increased protein half-life in these meningioma cells and therefore a significant CTGF protein level reduction might take longer than 48 hours to perceive.

Interestingly, incubation of NF2 null schwannoma cell line HEI193 cells with 1 µM and 10 µM of VT2 for 7 days caused a significant decrease of CTGF protein levels. Moreover, treating primary human schwannoma cells with 2 µM of VT3 for 7 days resulted in a significant reduction of CTGF protein expression (Laraba *et al.*, 2022). Accordingly, CTGF protein expression was observed to be significantly downregulated in the sciatic nerves of 3 and 5 month old NF2 sKO mice after being gavaged with VT1 or VT2 for 21 days, reversing the significant upregulation of CTGF protein expression in NF2 sKO sciatic nerves compared to control (Laraba *et al.*, 2022).

4.18.5 Stronger effect of Pan-TEAD inhibitors on CTGF expression than on TEAD expression

As mentioned before, Pan-TEAD palmitoylation inhibitors did not have a significant effect on TEAD protein expression in Merlin null and Merlin positive primary human meningioma cells (Figures 3.14.4 and 3.14.6).

In contrast, treating primary human schwannoma cells for 7 days with 2 µM of VT3 caused a visible decrease in the protein levels of TEAD1 - 4. Furthermore, while Pan-TEAD protein expression was significantly heightened in the sciatic nerves of 3 and 5 month old NF2 sKO mice compared to controls, only treatment with VT2 for 21 days managed to significantly decrease Pan-TEAD protein levels while VT1 failed to do so (Laraba *et al.*, 2022). The reason for this discrepancy might be the higher concentration of VT2 given to the mice (VT1: 10 mg/kg; VT2: 30 mg/kg), thereby having a more pronounced and therefore significant effect on Pan-TEAD protein expression. Additionally, it was reported that VT1 also did not affect TEAD protein levels when used in tumour cells at a concentration of 3 µM overnight or for 20 hours (Tang *et al.*, 2021).

Furthermore, TEADs appear to have a considerably longer protein half-life than CTGF. For example, TEAD4 has been shown to possess a half-life of more than 24 hours (Kim & Gumbiner, 2019) while CTGF's half-life is somewhere between 60 and 90 minutes (Ryseck *et al.*, 1991). Moreover, CTGF is a direct YAP-TEAD transcription target (Zhao *et al.*, 2008) and therefore CTGF expression will in all likelihood be affected more quickly than the TEAD protein levels.

Taking all of these observations in consideration, it appears as if Pan-TEAD palmitoylation inhibitors have a stronger effect on CTGF protein expression than on Pan-TEAD protein expression, possibly in part due to their distinctions in protein half-lives and their relative position in the Hippo signaling pathway. Furthermore, it seems that the ability of Pan-TEAD palmitoylation inhibitors to significantly decrease Pan-TEAD protein expression might be dependent on the variant of Pan-TEAD inhibitor (e.g. VT2 was effective but not VT1) and on the concentration and time period which the respective Pan-TEAD inhibitor is used for.

4.19 Limitations of the used Postn-Cre schwannoma model

As previously mentioned (see section 4.2), Postn-Cre driven knockout mice could only be kept up to 9 months of age due to heightened mortality, possibly caused by the appearance of substantially sized schwannomas and MPNSTs (Gehlhausen *et al.*, 2015). This naturally reduces the amount of time one would have to run drug trials, especially considering the slow growth of the schwannomas in this murine model. The occurrence of MPNSTs also illustrates that this schwannoma model is not ideal, given that MPNSTs are only seldom seen in NF2 patients and seemingly only in those who have undergone radiotherapy (see Introduction section 1.6). Finally, meningiomas and ependymomas unfortunately do not develop in this mouse model (Gehlhausen *et al.*, 2015) which solely reproduces the schwannoma aspect of NF2.

4.20 Future work

A few possibilities to continue/expand this work would be discerning the mechanism by which YAP/TAZ impairment seems to heighten apoptotic rates (see section 4.9), determining the proportions of M1 and M2-like macrophages found in the different genotypes and timepoints (section 4.11) and comparing hearing and balance impairments of NF2/YAP and NF2/TAZ mice to NF2 sKO and control mice.

Moreover, the results of macrophage depletion (see section 4.11), different treatments with losartan or Pan-TEAD S-autopalmitoylation inhibitors alone or in combination with one another (sections 4.15 and 4.17) or with for example MEK inhibitor trametinib (White *et al.*, 2019) could be explored regarding hearing and balance. Additionally, the influence of such therapeutic interventions on proliferation rates, non-neuronal/neuronal cell composition and apoptosis in DRGs could be scrutinized. Such treatment effects in more pathologically accurate locations such as dorsal nerve roots, VGs, vestibular and cochlear nerves and especially the CPA would also be very interesting to see.

One could also look into which collagen types can be found within the schwannomas of the Postn-Cre mouse model (section 4.13) or why CTGF protein expression is not affected in Merlin positive primary human meningioma cells after Pan-TEAD inhibition (section 4.18.4). Furthermore, the potential presence of other immune cells besides macrophages such as T lymphocytes in general (CD3+ cells) and cytotoxic T lymphocytes in particular (CD3+ CD8+ cells) in the Postn-Cre mouse schwannomas could be investigated.

Finally, it might be worthwhile to attempt the creation of an even more accurate NF2 mouse model. By adding a Cre-Recombinase under control of the Prostaglandin D_2 synthase promoter (PGDS-Cre (Kalamarides *et al.*, 2011)) to the Cre-Recombinase under the control of the Postn-Cre promoter (Postn-Cre) in $NF2^{fl/fl}$ mice, the resulting Postn-Cre+ PGDS-Cre+ $NF2^{fl/fl}$ mice might spontaneously develop both schwannomas and meningiomas (Gehlhausen *et al.*, 2015; Kalamarides *et al.*, 2011). This would permit the direct comparison of the effects of potential treatments on schwannomas and meningiomas, eventually allowing the discovery of a single treatment effective for both of these tumours.

4.21 Conclusion

In conclusion, these results indicate that NF2 loss heightens glial cell proliferation (% EdU positive nuclei) and macrophage numbers (% Iba1 positive cells) compared to control and an additional loss of YAP or TAZ reduces glial cell proliferation and macrophage numbers (compared to NF2 sKO). Moreover, these observations are most likely valid in all sites of schwannoma formation in the Postn-Cre driven schwannoma mouse model which I used. Also, NF2/TAZ dKO appears to mitigate the effects of NF2 sKO and NF2/YAP dKO schwannoma growth, possibly by promoting apoptotic cell death. Furthermore, the Vivace Pan-TEAD S-autopalmitoylation inhibitors were shown to be effective in NF2-deficient tumours, namely in schwannoma *in vivo* (Laraba *et al.*, 2022), meningioma *in vitro* (see Results) and mesothelioma *in vivo* (Tang *et al.*, 2021). Finally, current data makes it conceivable that the Vivace Pan-TEAD S-autopalmitoylation inhibitors significantly inhibited NF2 sKO VG growth due to a dual effect of significantly lowering glial cell proliferation and significantly increasing the apoptotic rate.

5. References

Achkova, D. & Maher, J. (2016) 'Role of the colony-stimulating factor (CSF)/CSF-1 receptor axis in cancer'. *Biochem Soc Trans*, 44 (2), pp. 333-341.

Adams, C. L., Ercolano, E., Ferluga, S., Sofela, A., Dave, F., Negroni, C., Kurian, K. M., Hilton, D. A. & Hanemann, C. O. (2020) 'A Rapid Robust Method for Subgrouping Non-NF2 Meningiomas According to Genotype and Detection of Lower Levels of M2 Macrophages in AKT1 E17K Mutated Tumours'. *Int J Mol Sci*, 21 (4),

Afik, R., Zigmond, E., Vugman, M., Klepfish, M., Shimshoni, E., Pasmanik-Chor, M., Shenoy, A., Bassat, E., Halpern, Z., Geiger, T., Sagi, I. & Varol, C. (2016) 'Tumor macrophages are pivotal constructors of tumor collagenous matrix'. *J Exp Med*, 213 (11), pp. 2315-2331.

Agnihotri, S., Gugel, I., Remke, M., Bornemann, A., Pantazis, G., Mack, S. C., Shih, D., Singh, S. K., Sabha, N., Taylor, M. D., Tatagiba, M., Zadeh, G. & Krischek, B. (2014) 'Gene-expression profiling elucidates molecular signaling networks that can be therapeutically targeted in vestibular schwannoma'. *J Neurosurg*, 121 (6), pp. 1434-1445.

Agnihotri, S., Jalali, S., Wilson, M. R., Danesh, A., Li, M., Klironomos, G., Krieger, J. R., Mansouri, A., Khan, O., Mamatjan, Y., Landon-Brace, N., Tung, T., Dowar, M., Li, T., Bruce, J. P., Burrell, K. E., Tonge, P. D., Alamsahebpour, A., Krischek, B., Agarwalla, P. K., Bi, W. L., Dunn, I. F., Beroukhim, R., Fehlings, M. G., Bril, V., Pagnotta, S. M., Iavarone, A., Pugh, T. J., Aldape, K. D. & Zadeh, G. (2016) 'The genomic landscape of schwannoma'. *Nat Genet*, 48 (11), pp. 1339-1348.

Ahmad, Z., Brown, C. M., Patel, A. K., Ryan, A. F., Ongkeko, R. & Doherty, J. K. (2010) 'Merlin knockdown in human Schwann cells: clues to vestibular schwannoma tumorigenesis'. *Otol Neurotol*, 31 (3), pp. 460-466.

Ahronowitz, I., Xin, W., Kiely, R., Sims, K., MacCollin, M. & Nunes, F. P. (2007) 'Mutational spectrum of the NF2 gene: a meta-analysis of 12 years of research and diagnostic laboratory findings'. *Hum Mutat*, 28 (1), pp. 1-12.

Alfthan, K., Heiska, L., Grönholm, M., Renkema, G. H. & Carpén, O. (2004) 'Cyclic AMP-dependent protein kinase phosphorylates merlin at serine 518 independently of p21-activated kinase and promotes merlin-ezrin heterodimerization'. *J Biol Chem*, 279 (18), pp. 18559-18566.

Ali Khajeh, J., Ju, J. H., Atchiba, M., Allaire, M., Stanley, C., Heller, W. T., Callaway, D. J. & Bu, Z. (2014) 'Molecular conformation of the full-length tumor suppressor NF2/Merlin--a small-angle neutron scattering study'. *J Mol Biol*, 426 (15), pp. 2755-2768.

Alonso, M. E., Bello, M. J., Gonzalez-Gomez, P., Arjona, D., de Campos, J. M., Gutierrez, M. & Rey, J. A. (2004) 'Aberrant CpG island methylation of multiple genes in ependymal tumors'. *J Neurooncol*, 67 (1-2), pp. 159-165.

Altomare, D. A., Vaslet, C. A., Skele, K. L., De Rienzo, A., Devarajan, K., Jhanwar, S. C., McClatchey, A. I., Kane, A. B. & Testa, J. R. (2005) 'A mouse model recapitulating molecular features of human mesothelioma'. *Cancer Res*, 65 (18), pp. 8090-8095.

Ammoun, S., Cunliffe, C. H., Allen, J. C., Chiriboga, L., Giancotti, F. G., Zagzag, D., Hanemann, C. O. & Karajannis, M. A. (2010) 'ErbB/HER receptor activation and preclinical efficacy of lapatinib in vestibular schwannoma'. *Neuro Oncol*, 12 (8), pp. 834-843.

Ammoun, S., Flaiz, C., Ristic, N., Schuldt, J. & Hanemann, C. O. (2008) 'Dissecting and targeting the growth factor-dependent and growth factor-independent extracellular signal-regulated kinase pathway in human schwannoma'. *Cancer Res*, 68 (13), pp. 5236-5245.

Ammoun, S., Provenzano, L., Zhou, L., Barczyk, M., Evans, K., Hilton, D. A., Hafizi, S. & Hanemann, C. O. (2014) 'Axl/Gas6/NFκB signalling in schwannoma pathological proliferation, adhesion and survival'. *Oncogene*, 33 (3), pp. 336-346.

Ammoun, S., Schmid, M. C., Ristic, N., Zhou, L., Hilton, D., Ercolano, E., Carroll, C. & Hanemann, C. O. (2012) 'The role of insulin-like growth factors signaling in merlin-deficient human schwannomas'. *Glia*, 60 (11), pp. 1721-1733.

Ammoun, S., Schmid, M. C., Zhou, L., Hilton, D. A., Barczyk, M. & Hanemann, C. O. (2015) 'The p53/mouse double minute 2 homolog complex deregulation in merlin-deficient tumours'. *Mol Oncol*, 9 (1), pp. 236-248.

An, Y., Adams, J. R., Hollern, D. P., Zhao, A., Chang, S. G., Gams, M. S., Chung, P. E. D., He, X., Jangra, R., Shah, J. S., Yang, J., Beck, L. A., Raghuram, N., Kozma, K. J., Loch, A. J., Wang, W., Fan, C., Done, S. J., Zacksenhaus, E., Guidos, C. J., Perou, C. M. & Egan, S. E. (2018) 'Cdh1 and Pik3ca Mutations Cooperate to Induce Immune-Related Invasive Lobular Carcinoma of the Breast'. *Cell Rep*, 25 (3), pp. 702-714.e706.

Anbanandam, A., Albarado, D. C., Nguyen, C. T., Halder, G., Gao, X. & Veeraraghavan, S. (2006) 'Insights into transcription enhancer factor 1 (TEF-1) activity from the solution structure of the TEA domain'. *Proc Natl Acad Sci U S A*, 103 (46), pp. 17225-17230.

Antinheimo, J., Haapasalo, H., Haltia, M., Tatagiba, M., Thomas, S., Brandis, A., Sainio, M., Carpen, O., Samii, M. & Jääskeläinen, J. (1997) 'Proliferation potential and histological features in neurofibromatosis 2-associated and sporadic meningiomas'. *J Neurosurg*, 87 (4), pp. 610-614.

Antonescu, C. R., Le Loarer, F., Mosquera, J. M., Sboner, A., Zhang, L., Chen, C. L., Chen, H. W., Pathan, N., Krausz, T., Dickson, B. C., Weinreb, I., Rubin, M. A., Hameed, M. & Fletcher, C. D. (2013) 'Novel YAP1-TFE3 fusion defines a distinct subset of epithelioid hemangioendothelioma'. *Genes Chromosomes Cancer*, 52 (8), pp. 775-784.

Ao, J. Y., Zhu, X. D., Chai, Z. T., Cai, H., Zhang, Y. Y., Zhang, K. Z., Kong, L. Q., Zhang, N., Ye, B. G., Ma, D. N. & Sun, H. C. (2017) 'Colony-Stimulating Factor 1 Receptor Blockade Inhibits Tumor Growth by

Altering the Polarization of Tumor-Associated Macrophages in Hepatocellular Carcinoma'. *Mol Cancer Ther*, 16 (8), pp. 1544-1554.

Aragona, M., Panciera, T., Manfrin, A., Giulitti, S., Michielin, F., Elvassore, N., Dupont, S. & Piccolo, S. (2013) 'A mechanical checkpoint controls multicellular growth through YAP/TAZ regulation by actin-processing factors'. *Cell*, 154 (5), pp. 1047-1059.

Arakawa, H., Hayashi, N., Nagase, H., Ogawa, M. & Nakamura, Y. (1994) 'Alternative splicing of the NF2 gene and its mutation analysis of breast and colorectal cancers'. *Hum Mol Genet*, 3 (4), pp. 565-568.

Asthagiri, A. R., Parry, D. M., Butman, J. A., Kim, H. J., Tsilou, E. T., Zhuang, Z. & Lonser, R. R. (2009) 'Neurofibromatosis type 2'. *Lancet*, 373 (9679), pp. 1974-1986.

Aylon, Y., Michael, D., Shmueli, A., Yabuta, N., Nojima, H. & Oren, M. (2006) 'A positive feedback loop between the p53 and Lats2 tumor suppressors prevents tetraploidization'. *Genes Dev*, 20 (19), pp. 2687-2700.

Azzolin, L., Panciera, T., Soligo, S., Enzo, E., Bicciato, S., Dupont, S., Bresolin, S., Frasson, C., Basso, G., Guzzardo, V., Fassina, A., Cordenonsi, M. & Piccolo, S. (2014) 'YAP/TAZ incorporation in the beta-catenin destruction complex orchestrates the Wnt response'. *Cell*, 158 (1), pp. 157-170.

Bae, S. J., Ni, L., Osinski, A., Tomchick, D. R., Brautigam, C. A. & Luo, X. (2017) 'SAV1 promotes Hippo kinase activation through antagonizing the PP2A phosphatase STRIPAK'. *Elife*, 6

Bai, Y., Liu, Y. J., Wang, H., Xu, Y., Stamenkovic, I. & Yu, Q. (2007) 'Inhibition of the hyaluronan-CD44 interaction by merlin contributes to the tumor-suppressor activity of merlin'. *Oncogene*, 26 (6), pp. 836-850.

Baia, G. S., Caballero, O. L., Orr, B. A., Lal, A., Ho, J. S., Cowdrey, C., Tihan, T., Mawrin, C. & Riggins, G. J. (2012) 'Yes-associated protein 1 is activated and functions as an oncogene in meningiomas'. *Mol Cancer Res*, 10 (7), pp. 904-913.

Barth, M., Montalbetti, C. & Spitzer, L. (2017) 'Preparation of New 4-(1, 1-Dioxo-1, 2-benzothiazol-3-yl) hydrazono] methyl]-2-methoxyphenols as Inhibitors of the YAP/TAZ-TEAD Interaction and Their Use in the Treatment of Malignant Mesothelioma'. *PCT Int. Appl. WO*, 2017064277 pp. A1.

Baser, M. E., De Rienzo, A., Altomare, D., Balsara, B. R., Hedrick, N. M., Gutmann, D. H., Pitts, L. H., Jackler, R. K. & Testa, J. R. (2002a) 'Neurofibromatosis 2 and malignant mesothelioma'. *Neurology*, 59 (2), pp. 290-291.

Baser, M. E., Evans, D. G., Jackler, R. K., Sujansky, E. & Rubenstein, A. (2000) 'Neurofibromatosis 2, radiosurgery and malignant nervous system tumours'. *Br J Cancer*, 82 (4), pp. 998.

Baser, M. E., Friedman, J. M., Aeschliman, D., Joe, H., Wallace, A. J., Ramsden, R. T. & Evans, D. G. (2002b) 'Predictors of the risk of mortality in neurofibromatosis 2'. *Am J Hum Genet*, 71 (4), pp. 715-723.

Baser, M. E., Friedman, J. M. & Evans, D. G. (2006) 'Increasing the specificity of diagnostic criteria for schwannomatosis'. *Neurology*, 66 (5), pp. 730-732.

Baser, M. E., Kuramoto, L., Woods, R., Joe, H., Friedman, J. M., Wallace, A. J., Ramsden, R. T., Olschwang, S., Bijlsma, E., Kalamarides, M., Papi, L., Kato, R., Carroll, J., Lázaro, C., Joncourt, F., Parry, D. M., Rouleau, G. A. & Evans, D. G. (2005a) 'The location of constitutional neurofibromatosis 2 (NF2) splice site mutations is associated with the severity of NF2'. *J Med Genet*, 42 (7), pp. 540-546.

Baser, M. E., Mautner, V. F., Parry, D. M. & Evans, D. G. (2005b) 'Methodological issues in longitudinal studies: vestibular schwannoma growth rates in neurofibromatosis 2'. *J Med Genet*, 42 (12), pp. 903-906.

Bashour, A. M., Meng, J. J., Ip, W., MacCollin, M. & Ratner, N. (2002) 'The neurofibromatosis type 2 gene product, merlin, reverses the F-actin cytoskeletal defects in primary human Schwannoma cells'. *Mol Cell Biol*, 22 (4), pp. 1150-1157.

Basu, S., Totty, N. F., Irwin, M. S., Sudol, M. & Downward, J. (2003) 'Akt phosphorylates the Yes-associated protein, YAP, to induce interaction with 14-3-3 and attenuation of p73-mediated apoptosis'. *Mol Cell*, 11 (1), pp. 11-23.

Baumgartner, R., Poernbacher, I., Buser, N., Hafen, E. & Stocker, H. (2010) 'The WW domain protein Kibra acts upstream of Hippo in Drosophila'. *Dev Cell*, 18 (2), pp. 309-316.

Belandia, B. & Parker, M. G. (2000) 'Functional interaction between the p160 coactivator proteins and the transcriptional enhancer factor family of transcription factors'. *J Biol Chem*, 275 (40), pp. 30801-30805.

Benhaddou, A., Keime, C., Ye, T., Morlon, A., Michel, I., Jost, B., Mengus, G. & Davidson, I. (2012) 'Transcription factor TEAD4 regulates expression of myogenin and the unfolded protein response genes during C2C12 cell differentiation'. *Cell Death Differ*, 19 (2), pp. 220-231.

Beyer, T. A., Weiss, A., Khomchuk, Y., Huang, K., Ogunjimi, A. A., Varelas, X. & Wrana, J. L. (2013) 'Switch enhancers interpret TGF-β and Hippo signaling to control cell fate in human embryonic stem cells'. *Cell Rep*, 5 (6), pp. 1611-1624.

Bi, W. L., Abedalthagafi, M., Horowitz, P., Agarwalla, P. K., Mei, Y., Aizer, A. A., Brewster, R., Dunn, G. P., Al-Mefty, O., Alexander, B. M., Santagata, S., Beroukhim, R. & Dunn, I. F. (2016) 'Genomic landscape of intracranial meningiomas'. *J Neurosurg*, 125 (3), pp. 525-535.

Bianchi, A. B., Hara, T., Ramesh, V., Gao, J., Klein-Szanto, A. J., Morin, F., Menon, A. G., Trofatter, J. A., Gusella, J. F., Seizinger, B. R. & et al. (1994) 'Mutations in transcript isoforms of the neurofibromatosis 2 gene in multiple human tumour types'. *Nat Genet*, 6 (2), pp. 185-192.

Bianchi, A. B., Mitsunaga, S. I., Cheng, J. Q., Klein, W. M., Jhanwar, S. C., Seizinger, B., Kley, N., Klein-Szanto, A. J. & Testa, J. R. (1995) 'High frequency of inactivating mutations in the neurofibromatosis type 2 gene (NF2) in primary malignant mesotheliomas'. *Proc Natl Acad Sci U S A*, 92 (24), pp. 10854-10858.

Blakeley, J. O., Ye, X., Duda, D. G., Halpin, C. F., Bergner, A. L., Muzikansky, A., Merker, V. L., Gerstner, E. R., Fayad, L. M., Ahlawat, S., Jacobs, M. A., Jain, R. K., Zalewski, C., Dombi, E., Widemann, B. C. & Plotkin, S. R. (2016) 'Efficacy and Biomarker Study of Bevacizumab for Hearing Loss Resulting From Neurofibromatosis Type 2-Associated Vestibular Schwannomas'. *J Clin Oncol*, 34 (14), pp. 1669-1675.

Boggiano, J. C., Vanderzalm, P. J. & Fehon, R. G. (2011) 'Tao-1 phosphorylates Hippo/MST kinases to regulate the Hippo-Salvador-Warts tumor suppressor pathway'. *Dev Cell*, 21 (5), pp. 888-895.

Boin, A., Couvelard, A., Couderc, C., Brito, I., Filipescu, D., Kalamarides, M., Bedossa, P., De Koning, L., Danelsky, C., Dubois, T., Hupé, P., Louvard, D. & Lallemand, D. (2014) 'Proteomic screening identifies a YAP-driven signaling network linked to tumor cell proliferation in human schwannomas'. *Neuro Oncol*, 16 (9), pp. 1196-1209.

Bokhovchuk, F., Mesrouze, Y., Delaunay, C., Martin, T., Villard, F., Meyerhofer, M., Fontana, P., Zimmermann, C., Erdmann, D., Furet, P., Scheufler, C., Schmelzle, T. & Chène, P. (2020) 'Identification of FAM181A and FAM181B as new interactors with the TEAD transcription factors'. *Protein Sci*, 29 (2), pp. 509-520.

Bokhovchuk, F., Mesrouze, Y., Izaac, A., Meyerhofer, M., Zimmermann, C., Fontana, P., Schmelzle, T., Erdmann, D., Furet, P., Kallen, J. & Chène, P. (2019) 'Molecular and structural characterization of a TEAD mutation at the origin of Sveinsson's chorioretinal atrophy'. *Febs j*, 286 (12), pp. 2381-2398.

Bonde, A. K., Tischler, V., Kumar, S., Soltermann, A. & Schwendener, R. A. (2012) 'Intratumoral macrophages contribute to epithelial-mesenchymal transition in solid tumors'. *BMC Cancer*, 12 pp. 35.

Bonilla, X., Parmentier, L., King, B., Bezrukov, F., Kaya, G., Zoete, V., Seplyarskiy, V. B., Sharpe, H. J., McKee, T., Letourneau, A., Ribaux, P. G., Popadin, K., Basset-Seguin, N., Ben Chaabene, R., Santoni, F. A., Andrianova, M. A., Guipponi, M., Garieri, M., Verdan, C., Grosdemange, K., Sumara, O., Eilers, M., Aifantis, I., Michielin, O., de Sauvage, F. J., Antonarakis, S. E. & Nikolaev, S. I. (2016) 'Genomic analysis identifies new drivers and progression pathways in skin basal cell carcinoma'. *Nat Genet*, 48 (4), pp. 398-406.

Bosco, E. E., Nakai, Y., Hennigan, R. F., Ratner, N. & Zheng, Y. (2010) 'NF2-deficient cells depend on the Rac1-canonical Wnt signaling pathway to promote the loss of contact inhibition of proliferation'. *Oncogene*, 29 (17), pp. 2540-2549.

Bourguignon, L. Y., Gilad, E., Peyrollier, K., Brightman, A. & Swanson, R. A. (2007) 'Hyaluronan-CD44 interaction stimulates Rac1 signaling and PKN gamma kinase activation leading to cytoskeleton function and cell migration in astrocytes'. *J Neurochem*, 101 (4), pp. 1002-1017.

Bourguignon, L. Y., Zhu, H., Shao, L. & Chen, Y. W. (2000) 'CD44 interaction with tiam1 promotes Rac1 signaling and hyaluronic acid-mediated breast tumor cell migration'. *J Biol Chem*, 275 (3), pp. 1829-1838.

Bouzas, E. A., Parry, D. M., Eldridge, R. & Kaiser-Kupfer, M. I. (1992) 'Familial occurrence of combined pigment epithelial and retinal hamartomas associated with neurofibromatosis 2'. *Retina*, 12 (2), pp. 103-107.

Brackmann, D. E., Fayad, J. N., Slattery, W. H., 3rd, Friedman, R. A., Day, J. D., Hitselberger, W. E. & Owens, R. M. (2001) 'Early proactive management of vestibular schwannomas in neurofibromatosis type 2'. *Neurosurgery*, 49 (2), pp. 274-280; discussion 280-273.

Brastianos, P. K., Horowitz, P. M., Santagata, S., Jones, R. T., McKenna, A., Getz, G., Ligon, K. L., Palescandolo, E., Van Hummelen, P., Ducar, M. D., Raza, A., Sunkavalli, A., Macconaill, L. E., Stemmer-Rachamimov, A. O., Louis, D. N., Hahn, W. C., Dunn, I. F. & Beroukhim, R. (2013) 'Genomic sequencing of meningiomas identifies oncogenic SMO and AKT1 mutations'. *Nat Genet*, 45 (3), pp. 285-289.

Bueno, R., Stawiski, E. W., Goldstein, L. D., Durinck, S., De Rienzo, A., Modrusan, Z., Gnad, F., Nguyen, T. T., Jaiswal, B. S., Chirieac, L. R., Sciaranghella, D., Dao, N., Gustafson, C. E., Munir, K. J., Hackney, J. A., Chaudhuri, A., Gupta, R., Guillory, J., Toy, K., Ha, C., Chen, Y. J., Stinson, J., Chaudhuri, S., Zhang, N., Wu, T. D., Sugarbaker, D. J., de Sauvage, F. J., Richards, W. G. & Seshagiri, S. (2016) 'Comprehensive genomic analysis of malignant pleural mesothelioma identifies recurrent mutations, gene fusions and splicing alterations'. *Nat Genet*, 48 (4), pp. 407-416.

Bum-Erdene, K., Zhou, D., Gonzalez-Gutierrez, G., Ghozayel, M. K., Si, Y., Xu, D., Shannon, H. E., Bailey, B. J., Corson, T. W., Pollok, K. E., Wells, C. D. & Meroueh, S. O. (2019) 'Small-Molecule Covalent Modification of Conserved Cysteine Leads to Allosteric Inhibition of the TEAD·Yap Protein-Protein Interaction'. *Cell Chem Biol*, 26 (3), pp. 378-389.e313.

Bürglin, T. R. (1991) 'The TEA domain: a novel, highly conserved DNA-binding motif'. *Cell*, 66 (1), pp. 11-12.

Burns, S. S., Akhmametyeva, E. M., Oblinger, J. L., Bush, M. L., Huang, J., Senner, V., Chen, C. S., Jacob, A., Welling, D. B. & Chang, L. S. (2013) 'Histone deacetylase inhibitor AR-42 differentially affects cell-cycle transit in meningeal and meningioma cells, potently inhibiting NF2-deficient meningioma growth'. *Cancer Res*, 73 (2), pp. 792-803.

Bush, M. L., Oblinger, J., Brendel, V., Santarelli, G., Huang, J., Akhmametyeva, E. M., Burns, S. S., Wheeler, J., Davis, J., Yates, C. W., Chaudhury, A. R., Kulp, S., Chen, C. S., Chang, L. S., Welling, D. B. &

Jacob, A. (2011) 'AR42, a novel histone deacetylase inhibitor, as a potential therapy for vestibular schwannomas and meningiomas'. *Neuro Oncol*, 13 (9), pp. 983-999.

Čačev, T., Aralica, G., Lončar, B. & Kapitanović, S. (2014) 'Loss of NF2/Merlin expression in advanced sporadic colorectal cancer'. *Cell Oncol (Dordr)*, 37 (1), pp. 69-77.

Caffo, M., Caruso, G., Galatioto, S., Meli, F., Cacciola, F., Germanò, A., Alafaci, C. & Tomasello, F. (2008) 'Immunohistochemical study of the extracellular matrix proteins laminin, fibronectin and type IV collagen in secretory meningiomas'. *J Clin Neurosci*, 15 (7), pp. 806-811.

Cai, J., Maitra, A., Anders, R. A., Taketo, M. M. & Pan, D. (2015) 'β-Catenin destruction complex-independent regulation of Hippo-YAP signaling by APC in intestinal tumorigenesis'. *Genes Dev*, 29 (14), pp. 1493-1506.

Cai, J., Song, X., Wang, W., Watnick, T., Pei, Y., Qian, F. & Pan, D. (2018) 'A RhoA-YAP-c-Myc signaling axis promotes the development of polycystic kidney disease'. *Genes Dev*, 32 (11-12), pp. 781-793.

Calvo, F., Ege, N., Grande-Garcia, A., Hooper, S., Jenkins, R. P., Chaudhry, S. I., Harrington, K., Williamson, P., Moeendarbary, E., Charras, G. & Sahai, E. (2013) 'Mechanotransduction and YAP-dependent matrix remodelling is required for the generation and maintenance of cancer-associated fibroblasts'. *Nat Cell Biol*, 15 (6), pp. 637-646.

Camargo, F. D., Gokhale, S., Johnnidis, J. B., Fu, D., Bell, G. W., Jaenisch, R. & Brummelkamp, T. R. (2007) 'YAP1 increases organ size and expands undifferentiated progenitor cells'. *Curr Biol*, 17 (23), pp. 2054-2060.

Cao, J. J., Zhao, X. M., Wang, D. L., Chen, K. H., Sheng, X., Li, W. B., Li, M. C., Liu, W. J. & He, J. (2014) 'YAP is overexpressed in clear cell renal cell carcinoma and its knockdown reduces cell proliferation and induces cell cycle arrest and apoptosis'. *Oncol Rep*, 32 (4), pp. 1594-1600.

Cao, X., Pfaff, S. L. & Gage, F. H. (2008) 'YAP regulates neural progenitor cell number via the TEA domain transcription factor'. *Genes Dev*, 22 (23), pp. 3320-3334.

Cattin, A. L., Burden, J. J., Van Emmenis, L., Mackenzie, F. E., Hoving, J. J., Garcia Calavia, N., Guo, Y., McLaughlin, M., Rosenberg, L. H., Quereda, V., Jamecna, D., Napoli, I., Parrinello, S., Enver, T., Ruhrberg, C. & Lloyd, A. C. (2015) 'Macrophage-Induced Blood Vessels Guide Schwann Cell-Mediated Regeneration of Peripheral Nerves'. *Cell*, 162 (5), pp. 1127-1139.

Cayé-Thomasen, P., Werther, K., Nalla, A., Bøg-Hansen, T. C., Nielsen, H. J., Stangerup, S. E. & Thomsen, J. (2005) 'VEGF and VEGF receptor-1 concentration in vestibular schwannoma homogenates correlates to tumor growth rate'. *Otol Neurotol*, 26 (1), pp. 98-101.

Cebola, I., Rodríguez-Seguí, S. A., Cho, C. H., Bessa, J., Rovira, M., Luengo, M., Chhatriwala, M., Berry, A., Ponsa-Cobas, J., Maestro, M. A., Jennings, R. E., Pasquali, L., Morán, I., Castro, N., Hanley, N. A.,

Gomez-Skarmeta, J. L., Vallier, L. & Ferrer, J. (2015) 'TEAD and YAP regulate the enhancer network of human embryonic pancreatic progenitors'. *Nat Cell Biol*, 17 (5), pp. 615-626.

Chan, P., Han, X., Zheng, B., DeRan, M., Yu, J., Jarugumilli, G. K., Deng, H., Pan, D., Luo, X. & Wu, X. (2016) 'Autopalmitoylation of TEAD proteins regulates transcriptional output of the Hippo pathway'. *Nat Chem Biol*, 12 (4), pp. 282-289.

Chan, S. W., Lim, C. J., Chong, Y. F., Pobbati, A. V., Huang, C. & Hong, W. (2011) 'Hippo pathway-independent restriction of TAZ and YAP by angiomotin'. *J Biol Chem*, 286 (9), pp. 7018-7026.

Chan, S. W., Lim, C. J., Loo, L. S., Chong, Y. F., Huang, C. & Hong, W. (2009) 'TEADs mediate nuclear retention of TAZ to promote oncogenic transformation'. *J Biol Chem*, 284 (21), pp. 14347-14358.

Chang, L., Azzolin, L., Di Biagio, D., Zanconato, F., Battilana, G., Lucon Xiccato, R., Aragona, M., Giulitti, S., Panciera, T., Gandin, A., Sigismondo, G., Krijgsveld, J., Fassan, M., Brusatin, G., Cordenonsi, M. & Piccolo, S. (2018) 'The SWI/SNF complex is a mechanoregulated inhibitor of YAP and TAZ'. *Nature*, 563 (7730), pp. 265-269.

Chang, U. K., Choe, W. J., Chung, S. K., Chung, C. K. & Kim, H. J. (2002) 'Surgical outcome and prognostic factors of spinal intramedullary ependymomas in adults'. *J Neurooncol*, 57 (2), pp. 133-139.

Chanmee, T., Ontong, P., Konno, K. & Itano, N. (2014) 'Tumor-associated macrophages as major players in the tumor microenvironment'. *Cancers (Basel)*, 6 (3), pp. 1670-1690.

Chen, C. S., Weng, S. C., Tseng, P. H., Lin, H. P. & Chen, C. S. (2005) 'Histone acetylation-independent effect of histone deacetylase inhibitors on Akt through the reshuffling of protein phosphatase 1 complexes'. *J Biol Chem*, 280 (46), pp. 38879-38887.

Chen, H. H., Maeda, T., Mullett, S. J. & Stewart, A. F. (2004) 'Transcription cofactor Vgl-2 is required for skeletal muscle differentiation'. *Genesis*, 39 (4), pp. 273-279.

Chen, H. H., Mullett, S. J. & Stewart, A. F. (2004) 'Vgl-4, a novel member of the vestigial-like family of transcription cofactors, regulates alpha1-adrenergic activation of gene expression in cardiac myocytes'. *J Biol Chem*, 279 (29), pp. 30800-30806.

Chen, H. Y., Yu, S. L., Ho, B. C., Su, K. Y., Hsu, Y. C., Chang, C. S., Li, Y. C., Yang, S. Y., Hsu, P. Y., Ho, H., Chang, Y. H., Chen, C. Y., Yang, H. I., Hsu, C. P., Yang, T. Y., Chen, K. C., Hsu, K. H., Tseng, J. S., Hsia, J. Y., Chuang, C. Y., Yuan, S., Lee, M. H., Liu, C. H., Wu, G. I., Hsiung, C. A., Chen, Y. M., Wang, C. L., Huang, M. S., Yu, C. J., Chen, K. Y., Tsai, Y. H., Su, W. C., Chen, H. W., Chen, J. J., Chen, C. J., Chang, G. C., Yang, P. C. & Li, K. C. (2015a) 'R331W Missense Mutation of Oncogene YAP1 Is a Germline Risk Allele for Lung Adenocarcinoma With Medical Actionability'. *J Clin Oncol*, 33 (20), pp. 2303-2310.

Chen, L., Chan, S. W., Zhang, X., Walsh, M., Lim, C. J., Hong, W. & Song, H. (2010) 'Structural basis of YAP recognition by TEAD4 in the hippo pathway'. *Genes Dev*, 24 (3), pp. 290-300.

Chen, Q., Zhang, N., Gray, R. S., Li, H., Ewald, A. J., Zahnow, C. A. & Pan, D. (2014) 'A temporal requirement for Hippo signaling in mammary gland differentiation, growth, and tumorigenesis'. *Genes Dev*, 28 (5), pp. 432-437.

Chen, Q., Zhang, N., Xie, R., Wang, W., Cai, J., Choi, K. S., David, K. K., Huang, B., Yabuta, N., Nojima, H., Anders, R. A. & Pan, D. (2015b) 'Homeostatic control of Hippo signaling activity revealed by an endogenous activating mutation in YAP'. *Genes Dev*, 29 (12), pp. 1285-1297.

Chen, Z., Li, S., Mo, J., Hawley, E., Wang, Y., He, Y., Brosseau, J. P., Shipman, T., Clapp, D. W., Carroll, T. J. & Le, L. Q. (2020) 'Schwannoma development is mediated by Hippo pathway dysregulation and modified by RAS/MAPK signaling'. *JCI Insight*, 5 (20),

Chen, Z., Mo, J., Brosseau, J. P., Shipman, T., Wang, Y., Liao, C. P., Cooper, J. M., Allaway, R. J., Gosline, S. J. C., Guinney, J., Carroll, T. J. & Le, L. Q. (2019) 'Spatiotemporal Loss of NF1 in Schwann Cell Lineage Leads to Different Types of Cutaneous Neurofibroma Susceptible to Modification by the Hippo Pathway'. *Cancer Discov*, 9 (1), pp. 114-129.

Cheng, J. Q., Lee, W. C., Klein, M. A., Cheng, G. Z., Jhanwar, S. C. & Testa, J. R. (1999) 'Frequent mutations of NF2 and allelic loss from chromosome band 22q12 in malignant mesothelioma: evidence for a two-hit mechanism of NF2 inactivation'. *Genes Chromosomes Cancer*, 24 (3), pp. 238-242.

Cho, Y. S., Zhu, J., Li, S., Wang, B., Han, Y. & Jiang, J. (2018) 'Regulation of Yki/Yap subcellular localization and Hpo signaling by a nuclear kinase PRP4K'. *Nat Commun*, 9 (1), pp. 1657.

Chow, H. Y., Dong, B., Duron, S. G., Campbell, D. A., Ong, C. C., Hoeflich, K. P., Chang, L. S., Welling, D. B., Yang, Z. J. & Chernoff, J. (2015) 'Group I Paks as therapeutic targets in NF2-deficient meningioma'. *Oncotarget*, 6 (4), pp. 1981-1994.

Clark, V. E., Erson-Omay, E. Z., Serin, A., Yin, J., Cotney, J., Ozduman, K., Avsar, T., Li, J., Murray, P. B., Henegariu, O., Yilmaz, S., Gunel, J. M., Carrion-Grant, G., Yilmaz, B., Grady, C., Tanrikulu, B., Bakircioglu, M., Kaymakcalan, H., Caglayan, A. O., Sencar, L., Ceyhun, E., Atik, A. F., Bayri, Y., Bai, H., Kolb, L. E., Hebert, R. M., Omay, S. B., Mishra-Gorur, K., Choi, M., Overton, J. D., Holland, E. C., Mane, S., State, M. W., Bilguvar, K., Baehring, J. M., Gutin, P. H., Piepmeier, J. M., Vortmeyer, A., Brennan, C. W., Pamir, M. N., Kilic, T., Lifton, R. P., Noonan, J. P., Yasuno, K. & Gunel, M. (2013) 'Genomic analysis of non-NF2 meningiomas reveals mutations in TRAF7, KLF4, AKT1, and SMO'. *Science*, 339 (6123), pp. 1077-1080.

Clark, V. E., Harmancı, A. S., Bai, H., Youngblood, M. W., Lee, T. I., Baranoski, J. F., Ercan-Sencicek, A. G., Abraham, B. J., Weintraub, A. S., Hnisz, D., Simon, M., Krischek, B., Erson-Omay, E. Z., Henegariu, O., Carrión-Grant, G., Mishra-Gorur, K., Durán, D., Goldmann, J. E., Schramm, J., Goldbrunner, R., Piepmeier, J. M., Vortmeyer, A. O., Günel, J. M., Bilgüvar, K., Yasuno, K., Young, R. A. & Günel, M. (2016) 'Recurrent somatic mutations in POLR2A define a distinct subset of meningiomas'. *Nat Genet*, 48 (10), pp. 1253-1259.

Cloughesy, T. F., Yoshimoto, K., Nghiemphu, P., Brown, K., Dang, J., Zhu, S., Hsueh, T., Chen, Y., Wang, W., Youngkin, D., Liau, L., Martin, N., Becker, D., Bergsneider, M., Lai, A., Green, R., Oglesby, T., Koleto, M., Trent, J., Horvath, S., Mischel, P. S., Mellinghoff, I. K. & Sawyers, C. L. (2008) 'Antitumor activity of rapamycin in a Phase I trial for patients with recurrent PTEN-deficient glioblastoma'. *PLoS Med*, 5 (1), pp. e8.

Colegio, O. R., Chu, N. Q., Szabo, A. L., Chu, T., Rhebergen, A. M., Jairam, V., Cyrus, N., Brokowski, C. E., Eisenbarth, S. C., Phillips, G. M., Cline, G. W., Phillips, A. J. & Medzhitov, R. (2014) 'Functional polarization of tumour-associated macrophages by tumour-derived lactic acid'. *Nature*, 513 (7519), pp. 559-563.

Cooper, J. & Giancotti, F. G. (2014) 'Molecular insights into NF2/Merlin tumor suppressor function'. *FEBS Lett*, 588 (16), pp. 2743-2752.

Cordenonsi, M., Zanconato, F., Azzolin, L., Forcato, M., Rosato, A., Frasson, C., Inui, M., Montagner, M., Parenti, A. R., Poletti, A., Daidone, M. G., Dupont, S., Basso, G., Bicciato, S. & Piccolo, S. (2011) 'The Hippo transducer TAZ confers cancer stem cell-related traits on breast cancer cells'. *Cell*, 147 (4), pp. 759-772.

Cottini, F., Hideshima, T., Xu, C., Sattler, M., Dori, M., Agnelli, L., ten Hacken, E., Bertilaccio, M. T., Antonini, E., Neri, A., Ponzoni, M., Marcatti, M., Richardson, P. G., Carrasco, R., Kimmelman, A. C., Wong, K. K., Caligaris-Cappio, F., Blandino, G., Kuehl, W. M., Anderson, K. C. & Tonon, G. (2014) 'Rescue of Hippo coactivator YAP1 triggers DNA damage-induced apoptosis in hematological cancers'. *Nat Med*, 20 (6), pp. 599-606.

Cotton, J. L., Li, Q., Ma, L., Park, J. S., Wang, J., Ou, J., Zhu, L. J., Ip, Y. T., Johnson, R. L. & Mao, J. (2017) 'YAP/TAZ and Hedgehog Coordinate Growth and Patterning in Gastrointestinal Mesenchyme'. *Dev Cell*, 43 (1), pp. 35-47.e34.

Couldwell, W. T., Fukushima, T., Giannotta, S. L. & Weiss, M. H. (1996) 'Petroclival meningiomas: surgical experience in 109 cases'. *J Neurosurg*, 84 (1), pp. 20-28.

Couldwell, W. T., Kan, P., Liu, J. K. & Apfelbaum, R. I. (2006) 'Decompression of cavernous sinus meningioma for preservation and improvement of cranial nerve function. Technical note'. *J Neurosurg*, 105 (1), pp. 148-152.

Croci, O., De Fazio, S., Biagioni, F., Donato, E., Caganova, M., Curti, L., Doni, M., Sberna, S., Aldeghi, D., Biancotto, C., Verrecchia, A., Olivero, D., Amati, B. & Campaner, S. (2017) 'Transcriptional integration of mitogenic and mechanical signals by Myc and YAP'. *Genes Dev*, 31 (20), pp. 2017-2022.

Crook, Z. R., Sevilla, G. P., Friend, D., Brusniak, M. Y., Bandaranayake, A. D., Clarke, M., Gewe, M., Mhyre, A. J., Baker, D., Strong, R. K., Bradley, P. & Olson, J. M. (2017) 'Mammalian display screening of diverse cystine-dense peptides for difficult to drug targets'. *Nat Commun*, 8 (1), pp. 2244.

Curiel, T. J., Coukos, G., Zou, L., Alvarez, X., Cheng, P., Mottram, P., Evdemon-Hogan, M., Conejo-Garcia, J. R., Zhang, L., Burow, M., Zhu, Y., Wei, S., Kryczek, I., Daniel, B., Gordon, A., Myers, L.,

Lackner, A., Disis, M. L., Knutson, K. L., Chen, L. & Zou, W. (2004) 'Specific recruitment of regulatory T cells in ovarian carcinoma fosters immune privilege and predicts reduced survival'. *Nat Med*, 10 (9), pp. 942-949.

Currey, L., Thor, S. & Piper, M. (2021) 'TEAD family transcription factors in development and disease'. *Development*, 148 (12),

Cushing, H. (1917) *Tumors of the Nervus Acusticus and the Syndrome of the Cerebellopontile Angle.* WB Saunders.

Dai, X., Liu, H., Shen, S., Guo, X., Yan, H., Ji, X., Li, L., Huang, J., Feng, X. H. & Zhao, B. (2015) 'YAP activates the Hippo pathway in a negative feedback loop'. *Cell Res*, 25 (10), pp. 1175-1178.

Dasari, V. R., Mazack, V., Feng, W., Nash, J., Carey, D. J. & Gogoi, R. (2017) 'Verteporfin exhibits YAP-independent anti-proliferative and cytotoxic effects in endometrial cancer cells'. *Oncotarget*, 8 (17), pp. 28628-28640.

de Vries, M., Briaire-de Bruijn, I., Malessy, M. J., de Bruine, S. F., van der Mey, A. G. & Hogendoorn, P. C. (2013) 'Tumor-associated macrophages are related to volumetric growth of vestibular schwannomas'. *Otol Neurotol*, 34 (2), pp. 347-352.

de Vries, M., Hogendoorn, P. C., Briaire-de Bruyn, I., Malessy, M. J. & van der Mey, A. G. (2012) 'Intratumoral hemorrhage, vessel density, and the inflammatory reaction contribute to volume increase of sporadic vestibular schwannomas'. *Virchows Arch*, 460 (6), pp. 629-636.

Deel, M. D., Slemmons, K. K., Hinson, A. R., Genadry, K. C., Burgess, B. A., Crose, L. E. S., Kuprasertkul, N., Oristian, K. M., Bentley, R. C. & Linardic, C. M. (2018) 'The Transcriptional Coactivator TAZ Is a Potent Mediator of Alveolar Rhabdomyosarcoma Tumorigenesis'. *Clin Cancer Res*, 24 (11), pp. 2616-2630.

Deng, H., Wang, W., Yu, J., Zheng, Y., Qing, Y. & Pan, D. (2015) 'Spectrin regulates Hippo signaling by modulating cortical actomyosin activity'. *Elife*, 4 pp. e06567.

Denning, T. L., Wang, Y. C., Patel, S. R., Williams, I. R. & Pulendran, B. (2007) 'Lamina propria macrophages and dendritic cells differentially induce regulatory and interleukin 17-producing T cell responses'. *Nat Immunol*, 8 (10), pp. 1086-1094.

DeRan, M., Yang, J., Shen, C. H., Peters, E. C., Fitamant, J., Chan, P., Hsieh, M., Zhu, S., Asara, J. M., Zheng, B., Bardeesy, N., Liu, J. & Wu, X. (2014) 'Energy stress regulates hippo-YAP signaling involving AMPK-mediated regulation of angiomotin-like 1 protein'. *Cell Rep*, 9 (2), pp. 495-503.

Diepenbruck, M., Waldmeier, L., Ivanek, R., Berninger, P., Arnold, P., van Nimwegen, E. & Christofori, G. (2014) 'Tead2 expression levels control the subcellular distribution of Yap and Taz, zyxin expression and epithelial-mesenchymal transition'. *J Cell Sci*, 127 (Pt 7), pp. 1523-1536.

Ding, Y., He, J., Huang, J., Yu, T., Shi, X., Zhang, T., Yan, G., Chen, S. & Peng, C. (2019) 'Harmine induces anticancer activity in breast cancer cells via targeting TAZ'. *Int J Oncol*, 54 (6), pp. 1995-2004.

Dong, J., Feldmann, G., Huang, J., Wu, S., Zhang, N., Comerford, S. A., Gayyed, M. F., Anders, R. A., Maitra, A. & Pan, D. (2007) 'Elucidation of a universal size-control mechanism in Drosophila and mammals'. *Cell*, 130 (6), pp. 1120-1133.

Dow, G., Biggs, N., Evans, G., Gillespie, J., Ramsden, R. & King, A. (2005) 'Spinal tumors in neurofibromatosis type 2. Is emerging knowledge of genotype predictive of natural history?'. *J Neurosurg Spine*, 2 (5), pp. 574-579.

Dupont, S., Morsut, L., Aragona, M., Enzo, E., Giulitti, S., Cordenonsi, M., Zanconato, F., Le Digabel, J., Forcato, M., Bicciato, S., Elvassore, N. & Piccolo, S. (2011) 'Role of YAP/TAZ in mechanotransduction'. *Nature*, 474 (7350), pp. 179-183.

Ege, N., Dowbaj, A. M., Jiang, M., Howell, M., Hooper, S., Foster, C., Jenkins, R. P. & Sahai, E. (2018) 'Quantitative Analysis Reveals that Actin and Src-Family Kinases Regulate Nuclear YAP1 and Its Export'. *Cell Syst*, 6 (6), pp. 692-708.e613.

Egelhoff, J. C., Bates, D. J., Ross, J. S., Rothner, A. D. & Cohen, B. H. (1992) 'Spinal MR findings in neurofibromatosis types 1 and 2'. *AJNR Am J Neuroradiol*, 13 (4), pp. 1071-1077.

Ehsanian, R., Brown, M., Lu, H., Yang, X. P., Pattatheyil, A., Yan, B., Duggal, P., Chuang, R., Doondeea, J., Feller, S., Sudol, M., Chen, Z. & Van Waes, C. (2010) 'YAP dysregulation by phosphorylation or ΔNp63-mediated gene repression promotes proliferation, survival and migration in head and neck cancer subsets'. *Oncogene*, 29 (46), pp. 6160-6171.

Elosegui-Artola, A., Andreu, I., Beedle, A. E. M., Lezamiz, A., Uroz, M., Kosmalska, A. J., Oria, R., Kechagia, J. Z., Rico-Lastres, P., Le Roux, A. L., Shanahan, C. M., Trepat, X., Navajas, D., Garcia-Manyes, S. & Roca-Cusachs, P. (2017) 'Force Triggers YAP Nuclear Entry by Regulating Transport across Nuclear Pores'. *Cell*, 171 (6), pp. 1397-1410.e1314.

Enzo, E., Santinon, G., Pocaterra, A., Aragona, M., Bresolin, S., Forcato, M., Grifoni, D., Pession, A., Zanconato, F., Guzzo, G., Bicciato, S. & Dupont, S. (2015) 'Aerobic glycolysis tunes YAP/TAZ transcriptional activity'. *Embo j*, 34 (10), pp. 1349-1370.

Epstein, F. J., Farmer, J. P. & Freed, D. (1992) 'Adult intramedullary astrocytomas of the spinal cord'. *J Neurosurg*, 77 (3), pp. 355-359.

Epstein, F. J., Farmer, J. P. & Freed, D. (1993) 'Adult intramedullary spinal cord ependymomas: the result of surgery in 38 patients'. *J Neurosurg*, 79 (2), pp. 204-209.

Erkes, D. A., Rosenbaum, S. R., Field, C. O., Chervoneva, I., Villanueva, J. & Aplin, A. E. (2020) 'PLX3397 inhibits the accumulation of intra-tumoral macrophages and improves bromodomain and extra-terminal inhibitor efficacy in melanoma'. *Pigment Cell Melanoma Res*, 33 (2), pp. 372-377.

Evans, D. G., Birch, J. M. & Ramsden, R. T. (1999) 'Paediatric presentation of type 2 neurofibromatosis'. *Arch Dis Child*, 81 (6), pp. 496-499.

Evans, D. G., Birch, J. M., Ramsden, R. T., Sharif, S. & Baser, M. E. (2006) 'Malignant transformation and new primary tumours after therapeutic radiation for benign disease: substantial risks in certain tumour prone syndromes'. *J Med Genet*, 43 (4), pp. 289-294.

Evans, D. G., Huson, S. M., Donnai, D., Neary, W., Blair, V., Newton, V. & Harris, R. (1992a) 'A clinical study of type 2 neurofibromatosis'. *Q J Med*, 84 (304), pp. 603-618.

Evans, D. G., Huson, S. M., Donnai, D., Neary, W., Blair, V., Teare, D., Newton, V., Strachan, T., Ramsden, R. & Harris, R. (1992b) 'A genetic study of type 2 neurofibromatosis in the United Kingdom. I. Prevalence, mutation rate, fitness, and confirmation of maternal transmission effect on severity'. *J Med Genet*, 29 (12), pp. 841-846.

Evans, D. G., Moran, A., King, A., Saeed, S., Gurusinghe, N. & Ramsden, R. (2005) 'Incidence of vestibular schwannoma and neurofibromatosis 2 in the North West of England over a 10-year period: higher incidence than previously thought'. *Otol Neurotol*, 26 (1), pp. 93-97.

Evans, D. G., Ramsden, R. T., Shenton, A., Gokhale, C., Bowers, N. L., Huson, S. M., Pichert, G. & Wallace, A. (2007) 'Mosaicism in neurofibromatosis type 2: an update of risk based on uni/bilaterality of vestibular schwannoma at presentation and sensitive mutation analysis including multiple ligation-dependent probe amplification'. *J Med Genet*, 44 (7), pp. 424-428.

Evans, D. G., Trueman, L., Wallace, A., Collins, S. & Strachan, T. (1998) 'Genotype/phenotype correlations in type 2 neurofibromatosis (NF2): evidence for more severe disease associated with truncating mutations'. *J Med Genet*, 35 (6), pp. 450-455.

Fan, R., Kim, N. G. & Gumbiner, B. M. (2013) 'Regulation of Hippo pathway by mitogenic growth factors via phosphoinositide 3-kinase and phosphoinositide-dependent kinase-1'. *Proc Natl Acad Sci U S A*, 110 (7), pp. 2569-2574.

Feiling, A. & Ward, E. (1920) 'A FAMILIAL FORM OF ACOUSTIC TUMOUR'. *Br Med J*, 1 (3093), pp. 496-497.

Feng, J., Yang, H., Zhang, Y., Wei, H., Zhu, Z., Zhu, B., Yang, M., Cao, W., Wang, L. & Wu, Z. (2017) 'Tumor cell-derived lactate induces TAZ-dependent upregulation of PD-L1 through GPR81 in human lung cancer cells'. *Oncogene*, 36 (42), pp. 5829-5839.

Feng, X., Degese, M. S., Iglesias-Bartolome, R., Vaque, J. P., Molinolo, A. A., Rodrigues, M., Zaidi, M. R., Ksander, B. R., Merlino, G., Sodhi, A., Chen, Q. & Gutkind, J. S. (2014) 'Hippo-independent

activation of YAP by the GNAQ uveal melanoma oncogene through a trio-regulated rho GTPase signaling circuitry'. *Cancer Cell*, 25 (6), pp. 831-845.

Feng, Y., Liang, Y., Zhu, X., Wang, M., Gui, Y., Lu, Q., Gu, M., Xue, X., Sun, X., He, W., Yang, J., Johnson, R. L. & Dai, C. (2018) 'The signaling protein Wnt5a promotes TGFβ1-mediated macrophage polarization and kidney fibrosis by inducing the transcriptional regulators Yap/Taz'. *J Biol Chem*, 293 (50), pp. 19290-19302.

Fernandez-Valle, C., Tang, Y., Ricard, J., Rodenas-Ruano, A., Taylor, A., Hackler, E., Biggerstaff, J. & Iacovelli, J. (2002) 'Paxillin binds schwannomin and regulates its density-dependent localization and effect on cell morphology'. *Nat Genet*, 31 (4), pp. 354-362.

Fernandez, L. A., Northcott, P. A., Dalton, J., Fraga, C., Ellison, D., Angers, S., Taylor, M. D. & Kenney, A. M. (2009) 'YAP1 is amplified and up-regulated in hedgehog-associated medulloblastomas and mediates Sonic hedgehog-driven neural precursor proliferation'. *Genes Dev*, 23 (23), pp. 2729-2741.

Ferrante, L., Mastronardi, L., Celli, P., Lunardi, P., Acqui, M. & Fortuna, A. (1992) 'Intramedullary spinal cord ependymomas--a study of 45 cases with long-term follow-up'. *Acta Neurochir (Wien)*, 119 (1-4), pp. 74-79.

Fex Svenningsen, A., Colman, D. R. & Pedraza, L. (2004) 'Satellite cells of dorsal root ganglia are multipotential glial precursors'. *Neuron Glia Biol*, 1 (1), pp. 85-93.

Figeac, N., Mohamed, A. D., Sun, C., Schönfelder, M., Matallanas, D., Garcia-Munoz, A., Missiaglia, E., Collie-Duguid, E., De Mello, V., Pobbati, A. V., Pruller, J., Jaka, O., Harridge, S. D. R., Hong, W., Shipley, J., Vargesson, N., Zammit, P. S. & Wackerhage, H. (2019) 'VGLL3 operates via TEAD1, TEAD3 and TEAD4 to influence myogenesis in skeletal muscle'. *J Cell Sci*, 132 (13),

Filler, A. G., Maravilla, K. R. & Tsuruda, J. S. (2004) 'MR neurography and muscle MR imaging for image diagnosis of disorders affecting the peripheral nerves and musculature'. *Neurol Clin*, 22 (3), pp. 643-682, vi-vii.

Fisher, L. M., Doherty, J. K., Lev, M. H. & Slattery, W. H., 3rd (2007) 'Distribution of nonvestibular cranial nerve schwannomas in neurofibromatosis 2'. *Otol Neurotol*, 28 (8), pp. 1083-1090.

Flaiz, C., Ammoun, S., Biebl, A. & Hanemann, C. O. (2009) 'Altered adhesive structures and their relation to RhoGTPase activation in merlin-deficient Schwannoma'. *Brain Pathol*, 19 (1), pp. 27-38.

Flaiz, C., Utermark, T., Parkinson, D. B., Poetsch, A. & Hanemann, C. O. (2008) 'Impaired intercellular adhesion and immature adherens junctions in merlin-deficient human primary schwannoma cells'. *Glia*, 56 (5), pp. 506-515.

Fletcher, G. C., Elbediwy, A., Khanal, I., Ribeiro, P. S., Tapon, N. & Thompson, B. J. (2015) 'The Spectrin cytoskeleton regulates the Hippo signalling pathway'. *Embo j*, 34 (7), pp. 940-954.

Fleury-Feith, J., Lecomte, C., Renier, A., Matrat, M., Kheuang, L., Abramowski, V., Levy, F., Janin, A., Giovannini, M. & Jaurand, M. C. (2003) 'Hemizygosity of Nf2 is associated with increased susceptibility to asbestos-induced peritoneal tumours'. *Oncogene*, 22 (24), pp. 3799-3805.

Fogg, V. C., Liu, C. J. & Margolis, B. (2005) 'Multiple regions of Crumbs3 are required for tight junction formation in MCF10A cells'. *J Cell Sci*, 118 (Pt 13), pp. 2859-2869.

Forde, C., King, A. T., Rutherford, S. A., Hammerbeck-Ward, C., Lloyd, S. K., Freeman, S. R., Pathmanaban, O. N., Stapleton, E., Thomas, O. M., Laitt, R. D., Stivaros, S., Kilday, J. P., Vassallo, G., McBain, C., Kerrigan, S., Smith, M. J., McCabe, M. G., Harkness, E. F. & Evans, D. G. (2021) 'Disease course of neurofibromatosis type 2: a 30-year follow-up study of 353 patients seen at a single institution'. *Neuro Oncol*, 23 (7), pp. 1113-1124.

Franklin, R. A., Liao, W., Sarkar, A., Kim, M. V., Bivona, M. R., Liu, K., Pamer, E. G. & Li, M. O. (2014) 'The cellular and molecular origin of tumor-associated macrophages'. *Science*, 344 (6186), pp. 921-925.

Friedrich, S., Schwabe, K., Klein, R., Krusche, C. A., Krauss, J. K. & Nakamura, M. (2012) 'Comparative morphological and immunohistochemical study of human meningioma after intracranial transplantation into nude mice'. *J Neurosci Methods*, 205 (1), pp. 1-9.

Galli, G. G., Carrara, M., Yuan, W. C., Valdes-Quezada, C., Gurung, B., Pepe-Mooney, B., Zhang, T., Geeven, G., Gray, N. S., de Laat, W., Calogero, R. A. & Camargo, F. D. (2015) 'YAP Drives Growth by Controlling Transcriptional Pause Release from Dynamic Enhancers'. *Mol Cell*, 60 (2), pp. 328-337.

Ganem, N. J., Cornils, H., Chiu, S. Y., O'Rourke, K. P., Arnaud, J., Yimlamai, D., Théry, M., Camargo, F. D. & Pellman, D. (2014) 'Cytokinesis failure triggers hippo tumor suppressor pathway activation'. *Cell*, 158 (4), pp. 833-848.

Gao, T., Zhou, D., Yang, C., Singh, T., Penzo-Méndez, A., Maddipati, R., Tzatsos, A., Bardeesy, N., Avruch, J. & Stanger, B. Z. (2013) 'Hippo signaling regulates differentiation and maintenance in the exocrine pancreas'. *Gastroenterology*, 144 (7), pp. 1543-1553, 1553.e1541.

Gao, X., Zhang, L., Jia, Q., Tang, L., Guo, W., Wang, T., Wu, Z., Zhou, W., Li, Z. & Xiao, J. (2020) 'Whole Genome Sequencing Identifies Key Genes in Spinal Schwannoma'. *Front Genet*, 11 pp. 507816.

Garcia, C. & Gutmann, D. H. (2014) 'Nf2/Merlin controls spinal cord neural progenitor function in a Rac1/ErbB2-dependent manner'. *PLoS One*, 9 (5), pp. e97320.

Gardner, W. & FRAZIER, C. H. (1930) 'Bilateral acoustic neurofibromas: a clinical study and field survey of a family of five generations with bilateral deafness in thirty-eight members'. *Archives of Neurology & Psychiatry*, 23 (2), pp. 266-302.

Gehlhausen, J. R., Park, S. J., Hickox, A. E., Shew, M., Staser, K., Rhodes, S. D., Menon, K., Lajiness, J. D., Mwanthi, M., Yang, X., Yuan, J., Territo, P., Hutchins, G., Nalepa, G., Yang, F. C., Conway, S. J., Heinz, M. G., Stemmer-Rachamimov, A., Yates, C. W. & Wade Clapp, D. (2015) 'A murine model of neurofibromatosis type 2 that accurately phenocopies human schwannoma formation'. *Hum Mol Genet*, 24 (1), pp. 1-8.

Geissler, K. J., Jung, M. J., Riecken, L. B., Sperka, T., Cui, Y., Schacke, S., Merkel, U., Markwart, R., Rubio, I., Than, M. E., Breithaupt, C., Peuker, S., Seifert, R., Kaupp, U. B., Herrlich, P. & Morrison, H. (2013) 'Regulation of Son of sevenless by the membrane-actin linker protein ezrin'. *Proc Natl Acad Sci U S A*, 110 (51), pp. 20587-20592.

Genevet, A., Wehr, M. C., Brain, R., Thompson, B. J. & Tapon, N. (2010) 'Kibra is a regulator of the Salvador/Warts/Hippo signaling network'. *Dev Cell*, 18 (2), pp. 300-308.

Geng, J., Sun, X., Wang, P., Zhang, S., Wang, X., Wu, H., Hong, L., Xie, C., Li, X., Zhao, H., Liu, Q., Jiang, M., Chen, Q., Zhang, J., Li, Y., Song, S., Wang, H. R., Zhou, R., Johnson, R. L., Chien, K. Y., Lin, S. C., Han, J., Avruch, J., Chen, L. & Zhou, D. (2015) 'Kinases Mst1 and Mst2 positively regulate phagocytic induction of reactive oxygen species and bactericidal activity'. *Nat Immunol*, 16 (11), pp. 1142-1152.

George, D., Ahrens, P. & Lambert, S. (2018) 'Satellite glial cells represent a population of developmentally arrested Schwann cells'. *Glia*, 66 (7), pp. 1496-1506.

George, N. M., Day, C. E., Boerner, B. P., Johnson, R. L. & Sarvetnick, N. E. (2012) 'Hippo signaling regulates pancreas development through inactivation of Yap'. *Mol Cell Biol*, 32 (24), pp. 5116-5128.

Gibault, F., Bailly, F., Corvaisier, M., Coevoet, M., Huet, G., Melnyk, P. & Cotelle, P. (2017) 'Molecular Features of the YAP Inhibitor Verteporfin: Synthesis of Hexasubstituted Dipyrrins as Potential Inhibitors of YAP/TAZ, the Downstream Effectors of the Hippo Pathway'. *ChemMedChem*, 12 (12), pp. 954-961.

Gijtenbeek, J. M., Gabreëls-Festen, A. A., Lammens, M., Zwarts, M. J. & van Engelen, B. G. (2001) 'Mononeuropathy multiplex as the initial manifestation of neurofibromatosis type 2'. *Neurology*, 56 (12), pp. 1766-1768.

Gilbert, M. R., Ruda, R. & Soffietti, R. (2010) 'Ependymomas in adults'. *Curr Neurol Neurosci Rep*, 10 (3), pp. 240-247.

Giovannini, M., Bonne, N. X., Vitte, J., Chareyre, F., Tanaka, K., Adams, R., Fisher, L. M., Valeyrie-Allanore, L., Wolkenstein, P., Goutagny, S. & Kalamarides, M. (2014) 'mTORC1 inhibition delays growth of neurofibromatosis type 2 schwannoma'. *Neuro Oncol*, 16 (4), pp. 493-504.

Giovannini, M., Robanus-Maandag, E., Niwa-Kawakita, M., van der Valk, M., Woodruff, J. M., Goutebroze, L., Merel, P., Berns, A. & Thomas, G. (1999) 'Schwann cell hyperplasia and tumors in transgenic mice expressing a naturally occurring mutant NF2 protein'. *Genes Dev*, 13 (8), pp. 978-986.

Giovannini, M., Robanus-Maandag, E., van der Valk, M., Niwa-Kawakita, M., Abramowski, V., Goutebroze, L., Woodruff, J. M., Berns, A. & Thomas, G. (2000) 'Conditional biallelic Nf2 mutation in the mouse promotes manifestations of human neurofibromatosis type 2'. *Genes Dev*, 14 (13), pp. 1617-1630.

Gladden, A. B., Hebert, A. M., Schneeberger, E. E. & McClatchey, A. I. (2010) 'The NF2 tumor suppressor, Merlin, regulates epidermal development through the establishment of a junctional polarity complex'. *Dev Cell*, 19 (5), pp. 727-739.

Gogineni, V. R., Nalla, A. K., Gupta, R., Dinh, D. H., Klopfenstein, J. D. & Rao, J. S. (2011) 'Chk2-mediated G2/M cell cycle arrest maintains radiation resistance in malignant meningioma cells'. *Cancer Lett*, 313 (1), pp. 64-75.

Gonzalez-Agosti, C., Wiederhold, T., Herndon, M. E., Gusella, J. & Ramesh, V. (1999) 'Interdomain interaction of merlin isoforms and its influence on intermolecular binding to NHE-RF'. *J Biol Chem*, 274 (48), pp. 34438-34442.

Gonzalez-Gomez, P., Bello, M. J., Alonso, M. E., Lomas, J., Arjona, D., Campos, J. M., Vaquero, J., Isla, A., Lassaletta, L., Gutierrez, M., Sarasa, J. L. & Rey, J. A. (2003) 'CpG island methylation in sporadic and neurofibromatis type 2-associated schwannomas'. *Clin Cancer Res*, 9 (15), pp. 5601-5606.

Goudreault, M., D'Ambrosio, L. M., Kean, M. J., Mullin, M. J., Larsen, B. G., Sanchez, A., Chaudhry, S., Chen, G. I., Sicheri, F., Nesvizhskii, A. I., Aebersold, R., Raught, B. & Gingras, A. C. (2009) 'A PP2A phosphatase high density interaction network identifies a novel striatin-interacting phosphatase and kinase complex linked to the cerebral cavernous malformation 3 (CCM3) protein'. *Mol Cell Proteomics*, 8 (1), pp. 157-171.

Goulev, Y., Fauny, J. D., Gonzalez-Marti, B., Flagiello, D., Silber, J. & Zider, A. (2008) 'SCALLOPED interacts with YORKIE, the nuclear effector of the hippo tumor-suppressor pathway in Drosophila'. *Curr Biol*, 18 (6), pp. 435-441.

Goutagny, S., Nault, J. C., Mallet, M., Henin, D., Rossi, J. Z. & Kalamarides, M. (2014) 'High incidence of activating TERT promoter mutations in meningiomas undergoing malignant progression'. *Brain Pathol*, 24 (2), pp. 184-189.

Goutagny, S., Raymond, E., Esposito-Farese, M., Trunet, S., Mawrin, C., Bernardeschi, D., Larroque, B., Sterkers, O., Giovannini, M. & Kalamarides, M. (2015) 'Phase II study of mTORC1 inhibition by everolimus in neurofibromatosis type 2 patients with growing vestibular schwannomas'. *J Neurooncol*, 122 (2), pp. 313-320.

Graillon, T., Sanson, M., Campello, C., Idbaih, A., Peyre, M., Peyrière, H., Basset, N., Autran, D., Roche, C., Kalamarides, M., Roche, P. H., Fuentes, S., Tabouret, E., Barrie, M., Cohen, A., Honoré, S., Boucekine, M., Baumstarck, K., Figarella-Branger, D., Barlier, A., Dufour, H. & Chinot, O. L. (2020) 'Everolimus and Octreotide for Patients with Recurrent Meningioma: Results from the Phase II CEVOREM Trial'. *Clin Cancer Res*, 26 (3), pp. 552-557.

Griffin, J. W., George, R. & Ho, T. (1993) 'Macrophage systems in peripheral nerves. A review'. *J Neuropathol Exp Neurol*, 52 (6), pp. 553-560.

Grönholm, M., Sainio, M., Zhao, F., Heiska, L., Vaheri, A. & Carpén, O. (1999) 'Homotypic and heterotypic interaction of the neurofibromatosis 2 tumor suppressor protein merlin and the ERM protein ezrin'. *J Cell Sci*, 112 (Pt 6) pp. 895-904.

Guo, P., Lee, C. H., Lei, H., Zheng, Y., Pulgar Prieto, K. D. & Pan, D. (2019) 'Nerfin-1 represses transcriptional output of Hippo signaling in cell competition'. *Elife*, 8

Guo, X., Zhao, Y., Yan, H., Yang, Y., Shen, S., Dai, X., Ji, X., Ji, F., Gong, X. G., Li, L., Bai, X., Feng, X. H., Liang, T., Ji, J., Chen, L., Wang, H. & Zhao, B. (2017) 'Single tumor-initiating cells evade immune clearance by recruiting type II macrophages'. *Genes Dev*, 31 (3), pp. 247-259.

Gupta, M., Kogut, P., Davis, F. J., Belaguli, N. S., Schwartz, R. J. & Gupta, M. P. (2001) 'Physical interaction between the MADS box of serum response factor and the TEA/ATTS DNA-binding domain of transcription enhancer factor-1'. *J Biol Chem*, 276 (13), pp. 10413-10422.

Gupta, M. P., Kogut, P. & Gupta, M. (2000) 'Protein kinase-A dependent phosphorylation of transcription enhancer factor-1 represses its DNA-binding activity but enhances its gene activation ability'. *Nucleic Acids Res*, 28 (16), pp. 3168-3177.

Gutmann, D. H., Giordano, M. J., Fishback, A. S. & Guha, A. (1997) 'Loss of merlin expression in sporadic meningiomas, ependymomas and schwannomas'. *Neurology*, 49 (1), pp. 267-270.

Haemmerle, M., Taylor, M. L., Gutschner, T., Pradeep, S., Cho, M. S., Sheng, J., Lyons, Y. M., Nagaraja, A. S., Dood, R. L., Wen, Y., Mangala, L. S., Hansen, J. M., Rupaimoole, R., Gharpure, K. M., Rodriguez-Aguayo, C., Yim, S. Y., Lee, J. S., Ivan, C., Hu, W., Lopez-Berestein, G., Wong, S. T., Karlan, B. Y., Levine, D. A., Liu, J., Afshar-Kharghan, V. & Sood, A. K. (2017) 'Platelets reduce anoikis and promote metastasis by activating YAP1 signaling'. *Nat Commun*, 8 (1), pp. 310.

Hagel, C., Lindenau, M., Lamszus, K., Kluwe, L., Stavrou, D. & Mautner, V. F. (2002) 'Polyneuropathy in neurofibromatosis 2: clinical findings, molecular genetics and neuropathological alterations in sural nerve biopsy specimens'. *Acta Neuropathol*, 104 (2), pp. 179-187.

Hagenbeek, T. J., Webster, J. D., Kljavin, N. M., Chang, M. T., Pham, T., Lee, H. J., Klijn, C., Cai, A. G., Totpal, K., Ravishankar, B., Yang, N., Lee, D. H., Walsh, K. B., Hatzivassiliou, G., de la Cruz, C. C., Gould, S. E., Wu, X., Lee, W. P., Yang, S., Zhang, Z., Gu, Q., Ji, Q., Jackson, E. L., Lim, D. S. & Dey, A. (2018) 'The Hippo pathway effector TAZ induces TEAD-dependent liver inflammation and tumors'. *Sci Signal*, 11 (547),

Halliday, D., Emmanouil, B., Pretorius, P., MacKeith, S., Painter, S., Tomkins, H., Evans, D. G. & Parry, A. (2017) 'Genetic Severity Score predicts clinical phenotype in NF2'. *J Med Genet*, 54 (10), pp. 657-664.

Hamaratoglu, F., Willecke, M., Kango-Singh, M., Nolo, R., Hyun, E., Tao, C., Jafar-Nejad, H. & Halder, G. (2006) 'The tumour-suppressor genes NF2/Merlin and Expanded act through Hippo signalling to regulate cell proliferation and apoptosis'. *Nat Cell Biol*, 8 (1), pp. 27-36.

Han, J., Daniel, J. C. & Pappas, G. D. (1996) 'Expression of type VI collagen in psammoma bodies: immunofluorescence studies on two fresh human meningiomas'. *Acta Cytol*, 40 (2), pp. 177-181.

Hanahan, D. & Weinberg, R. A. (2000) 'The hallmarks of cancer'. *Cell*, 100 (1), pp. 57-70.

Hanemann, C. O., Diebold, R. & Kaufmann, D. (2007) 'Role of NF2 haploinsufficiency in NF2-associated polyneuropathy'. *Brain Pathol*, 17 (4), pp. 371-376.

Hansen, C. G., Ng, Y. L., Lam, W. L., Plouffe, S. W. & Guan, K. L. (2015) 'The Hippo pathway effectors YAP and TAZ promote cell growth by modulating amino acid signaling to mTORC1'. *Cell Res*, 25 (12), pp. 1299-1313.

Hansen, M. R., Roehm, P. C., Chatterjee, P. & Green, S. H. (2006) 'Constitutive neuregulin-1/ErbB signaling contributes to human vestibular schwannoma proliferation'. *Glia*, 53 (6), pp. 593-600.

Hartmann, C., Sieberns, J., Gehlhaar, C., Simon, M., Paulus, W. & von Deimling, A. (2006) 'NF2 mutations in secretory and other rare variants of meningiomas'. *Brain Pathol*, 16 (1), pp. 15-19.

Harvey, K. F., Pfleger, C. M. & Hariharan, I. K. (2003) 'The Drosophila Mst ortholog, hippo, restricts growth and cell proliferation and promotes apoptosis'. *Cell*, 114 (4), pp. 457-467.

Hawley, E., Gehlhausen, J., Karchugina, S., Chow, H. Y., Araiza-Olivera, D., Radu, M., Smith, A., Burks, C., Jiang, L., Li, X., Bessler, W., Masters, A., Edwards, D., Burgin, C., Jones, D., Yates, C., Clapp, D. W., Chernoff, J. & Park, S. J. (2021) 'PAK1 inhibition reduces tumor size and extends the lifespan of mice in a genetically engineered mouse model of Neurofibromatosis Type 2 (NF2)'. *Hum Mol Genet*, 30 (17), pp. 1607-1617.

He, C., Mao, D., Hua, G., Lv, X., Chen, X., Angeletti, P. C., Dong, J., Remmenga, S. W., Rodabaugh, K. J., Zhou, J., Lambert, P. F., Yang, P., Davis, J. S. & Wang, C. (2015) 'The Hippo/YAP pathway interacts with EGFR signaling and HPV oncoproteins to regulate cervical cancer progression'. *EMBO Mol Med*, 7 (11), pp. 1426-1449.

Heallen, T., Zhang, M., Wang, J., Bonilla-Claudio, M., Klysik, E., Johnson, R. L. & Martin, J. F. (2011) 'Hippo pathway inhibits Wnt signaling to restrain cardiomyocyte proliferation and heart size'. *Science*, 332 (6028), pp. 458-461.

Health, N. I. o. (1988) 'National Institutes of health consensus development conference statement: neurofibromatosis'. *Neurofibromatosis*, 1 pp. 172-178.

Hennigan, R. F., Foster, L. A., Chaiken, M. F., Mani, T., Gomes, M. M., Herr, A. B. & Ip, W. (2010) 'Fluorescence resonance energy transfer analysis of merlin conformational changes'. *Mol Cell Biol*, 30 (1), pp. 54-67.

Hergovich, A. (2016) 'The Roles of NDR Protein Kinases in Hippo Signalling'. *Genes (Basel)*, 7 (5),

Hermann, A., Wennmann, D. O., Gromnitza, S., Edeling, M., Van Marck, V., Sudol, M., Schaefer, L., Duning, K., Weide, T., Pavenstädt, H. & Kremerskothen, J. (2018) 'WW and C2 domain-containing proteins regulate hepatic cell differentiation and tumorigenesis through the hippo signaling pathway'. *Hepatology*, 67 (4), pp. 1546-1559.

Herrlich, P., Morrison, H., Sleeman, J., Orian-Rousseau, V., König, H., Weg-Remers, S. & Ponta, H. (2000) 'CD44 acts both as a growth- and invasiveness-promoting molecule and as a tumor-suppressing cofactor'. *Ann N Y Acad Sci*, 910 pp. 106-118; discussion 118-120.

Hiemer, S. E., Szymaniak, A. D. & Varelas, X. (2014) 'The transcriptional regulators TAZ and YAP direct transforming growth factor β-induced tumorigenic phenotypes in breast cancer cells'. *J Biol Chem*, 289 (19), pp. 13461-13474.

Hilton, D. A., Ristic, N. & Hanemann, C. O. (2009) 'Activation of ERK, AKT and JNK signalling pathways in human schwannomas in situ'. *Histopathology*, 55 (6), pp. 744-749.

Holden, J. K., Crawford, J. J., Noland, C. L., Schmidt, S., Zbieg, J. R., Lacap, J. A., Zang, R., Miller, G. M., Zhang, Y., Beroza, P., Reja, R., Lee, W., Tom, J. Y. K., Fong, R., Steffek, M., Clausen, S., Hagenbeek, T. J., Hu, T., Zhou, Z., Shen, H. C. & Cunningham, C. N. (2020) 'Small Molecule Dysregulation of TEAD Lipidation Induces a Dominant-Negative Inhibition of Hippo Pathway Signaling'. *Cell Rep*, 31 (12), pp. 107809.

Holden, J. K. & Cunningham, C. N. (2018) 'Targeting the Hippo Pathway and Cancer through the TEAD Family of Transcription Factors'. *Cancers (Basel)*, 10 (3),

Holmgaard, R. B., Zamarin, D., Lesokhin, A., Merghoub, T. & Wolchok, J. D. (2016) 'Targeting myeloid-derived suppressor cells with colony stimulating factor-1 receptor blockade can reverse immune resistance to immunotherapy in indoleamine 2,3-dioxygenase-expressing tumors'. *EBioMedicine*, 6 pp. 50-58.

Honda, M., Hidaka, K., Fukada, S. I., Sugawa, R., Shirai, M., Ikawa, M. & Morisaki, T. (2017) 'Vestigial-like 2 contributes to normal muscle fiber type distribution in mice'. *Sci Rep*, 7 (1), pp. 7168.

Hong, A. W., Meng, Z., Yuan, H. X., Plouffe, S. W., Moon, S., Kim, W., Jho, E. H. & Guan, K. L. (2017) 'Osmotic stress-induced phosphorylation by NLK at Ser128 activates YAP'. *EMBO Rep*, 18 (1), pp. 72-86.

Hong, J. H., Hwang, E. S., McManus, M. T., Amsterdam, A., Tian, Y., Kalmukova, R., Mueller, E., Benjamin, T., Spiegelman, B. M., Sharp, P. A., Hopkins, N. & Yaffe, M. B. (2005) 'TAZ, a transcriptional modulator of mesenchymal stem cell differentiation'. *Science*, 309 (5737), pp. 1074-1078.

Hoshimaru, M., Koyama, T., Hashimoto, N. & Kikuchi, H. (1999) 'Results of microsurgical treatment for intramedullary spinal cord ependymomas: analysis of 36 cases'. *Neurosurgery*, 44 (2), pp. 264-269.

Houshmandi, S. S., Emnett, R. J., Giovannini, M. & Gutmann, D. H. (2009) 'The neurofibromatosis 2 protein, merlin, regulates glial cell growth in an ErbB2- and Src-dependent manner'. *Mol Cell Biol*, 29 (6), pp. 1472-1486.

Hu, C., Yu, M., Li, C., Wang, Y., Li, X., Ulrich, B., Su, R., Dong, L., Weng, H., Huang, H., Jiang, X., Chen, J. & Jin, J. (2020) 'miR-550-1 functions as a tumor suppressor in acute myeloid leukemia via the hippo signaling pathway'. *Int J Biol Sci*, 16 (15), pp. 2853-2867.

Huang, H. Y., Park, N., Erlandson, R. A. & Antonescu, C. R. (2004) 'Immunohistochemical and ultrastructural comparative study of external lamina structure in 31 cases of cellular, classical, and melanotic schwannomas'. *Appl Immunohistochem Mol Morphol*, 12 (1), pp. 50-58.

Huang, V., Bergner, A. L., Halpin, C., Merker, V. L., Sheridan, M. R., Widemann, B. C., Blakeley, J. O. & Plotkin, S. R. (2018) 'Improvement in Patient-reported Hearing After Treatment With Bevacizumab in People With Neurofibromatosis Type 2'. *Otol Neurotol*, 39 (5), pp. 632-638.

Huang, Y. J., Yang, C. K., Wei, P. L., Huynh, T. T., Whang-Peng, J., Meng, T. C., Hsiao, M., Tzeng, Y. M., Wu, A. T. & Yen, Y. (2017) 'Ovatodiolide suppresses colon tumorigenesis and prevents polarization of M2 tumor-associated macrophages through YAP oncogenic pathways'. *J Hematol Oncol*, 10 (1), pp. 60.

Huh, H. D., Kim, D. H., Jeong, H. S. & Park, H. W. (2019) 'Regulation of TEAD Transcription Factors in Cancer Biology'. *Cells*, 8 (6),

Hulsebos, T. J., Plomp, A. S., Wolterman, R. A., Robanus-Maandag, E. C., Baas, F. & Wesseling, P. (2007) 'Germline mutation of INI1/SMARCB1 in familial schwannomatosis'. *Am J Hum Genet*, 80 (4), pp. 805-810.

Iglesias-Bartolome, R., Torres, D., Marone, R., Feng, X., Martin, D., Simaan, M., Chen, M., Weinstein, L. S., Taylor, S. S., Molinolo, A. A. & Gutkind, J. S. (2015) 'Inactivation of a Gα(s)-PKA tumour suppressor pathway in skin stem cells initiates basal-cell carcinogenesis'. *Nat Cell Biol*, 17 (6), pp. 793-803.

Ivashkiv, L. B. (2013) 'Epigenetic regulation of macrophage polarization and function'. *Trends Immunol*, 34 (5), pp. 216-223.

Iwami, K., Natsume, A., Ohno, M., Ikeda, H., Mineno, J., Nukaya, I., Okamoto, S., Fujiwara, H., Yasukawa, M., Shiku, H. & Wakabayashi, T. (2013) 'Adoptive transfer of genetically modified Wilms' tumor 1-specific T cells in a novel malignant skull base meningioma model'. *Neuro Oncol*, 15 (6), pp. 747-758.

Iwata, A., Kunimoto, M. & Inoue, K. (1998) 'Schwann cell proliferation as the cause of peripheral neuropathy in neurofibromatosis-2'. *J Neurol Sci*, 156 (2), pp. 201-204.

Jablonski, K. A., Amici, S. A., Webb, L. M., Ruiz-Rosado Jde, D., Popovich, P. G., Partida-Sanchez, S. & Guerau-de-Arellano, M. (2015) 'Novel Markers to Delineate Murine M1 and M2 Macrophages'. *PLoS One*, 10 (12), pp. e0145342.

Jacob, A., Lee, T. X., Neff, B. A., Miller, S., Welling, B. & Chang, L. S. (2008) 'Phosphatidylinositol 3-kinase/AKT pathway activation in human vestibular schwannoma'. *Otol Neurotol*, 29 (1), pp. 58-68.

Jacob, A., Oblinger, J., Bush, M. L., Brendel, V., Santarelli, G., Chaudhury, A. R., Kulp, S., La Perle, K. M., Chen, C. S., Chang, L. S. & Welling, D. B. (2012) 'Preclinical validation of AR42, a novel histone deacetylase inhibitor, as treatment for vestibular schwannomas'. *Laryngoscope*, 122 (1), pp. 174-189.

Jacquemin, P., Hwang, J. J., Martial, J. A., Dollé, P. & Davidson, I. (1996) 'A novel family of developmentally regulated mammalian transcription factors containing the TEA/ATTS DNA binding domain'. *J Biol Chem*, 271 (36), pp. 21775-21785.

James, M. F., Han, S., Polizzano, C., Plotkin, S. R., Manning, B. D., Stemmer-Rachamimov, A. O., Gusella, J. F. & Ramesh, V. (2009) 'NF2/merlin is a novel negative regulator of mTOR complex 1, and activation of mTORC1 is associated with meningioma and schwannoma growth'. *Mol Cell Biol*, 29 (15), pp. 4250-4261.

James, M. F., Stivison, E., Beauchamp, R., Han, S., Li, H., Wallace, M. R., Gusella, J. F., Stemmer-Rachamimov, A. O. & Ramesh, V. (2012) 'Regulation of mTOR complex 2 signaling in neurofibromatosis 2-deficient target cell types'. *Mol Cancer Res*, 10 (5), pp. 649-659.

Janse van Rensburg, H. J., Azad, T., Ling, M., Hao, Y., Snetsinger, B., Khanal, P., Minassian, L. M., Graham, C. H., Rauh, M. J. & Yang, X. (2018) 'The Hippo Pathway Component TAZ Promotes Immune Evasion in Human Cancer through PD-L1'. *Cancer Res*, 78 (6), pp. 1457-1470.

Ji, H., Ramsey, M. R., Hayes, D. N., Fan, C., McNamara, K., Kozlowski, P., Torrice, C., Wu, M. C., Shimamura, T., Perera, S. A., Liang, M. C., Cai, D., Naumov, G. N., Bao, L., Contreras, C. M., Li, D., Chen, L., Krishnamurthy, J., Koivunen, J., Chirieac, L. R., Padera, R. F., Bronson, R. T., Lindeman, N. I., Christiani, D. C., Lin, X., Shapiro, G. I., Jänne, P. A., Johnson, B. E., Meyerson, M., Kwiatkowski, D. J., Castrillon, D. H., Bardeesy, N., Sharpless, N. E. & Wong, K. K. (2007) 'LKB1 modulates lung cancer differentiation and metastasis'. *Nature*, 448 (7155), pp. 807-810.

Ji, S., Liu, Q., Zhang, S., Chen, Q., Wang, C., Zhang, W., Xiao, C., Li, Y., Nian, C., Li, J., Li, J., Geng, J., Hong, L., Xie, C., He, Y., Chen, X., Li, X., Yin, Z. Y., You, H., Lin, K. H., Wu, Q., Yu, C., Johnson, R. L.,

Wang, L., Chen, L., Wang, F. & Zhou, D. (2019) 'FGF15 Activates Hippo Signaling to Suppress Bile Acid Metabolism and Liver Tumorigenesis'. *Dev Cell*, 48 (4), pp. 460-474.e469.

Jia, J., Zhang, W., Wang, B., Trinko, R. & Jiang, J. (2003) 'The Drosophila Ste20 family kinase dMST functions as a tumor suppressor by restricting cell proliferation and promoting apoptosis'. *Genes Dev*, 17 (20), pp. 2514-2519.

Jiang, S. W., Desai, D., Khan, S. & Eberhardt, N. L. (2000) 'Cooperative binding of TEF-1 to repeated GGAATG-related consensus elements with restricted spatial separation and orientation'. *DNA Cell Biol*, 19 (8), pp. 507-514.

Jiang, S. W., Dong, M., Trujillo, M. A., Miller, L. J. & Eberhardt, N. L. (2001) 'DNA binding of TEA/ATTS domain factors is regulated by protein kinase C phosphorylation in human choriocarcinoma cells'. *J Biol Chem*, 276 (26), pp. 23464-23470.

Jiao, S., Li, C., Hao, Q., Miao, H., Zhang, L., Li, L. & Zhou, Z. (2017) 'VGLL4 targets a TCF4-TEAD4 complex to coregulate Wnt and Hippo signalling in colorectal cancer'. *Nat Commun*, 8 pp. 14058.

Jiao, S., Wang, H., Shi, Z., Dong, A., Zhang, W., Song, X., He, F., Wang, Y., Zhang, Z., Wang, W., Wang, X., Guo, T., Li, P., Zhao, Y., Ji, H., Zhang, L. & Zhou, Z. (2014) 'A peptide mimicking VGLL4 function acts as a YAP antagonist therapy against gastric cancer'. *Cancer Cell*, 25 (2), pp. 166-180.

Jin, H., Sperka, T., Herrlich, P. & Morrison, H. (2006) 'Tumorigenic transformation by CPI-17 through inhibition of a merlin phosphatase'. *Nature*, 442 (7102), pp. 576-579.

Jin, X., Zhao, W., Zhou, P. & Niu, T. (2018) 'YAP knockdown inhibits proliferation and induces apoptosis of human prostate cancer DU145 cells'. *Mol Med Rep*, 17 (3), pp. 3783-3788.

Jinushi, M., Chiba, S., Yoshiyama, H., Masutomi, K., Kinoshita, I., Dosaka-Akita, H., Yagita, H., Takaoka, A. & Tahara, H. (2011) 'Tumor-associated macrophages regulate tumorigenicity and anticancer drug responses of cancer stem/initiating cells'. *Proc Natl Acad Sci U S A*, 108 (30), pp. 12425-12430.

Johnson, M. D., Okedli, E., Woodard, A., Toms, S. A. & Allen, G. S. (2002) 'Evidence for phosphatidylinositol 3-kinase-Akt-p7S6K pathway activation and transduction of mitogenic signals by platelet-derived growth factor in meningioma cells'. *J Neurosurg*, 97 (3), pp. 668-675.

Justice, R. W., Zilian, O., Woods, D. F., Noll, M. & Bryant, P. J. (1995) 'The Drosophila tumor suppressor gene warts encodes a homolog of human myotonic dystrophy kinase and is required for the control of cell shape and proliferation'. *Genes Dev*, 9 (5), pp. 534-546.

Kaan, H. Y. K., Sim, A. Y. L., Tan, S. K. J., Verma, C. & Song, H. (2017) 'Targeting YAP/TAZ-TEAD protein-protein interactions using fragment-based and computational modeling approaches'. *PLoS One*, 12 (6), pp. e0178381.

Kaempchen, K., Mielke, K., Utermark, T., Langmesser, S. & Hanemann, C. O. (2003) 'Upregulation of the Rac1/JNK signaling pathway in primary human schwannoma cells'. *Hum Mol Genet*, 12 (11), pp. 1211-1221.

Kalamarides, M., Niwa-Kawakita, M., Leblois, H., Abramowski, V., Perricaudet, M., Janin, A., Thomas, G., Gutmann, D. H. & Giovannini, M. (2002) 'Nf2 gene inactivation in arachnoidal cells is rate-limiting for meningioma development in the mouse'. *Genes Dev*, 16 (9), pp. 1060-1065.

Kalamarides, M., Stemmer-Rachamimov, A. O., Niwa-Kawakita, M., Chareyre, F., Taranchon, E., Han, Z. Y., Martinelli, C., Lusis, E. A., Hegedus, B., Gutmann, D. H. & Giovannini, M. (2011) 'Identification of a progenitor cell of origin capable of generating diverse meningioma histological subtypes'. *Oncogene*, 30 (20), pp. 2333-2344.

Kalamarides, M., Stemmer-Rachamimov, A. O., Takahashi, M., Han, Z. Y., Chareyre, F., Niwa-Kawakita, M., Black, P. M., Carroll, R. S. & Giovannini, M. (2008) 'Natural history of meningioma development in mice reveals: a synergy of Nf2 and p16(Ink4a) mutations'. *Brain Pathol*, 18 (1), pp. 62-70.

Kalinski, P. (2012) 'Regulation of immune responses by prostaglandin E2'. *J Immunol*, 188 (1), pp. 21-28.

Kanai, F., Marignani, P. A., Sarbassova, D., Yagi, R., Hall, R. A., Donowitz, M., Hisaminato, A., Fujiwara, T., Ito, Y., Cantley, L. C. & Yaffe, M. B. (2000) 'TAZ: a novel transcriptional co-activator regulated by interactions with 14-3-3 and PDZ domain proteins'. *Embo j*, 19 (24), pp. 6778-6791.

Kaneda, A., Seike, T., Danjo, T., Nakajima, T., Otsubo, N., Yamaguchi, D., Tsuji, Y., Hamaguchi, K., Yasunaga, M., Nishiya, Y., Suzuki, M., Saito, J. I., Yatsunami, R., Nakamura, S., Sekido, Y. & Mori, K. (2020) 'The novel potent TEAD inhibitor, K-975, inhibits YAP1/TAZ-TEAD protein-protein interactions and exerts an anti-tumor effect on malignant pleural mesothelioma'. *Am J Cancer Res*, 10 (12), pp. 4399-4415.

Kaneda, A., Seike, T., Uemori, T., Myojo, K., Aida, K., Danjo, T., Nakajima, T., Yamaguchi, D., Hamada, T. & Tsuji, Y. (2019) 'Discovery of a first-in-class TEAD inhibitor which directly inhibits YAP/TAZ-TEAD protein-protein interaction and shows a potent anti-tumor effect in malignant pleural mesothelioma'.[in AACR. (Accessed:Kaneda, A., Seike, T., Uemori, T., Myojo, K., Aida, K., Danjo, T., Nakajima, T., Yamaguchi, D., Hamada, T. & Tsuji, Y.

Kanter, W. R., Eldridge, R., Fabricant, R., Allen, J. C. & Koerber, T. (1980) 'Central neurofibromatosis with bilateral acoustic neuroma: genetic, clinical and biochemical distinctions from peripheral neurofibromatosis'. *Neurology*, 30 (8), pp. 851-859.

Kapoor, A., Yao, W., Ying, H., Hua, S., Liewen, A., Wang, Q., Zhong, Y., Wu, C. J., Sadanandam, A., Hu, B., Chang, Q., Chu, G. C., Al-Khalil, R., Jiang, S., Xia, H., Fletcher-Sananikone, E., Lim, C., Horwitz, G. I., Viale, A., Pettazzoni, P., Sanchez, N., Wang, H., Protopopov, A., Zhang, J., Heffernan, T., Johnson, R.

L., Chin, L., Wang, Y. A., Draetta, G. & DePinho, R. A. (2014) 'Yap1 activation enables bypass of oncogenic Kras addiction in pancreatic cancer'. *Cell*, 158 (1), pp. 185-197.

Karajannis, M. A., Legault, G., Hagiwara, M., Ballas, M. S., Brown, K., Nusbaum, A. O., Hochman, T., Goldberg, J. D., Koch, K. M., Golfinos, J. G., Roland, J. T. & Allen, J. C. (2012) 'Phase II trial of lapatinib in adult and pediatric patients with neurofibromatosis type 2 and progressive vestibular schwannomas'. *Neuro Oncol*, 14 (9), pp. 1163-1170.

Karajannis, M. A., Legault, G., Hagiwara, M., Giancotti, F. G., Filatov, A., Derman, A., Hochman, T., Goldberg, J. D., Vega, E., Wisoff, J. H., Golfinos, J. G., Merkelson, A., Roland, J. T. & Allen, J. C. (2014) 'Phase II study of everolimus in children and adults with neurofibromatosis type 2 and progressive vestibular schwannomas'. *Neuro Oncol*, 16 (2), pp. 292-297.

Kawashima, M., Suzuki, S. O., Yamashima, T., Fukui, M. & Iwaki, T. (2001) 'Prostaglandin D synthase (beta-trace) in meningeal hemangiopericytoma'. *Mod Pathol*, 14 (3), pp. 197-201.

Keshet, R., Adler, J., Ricardo Lax, I., Shanzer, M., Porat, Z., Reuven, N. & Shaul, Y. (2015) 'c-Abl antagonizes the YAP oncogenic function'. *Cell Death Differ*, 22 (6), pp. 935-945.

Kessenbrock, K., Plaks, V. & Werb, Z. (2010) 'Matrix metalloproteinases: regulators of the tumor microenvironment'. *Cell*, 141 (1), pp. 52-67.

Kida, Y., Kobayashi, T., Tanaka, T. & Mori, Y. (2000) 'Radiosurgery for bilateral neurinomas associated with neurofibromatosis type 2'. *Surg Neurol*, 53 (4), pp. 383-389; discussion 389-390.

Kilpatrick, T. J., Hjorth, R. J. & Gonzales, M. F. (1992) 'A case of neurofibromatosis 2 presenting with a mononeuritis multiplex'. *J Neurol Neurosurg Psychiatry*, 55 (5), pp. 391-393.

Kim, K., Heo, K., Choi, J., Jackson, S., Kim, H., Xiong, Y. & An, W. (2012) 'Vpr-binding protein antagonizes p53-mediated transcription via direct interaction with H3 tail'. *Mol Cell Biol*, 32 (4), pp. 783-796.

Kim, M., Kim, M., Lee, S., Kuninaka, S., Saya, H., Lee, H., Lee, S. & Lim, D. S. (2013) 'cAMP/PKA signalling reinforces the LATS-YAP pathway to fully suppress YAP in response to actin cytoskeletal changes'. *Embo j*, 32 (11), pp. 1543-1555.

Kim, M., Kim, T., Johnson, R. L. & Lim, D. S. (2015) 'Transcriptional co-repressor function of the hippo pathway transducers YAP and TAZ'. *Cell Rep*, 11 (2), pp. 270-282.

Kim, M. H., Kim, C. G., Kim, S. K., Shin, S. J., Choe, E. A., Park, S. H., Shin, E. C. & Kim, J. (2018a) 'YAP-Induced PD-L1 Expression Drives Immune Evasion in BRAFi-Resistant Melanoma'. *Cancer Immunol Res*, 6 (3), pp. 255-266.

Kim, N. G. & Gumbiner, B. M. (2015) 'Adhesion to fibronectin regulates Hippo signaling via the FAK-Src-PI3K pathway'. *J Cell Biol*, 210 (3), pp. 503-515.

Kim, N. G. & Gumbiner, B. M. (2019) 'Cell contact and Nf2/Merlin-dependent regulation of TEAD palmitoylation and activity'. *Proc Natl Acad Sci U S A*, 116 (20), pp. 9877-9882.

Kim, N. G., Koh, E., Chen, X. & Gumbiner, B. M. (2011) 'E-cadherin mediates contact inhibition of proliferation through Hippo signaling-pathway components'. *Proc Natl Acad Sci U S A*, 108 (29), pp. 11930-11935.

Kim, T., Hwang, D., Lee, D., Kim, J. H., Kim, S. Y. & Lim, D. S. (2017) 'MRTF potentiates TEAD-YAP transcriptional activity causing metastasis'. *Embo j*, 36 (4), pp. 520-535.

Kim, W., Khan, S. K., Liu, Y., Xu, R., Park, O., He, Y., Cha, B., Gao, B. & Yang, Y. (2018b) 'Hepatic Hippo signaling inhibits protumoural microenvironment to suppress hepatocellular carcinoma'. *Gut*, 67 (9), pp. 1692-1703.

Kimura, Y., Koga, H., Araki, N., Mugita, N., Fujita, N., Takeshima, H., Nishi, T., Yamashima, T., Saido, T. C., Yamasaki, T., Moritake, K., Saya, H. & Nakao, M. (1998) 'The involvement of calpain-dependent proteolysis of the tumor suppressor NF2 (merlin) in schwannomas and meningiomas'. *Nat Med*, 4 (8), pp. 915-922.

King, A. T., Rutherford, S. A., Hammerbeck-Ward, C., Lloyd, S. K., Freeman, S. M., Pathmanaban, O. N., Rodriguez-Valero, M., Thomas, O. M., Laitt, R. D., Stivaros, S., Kellett, M. & Evans, D. G. (2018a) 'High-Grade Glioma is not a Feature of Neurofibromatosis Type 2 in the Unirradiated Patient'. *Neurosurgery*, 83 (2), pp. 193-196.

King, A. T., Rutherford, S. A., Hammerbeck-Ward, C., Lloyd, S. K., Freeman, S. R., Pathmanaban, O. N., Kellett, M., Obholzer, R., Afridi, S., Axon, P., Halliday, D., Parry, A., Thomas, O. M., Laitt, R. D., McCabe, M. G., Stivaros, S., Erridge, S. & Evans, D. G. (2018b) 'Malignant Peripheral Nerve Sheath Tumors are not a Feature of Neurofibromatosis Type 2 in the Unirradiated Patient'. *Neurosurgery*, 83 (1), pp. 38-42.

Kino, T., Takeshima, H., Nakao, M., Nishi, T., Yamamoto, K., Kimura, T., Saito, Y., Kochi, M., Kuratsu, J., Saya, H. & Ushio, Y. (2001) 'Identification of the cis-acting region in the NF2 gene promoter as a potential target for mutation and methylation-dependent silencing in schwannoma'. *Genes Cells*, 6 (5), pp. 441-454.

Kissil, J. L., Johnson, K. C., Eckman, M. S. & Jacks, T. (2002) 'Merlin phosphorylation by p21-activated kinase 2 and effects of phosphorylation on merlin localization'. *J Biol Chem*, 277 (12), pp. 10394-10399.

Kissil, J. L., Wilker, E. W., Johnson, K. C., Eckman, M. S., Yaffe, M. B. & Jacks, T. (2003) 'Merlin, the product of the Nf2 tumor suppressor gene, is an inhibitor of the p21-activated kinase, Pak1'. *Mol Cell*, 12 (4), pp. 841-849.

Klein, D., Patzkó, Á., Schreiber, D., van Hauwermeiren, A., Baier, M., Groh, J., West, B. L. & Martini, R. (2015) 'Targeting the colony stimulating factor 1 receptor alleviates two forms of Charcot-Marie-Tooth disease in mice'. *Brain*, 138 (Pt 11), pp. 3193-3205.

Kluwe, L. & Mautner, V. F. (1998) 'Mosaicism in sporadic neurofibromatosis 2 patients'. *Hum Mol Genet*, 7 (13), pp. 2051-2055.

Knight, J. F., Shepherd, C. J., Rizzo, S., Brewer, D., Jhavar, S., Dodson, A. R., Cooper, C. S., Eeles, R., Falconer, A., Kovacs, G., Garrett, M. D., Norman, A. R., Shipley, J. & Hudson, D. L. (2008) 'TEAD1 and c-Cbl are novel prostate basal cell markers that correlate with poor clinical outcome in prostate cancer'. *Br J Cancer*, 99 (11), pp. 1849-1858.

Knudson, A. G., Jr. (1971) 'Mutation and cancer: statistical study of retinoblastoma'. *Proc Natl Acad Sci U S A*, 68 (4), pp. 820-823.

Kondziolka, D., Levy, E. I., Niranjan, A., Flickinger, J. C. & Lunsford, L. D. (1999) 'Long-term outcomes after meningioma radiosurgery: physician and patient perspectives'. *J Neurosurg*, 91 (1), pp. 44-50.

Koontz, L. M., Liu-Chittenden, Y., Yin, F., Zheng, Y., Yu, J., Huang, B., Chen, Q., Wu, S. & Pan, D. (2013) 'The Hippo effector Yorkie controls normal tissue growth by antagonizing scalloped-mediated default repression'. *Dev Cell*, 25 (4), pp. 388-401.

Korkaya, H., Liu, S. & Wicha, M. S. (2011) 'Regulation of cancer stem cells by cytokine networks: attacking cancer's inflammatory roots'. *Clin Cancer Res*, 17 (19), pp. 6125-6129.

Koutsimpelas, D., Ruerup, G., Mann, W. J. & Brieger, J. (2012) 'Lack of neurofibromatosis type 2 gene promoter methylation in sporadic vestibular schwannomas'. *ORL J Otorhinolaryngol Relat Spec*, 74 (1), pp. 33-37.

Kressel, M. & Schmucker, B. (2002) 'Nucleocytoplasmic transfer of the NF2 tumor suppressor protein merlin is regulated by exon 2 and a CRM1-dependent nuclear export signal in exon 15'. *Hum Mol Genet*, 11 (19), pp. 2269-2278.

Krneta, T., Gillgrass, A., Poznanski, S., Chew, M., Lee, A. J., Kolb, M. & Ashkar, A. A. (2017) 'M2-polarized and tumor-associated macrophages alter NK cell phenotype and function in a contact-dependent manner'. *J Leukoc Biol*, 101 (1), pp. 285-295.

Kuang, D. M., Zhao, Q., Peng, C., Xu, J., Zhang, J. P., Wu, C. & Zheng, L. (2009) 'Activated monocytes in peritumoral stroma of hepatocellular carcinoma foster immune privilege and disease progression through PD-L1'. *J Exp Med*, 206 (6), pp. 1327-1337.

Kuo, H. C., Chu, C. C., Jung, S. M. & Huang, C. C. (2004) 'An unusual clinical course of peripheral neuropathy in neurofibromatosis type 2'. *J Clin Neuromuscul Dis*, 5 (4), pp. 195-201.

Kwon, M. J., Sung, C. O., Kang, S. Y., Do, I. G. & Suh, Y. L. (2013) 'Differential expression of extracellular matrix-related genes in rare variants of meningioma'. *Hum Pathol*, 44 (2), pp. 260-268.

Lai, D., Ho, K. C., Hao, Y. & Yang, X. (2011) 'Taxol resistance in breast cancer cells is mediated by the hippo pathway component TAZ and its downstream transcriptional targets Cyr61 and CTGF'. *Cancer Res*, 71 (7), pp. 2728-2738.

Lai, D. & Yang, X. (2013) 'BMP4 is a novel transcriptional target and mediator of mammary cell migration downstream of the Hippo pathway component TAZ'. *Cell Signal*, 25 (8), pp. 1720-1728.

Lai, Z. C., Wei, X., Shimizu, T., Ramos, E., Rohrbaugh, M., Nikolaidis, N., Ho, L. L. & Li, Y. (2005) 'Control of cell proliferation and apoptosis by mob as tumor suppressor, mats'. *Cell*, 120 (5), pp. 675-685.

LaJeunesse, D. R., McCartney, B. M. & Fehon, R. G. (1998) 'Structural analysis of Drosophila merlin reveals functional domains important for growth control and subcellular localization'. *J Cell Biol*, 141 (7), pp. 1589-1599.

Lallemand, D., Manent, J., Couvelard, A., Watilliaux, A., Siena, M., Chareyre, F., Lampin, A., Niwa-Kawakita, M., Kalamarides, M. & Giovannini, M. (2009) 'Merlin regulates transmembrane receptor accumulation and signaling at the plasma membrane in primary mouse Schwann cells and in human schwannomas'. *Oncogene*, 28 (6), pp. 854-865.

Lallemand, D., Saint-Amaux, A. L. & Giovannini, M. (2009) 'Tumor-suppression functions of merlin are independent of its role as an organizer of the actin cytoskeleton in Schwann cells'. *J Cell Sci*, 122 (Pt 22), pp. 4141-4149.

Lamar, J. M., Stern, P., Liu, H., Schindler, J. W., Jiang, Z. G. & Hynes, R. O. (2012) 'The Hippo pathway target, YAP, promotes metastasis through its TEAD-interaction domain'. *Proc Natl Acad Sci U S A*, 109 (37), pp. E2441-2450.

Laraba, L., Hillson, L., de Guibert, J. G., Hewitt, A., Jaques, M. R., Tang, T. T., Post, L., Ercolano, E., Rai, G., Yang, S. M., Jagger, D. J., Woznica, W., Edwards, P., Shivane, A. G., Hanemann, C. O. & Parkinson, D. B. (2022) 'Inhibition of YAP/TAZ-driven TEAD activity prevents growth of NF2-null schwannoma and meningioma'. *Brain*,

Larson, J. J., van Loveren, H. R., Balko, M. G. & Tew, J. M., Jr. (1995) 'Evidence of meningioma infiltration into cranial nerves: clinical implications for cavernous sinus meningiomas'. *J Neurosurg*, 83 (4), pp. 596-599.

Lau, Y. K., Murray, L. B., Houshmandi, S. S., Xu, Y., Gutmann, D. H. & Yu, Q. (2008) 'Merlin is a potent inhibitor of glioma growth'. *Cancer Res*, 68 (14), pp. 5733-5742.

Laulajainen, M., Muranen, T., Carpen, O. & Gronholm, M. (2008) 'Protein kinase A-mediated phosphorylation of the NF2 tumor suppressor protein merlin at serine 10 affects the actin cytoskeleton'. *Oncogene*, 27 (23), pp. 3233-3243.

Laulajainen, M., Muranen, T., Nyman, T. A., Carpén, O. & Grönholm, M. (2011) 'Multistep phosphorylation by oncogenic kinases enhances the degradation of the NF2 tumor suppressor merlin'. *Neoplasia*, 13 (7), pp. 643-652.

Lawrence, T. & Natoli, G. (2011) 'Transcriptional regulation of macrophage polarization: enabling diversity with identity'. *Nat Rev Immunol*, 11 (11), pp. 750-761.

LeBlanc, L., Ramirez, N. & Kim, J. (2021) 'Context-dependent roles of YAP/TAZ in stem cell fates and cancer'. *Cell Mol Life Sci*, 78 (9), pp. 4201-4219.

Lee, D. H., Park, J. O., Kim, T. S., Kim, S. K., Kim, T. H., Kim, M. C., Park, G. S., Kim, J. H., Kuninaka, S., Olson, E. N., Saya, H., Kim, S. Y., Lee, H. & Lim, D. S. (2016) 'LATS-YAP/TAZ controls lineage specification by regulating TGFβ signaling and Hnf4α expression during liver development'. *Nat Commun*, 7 pp. 11961.

Lee, H. J., Diaz, M. F., Price, K. M., Ozuna, J. A., Zhang, S., Sevick-Muraca, E. M., Hagan, J. P. & Wenzel, P. L. (2017) 'Fluid shear stress activates YAP1 to promote cancer cell motility'. *Nat Commun*, 8 pp. 14122.

Lee, J. M., Lee, J. S., Kim, H., Kim, K., Park, H., Kim, J. Y., Lee, S. H., Kim, I. S., Kim, J., Lee, M., Chung, C. H., Seo, S. B., Yoon, J. B., Ko, E., Noh, D. Y., Kim, K. I., Kim, K. K. & Baek, S. H. (2012) 'EZH2 generates a methyl degron that is recognized by the DCAF1/DDB1/CUL4 E3 ubiquitin ligase complex'. *Mol Cell*, 48 (4), pp. 572-586.

Lee, K. P., Lee, J. H., Kim, T. S., Kim, T. H., Park, H. D., Byun, J. S., Kim, M. C., Jeong, W. I., Calvisi, D. F., Kim, J. M. & Lim, D. S. (2010) 'The Hippo-Salvador pathway restrains hepatic oval cell proliferation, liver size, and liver tumorigenesis'. *Proc Natl Acad Sci U S A*, 107 (18), pp. 8248-8253.

Lee, M., Rezai, A. R., Freed, D. & Epstein, F. J. (1996) 'Intramedullary spinal cord tumors in neurofibromatosis'. *Neurosurgery*, 38 (1), pp. 32-37.

Lee, P. C. & Machner, M. P. (2018) 'The Legionella Effector Kinase LegK7 Hijacks the Host Hippo Pathway to Promote Infection'. *Cell Host Microbe*, 24 (3), pp. 429-438.e426.

Lee, T. X., Packer, M. D., Huang, J., Akhmametyeva, E. M., Kulp, S. K., Chen, C. S., Giovannini, M., Jacob, A., Welling, D. B. & Chang, L. S. (2009) 'Growth inhibitory and anti-tumour activities of OSU-03012, a novel PDK-1 inhibitor, on vestibular schwannoma and malignant schwannoma cells'. *Eur J Cancer*, 45 (9), pp. 1709-1720.

Lee, W. H. (1990) 'Characterization of a newly established malignant meningioma cell line of the human brain: IOMM-Lee'. *Neurosurgery*, 27 (3), pp. 389-395; discussion 396.

Lehtinen, M. K., Yuan, Z., Boag, P. R., Yang, Y., Villén, J., Becker, E. B., DiBacco, S., de la Iglesia, N., Gygi, S., Blackwell, T. K. & Bonni, A. (2006) 'A conserved MST-FOXO signaling pathway mediates oxidative-stress responses and extends life span'. *Cell*, 125 (5), pp. 987-1001.

Lei, Q. Y., Zhang, H., Zhao, B., Zha, Z. Y., Bai, F., Pei, X. H., Zhao, S., Xiong, Y. & Guan, K. L. (2008) 'TAZ promotes cell proliferation and epithelial-mesenchymal transition and is inhibited by the hippo pathway'. *Mol Cell Biol*, 28 (7), pp. 2426-2436.

Lesokhin, A. M., Hohl, T. M., Kitano, S., Cortez, C., Hirschhorn-Cymerman, D., Avogadri, F., Rizzuto, G. A., Lazarus, J. J., Pamer, E. G., Houghton, A. N., Merghoub, T. & Wolchok, J. D. (2012) 'Monocytic CCR2(+) myeloid-derived suppressor cells promote immune escape by limiting activated CD8 T-cell infiltration into the tumor microenvironment'. *Cancer Res*, 72 (4), pp. 876-886.

Levy, D., Adamovich, Y., Reuven, N. & Shaul, Y. (2007) 'The Yes-associated protein 1 stabilizes p73 by preventing Itch-mediated ubiquitination of p73'. *Cell Death Differ*, 14 (4), pp. 743-751.

Levy, D., Adamovich, Y., Reuven, N. & Shaul, Y. (2008) 'Yap1 phosphorylation by c-Abl is a critical step in selective activation of proapoptotic genes in response to DNA damage'. *Mol Cell*, 29 (3), pp. 350-361.

Lewis, D., Roncaroli, F., Agushi, E., Mosses, D., Williams, R., Li, K. L., Zhu, X., Hinz, R., Atkinson, R., Wadeson, A., Hulme, S., Mayers, H., Stapleton, E., Lloyd, S. K. L., Freeman, S. R., Rutherford, S. A., Hammerbeck-Ward, C., Evans, D. G., Pathmanaban, O., Jackson, A., King, A. T. & Coope, D. J. (2019) 'Inflammation and vascular permeability correlate with growth in sporadic vestibular schwannoma'. *Neuro Oncol*, 21 (3), pp. 314-325.

Li, J., Li, Z., Wu, Y., Diao, P., Zhang, W., Wang, Y., Yang, J. & Cheng, J. (2019a) 'Overexpression of lncRNA WWTR1-AS1 associates with tumor aggressiveness and unfavorable survival in head-neck squamous cell carcinoma'. *J Cell Biochem*, 120 (10), pp. 18266-18277.

Li, M., Chen, J., Yu, X., Xu, S., Li, D., Zheng, Q. & Yin, Y. (2019b) 'Myricetin Suppresses the Propagation of Hepatocellular Carcinoma via Down-Regulating Expression of YAP'. *Cells*, 8 (4),

Li, N., Batzer, A., Daly, R., Yajnik, V., Skolnik, E., Chardin, P., Bar-Sagi, D., Margolis, B. & Schlessinger, J. (1993) 'Guanine-nucleotide-releasing factor hSos1 binds to Grb2 and links receptor tyrosine kinases to Ras signalling'. *Nature*, 363 (6424), pp. 85-88.

Li, P., Silvis, M. R., Honaker, Y., Lien, W. H., Arron, S. T. & Vasioukhin, V. (2016a) 'αE-catenin inhibits a Src-YAP1 oncogenic module that couples tyrosine kinases and the effector of Hippo signaling pathway'. *Genes Dev*, 30 (7), pp. 798-811.

Li, Q., Li, S., Mana-Capelli, S., Roth Flach, R. J., Danai, L. V., Amcheslavsky, A., Nie, Y., Kaneko, S., Yao, X., Chen, X., Cotton, J. L., Mao, J., McCollum, D., Jiang, J., Czech, M. P., Xu, L. & Ip, Y. T. (2014a) 'The conserved misshapen-warts-Yorkie pathway acts in enteroblasts to regulate intestinal stem cells in Drosophila'. *Dev Cell*, 31 (3), pp. 291-304.

Li, Q., Sun, Y., Jarugumilli, G. K., Liu, S., Dang, K., Cotton, J. L., Xiol, J., Chan, P. Y., DeRan, M., Ma, L., Li, R., Zhu, L. J., Li, J. H., Leiter, A. B., Ip, Y. T., Camargo, F. D., Luo, X., Johnson, R. L., Wu, X. & Mao, J. (2020) 'Lats1/2 Sustain Intestinal Stem Cells and Wnt Activation through TEAD-Dependent and Independent Transcription'. *Cell Stem Cell*, 26 (5), pp. 675-692.e678.

Li, S., Shen, D., Shao, J., Crowder, R., Liu, W., Prat, A., He, X., Liu, S., Hoog, J., Lu, C., Ding, L., Griffith, O. L., Miller, C., Larson, D., Fulton, R. S., Harrison, M., Mooney, T., McMichael, J. F., Luo, J., Tao, Y., Goncalves, R., Schlosberg, C., Hiken, J. F., Saied, L., Sanchez, C., Giuntoli, T., Bumb, C., Cooper, C., Kitchens, R. T., Lin, A., Phommaly, C., Davies, S. R., Zhang, J., Kavuri, M. S., McEachern, D., Dong, Y. Y., Ma, C., Pluard, T., Naughton, M., Bose, R., Suresh, R., McDowell, R., Michel, L., Aft, R., Gillanders, W., DeSchryver, K., Wilson, R. K., Wang, S., Mills, G. B., Gonzalez-Angulo, A., Edwards, J. R., Maher, C., Perou, C. M., Mardis, E. R. & Ellis, M. J. (2013) 'Endocrine-therapy-resistant ESR1 variants revealed by genomic characterization of breast-cancer-derived xenografts'. *Cell Rep*, 4 (6), pp. 1116-1130.

Li, W., Cooper, J., Zhou, L., Yang, C., Erdjument-Bromage, H., Zagzag, D., Snuderl, M., Ladanyi, M., Hanemann, C. O., Zhou, P., Karajannis, M. A. & Giancotti, F. G. (2014b) 'Merlin/NF2 loss-driven tumorigenesis linked to CRL4(DCAF1)-mediated inhibition of the hippo pathway kinases Lats1 and 2 in the nucleus'. *Cancer Cell*, 26 (1), pp. 48-60.

Li, W., Dong, S., Wei, W., Wang, G., Zhang, A., Pu, P. & Jia, Z. (2016b) 'The role of transcriptional coactivator TAZ in gliomas'. *Oncotarget*, 7 (50), pp. 82686-82699.

Li, W., Xiao, J., Zhou, X., Xu, M., Hu, C., Xu, X., Lu, Y., Liu, C., Xue, S., Nie, L., Zhang, H., Li, Z., Zhang, Y., Ji, F., Hui, L., Tao, W., Wei, B. & Wang, H. (2015a) 'STK4 regulates TLR pathways and protects against chronic inflammation-related hepatocellular carcinoma'. *J Clin Invest*, 125 (11), pp. 4239-4254.

Li, W., You, L., Cooper, J., Schiavon, G., Pepe-Caprio, A., Zhou, L., Ishii, R., Giovannini, M., Hanemann, C. O., Long, S. B., Erdjument-Bromage, H., Zhou, P., Tempst, P. & Giancotti, F. G. (2010) 'Merlin/NF2 suppresses tumorigenesis by inhibiting the E3 ubiquitin ligase CRL4(DCAF1) in the nucleus'. *Cell*, 140 (4), pp. 477-490.

Li, X., Wang, W., Wang, J., Malovannaya, A., Xi, Y., Li, W., Guerra, R., Hawke, D. H., Qin, J. & Chen, J. (2015b) 'Proteomic analyses reveal distinct chromatin-associated and soluble transcription factor complexes'. *Mol Syst Biol*, 11 (1), pp. 775.

Li, Y., Li, L., Zhu, M., Ye, L. & Yang, Q. (2017) 'Upregulation of Yes-associated protein and transcriptional co-activator with PDZ-binding motif influences the behavior of LOVO human colon adenocarcinoma cells'. *Exp Ther Med*, 14 (4), pp. 3831-3835.

Li, Y., Liu, S., Ng, E. Y., Li, R., Poulsen, A., Hill, J., Pobbati, A. V., Hung, A. W., Hong, W., Keller, T. H. & Kang, C. (2018) 'Structural and ligand-binding analysis of the YAP-binding domain of transcription factor TEAD4'. *Biochem J*, 475 (12), pp. 2043-2055.

Li, Y., Tennekoon, G. I., Birnbaum, M., Marchionni, M. A. & Rutkowski, J. L. (2001) 'Neuregulin signaling through a PI3K/Akt/Bad pathway in Schwann cell survival'. *Mol Cell Neurosci*, 17 (4), pp. 761-767.

Liang, K., Zhou, G., Zhang, Q., Li, J. & Zhang, C. (2014a) 'Expression of hippo pathway in colorectal cancer'. *Saudi J Gastroenterol*, 20 (3), pp. 188-194.

Liang, N., Zhang, C., Dill, P., Panasyuk, G., Pion, D., Koka, V., Gallazzini, M., Olson, E. N., Lam, H., Henske, E. P., Dong, Z., Apte, U., Pallet, N., Johnson, R. L., Terzi, F., Kwiatkowski, D. J., Scoazec, J. Y., Martignoni, G. & Pende, M. (2014b) 'Regulation of YAP by mTOR and autophagy reveals a therapeutic target of tuberous sclerosis complex'. *J Exp Med*, 211 (11), pp. 2249-2263.

Lin, K. C., Moroishi, T., Meng, Z., Jeong, H. S., Plouffe, S. W., Sekido, Y., Han, J., Park, H. W. & Guan, K. L. (2017) 'Regulation of Hippo pathway transcription factor TEAD by p38 MAPK-induced cytoplasmic translocation'. *Nat Cell Biol*, 19 (8), pp. 996-1002.

Lin, Z., Guo, H., Cao, Y., Zohrabian, S., Zhou, P., Ma, Q., VanDusen, N., Guo, Y., Zhang, J., Stevens, S. M., Liang, F., Quan, Q., van Gorp, P. R., Li, A., Dos Remedios, C., He, A., Bezzerides, V. J. & Pu, W. T. (2016) 'Acetylation of VGLL4 Regulates Hippo-YAP Signaling and Postnatal Cardiac Growth'. *Dev Cell*, 39 (4), pp. 466-479.

Linde, N., Lederle, W., Depner, S., van Rooijen, N., Gutschalk, C. M. & Mueller, M. M. (2012) 'Vascular endothelial growth factor-induced skin carcinogenesis depends on recruitment and alternative activation of macrophages'. *J Pathol*, 227 (1), pp. 17-28.

Lindsley, A., Snider, P., Zhou, H., Rogers, R., Wang, J., Olaopa, M., Kruzynska-Frejtag, A., Koushik, S. V., Lilly, B., Burch, J. B., Firulli, A. B. & Conway, S. J. (2007) 'Identification and characterization of a novel Schwann and outflow tract endocardial cushion lineage-restricted periostin enhancer'. *Dev Biol*, 307 (2), pp. 340-355.

Liu-Chittenden, Y., Huang, B., Shim, J. S., Chen, Q., Lee, S. J., Anders, R. A., Liu, J. O. & Pan, D. (2012) 'Genetic and pharmacological disruption of the TEAD-YAP complex suppresses the oncogenic activity of YAP'. *Genes Dev*, 26 (12), pp. 1300-1305.

Liu, C. Y., Zha, Z. Y., Zhou, X., Zhang, H., Huang, W., Zhao, D., Li, T., Chan, S. W., Lim, C. J., Hong, W., Zhao, S., Xiong, Y., Lei, Q. Y. & Guan, K. L. (2010) 'The hippo tumor pathway promotes TAZ degradation by phosphorylating a phosphodegron and recruiting the SCF{beta}-TrCP E3 ligase'. *J Biol Chem*, 285 (48), pp. 37159-37169.

Liu, D., Song, L., Wei, J., Courtney, A. N., Gao, X., Marinova, E., Guo, L., Heczey, A., Asgharzadeh, S., Kim, E., Dotti, G. & Metelitsa, L. S. (2012) 'IL-15 protects NKT cells from inhibition by tumor-associated macrophages and enhances antimetastatic activity'. *J Clin Invest*, 122 (6), pp. 2221-2233.

Liu, F., Lagares, D., Choi, K. M., Stopfer, L., Marinković, A., Vrbanac, V., Probst, C. K., Hiemer, S. E., Sisson, T. H., Horowitz, J. C., Rosas, I. O., Fredenburgh, L. E., Feghali-Bostwick, C., Varelas, X., Tager,

A. M. & Tschumperlin, D. J. (2015a) 'Mechanosignaling through YAP and TAZ drives fibroblast activation and fibrosis'. *Am J Physiol Lung Cell Mol Physiol*, 308 (4), pp. L344-357.

Liu, G., Yu, F. X., Kim, Y. C., Meng, Z., Naipauer, J., Looney, D. J., Liu, X., Gutkind, J. S., Mesri, E. A. & Guan, K. L. (2015b) 'Kaposi sarcoma-associated herpesvirus promotes tumorigenesis by modulating the Hippo pathway'. *Oncogene*, 34 (27), pp. 3536-3546.

Liu, J., Zhang, N., Li, Q., Zhang, W., Ke, F., Leng, Q., Wang, H., Chen, J. & Wang, H. (2011) 'Tumor-associated macrophages recruit CCR6+ regulatory T cells and promote the development of colorectal cancer via enhancing CCL20 production in mice'. *PLoS One*, 6 (4), pp. e19495.

Liu, X., Kong, C. & Zhang, Z. (2018) 'miR-130b promotes bladder cancer cell proliferation, migration and invasion by targeting VGLL4'. *Oncol Rep*, 39 (5), pp. 2324-2332.

Liu, X., Li, H., Rajurkar, M., Li, Q., Cotton, J. L., Ou, J., Zhu, L. J., Goel, H. L., Mercurio, A. M., Park, J. S., Davis, R. J. & Mao, J. (2016a) 'Tead and AP1 Coordinate Transcription and Motility'. *Cell Rep*, 14 (5), pp. 1169-1180.

Liu, X., Yang, N., Figel, S. A., Wilson, K. E., Morrison, C. D., Gelman, I. H. & Zhang, J. (2013) 'PTPN14 interacts with and negatively regulates the oncogenic function of YAP'. *Oncogene*, 32 (10), pp. 1266-1273.

Liu, Y., Wang, G., Yang, Y., Mei, Z., Liang, Z., Cui, A., Wu, T., Liu, C. Y. & Cui, L. (2016b) 'Increased TEAD4 expression and nuclear localization in colorectal cancer promote epithelial-mesenchymal transition and metastasis in a YAP-independent manner'. *Oncogene*, 35 (21), pp. 2789-2800.

Lloyd, S. K. & Evans, D. G. (2013) 'Neurofibromatosis type 2 (NF2): diagnosis and management'. *Handb Clin Neurol*, 115 pp. 957-967.

Lomas, J., Bello, M. J., Arjona, D., Alonso, M. E., Martinez-Glez, V., Lopez-Marin, I., Amiñoso, C., de Campos, J. M., Isla, A., Vaquero, J. & Rey, J. A. (2005) 'Genetic and epigenetic alteration of the NF2 gene in sporadic meningiomas'. *Genes Chromosomes Cancer*, 42 (3), pp. 314-319.

López-Lago, M. A., Okada, T., Murillo, M. M., Socci, N. & Giancotti, F. G. (2009) 'Loss of the tumor suppressor gene NF2, encoding merlin, constitutively activates integrin-dependent mTORC1 signaling'. *Mol Cell Biol*, 29 (15), pp. 4235-4249.

Lorsbach, R. B., Murphy, W. J., Lowenstein, C. J., Snyder, S. H. & Russell, S. W. (1993) 'Expression of the nitric oxide synthase gene in mouse macrophages activated for tumor cell killing. Molecular basis for the synergy between interferon-gamma and lipopolysaccharide'. *J Biol Chem*, 268 (3), pp. 1908-1913.

Lowenstein, C. J., Alley, E. W., Raval, P., Snowman, A. M., Snyder, S. H., Russell, S. W. & Murphy, W. J. (1993) 'Macrophage nitric oxide synthase gene: two upstream regions mediate induction by interferon gamma and lipopolysaccharide'. *Proc Natl Acad Sci U S A*, 90 (20), pp. 9730-9734.

Lu, H., Clauser, K. R., Tam, W. L., Frose, J., Ye, X., Eaton, E. N., Reinhardt, F., Donnenberg, V. S., Bhargava, R., Carr, S. A. & Weinberg, R. A. (2014) 'A breast cancer stem cell niche supported by juxtacrine signalling from monocytes and macrophages'. *Nat Cell Biol*, 16 (11), pp. 1105-1117.

Lu, L., Li, Y., Kim, S. M., Bossuyt, W., Liu, P., Qiu, Q., Wang, Y., Halder, G., Finegold, M. J., Lee, J. S. & Johnson, R. L. (2010) 'Hippo signaling is a potent in vivo growth and tumor suppressor pathway in the mammalian liver'. *Proc Natl Acad Sci U S A*, 107 (4), pp. 1437-1442.

Lu, W., Wang, J., Li, Y., Tao, H., Xiong, H., Lian, F., Gao, J., Ma, H., Lu, T., Zhang, D., Ye, X., Ding, H., Yue, L., Zhang, Y., Tang, H., Zhang, N., Yang, Y., Jiang, H., Chen, K., Zhou, B. & Luo, C. (2019) 'Discovery and biological evaluation of vinylsulfonamide derivatives as highly potent, covalent TEAD autopalmitoylation inhibitors'. *Eur J Med Chem*, 184 pp. 111767.

Ma, B., Chen, Y., Chen, L., Cheng, H., Mu, C., Li, J., Gao, R., Zhou, C., Cao, L., Liu, J., Zhu, Y., Chen, Q. & Wu, S. (2015) 'Hypoxia regulates Hippo signalling through the SIAH2 ubiquitin E3 ligase'. *Nat Cell Biol*, 17 (1), pp. 95-103.

MacDonald, K. P., Rowe, V., Bofinger, H. M., Thomas, R., Sasmono, T., Hume, D. A. & Hill, G. R. (2005) 'The colony-stimulating factor 1 receptor is expressed on dendritic cells during differentiation and regulates their expansion'. *J Immunol*, 175 (3), pp. 1399-1405.

Madisen, L., Zwingman, T. A., Sunkin, S. M., Oh, S. W., Zariwala, H. A., Gu, H., Ng, L. L., Palmiter, R. D., Hawrylycz, M. J., Jones, A. R., Lein, E. S. & Zeng, H. (2010) 'A robust and high-throughput Cre reporting and characterization system for the whole mouse brain'. *Nat Neurosci*, 13 (1), pp. 133-140.

Maeda, T., Gupta, M. P. & Stewart, A. F. (2002) 'TEF-1 and MEF2 transcription factors interact to regulate muscle-specific promoters'. *Biochem Biophys Res Commun*, 294 (4), pp. 791-797.

Mahler, J. F., Stokes, W., Mann, P. C., Takaoka, M. & Maronpot, R. R. (1996) 'Spontaneous lesions in aging FVB/N mice'. *Toxicol Pathol*, 24 (6), pp. 710-716.

Mahoney, W. M., Jr., Hong, J. H., Yaffe, M. B. & Farrance, I. K. (2005) 'The transcriptional co-activator TAZ interacts differentially with transcriptional enhancer factor-1 (TEF-1) family members'. *Biochem J*, 388 (Pt 1), pp. 217-225.

Makarova, O., Roh, M. H., Liu, C. J., Laurinec, S. & Margolis, B. (2003) 'Mammalian Crumbs3 is a small transmembrane protein linked to protein associated with Lin-7 (Pals1)'. *Gene*, 302 (1-2), pp. 21-29.

Malhotra, A., Shibata, Y., Hall, I. M. & Dutta, A. (2013) 'Chromosomal structural variations during progression of a prostate epithelial cell line to a malignant metastatic state inactivate the NF2, NIPSNAP1, UGT2B17, and LPIN2 genes'. *Cancer Biol Ther*, 14 (9), pp. 840-852.

Mani, T., Hennigan, R. F., Foster, L. A., Conrady, D. G., Herr, A. B. & Ip, W. (2011) 'FERM domain phosphoinositide binding targets merlin to the membrane and is essential for its growth-suppressive function'. *Mol Cell Biol*, 31 (10), pp. 1983-1996.

Manning, S. A., Dent, L. G., Kondo, S., Zhao, Z. W., Plachta, N. & Harvey, K. F. (2018) 'Dynamic Fluctuations in Subcellular Localization of the Hippo Pathway Effector Yorkie In Vivo'. *Curr Biol*, 28 (10), pp. 1651-1660.e1654.

Mantovani, A. & Allavena, P. (2015) 'The interaction of anticancer therapies with tumor-associated macrophages'. *J Exp Med*, 212 (4), pp. 435-445.

Mantovani, A., Biswas, S. K., Galdiero, M. R., Sica, A. & Locati, M. (2013) 'Macrophage plasticity and polarization in tissue repair and remodelling'. *J Pathol*, 229 (2), pp. 176-185.

Marks, M., Pennimpede, T., Lange, L., Grote, P., Herrmann, B. G. & Wittler, L. (2016) 'Analysis of the Fam181 gene family during mouse development reveals distinct strain-specific expression patterns, suggesting a role in nervous system development and function'. *Gene*, 575 (2 Pt 2), pp. 438-451.

Martinez, F. O. & Gordon, S. (2014) 'The M1 and M2 paradigm of macrophage activation: time for reassessment'. *F1000Prime Rep*, 6 pp. 13.

Mathieu, D., Kondziolka, D., Flickinger, J. C., Niranjan, A., Williamson, R., Martin, J. J. & Lunsford, L. D. (2007) 'Stereotactic radiosurgery for vestibular schwannomas in patients with neurofibromatosis type 2: an analysis of tumor control, complications, and hearing preservation rates'. *Neurosurgery*, 60 (3), pp. 460-468; discussion 468-470.

Mautner, V. F., Lindenau, M., Baser, M. E., Hazim, W., Tatagiba, M., Haase, W., Samii, M., Wais, R. & Pulst, S. M. (1996) 'The neuroimaging and clinical spectrum of neurofibromatosis 2'. *Neurosurgery*, 38 (5), pp. 880-885; discussion 885-886.

Mautner, V. F., Lindenau, M., Baser, M. E., Kluwe, L. & Gottschalk, J. (1997) 'Skin abnormalities in neurofibromatosis 2'. *Arch Dermatol*, 133 (12), pp. 1539-1543.

Mautner, V. F., Nguyen, R., Kutta, H., Fuensterer, C., Bokemeyer, C., Hagel, C., Friedrich, R. E. & Panse, J. (2010) 'Bevacizumab induces regression of vestibular schwannomas in patients with neurofibromatosis type 2'. *Neuro Oncol*, 12 (1), pp. 14-18.

Mautner, V. F., Tatagiba, M., Lindenau, M., Fünsterer, C., Pulst, S. M., Baser, M. E., Kluwe, L. & Zanella, F. E. (1995) 'Spinal tumors in patients with neurofibromatosis type 2: MR imaging study of frequency, multiplicity, and variety'. *AJR Am J Roentgenol*, 165 (4), pp. 951-955.

Mawrin, C., Sasse, T., Kirches, E., Kropf, S., Schneider, T., Grimm, C., Pambor, C., Vorwerk, C. K., Firsching, R., Lendeckel, U. & Dietzmann, K. (2005) 'Different activation of mitogen-activated protein kinase and Akt signaling is associated with aggressive phenotype of human meningiomas'. *Clin Cancer Res*, 11 (11), pp. 4074-4082.

Mayfrank, L., Mohadjer, M. & Wullich, B. (1990) 'Intracranial calcified deposits in neurofibromatosis type 2. A CT study of 11 cases'. *Neuroradiology*, 32 (1), pp. 33-37.

Mazzoni, A., Bronte, V., Visintin, A., Spitzer, J. H., Apolloni, E., Serafini, P., Zanovello, P. & Segal, D. M. (2002) 'Myeloid suppressor lines inhibit T cell responses by an NO-dependent mechanism'. *J Immunol*, 168 (2), pp. 689-695.

McClatchey, A. I. & Giovannini, M. (2005) 'Membrane organization and tumorigenesis--the NF2 tumor suppressor, Merlin'. *Genes Dev*, 19 (19), pp. 2265-2277.

McClatchey, A. I., Saotome, I., Ramesh, V., Gusella, J. F. & Jacks, T. (1997) 'The Nf2 tumor suppressor gene product is essential for extraembryonic development immediately prior to gastrulation'. *Genes Dev*, 11 (10), pp. 1253-1265.

McCormick, P. C., Torres, R., Post, K. D. & Stein, B. M. (1990) 'Intramedullary ependymoma of the spinal cord'. *J Neurosurg*, 72 (4), pp. 523-532.

McGuire, C. S., Sainani, K. L. & Fisher, P. G. (2009) 'Incidence patterns for ependymoma: a surveillance, epidemiology, and end results study'. *J Neurosurg*, 110 (4), pp. 725-729.

McNeill, H. & Reginensi, A. (2017) 'Lats1/2 Regulate Yap/Taz to Control Nephron Progenitor Epithelialization and Inhibit Myofibroblast Formation'. *J Am Soc Nephrol*, 28 (3), pp. 852-861.

Mehra, R., Vats, P., Cieslik, M., Cao, X., Su, F., Shukla, S., Udager, A. M., Wang, R., Pan, J., Kasaian, K., Lonigro, R., Siddiqui, J., Premkumar, K., Palapattu, G., Weizer, A., Hafez, K. S., Wolf, J. S., Jr., Sangoi, A. R., Trpkov, K., Osunkoya, A. O., Zhou, M., Giannico, G., McKenney, J. K., Dhanasekaran, S. M. & Chinnaiyan, A. M. (2016) 'Biallelic Alteration and Dysregulation of the Hippo Pathway in Mucinous Tubular and Spindle Cell Carcinoma of the Kidney'. *Cancer Discov*, 6 (11), pp. 1258-1266.

Mei, Y., Bi, W. L., Greenwald, N. F., Agar, N. Y., Beroukhim, R., Dunn, G. P. & Dunn, I. F. (2017) 'Genomic profile of human meningioma cell lines'. *PLoS One*, 12 (5), pp. e0178322.

Meng, F., Zhou, R., Wu, S., Zhang, Q., Jin, Q., Zhou, Y., Plouffe, S. W., Liu, S., Song, H., Xia, Z., Zhao, B., Ye, S., Feng, X. H., Guan, K. L., Zou, J. & Xu, P. (2016) 'Mst1 shuts off cytosolic antiviral defense through IRF3 phosphorylation'. *Genes Dev*, 30 (9), pp. 1086-1100.

Meng, Z., Moroishi, T., Mottier-Pavie, V., Plouffe, S. W., Hansen, C. G., Hong, A. W., Park, H. W., Mo, J. S., Lu, W., Lu, S., Flores, F., Yu, F. X., Halder, G. & Guan, K. L. (2015) 'MAP4K family kinases act in parallel to MST1/2 to activate LATS1/2 in the Hippo pathway'. *Nat Commun*, 6 pp. 8357.

Meng, Z., Qiu, Y., Lin, K. C., Kumar, A., Placone, J. K., Fang, C., Wang, K. C., Lu, S., Pan, M., Hong, A. W., Moroishi, T., Luo, M., Plouffe, S. W., Diao, Y., Ye, Z., Park, H. W., Wang, X., Yu, F. X., Chien, S., Wang, C. Y., Ren, B., Engler, A. J. & Guan, K. L. (2018) 'RAP2 mediates mechanoresponses of the Hippo pathway'. *Nature*, 560 (7720), pp. 655-660.

Mesrouze, Y., Meyerhofer, M., Bokhovchuk, F., Fontana, P., Zimmermann, C., Martin, T., Delaunay, C., Izaac, A., Kallen, J., Schmelzle, T., Erdmann, D. & Chène, P. (2017) 'Effect of the acylation of TEAD4 on its interaction with co-activators YAP and TAZ'. *Protein Sci*, 26 (12), pp. 2399-2409.

Meyers, S. M., Gutman, F. A., Kaye, L. D. & Rothner, A. D. (1995) 'Retinal changes associated with neurofibromatosis 2'. *Trans Am Ophthalmol Soc*, 93 pp. 245-252; discussion 252-247.

Miao, J., Hsu, P. C., Yang, Y. L., Xu, Z., Dai, Y., Wang, Y., Chan, G., Huang, Z., Hu, B., Li, H., Jablons, D. M. & You, L. (2017) 'YAP regulates PD-L1 expression in human NSCLC cells'. *Oncotarget*, 8 (70), pp. 114576-114587.

Michelhaugh, S. K., Guastella, A. R., Varadarajan, K., Klinger, N. V., Parajuli, P., Ahmad, A., Sethi, S., Aboukameel, A., Kiousis, S., Zitron, I. M., Ebrahim, S. A., Polin, L. A., Sarkar, F. H., Bollig-Fischer, A. & Mittal, S. (2015) 'Development of patient-derived xenograft models from a spontaneously immortal low-grade meningioma cell line, KCI-MENG1'. *J Transl Med*, 13 pp. 227.

Mindos, T., Dun, X. P., North, K., Doddrell, R. D., Schulz, A., Edwards, P., Russell, J., Gray, B., Roberts, S. L., Shivane, A., Mortimer, G., Pirie, M., Zhang, N., Pan, D., Morrison, H. & Parkinson, D. B. (2017) 'Merlin controls the repair capacity of Schwann cells after injury by regulating Hippo/YAP activity'. *J Cell Biol*, 216 (2), pp. 495-510.

Mishra, P., Singh, U., Pandey, C. M., Mishra, P. & Pandey, G. (2019) 'Application of student's t-test, analysis of variance, and covariance'. *Ann Card Anaesth*, 22 (4), pp. 407-411.

Miyanaga, A., Masuda, M., Tsuta, K., Kawasaki, K., Nakamura, Y., Sakuma, T., Asamura, H., Gemma, A. & Yamada, T. (2015) 'Hippo pathway gene mutations in malignant mesothelioma: revealed by RNA and targeted exon sequencing'. *J Thorac Oncol*, 10 (5), pp. 844-851.

Mo, J. S., Meng, Z., Kim, Y. C., Park, H. W., Hansen, C. G., Kim, S., Lim, D. S. & Guan, K. L. (2015) 'Cellular energy stress induces AMPK-mediated regulation of YAP and the Hippo pathway'. *Nat Cell Biol*, 17 (4), pp. 500-510.

Mohseni, M., Sun, J., Lau, A., Curtis, S., Goldsmith, J., Fox, V. L., Wei, C., Frazier, M., Samson, O., Wong, K. K., Kim, C. & Camargo, F. D. (2014) 'A genetic screen identifies an LKB1-MARK signalling axis controlling the Hippo-YAP pathway'. *Nat Cell Biol*, 16 (1), pp. 108-117.

Moon, S., Kim, W., Kim, S., Kim, Y., Song, Y., Bilousov, O., Kim, J., Lee, T., Cha, B., Kim, M., Kim, H., Katanaev, V. L. & Jho, E. H. (2017) 'Phosphorylation by NLK inhibits YAP-14-3-3-interactions and induces its nuclear localization'. *EMBO Rep*, 18 (1), pp. 61-71.

Morales, F. C., Molina, J. R., Hayashi, Y. & Georgescu, M. M. (2010) 'Overexpression of ezrin inactivates NF2 tumor suppressor in glioblastoma'. *Neuro Oncol*, 12 (6), pp. 528-539.

Mori, T., Gotoh, S., Shirakawa, M. & Hakoshima, T. (2014) 'Structural basis of DDB1-and-Cullin 4-associated Factor 1 (DCAF1) recognition by merlin/NF2 and its implication in tumorigenesis by CD44-mediated inhibition of merlin suppression of DCAF1 function'. *Genes Cells*, 19 (8), pp. 603-619.

Moroishi, T., Park, H. W., Qin, B., Chen, Q., Meng, Z., Plouffe, S. W., Taniguchi, K., Yu, F. X., Karin, M., Pan, D. & Guan, K. L. (2015) 'A YAP/TAZ-induced feedback mechanism regulates Hippo pathway homeostasis'. *Genes Dev*, 29 (12), pp. 1271-1284.

Morrison, H., Sherman, L. S., Legg, J., Banine, F., Isacke, C., Haipek, C. A., Gutmann, D. H., Ponta, H. & Herrlich, P. (2001) 'The NF2 tumor suppressor gene product, merlin, mediates contact inhibition of growth through interactions with CD44'. *Genes Dev*, 15 (8), pp. 968-980.

Morrison, H., Sperka, T., Manent, J., Giovannini, M., Ponta, H. & Herrlich, P. (2007) 'Merlin/neurofibromatosis type 2 suppresses growth by inhibiting the activation of Ras and Rac'. *Cancer Res*, 67 (2), pp. 520-527.

Moyhuddin, A., Baser, M. E., Watson, C., Purcell, S., Ramsden, R. T., Heiberg, A., Wallace, A. J. & Evans, D. G. (2003) 'Somatic mosaicism in neurofibromatosis 2: prevalence and risk of disease transmission to offspring'. *J Med Genet*, 40 (6), pp. 459-463.

Murakami, H., Mizuno, T., Taniguchi, T., Fujii, M., Ishiguro, F., Fukui, T., Akatsuka, S., Horio, Y., Hida, T., Kondo, Y., Toyokuni, S., Osada, H. & Sekido, Y. (2011) 'LATS2 is a tumor suppressor gene of malignant mesothelioma'. *Cancer Res*, 71 (3), pp. 873-883.

Murakami, S., Shahbazian, D., Surana, R., Zhang, W., Chen, H., Graham, G. T., White, S. M., Weiner, L. M. & Yi, C. (2017) 'Yes-associated protein mediates immune reprogramming in pancreatic ductal adenocarcinoma'. *Oncogene*, 36 (9), pp. 1232-1244.

Murdoch, C., Muthana, M., Coffelt, S. B. & Lewis, C. E. (2008) 'The role of myeloid cells in the promotion of tumour angiogenesis'. *Nat Rev Cancer*, 8 (8), pp. 618-631.

Murray, L. B., Lau, Y. K. & Yu, Q. (2012) 'Merlin is a negative regulator of human melanoma growth'. *PLoS One*, 7 (8), pp. e43295.

Murray, P. J., Allen, J. E., Biswas, S. K., Fisher, E. A., Gilroy, D. W., Goerdt, S., Gordon, S., Hamilton, J. A., Ivashkiv, L. B., Lawrence, T., Locati, M., Mantovani, A., Martinez, F. O., Mege, J. L., Mosser, D. M., Natoli, G., Saeij, J. P., Schultze, J. L., Shirey, K. A., Sica, A., Suttles, J., Udalova, I., van Ginderachter, J. A., Vogel, S. N. & Wynn, T. A. (2014) 'Macrophage activation and polarization: nomenclature and experimental guidelines'. *Immunity*, 41 (1), pp. 14-20.

Nakai, Y., Zheng, Y., MacCollin, M. & Ratner, N. (2006) 'Temporal control of Rac in Schwann cell-axon interaction is disrupted in NF2-mutant schwannoma cells'. *J Neurosci*, 26 (13), pp. 3390-3395.

Nash, P., Tang, X., Orlicky, S., Chen, Q., Gertler, F. B., Mendenhall, M. D., Sicheri, F., Pawson, T. & Tyers, M. (2001) 'Multisite phosphorylation of a CDK inhibitor sets a threshold for the onset of DNA replication'. *Nature*, 414 (6863), pp. 514-521.

Neto-Silva, R. M., de Beco, S. & Johnston, L. A. (2010) 'Evidence for a growth-stabilizing regulatory feedback mechanism between Myc and Yorkie, the Drosophila homolog of Yap'. *Dev Cell*, 19 (4), pp. 507-520.

Nguyen, H. T., Hong, X., Tan, S., Chen, Q., Chan, L., Fivaz, M., Cohen, S. M. & Voorhoeve, P. M. (2014) 'Viral small T oncoproteins transform cells by alleviating hippo-pathway-mediated inhibition of the YAP proto-oncogene'. *Cell Rep*, 8 (3), pp. 707-713.

Nguyen, R., Reczek, D. & Bretscher, A. (2001) 'Hierarchy of merlin and ezrin N- and C-terminal domain interactions in homo- and heterotypic associations and their relationship to binding of scaffolding proteins EBP50 and E3KARP'. *J Biol Chem*, 276 (10), pp. 7621-7629.

Ni, L., Li, S., Yu, J., Min, J., Brautigam, C. A., Tomchick, D. R., Pan, D. & Luo, X. (2013) 'Structural basis for autoactivation of human Mst2 kinase and its regulation by RASSF5'. *Structure*, 21 (10), pp. 1757-1768.

Ni, L., Zheng, Y., Hara, M., Pan, D. & Luo, X. (2015) 'Structural basis for Mob1-dependent activation of the core Mst-Lats kinase cascade in Hippo signaling'. *Genes Dev*, 29 (13), pp. 1416-1431.

Ni, X., Tao, J., Barbi, J., Chen, Q., Park, B. V., Li, Z., Zhang, N., Lebid, A., Ramaswamy, A., Wei, P., Zheng, Y., Zhang, X., Wu, X., Vignali, P., Yang, C. P., Li, H., Pardoll, D., Lu, L., Pan, D. & Pan, F. (2018) 'YAP Is Essential for Treg-Mediated Suppression of Antitumor Immunity'. *Cancer Discov*, 8 (8), pp. 1026-1043.

Nigim, F., Esaki, S., Hood, M., Lelic, N., James, M. F., Ramesh, V., Stemmer-Rachamimov, A., Cahill, D. P., Brastianos, P. K., Rabkin, S. D., Martuza, R. L. & Wakimoto, H. (2016) 'A new patient-derived orthotopic malignant meningioma model treated with oncolytic herpes simplex virus'. *Neuro Oncol*, 18 (9), pp. 1278-1287.

Nishio, M., Sugimachi, K., Goto, H., Wang, J., Morikawa, T., Miyachi, Y., Takano, Y., Hikasa, H., Itoh, T., Suzuki, S. O., Kurihara, H., Aishima, S., Leask, A., Sasaki, T., Nakano, T., Nishina, H., Nishikawa, Y., Sekido, Y., Nakao, K., Shin-Ya, K., Mimori, K. & Suzuki, A. (2016) 'Dysregulated YAP1/TAZ and TGF-β signaling mediate hepatocarcinogenesis in Mob1a/1b-deficient mice'. *Proc Natl Acad Sci U S A*, 113 (1), pp. E71-80.

Noland, C. L., Gierke, S., Schnier, P. D., Murray, J., Sandoval, W. N., Sagolla, M., Dey, A., Hannoush, R. N., Fairbrother, W. J. & Cunningham, C. N. (2016) 'Palmitoylation of TEAD Transcription Factors Is Required for Their Stability and Function in Hippo Pathway Signaling'. *Structure*, 24 (1), pp. 179-186.

Noy, R. & Pollard, J. W. (2014) 'Tumor-associated macrophages: from mechanisms to therapy'. *Immunity*, 41 (1), pp. 49-61.

Nunes, F. & MacCollin, M. (2003) 'Neurofibromatosis 2 in the pediatric population'. *J Child Neurol*, 18 (10), pp. 718-724.

O'Reilly, K. E., Rojo, F., She, Q. B., Solit, D., Mills, G. B., Smith, D., Lane, H., Hofmann, F., Hicklin, D. J., Ludwig, D. L., Baselga, J. & Rosen, N. (2006) 'mTOR inhibition induces upstream receptor tyrosine kinase signaling and activates Akt'. *Cancer Res*, 66 (3), pp. 1500-1508.

Obremski, V. J., Hall, A. M. & Fernandez-Valle, C. (1998) 'Merlin, the neurofibromatosis type 2 gene product, and beta1 integrin associate in isolated and differentiating Schwann cells'. *J Neurobiol*, 37 (4), pp. 487-501.

Oda, Y., Kawahara, E., Minamoto, T., Ueda, Y., Ikeda, K., Nagai, Y. & Nakanishi, I. (1988) 'Immunohistochemical studies on the tissue localization of collagen types I, III, IV, V and VI in schwannomas. Correlation with ultrastructural features of the extracellular matrix'. *Virchows Arch B Cell Pathol Incl Mol Pathol*, 56 (3), pp. 153-163.

Ogawa, K., Oguchi, M., Nakashima, Y. & Yamabe, H. (1989) 'Distribution of collagen type IV in brain tumors: an immunohistochemical study'. *J Neurooncol*, 7 (4), pp. 357-366.

Oh, H., Slattery, M., Ma, L., White, K. P., Mann, R. S. & Irvine, K. D. (2014) 'Yorkie promotes transcription by recruiting a histone methyltransferase complex'. *Cell Rep*, 8 (2), pp. 449-459.

Oh, J. E., Ohta, T., Satomi, K., Foll, M., Durand, G., McKay, J., Le Calvez-Kelm, F., Mittelbronn, M., Brokinkel, B., Paulus, W. & Ohgaki, H. (2015) 'Alterations in the NF2/LATS1/LATS2/YAP Pathway in Schwannomas'. *J Neuropathol Exp Neurol*, 74 (10), pp. 952-959.

Oh, S. A. & Li, M. O. (2013) 'TGF-beta: guardian of T cell function'. *J Immunol*, 191 (8), pp. 3973-3979.

Ojalvo, L. S., King, W., Cox, D. & Pollard, J. W. (2009) 'High-density gene expression analysis of tumor-associated macrophages from mouse mammary tumors'. *Am J Pathol*, 174 (3), pp. 1048-1064.

Oka, T., Remue, E., Meerschaert, K., Vanloo, B., Boucherie, C., Gfeller, D., Bader, G. D., Sidhu, S. S., Vandekerckhove, J., Gettemans, J. & Sudol, M. (2010) 'Functional complexes between YAP2 and ZO-2 are PDZ domain-dependent, and regulate YAP2 nuclear localization and signalling'. *Biochem J*, 432 (3), pp. 461-472.

Okada, T., Lopez-Lago, M. & Giancotti, F. G. (2005) 'Merlin/NF-2 mediates contact inhibition of growth by suppressing recruitment of Rac to the plasma membrane'. *J Cell Biol*, 171 (2), pp. 361-371.

Okano, A., Miyawaki, S., Hongo, H., Dofuku, S., Teranishi, Y., Mitsui, J., Tanaka, M., Shin, M., Nakatomi, H. & Saito, N. (2021) 'Associations of pathological diagnosis and genetic abnormalities in meningiomas with the embryological origins of the meninges'. *Sci Rep*, 11 (1), pp. 6987.

Oliferenko, S., Kaverina, I., Small, J. V. & Huber, L. A. (2000) 'Hyaluronic acid (HA) binding to CD44 activates Rac1 and induces lamellipodia outgrowth'. *J Cell Biol*, 148 (6), pp. 1159-1164.

Omeis, I., Hillard, V. H., Braun, A., Benzil, D. L., Murali, R. & Harter, D. H. (2006) 'Meningioangiomatosis associated with neurofibromatosis: report of 2 cases in a single family and review of the literature'. *Surg Neurol*, 65 (6), pp. 595-603.

Ooki, T., Murata-Kamiya, N., Takahashi-Kanemitsu, A., Wu, W. & Hatakeyama, M. (2019) 'High-Molecular-Weight Hyaluronan Is a Hippo Pathway Ligand Directing Cell Density-Dependent Growth Inhibition via PAR1b'. *Dev Cell*, 49 (4), pp. 590-604.e599.

Osorio, D. S., Hu, J., Mitchell, C., Allen, J. C., Stanek, J., Hagiwara, M. & Karajannis, M. A. (2018) 'Effect of lapatinib on meningioma growth in adults with neurofibromatosis type 2'. *J Neurooncol*, 139 (3), pp. 749-755.

Ota, M. & Sasaki, H. (2008) 'Mammalian Tead proteins regulate cell proliferation and contact inhibition as transcriptional mediators of Hippo signaling'. *Development*, 135 (24), pp. 4059-4069.

Otsuka, G., Saito, K., Nagatani, T. & Yoshida, J. (2003) 'Age at symptom onset and long-term survival in patients with neurofibromatosis Type 2'. *J Neurosurg*, 99 (3), pp. 480-483.

Oudhoff, M. J., Freeman, S. A., Couzens, A. L., Antignano, F., Kuznetsova, E., Min, P. H., Northrop, J. P., Lehnertz, B., Barsyte-Lovejoy, D., Vedadi, M., Arrowsmith, C. H., Nishina, H., Gold, M. R., Rossi, F. M., Gingras, A. C. & Zaph, C. (2013) 'Control of the hippo pathway by Set7-dependent methylation of Yap'. *Dev Cell*, 26 (2), pp. 188-194.

Overweg-Plandsoen, W. C., Brouwer-Mladin, R., Merel, P., de Vries, L. & Bijlsma, E. K. (1996) 'Neurofibromatosis type 2 in an adolescent boy with polyneuropathy and a mutation in the NF2 gene'. *J Neurol*, 243 (10), pp. 724-726.

Pachow, D., Andrae, N., Kliese, N., Angenstein, F., Stork, O., Wilisch-Neumann, A., Kirches, E. & Mawrin, C. (2013) 'mTORC1 inhibitors suppress meningioma growth in mouse models'. *Clin Cancer Res*, 19 (5), pp. 1180-1189.

Pajtler, K. W., Witt, H., Sill, M., Jones, D. T., Hovestadt, V., Kratochwil, F., Wani, K., Tatevossian, R., Punchihewa, C., Johann, P., Reimand, J., Warnatz, H. J., Ryzhova, M., Mack, S., Ramaswamy, V., Capper, D., Schweizer, L., Sieber, L., Wittmann, A., Huang, Z., van Sluis, P., Volckmann, R., Koster, J., Versteeg, R., Fults, D., Toledano, H., Avigad, S., Hoffman, L. M., Donson, A. M., Foreman, N., Hewer, E., Zitterbart, K., Gilbert, M., Armstrong, T. S., Gupta, N., Allen, J. C., Karajannis, M. A., Zagzag, D., Hasselblatt, M., Kulozik, A. E., Witt, O., Collins, V. P., von Hoff, K., Rutkowski, S., Pietsch, T., Bader, G., Yaspo, M. L., von Deimling, A., Lichter, P., Taylor, M. D., Gilbertson, R., Ellison, D. W., Aldape, K., Korshunov, A., Kool, M. & Pfister, S. M. (2015) 'Molecular Classification of Ependymal Tumors across All CNS Compartments, Histopathological Grades, and Age Groups'. *Cancer Cell*, 27 (5), pp. 728-743.

Pantalacci, S., Tapon, N. & Léopold, P. (2003) 'The Salvador partner Hippo promotes apoptosis and cell-cycle exit in Drosophila'. *Nat Cell Biol*, 5 (10), pp. 921-927.

Paramasivam, M., Sarkeshik, A., Yates, J. R., 3rd, Fernandes, M. J. & McCollum, D. (2011) 'Angiomotin family proteins are novel activators of the LATS2 kinase tumor suppressor'. *Mol Biol Cell*, 22 (19), pp. 3725-3733.

Park, H. W., Kim, Y. C., Yu, B., Moroishi, T., Mo, J. S., Plouffe, S. W., Meng, Z., Lin, K. C., Yu, F. X., Alexander, C. M., Wang, C. Y. & Guan, K. L. (2015) 'Alternative Wnt Signaling Activates YAP/TAZ'. *Cell*, 162 (4), pp. 780-794.

Park, R., Moon, U. Y., Park, J. Y., Hughes, L. J., Johnson, R. L., Cho, S. H. & Kim, S. (2016a) 'Yap is required for ependymal integrity and is suppressed in LPA-induced hydrocephalus'. *Nat Commun*, 7 pp. 10329.

Park, Y. Y., Sohn, B. H., Johnson, R. L., Kang, M. H., Kim, S. B., Shim, J. J., Mangala, L. S., Kim, J. H., Yoo, J. E., Rodriguez-Aguayo, C., Pradeep, S., Hwang, J. E., Jang, H. J., Lee, H. S., Rupaimoole, R., Lopez-Berestein, G., Jeong, W., Park, I. S., Park, Y. N., Sood, A. K., Mills, G. B. & Lee, J. S. (2016b) 'Yes-associated protein 1 and transcriptional coactivator with PDZ-binding motif activate the mammalian target of rapamycin complex 1 pathway by regulating amino acid transporters in hepatocellular carcinoma'. *Hepatology*, 63 (1), pp. 159-172.

Parry, D. M., Eldridge, R., Kaiser-Kupfer, M. I., Bouzas, E. A., Pikus, A. & Patronas, N. (1994) 'Neurofibromatosis 2 (NF2): clinical characteristics of 63 affected individuals and clinical evidence for heterogeneity'. *Am J Med Genet*, 52 (4), pp. 450-461.

Parry, D. M., MacCollin, M. M., Kaiser-Kupfer, M. I., Pulaski, K., Nicholson, H. S., Bolesta, M., Eldridge, R. & Gusella, J. F. (1996) 'Germ-line mutations in the neurofibromatosis 2 gene: correlations with disease severity and retinal abnormalities'. *Am J Hum Genet*, 59 (3), pp. 529-539.

Pathmanaban, O. N., Sadler, K. V., Kamaly-Asl, I. D., King, A. T., Rutherford, S. A., Hammerbeck-Ward, C., McCabe, M. G., Kilday, J. P., Beetz, C., Poplawski, N. K., Evans, D. G. & Smith, M. J. (2017) 'Association of Genetic Predisposition With Solitary Schwannoma or Meningioma in Children and Young Adults'. *JAMA Neurol*, 74 (9), pp. 1123-1129.

Patronas, N. J., Courcoutsakis, N., Bromley, C. M., Katzman, G. L., MacCollin, M. & Parry, D. M. (2001) 'Intramedullary and spinal canal tumors in patients with neurofibromatosis 2: MR imaging findings and correlation with genotype'. *Radiology*, 218 (2), pp. 434-442.

Paulus, W., Sage, E. H., Liszka, U., Iruela-Arispe, M. L. & Jellinger, K. (1991) 'Increased levels of type VIII collagen in human brain tumours compared to normal brain tissue and non-neoplastic cerebral disorders'. *Br J Cancer*, 63 (3), pp. 367-371.

Pavel, M., Renna, M., Park, S. J., Menzies, F. M., Ricketts, T., Füllgrabe, J., Ashkenazi, A., Frake, R. A., Lombarte, A. C., Bento, C. F., Franze, K. & Rubinsztein, D. C. (2018) 'Contact inhibition controls cell survival and proliferation via YAP/TAZ-autophagy axis'. *Nat Commun*, 9 (1), pp. 2961.

Pefani, D. E., Pankova, D., Abraham, A. G., Grawenda, A. M., Vlahov, N., Scrace, S. & E, O. N. (2016) 'TGF-β Targets the Hippo Pathway Scaffold RASSF1A to Facilitate YAP/SMAD2 Nuclear Translocation'. *Mol Cell*, 63 (1), pp. 156-166.

Pelton, P. D., Sherman, L. S., Rizvi, T. A., Marchionni, M. A., Wood, P., Friedman, R. A. & Ratner, N. (1998) 'Ruffling membrane, stress fiber, cell spreading and proliferation abnormalities in human Schwannoma cells'. *Oncogene*, 17 (17), pp. 2195-2209.

Peng, C., Zhu, Y., Zhang, W., Liao, Q., Chen, Y., Zhao, X., Guo, Q., Shen, P., Zhen, B., Qian, X., Yang, D., Zhang, J. S., Xiao, D., Qin, W. & Pei, H. (2017) 'Regulation of the Hippo-YAP Pathway by Glucose Sensor O-GlcNAcylation'. *Mol Cell*, 68 (3), pp. 591-604.e595.

Perry, A., Giannini, C., Raghavan, R., Scheithauer, B. W., Banerjee, R., Margraf, L., Bowers, D. C., Lytle, R. A., Newsham, I. F. & Gutmann, D. H. (2001) 'Aggressive phenotypic and genotypic features in pediatric and NF2-associated meningiomas: a clinicopathologic study of 53 cases'. *J Neuropathol Exp Neurol*, 60 (10), pp. 994-1003.

Perry, A., Graffeo, C. S., Carlstrom, L. P., Raghunathan, A., Driscoll, C. L. W., Neff, B. A., Carlson, M. L., Parney, I. F., Link, M. J. & Van Gompel, J. J. (2019) 'Predominance of M1 subtype among tumor-associated macrophages in phenotypically aggressive sporadic vestibular schwannoma'. *J Neurosurg*, pp. 1-9.

Petrilli, A., Bott, M. & Fernández-Valle, C. (2013) 'Inhibition of SIRT2 in merlin/NF2-mutant Schwann cells triggers necrosis'. *Oncotarget*, 4 (12), pp. 2354-2365.

Petrilli, A., Copik, A., Posadas, M., Chang, L. S., Welling, D. B., Giovannini, M. & Fernández-Valle, C. (2014a) 'LIM domain kinases as potential therapeutic targets for neurofibromatosis type 2'. *Oncogene*, 33 (27), pp. 3571-3582.

Petrilli, A. M. & Fernández-Valle, C. (2016) 'Role of Merlin/NF2 inactivation in tumor biology'. *Oncogene*, 35 (5), pp. 537-548.

Petrilli, A. M., Fuse, M. A., Donnan, M. S., Bott, M., Sparrow, N. A., Tondera, D., Huffziger, J., Frenzel, C., Malany, C. S., Echeverri, C. J., Smith, L. & Fernández-Valle, C. (2014b) 'A chemical biology approach identified PI3K as a potential therapeutic target for neurofibromatosis type 2'. *Am J Transl Res*, 6 (5), pp. 471-493.

Peyre, M., Salaud, C., Clermont-Taranchon, E., Niwa-Kawakita, M., Goutagny, S., Mawrin, C., Giovannini, M. & Kalamarides, M. (2015) 'PDGF activation in PGDS-positive arachnoid cells induces meningioma formation in mice promoting tumor progression in combination with Nf2 and Cdkn2ab loss'. *Oncotarget*, 6 (32), pp. 32713-32722.

Peyre, M., Stemmer-Rachamimov, A., Clermont-Taranchon, E., Quentin, S., El-Taraya, N., Walczak, C., Volk, A., Niwa-Kawakita, M., Karboul, N., Giovannini, M. & Kalamarides, M. (2013) 'Meningioma progression in mice triggered by Nf2 and Cdkn2ab inactivation'. *Oncogene*, 32 (36), pp. 4264-4272.

Pineau, P., Marchio, A., Nagamori, S., Seki, S., Tiollais, P. & Dejean, A. (2003) 'Homozygous deletion scanning in hepatobiliary tumor cell lines reveals alternative pathways for liver carcinogenesis'. *Hepatology*, 37 (4), pp. 852-861.

Piotrowski, A., Xie, J., Liu, Y. F., Poplawski, A. B., Gomes, A. R., Madanecki, P., Fu, C., Crowley, M. R., Crossman, D. K., Armstrong, L., Babovic-Vuksanovic, D., Bergner, A., Blakeley, J. O., Blumenthal, A. L., Daniels, M. S., Feit, H., Gardner, K., Hurst, S., Kobelka, C., Lee, C., Nagy, R., Rauen, K. A., Slopis, J. M., Suwannarat, P., Westman, J. A., Zanko, A., Korf, B. R. & Messiaen, L. M. (2014) 'Germline loss-of-function mutations in LZTR1 predispose to an inherited disorder of multiple schwannomas'. *Nat Genet*, 46 (2), pp. 182-187.

Plotkin, S. R., Duda, D. G., Muzikansky, A., Allen, J., Blakeley, J., Rosser, T., Campian, J. L., Clapp, D. W., Fisher, M. J., Tonsgard, J., Ullrich, N., Thomas, C., Cutter, G., Korf, B., Packer, R. & Karajannis, M. A. (2019) 'Multicenter, Prospective, Phase II and Biomarker Study of High-Dose Bevacizumab as Induction Therapy in Patients With Neurofibromatosis Type 2 and Progressive Vestibular Schwannoma'. *J Clin Oncol*, 37 (35), pp. 3446-3454.

Plotkin, S. R., Merker, V. L., Halpin, C., Jennings, D., McKenna, M. J., Harris, G. J. & Barker, F. G., 2nd (2012) 'Bevacizumab for progressive vestibular schwannoma in neurofibromatosis type 2: a retrospective review of 31 patients'. *Otol Neurotol*, 33 (6), pp. 1046-1052.

Plotkin, S. R., O'Donnell, C. C., Curry, W. T., Bove, C. M., MacCollin, M. & Nunes, F. P. (2011) 'Spinal ependymomas in neurofibromatosis Type 2: a retrospective analysis of 55 patients'. *J Neurosurg Spine*, 14 (4), pp. 543-547.

Plotkin, S. R., Stemmer-Rachamimov, A. O., Barker, F. G., 2nd, Halpin, C., Padera, T. P., Tyrrell, A., Sorensen, A. G., Jain, R. K. & di Tomaso, E. (2009) 'Hearing improvement after bevacizumab in patients with neurofibromatosis type 2'. *N Engl J Med*, 361 (4), pp. 358-367.

Plouffe, S. W., Meng, Z., Lin, K. C., Lin, B., Hong, A. W., Chun, J. V. & Guan, K. L. (2016) 'Characterization of Hippo Pathway Components by Gene Inactivation'. *Mol Cell*, 64 (5), pp. 993-1008.

Pobbati, A. V., Chan, S. W., Lee, I., Song, H. & Hong, W. (2012) 'Structural and functional similarity between the Vgll1-TEAD and the YAP-TEAD complexes'. *Structure*, 20 (7), pp. 1135-1140.

Pobbati, A. V., Han, X., Hung, A. W., Weiguang, S., Huda, N., Chen, G. Y., Kang, C., Chia, C. S., Luo, X., Hong, W. & Poulsen, A. (2015) 'Targeting the Central Pocket in Human Transcription Factor TEAD as a Potential Cancer Therapeutic Strategy'. *Structure*, 23 (11), pp. 2076-2086.

Pobbati, A. V. & Hong, W. (2020) 'A combat with the YAP/TAZ-TEAD oncoproteins for cancer therapy'. *Theranostics*, 10 (8), pp. 3622-3635.

Poernbacher, I., Baumgartner, R., Marada, S. K., Edwards, K. & Stocker, H. (2012) 'Drosophila Pez acts in Hippo signaling to restrict intestinal stem cell proliferation'. *Curr Biol*, 22 (5), pp. 389-396.

Poitelon, Y., Lopez-Anido, C., Catignas, K., Berti, C., Palmisano, M., Williamson, C., Ameroso, D., Abiko, K., Hwang, Y., Gregorieff, A., Wrana, J. L., Asmani, M., Zhao, R., Sim, F. J., Wrabetz, L., Svaren, J. & Feltri, M. L. (2016) 'YAP and TAZ control peripheral myelination and the expression of laminin receptors in Schwann cells'. *Nat Neurosci*, 19 (7), pp. 879-887.

Poon, C. L., Lin, J. I., Zhang, X. & Harvey, K. F. (2011) 'The sterile 20-like kinase Tao-1 controls tissue growth by regulating the Salvador-Warts-Hippo pathway'. *Dev Cell*, 21 (5), pp. 896-906.

Poulikakos, P. I., Xiao, G. H., Gallagher, R., Jablonski, S., Jhanwar, S. C. & Testa, J. R. (2006) 'Re-expression of the tumor suppressor NF2/merlin inhibits invasiveness in mesothelioma cells and negatively regulates FAK'. *Oncogene*, 25 (44), pp. 5960-5968.

Praskova, M., Khoklatchev, A., Ortiz-Vega, S. & Avruch, J. (2004) 'Regulation of the MST1 kinase by autophosphorylation, by the growth inhibitory proteins, RASSF1 and NORE1, and by Ras'. *Biochem J*, 381 (Pt 2), pp. 453-462.

Praskova, M., Xia, F. & Avruch, J. (2008) 'MOBKL1A/MOBKL1B phosphorylation by MST1 and MST2 inhibits cell proliferation'. *Curr Biol*, 18 (5), pp. 311-321.

Proctor, D. T., Huang, J., Lama, S., Albakr, A., Van Marle, G. & Sutherland, G. R. (2019) 'Tumor-associated macrophage infiltration in meningioma'. *Neurooncol Adv*, 1 (1), pp. vdz018.

Puttmann, S., Senner, V., Braune, S., Hillmann, B., Exeler, R., Rickert, C. H. & Paulus, W. (2005) 'Establishment of a benign meningioma cell line by hTERT-mediated immortalization'. *Lab Invest*, 85 (9), pp. 1163-1171.

Pykett, M. J., Murphy, M., Harnish, P. R. & George, D. L. (1994) 'The neurofibromatosis 2 (NF2) tumor suppressor gene encodes multiple alternatively spliced transcripts'. *Hum Mol Genet*, 3 (4), pp. 559-564.

Qi, Q., Liu, X., Brat, D. J. & Ye, K. (2014) 'Merlin sumoylation is required for its tumor suppressor activity'. *Oncogene*, 33 (41), pp. 4893-4903.

Qi, Y., Yu, J., Han, W., Fan, X., Qian, H., Wei, H., Tsai, Y. H., Zhao, J., Zhang, W., Liu, Q., Meng, S., Wang, Y. & Wang, Z. (2016) 'A splicing isoform of TEAD4 attenuates the Hippo-YAP signalling to inhibit tumour proliferation'. *Nat Commun*, 7 pp. ncomms11840.

Qian, B., Deng, Y., Im, J. H., Muschel, R. J., Zou, Y., Li, J., Lang, R. A. & Pollard, J. W. (2009) 'A distinct macrophage population mediates metastatic breast cancer cell extravasation, establishment and growth'. *PLoS One*, 4 (8), pp. e6562.

Qian, B. Z., Li, J., Zhang, H., Kitamura, T., Zhang, J., Campion, L. R., Kaiser, E. A., Snyder, L. A. & Pollard, J. W. (2011) 'CCL2 recruits inflammatory monocytes to facilitate breast-tumour metastasis'. *Nature*, 475 (7355), pp. 222-225.

Qing, Y., Yin, F., Wang, W., Zheng, Y., Guo, P., Schozer, F., Deng, H. & Pan, D. (2014) 'The Hippo effector Yorkie activates transcription by interacting with a histone methyltransferase complex through Ncoa6'. *Elife*, 3

Quail, D. F. & Joyce, J. A. (2013) 'Microenvironmental regulation of tumor progression and metastasis'. *Nat Med*, 19 (11), pp. 1423-1437.

Ragel, B. T., Elam, I. L., Gillespie, D. L., Flynn, J. R., Kelly, D. A., Mabey, D., Feng, H., Couldwell, W. T. & Jensen, R. L. (2008) 'A novel model of intracranial meningioma in mice using luciferase-expressing meningioma cells. Laboratory investigation'. *J Neurosurg*, 108 (2), pp. 304-310.

Ragge, N. K., Baser, M. E., Klein, J., Nechiporuk, A., Sainz, J., Pulst, S. M. & Riccardi, V. M. (1995) 'Ocular abnormalities in neurofibromatosis 2'. *Am J Ophthalmol*, 120 (5), pp. 634-641.

Ragni, C. V., Diguet, N., Le Garrec, J. F., Novotova, M., Resende, T. P., Pop, S., Charon, N., Guillemot, L., Kitasato, L., Badouel, C., Dufour, A., Olivo-Marin, J. C., Trouvé, A., McNeill, H. & Meilhac, S. M. (2017) 'Amotl1 mediates sequestration of the Hippo effector Yap1 downstream of Fat4 to restrict heart growth'. *Nat Commun*, 8 pp. 14582.

Rajbhandari, P., Lopez, G., Capdevila, C., Salvatori, B., Yu, J., Rodriguez-Barrueco, R., Martinez, D., Yarmarkovich, M., Weichert-Leahey, N., Abraham, B. J., Alvarez, M. J., Iyer, A., Harenza, J. L., Oldridge, D., De Preter, K., Koster, J., Asgharzadeh, S., Seeger, R. C., Wei, J. S., Khan, J., Vandesompele, J., Mestdagh, P., Versteeg, R., Look, A. T., Young, R. A., Iavarone, A., Lasorella, A., Silva, J. M., Maris, J. M. & Califano, A. (2018) 'Cross-Cohort Analysis Identifies a TEAD4-MYCN Positive Feedback Loop as the Core Regulatory Element of High-Risk Neuroblastoma'. *Cancer Discov*, 8 (5), pp. 582-599.

Reggiani, F., Gobbi, G., Ciarrocchi, A. & Sancisi, V. (2021) 'YAP and TAZ Are Not Identical Twins'. *Trends Biochem Sci*, 46 (2), pp. 154-168.

Reinhold, W. C., Varma, S., Sousa, F., Sunshine, M., Abaan, O. D., Davis, S. R., Reinhold, S. W., Kohn, K. W., Morris, J., Meltzer, P. S., Doroshow, J. H. & Pommier, Y. (2014) 'NCI-60 whole exome sequencing and pharmacological CellMiner analyses'. *PLoS One*, 9 (7), pp. e101670.

Rennie, A. T., Side, L., Kerr, R. S., Anslow, P. & Pretorius, P. (2008) 'Intramedullary tumours in patients with neurofibromatosis type 2: MRI features associated with a favourable prognosis'. *Clin Radiol*, 63 (2), pp. 193-200.

Ribas, R., Moncaut, N., Siligan, C., Taylor, K., Cross, J. W., Rigby, P. W. & Carvajal, J. J. (2011) 'Members of the TEAD family of transcription factors regulate the expression of Myf5 in ventral somitic compartments'. *Dev Biol*, 355 (2), pp. 372-380.

Roche, P. H., Régis, J., Pellet, W., Thomassin, J. M., Grégoire, R., Dufour, H. & Peragut, J. C. (2000) '[Neurofibromatosis type 2. Preliminary results of gamma knife radiosurgery of vestibular schwannomas]'. *Neurochirurgie*, 46 (4), pp. 339-353; discussion 354.

Rong, R., Surace, E. I., Haipek, C. A., Gutmann, D. H. & Ye, K. (2004a) 'Serine 518 phosphorylation modulates merlin intramolecular association and binding to critical effectors important for NF2 growth suppression'. *Oncogene*, 23 (52), pp. 8447-8454.

Rong, R., Tang, X., Gutmann, D. H. & Ye, K. (2004b) 'Neurofibromatosis 2 (NF2) tumor suppressor merlin inhibits phosphatidylinositol 3-kinase through binding to PIKE-L'. *Proc Natl Acad Sci U S A*, 101 (52), pp. 18200-18205.

Rouleau, G. A., Merel, P., Lutchman, M., Sanson, M., Zucman, J., Marineau, C., Hoang-Xuan, K., Demczuk, S., Desmaze, C., Plougastel, B. & et al. (1993) 'Alteration in a new gene encoding a putative membrane-organizing protein causes neuro-fibromatosis type 2'. *Nature*, 363 (6429), pp. 515-521.

Rouleau, G. A., Wertelecki, W., Haines, J. L., Hobbs, W. J., Trofatter, J. A., Seizinger, B. R., Martuza, R. L., Superneau, D. W., Conneally, P. M. & Gusella, J. F. (1987) 'Genetic linkage of bilateral acoustic neurofibromatosis to a DNA marker on chromosome 22'. *Nature*, 329 (6136), pp. 246-248.

Rowe, J., Grainger, A., Walton, L., Radatz, M. & Kemeny, A. (2007) 'Safety of radiosurgery applied to conditions with abnormal tumor suppressor genes'. *Neurosurgery*, 60 (5), pp. 860-864; discussion 860-864.

Rowe, J. G., Radatz, M. W., Walton, L., Soanes, T., Rodgers, J. & Kemeny, A. A. (2003) 'Clinical experience with gamma knife stereotactic radiosurgery in the management of vestibular schwannomas secondary to type 2 neurofibromatosis'. *J Neurol Neurosurg Psychiatry*, 74 (9), pp. 1288-1293.

Ruffell, B., Chang-Strachan, D., Chan, V., Rosenbusch, A., Ho, C. M., Pryer, N., Daniel, D., Hwang, E. S., Rugo, H. S. & Coussens, L. M. (2014) 'Macrophage IL-10 blocks CD8+ T cell-dependent responses to chemotherapy by suppressing IL-12 expression in intratumoral dendritic cells'. *Cancer Cell*, 26 (5), pp. 623-637.

Ruggieri, M., Iannetti, P., Polizzi, A., La Mantia, I., Spalice, A., Giliberto, O., Platania, N., Gabriele, A. L., Albanese, V. & Pavone, L. (2005) 'Earliest clinical manifestations and natural history of neurofibromatosis type 2 (NF2) in childhood: a study of 24 patients'. *Neuropediatrics*, 36 (1), pp. 21-34.

Ryseck, R. P., Macdonald-Bravo, H., Mattéi, M. G. & Bravo, R. (1991) 'Structure, mapping, and expression of fisp-12, a growth factor-inducible gene encoding a secreted cysteine-rich protein'. *Cell Growth Differ*, 2 (5), pp. 225-233.

Sagers, J. E., Sahin, M. I., Moon, I., Ahmed, S. G., Stemmer-Rachamimov, A., Brenner, G. J. & Stankovic, K. M. (2019) 'NLRP3 inflammasome activation in human vestibular schwannoma: Implications for tumor-induced hearing loss'. *Hear Res*, 381 pp. 107770.

Sainio, M., Zhao, F., Heiska, L., Turunen, O., den Bakker, M., Zwarthoff, E., Lutchman, M., Rouleau, G. A., Jääskeläinen, J., Vaheri, A. & Carpén, O. (1997) 'Neurofibromatosis 2 tumor suppressor protein

colocalizes with ezrin and CD44 and associates with actin-containing cytoskeleton'. *J Cell Sci*, 110 (Pt 18) pp. 2249-2260.

Sainz, J., Huynh, D. P., Figueroa, K., Ragge, N. K., Baser, M. E. & Pulst, S. M. (1994) 'Mutations of the neurofibromatosis type 2 gene and lack of the gene product in vestibular schwannomas'. *Hum Mol Genet*, 3 (6), pp. 885-891.

Sakamoto, K. M., Kim, K. B., Kumagai, A., Mercurio, F., Crews, C. M. & Deshaies, R. J. (2001) 'Protacs: chimeric molecules that target proteins to the Skp1-Cullin-F box complex for ubiquitination and degradation'. *Proc Natl Acad Sci U S A*, 98 (15), pp. 8554-8559.

Salokorpi, N., Yrjänä, S., Tuominen, H., Karttunen, A., Heljasvaara, R., Pihlajaniemi, T., Heikkinen, E. & Koivukangas, J. (2013) 'Expression of VEGF and collagen XVIII in meningiomas: correlations with histopathological and MRI characteristics'. *Acta Neurochir (Wien)*, 155 (6), pp. 989-996; discussion 996.

Samanta, S., Guru, S., Elaimy, A. L., Amante, J. J., Ou, J., Yu, J., Zhu, L. J. & Mercurio, A. M. (2018) 'IMP3 Stabilization of WNT5B mRNA Facilitates TAZ Activation in Breast Cancer'. *Cell Rep*, 23 (9), pp. 2559-2567.

Samii, M., Matthies, C. & Tatagiba, M. (1997) 'Management of vestibular schwannomas (acoustic neuromas): auditory and facial nerve function after resection of 120 vestibular schwannomas in patients with neurofibromatosis 2'. *Neurosurgery*, 40 (4), pp. 696-705; discussion 705-696.

Sanchez-Vega, F., Mina, M., Armenia, J., Chatila, W. K., Luna, A., La, K. C., Dimitriadoy, S., Liu, D. L., Kantheti, H. S., Saghafinia, S., Chakravarty, D., Daian, F., Gao, Q., Bailey, M. H., Liang, W. W., Foltz, S. M., Shmulevich, I., Ding, L., Heins, Z., Ochoa, A., Gross, B., Gao, J., Zhang, H., Kundra, R., Kandoth, C., Bahceci, I., Dervishi, L., Dogrusoz, U., Zhou, W., Shen, H., Laird, P. W., Way, G. P., Greene, C. S., Liang, H., Xiao, Y., Wang, C., Iavarone, A., Berger, A. H., Bivona, T. G., Lazar, A. J., Hammer, G. D., Giordano, T., Kwong, L. N., McArthur, G., Huang, C., Tward, A. D., Frederick, M. J., McCormick, F., Meyerson, M., Van Allen, E. M., Cherniack, A. D., Ciriello, G., Sander, C. & Schultz, N. (2018) 'Oncogenic Signaling Pathways in The Cancer Genome Atlas'. *Cell*, 173 (2), pp. 321-337.e310.

Sangaletti, S., Di Carlo, E., Gariboldi, S., Miotti, S., Cappetti, B., Parenza, M., Rumio, C., Brekken, R. A., Chiodoni, C. & Colombo, M. P. (2008) 'Macrophage-derived SPARC bridges tumor cell-extracellular matrix interactions toward metastasis'. *Cancer Res*, 68 (21), pp. 9050-9059.

Savage, N. D., de Boer, T., Walburg, K. V., Joosten, S. A., van Meijgaarden, K., Geluk, A. & Ottenhoff, T. H. (2008) 'Human anti-inflammatory macrophages induce Foxp3+ GITR+ CD25+ regulatory T cells, which suppress via membrane-bound TGFbeta-1'. *J Immunol*, 181 (3), pp. 2220-2226.

Scherer, S. S. & Gutmann, D. H. (1996) 'Expression of the neurofibromatosis 2 tumor suppressor gene product, merlin, in Schwann cells'. *J Neurosci Res*, 46 (5), pp. 595-605.

Schieffer, K. M., Agarwal, V., LaHaye, S., Miller, K. E., Koboldt, D. C., Lichtenberg, T., Leraas, K., Brennan, P., Kelly, B. J., Crist, E., Rusin, J., Finlay, J. L., Osorio, D. S., Sribnick, E. A., Leonard, J. R.,

Feldman, A., Orr, B. A., Serrano, J., Vasudevaraja, V., Snuderl, M., White, P., Magrini, V., Wilson, R. K., Mardis, E. R., Boué, D. R. & Cottrell, C. E. (2021) 'YAP1-FAM118B Fusion Defines a Rare Subset of Childhood and Young Adulthood Meningiomas'. *Am J Surg Pathol*, 45 (3), pp. 329-340.

Schlegelmilch, K., Mohseni, M., Kirak, O., Pruszak, J., Rodriguez, J. R., Zhou, D., Kreger, B. T., Vasioukhin, V., Avruch, J., Brummelkamp, T. R. & Camargo, F. D. (2011) 'Yap1 acts downstream of alpha-catenin to control epidermal proliferation'. *Cell*, 144 (5), pp. 782-795.

Schulz, A., Baader, S. L., Niwa-Kawakita, M., Jung, M. J., Bauer, R., Garcia, C., Zoch, A., Schacke, S., Hagel, C., Mautner, V. F., Hanemann, C. O., Dun, X. P., Parkinson, D. B., Weis, J., Schröder, J. M., Gutmann, D. H., Giovannini, M. & Morrison, H. (2013) 'Merlin isoform 2 in neurofibromatosis type 2-associated polyneuropathy'. *Nat Neurosci*, 16 (4), pp. 426-433.

Schulz, A., Buttner, R., Hagel, C., Baader, S. L., Kluwe, L., Salamon, J., Mautner, V. F., Mindos, T., Parkinson, D. B., Gehlhausen, J. R., Clapp, D. W. & Morrison, H. (2016) 'The importance of nerve microenvironment for schwannoma development'. *Acta Neuropathol*, 132 (2), pp. 289-307.

Schulz, A., Kyselyova, A., Baader, S. L., Jung, M. J., Zoch, A., Mautner, V. F., Hagel, C. & Morrison, H. (2014) 'Neuronal merlin influences ERBB2 receptor expression on Schwann cells through neuregulin 1 type III signalling'. *Brain*, 137 (Pt 2), pp. 420-432.

Schulz, C., Gomez Perdiguero, E., Chorro, L., Szabo-Rogers, H., Cagnard, N., Kierdorf, K., Prinz, M., Wu, B., Jacobsen, S. E., Pollard, J. W., Frampton, J., Liu, K. J. & Geissmann, F. (2012) 'A lineage of myeloid cells independent of Myb and hematopoietic stem cells'. *Science*, 336 (6077), pp. 86-90.

Schwitalla, S., Fingerle, A. A., Cammareri, P., Nebelsiek, T., Goktuna, S. I., Ziegler, P. K., Canli, O., Heijmans, J., Huels, D. J., Moreaux, G., Rupec, R. A., Gerhard, M., Schmid, R., Barker, N., Clevers, H., Lang, R., Neumann, J., Kirchner, T., Taketo, M. M., van den Brink, G. R., Sansom, O. J., Arkan, M. C. & Greten, F. R. (2013) 'Intestinal tumorigenesis initiated by dedifferentiation and acquisition of stem-cell-like properties'. *Cell*, 152 (1-2), pp. 25-38.

Seizinger, B. R., Rouleau, G. A., Ozelius, L. J., Lane, A. H., Faryniarz, A. G., Chao, M. V., Huson, S., Korf, B. R., Parry, D. M., Pericak-Vance, M. A. & et al. (1987) 'Genetic linkage of von Recklinghausen neurofibromatosis to the nerve growth factor receptor gene'. *Cell*, 49 (5), pp. 589-594.

Sekido, Y., Pass, H. I., Bader, S., Mew, D. J., Christman, M. F., Gazdar, A. F. & Minna, J. D. (1995) 'Neurofibromatosis type 2 (NF2) gene is somatically mutated in mesothelioma but not in lung cancer'. *Cancer Res*, 55 (6), pp. 1227-1231.

Sekine, S., Kiyono, T., Ryo, E., Ogawa, R., Wakai, S., Ichikawa, H., Suzuki, K., Arai, S., Tsuta, K., Ishida, M., Sasajima, Y., Goshima, N., Yamazaki, N. & Mori, T. (2019) 'Recurrent YAP1-MAML2 and YAP1-NUTM1 fusions in poroma and porocarcinoma'. *J Clin Invest*, 129 (9), pp. 3827-3832.

Seo, E., Basu-Roy, U., Gunaratne, P. H., Coarfa, C., Lim, D. S., Basilico, C. & Mansukhani, A. (2013) 'SOX2 regulates YAP1 to maintain stemness and determine cell fate in the osteo-adipo lineage'. *Cell Rep*, 3 (6), pp. 2075-2087.

Serrano, I., McDonald, P. C., Lock, F., Muller, W. J. & Dedhar, S. (2013) 'Inactivation of the Hippo tumour suppressor pathway by integrin-linked kinase'. *Nat Commun*, 4 pp. 2976.

Shalem, O., Sanjana, N. E., Hartenian, E., Shi, X., Scott, D. A., Mikkelson, T., Heckl, D., Ebert, B. L., Root, D. E., Doench, J. G. & Zhang, F. (2014) 'Genome-scale CRISPR-Cas9 knockout screening in human cells'. *Science*, 343 (6166), pp. 84-87.

Shao, D. D., Xue, W., Krall, E. B., Bhutkar, A., Piccioni, F., Wang, X., Schinzel, A. C., Sood, S., Rosenbluh, J., Kim, J. W., Zwang, Y., Roberts, T. M., Root, D. E., Jacks, T. & Hahn, W. C. (2014) 'KRAS and YAP1 converge to regulate EMT and tumor survival'. *Cell*, 158 (1), pp. 171-184.

Shaw, R. J., McClatchey, A. I. & Jacks, T. (1998) 'Regulation of the neurofibromatosis type 2 tumor suppressor protein, merlin, by adhesion and growth arrest stimuli'. *J Biol Chem*, 273 (13), pp. 7757-7764.

Shaw, R. J., Paez, J. G., Curto, M., Yaktine, A., Pruitt, W. M., Saotome, I., O'Bryan, J. P., Gupta, V., Ratner, N., Der, C. J., Jacks, T. & McClatchey, A. I. (2001) 'The Nf2 tumor suppressor, merlin, functions in Rac-dependent signaling'. *Dev Cell*, 1 (1), pp. 63-72.

Sheikh, H. A., Tometsko, M., Niehouse, L., Aldeeb, D., Swalsky, P., Finkelstein, S., Barnes, E. L. & Hunt, J. L. (2004) 'Molecular genotyping of medullary thyroid carcinoma can predict tumor recurrence'. *Am J Surg Pathol*, 28 (1), pp. 101-106.

Sheng, X., Li, W. B., Wang, D. L., Chen, K. H., Cao, J. J., Luo, Z., He, J., Li, M. C., Liu, W. J. & Yu, C. (2015) 'YAP is closely correlated with castration-resistant prostate cancer, and downregulation of YAP reduces proliferation and induces apoptosis of PC-3 cells'. *Mol Med Rep*, 12 (4), pp. 4867-4876.

Sher, I., Hanemann, C. O., Karplus, P. A. & Bretscher, A. (2012) 'The tumor suppressor merlin controls growth in its open state, and phosphorylation converts it to a less-active more-closed state'. *Dev Cell*, 22 (4), pp. 703-705.

Sherman, L., Xu, H. M., Geist, R. T., Saporito-Irwin, S., Howells, N., Ponta, H., Herrlich, P. & Gutmann, D. H. (1997) 'Interdomain binding mediates tumor growth suppression by the NF2 gene product'. *Oncogene*, 15 (20), pp. 2505-2509.

Sherman, L. S., Rizvi, T. A., Karyala, S. & Ratner, N. (2000) 'CD44 enhances neuregulin signaling by Schwann cells'. *J Cell Biol*, 150 (5), pp. 1071-1084.

Shi, Y., Cao, T., Sun, Y., Xia, J., Wang, P. & Ma, J. (2019) 'Nitidine Chloride inhibits cell proliferation and invasion via downregulation of YAP expression in prostate cancer cells'. *Am J Transl Res*, 11 (2), pp. 709-720.

Shimizu, T., Seto, A., Maita, N., Hamada, K., Tsukita, S., Tsukita, S. & Hakoshima, T. (2002) 'Structural basis for neurofibromatosis type 2. Crystal structure of the merlin FERM domain'. *J Biol Chem*, 277 (12), pp. 10332-10336.

Shin, E. K., Lee, S. H., Cho, S. H., Jung, S., Yoon, S. H., Park, S. W., Park, J. S., Uh, S. T., Kim, Y. K., Kim, Y. H., Choi, J. S., Park, B. L., Shin, H. D. & Park, C. S. (2010) 'Association between colony-stimulating factor 1 receptor gene polymorphisms and asthma risk'. *Hum Genet*, 128 (3), pp. 293-302.

Shreberk-Shaked, M., Dassa, B., Sinha, S., Di Agostino, S., Azuri, I., Mukherjee, S., Aylon, Y., Blandino, G., Ruppin, E. & Oren, M. (2020) 'A Division of Labor between YAP and TAZ in Non-Small Cell Lung Cancer'. *Cancer Res*, 80 (19), pp. 4145-4157.

Shrestha, Y., Schafer, E. J., Boehm, J. S., Thomas, S. R., He, F., Du, J., Wang, S., Barretina, J., Weir, B. A., Zhao, J. J., Polyak, K., Golub, T. R., Beroukhim, R. & Hahn, W. C. (2012) 'PAK1 is a breast cancer oncogene that coordinately activates MAPK and MET signaling'. *Oncogene*, 31 (29), pp. 3397-3408.

Sica, A. & Mantovani, A. (2012) 'Macrophage plasticity and polarization: in vivo veritas'. *J Clin Invest*, 122 (3), pp. 787-795.

Siddiqui, A. A. & Shah, A. A. (2004) 'Complete surgical excision of intramedullary schwannoma at the craniovertebral junction in neurofibromatosis type-2'. *Br J Neurosurg*, 18 (2), pp. 193-196.

Sievers, P., Chiang, J., Schrimpf, D., Stichel, D., Paramasivam, N., Sill, M., Gayden, T., Casalini, B., Reuss, D. E., Dalton, J., Pajtler, K. W., Hänggi, D., Herold-Mende, C., Rushing, E., Korshunov, A., Mawrin, C., Weller, M., Schlesner, M., Wick, W., Jabado, N., Jones, D. T. W., Pfister, S. M., von Deimling, A., Ellison, D. W. & Sahm, F. (2020) 'YAP1-fusions in pediatric NF2-wildtype meningioma'. *Acta Neuropathol*, 139 (1), pp. 215-218.

Silvis, M. R., Kreger, B. T., Lien, W. H., Klezovitch, O., Rudakova, G. M., Camargo, F. D., Lantz, D. M., Seykora, J. T. & Vasioukhin, V. (2011) 'alpha-catenin is a tumor suppressor that controls cell accumulation by regulating the localization and activity of the transcriptional coactivator Yap1'. *Sci Signal*, 4 (174), pp. ra33.

Simon, E., Faucheux, C., Zider, A., Thézé, N. & Thiébaud, P. (2016) 'From vestigial to vestigial-like: the Drosophila gene that has taken wing'. *Dev Genes Evol*, 226 (4), pp. 297-315.

Skibinski, A., Breindel, J. L., Prat, A., Galván, P., Smith, E., Rolfs, A., Gupta, P. B., LaBaer, J. & Kuperwasser, C. (2014) 'The Hippo transducer TAZ interacts with the SWI/SNF complex to regulate breast epithelial lineage commitment'. *Cell Rep*, 6 (6), pp. 1059-1072.

Slemmons, K. K., Crose, L. E., Rudzinski, E., Bentley, R. C. & Linardic, C. M. (2015) 'Role of the YAP Oncoprotein in Priming Ras-Driven Rhabdomyosarcoma'. *PLoS One*, 10 (10), pp. e0140781.

Smole, Z., Thoma, C. R., Applegate, K. T., Duda, M., Gutbrodt, K. L., Danuser, G. & Krek, W. (2014) 'Tumor suppressor NF2/Merlin is a microtubule stabilizer'. *Cancer Res*, 74 (1), pp. 353-362.

Sobel, R. A. (1993) 'Vestibular (acoustic) schwannomas: histologic features in neurofibromatosis 2 and in unilateral cases'. *J Neuropathol Exp Neurol*, 52 (2), pp. 106-113.

Song, H., Mak, K. K., Topol, L., Yun, K., Hu, J., Garrett, L., Chen, Y., Park, O., Chang, J., Simpson, R. M., Wang, C. Y., Gao, B., Jiang, J. & Yang, Y. (2010) 'Mammalian Mst1 and Mst2 kinases play essential roles in organ size control and tumor suppression'. *Proc Natl Acad Sci U S A*, 107 (4), pp. 1431-1436.

Song, S., Honjo, S., Jin, J., Chang, S. S., Scott, A. W., Chen, Q., Kalhor, N., Correa, A. M., Hofstetter, W. L., Albarracin, C. T., Wu, T. T., Johnson, R. L., Hung, M. C. & Ajani, J. A. (2015) 'The Hippo Coactivator YAP1 Mediates EGFR Overexpression and Confers Chemoresistance in Esophageal Cancer'. *Clin Cancer Res*, 21 (11), pp. 2580-2590.

Sorrentino, G., Ruggeri, N., Specchia, V., Cordenonsi, M., Mano, M., Dupont, S., Manfrin, A., Ingallina, E., Sommaggio, R., Piazza, S., Rosato, A., Piccolo, S. & Del Sal, G. (2014) 'Metabolic control of YAP and TAZ by the mevalonate pathway'. *Nat Cell Biol*, 16 (4), pp. 357-366.

Sperfeld, A. D., Hein, C., Schröder, J. M., Ludolph, A. C. & Hanemann, C. O. (2002) 'Occurrence and characterization of peripheral nerve involvement in neurofibromatosis type 2'. *Brain*, 125 (Pt 5), pp. 996-1004.

Stanley, E. R. & Chitu, V. (2014) 'CSF-1 receptor signaling in myeloid cells'. *Cold Spring Harb Perspect Biol*, 6 (6),

Stein, C., Bardet, A. F., Roma, G., Bergling, S., Clay, I., Ruchti, A., Agarinis, C., Schmelzle, T., Bouwmeester, T., Schübeler, D. & Bauer, A. (2015) 'YAP1 Exerts Its Transcriptional Control via TEAD-Mediated Activation of Enhancers'. *PLoS Genet*, 11 (8), pp. e1005465.

Stickney, J. T., Bacon, W. C., Rojas, M., Ratner, N. & Ip, W. (2004) 'Activation of the tumor suppressor merlin modulates its interaction with lipid rafts'. *Cancer Res*, 64 (8), pp. 2717-2724.

Strano, S., Munarriz, E., Rossi, M., Castagnoli, L., Shaul, Y., Sacchi, A., Oren, M., Sudol, M., Cesareni, G. & Blandino, G. (2001) 'Physical interaction with Yes-associated protein enhances p73 transcriptional activity'. *J Biol Chem*, 276 (18), pp. 15164-15173.

Straßburger, K., Tiebe, M., Pinna, F., Breuhahn, K. & Teleman, A. A. (2012) 'Insulin/IGF signaling drives cell proliferation in part via Yorkie/YAP'. *Dev Biol*, 367 (2), pp. 187-196.

Striedinger, K., VandenBerg, S. R., Baia, G. S., McDermott, M. W., Gutmann, D. H. & Lal, A. (2008) 'The neurofibromatosis 2 tumor suppressor gene product, merlin, regulates human meningioma cell growth by signaling through YAP'. *Neoplasia*, 10 (11), pp. 1204-1212.

Stuehr, D. J. & Marletta, M. A. (1985) 'Mammalian nitrate biosynthesis: mouse macrophages produce nitrite and nitrate in response to Escherichia coli lipopolysaccharide'. *Proc Natl Acad Sci U S A*, 82 (22), pp. 7738-7742.

Su, T., Ludwig, M. Z., Xu, J. & Fehon, R. G. (2017) 'Kibra and Merlin Activate the Hippo Pathway Spatially Distinct from and Independent of Expanded'. *Dev Cell*, 40 (5), pp. 478-490.e473.

Sughrue, M. E., Kaur, R., Kane, A. J., Rutkowski, M. J., Yang, I., Pitts, L. H., Tihan, T. & Parsa, A. T. (2011) 'Intratumoral hemorrhage and fibrosis in vestibular schwannoma: a possible mechanism for hearing loss'. *J Neurosurg*, 114 (2), pp. 386-393.

Sun, Z., Xu, R., Li, X., Ren, W., Ou, C., Wang, Q., Zhang, H., Zhang, X., Ma, J., Wang, H. & Li, G. (2015) 'Prognostic Value of Yes-Associated Protein 1 (YAP1) in Various Cancers: A Meta-Analysis'. *PLoS One*, 10 (8), pp. e0135119.

Surace, E. I., Haipek, C. A. & Gutmann, D. H. (2004) 'Effect of merlin phosphorylation on neurofibromatosis 2 (NF2) gene function'. *Oncogene*, 23 (2), pp. 580-587.

Szulzewsky, F., Arora, S., Arakaki, A. K. S., Sievers, P., Almiron Bonnin, D. A., Paddison, P. J., Sahm, F., Cimino, P. J., Gujral, T. S. & Holland, E. C. (2022) 'Both YAP1-MAML2 and constitutively active YAP1 drive the formation of tumors that resemble NF2 mutant meningiomas in mice'. *Genes Dev*,

Tamm, C., Böwer, N. & Annerén, C. (2011) 'Regulation of mouse embryonic stem cell self-renewal by a Yes-YAP-TEAD2 signaling pathway downstream of LIF'. *J Cell Sci*, 124 (Pt 7), pp. 1136-1144.

Tamura, R., Fujioka, M., Morimoto, Y., Ohara, K., Kosugi, K., Oishi, Y., Sato, M., Ueda, R., Fujiwara, H., Hikichi, T., Noji, S., Oishi, N., Ogawa, K., Kawakami, Y., Ohira, T., Yoshida, K. & Toda, M. (2019) 'A VEGF receptor vaccine demonstrates preliminary efficacy in neurofibromatosis type 2'. *Nat Commun*, 10 (1), pp. 5758.

Tanaka, K., Sato, C., Maeda, Y., Koike, M., Matsutani, M., Yamada, K. & Miyaki, M. (1989) 'Establishment of a human malignant meningioma cell line with amplified c-myc oncogene'. *Cancer*, 64 (11), pp. 2243-2249.

Tanas, M. R., Sboner, A., Oliveira, A. M., Erickson-Johnson, M. R., Hespelt, J., Hanwright, P. J., Flanagan, J., Luo, Y., Fenwick, K., Natrajan, R., Mitsopoulos, C., Zvelebil, M., Hoch, B. L., Weiss, S. W., Debiec-Rychter, M., Sciot, R., West, R. B., Lazar, A. J., Ashworth, A., Reis-Filho, J. S., Lord, C. J., Gerstein, M. B., Rubin, M. A. & Rubin, B. P. (2011) 'Identification of a disease-defining gene fusion in epithelioid hemangioendothelioma'. *Sci Transl Med*, 3 (98), pp. 98ra82.

Tang, T. T., Konradi, A. W., Feng, Y., Peng, X., Ma, M., Li, J., Yu, F. X., Guan, K. L. & Post, L. (2021) 'Small Molecule Inhibitors of TEAD Auto-palmitoylation Selectively Inhibit Proliferation and Tumor Growth of NF2-deficient Mesothelioma'. *Mol Cancer Ther*, 20 (6), pp. 986-998.

Tang, X., Jang, S. W., Wang, X., Liu, Z., Bahr, S. M., Sun, S. Y., Brat, D., Gutmann, D. H. & Ye, K. (2007) 'Akt phosphorylation regulates the tumour-suppressor merlin through ubiquitination and degradation'. *Nat Cell Biol*, 9 (10), pp. 1199-1207.

Taniguchi, K., Moroishi, T., de Jong, P. R., Krawczyk, M., Grebbin, B. M., Luo, H., Xu, R. H., Golob-Schwarzl, N., Schweiger, C., Wang, K., Di Caro, G., Feng, Y., Fearon, E. R., Raz, E., Kenner, L., Farin, H. F., Guan, K. L., Haybaeck, J., Datz, C., Zhang, K. & Karin, M. (2017) 'YAP-IL-6ST autoregulatory loop activated on APC loss controls colonic tumorigenesis'. *Proc Natl Acad Sci U S A*, 114 (7), pp. 1643-1648.

Tapon, N., Harvey, K. F., Bell, D. W., Wahrer, D. C., Schiripo, T. A., Haber, D. & Hariharan, I. K. (2002) 'salvador Promotes both cell cycle exit and apoptosis in Drosophila and is mutated in human cancer cell lines'. *Cell*, 110 (4), pp. 467-478.

Thaxton, C., Lopera, J., Bott, M., Baldwin, M. E., Kalidas, P. & Fernandez-Valle, C. (2007) 'Phosphorylation of the NF2 tumor suppressor in Schwann cells is mediated by Cdc42-Pak and requires paxillin binding'. *Mol Cell Neurosci*, 34 (2), pp. 231-242.

Thaxton, C., Lopera, J., Bott, M. & Fernandez-Valle, C. (2008) 'Neuregulin and laminin stimulate phosphorylation of the NF2 tumor suppressor in Schwann cells by distinct protein kinase A and p21-activated kinase-dependent pathways'. *Oncogene*, 27 (19), pp. 2705-2715.

Thomas, P. K., King, R. H., Chiang, T. R., Scaravilli, F., Sharma, A. K. & Downie, A. W. (1990) 'Neurofibromatous neuropathy'. *Muscle Nerve*, 13 (2), pp. 93-101.

Thurneysen, C., Opitz, I., Kurtz, S., Weder, W., Stahel, R. A. & Felley-Bosco, E. (2009) 'Functional inactivation of NF2/merlin in human mesothelioma'. *Lung Cancer*, 64 (2), pp. 140-147.

Tian, W., Yu, J., Tomchick, D. R., Pan, D. & Luo, X. (2010) 'Structural and functional analysis of the YAP-binding domain of human TEAD2'. *Proc Natl Acad Sci U S A*, 107 (16), pp. 7293-7298.

Tikoo, A., Varga, M., Ramesh, V., Gusella, J. & Maruta, H. (1994) 'An anti-Ras function of neurofibromatosis type 2 gene product (NF2/Merlin)'. *J Biol Chem*, 269 (38), pp. 23387-23390.

Trivedi, R., Byrne, J., Huson, S. M. & Donaghy, M. (2000) 'Focal amyotrophy in neurofibromatosis 2'. *J Neurol Neurosurg Psychiatry*, 69 (2), pp. 257-261.

Trofatter, J. A., MacCollin, M. M., Rutter, J. L., Murrell, J. R., Duyao, M. P., Parry, D. M., Eldridge, R., Kley, N., Menon, A. G., Pulaski, K. & et al. (1993) 'A novel moesin-, ezrin-, radixin-like gene is a candidate for the neurofibromatosis 2 tumor suppressor'. *Cell*, 72 (5), pp. 791-800.

Truett, G. E., Heeger, P., Mynatt, R. L., Truett, A. A., Walker, J. A. & Warman, M. L. (2000) 'Preparation of PCR-quality mouse genomic DNA with hot sodium hydroxide and tris (HotSHOT)'. *Biotechniques*, 29 (1), pp. 52, 54.

Tuchen, M., Wilisch-Neumann, A., Daniel, E. A., Baldauf, L., Pachow, D., Scholz, J., Angenstein, F., Stork, O., Kirches, E. & Mawrin, C. (2017) 'Receptor tyrosine kinase inhibition by regorafenib/sorafenib inhibits growth and invasion of meningioma cells'. *Eur J Cancer*, 73 pp. 9-21.

Udan, R. S., Kango-Singh, M., Nolo, R., Tao, C. & Halder, G. (2003) 'Hippo promotes proliferation arrest and apoptosis in the Salvador/Warts pathway'. *Nat Cell Biol*, 5 (10), pp. 914-920.

Varelas, X., Sakuma, R., Samavarchi-Tehrani, P., Peerani, R., Rao, B. M., Dembowy, J., Yaffe, M. B., Zandstra, P. W. & Wrana, J. L. (2008) 'TAZ controls Smad nucleocytoplasmic shuttling and regulates human embryonic stem-cell self-renewal'. *Nat Cell Biol*, 10 (7), pp. 837-848.

Varelas, X., Samavarchi-Tehrani, P., Narimatsu, M., Weiss, A., Cockburn, K., Larsen, B. G., Rossant, J. & Wrana, J. L. (2010) 'The Crumbs complex couples cell density sensing to Hippo-dependent control of the TGF-β-SMAD pathway'. *Dev Cell*, 19 (6), pp. 831-844.

Vassilev, A., Kaneko, K. J., Shu, H., Zhao, Y. & DePamphilis, M. L. (2001) 'TEAD/TEF transcription factors utilize the activation domain of YAP65, a Src/Yes-associated protein localized in the cytoplasm'. *Genes Dev*, 15 (10), pp. 1229-1241.

Viskochil, D., Buchberg, A. M., Xu, G., Cawthon, R. M., Stevens, J., Wolff, R. K., Culver, M., Carey, J. C., Copeland, N. G., Jenkins, N. A. & et al. (1990) 'Deletions and a translocation interrupt a cloned gene at the neurofibromatosis type 1 locus'. *Cell*, 62 (1), pp. 187-192.

von Gise, A., Lin, Z., Schlegelmilch, K., Honor, L. B., Pan, G. M., Buck, J. N., Ma, Q., Ishiwata, T., Zhou, B., Camargo, F. D. & Pu, W. T. (2012) 'YAP1, the nuclear target of Hippo signaling, stimulates heart growth through cardiomyocyte proliferation but not hypertrophy'. *Proc Natl Acad Sci U S A*, 109 (7), pp. 2394-2399.

Wada, K., Itoga, K., Okano, T., Yonemura, S. & Sasaki, H. (2011) 'Hippo pathway regulation by cell morphology and stress fibers'. *Development*, 138 (18), pp. 3907-3914.

Wallace, M. R., Marchuk, D. A., Andersen, L. B. & Collins, F. S. (1990a) 'Response: Type 1 Neurofibromatosis Gene: Correction'. *Science*, 250 (4988), pp. 1749-1749.

Wallace, M. R., Marchuk, D. A., Andersen, L. B., Letcher, R., Odeh, H. M., Saulino, A. M., Fountain, J. W., Brereton, A., Nicholson, J., Mitchell, A. L. & et al. (1990b) 'Type 1 neurofibromatosis gene: identification of a large transcript disrupted in three NF1 patients'. *Science*, 249 (4965), pp. 181-186.

Wan, S., Zhao, E., Kryczek, I., Vatan, L., Sadovskaya, A., Ludema, G., Simeone, D. M., Zou, W. & Welling, T. H. (2014) 'Tumor-associated macrophages produce interleukin 6 and signal via STAT3 to promote expansion of human hepatocellular carcinoma stem cells'. *Gastroenterology*, 147 (6), pp. 1393-1404.

Wang, C., Nie, Z., Zhou, Z., Zhang, H., Liu, R., Wu, J., Qin, J., Ma, Y., Chen, L., Li, S., Chen, W., Li, F., Shi, P., Wu, Y., Shen, J. & Chen, C. (2015a) 'The interplay between TEAD4 and KLF5 promotes breast cancer partially through inhibiting the transcription of p27Kip1'. *Oncotarget*, 6 (19), pp. 17685-17697.

Wang, G., Lu, X., Dey, P., Deng, P., Wu, C. C., Jiang, S., Fang, Z., Zhao, K., Konaparthi, R., Hua, S., Zhang, J., Li-Ning-Tapia, E. M., Kapoor, A., Wu, C. J., Patel, N. B., Guo, Z., Ramamoorthy, V., Tieu, T. N., Heffernan, T., Zhao, D., Shang, X., Khadka, S., Hou, P., Hu, B., Jin, E. J., Yao, W., Pan, X., Ding, Z., Shi, Y., Li, L., Chang, Q., Troncoso, P., Logothetis, C. J., McArthur, M. J., Chin, L., Wang, Y. A. & DePinho, R. A. (2016a) 'Targeting YAP-Dependent MDSC Infiltration Impairs Tumor Progression'. *Cancer Discov*, 6 (1), pp. 80-95.

Wang, L., Luo, J. Y., Li, B., Tian, X. Y., Chen, L. J., Huang, Y., Liu, J., Deng, D., Lau, C. W., Wan, S., Ai, D., Mak, K. K., Tong, K. K., Kwan, K. M., Wang, N., Chiu, J. J., Zhu, Y. & Huang, Y. (2016b) 'Integrin-YAP/TAZ-JNK cascade mediates atheroprotective effect of unidirectional shear flow'. *Nature*, 540 (7634), pp. 579-582.

Wang, S., Liechty, B., Patel, S., Weber, J. S., Hollmann, T. J., Snuderl, M. & Karajannis, M. A. (2018a) 'Programmed death ligand 1 expression and tumor infiltrating lymphocytes in neurofibromatosis type 1 and 2 associated tumors'. *J Neurooncol*, 138 (1), pp. 183-190.

Wang, S., Xie, F., Chu, F., Zhang, Z., Yang, B., Dai, T., Gao, L., Wang, L., Ling, L., Jia, J., van Dam, H., Jin, J., Zhang, L. & Zhou, F. (2017) 'YAP antagonizes innate antiviral immunity and is targeted for lysosomal degradation through IKKε-mediated phosphorylation'. *Nat Immunol*, 18 (7), pp. 733-743.

Wang, W., Huang, J., Wang, X., Yuan, J., Li, X., Feng, L., Park, J. I. & Chen, J. (2012) 'PTPN14 is required for the density-dependent control of YAP1'. *Genes Dev*, 26 (17), pp. 1959-1971.

Wang, W., Li, N., Li, X., Tran, M. K., Han, X. & Chen, J. (2015b) 'Tankyrase Inhibitors Target YAP by Stabilizing Angiomotin Family Proteins'. *Cell Rep*, 13 (3), pp. 524-532.

Wang, W., Xiao, Z. D., Li, X., Aziz, K. E., Gan, B., Johnson, R. L. & Chen, J. (2015c) 'AMPK modulates Hippo pathway activity to regulate energy homeostasis'. *Nat Cell Biol*, 17 (4), pp. 490-499.

Wang, X., Wu, B. & Zhong, Z. (2018) 'Downregulation of YAP inhibits proliferation, invasion and increases cisplatin sensitivity in human hepatocellular carcinoma cells'. *Oncol Lett*, 16 (1), pp. 585-593.

Wang, Y., Xu, X., Maglic, D., Dill, M. T., Mojumdar, K., Ng, P. K., Jeong, K. J., Tsang, Y. H., Moreno, D., Bhavana, V. H., Peng, X., Ge, Z., Chen, H., Li, J., Chen, Z., Zhang, H., Han, L., Du, D., Creighton, C. J., Mills, G. B., Camargo, F. & Liang, H. (2018b) 'Comprehensive Molecular Characterization of the Hippo Signaling Pathway in Cancer'. *Cell Rep*, 25 (5), pp. 1304-1317.e1305.

Wang, Y., Zhu, Y., Gu, Y., Ma, M., Wang, Y., Qi, S., Zeng, Y., Zhu, R., Wang, X., Yu, P., Xu, J., Shu, Y. & Yu, F. X. (2021) 'Stabilization of Motin family proteins in NF2-deficient cells prevents full activation of YAP/TAZ and rapid tumorigenesis'. *Cell Rep*, 36 (8), pp. 109596.

Wang, Z., Wu, Y., Wang, H., Zhang, Y., Mei, L., Fang, X., Zhang, X., Zhang, F., Chen, H., Liu, Y., Jiang, Y., Sun, S., Zheng, Y., Li, N. & Huang, L. (2014) 'Interplay of mevalonate and Hippo pathways regulates RHAMM transcription via YAP to modulate breast cancer cell motility'. *Proc Natl Acad Sci U S A*, 111 (1), pp. E89-98.

Wellenreuther, R., Kraus, J. A., Lenartz, D., Menon, A. G., Schramm, J., Louis, D. N., Ramesh, V., Gusella, J. F., Wiestler, O. D. & von Deimling, A. (1995) 'Analysis of the neurofibromatosis 2 gene reveals molecular variants of meningioma'. *Am J Pathol*, 146 (4), pp. 827-832.

Wells, C. D., Fawcett, J. P., Traweger, A., Yamanaka, Y., Goudreault, M., Elder, K., Kulkarni, S., Gish, G., Virag, C., Lim, C., Colwill, K., Starostine, A., Metalnikov, P. & Pawson, T. (2006) 'A Rich1/Amot complex regulates the Cdc42 GTPase and apical-polarity proteins in epithelial cells'. *Cell*, 125 (3), pp. 535-548.

Wentworth, S., Pinn, M., Bourland, J. D., Deguzman, A. F., Ekstrand, K., Ellis, T. L., Glazier, S. S., McMullen, K. P., Munley, M., Stieber, V. W., Tatter, S. B. & Shaw, E. G. (2009) 'Clinical experience with radiation therapy in the management of neurofibromatosis-associated central nervous system tumors'. *Int J Radiat Oncol Biol Phys*, 73 (1), pp. 208-213.

West, A. P., Brodsky, I. E., Rahner, C., Woo, D. K., Erdjument-Bromage, H., Tempst, P., Walsh, M. C., Choi, Y., Shadel, G. S. & Ghosh, S. (2011) 'TLR signalling augments macrophage bactericidal activity through mitochondrial ROS'. *Nature*, 472 (7344), pp. 476-480.

White, S. M., Avantaggiati, M. L., Nemazanyy, I., Di Poto, C., Yang, Y., Pende, M., Gibney, G. T., Ressom, H. W., Field, J., Atkins, M. B. & Yi, C. (2019) 'YAP/TAZ Inhibition Induces Metabolic and Signaling Rewiring Resulting in Targetable Vulnerabilities in NF2-Deficient Tumor Cells'. *Dev Cell*, 49 (3), pp. 425-443.e429.

Wickremesekera, A., Hovens, C. M. & Kaye, A. H. (2007) 'Expression of ErbB-1 and 2 in vestibular schwannomas'. *J Clin Neurosci*, 14 (12), pp. 1199-1206.

Wickremesekera, A., Hovens, C. M. & Kaye, A. H. (2010) 'Expression of ErbB-1 and ErbB-2 in meningioma'. *J Clin Neurosci*, 17 (9), pp. 1155-1158.

Wiemels, J., Wrensch, M. & Claus, E. B. (2010) 'Epidemiology and etiology of meningioma'. *J Neurooncol*, 99 (3), pp. 307-314.

Wiestler, O. D., von Siebenthal, K., Schmitt, H. P., Feiden, W. & Kleihues, P. (1989) 'Distribution and immunoreactivity of cerebral micro-hamartomas in bilateral acoustic neurofibromatosis (neurofibromatosis 2)'. *Acta Neuropathol*, 79 (2), pp. 137-143.

Wishart, J. H. (1822) 'Case of Tumours in the Skull, Dura Mater, and Brain'. *Edinb Med Surg J*, 18 (72), pp. 393-397.

Wu, H., Wei, L., Fan, F., Ji, S., Zhang, S., Geng, J., Hong, L., Fan, X., Chen, Q., Tian, J., Jiang, M., Sun, X., Jin, C., Yin, Z. Y., Liu, Q., Zhang, J., Qin, F., Lin, K. H., Yu, J. S., Deng, X., Wang, H. R., Zhao, B., Johnson, R. L., Chen, L. & Zhou, D. (2015) 'Integration of Hippo signalling and the unfolded protein response to restrain liver overgrowth and tumorigenesis'. *Nat Commun*, 6 pp. 6239.

Wu, L., Vasilijic, S., Sun, Y., Chen, J., Landegger, L. D., Zhang, Y., Zhou, W., Ren, J., Early, S., Yin, Z., Ho, W. W., Zhang, N., Gao, X., Lee, G. Y., Datta, M., Sagers, J. E., Brown, A., Muzikansky, A., Stemmer-Rachamimov, A., Zhang, L., Plotkin, S. R., Jain, R. K., Stankovic, K. M. & Xu, L. (2021) 'Losartan prevents tumor-induced hearing loss and augments radiation efficacy in NF2 schwannoma rodent models'. *Sci Transl Med*, 13 (602),

Wu, S., Huang, J., Dong, J. & Pan, D. (2003) 'hippo encodes a Ste-20 family protein kinase that restricts cell proliferation and promotes apoptosis in conjunction with salvador and warts'. *Cell*, 114 (4), pp. 445-456.

Wu, S., Liu, Y., Zheng, Y., Dong, J. & Pan, D. (2008) 'The TEAD/TEF family protein Scalloped mediates transcriptional output of the Hippo growth-regulatory pathway'. *Dev Cell*, 14 (3), pp. 388-398.

Wu, X. (2020) 'Tead transcription factor autopalmitoylation inhibitors'.[in Google Patents. (Accessed:Wu, X.

Wyckoff, J. B., Wang, Y., Lin, E. Y., Li, J. F., Goswami, S., Stanley, E. R., Segall, J. E., Pollard, J. W. & Condeelis, J. (2007) 'Direct visualization of macrophage-assisted tumor cell intravasation in mammary tumors'. *Cancer Res*, 67 (6), pp. 2649-2656.

Wynn, T. A., Chawla, A. & Pollard, J. W. (2013) 'Macrophage biology in development, homeostasis and disease'. *Nature*, 496 (7446), pp. 445-455.

Xiao, G. H., Beeser, A., Chernoff, J. & Testa, J. R. (2002) 'p21-activated kinase links Rac/Cdc42 signaling to merlin'. *J Biol Chem*, 277 (2), pp. 883-886.

Xiao, G. H., Gallagher, R., Shetler, J., Skele, K., Altomare, D. A., Pestell, R. G., Jhanwar, S. & Testa, J. R. (2005) 'The NF2 tumor suppressor gene product, merlin, inhibits cell proliferation and cell cycle progression by repressing cyclin D1 expression'. *Mol Cell Biol*, 25 (6), pp. 2384-2394.

Xiao, J. H., Davidson, I., Matthes, H., Garnier, J. M. & Chambon, P. (1991) 'Cloning, expression, and transcriptional properties of the human enhancer factor TEF-1'. *Cell*, 65 (4), pp. 551-568.

Xin, M., Kim, Y., Sutherland, L. B., Qi, X., McAnally, J., Schwartz, R. J., Richardson, J. A., Bassel-Duby, R. & Olson, E. N. (2011) 'Regulation of insulin-like growth factor signaling by Yap governs cardiomyocyte proliferation and embryonic heart size'. *Sci Signal*, 4 (196), pp. ra70.

Xu, T., Wang, W., Zhang, S., Stewart, R. A. & Yu, W. (1995) 'Identifying tumor suppressors in genetic mosaics: the Drosophila lats gene encodes a putative protein kinase'. *Development*, 121 (4), pp. 1053-1063.

Xue, J., Schmidt, S. V., Sander, J., Draffehn, A., Krebs, W., Quester, I., De Nardo, D., Gohel, T. D., Emde, M., Schmidleithner, L., Ganesan, H., Nino-Castro, A., Mallmann, M. R., Labzin, L., Theis, H., Kraut, M., Beyer, M., Latz, E., Freeman, T. C., Ulas, T. & Schultze, J. L. (2014) 'Transcriptome-based

network analysis reveals a spectrum model of human macrophage activation'. *Immunity*, 40 (2), pp. 274-288.

Yaegashi, S., Sachse, R., Ohuchi, N., Mori, S. & Sekiya, T. (1995) 'Low incidence of a nucleotide sequence alteration of the neurofibromatosis 2 gene in human breast cancers'. *Jpn J Cancer Res*, 86 (10), pp. 929-933.

Yang, J., Liao, D., Chen, C., Liu, Y., Chuang, T. H., Xiang, R., Markowitz, D., Reisfeld, R. A. & Luo, Y. (2013a) 'Tumor-associated macrophages regulate murine breast cancer stem cells through a novel paracrine EGFR/Stat3/Sox-2 signaling pathway'. *Stem Cells*, 31 (2), pp. 248-258.

Yang, N., Morrison, C. D., Liu, P., Miecznikowski, J., Bshara, W., Han, S., Zhu, Q., Omilian, A. R., Li, X. & Zhang, J. (2012) 'TAZ induces growth factor-independent proliferation through activation of EGFR ligand amphiregulin'. *Cell Cycle*, 11 (15), pp. 2922-2930.

Yang, S., Zhang, L., Liu, M., Chong, R., Ding, S. J., Chen, Y. & Dong, J. (2013b) 'CDK1 phosphorylation of YAP promotes mitotic defects and cell motility and is essential for neoplastic transformation'. *Cancer Res*, 73 (22), pp. 6722-6733.

Yao, F., Zhou, Z., Kim, J., Hang, Q., Xiao, Z., Ton, B. N., Chang, L., Liu, N., Zeng, L., Wang, W., Wang, Y., Zhang, P., Hu, X., Su, X., Liang, H., Sun, Y. & Ma, L. (2018) 'SKP2- and OTUD1-regulated non-proteolytic ubiquitination of YAP promotes YAP nuclear localization and activity'. *Nat Commun*, 9 (1), pp. 2269.

Yasunami, M., Suzuki, K. & Ohkubo, H. (1996) 'A novel family of TEA domain-containing transcription factors with distinct spatiotemporal expression patterns'. *Biochem Biophys Res Commun*, 228 (2), pp. 365-370.

Ydens, E., Cauwels, A., Asselbergh, B., Goethals, S., Peeraer, L., Lornet, G., Almeida-Souza, L., Van Ginderachter, J. A., Timmerman, V. & Janssens, S. (2012) 'Acute injury in the peripheral nervous system triggers an alternative macrophage response'. *J Neuroinflammation*, 9 pp. 176.

Ye, K. (2007) 'Phosphorylation of merlin regulates its stability and tumor suppressive activity'. *Cell Adh Migr*, 1 (4), pp. 196-198.

Yeung, J., Yaghoobi, V., Miyagishima, D., Vesely, M. D., Zhang, T., Badri, T., Nassar, A., Han, X., Sanmamed, M. F., Youngblood, M., Peyre, M., Kalamarides, M., Rimm, D. L., Gunel, M. & Chen, L. (2021) 'Targeting the CSF1/CSF1R axis is a potential treatment strategy for malignant meningiomas'. *Neuro Oncol*, 23 (11), pp. 1922-1935.

Yi, C., Shen, Z., Stemmer-Rachamimov, A., Dawany, N., Troutman, S., Showe, L. C., Liu, Q., Shimono, A., Sudol, M., Holmgren, L., Stanger, B. Z. & Kissil, J. L. (2013) 'The p130 isoform of angiomotin is required for Yap-mediated hepatic epithelial cell proliferation and tumorigenesis'. *Sci Signal*, 6 (291), pp. ra77.

Yi, C., Troutman, S., Fera, D., Stemmer-Rachamimov, A., Avila, J. L., Christian, N., Persson, N. L., Shimono, A., Speicher, D. W., Marmorstein, R., Holmgren, L. & Kissil, J. L. (2011) 'A tight junction-associated Merlin-angiomotin complex mediates Merlin's regulation of mitogenic signaling and tumor suppressive functions'. *Cancer Cell*, 19 (4), pp. 527-540.

Yi, J., Lu, L., Yanger, K., Wang, W., Sohn, B. H., Stanger, B. Z., Zhang, M., Martin, J. F., Ajani, J. A., Chen, J., Lee, J. S., Song, S. & Johnson, R. L. (2016) 'Large tumor suppressor homologs 1 and 2 regulate mouse liver progenitor cell proliferation and maturation through antagonism of the coactivators YAP and TAZ'. *Hepatology*, 64 (5), pp. 1757-1772.

Yin, F., Yu, J., Zheng, Y., Chen, Q., Zhang, N. & Pan, D. (2013) 'Spatial organization of Hippo signaling at the plasma membrane mediated by the tumor suppressor Merlin/NF2'. *Cell*, 154 (6), pp. 1342-1355.

Yokoyama, T., Osada, H., Murakami, H., Tatematsu, Y., Taniguchi, T., Kondo, Y., Yatabe, Y., Hasegawa, Y., Shimokata, K., Horio, Y., Hida, T. & Sekido, Y. (2008) 'YAP1 is involved in mesothelioma development and negatively regulated by Merlin through phosphorylation'. *Carcinogenesis*, 29 (11), pp. 2139-2146.

Yoo, N. J., Park, S. W. & Lee, S. H. (2012) 'Mutational analysis of tumour suppressor gene NF2 in common solid cancers and acute leukaemias'. *Pathology*, 44 (1), pp. 29-32.

Youngblood, M. W., Duran, D., Montejo, J. D., Li, C., Omay, S. B., Özduman, K., Sheth, A. H., Zhao, A. Y., Tyrtova, E., Miyagishima, D. F., Fomchenko, E. I., Hong, C. S., Clark, V. E., Riche, M., Peyre, M., Boetto, J., Sohrabi, S., Koljaka, S., Baranoski, J. F., Knight, J., Zhu, H., Pamir, M. N., Avşar, T., Kilic, T., Schramm, J., Timmer, M., Goldbrunner, R., Gong, Y., Bayri, Y., Amankulor, N., Hamilton, R. L., Bilguvar, K., Tikhonova, I., Tomak, P. R., Huttner, A., Simon, M., Krischek, B., Kalamarides, M., Erson-Omay, E. Z., Moliterno, J. & Günel, M. (2019) 'Correlations between genomic subgroup and clinical features in a cohort of more than 3000 meningiomas'. *J Neurosurg*, pp. 1-10.

Yu, C., Zhang, Y. L., Pan, W. W., Li, X. M., Wang, Z. W., Ge, Z. J., Zhou, J. J., Cang, Y., Tong, C., Sun, Q. Y. & Fan, H. Y. (2013a) 'CRL4 complex regulates mammalian oocyte survival and reprogramming by activation of TET proteins'. *Science*, 342 (6165), pp. 1518-1521.

Yu, F. X., Luo, J., Mo, J. S., Liu, G., Kim, Y. C., Meng, Z., Zhao, L., Peyman, G., Ouyang, H., Jiang, W., Zhao, J., Chen, X., Zhang, L., Wang, C. Y., Bastian, B. C., Zhang, K. & Guan, K. L. (2014) 'Mutant Gq/11 promote uveal melanoma tumorigenesis by activating YAP'. *Cancer Cell*, 25 (6), pp. 822-830.

Yu, F. X., Zhang, Y., Park, H. W., Jewell, J. L., Chen, Q., Deng, Y., Pan, D., Taylor, S. S., Lai, Z. C. & Guan, K. L. (2013b) 'Protein kinase A activates the Hippo pathway to modulate cell proliferation and differentiation'. *Genes Dev*, 27 (11), pp. 1223-1232.

Yu, F. X., Zhao, B., Panupinthu, N., Jewell, J. L., Lian, I., Wang, L. H., Zhao, J., Yuan, H., Tumaneng, K., Li, H., Fu, X. D., Mills, G. B. & Guan, K. L. (2012) 'Regulation of the Hippo-YAP pathway by G-protein-coupled receptor signaling'. *Cell*, 150 (4), pp. 780-791.

Yu, J., Zheng, Y., Dong, J., Klusza, S., Deng, W. M. & Pan, D. (2010) 'Kibra functions as a tumor suppressor protein that regulates Hippo signaling in conjunction with Merlin and Expanded'. *Dev Cell*, 18 (2), pp. 288-299.

Yuan, X., Klein, D., Kerscher, S., West, B. L., Weis, J., Katona, I. & Martini, R. (2018) 'Macrophage Depletion Ameliorates Peripheral Neuropathy in Aging Mice'. *J Neurosci*, 38 (19), pp. 4610-4620.

Zanconato, F., Forcato, M., Battilana, G., Azzolin, L., Quaranta, E., Bodega, B., Rosato, A., Bicciato, S., Cordenonsi, M. & Piccolo, S. (2015) 'Genome-wide association between YAP/TAZ/TEAD and AP-1 at enhancers drives oncogenic growth'. *Nat Cell Biol*, 17 (9), pp. 1218-1227.

Zender, L., Spector, M. S., Xue, W., Flemming, P., Cordon-Cardo, C., Silke, J., Fan, S. T., Luk, J. M., Wigler, M., Hannon, G. J., Mu, D., Lucito, R., Powers, S. & Lowe, S. W. (2006) 'Identification and validation of oncogenes in liver cancer using an integrative oncogenomic approach'. *Cell*, 125 (7), pp. 1253-1267.

Zeng, Y., Stauffer, S., Zhou, J., Chen, X., Chen, Y. & Dong, J. (2017) 'Cyclin-dependent kinase 1 (CDK1)-mediated mitotic phosphorylation of the transcriptional co-repressor Vgll4 inhibits its tumor-suppressing activity'. *J Biol Chem*, 292 (36), pp. 15028-15038.

Zhan, T., Huang, X., Tian, X., Chen, X., Ding, Y., Luo, H. & Zhang, Y. (2018) 'Downregulation of MicroRNA-455-3p Links to Proliferation and Drug Resistance of Pancreatic Cancer Cells via Targeting TAZ'. *Mol Ther Nucleic Acids*, 10 pp. 215-226.

Zhang, E., Shen, B., Mu, X., Qin, Y., Zhang, F., Liu, Y., Xiao, J., Zhang, P., Wang, C., Tan, M. & Fan, Y. (2016) 'Ubiquitin-specific protease 11 (USP11) functions as a tumor suppressor through deubiquitinating and stabilizing VGLL4 protein'. *Am J Cancer Res*, 6 (12), pp. 2901-2909.

Zhang, H., Liu, C. Y., Zha, Z. Y., Zhao, B., Yao, J., Zhao, S., Xiong, Y., Lei, Q. Y. & Guan, K. L. (2009a) 'TEAD transcription factors mediate the function of TAZ in cell growth and epithelial-mesenchymal transition'. *J Biol Chem*, 284 (20), pp. 13355-13362.

Zhang, H., Pasolli, H. A. & Fuchs, E. (2011) 'Yes-associated protein (YAP) transcriptional coactivator functions in balancing growth and differentiation in skin'. *Proc Natl Acad Sci U S A*, 108 (6), pp. 2270-2275.

Zhang, H., Ramakrishnan, S. K., Triner, D., Centofanti, B., Maitra, D., Győrffy, B., Sebolt-Leopold, J. S., Dame, M. K., Varani, J., Brenner, D. E., Fearon, E. R., Omary, M. B. & Shah, Y. M. (2015a) 'Tumor-selective proteotoxicity of verteporfin inhibits colon cancer progression independently of YAP1'. *Sci Signal*, 8 (397), pp. ra98.

Zhang, H. Y., Yang, G. H., Chen, H. J., Wei, B., Ke, Q., Guo, H., Ye, L., Bu, H., Yang, K. & Zhang, Y. H. (2005) 'Clinicopathological, immunohistochemical, and ultrastructural study of 13 cases of melanotic schwannoma'. *Chin Med J (Engl)*, 118 (17), pp. 1451-1461.

Zhang, J., Ji, J. Y., Yu, M., Overholtzer, M., Smolen, G. A., Wang, R., Brugge, J. S., Dyson, N. J. & Haber, D. A. (2009b) 'YAP-dependent induction of amphiregulin identifies a non-cell-autonomous component of the Hippo pathway'. *Nat Cell Biol*, 11 (12), pp. 1444-1450.

Zhang, L., Ren, F., Zhang, Q., Chen, Y., Wang, B. & Jiang, J. (2008) 'The TEAD/TEF family of transcription factor Scalloped mediates Hippo signaling in organ size control'. *Dev Cell*, 14 (3), pp. 377-387.

Zhang, L., Tang, F., Terracciano, L., Hynx, D., Kohler, R., Bichet, S., Hess, D., Cron, P., Hemmings, B. A., Hergovich, A. & Schmitz-Rohmer, D. (2015b) 'NDR functions as a physiological YAP1 kinase in the intestinal epithelium'. *Curr Biol*, 25 (3), pp. 296-305.

Zhang, N., Bai, H., David, K. K., Dong, J., Zheng, Y., Cai, J., Giovannini, M., Liu, P., Anders, R. A. & Pan, D. (2010) 'The Merlin/NF2 tumor suppressor functions through the YAP oncoprotein to regulate tissue homeostasis in mammals'. *Dev Cell*, 19 (1), pp. 27-38.

Zhang, Q., Meng, F., Chen, S., Plouffe, S. W., Wu, S., Liu, S., Li, X., Zhou, R., Wang, J., Zhao, B., Liu, J., Qin, J., Zou, J., Feng, X. H., Guan, K. L. & Xu, P. (2017) 'Hippo signalling governs cytosolic nucleic acid sensing through YAP/TAZ-mediated TBK1 blockade'. *Nat Cell Biol*, 19 (4), pp. 362-374.

Zhang, S., Zhang, H., Ghia, E. M., Huang, J., Wu, L., Zhang, J., Lam, S., Lei, Y., He, J., Cui, B., Widhopf, G. F., 2nd, Yu, J., Schwab, R., Messer, K., Jiang, W., Parker, B. A., Carson, D. A. & Kipps, T. J. (2019) 'Inhibition of chemotherapy resistant breast cancer stem cells by a ROR1 specific antibody'. *Proc Natl Acad Sci U S A*, 116 (4), pp. 1370-1377.

Zhang, W., Gao, Y., Li, P., Shi, Z., Guo, T., Li, F., Han, X., Feng, Y., Zheng, C., Wang, Z., Li, F., Chen, H., Zhou, Z., Zhang, L. & Ji, H. (2014a) 'VGLL4 functions as a new tumor suppressor in lung cancer by negatively regulating the YAP-TEAD transcriptional complex'. *Cell Research*, 24 (3), pp. 331-343.

Zhang, W., Li, J., Wu, Y., Ge, H., Song, Y., Wang, D., Yuan, H., Jiang, H., Wang, Y. & Cheng, J. (2018a) 'TEAD4 overexpression promotes epithelial-mesenchymal transition and associates with aggressiveness and adverse prognosis in head neck squamous cell carcinoma'. *Cancer Cell Int*, 18 pp. 178.

Zhang, W., Xu, J., Li, J., Guo, T., Jiang, D., Feng, X., Ma, X., He, L., Wu, W., Yin, M., Ge, L., Wang, Z., Ho, M. S., Zhao, Y., Fei, Z. & Zhang, L. (2018b) 'The TEA domain family transcription factor TEAD4 represses murine adipogenesis by recruiting the cofactors VGLL4 and CtBP2 into a transcriptional complex'. *J Biol Chem*, 293 (44), pp. 17119-17134.

Zhang, Y. L., Li, Q., Yang, X. M., Fang, F., Li, J., Wang, Y. H., Yang, Q., Zhu, L., Nie, H. Z., Zhang, X. L., Feng, M. X., Jiang, S. H., Tian, G. A., Hu, L. P., Lee, H. Y., Lee, S. J., Xia, Q. & Zhang, Z. G. (2018c) 'SPON2 Promotes M1-like Macrophage Recruitment and Inhibits Hepatocellular Carcinoma Metastasis by Distinct Integrin-Rho GTPase-Hippo Pathways'. *Cancer Res*, 78 (9), pp. 2305-2317.

Zhang, Z., Lin, Z., Zhou, Z., Shen, H. C., Yan, S. F., Mayweg, A. V., Xu, Z., Qin, N., Wong, J. C., Zhang, Z., Rong, Y., Fry, D. C. & Hu, T. (2014b) 'Structure-Based Design and Synthesis of Potent Cyclic Peptides Inhibiting the YAP-TEAD Protein-Protein Interaction'. *ACS Med Chem Lett*, 5 (9), pp. 993-998.

Zhao, B., Li, L., Lu, Q., Wang, L. H., Liu, C. Y., Lei, Q. & Guan, K. L. (2011) 'Angiomotin is a novel Hippo pathway component that inhibits YAP oncoprotein'. *Genes Dev*, 25 (1), pp. 51-63.

Zhao, B., Li, L., Tumaneng, K., Wang, C. Y. & Guan, K. L. (2010) 'A coordinated phosphorylation by Lats and CK1 regulates YAP stability through SCF(beta-TRCP)'. *Genes Dev*, 24 (1), pp. 72-85.

Zhao, B., Li, L., Wang, L., Wang, C. Y., Yu, J. & Guan, K. L. (2012) 'Cell detachment activates the Hippo pathway via cytoskeleton reorganization to induce anoikis'. *Genes Dev*, 26 (1), pp. 54-68.

Zhao, B., Wei, X., Li, W., Udan, R. S., Yang, Q., Kim, J., Xie, J., Ikenoue, T., Yu, J., Li, L., Zheng, P., Ye, K., Chinnaiyan, A., Halder, G., Lai, Z. C. & Guan, K. L. (2007) 'Inactivation of YAP oncoprotein by the Hippo pathway is involved in cell contact inhibition and tissue growth control'. *Genes Dev*, 21 (21), pp. 2747-2761.

Zhao, B., Ye, X., Yu, J., Li, L., Li, W., Li, S., Yu, J., Lin, J. D., Wang, C. Y., Chinnaiyan, A. M., Lai, Z. C. & Guan, K. L. (2008) 'TEAD mediates YAP-dependent gene induction and growth control'. *Genes Dev*, 22 (14), pp. 1962-1971.

Zhao, F., Yang, Z., Chen, Y., Zhou, Q., Zhang, J., Liu, J., Wang, B., He, Q., Zhang, L., Yu, Y. & Liu, P. (2018a) 'Deregulation of the Hippo Pathway Promotes Tumor Cell Proliferation Through YAP Activity in Human Sporadic Vestibular Schwannoma'. *World Neurosurg*, 117 pp. e269-e279.

Zhao, L., Guan, H., Song, C., Wang, Y., Liu, C., Cai, C., Zhu, H., Liu, H., Zhao, L. & Xiao, J. (2018b) 'YAP1 is essential for osteoclastogenesis through a TEADs-dependent mechanism'. *Bone*, 110 pp. 177-186.

Zhao, Y., Liu, P., Zhang, N., Chen, J., Landegger, L. D., Wu, L., Zhao, F., Zhao, Y., Zhang, Y., Zhang, J., Fujita, T., Stemmer-Rachamimov, A., Ferraro, G. B., Liu, H., Muzikansky, A., Plotkin, S. R., Stankovic, K. M., Jain, R. K. & Xu, L. (2018c) 'Targeting the cMET pathway augments radiation response without adverse effect on hearing in NF2 schwannoma models'. *Proc Natl Acad Sci U S A*, 115 (9), pp. E2077-e2084.

Zheng, Y. & Pan, D. (2019) 'The Hippo Signaling Pathway in Development and Disease'. *Dev Cell*, 50 (3), pp. 264-282.

Zheng, Y., Wang, W., Liu, B., Deng, H., Uster, E. & Pan, D. (2015) 'Identification of Happyhour/MAP4K as Alternative Hpo/Mst-like Kinases in the Hippo Kinase Cascade'. *Dev Cell*, 34 (6), pp. 642-655.

Zhou, D., Conrad, C., Xia, F., Park, J. S., Payer, B., Yin, Y., Lauwers, G. Y., Thasler, W., Lee, J. T., Avruch, J. & Bardeesy, N. (2009) 'Mst1 and Mst2 maintain hepatocyte quiescence and suppress hepatocellular carcinoma development through inactivation of the Yap1 oncogene'. *Cancer Cell*, 16 (5), pp. 425-438.

Zhou, G. X., Li, X. Y., Zhang, Q., Zhao, K., Zhang, C. P., Xue, C. H., Yang, K. & Tian, Z. B. (2013) 'Effects of the hippo signaling pathway in human gastric cancer'. *Asian Pac J Cancer Prev*, 14 (9), pp. 5199-5205.

Zhou, L., Ercolano, E., Ammoun, S., Schmid, M. C., Barczyk, M. A. & Hanemann, C. O. (2011) 'Merlin-deficient human tumors show loss of contact inhibition and activation of Wnt/β-catenin signaling linked to the PDGFR/Src and Rac/PAK pathways'. *Neoplasia*, 13 (12), pp. 1101-1112.

Zhou, T. Y., Zhou, Y. L., Qian, M. J., Fang, Y. Z., Ye, S., Xin, W. X., Yang, X. C. & Wu, H. H. (2018) 'Interleukin-6 induced by YAP in hepatocellular carcinoma cells recruits tumor-associated macrophages'. *J Pharmacol Sci*, 138 (2), pp. 89-95.

Zhou, X., Li, W., Wang, S., Zhang, P., Wang, Q., Xiao, J., Zhang, C., Zheng, X., Xu, X., Xue, S., Hui, L., Ji, H., Wei, B. & Wang, H. (2019) 'YAP Aggravates Inflammatory Bowel Disease by Regulating M1/M2 Macrophage Polarization and Gut Microbial Homeostasis'. *Cell Rep*, 27 (4), pp. 1176-1189.e1175.

Zhou, Y., Huang, T., Zhang, J., Wong, C. C., Zhang, B., Dong, Y., Wu, F., Tong, J. H. M., Wu, W. K. K., Cheng, A. S. L., Yu, J., Kang, W. & To, K. F. (2017) 'TEAD1/4 exerts oncogenic role and is negatively regulated by miR-4269 in gastric tumorigenesis'. *Oncogene*, 36 (47), pp. 6518-6530.

Zhou, Z., Hu, T., Xu, Z., Lin, Z., Zhang, Z., Feng, T., Zhu, L., Rong, Y., Shen, H., Luk, J. M., Zhang, X. & Qin, N. (2015) 'Targeting Hippo pathway by specific interruption of YAP-TEAD interaction using cyclic YAP-like peptides'. *Faseb j*, 29 (2), pp. 724-732.

Zhou, Z., Zhu, J. S., Gao, C. P., Li, L. P., Zhou, C., Wang, H. & Liu, X. G. (2016) 'siRNA targeting YAP gene inhibits gastric carcinoma growth and tumor metastasis in SCID mice'. *Oncol Lett*, 11 (4), pp. 2806-2814.

Zhu, C., Li, L., Zhang, Z., Bi, M., Wang, H., Su, W., Hernandez, K., Liu, P., Chen, J., Chen, M., Huang, T. H., Chen, L. & Liu, Z. (2019) 'A Non-canonical Role of YAP/TEAD Is Required for Activation of Estrogen-Regulated Enhancers in Breast Cancer'. *Mol Cell*, 75 (4), pp. 791-806.e798.

Zoch, A., Mayerl, S., Schulz, A., Greither, T., Frappart, L., Rübsam, J., Heuer, H., Giovannini, M. & Morrison, H. (2015) 'Merlin Isoforms 1 and 2 Both Act as Tumour Suppressors and Are Required for Optimal Sperm Maturation'. *PLoS One*, 10 (8), pp. e0129151.

6. Appendix

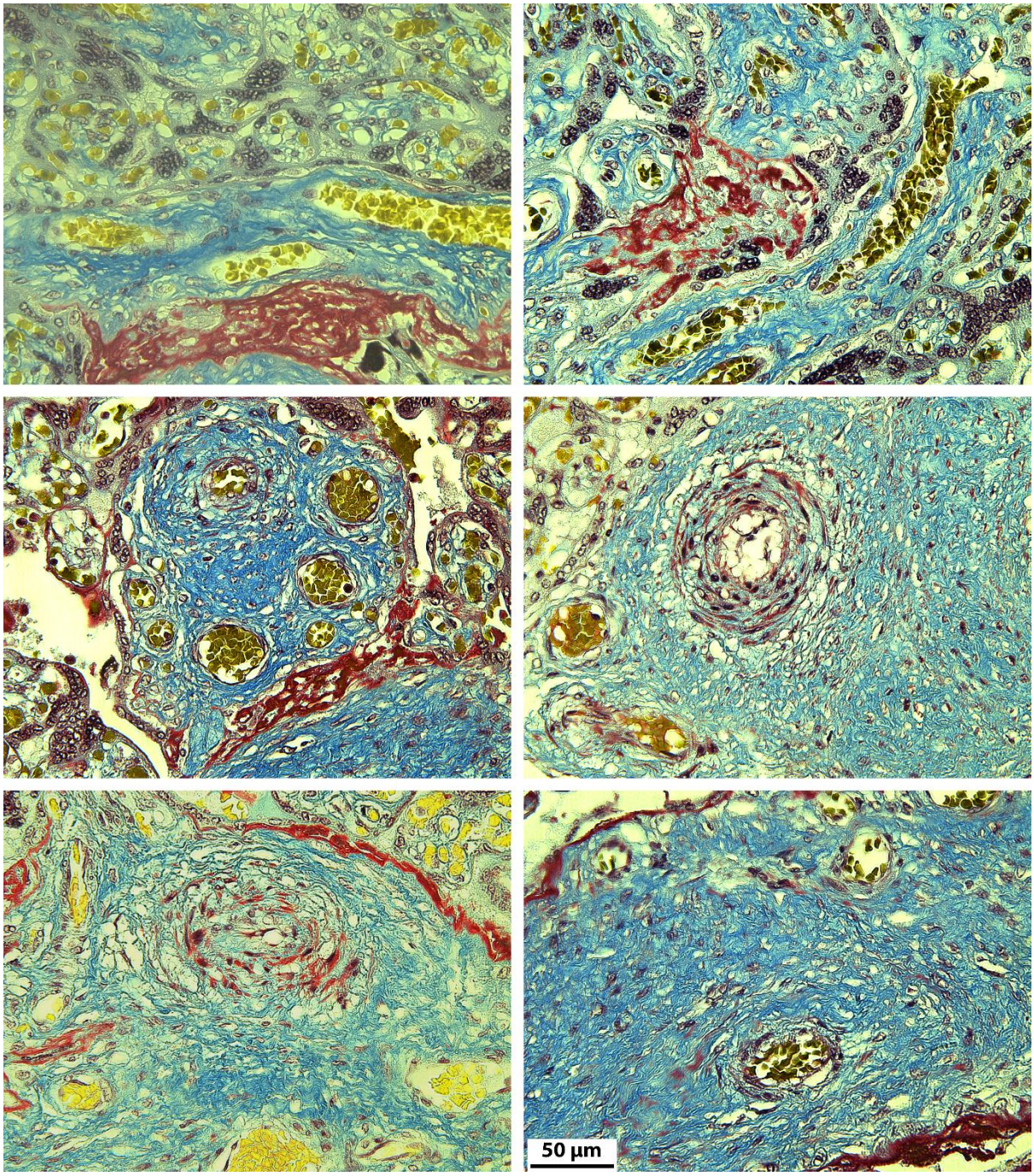

Figure 6.1: Martius Scarlet Blue (MSB) control stainings on paraffin sections of human tonsil tissue *by Philip Edwards of the Cellular and Anatomical Pathology Department of Derriford Hospital. Collagen in blue; muscle in pale red; fibrin in red; red blood cells in yellow/orange; nuclei in purple/blue. Scale bar = 50 µm in all images.*

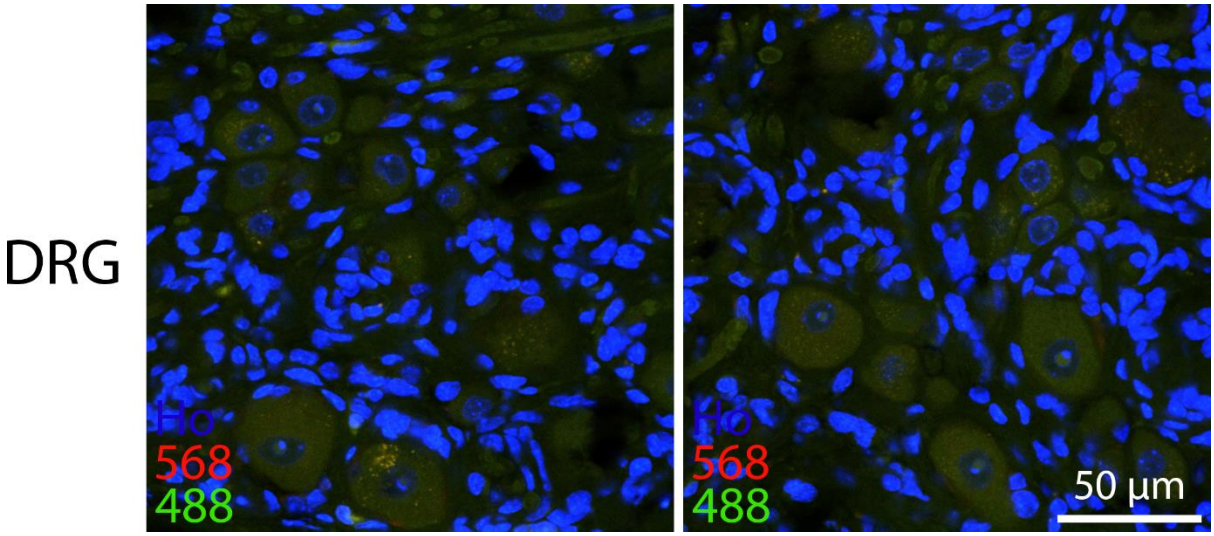

***Figure 6.2: Images of frozen DRG tissue stained without primary anti-Collagen IV and anti-Neurofilament antibodies**, only with the secondary antibodies anti-Rabbit Alexa Fluor 568 = 568 and anti-Chicken Alexa Fluor 488 = 488 plus DNA dye Hoechst (Ho). Scale bar = 50 µm in both images.*

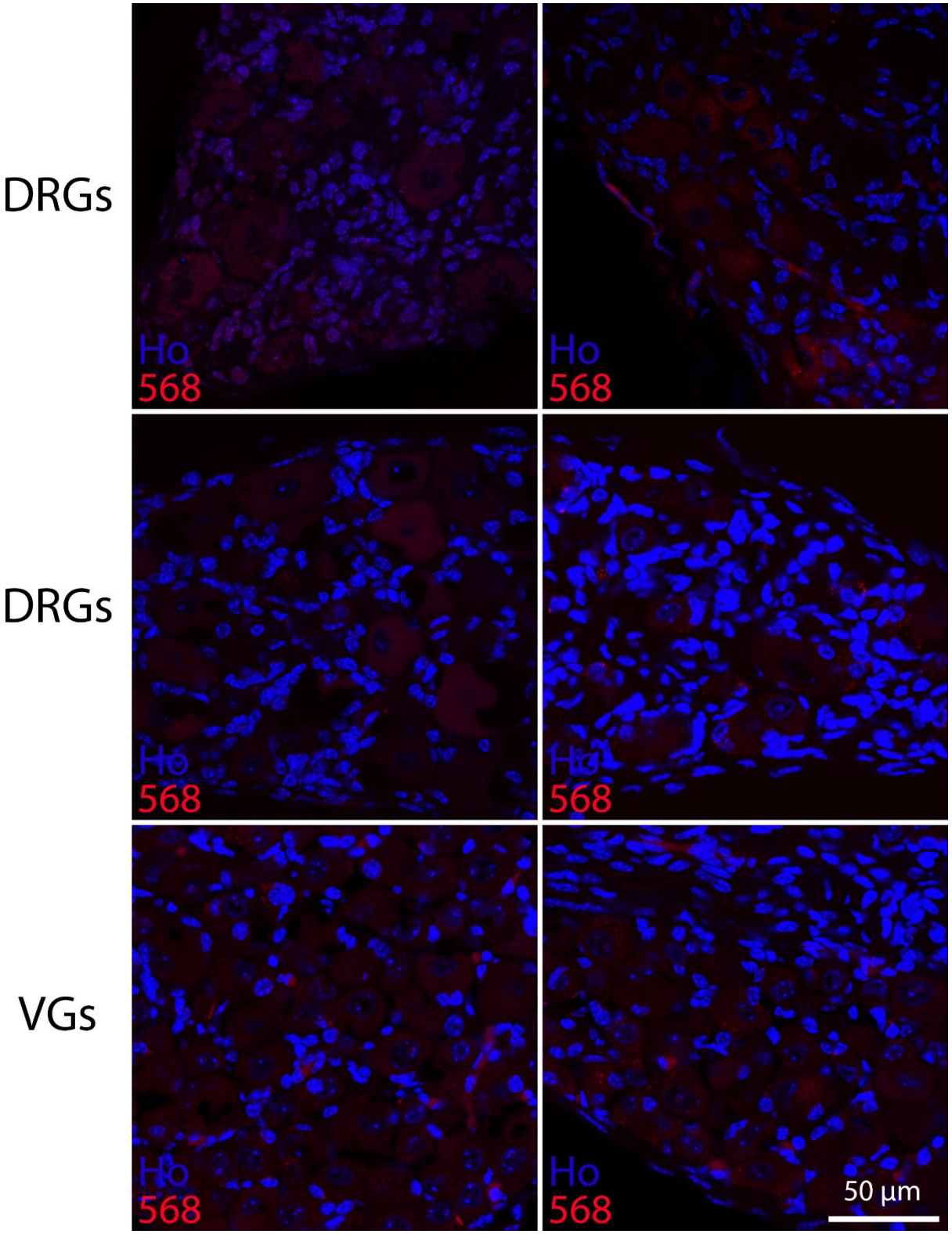

***Figure 6.3: Images of frozen DRG and VG sections stained without primary anti-Iba1 antibody**, only with secondary antibody (anti-Rabbit Alexa Fluor 568 = 568) plus DNA dye Hoechst (Ho). Scale bar = 50 µm in all images.*

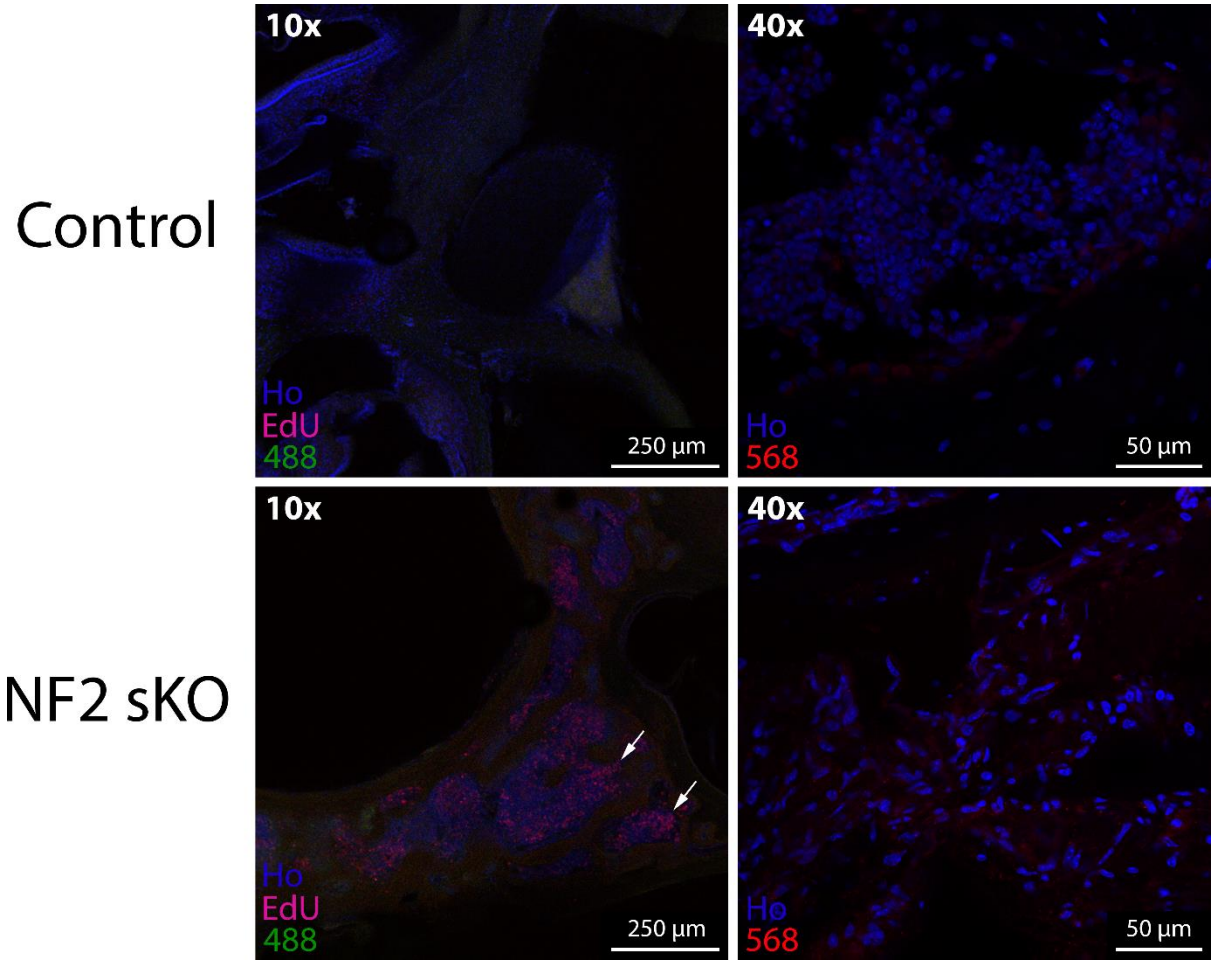

Figure 6.4: Agarose cochlea sections stained without primary anti-Iba1 antibody*, only with secondary antibodies and DNA dye Hoechst (Ho); anti-Rabbit Alexa Fluor 488 = 488 and EdU on the left and anti-Rabbit Alexa Fluor 568 = 568 without EdU on the right. Images as with 10x and 40x microscope objectives, indicated in upper left corner of each image. Scale bars = 250 µm (in 10x) and 50 µm (in 40x).*

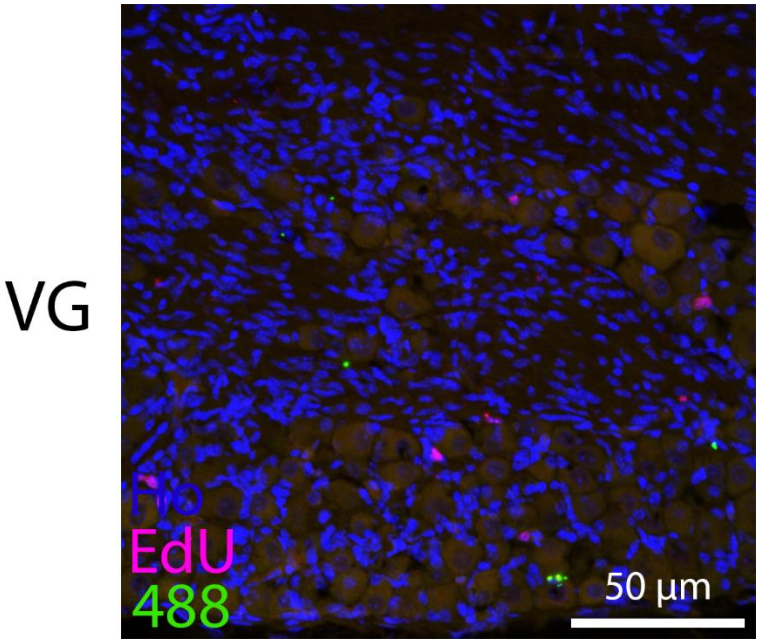

***Figure 6.5: Frozen VG tissue stained without primary anti-Neurofilament antibody**, only with secondary antibody anti-Chicken Alexa Fluor 488 = 488 plus EdU and DNA dye Hoechst (Ho). Scale bar = 50 µm.*

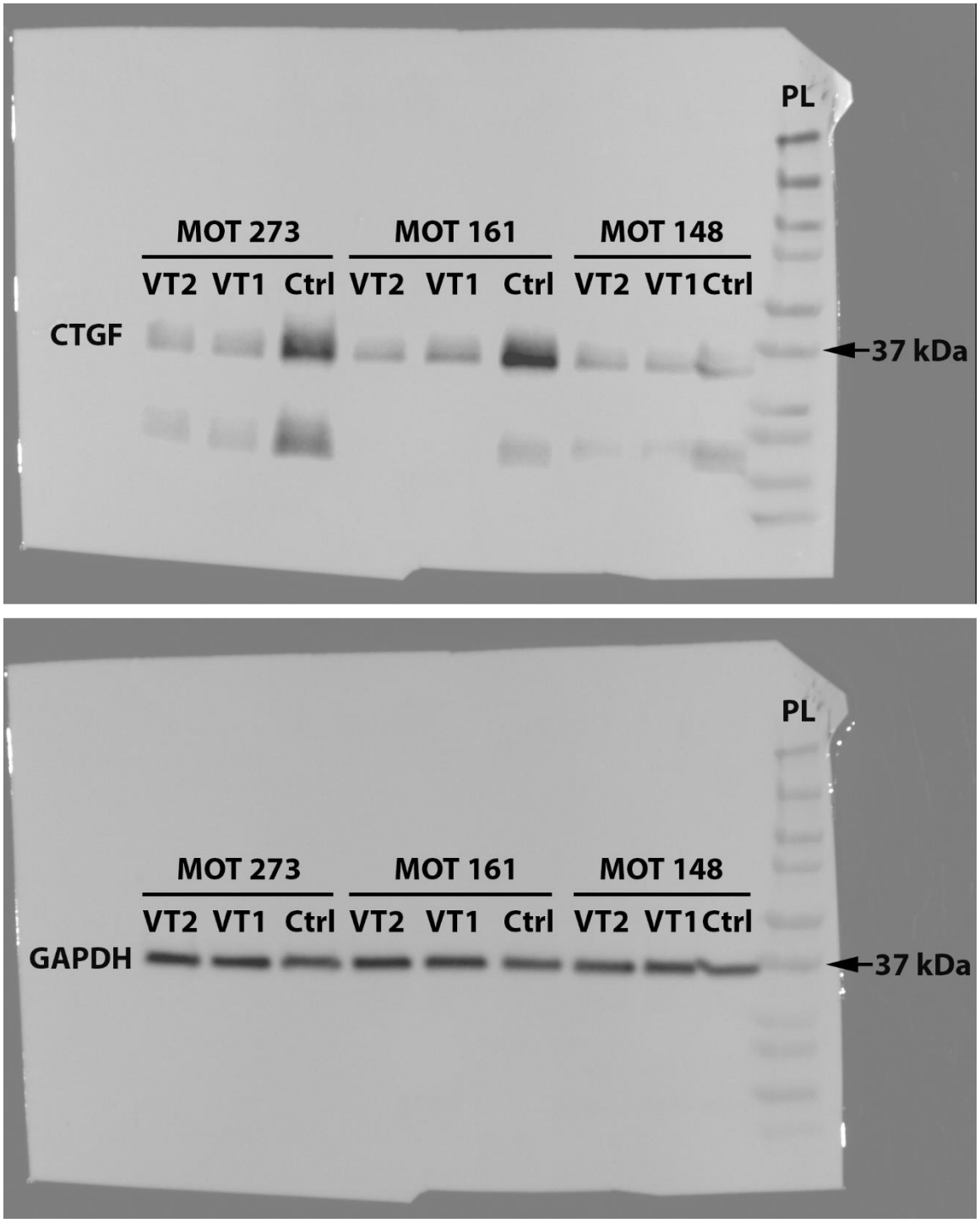

Figure 6.6: Images of complete PVDF membranes whose bands are seen in Figure 3.14.1*. PVDF membranes with the protein lysates from Merlin null primary human meningioma cells MOT 273, 161 and 148 treated with 1μM of VT1 or VT2 or with Ctrl (DMSO vehicle) for 48 hours incubated with anti-CTGF primary antibody (top image). Same PVDF membrane was incubated with anti-GAPDH primary antibody after stripping (bottom image). CTGF and GAPDH protein bands visible at 37 kilodalton (kDa). PL = protein ladder.*

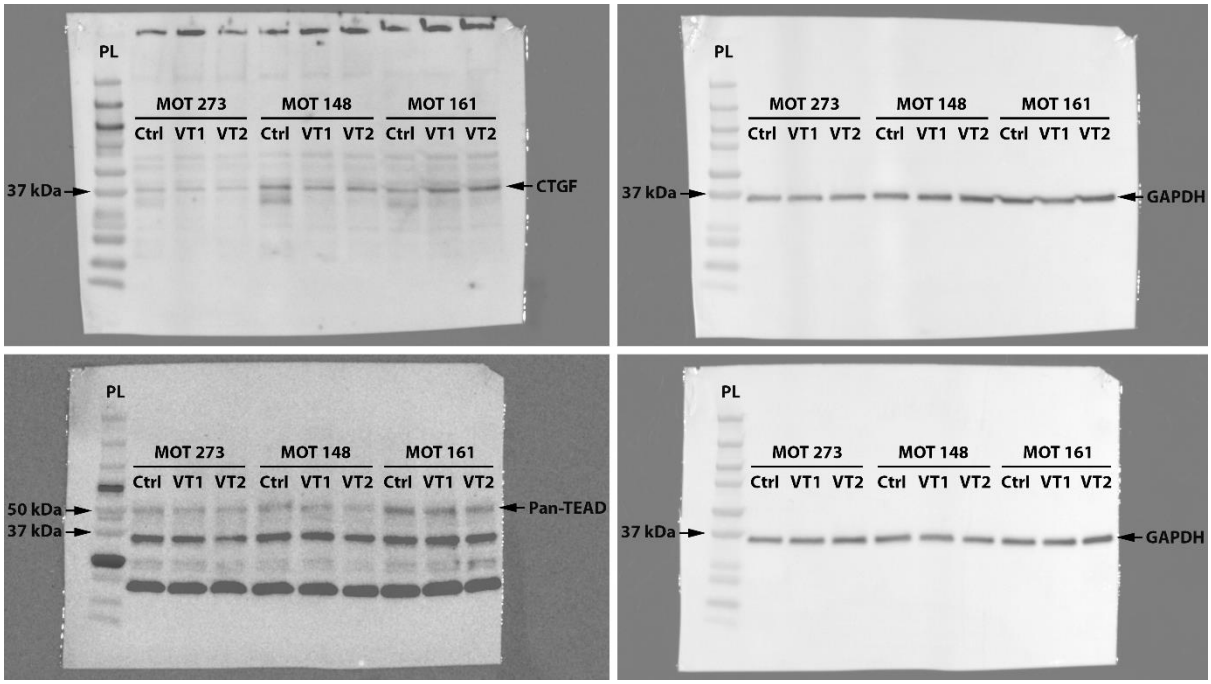

Figure 6.7: Images of uncropped PVDF membranes whose bands are seen in Figure 3.14.3*. PVDF membranes with the protein lysates from Merlin null primary human meningioma cells MOT 273, 148 and 161 treated with 1μM of VT1 or VT2 or with Ctrl (DMSO vehicle) for 48 hours incubated with anti-CTGF or anti-Pan-TEAD primary antibodies (on the left). Both PVDF membranes incubated with anti-GAPDH primary antibody after stripping (images seen next to respective PVDF membranes on the right). CTGF and GAPDH protein bands can be seen at 37 kDa, Pan-TEAD protein bands at 50 kDa. PL = protein ladder.*

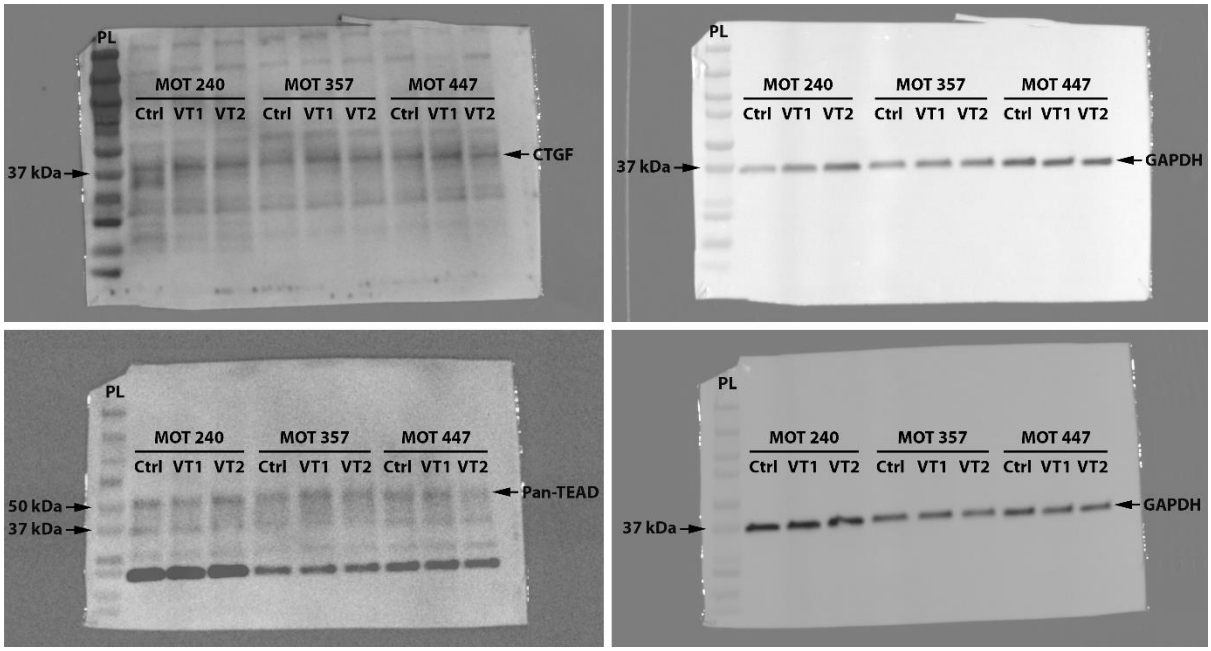

Figure 6.8: Images of whole PVDF membranes whose bands are visible in Figure 3.14.5. *PVDF membranes with the protein lysates from Merlin positive primary human meningioma cells MOT 240, 357 and 447 treated for 48 hours with 1µM of VT1 or VT2 or with Ctrl (DMSO vehicle) incubated with anti-CTGF or anti-Pan-TEAD primary antibodies (on the left). After stripping, both PVDF membranes incubated with anti-GAPDH primary antibody (images seen next to respective PVDF membranes on the right). Pan-TEAD protein bands visible at 50 kDa, CTGF and GAPDH protein bands at 37 kDa. PL = protein ladder.*